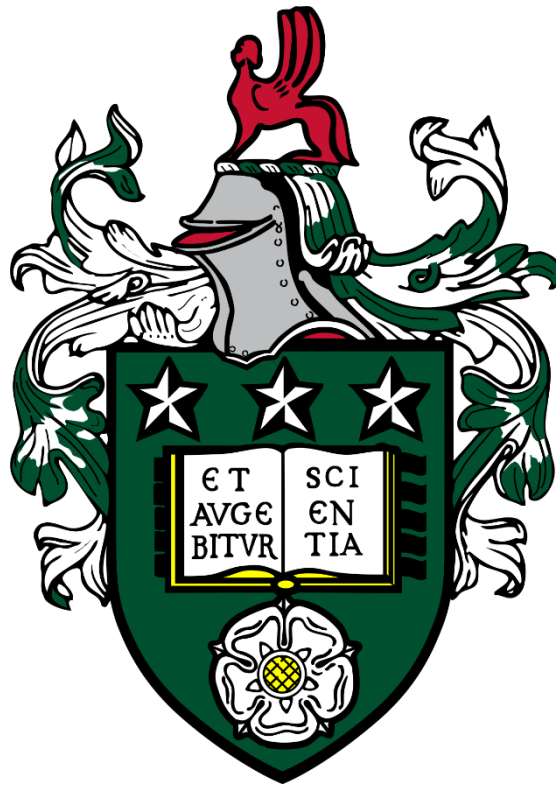


# THE BIOMECHANICAL AND WEAR PERFORMANCE OF A TOTAL ANKLE REPLACEMENT

James David Hopwood

Submitted in accordance with the requirements for the degree of  
Doctor of Philosophy



The University of Leeds

Institute of Medical and Biological Engineering

School of Mechanical Engineering

November 2022

The candidate confirms that the work submitted is his own and that appropriate credit has been given where reference has been made to the work of others.

This copy has been supplied on the understanding that it is copyright material and that no quotation from the thesis may be published without proper acknowledgement

© 2022 The University of Leeds and James David Hopwood

The right of James David Hopwood to be identified as Author of this work has been asserted by him in accordance with the Copyright, Designs and Patents Act 1988.

My PhD is dedicated to the memories of my Nan (Valerie Hopwood) and  
Papa (Geoffrey Hopwood)

Forever in our thoughts, always in our hearts



## ACKNOWLEDGEMENTS

Submitting this thesis after nearly a decade at the University of Leeds, it's safe to say I've made myself at home here...or did I overstay my welcome? Throughout the highs and lows of my PhD journey, I have been fortunate to meet an abundance of individuals who ultimately made this project possible.

I would firstly like to express my sincere gratitude to my supervisors Dr. Claire Brockett, Prof. Anthony Redmond and Dr. Graham Chapman for their continuing help and support throughout the duration of my PhD. Their guidance, expertise and constant encouragement has been invaluable to the planning, execution, and completion of this thesis. I would especially like to thank Dr. Brockett, who as well as playing the lead supervisory role, has significantly contributed to my professional development as an academic researcher. I admire the dedication she has to each of her PhD students and feel very fortunate to have been one of them (#imbeankles).

My utmost appreciation must extend to the Institute of Medical and Biological Engineering (iMBE) technical team: Phil Wood; Camille Hammersley; Andrew Stockdale; Dec Isaac; Keith Dyer; Sam Burdon; Rhys Moore; Jane Cardie; and Irvin Homan. In particular, I would like to thank Phil Wood for dedicating his time and effort in assisting me throughout my testing (even when I did manage to break the simulator on a number of occasions!) Further to this, I would like to acknowledge the high-class facilities and equipment provided by iMBE, which was necessary for the completion of this body of work.

I am extremely thankful for the contributions of Dr. Laura Richards and Dr. Simon Collins, my industrial sponsors from MatOrtho Ltd, for their invaluable product insight, active involvement and provision of all the samples used within this project. I would also like to recognise the team at the Nottingham Trent Gait Laboratory, in particular, Dr. Cleveland Barnett and Jodie Levick, for their technical guidance and expertise.

I would like to acknowledge the financial support received from the Engineering and Physical Sciences Research Council (EPSRC) Centre for Doctoral Training in Tissue Engineering and Regenerative Medicine, MatOrtho Ltd and the Centre for Sport, Exercise and Osteoarthritis Research, Versus Arthritis.

A special thanks goes to all of the participants who gave up their valuable time to take part in the studies. They are the ones that made this research possible, and for that I would like to express my deepest appreciation.

To all of those who I have had the pleasure of living and working with throughout my PhD, thank you for making this such an enjoyable journey and giving me unforgettable memories that I will cherish forever. Special mentions include: Matt Sullivan; Paddy Lawson; Simon Williams;

Kern Cowell; Dave Rochelle; Danny White; Lizzy Young; the Ankle Research Group; Rat Mansion; and The Longest Yard.

I am forever grateful to my girlfriend Louise (and the gang!), for her unwavering patience, proof reading skills, love and most importantly, putting up with my continuous narration of how my write up was going each and every day.

Above all, I would like to thank my parents (Dave and Joanne), as well as my two younger brothers (Jonny and Ben), for offering their unfaltering support, optimism and reassurance throughout my time at university, and for helping me to get to where I find myself in life now.

Just remember, that every time you meet me now, it will be a doctor's appointment!

## ABSTRACT

Total ankle replacement (TAR) is an alternative to ankle arthrodesis (AA), which consists of replacing the degenerated joint with a mechanical motion-preserving alternative. TAR is still not considered as clinically successful as hip and knee replacements, with approximately 45-91% survivorship at 15 years. This is primarily due to implant loosening, which has been associated with wear-mediated osteolysis. The development of a successful TAR has been further restricted by limited pre-clinical testing and biomechanical analyses compared to hip and knee joints. The research in this thesis aimed to assess the biomechanical and wear performance of a third generation mobile-bearing TAR.

The wear performance of the BOX® ankle (MatOrtho Ltd, Leatherhead, UK) was determined through a series of four implant and simulator parameter based studies: (1) implant size; (2) accelerated artificial ageing; (3) simulator type; and (4) simulator input profiles. Different sizes of the device were evaluated in two types of mechanical knee simulators (pneumatic and electromechanical) for up to 5 million cycles (Mc), under varying loads and kinematics (University of Leeds and ISO 22622:2019), aiming to replicate an ankle gait cycle. Gravimetric measurements of polyethylene wear were taken every Mc, while simulator input following, topographic changes, and visual damage wear modes were also reported. No statistically significant differences in the mean wear rate were determined between implant sizes, simulator type or simulator input profiles, with each wear rate comparing well to the ankle simulator literature. The artificially aged inserts exhibited increased wear rates during the steady-state wear phase, but showed no indication of structural failure. The biomechanical performance of the implant was investigated through three-dimensional gait analysis. A BOX® ankle patient cohort (n = 6) was compared against AA patients (n = 9) and a mixed TAR patient group (n = 6). A multi-segment foot model (MFM) was used to calculate peak and ROM kinematics of the hindfoot, midfoot and forefoot segments, while kinetic and kinematics parameters were determined for the hip and knee joints. Spatiotemporal parameters and patient reported outcome measures were also assessed. The range of hindfoot sagittal motion was greater in both TAR cohorts compared to the AA cohort, while the AA patients displayed hypermobility at the distal foot segments. The outcome of this study further emphasizes the clinical relevance of using a MFM and suggests surgical decision making should consider the effect of treatment options on the distally located foot joints.

To summarise, the thesis highlighted the influence of a variety of implant and simulator parameters on TAR wear simulation, alongside the improved biomechanical function of TAR when compared to AA. The study provided a useful benchmark for future TAR wear simulations, which should aim to develop a clinically relevant wear simulation protocol, under a variety of activities of daily living, to further understand the biomechanical and wear performance of a TAR.

# CONTENTS

<b>ACKNOWLEDGEMENTS</b> .....	<b>iii</b>
<b>ABSTRACT</b> .....	<b>v</b>
<b>LIST OF FIGURES</b> .....	<b>xii</b>
<b>LIST OF TABLES</b> .....	<b>xix</b>
<b>DISSEMINATION OF RESEARCH</b> .....	<b>1</b>
<b>ABBREVIATION LIST</b> .....	<b>2</b>
<b>ANATOMICAL TERMINOLOGY</b> .....	<b>4</b>
<b>INTRODUCTION</b> .....	<b>6</b>
<b>AIMS AND OBJECTIVES</b> .....	<b>7</b>
<b>THESIS OUTLINE</b> .....	<b>9</b>
<b>CHAPTER 1: LITERATURE REVIEW</b> .....	<b>10</b>
1.1    Ankle Joint Complex Anatomy and Function .....	11
1.2    Biomechanics of the Ankle .....	13
1.2.1    Anatomical Planes and Axes.....	13
1.2.2    Motions of the Ankle Joint Complex.....	14
1.2.3    Axis of Rotation.....	15
1.2.4    Range of Motion.....	17
1.2.5    Gait Cycle and Events .....	17
1.2.6    Ankle Forces .....	20
1.3    Ankle Arthritis.....	21
1.4    Treatment of Ankle Arthritis.....	22
1.4.1    Non-surgical Interventions .....	22
1.4.2    Surgical Interventions .....	23
1.4.3    Ankle Arthrodesis.....	23
1.4.4    Total Ankle Replacement.....	25
1.4.4.1    History and Design Development .....	25
1.4.4.2    Survivorship.....	27
1.4.4.3    Complications.....	28
1.4.5    Biomechanics of Total Ankle Replacements .....	29
1.4.6    Biomechanical Differences between Arthrodesis and Replacement.....	30
1.4.7    The Bologna-Oxford Ankle.....	32
1.5    Fundamentals of Biotribology.....	34
1.5.1    Friction.....	34
1.5.2    Lubrication .....	35
1.5.3    Wear.....	38
1.6    Wear Simulation.....	41
1.6.1    Simulator Inputs .....	44

1.6.2	Wear Rates and Limitations.....	45
1.6.3	Conventional versus Cross-linked Polyethylene.....	48
1.6.4	Force versus Displacement Control.....	49
1.6.5	Simulator Lubrication.....	49
1.6.6	Fixed versus Mobile Design.....	50
1.6.7	Wear Simulator Summary.....	51
1.7	Summary of the Literature Review.....	51
<b>CHAPTER 2: METHOD DEVELOPMENT.....</b>		<b>53</b>
2.1	Introduction.....	54
2.2	Materials.....	54
2.3	Simulator Methods.....	55
2.3.1	Simulator Inputs.....	56
2.3.1.1	Axial Load.....	56
2.3.1.2	Flexion/Extension.....	57
2.3.1.3	Internal/External Rotation.....	57
2.3.1.4	Anterior/Posterior Displacement.....	58
2.3.2	Simulator Input Translation.....	59
2.3.3	Talar Fixtures.....	60
2.3.4	Component Set-up.....	60
2.3.5	Contact Areas.....	60
2.3.6	Calibration.....	61
2.3.7	Simulation Preparation.....	62
2.3.8	Frequency.....	62
2.3.9	Lubrication.....	62
2.4	Gravimetric Measurement Method.....	63
2.5	Simulation Duration and Serum Changes.....	64
2.6	Loading and Kinematic Performance.....	64
2.7	Surface Roughness Measurements.....	65
2.8	Visual Surface Damage Modes.....	69
2.9	Retrievals Analysis.....	70
<b>CHAPTER 3: THE EFFECT OF IMPLANT PARAMETERS ON THE WEAR OF A TOTAL ANKLE REPLACEMENT.....</b>		<b>71</b>
3.1	Introduction.....	72
3.2	Materials.....	73
3.2.1	The Simulator and Calibration Set-up.....	74
3.2.3	Simulator Inputs.....	76
3.3	Methods.....	77
3.4	Results.....	79
3.4.1	Simulator Loading and Kinematic Performance.....	79

3.4.2	Wear Rate Comparison .....	84
3.4.3	Surface Topographic Results .....	88
3.4.4	Superior Insert Visual Comparison .....	91
3.5	Discussion.....	96
3.5.1	The Wear Effects of Implant Size .....	96
3.5.2	The Wear Effects of Accelerated Artificial Ageing .....	100
3.5.3	Wear Rate Comparison .....	103
3.5.4	Damage Mode Comparison.....	106
3.6	Conclusion.....	109
<b>CHAPTER 4: THE EFFECT OF SIMULATOR PARAMETERS ON THE WEAR OF A TOTAL ANKLE REPLACEMENT .....</b>		<b>110</b>
4.1	Introduction.....	111
4.2	Materials .....	112
4.2.1	The Simulator and Calibration Set-up.....	113
4.2.2	Simulator Kinetics and Kinematics .....	113
4.3	Methods .....	114
4.4	Results .....	117
4.4.1	Simulator Loading and Kinematic Performance.....	117
4.4.2	Wear Rate Comparison .....	122
4.4.3	Surface Topographic Results .....	125
4.4.4	Visual Damage Mode Comparison.....	128
4.5	Discussion.....	132
4.5.1	Wear Rate Comparison .....	132
4.5.2	Simulator Loading and Kinematic Performance.....	133
4.5.3	Surface Analysis and Damage Modes .....	138
4.4	Conclusion.....	140
<b>CHAPTER 5: BIOMECHANICAL PERFORMANCE OF ANKLE ARTHRODESIS AND TOTAL ANKLE REPLACEMENTS DURING OVERGROUND WALKING</b>		<b>141</b>
5.1	Introduction.....	142
5.2	Methods .....	145
5.2.1	Ethics for Data Collection .....	145
5.2.2	Pilot Study.....	145
5.2.3	Gait Laboratory Set-up.....	146
5.2.3.1	Motion Capture Equipment.....	146
5.2.3.2	Calibration of the 3D Volume .....	147
5.2.3	Participant Information.....	148
5.2.4	Patient Reported Outcomes .....	149
5.2.5	Participant Preparation .....	150
5.2.6	Data Collection.....	153

5.2.7	Data Processing .....	154
5.2.8	Data Analysis.....	155
5.2.9	Statistical Analysis.....	158
5.3	Results .....	158
5.3.1	Patient Reported Outcome Measures .....	158
5.3.2	Spatiotemporal Parameters .....	158
5.3.3	Hip Kinematics .....	159
5.3.4	Knee Kinematics .....	161
5.3.5	Single-segment Foot Model Kinematics.....	163
5.3.6	Multi-segment Foot Model Kinematics.....	165
5.3.6.1	Hindfoot (Segment) Kinematics .....	165
5.3.6.2	Midfoot (Segment) Kinematics.....	167
5.3.6.3	Forefoot (Segment) Kinematics.....	169
5.3.6.4	Forefoot-to-Hindfoot (Segment) Kinematics.....	169
5.3.7	Ground Reaction Forces.....	172
5.3.8	Joint Moments .....	173
5.3.8.1	Hip Moments .....	173
5.3.8.2	Knee Moments.....	174
5.3.8.3	Ankle Moments.....	175
5.3.9	Joint Power.....	176
5.4	Discussion.....	178
5.4.1	Multi-segment Foot Model Kinematics.....	179
5.4.2	Single-segment Foot Model Kinematics.....	184
5.4.3	Ankle Moment and Power.....	186
5.4.4	Proximal Joint Kinetics and Kinematics.....	187
5.4.5	Ground Reaction Forces.....	189
5.4.6	Spatiotemporal Outcomes .....	190
5.4.7	Patient Reported Outcome Measures .....	191
5.4.8	Implant Design .....	192
5.5	Conclusion.....	193
<b>CHAPTER 6: OVERALL DISCUSSIONS, CONCLUSIONS AND FUTURE WORK</b>		<b>194</b>
6.1	Overall Discussion .....	195
6.1.1	Wear Effects of Implant and Simulator Parameters.....	196
6.1.2	Biomechanical Effects of Ankle Arthrodesis and Total Ankle Replacement..	206
6.1.3	Biomechanical versus Wear Performance .....	208
6.1.4	Target Product Profile for Future Wear Simulator Studies.....	212
6.2	Limitations .....	214
6.2.1	Pre-clinical Wear Simulation.....	214

6.2.1.1	Simulator .....	214
6.2.1.2	Experimental Protocol.....	215
6.2.1.3	Gravimetric Wear Assessment.....	218
6.2.1.4	Surface Topographic Assessment.....	221
6.2.2	Gait Analysis .....	224
6.2.2.1	Participant Population.....	224
6.2.2.2	Data Collection .....	225
6.2.2.3	Data Analysis.....	228
6.3	Overall Conclusions .....	228
6.3.1	Wear Effects of Implant Parameters.....	228
6.3.2	Wear Effects of Simulator Parameters.....	229
6.3.3	Biomechanical Effects of Ankle Arthrodesis and Total Ankle Replacement.....	229
6.4	Directions of Future Research .....	230
<b>REFERENCE LIST .....</b>		<b>237</b>
<b>APPENDIX A: ENGINEERING DRAWINGS .....</b>		<b>291</b>
A.1	ProSim Pneumatic Knee Simulator (KSpn) Medium Sized Delrin Fixture.....	292
A.2	ProSim Pneumatic Knee Simulator (KSpn) Extra Small Sized Delrin Fixture.....	293
A.3	ProSim Electromechanical Knee Simulator (KSem) Small Sized Delrin Fixture .....	294
<b>APPENDIX B: EXAMPLE SIMULATOR CALIBRATION REPORT (STATION 1)</b> .....		<b>295</b>
B.1	Axial Force.....	296
B.2	Anterior-Posterior Force.....	297
B.3	Medial-Lateral Force .....	297
B.4	Tibial Rotation Torque Calibration Report For Station 1 .....	297
B.5	Flexion-Extension Torque (+) .....	298
B.6	Flexion-Extension Torque (-).....	298
B.7	Abduction-Adduction Torque (+).....	299
B.8	Abduction-Adduction Torque (-) .....	299
B.9	Anterior-Posterior Displacement.....	300
<b>APPENDIX C: SIMULATOR CALIBRATION RECORD .....</b>		<b>301</b>
C.1	Calibration Record for ProSim Pneumatic Knee Simulator (KSpn) – Implant Size Study (Test 1).....	302
C.2	Calibration Record for ProSim Pneumatic Knee Simulator (KSpn) – Implant Size Study (Test 2).....	304
C.3	Calibration Record for ProSim Electromechanical Knee Simulator (KSem) – Simulator Type and ISO Standard Studies .....	306
C.4	Calibration Record for ProSim Electromechanical Knee Simulator (KSem) – Accelerated Artificially Aged Study.....	307
<b>APPENDIX D: SERUM CERTIFICATE OF ANALYSIS .....</b>		<b>308</b>
D.1	Serum Protein Concentration for the Implant Size Study (Test 1) .....	309

D.2	Serum Protein Concentration for the Implant Size (Test 2), Simulator Type and ISO Standard Studies .....	310
D.3	Serum Protein Concentration for the Accelerated Artificially Aged Study.....	311
<b>APPENDIX E: SURFACE TOPOGRAPHIC MEASUREMENTS FOR EACH WEAR SIMULATOR STUDY .....</b>		<b>312</b>
E.1	Implant Size.....	313
E.2	Accelerated Artificial Ageing .....	315
E.3	Simulator Type.....	317
E.4	Simulator Inputs .....	318
<b>APPENDIX F: ETHICAL APPROVAL.....</b>		<b>320</b>
F.1	University of Leeds Ethics Committee Approval .....	321
F.2	Nottingham Trent University Ethics Committee Approval.....	322
F.3	NHS East of Scotland Research Ethics Service Approval .....	323
F.4	NHS Health Research Authority (HRA) and Health and Care Research Wales (HCRW) Approval Letter .....	324
F.5	Integrated Research Application System (IRAS) Final Document Checklist for HRA Approval .....	326
<b>APPENDIX G: PILOT GAIT STUDY.....</b>		<b>327</b>
G.1	Introduction.....	328
G.2	Methods .....	329
G.3	Results .....	331
G.4	Discussion and Conclusion.....	346
<b>APPENDIX H: VISUAL 3D PIPELINE COMMANDS .....</b>		<b>347</b>

## LIST OF FIGURES

Figure 1. Schematic image of the bones of the right foot. Adapted from Hamill et al. (2021)...	11
Figure 2. Sagittal view of the joints associated with the AJC. Adapted from Nordin and Frankel (2021). .....	12
Figure 3. Lateral view of the ligaments of the ankle (Nordin and Frankel, 2021).....	13
Figure 4. The three anatomical planes of motion and anatomical positioning terminology. ....	14
Figure 5. Motions of the ankle: Dorsi-/Plantarflexion (A), Abduction/Adduction (B), Inversion/Eversion (C).....	15
Figure 6. Subtalar joint axis in the anterior-posterior (left) and lateral (right) views demonstrating inclination and deviation respectively. Adapted from Jastifer and Gustafson (2014). .....	16
Figure 7. A representation of the subtalar joint as a mitred hinge. Adapted from Inman (1976). .....	17
Figure 8. The level walking gait cycle broken down into its sub-phases (right foot). Adapted from Hamill et al. (2021).....	19
Figure 9. The ankle and subtalar joint motions in the sagittal and frontal planes, respectively, during a natural walking gait cycle. Adapted from Sammarco and Hockenbury (2012). .....	20
Figure 10. Lateral and anteroposterior post-operative weight-bearing radiographs of an ankle arthrodesis fixation. Adapted from Brodsky et al. (2016). .....	24
Figure 11. AP and lateral weight-bearing radiographs at 7 years follow-up following a mobile-bearing device. Adapted from Giannini (2013).....	25
Figure 12. Schematic of a fixed (left) and mobile (right) TAR, consisting of metallic tibial and talar components and an UHMWPE meniscal insert. ....	27
Figure 13. Indications for the first revisions following primary TAR (NJR, 2021). .....	29
Figure 14. The three components of the BOX® ankle: tibial component (above), UHMWPE meniscal component (in between), talar component (below). Adapted from the MatOrtho Ltd Operative Technique (MatOrtho Ltd, 2015).....	33
Figure 15. Free body diagram of forces in sliding contact, where the (W) is the weight of the body, (N) is the normal force exerted by the surface, (P) is the horizontal external force, and (T) is the frictional force exerted by the surface.....	34
Figure 16. Microscopic detail of a real surface contact, displaying asperities on the articulating surfaces. ....	35
Figure 17. Stribeck curve used to demonstrate the lubrication regime.....	37
Figure 18. Schematic of periprosthetic inflammation and aseptic osteolysis. Adapted from Cobelli et al. (2011).....	40
Figure 19. Six station predominately pneumatic driven ProSim Knee Simulator (KSpn; Simulation Solutions, Stockport, UK).....	56
Figure 20. Axes of rotation and translation on a knee simulator for a left ankle. ....	57

Figure 21. Knee simulator input profiles (UoL) for AL (red), FE (blue), tibial IER (yellow), and AP displacement (green). Adapted from Smyth et al. (2017). .....	58
Figure 22. Schematic drawing demonstrating the loads and motions of a left-sided device (left) relative to the inverted simulator positioning (right). Adapted from MatOrtho (2020).....	59
Figure 23. Tibial and talar component setup within ProSim Pneumatic Knee Simulator (KSpn; Simulation Solutions, Stockport, UK).....	60
Figure 24. Contact areas of the talar (left), UHMWPE insert (middle), and tibial (right) components, demonstrating central alignment.....	61
Figure 25. ProSim Pneumatic Knee Simulator (KSpn) load (left) and rotation/displacement (right) calibration set-up.....	62
Figure 26. Form Talysurf PGI800 (A) used to measure the surface roughness of the UHMWPE insert (B), tibial (C), and talar (D) articulating surfaces.....	66
Figure 27. The segmentation process for the talar (left) and superior insert (right) roughness traces. ....	67
Figure 28. Sample traces of the tibia (A), superior insert (B), inferior insert (C) and talus (D) articulating surfaces of the BOX® ankle.....	67
Figure 29. Schematic showing 2D surface roughness parameters of interest for the TAR articulating surfaces. Adapted from Cowie and Jennings (2021). ....	68
Figure 30. Profiles with negative (top) and positive (bottom) skewness (Rsk) values. Adapted from Leach (2010). ....	69
Figure 31. Profiles with low (top) and high (bottom) values of Rku. Adapted from (Leach, 2010). ....	69
Figure 32. Three stations of the ProSim electromechanically driven knee simulator (KSem; Simulation Solutions, Stockport, UK).....	74
Figure 33. ProSim Electromechanical Knee Simulator (KSem): (A) AL, FE torque and abduction/adduction torque; (B) AP force; (C) tibial rotation torque; and (D) AP linear position. ....	76
Figure 34. ISO standard input profiles for AL (red), FE angle (blue), tibial IER angle (yellow), and AP displacement (green). Adapted from ISO 22622:2019.....	77
Figure 35. Simulator input (black) and output profiles (blue) (mean $\pm$ 95% CL, n = 6) across all stations for AL (A), FE angle (B), tibial IER angle (C) and AP displacement (D). ....	80
Figure 36. Simulator input (black) and output profiles for each station of KSpn for AL (A), FE angle (B), tibial IER angle (C) and AP displacement (D).....	81
Figure 37. Simulator inputs (black) and average outputs (red) (mean $\pm$ 95% CL, n = 5) across all the stations for AL (A), FE angle (B), tibial IER angle (C) and AP displacement (D). ....	82
Figure 38. Simulator input (black) and output profiles for each station of KSem for AL (A), FE angle (B), tibial IER angle (C) and AP displacement (D).....	83
Figure 39. Cumulative mean wear rates (mm <sup>3</sup> ) with $\pm$ 95% CL for the medium (red) and extra small (blue) sized implants after 5 Mc (n = 6 for both implant sizes).....	84

Figure 40. Mean run-in and steady-state wear rate (mm <sup>3</sup> /Mc) with ± 95% CL for the medium (M; red) and extra small (XS; blue) implants after 5 Mc (n = 6 for each implant size).....	85
Figure 41. Individual wear rates for the medium (M) and extra small (XS) sized inserts during each Mc (n = 6 for both implant sizes), with the colours representing the station within the pneumatic simulator. ....	85
Figure 42. Cumulative mean wear rates (mm <sup>3</sup> ) with ±95% CL for the small sized artificially aged implants after 5 Mc (n = 5). ....	86
Figure 43. Mean run-in (red) and steady-state (blue) wear rate (mm <sup>3</sup> /Mc) with ± 95% CL for the small artificially aged implants after 5 Mc (n = 5). ....	87
Figure 44. Individual wear rates for the small sized artificially aged inserts during each Mc (n = 5), with the colours representing the station within the pneumatic simulator.....	87
Figure 45. Five representative (two-dimensional) traces across the superior insert bearing surface used to determine the topographical parameters.....	88
Figure 46. Photographs of three medium (top) and extra small (bottom) superior insert surfaces after 5 Mc. Machining lines are no longer visible and there are clear signs of abrasive wear, burnishing and scratching.....	92
Figure 47. Damage modes on the superior bearing insert surface from both implant sizes after 5 Mc (n = 6 for both implant sizes): A-C = Burnishing; D-F = Scratching; G-I = Pitting; J-L = Abrasive wear; M-O = Material on the surface. Multiple damage modes were captured with the Alicona InfiniteFocus microscope (20x resolution).....	93
Figure 48. Photographs of the five aged small superior insert surface after 5 Mc. Machining lines are no longer visible and there are clear signs of abrasive wear, burnishing and scratching. ....	94
Figure 49. Damage modes on the superior bearing insert surface of the small sized artificially aged implants (n = 5): A-C = Burnishing; D-F = Scratching; G-I = Pitting; J-L = Abrasive wear; M-O = Material on the surface. Multiple damage modes were captured with the Alicona InfiniteFocus microscope (20x resolution).....	95
Figure 50. Six hypothetical surface profiles (red lines) with the same surface roughness value but with different surface texture characteristics (e.g. surface or kurtosis). ....	98
Figure 51. Wear tested surface of the BOX® ankle superior insert and the visual imprint from the conventional UHMWPE articulation on the tibial component (A) compared to that of an in vitro Zenith after 12 Mc (B) and Biomet AES retrieval (C). Adapted from Smyth et al. (2017). ....	108
Figure 52. ISO standard input profiles (red) compared to the previously simulated UoL (blue) input profiles for AL (A), FE angle (B), IER angle (C) and AP displacement (D).....	113
Figure 53. Schematic diagram with sign convention for the loading and kinematic profile directions from ISO 22622:2019 (A) and University of Leeds (Smyth et al., 2017) (B) of a left implant in the inverted position. ....	114
Figure 54. Sign convention and positive directions for the load and motion, shown for a left ankle joint-prosthesis. Adapted from ISO 22622:2019.....	115
Figure 55. Simulator input (black) and output profiles (red) (mean ± 95% CL, n = 6) across all stations for AL (A), FE angle (B), tibial IER angle (C) and AP displacement (D) from the electromechanical (red) and pneumatic (blue) simulators.....	118

Figure 56. Simulator input (black) and output profiles for each station of KSem (red) and KSpn (blue) for AL (A), FE angle (B), tibial IER angle (C) and AP displacement (D).....	119
Figure 57. Simulator input (black) and output profiles (red) (mean $\pm$ 95% CL, n = 6) across all stations for AL (A), FE angle (B), tibial IER angle (C) and AP displacement (D) for the duration of the simulation (2 Mc).....	121
Figure 58. Simulator input (black) and mean output profiles from each of the six stations for AL (A), FE angle (B), tibial IER angle (C) and AP displacement (D) for the duration of the simulation (2 Mc).....	122
Figure 59. Cumulative mean wear rates (mm <sup>3</sup> ) with $\pm$ 95% CL for the medium sized implants within the electromechanical (red) and pneumatic (blue) controlled simulators after 3 Mc (n = 5). .....	123
Figure 60. Mean run-in and steady-state wear rate (mm <sup>3</sup> /Mc) with $\pm$ 95% CL for the medium sized implants within the electromechanical (red) and pneumatic (blue) controlled simulators after 3 Mc (n = 5).....	124
Figure 61. Individual wear rates for the medium sized inserts during each Mc (n = 5), with the colours representing the station within the electromechanical simulator.....	124
Figure 62. Mean steady-state wear rate (mm <sup>3</sup> /Mc) with $\pm$ 95% CL for the medium sized implants simulated under ISO 22622:2019 (red) and University of Leeds (blue) loading and kinematic inputs for 2 Mc (n = 5). .....	125
Figure 63. Individual wear rates for the medium sized inserts during each Mc (n = 5), under ISO 22622:2019 loading and kinematic inputs. Each colour represents the specific station within the electromechanical simulator.....	126
Figure 64. Photographs of five medium sized superior insert surfaces after 3 Mc in the electromechanical simulator (KSem), under University of Leeds (UoL) loading and kinematic input profiles. Machining lines are no longer visible and there are clear signs of abrasive wear, burnishing and multidirectional scratching across the articulating surface. ....	128
Figure 65. Damage modes on the superior bearing insert surface of the five medium sized implants after 3 Mc (n = 5): A-C = Burnishing; D-F = Scratching; G-I = Pitting; J-L = Abrasive wear; M-O = Material on the surface. Multiple damage modes were captured with the Alicona InfiniteFocus microscope (20x resolution).....	129
Figure 66. Photographs of the six medium sized superior insert surfaces after 5 Mc, with the last 2 Mc being run under ISO 22622:2019 loading and kinematic input profiles. Machining lines are no longer visible and there are clear signs of abrasive wear, burnishing and multidirectional scratching across the whole articulating surface (n = 5).....	130
Figure 67. Damage modes on the superior bearing insert surface of the medium sized implants after an additional 2 Mc of ISO 22622:2019 loading and kinematic input profiles (n = 5): A-C = Burnishing; D-F = Scratching; G-I = Pitting; J-L = Abrasive wear; M-O = Material on the surface. Multiple damage modes were captured with the Alicona InfiniteFocus microscope (20x resolution). .....	131
Figure 68. Mean ( $\pm$ 95% CL) wear rate (mm <sup>3</sup> /Mc) for the Zenith (Corin Group PLC., Cirencester, UK) mid-range implant sizes for the six 2 Mc stages from Smyth et al. (2017) kinematic comparison study (n = 5). Adapted from Smyth et al. (2017). .....	136
Figure 69. The superior view of the Qualisys Oqus 3D motion capture system (blue area) and the smaller calibrated movement volume (pink area); and the Qualisys Oqus cameras (right) at the	

NTU gait laboratory. The force platforms (violet rectangles) are positioned in the middle of the movement volume to capture GRF data. ....	147
Figure 70. The Vicon Active Wand (Vicon MX, Oxford Metrics, UK) required for the calibration process at CAH. ....	148
Figure 71. The L-shaped reference structure and T-shaped wand (Qualisys™ Medical AB, Goteborg, Sweden) required for the calibration process at NTU. ....	148
Figure 72. Anatomical locations of the 36 marker model set in the anterior (left) and posterior (right) view .....	150
Figure 73. Four-marker semi-rigid thermoplastic shell used as tracking markers for the thigh (left) and thigh (right) during kinematic data collection.....	151
Figure 74. The IOR multi-segment foot model used to measure the kinematic data for the hindfoot, midfoot and forefoot segments. ....	152
Figure 75. Static trial (left) and the label list for the 36 reflective markers (right) within Qualisys software. ....	153
Figure 76. An example of a participant completing a successful trial within the movement area. ....	154
Figure 77. The marker set-up for the static condition (left) and the Visual 3D model created from the body segments. ....	155
Figure 78. Schematic of the ground reaction force waveform and vertical peaks (GRF1 <sub>MAX</sub> and GRF2 <sub>MAX</sub> ).....	157
Figure 79. Mean ( $\pm$ 95% CL) hip flexion (+)/extension (-) (A), adduction (+)/abduction (-) (B) and internal (+)/external (-) rotation (C) kinematic waveforms during the gait cycle, in patients with AA (blue), TAR (red) and BOX® ankle (green).....	160
Figure 80. Mean ( $\pm$ 95% CL) knee flexion (+)/extension (-) (A), adduction (+)/abduction (-) (B) and internal (+)/external (-) rotation (C) kinematic waveforms during the gait cycle, in patients with AA (blue), TAR (red) and BOX® ankle (green).....	162
Figure 81. Mean ( $\pm$ 95% CL) single-segment ankle dorsiflexion (+)/plantarflexion (-) (A), eversion (+)/inversion (-) (B) and adduction (+)/abduction (-) (C) kinematic waveforms during the gait cycle, in patients with AA (blue), TAR (red) and BOX® ankle (green). ....	164
Figure 82. Mean ( $\pm$ 95% CL) hindfoot segment dorsiflexion (+)/plantarflexion (-) (A), eversion (+)/inversion (-) (B) and adduction (+)/abduction (-) (C) kinematic waveforms during the gait cycle, in patients with AA (blue), TAR (red) and BOX® ankle (green). ....	166
Figure 83. Mean ( $\pm$ 95% CL) midfoot segment dorsiflexion (+) (A), eversion (+)/inversion (-) (B) and adduction (+)/abduction (-) (C) kinematic waveforms during the gait cycle, in patients with AA (blue), TAR (red) and BOX® ankle (green).....	168
Figure 84. Mean ( $\pm$ 95% CL) forefoot segment plantarflexion (-) (A), inversion (-) (B) and adduction (+)/abduction (-) (C) kinematic waveforms during the gait cycle, in patients with AA (blue), TAR (red) and BOX® ankle (green).....	170
Figure 85. Mean ( $\pm$ 95% CL) forefoot-to-hindfoot segment plantarflexion (-) (A), inversion (-) (B) and adduction (+)/abduction (-) (C) kinematic waveforms during the gait cycle, in patients with AA (blue), TAR (red) and BOX® ankle (green).....	171

Figure 86. Mean ( $\pm$ 95% CL) vertical GRF during the stance phase, in patients with AA (blue), TAR (red) and BOX® ankle (green). .....	172
Figure 87. Mean ( $\pm$ 95% CL) sagittal (A) and frontal (B) hip internal moments during the stance phase, in patients with AA (blue), TAR (red) and BOX® ankle (green). .....	173
Figure 88. Mean ( $\pm$ 95% CL) sagittal (A) and frontal (B) knee internal moments during the stance phase, in patients with AA (blue), TAR (red) and BOX® ankle (green). .....	174
Figure 89. Mean ( $\pm$ 95% CL) sagittal (A) and frontal (B) ankle internal moments during the stance phase, in patients with AA (blue), TAR (red) and BOX® ankle (green). .....	175
Figure 90. Mean ( $\pm$ 95% CL) sagittal hip (A), knee (B) and ankle (C) joint power during the stance phase, in patients with AA (blue), TAR (red) and BOX® ankle (green). .....	177
Figure 91. Current pre-clinical testing recommended flexion (+)/extension (-) (A) and tibial rotation (B) input profiles from the ISO 22622:2019 (blue) compared to the mean kinematic waveforms from the BOX® ankle patient cohort (red). .....	209
Figure 92. Mean ( $\pm$ 95% CL) hip flexion (+)/extension (-) (A), adduction (+)/abduction (-) (B) and internal (+)/external (-) rotation (C) kinematic waveforms during the gait cycle, of the participants at the Chapel Allerton Hospital (CAH; blue) and Nottingham Trent University (NTU; red) research sites. ....	333
Figure 93. Mean ( $\pm$ 95% CL) knee flexion (+)/extension (-) (A), adduction (+)/abduction (-) (B) and internal (+)/external (-) rotation (C) kinematic waveforms during the gait cycle, of the participants at the Chapel Allerton Hospital (CAH; blue) and Nottingham Trent University (NTU; red) research sites. ....	334
Figure 94. Mean ( $\pm$ 95% CL) single-segment ankle dorsiflexion (+)/plantarflexion (-) (A), eversion (+)/inversion (-) (B) and adduction (+)/abduction (-) (C) kinematic waveforms during the gait cycle, of the participants at the Chapel Allerton Hospital (CAH; blue) and Nottingham Trent University (NTU; red) research sites. ....	335
Figure 95. Mean ( $\pm$ 95% CL) hindfoot segment dorsiflexion (+)/plantarflexion (-) (A), eversion (+)/inversion (-) (B) and adduction (+)/abduction (-) (C) kinematic waveforms during the gait cycle, of the participants at the Chapel Allerton Hospital (CAH; blue) and Nottingham Trent University (NTU; red) research sites. ....	337
Figure 96. Mean ( $\pm$ 95% CL) midfoot segment dorsiflexion (+) (A), inversion (-) (B) and adduction (+)/abduction (-) (C) kinematic waveforms during the gait cycle, of the participants at the Chapel Allerton Hospital (CAH; blue) and Nottingham Trent University (NTU; red) research sites. ....	338
Figure 97. Mean ( $\pm$ 95% CL) forefoot segment plantarflexion (-) (A), inversion (-) (B) and adduction (+) (C) kinematic waveforms during the gait cycle, of the participants at Chapel Allerton Hospital (CAH; blue) and Nottingham Trent University (NTU; red) research sites. ....	339
Figure 98. Mean ( $\pm$ 95% CL) forefoot-to-hindfoot segment plantarflexion (-) (A), inversion (-) (B) and adduction (+)/abduction (-) (C) kinematic waveforms during the gait cycle, of the participants at Chapel Allerton Hospital (CAH; blue) and Nottingham Trent University (NTU; red) research sites. ....	340
Figure 99. Mean ( $\pm$ 95% CL) vertical GRF during the stance phase, of the participants at Chapel Allerton Hospital (CAH; blue) and Nottingham Trent University (NTU; red) research sites. ....	341

Figure 100. Mean ( $\pm$ 95% CL) sagittal (A) and frontal (B) hip internal moments during the stance phase, of the participants at Chapel Allerton Hospital (CAH; blue) and Nottingham Trent University (NTU; red) research sites. ....	342
Figure 101. Mean ( $\pm$ 95% CL) sagittal (A) and frontal (B) knee internal moments during the stance phase, of the participants at Chapel Allerton Hospital (CAH; blue) and Nottingham Trent University (NTU; red) research sites. ....	343
Figure 102. Mean ( $\pm$ 95% CL) sagittal (A) and frontal (B) ankle internal moments during the stance phase, of the participants at Chapel Allerton Hospital (CAH; blue) and Nottingham Trent University (NTU; red) research sites. ....	344
Figure 103. Mean ( $\pm$ 95% CL) sagittal hip (A), knee (B) and ankle (C) joint power during the stance phase, of the participants at Chapel Allerton Hospital (CAH; blue) and Nottingham Trent University (NTU; red) research sites. ....	345

## LIST OF TABLES

Table 1. Wear simulator study implant, material and manufacturing details.....	42
Table 2. Wear study simulation information. ....	43
Table 3. Applied ranges of load and motions in previous ankle wear simulations. ....	44
Table 4. Implant size dimensions for the extra small, small and medium BOX® ankle. ....	55
Table 5. ProSim Pneumatic Knee Simulator (KSpn) Simulator Controls.....	56
Table 6. Surface roughness trace information for the tibial component. ....	67
Table 7. Surface roughness trace information for the superior insert.....	67
Table 8. Surface roughness trace information for the inferior insert. ....	67
Table 9. Surface roughness trace information for the talar component. ....	67
Table 10. Retrieval damage modes as described by Hood et al. (1983). ....	70
Table 11. Bearing details for the medium, small and extra-small implant sizes.....	73
Table 12. Bearing details for the medium sized implants.....	112
Table 13. Comparison of peak inputs from University of Leeds (UoL) and ISO 22622:2019 profiles. ....	114
Table 14. Participant demographics for the three treatment option cohorts.....	149
Table 15. Location of the skin-mounted and tracking markers. ....	152
Table 16. Mean ( $\pm$ 95% CL) MOxFQ domain scores between the three patient cohorts. ....	158
Table 17. Mean ( $\pm$ 95% CL) spatiotemporal gait parameters for the three patient cohorts. ....	159
Table 18. Mean ( $\pm$ 95% CL) hip kinematics for the three patient cohorts. ....	159
Table 19. Mean ( $\pm$ 95% CL) knee kinematics for the three patient cohorts.....	161
Table 20. Mean ( $\pm$ 95% CL) single-segment foot kinematics for the three patient cohorts. ....	163
Table 21. Mean ( $\pm$ 95% CL) hindfoot kinematics for the three patient cohorts. ....	165
Table 22. Mean ( $\pm$ 95% CL) midfoot kinematics for the three patient cohorts.....	167
Table 23. Mean ( $\pm$ 95% CL) forefoot kinematics for the three patient cohorts. ....	169
Table 24. Mean ( $\pm$ 95% CL) forefoot-to-hindfoot kinematics for the three patient cohorts. ..	172
Table 25. Mean ( $\pm$ 95% CL) peak vertical ground reaction force for the three patient cohorts. ....	173
Table 26. Mean ( $\pm$ 95% CL) peak internal joint moments in the sagittal and frontal plane for the three patient cohorts.....	176
Table 27. Mean ( $\pm$ 95% CL) peak joint generated power for the three patient cohorts.....	176
Table 28. Comparison of peak and ROM parameters for flexion/extension and tibial rotation input from ISO 22622:2019 and patient specific profiles. ....	210
Table 29. A Target Product Profile for future wear simulations of a TAR.....	213

Table 30. Mean ( $\pm$ 95% CL) average surface roughness (Ra) measurements for each articulating surface of the medium (M) and extra small (XS) sized implants alongside the percentage change between the measurement stages (n = 6 for each implant size).....	313
Table 31. Mean ( $\pm$ 95% CL) maximum profile peak heights (Rp) measurements for each articulating surface of the medium (M) and extra small (XS) sized implants alongside the percentage change between the measurement stages (n = 6 for each implant size).....	313
Table 32. Mean ( $\pm$ 95% CL) maximum profile valley depth (Rv) measurements for each articulating surface of the medium (M) and extra small (XS) sized implants alongside the percentage change between the measurement stages (n = 6 for each implant size).....	314
Table 33. Mean ( $\pm$ 95% CL) surface skewness (Rsk) measurements for each articulating surface of the medium (M) and extra small (XS) sized implants alongside the percentage change between the measurement stages (n = 6 for each implant size).....	314
Table 34. Mean ( $\pm$ 95% CL) surface kurtosis (Rku) measurements for each articulating surface of the medium (M) and extra small (XS) sized implants alongside the percentage change between the measurement stages (n = 6 for each implant size).....	315
Table 35. Mean ( $\pm$ 95% CL) average surface roughness (Ra) measurements for each articulating surface of the small sized artificially aged implants alongside the percentage change between the measurement stages (n = 5). ....	315
Table 36. Mean ( $\pm$ 95% CL) maximum profile peak heights (Rp) measurements for each articulating surface of the small sized artificially aged implants alongside the percentage change between the measurement stages (n = 5).....	315
Table 37. Mean ( $\pm$ 95% CL) maximum profile valley depth (Rv) measurements for each articulating surface of the small sized artificially aged implants alongside the percentage change between the measurement stages (n = 5).....	316
Table 38. Mean ( $\pm$ 95% CL) surface skewness (Rsk) measurements for each articulating surface of the small sized artificially aged implants alongside the percentage change between the measurement stages (n = 5). ....	316
Table 39. Mean ( $\pm$ 95% CL) surface kurtosis (Rku) measurements for each articulating surface of the small sized artificially aged implants alongside the percentage change between the measurement stages (n = 5). ....	316
Table 40. Mean ( $\pm$ 95% CL) average surface roughness (Ra) measurements for each articulating surface of the medium sized implants alongside the percentage change between the measurement stages (n = 5). ....	317
Table 41. Mean ( $\pm$ 95% CL) maximum profile peak heights (Rp) measurements for each articulating surface of the medium sized implants alongside the percentage change between the measurement stages (n = 5). ....	317
Table 42. Mean ( $\pm$ 95% CL) maximum profile valley depth (Rv) measurements for each articulating surface of the medium sized implants alongside the percentage change between the measurement stages (n = 5). ....	317
Table 43. Mean ( $\pm$ 95% CL) surface skewness (Rsk) measurements for each articulating surface of the medium sized implants alongside the percentage change between the measurement stages (n = 5).....	318

Table 44. Mean ( $\pm$ 95% CL) surface kurtosis (Rku) measurements for each articulating surface of the medium sized implants alongside the percentage change between the measurement stages (n = 5).....	318
Table 45. Mean ( $\pm$ 95% CL) average surface roughness (Ra) measurements for each articulating surface of the medium sized implants alongside the percentage change between the measurement stages (n = 5).....	318
Table 46. Mean ( $\pm$ 95% CL) maximum profile peak heights (Rp) measurements for each articulating surface of the medium sized implants alongside the percentage change between measurement stages after 2 Mc of ISO 22622:2019 loading and kinematic input profiles.....	319
Table 47. Mean ( $\pm$ 95% CL) maximum profile valley depth (Rv) measurements for each articulating surface of the medium sized implants after 2 Mc of ISO 22622:2019 loading and kinematic input profiles. ....	319
Table 48. Mean ( $\pm$ 95% CL) surface skewness (Rsk) measurements for each articulating surface of the medium sized implants after 2 Mc of ISO 22622:2019 loading and kinematic input profiles. ....	319
Table 49. Mean ( $\pm$ 95% CL) surface kurtosis (Rku) measurements for each articulating surface of the medium sized implants after 2 Mc of ISO 22622:2019 loading and kinematic input profiles. ....	319
Table 50. Mean ( $\pm$ 95% CL) demographic data of the participants at both research sites.....	329
Table 51. Gait laboratory motion capture and force platform systems used at each research site. ....	330
Table 52. Mean ( $\pm$ 95% CL) spatiotemporal parameters for the participants at the two research sites.....	331
Table 53. Mean ( $\pm$ 95% CL) hip, knee and single-segment ankle kinematic parameters for the participants at the two research sites. ....	332
Table 54. Mean ( $\pm$ 95% CL) multi-segment foot segment kinematic parameters for the participants at the two research sites. ....	336
Table 55. Mean ( $\pm$ 95% CL) vertical ground reaction force parameters for the participants at the two research sites. ....	341
Table 56. Mean ( $\pm$ 95% CL) joint moment parameters for the participants at the two research sites.....	342
Table 57. Mean ( $\pm$ 95% CL) joint power parameters for the participants at the two research sites. ....	344

## **DISSEMINATION OF RESEARCH**

### **CONFERENCE AND ORAL PRESENTATIONS**

J. Hopwood, A. Redmond, G. Chapman, L. Richards, S. Collins, C. Brockett. 2021. The Effect of Artificial Ageing on the Wear of a Total Ankle Arthroplasty. Orthopaedic Research Society, Virtual Meeting (12<sup>th</sup>-16<sup>th</sup> February 2021).

J. Hopwood, A. Redmond, G. Chapman, L. Richards, S. Collins, C. Brockett. 2020. A Comparison of Electromechanical versus Pneumatic-Controlled Knee Simulators for the Wear Performance of a Total Ankle Replacement. British Orthopaedic Research Society, Virtual Meeting (8<sup>th</sup>-9<sup>th</sup> September 2020).

J. Hopwood, A. Redmond, G. Chapman, L. Richards, S. Collins, C. Brockett. 2019. Influence of Implant Size on the Wear Performance of a Total Ankle Arthroplasty. International Society for Technology in Arthroplasty 32nd Annual Congress, Toronto, Canada (2<sup>nd</sup>-5<sup>th</sup> October 2019).

J. Hopwood, A. Redmond, G. Chapman, L. Richards, S. Collins, C. Brockett. 2018. The Biomechanical and Wear Performance of Total Ankle Replacements. Tissue and Cell Engineering Society, Keele, UK (2<sup>nd</sup>-4<sup>th</sup> July 2018).

### **CONFERENCE POSTER PRESENTATIONS**

J. Hopwood, A. Redmond, G. Chapman, L. Richards, S. Collins, C. Brockett. 2019. Wear Performance of a Mobile Bearing Total Ankle Replacement. British Orthopaedic Research Society, Cardiff, UK (4<sup>th</sup>-6<sup>th</sup> September 2019).

J. Hopwood, A. Redmond, G. Chapman, L. Richards, S. Collins, C. Brockett. 2018. The Effect of Varying Implant Size on the Wear Performance of Total Ankle Replacements. British Orthopaedic Research Society, Leeds, UK (10<sup>th</sup>-11<sup>th</sup> September 2018).

## ABBREVIATION LIST

2D	Two-Dimensional
3D	Three-Dimensional
AA	Ankle Arthrodesis
ADL	Activities of Daily Living
AES	Ankle Evolutive System
AIM	Automatic Identification of Markers
AJC	Ankle Joint Complex
AL	Axial Load
AMTI	Advanced Mechanical Technology Incorporated
ANOVA	Analysis of Variance
AOFAS	American Orthopaedic Foot and Ankle Society
AOR	Axis of Rotation
AP	Anterior/Posterior
ASTM	American Society for Testing and Materials
BMI	Body Mass Index
BOX	Bologna-Oxford
BW	Body Weight
CAH	Chapel Allerton Hospital
CAST	Calibrated Anatomical System Technique
CoCrMo	Cobalt-Chrome-Molybdenum
CL	Confidence Limit
CMM	Coordinate Measuring Machines
DoF	Degrees of Freedom
EHL	Elastohydrodynamic Lubrication
FB	Fixed-Bearing
FDA	Food and Drug Administration
FE	Flexion/Extension
GRF	Ground Reaction Forces
HRA	Health Research Authority
IER	Internal/External Rotation
IOR	Istituti Ortopedici Rizzoli
ISB	International Society of Biomechanics
ISO	International Organisation for Standardisation
iMBE	Institute of Medical and Biological Engineering
KSem	Electromechanical Knee Simulator
KSpn	Pneumatic Knee Simulator

LCL	Lateral Collateral Ligaments
LVD'T	Linear Variable Differential Transformer
Mc	Million Cycles
MAUDE	Manufacturer and User Facility Device Experience
MB	Mobile-Bearing
MCL	Medial Collateral Ligaments
MFM	Multi-Segment Foot Model
ML	Medial-Lateral
MOxFQ	Manchester-Oxford Foot Questionnaire
NHS	National Health Service
NICE	National Institute for Health and Care Excellence
NJR	National Joint Registry
NTU	Nottingham Trent University
OA	Osteoarthritis
PID	Proportional-Integral-Derivative
PMMA	Polymethyl Methacrylate
PROMS	Patient Reported Outcome Measures
PTOA	Post-traumatic Osteoarthritis
QoL	Quality of Life
Ra	Average Surface Roughness
Rku	Surface Kurtosis
Rp	Maximum Profile Peak Height
Rsk	Surface Skewness
Rv	Maximum Profile Valley Depth
RCT	Randomised Control Trial
REC	Research Ethics Committee
ROM	Range of Motion
SEM	Scanning Electron Microscopy
SFM	Single-Segment Foot Model
SPSS	Statistical Package for Social Sciences
STA	Soft Tissue Artefacts
STAR	Scandinavian Total Ankle Replacement
TTP	Target Product Profile
μCT	Micro Computed Tomography

## **ANATOMICAL TERMINOLOGY**

In order to communicate specific information concerning human movement, specialised terminology is required to precisely identify body position and direction. All of the position and motion terminology presented in the thesis is relative to the universally accepted anatomical reference position. This is an erect standard position of the body, facing directly forward, including the arms hanging down at the sides of the body with the palms of the hand facing forward, and the feet placed slightly apart.

### **ANATOMICAL REFERENCE PLANES**

<b>Sagittal Plane</b>	The plane that bisects the body into right and left sides
<b>Frontal Plane</b>	The plane that bisects the body into front and back halves
<b>Transverse Plane</b>	A body plane that is perpendicular to the long axis of a segment or the body

### **ANATOMICAL POSITIONING TERMINOLOGY**

<b>Anterior</b>	A position in front of a designated reference point
<b>Posterior</b>	A position behind a designated reference point
<b>Medial</b>	A position relatively closer to the midline of the body
<b>Lateral</b>	A position relatively far from the midline of the body
<b>Proximal</b>	A position relatively closer to a designated reference point
<b>Distal</b>	A position relatively far from a designated reference point
<b>Superior</b>	A position above a designated reference point
<b>Inferior</b>	A position below a designated reference point

### **JOINT MOTION TERMINOLOGY**

<b>Flexion</b>	Movement of a segment toward an adjacent segment so that the angle between the two is decreased
<b>Extension</b>	Movement of a segment away from an adjacent segment so that the angle between the two segments is increased
<b>Abduction</b>	Sideways movement of the segment away from the midline or sagittal plane
<b>Adduction</b>	Sideways movement of a segment toward the midline or sagittal plane

<b>Plantarflexion</b>	Movement of the foot downward in the sagittal plane; movement away from the leg
<b>Dorsiflexion</b>	Rotation of the foot up in the sagittal plane; movement toward the leg
<b>Eversion</b>	The movement in which the lateral border of the foot lifts so that the sole of the foot faces away from the midline of the body
<b>Inversion</b>	The movement in which the medial border of the foot lifts so that the sole of the foot faces away from the midline of the body
<b>Internal Rotation</b>	Rotating the joint towards the midline
<b>External Rotation</b>	Rotating the joint away from the midline
<b>Pronation</b>	Subtalar pronation causes the plantar surface of the foot to face laterally
<b>Supination</b>	Subtalar supination causes the plantar surface of the foot to face medially

## INTRODUCTION

End-stage ankle osteoarthritis (OA) is a chronic debilitating disease characterised by progressive joint degeneration (Buckwalter et al., 2004), which can lead to considerable pain (Bloch et al., 2015) and functional impairments of the entire lower limb, causing difficulties during daily life activities, such as walking (Queen, 2017a; Deleu et al., 2021a). Ankle arthrodesis (AA) remains the gold-standard operative treatment strategy in patients suffering with end-stage ankle OA (Ferguson et al., 2019), which provides significant pain relief and well-documented long-term survivorship (Norvell et al., 2019; Lawton et al., 2020). It has however, been hypothesised that AA may potentially lead to altered gait mechanics and mechanical loads at the distal foot joints, which could lead to adjacent joint degeneration and further functional impairments (Pinsker et al., 2016). These disadvantages have encouraged motion preserving procedures such as total ankle replacement (TAR), which have been shown to conserve existing pre-operative sagittal ankle range of motion, increase the power generated at the ankle joint and improve walking speed post-surgery (Ingrosso et al., 2009; Brodsky et al., 2011; Deleu et al., 2022). However, there are limited studies which have directly compared the gait mechanics between AA and TAR, with many failing to determine the compensatory mechanisms that may be present at the distal foot joints or at the proximally located hip and knee joints. The majority of the gait based studies are also limited by relatively short-follow-up periods post-surgery.

Although TARs have the potential to improve gait mechanics, particularly at the distal foot joints, long-term survivorship remains unsatisfactory in comparison to AA (Maffulli et al., 2017) and that of hip and knee replacements (Palanca et al., 2018). Aseptic loosening is the main reason for the revision of TAR, which has been attributed to wear-mediated osteolysis through the production of wear debris (Schipper et al., 2017). As the survival rates of newer generation TARs are improving, there is an increased risk that wear-mediated osteolysis will become more prevalent (Smyth et al., 2017). Mechanical wear simulator studies have demonstrated that they are a powerful tool in predicting wear performance for varying prosthesis designs and bearing materials for total hip and knee replacements, under physiologically relevant conditions. However, TARs have not been subject to the same pre-clinical testing and are limited to a small number of studies, in which experimental protocols and input profiles widely vary. This makes it difficult to compare wear behaviour between different implants. Current TAR wear studies have also failed to recognise the influence of varying implant and simulator parameters on implant wear behaviour, which could explain the clinical failure of the device.

Pre-clinical *in vitro* simulations under varying implant and simulator parameters, alongside studies which investigate further the gait mechanics of TAR compared to the gold standard AA treatment option, are important in informing future device development, in regard to biomechanical and wear performance.

## AIMS AND OBJECTIVES

The main aim of this project was to understand the biomechanical and wear performance of a third generation mobile-bearing (MB) TAR, in current clinical use, using a combination of gait analysis and experimental simulation methodologies.

The proposed research aims were achieved through the three main objectives:

1. Determine the effect of varying implant parameters on the wear of a MB implant
2. Explore the effects of simulator parameters on the wear of a MB implant
3. Investigate biomechanical differences between AA and TAR patients using a lower limb and multi-segment foot model during overground walking at an intermediate follow-up period

The novelty of this work lies in the development and implementation of several wear simulations and gait analysis studies of a third generation MB TAR. The first novel component of the thesis examined the impact of different implant parameters on implant wear (Objective 1). The first of these was implant size, which is especially important given that surgeons must make the correct decision on implant size, to ensure a longer lasting device. Hip and knee studies have shown that increasing the implant size caused greater wear due to greater surface area and multidirectional motion at the bearing surfaces, but reduced the risk of insert dislocation. However, this has not been determined in TAR. Therefore, the first objective aimed to investigate whether size had an effect on TAR wear behaviour. The second parameter investigated was the impact of artificially aged polyethylene inserts on implant wear. All previous TAR wear studies used pristine polyethylene, which does not represent the material conditions *in situ* (being an oxygen rich environment undergoing radicalisation and release of free radicals). The risk of ageing and oxidation is even more concerning in ankles, due ankle implants being of a smaller size, increased contact mechanics, relative multidirectional motion and reduced polyethylene thickness when compared to hip and knee implants.

For the first time, ISO 22622:2019 profiles were used to determine the effect of simulator type and simulator input parameters on implant wear (Objective 2). Different simulator types (pneumatic and electromechanical) have previously been found to produce comparable wear results in hip and knee devices, but still needed to be understood for TAR due to the different contact mechanics and geometry of the device being measured. Improvements in kinematic following or differences in wear rates may lead to a preferred simulator type for future wear studies. Objective 2 also focused on comparing two different loading and kinematic input profiles, including the recently developed ISO 22622:2019. It was important to understand the effect of the ISO 22622:2019 profiles, to make sure they do not produce substantially different wear rates to previous wear studies, as well as confirming that the profiles do not result in the

production of adverse events such as insert dislocation. These profiles will likely be used as the benchmark for future wear testing.

The final objective (Objective 3) was to be the first study to combine the use of multi-segment foot modelling and lower limb biomechanical modelling to determine the differences in gait mechanics between TAR and AA patients at an intermediate follow-up period. Differences in kinematics and kinetics at the distally located foot joints and proximal hip and knee joints may be related to compensatory mechanisms and put patients at risk of requiring future surgical interventions. This study was also important to demonstrate that any improved wear rates determined as part of Objectives 1 and 2, compared to previous wear studies, may not guarantee *in vivo* performance.

The advancements of such methods will be crucial in the ongoing development of TAR, as well as enhancing clinical performance through understanding the envelope of TAR biomechanics and wear behaviour. This may also lead to TAR becoming the 'gold standard' choice for the treatment of end-stage ankle arthritis.

## THESIS OUTLINE

The thesis begins with a general review of the literature (Chapter 1), which includes background information on anatomy, function and biomechanics of the ankle joint complex. The review then considers ankle arthritis and the surgical interventions associated with the disease; namely AA and TAR. Next, an overview of the history and development of TARs is detailed, which considers designs, survivorship, complications, and biomechanical performance. The Chapter then presents a comparison of both treatments options with regard to patient functional outcomes and gait mechanics. Following this, a review of the fundamentals of biotribology and wear simulation studies of TARs is conducted. The Chapter concludes with the summary of the literature review.

Chapter 2 informs the reader of the general *in vitro* wear simulator methodologies under displacement control, which have been used in the wear studies detailed in Chapter 3 (Implant Parameters) and Chapter 4 (Simulator Parameters). Chapter 3 examines the influence of implant parameters on the wear behaviour of a mobile-bearing TAR. The Chapter is separated into two different wear studies, being implant size and accelerated artificial ageing. Chapter 4 investigates the impact of simulator parameters on the wear of the same mobile-bearing device. Again, the Chapter is separated into two wear studies (simulator type and simulator inputs). Both Chapters 3 and 4 compare the effect of the varying implant and simulator parameters on: simulator loading and kinematic following performance; wear rates; inter-station variability; topographical changes; and visual damage modes with respect to previously simulated and retrieved implants.

Chapter 5 details the use of three-dimensional motion capture to assess the gait differences in TAR and AA patients during overground level walking at an intermediate follow-up period post-surgery. The Chapter explores the use of a multi-segment foot model to determine kinematic differences between treatment options in the distally located joints of the foot. The Chapter also presents the differences in functional outcomes, spatiotemporal parameters, ground reaction forces, joint moments and power of the hip, knee and ankle.

Chapter 6 completes the main body of this thesis by providing a full discussion of the findings from each of the studies presented (Chapters 3-5). This Chapter also identifies the limitations associated with each study, as well as the implications, intentions for future work and concluding findings.

# **CHAPTER 1**

## **LITERATURE REVIEW**

# CHAPTER 1

## LITERATURE REVIEW

### 1.1 Ankle Joint Complex Anatomy and Function

The foot and ankle make up an intricate functional assembly of over twenty six irregularly shaped bones, thirty three joints, numerous tendons, ligaments and muscles responsible for our ability to support the weight of the body during static and dynamic locomotion (Kleipool and Blankevoort, 2010). The bones of the foot can be further divided into four functional regions: (1) the hindfoot which comprises of the talus and calcaneus; (2) the midfoot which comprises of the three cuneiforms, navicular and cuboid; (3) the forefoot which comprises of five metatarsals; and (4) the toes which comprise of five sets of phalanges, constructed of sixteen individual bones (Figure 1) (Levine et al., 2012). Although often referred to as the ‘ankle joint’, there are several articulations which facilitate motion of the foot. The ankle joint complex (AJC) is a multifaceted joint, consisting of the talocrural, subtalar and talocalcaneonavicular joints, which form a kinetic linkage system connecting the foot and lower limb, permitting the transfer of loads between the legs and feet (Grimston et al., 1993).

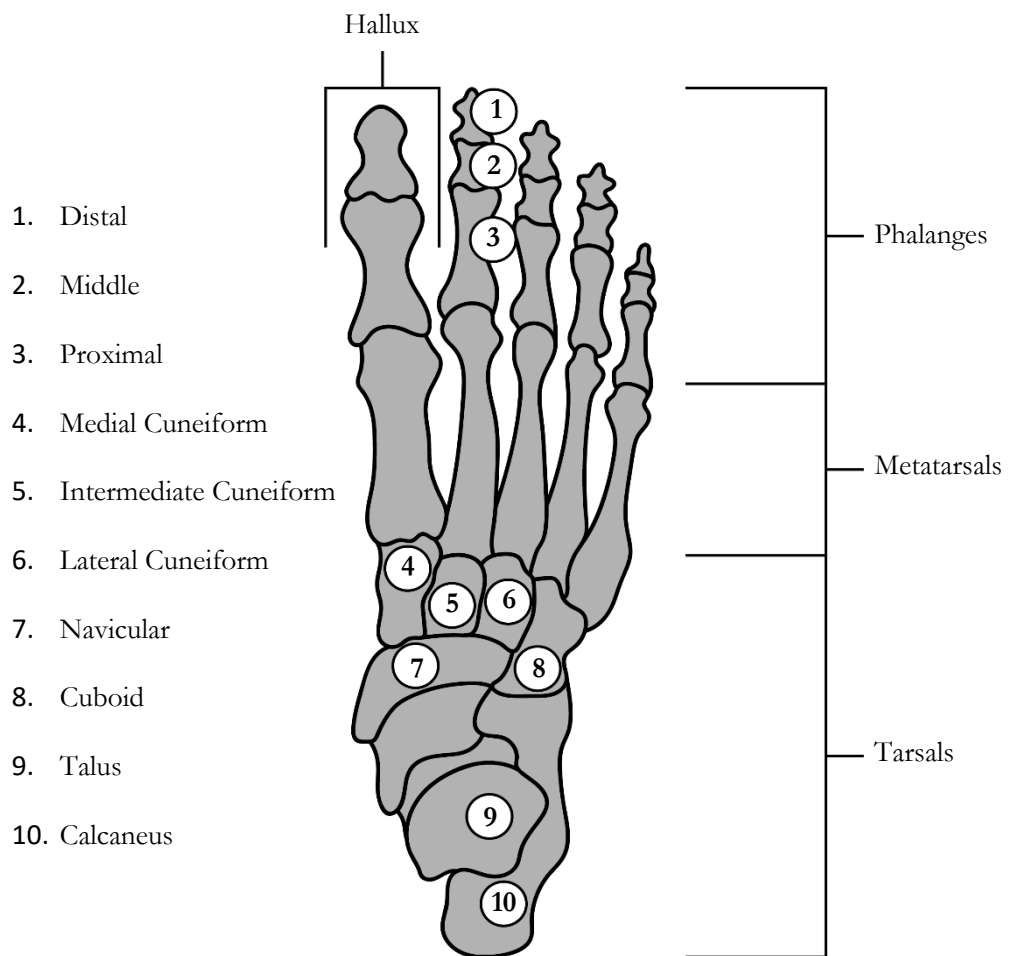


Figure 1. Schematic image of the bones of the right foot. Adapted from Hamill et al. (2021).

The talocrural (tibiotalar) joint is typically considered the “true ankle” joint and is established by the articulation of the inferior extremity of the tibia and fibula and the trochlea of the talus, as shown in Figure 2 (Michael et al., 2008). The talus is the most superior bone of the foot, consisting of a rounded head, neck and cuboidal body, which transmits the weight of the entire body of the foot (Hamill et al., 2021). The superior aspect of the body of the talus creates three joint surfaces (the trochlea; lateral malleolar facet; and medial malleolar facet), forming the articulation with the ankle mortise (Donatelli, 1985). The medial and lateral malleoli function together to restrain the talus, such that the talocrural joint primarily contributes to hinge like dorsi-/plantarflexion of the foot (Lundberg et al., 1989). The cone-shaped trochlea surface is formed from the talus being wider anteriorly than posteriorly, and the radius being smaller medially than laterally, suggesting the joint is most stable in dorsiflexion (Hertel, 2002).

The subtalar (talocalcaneal) joint consists of three articulations between the talus and calcaneus (Figure 2) (Jastifer and Gustafson, 2014). The calcaneus is the most posterior and largest bone of the foot, which is involved in the transfer of the weight of the body to the floor (Krähenbühl et al., 2016). The articulating facets of the inferior aspect of the talus have a concave structure, while the superior calcaneal surface is concentrically convex, resulting in the primary motions of inversion and eversion. The talocalcaneonavicular (transverse tarsal) joint is formed by the calcaneocuboid joint and the talonavicular joint. The talocalcaneonavicular joint shares a common axis of motion with the subtalar joint, which means it also contributes to inversion/eversion motion of the foot (Sarrafian, 1993).

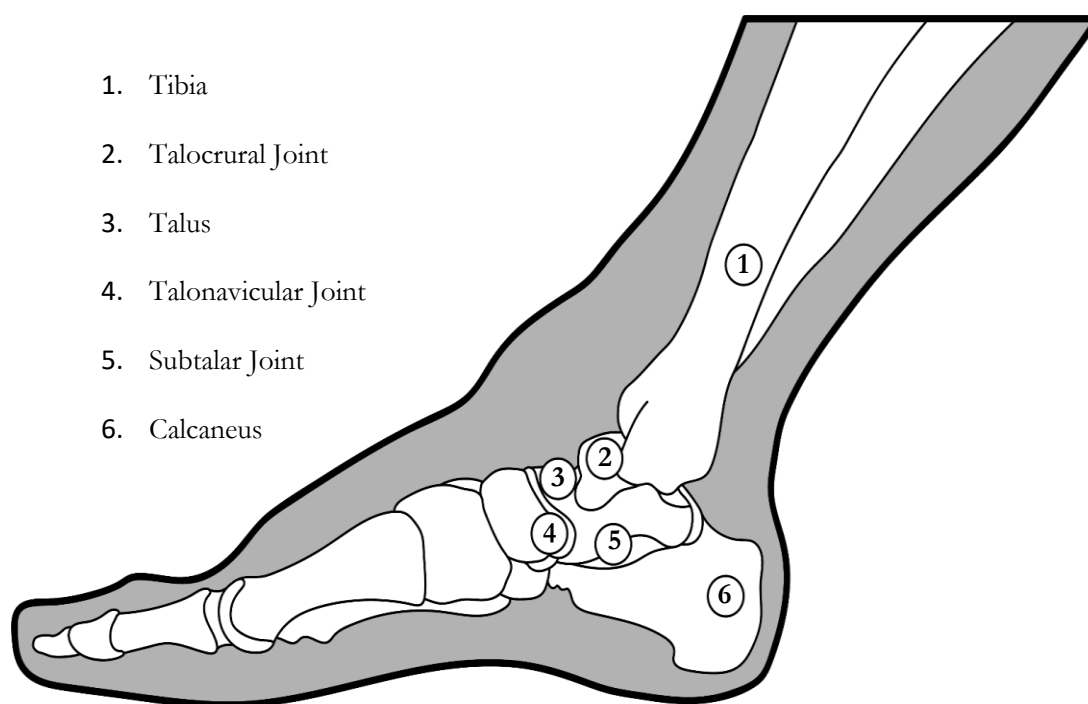


Figure 2. Sagittal view of the joints associated with the AJC. Adapted from Nordin and Frankel (2021).

The ligaments of the AJC play a fundamental role in providing stability during motion (Watanabe et al., 2012) and can be subdivided into lateral collateral ligaments (LCL), medial collateral ligaments (MCL), and ligaments of the tibiofibular syndesmosis (Golanó et al., 2010). The LCL consists of the anterior and posterior talofibular ligaments, and the calcaneofibular ligament, which provide resistance to inversion, varus stresses, and internal rotation (Figure 3) (Watanabe et al., 2012). The anterior talofibular ligament is at the greatest risk of injury, due to inversion injuries such as ankle sprains, which in turn, is the most common mechanism of ankle ligament injury (Lynch and Renström, 1999). The calcaneofibular ligament connects the talocrural and subtalar joints, ensuring stability of the subtalar joint (Golanó et al., 2010). The MCL consists of the tibionavicular, tibiocalcaneal and the anterior and posterior tibiotalar ligaments (Golanó et al., 2010). These ligaments work together to restrict eversion, valgus stresses, and external rotation within the ankle joint (Watanabe et al., 2012). The syndesmosis provides essential stability between the distal epiphyses of the tibia and fibula during activities of daily living (ADL) (Ebraheim et al., 2006).

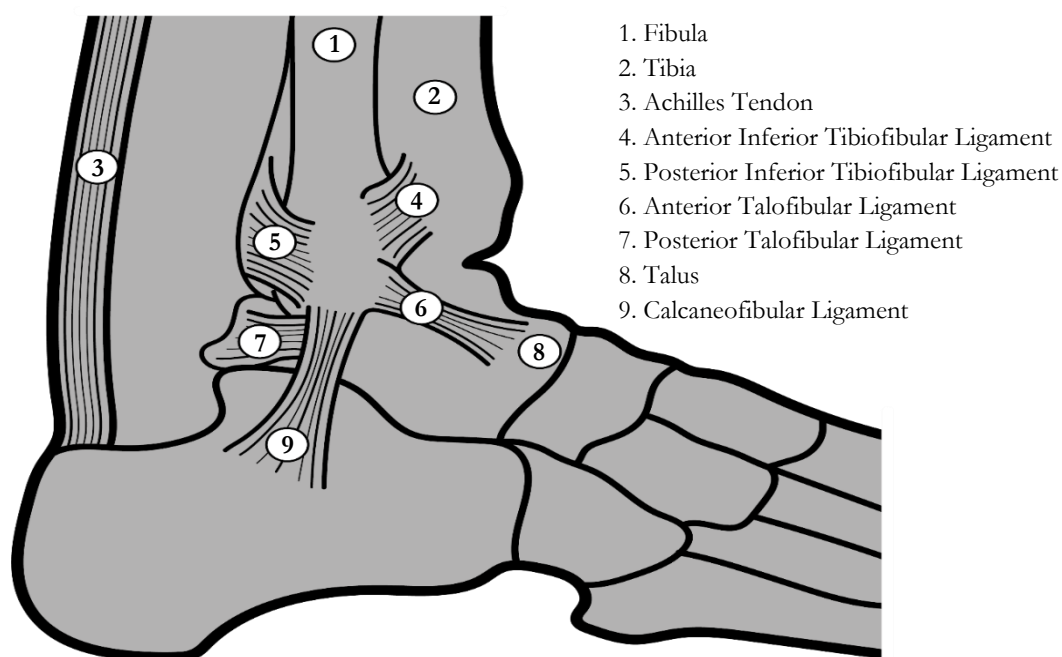


Figure 3. Lateral view of the ligaments of the ankle (Nordin and Frankel, 2021).

## 1.2 Biomechanics of the Ankle

### 1.2.1 Anatomical Planes and Axes

The AJC is efficient in producing multi-axial motion in all three anatomical (reference) planes of motion: sagittal (anteroposterior); frontal (coronal); and transverse (horizontal) (Figure 4). During motion, the body rotates around an imaginary axis of rotation (AOR), which passes through each joint. The three anatomical axes are commonly referred to as the mediolateral, anteroposterior

and longitudinal axes, which are perpendicular to the anatomical planes of motion and cause rotation in the sagittal, frontal and transverse planes, respectively (Nordin and Frankel, 2021).

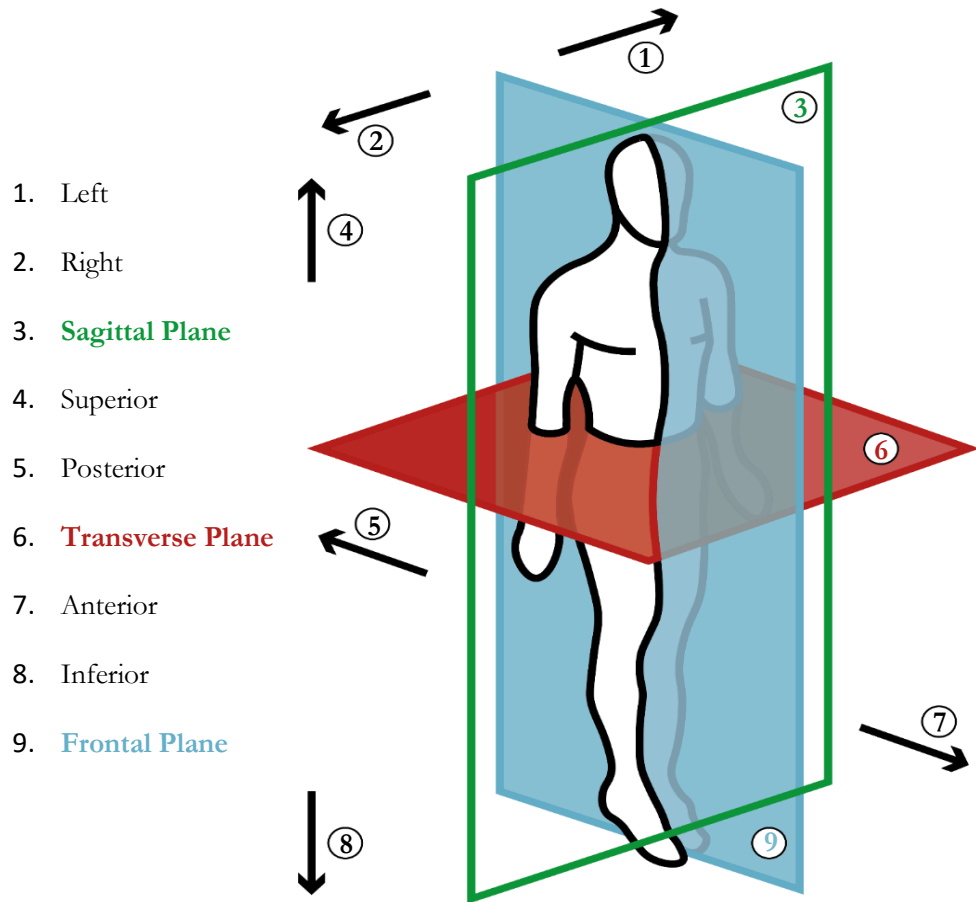


Figure 4. The three anatomical planes of motion and anatomical positioning terminology.

### 1.2.2 Motions of the Ankle Joint Complex

The AJC can rotate in all three planes of motion, allowing dorsi-/plantarflexion, inversion/eversion and abduction/adduction (internal/external rotation) in the sagittal, frontal and transverse planes, respectively (Figure 5) (Zwipp and Randt, 1994). In the sagittal plane, dorsiflexion is defined as the motion of the foot when the toes are raised off the ground, while plantarflexion occurs when the toes are pushed towards the ground (Snedeker and Wirth, 2012). Inversion occurs when the medial border of the foot lifts, causing the sole of the foot to tilt inwards, while eversion causes lifting of the lateral side of the foot and tilts the sole inwards towards the midline (Procter and Paul, 1982). Abduction is the motion where by the distal aspect is angled away from the midline of the body (lateral rotation), whereas adduction describes the motion of the distal aspect of the forefoot being angled in the direction of the midline (medial rotation) (Zwipp and Randt, 1994). Combinations of the individual planar orientations create three dimensional (3D) ‘triplanar’ motions commonly referred to as pronation and supination (Edington et al., 1990). Pronation is the amalgamation of dorsiflexion, eversion, and abduction, which causes the sole to face laterally. Supination is the opposite of pronation, in which the

combination of plantarflexion, inversion, and adduction causes the sole to face medially (McPoil and Knecht, 1985).

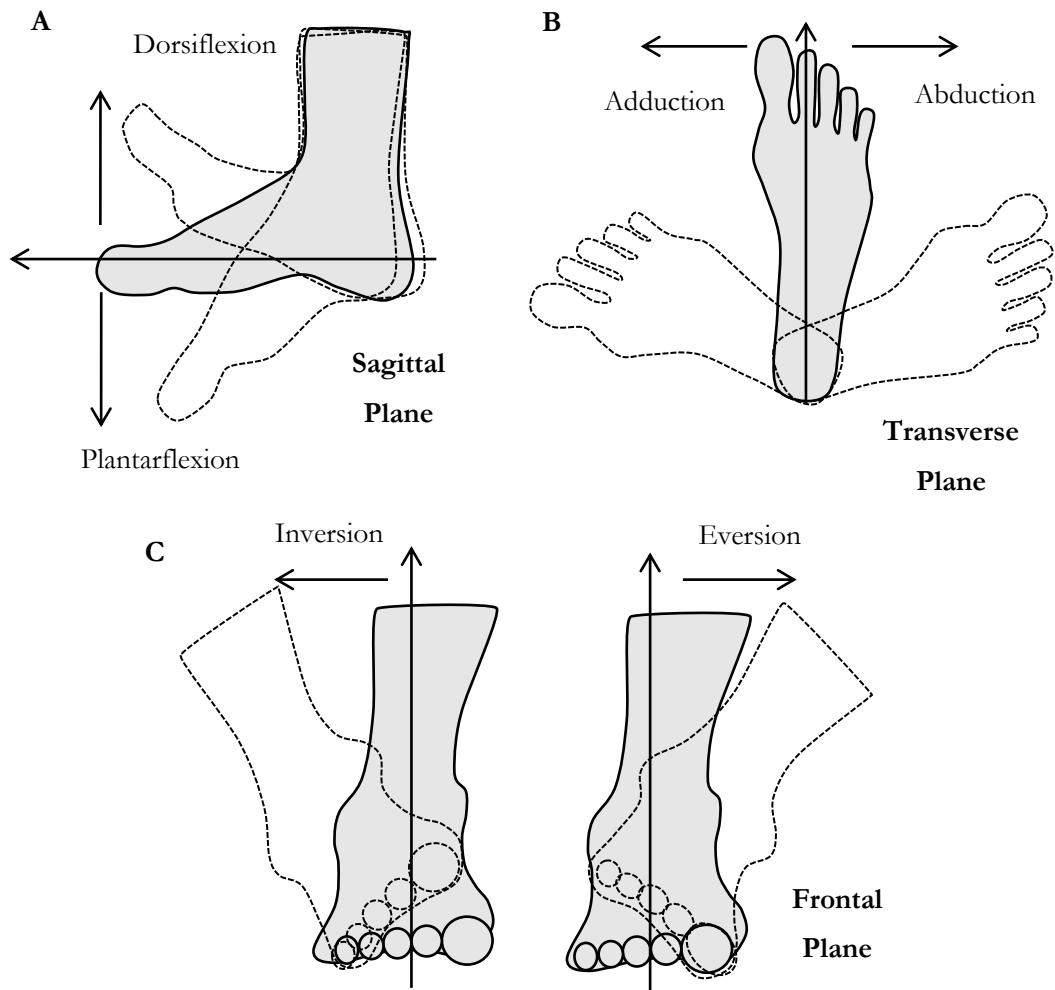


Figure 5. Motions of the ankle: Dorsi-/Plantarflexion (A), Abduction/Adduction (B), Inversion/Eversion (C).

### 1.2.3 Axis of Rotation

There remains a disagreement amongst researchers concerning the AOR for the joints of the AJC, with some individuals suggesting that the AJC is multi-axial. This is due to internal rotation that is produced during dorsiflexion and external rotation that occurs in plantarflexion (Siegler et al., 2014). Studies focused on defining talar anatomy, have highlighted differences in the medial and lateral aspects, signifying that the AOR of the talocrural joint differs as the motion changes (Barnett and Napier, 1952). It has been proposed that the AOR is inclined downwards and laterally during dorsiflexion, while being inclined upwards towards the lateral side of the ankle joint in plantarflexion (Barnett and Napier, 1952; Hicks, 1954). This finding was also supported by Lundberg et al. (1989), who implied that the talocrural joint possesses different axes for flexion, through applying known orientations of the AJC using roentgen stereophotogrammetry in 8 healthy participants. These changes between axes occurred gradually, particularly in the

frontal plane, with the dorsiflexion axes being inclined downwards and laterally compared with those of plantarflexion, which were inclined downwards and medially (Lundberg et al., 1989).

Other studies have determined that the talocrural joint is uniaxial in nature and works as a simple 'hinge' joint, with the simultaneous motion being produced as a result of its oblique axis (Inman, 1976; Sarrafian, 1993). Inman (1976) revealed that the lateral aspect of the trochlea remained perpendicular to the AOR, while the medial facet was inclined by 6°. The lateral facet of the trochlea was assumed to be circular in shape, while the medial aspect was elliptoid. The study also showed that in the frontal plane, the ankle joint axis was found to pass just below the tips of the malleoli (8°), inclining downwards and laterally. In the transverse plane, the axis was said to have gone through the centres of the malleoli, being inclined posterolaterally (Inman, 1976). However, a more recent computerised tomography based study of 26 healthy adults found that the trochlear surface of the talus can be modelled as a truncated conic saddle shape, orientated laterally compared to medially, as hypothesised by Inman (Siegler et al., 2014). The authors postulated that the compatible shape of the talus allows for triplanar motions of pronation and supination, while providing stability during inversion/eversion (Siegler et al., 2014). The subtalar joint possesses an oblique axis, which extends anteromedially from the talus to the posterolateral portion of the calcaneus (Donatelli, 1995). Using 46 cadaveric feet, the oblique axis has been found to produce a mean angle ( $\pm$  standard deviation) of  $41 \pm 9^\circ$  with the anteroposterior axis in the sagittal plane and  $23 \pm 11^\circ$  with the midline of the foot in the transverse plane (Figure 6) (Inman, 1976). The subtalar joint also acts as a torque converter during motion, resulting in tibial internal and external rotation during pronation and supination, which has been likened to a mitred hinge (Figure 7) (Donatelli, 1995).

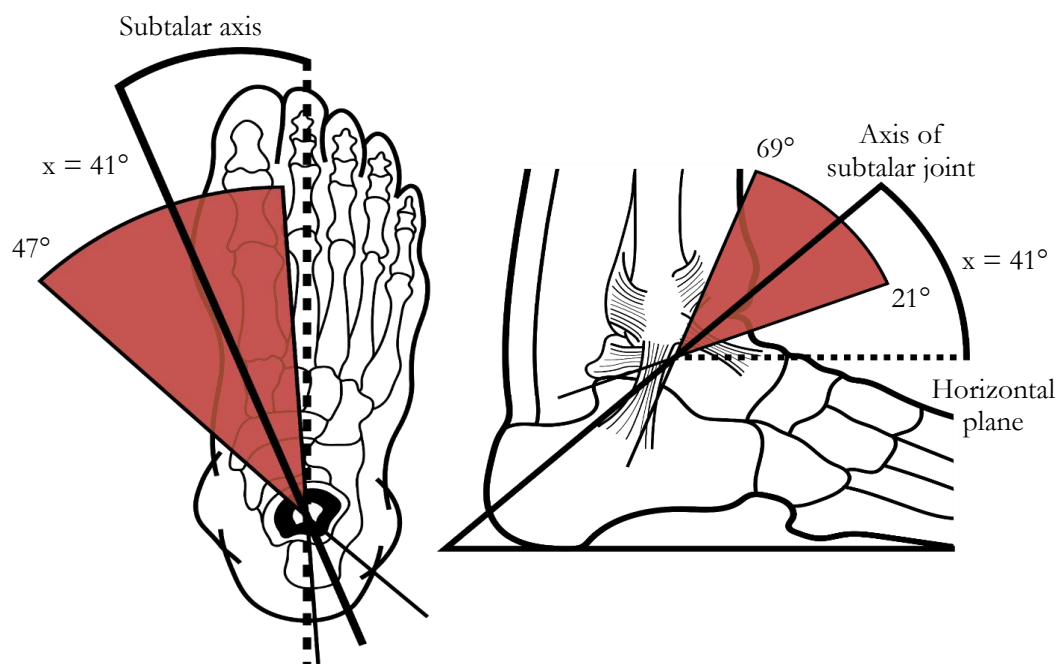


Figure 6. Subtalar joint axis in the anterior-posterior (left) and lateral (right) views demonstrating inclination and deviation respectively. Adapted from Jastifer and Gustafson (2014).

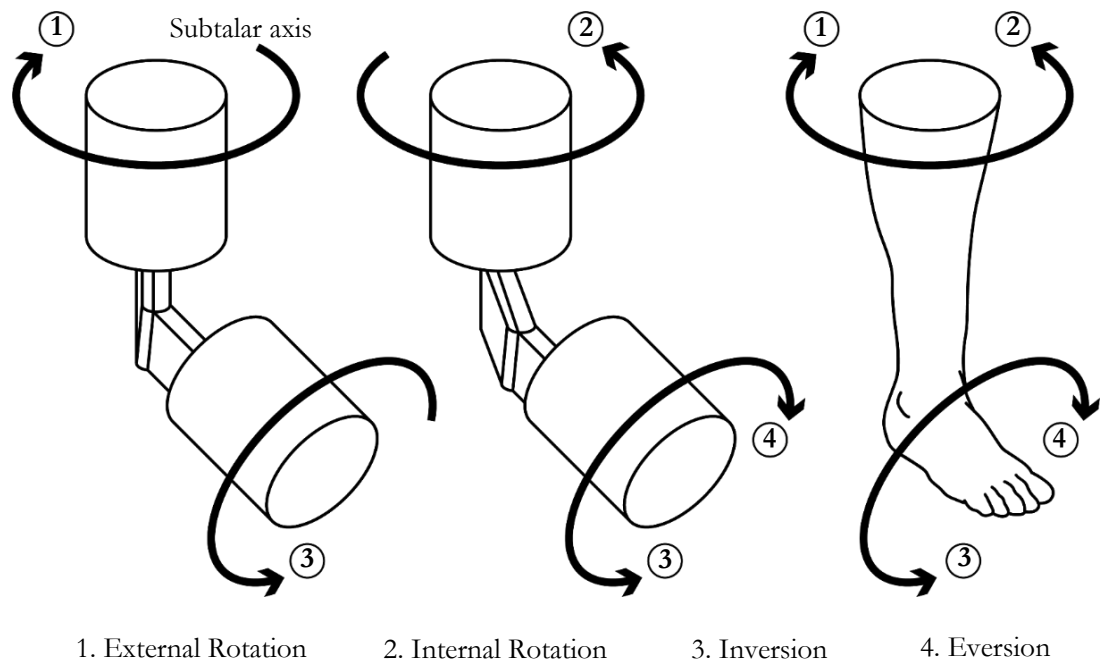


Figure 7. A representation of the subtalar joint as a mitred hinge. Adapted from Inman (1976).

#### 1.2.4 Range of Motion

Sagittal plane range of motion (ROM) represents the greatest amount of motion at the AJC, which is between 65°-70°, moving from 10°-20° of dorsiflexion through to 40°-55° of plantarflexion (Stauffer et al., 1977; Grimston et al., 1993). However, during ADL's, the required sagittal plane ROM is much lower, with a maximum of 30° for walking, 37° for stair ascent, and 56° for stair descent (Nordin and Frankel, 2021). Frontal plane ROM is approximately 35°, with a maximum inversion angle of 20°-30°, compared to 5°-10° for maximum eversion (Stauffer et al., 1977). Again, only 10°-15° of frontal plane motion is required during walking based activities (Sammarco and Hockenbury, 2012).

There is much debate throughout the ankle literature as to how much the talocrural and subtalar joints contribute to each other's motion. Historical research concluded that dorsi-/plantarflexion motion was solely accredited to the talocrural joint, while inversion/eversion occurred solely at the subtalar joint (Chen et al., 1988). However, dynamic magnetic resonance imaging techniques have been used to determine that most eversion occurred at the subtalar joint as predicted, but inversion motion was also found to occur at the talocrural joint (Sheehan et al., 2007). The improved understanding of talar geometry has also shown perceived motion in the subtalar joint may occur at the talocrural joint due to its saddle shape (Siegler et al., 2014).

#### 1.2.5 Gait Cycle and Events

Human locomotion is a cyclic process that is often referred to as the 'gait cycle', which is defined as the time intermission between two repeated events of walking (Levine et al., 2012). The gait cycle can be separated into two distinctive phases known as stance and swing (Stauffer et al., 1977). The former describes the process of the foot contacting the ground and accounts for 60%

of the gait cycle and the latter when the foot is not (Perry and Burnfield, 2010). While the gait cycle describes the motion of a single leg, the gait cycle of the contralateral limb is the same in healthy individuals, but time-shifted by 50%. The overlapping period of the stance phase in both limbs is known as the double-support period, representing the phase where both feet are on the ground simultaneously (Levine et al., 2012). The two phases of the gait cycle can be further separated into seven successive sub-phases: (1) loading response; (2) midstance; (3) terminal stance; (4) pre-swing; (5) initial swing; (6) mid-swing; and (7) terminal swing (Figure 8) (Whittle, 1996).

The loading response, corresponds to the double support period following initial contact with the ground (0-10%) (Perry and Burnfield 2010). Initial contact, also referred to as heel strike, is deemed the start of gait, with the foot and ankle in a relatively neutral position in the sagittal plane of motion (Figure 9). After initial contact, ankle plantarflexion occurs as the forefoot is lowered to the floor, pivoting around the calcaneus until the foot is flat on the ground. During initial contact, the foot is also typically in an inverted position leading to maximum eversion at midstance (Figure 9) (Michael et al., 2008). The midstance phase is associated with the neutral position of the foot and occurs during contralateral limb toe-off to heel rise (10-30%) (Levine et al., 2012). Throughout this phase, body weight (BW) is supported by a single limb, with the muscles surrounding the hip joint providing most of the stability required to maintain balance (Levine et al., 2012).

Terminal stance occurs during heel rise of the supporting limb, with the ankle joint attaining maximum dorsiflexion at 75% of stance (Levine et al., 2012). Subsequently, a rapid motion of plantarflexion occurs, coupled with tibial external rotation and forefoot supination, causing the calcaneus to lift off the ground. This continues until reaching maximum plantarflexion at toe-off (Figure 9) (Perry and Burnfield, 2010). Inversion begins to occur until toe-off (Figure 9), giving the foot rigidity to allow the heel to rise and push off into the swing phase (Nordin and Frankel, 2021).

The pre-swing phase begins at toe-off of the supporting foot and initial contact of the contralateral foot. This shorter double support period persists for approximately 10% of the gait cycle and is also known as the push-off or propulsion sub-phase (Levine et al., 2012). As the name suggests, the body accelerates forward as the foot acts as a rigid lever (Blackwood et al., 2005), pushing the body forward through the power generated primarily at the ankle (Levine et al., 2012). Throughout the initial swing phase, the foot swings across the mid-line of the body, acting as a 'pendulum', with the advancement of the lower limb (Levine et al., 2012). During mid-swing and terminal swing phases, the knee extends passively to prepare the foot for initial contact. The ankle progressively shifts from a plantarflexed position to a relatively neutral position at initial contact to begin the next gait cycle (Figure 9) (Perry and Burnfield, 2010).

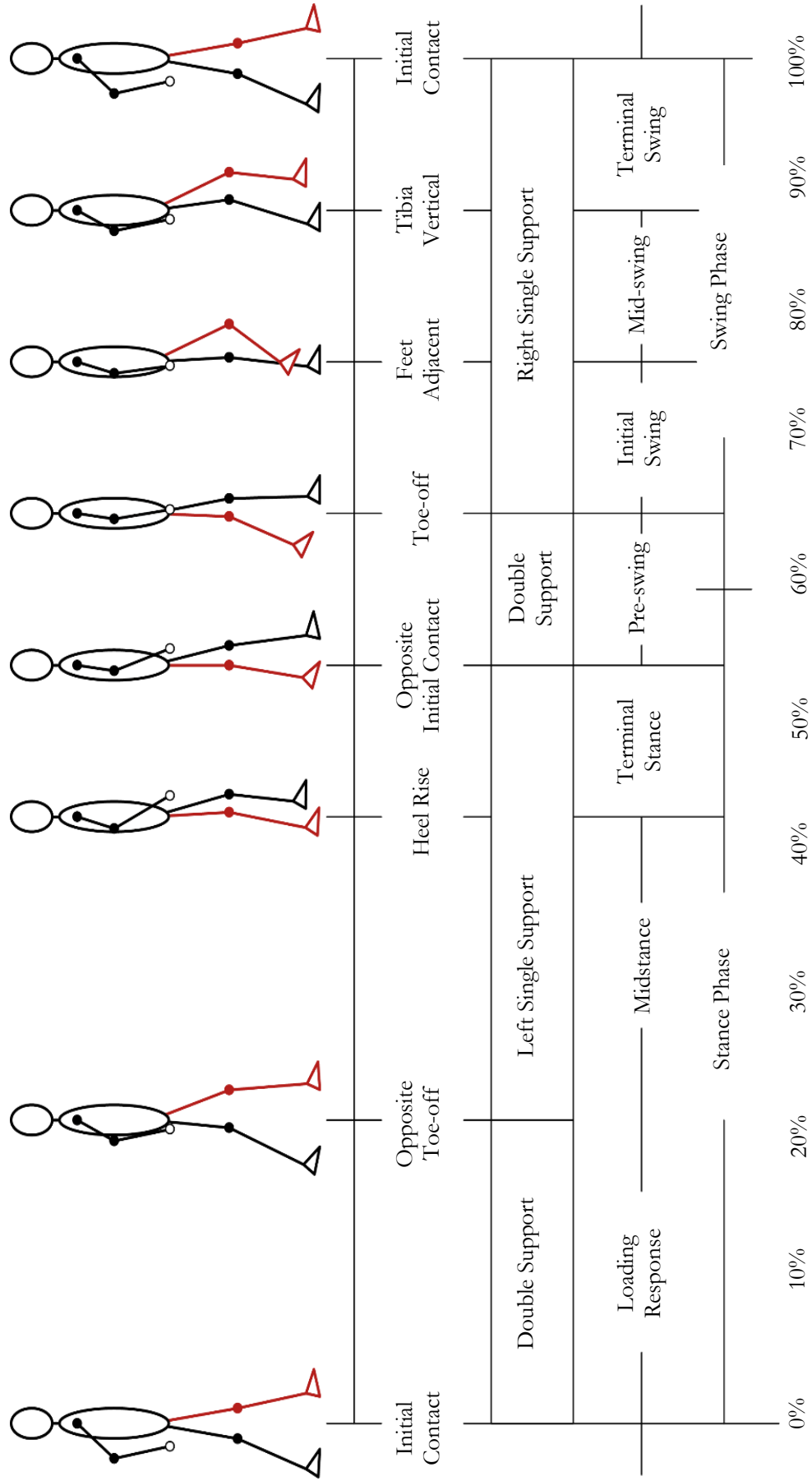


Figure 8. The level walking gait cycle broken down into its sub-phases (right foot). Adapted from Hamill et al. (2021).

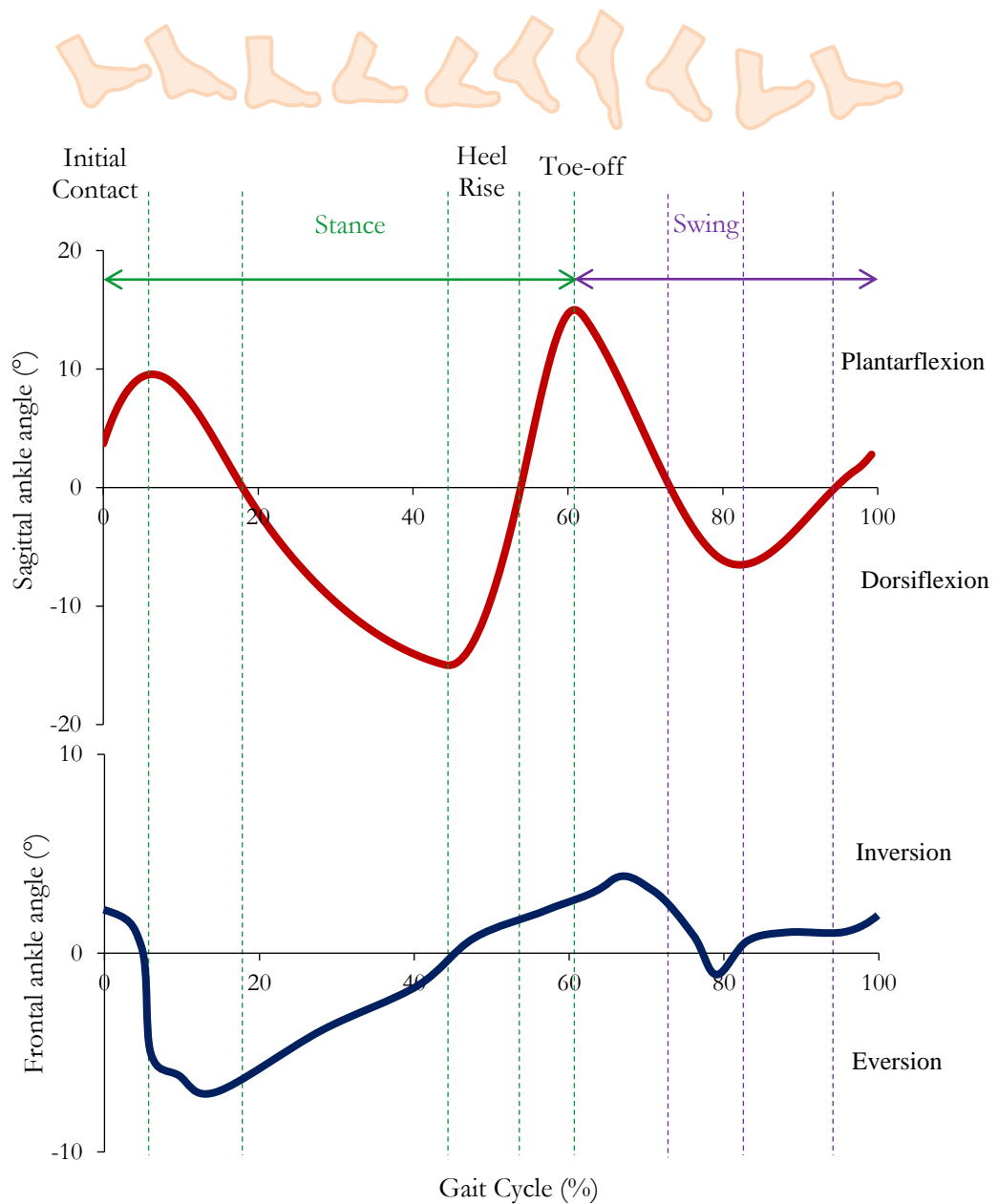


Figure 9. The ankle and subtalar joint motions in the sagittal and frontal planes, respectively, during a natural walking gait cycle. Adapted from Sammarco and Hockenbury (2012).

### 1.2.6 Ankle Forces

The talocrural joint bears a compressive force of approximately 5-7 times BW during the stance phase of walking (Michael et al., 2008), and up to 13 times BW during running (Burdett, 1982). Experimental studies have determined that approximately 83% of the load is transmitted through the tibia to the talus, with the remaining 17% transmitted through the fibula (Calhoun et al., 1994; Wang et al., 1996b). Of the load carried across the talocrural joint, between 77-90% is applied to the talar dome, with the remaining load (10-23%) being transferred across the medial and lateral talar facets (Michael et al., 2008). The load distribution is controlled by the forces at the ankle ligaments and their positional effects, with increased loads on the talar lateral facet during eversion and higher loads at the medial facet during inversion (Michael et al., 2008).

The talocrural joint has a relatively high level of congruency, meaning that despite the relatively high loads experienced during walking and varying ADLs, the load-bearing contact area of the talocrural joint is relatively large (11-13 cm<sup>2</sup>) (Michael et al., 2008). It has been proposed that the ankle possesses the highest weight bearing force per cm unit area than any other joint of the lower limb (Thomas and Daniels, 2003). The majority of studies have measured contact forces at the ankle through computational prediction or cadaveric experimentation. A cadaveric study applying a static load of 1500 N (approximately twice BW) in the neutral position, demonstrated a mean contact pressure of 9.9 MPa and a mean contact area of 483 mm<sup>2</sup>, which is substantially less than proposed values above (Kimizuka et al., 1980). A similar study using a lower load of 800 N, representing 1 times BW, produced a mean contact pressure of 1.84 MPa in the neutral ankle, 2.16 MPa in 20° of dorsiflexion and 2.14 MPa in 20° of plantarflexion (Wagner et al., 1992). The mobile axes of the ankle also allows the alignment of the AJC to adjust with changes in weight bearing, thus, reducing some of the contact stresses (Nordin and Frankel, 2021). However, the relatively high ROM and compressive loads that occur at the AJC, means that the ankle remains vulnerable to injury, which in some cases may subsequently lead to the degeneration within the joint.

### **1.3 Ankle Arthritis**

The most common pathology that can disrupt the ankles function is osteoarthritis (OA), which is characterised as a progressive cartilage degenerative disease (Hügler et al., 2012), with a population prevalence estimated to be 3.4% in people over 50 years of age (Murray et al., 2018). OA eventually causes the reduction in joint space, increased subchondral bone sclerosis, intra-articular inflammation and periarticular bone growth (Donell, 2019). Patients suffering with OA usually experience typical symptoms of joint pain, swelling, stiffness, impaired functional ability and reduced quality of life (QoL) (Thomas and Daniels, 2003; Buckwalter et al., 2004; Agel et al., 2005; Saltzman et al., 2006; Glazebrook et al., 2008; Hintermann and Ruiz, 2014). End-stage ankle OA has previously been shown to be as debilitating as end-stage hip OA, kidney disease and congestive heart failure (Saltzman et al., 2006; Glazebrook et al., 2008).

The number of cases of primary OA is considerably less common in the ankle joint compared to the proximal joints of the lower limb (Snedeker and Wirth, 2012), with approximately 47.7 per 100,000 individuals in the United Kingdom (UK) encountering this issue (Saltzman et al., 2006). The substantially lower occurrence rate of primary OA at the ankle joint is likely owed to the biomechanical and anatomical structure of the AJC (Adukia et al., 2020). Biomechanically, the sagittal ROM that occurs at the talocrural joint is substantially smaller than that of the hip and knee joints (Deleu et al., 2020a), which predisposes the proximal lower limb joints to developing primary OA (Thomas and Daniels, 2003). Anatomically, ankle cartilage has been found to be more stiff and resistant to mechanical damage (Shepherd and Seedhom, 1999). The cartilage at the ankle has also been shown to not generate matrix metalloproteinase 8 (MMP8) mRNA, an

enzyme known to be present in degenerative knee cartilage (Adams et al., 2015). Additionally, ankle cartilage tends to be less sensitive to the effects of cytokines, which have been associated to the advancement of primary OA (Adams et al., 2015; Pham et al., 2021).

Prior joint trauma is the most regular cause of ankle OA (Saltzman et al., 2005; Hintermann and Ruiz, 2014), accounting for between 65-80% of all cases, compared to 9.8% and 1.6% in knee and hip OA, respectively (Horisberger et al., 2009). The main predisposing causes of post-traumatic OA (PTOA) are ankle fracture (37.0%), persistent sprains (14.6%), pilon fracture (9.0%), tibial shaft fracture (8.5%), and osteochondral lesion of the talus (4.7%) (Saltzman et al., 2005). Ankle trauma and subsequent ankle OA is, therefore, more likely to affect younger and more active populations than in hip or knee OA (Hintermann and Ruiz, 2014). The average age of a patient requiring surgical intervention after PTOA is 51.5 years (Saltzman et al., 2005), while hip and knee OA patients commonly have surgical treatment at a later age of approximately 70 years (Thien et al., 2014). The earlier symptomatic onset of OA, compared to the proximal joints of the lower limb, means that patients may suffer over longer periods of time and the associated symptoms of OA must be endured to remain physically active and maintain their capacity to work (Hintermann and Ruiz, 2014).

## **1.4 Treatment of Ankle Arthritis**

The younger and more active population who suffer from PTOA present a new challenge with regard to selecting a surgical intervention that is reliable and long-lasting, in order to improve the functional capabilities and pain relief of patients suffering from end-stage ankle OA (Demetracopoulos et al., 2015).

### **1.4.1 Non-surgical Interventions**

Non-surgical interventions for ankle OA are the same as for other degenerative joints, comprising of approaches aimed at reducing weight bearing loads at the AJC (Castagnini et al., 2016). These surgical options include: physical activity modification to exercises such as swimming and cycling; weight reduction; withdrawal from high risk and impact sports; and the use of walking aids (Adukia et al., 2020). Arthritic patients may also benefit from shoe outsole adaptations (i.e., rocker sole) or foot orthotics to allow efficient forefoot motion and restrict movement at the AJC (Huang et al., 2006). In addition, the combined use of physiotherapy, analgesics, and anti-inflammatory medication should be recommended to patients with worsening conditions and before surgery is required (Bloch et al., 2015). Non-surgical treatments focus on pain management and slowing the progression of ankle degeneration. However, once end-stage ankle OA is reached, these treatment methods are considered completely ineffective and surgical interventions are a must (Bhatia, 2014).

### **1.4.2 Surgical Interventions**

There are several surgical interventions for patients suffering from end-stage ankle OA. Ankle debridement (ankle arthroscopy), utilises fibre optics, magnifying lenses and digital video monitors to visualise the ankle joint through minor incisions (Bluman et al., 2018). The main advantage of this treatment option is that it is a minimally invasive approach, coupled with a short recovery time (Bluman et al., 2018). However, the findings surrounding this technique remain inconsistent, particularly for patients suffering with end-stage ankle OA (Glazebrook et al., 2009). Supramalleolar osteotomy aims to realign the joint articular surface areas between the tibia and talus, thus increasing the contact area across the ankle to restore normal joint loading (Takakura et al., 1995). However, the survival rate of this realignment procedure was only 88% at a mean follow-up period of 5 years in 298 ankles (Krähenbühl et al., 2017). Distraction arthroplasty applies an external fixed or hinged distractor frame, designed to permit intermittent intra-articular fluid pressures and provide reprieve from mechanical stress on the cartilage (Martin et al., 2007). Previous research has demonstrated relatively beneficial results, with 9 of 16 patients (56.25%) presenting improved functional and pain outcomes at a short follow-up period of 41 months (Xu et al., 2017). On the other hand, the level of evidence of this technique remains insufficient and a significant proportion of younger patients require joint-sacrificing surgery in the mid-to-long term (Adukia et al., 2020).

Whilst each of these surgical interventions have their advantages, their clinical and functional findings remain inconsistent in patients suffering with end-stage ankle OA. Therefore, the remaining part of the section will concentrate on the two most common invasive surgical interventions for end-stage ankle OA: ankle arthrodesis (AA) and total ankle replacement (TAR).

### **1.4.3 Ankle Arthrodesis**

Introduced in 1879, AA, or ankle fusion, involves the restriction of movement at the AJC, through the artificial induction of joint ossification between the tibia and talus (Figure 10) (Cottino et al., 2012; Iwasa et al., 2014). AA is considered the gold-standard operative treatment strategy for surgeons in the treatment of end-stage ankle OA (Jordan et al., 2014; Lawton et al., 2020). There have been over thirty different operational techniques reported in the literature for AA (Nihal et al., 2008), with extensive data demonstrating significant pain relief and improved patient reported outcome measures (PROMs) (Lynch et al., 1988; Hendrickx et al., 2011; Norvell et al., 2019). Intermediate-to-long term revision rates of AA are also low, with a pooled mean rate of 6.3% at an average follow-up of 4 years post-surgery (Lawton et al., 2020). Consequently, younger patients suffering with ankle OA tend to have AA surgery, particularly when functioning under higher and repetitive loading (Kim et al., 2017). However, non-union (7.4%) and wound complication (6.5%) remain regular reasons for revision in the AA patient population (Lawton et al., 2020). There is also no acceptable 'salvage procedure' for AA patients, limiting the capacity for deformity corrections (Easley et al., 2002).



Figure 10. Lateral and anteroposterior post-operative weight-bearing radiographs of an ankle arthrodesis fixation. Adapted from Brodsky et al. (2016).

The major concern with AA surgery is the immobilisation of the joint itself. This has been associated with reduced walking velocity and ankle sagittal ROM in AA patients, compared with the unaffected contralateral limb or healthy participant cohorts during level walking (Mazur et al., 1979; Wu et al., 2000; Trouillier et al., 2002; Valderrabano et al., 2003; Beyaert et al., 2004; Thomas et al., 2006; Fuentes-Sanz et al., 2012). Conversely, other gait based studies have shown a minimal reduction in sagittal plane ROM at the AJC in arthritic patients treated with AA surgery (Hahn et al., 2012; Flavin et al., 2013), while Brodsky et al. (2016) demonstrated increased ankle joint ROM following AA at a short-term follow-up of 15 months. The authors of the latter study stated that regardless of the sagittal plane motion post-operatively, some AA patients experience mobility at the AJC rather than the anticipated increase in joint stiffness (Brodsky et al., 2016). These contradictory findings may be related to the methodological differences between the gait studies, with Brodsky et al. (2016) using a simplistic one-segment kinematic foot model, which has been shown to cause opposite kinematic results at the ankle joint during walking (Pothrat et al., 2015).

It is believed that the reduction in pain in the AJC following AA surgery may be a result of potential compensatory mechanics at the distal foot joints (Deleu et al., 2020a). A cadaveric gait simulation of a fused ankle demonstrated greater dorsiflexion and contact stresses at the forefoot joints during late stance (Demetracopoulos et al., 2016). Such compensatory motions may relate to alterations in adjacent joint contact mechanics, resulting in propagation of OA in the distally located joint (Demetracopoulos et al., 2016). A systematic review of 18 clinical studies showed the occurrence of subtalar OA ranged from 24% to 100%, while OA at the talonavicular and calcaneocuboid joint ranged between 18% to 77% following AA surgery (Ling et al., 2015). One

way to treat postulated adjacent-joint OA would be with additional immobilisation, thus creating a chain reaction, which can lead to eventual transtibial amputation (Greisberg et al., 2004).

Only recently, a 3D multi-segment foot model (MFM) was used to differentiate the joints of the hindfoot, midfoot and forefoot, in arthritic patients treated with AA (Eerdekens et al., 2020a). The study determined that there were no significant differences observed between the baseline and post-operative measurements, suggesting that the distally located joints did not undergo compensatory mechanisms at the 1 year post-operative follow-up. From a clinical point of view, this finding suggests that AA patients do not need to fear a loss of biomechanical functionality in their foot and ankle following surgery. However, it remains unclear as to whether the distally located joints to the AJC become constrained or hypermobile following AA at an intermediate-to-long-term follow-up post-surgery.

#### 1.4.4 Total Ankle Replacement

The disadvantages associated with AA surgery have encouraged the advancement and use of motion preserving surgical interventions such as TAR (Figure 11). This technology has been shown to result in the improved PROMs, preservation of ankle function and the potential to reduce the risk of developing adjacent joint degeneration (Deleu et al., 2020a).



Figure 11. AP and lateral weight-bearing radiographs at 7 years follow-up following a mobile-bearing device. Adapted from Giannini (2013).

##### 1.4.4.1 History and Design Development

Encouraged by the initial positive clinical outcomes of total hip replacements (THR) and total knee replacements (TKR), the first TAR was performed in 1970 (Lord and Marotte, 1973). The device was a simple 'hinged' design, comprising of a tibial component with a long stem, which was comparable to the femoral component of a THR. The talar component was manufactured from conventional ultra-high-molecular-weight polyethylene (UHMWPE).

Other first generation TARs were defined as being constrained or unconstrained devices. Constrained devices were categorised as being spherical, spheroidal, conical, or cylindrical in shape (Lewis, 1994). The design aimed to enhance stability during articulation (Vaughn et al., 1976), while reducing polyethylene wear by providing uniform force distribution across the bearing surface (Gougoulias et al., 2008). However, the issue with constrained devices was that the movement was limited to the sagittal plane and caused increased risk of loosening at the bone-implant interface during short-term follow-up (Coetzee et al., 2017). Unconstrained devices were typically trochlear, bi-spherical, concave-convex, and, convex-convex in design (Lewis, 1994). They had the advantage of increased ROM in all three planes of motion and reduced strain at the bone-implant interface (Gougoulias et al., 2008). Conversely, instability occurred as a result of excessive strain on the surrounding soft tissue, which was associated with increased UHMWPE wear (Gougoulias et al., 2008).

There were early encouraging PROMs with first generation TARs, however, high complication rates and failure were associated at longer-term follow ups, with recommendations for use only in elderly patients with limited physical demands (Lachiewicz, 1994). Both TAR designs required significant bone resection and required large volumes of polymethyl methacrylate cement fixation, which had been attributed to increased loosening, osteolysis and subsidence in the metallic components (Vickerstaff et al., 2007). The high failure rates in first generation TARs resulted in the concept being abandoned in favour of the more reliable AA surgical technique.

Researchers who identified problems with the early failing TAR designs considered this when developing second and third generation implants, which give additional consideration to replicating natural ankle anatomy (Vickerstaff et al., 2007). These devices are manufactured as either a two-part, fixed-bearing (FB) or three-part, mobile-bearing (MB) implants. FB designs are defined by the UHMWPE insert being fixed to the tibial component (Figure 12), enabling improved axial rotation and sagittal ROM (Vickerstaff et al., 2007). Compared to first generation designs, FB implants are fixated at the bone-implant interface through the use of a porous coating, which encourages osseointegration as opposed to cementation. This requires increased joint space, meaning more bone stock is maintained compared to first generation devices (Ianuzzi and Mkandawire, 2016).

The “constraint-conformity/congruency conflict” is more apparent in FB implants with entirely conforming articulating surfaces, which produce increased axial constraints and subsequent axial loosening torque (Gougoulias et al., 2008). Hypothetically, to decrease implant constraint, FB designs can only be partially conforming, resulting in higher polyethylene wear as a result of increased contact stresses at the articulating surfaces (Gougoulias et al., 2008). Therefore, reducing conformity is associated with increased UHMWPE wear, particularly where there is an imbalance, resulting in edge loading of the polyethylene insert, and ultimately device failure (Vickerstaff et al., 2007).

Despite the potential increased risk of higher contact stresses and subsequent wear associated with FB, the popularity for using this device design has further augmented with the introduction of fourth generation implant designs, such as the INFINITY™ (Wright Medical Group, Arlington, Tennessee, United States of America (USA)), which has a 65.2% market share in the UK in 2020 (NJR, 2021).

MB designs usually contain a flat tibial and curved talar metallic articulating surface, separated by a conforming UHMWPE meniscal insert (Figure 12). The design permits motion between the tibia and UHMWPE insert, allowing improved sagittal ROM compared to FB designs. This replicates rotational and translational freedom on the natural ankle, and reduces contact stresses at the bone-implant interface (Tochigi et al., 2005; Barg et al., 2015). The talar component in a MB has an increased contact area, due to the radius of curvature being longer than the talus of a natural ankle, preventing the likelihood of edge loading during motion (Hintermann, 2005). MB devices also decrease the volume of bone re-sectioning, resulting in a reduction of talar component subsidence (Gougoulis et al., 2008).

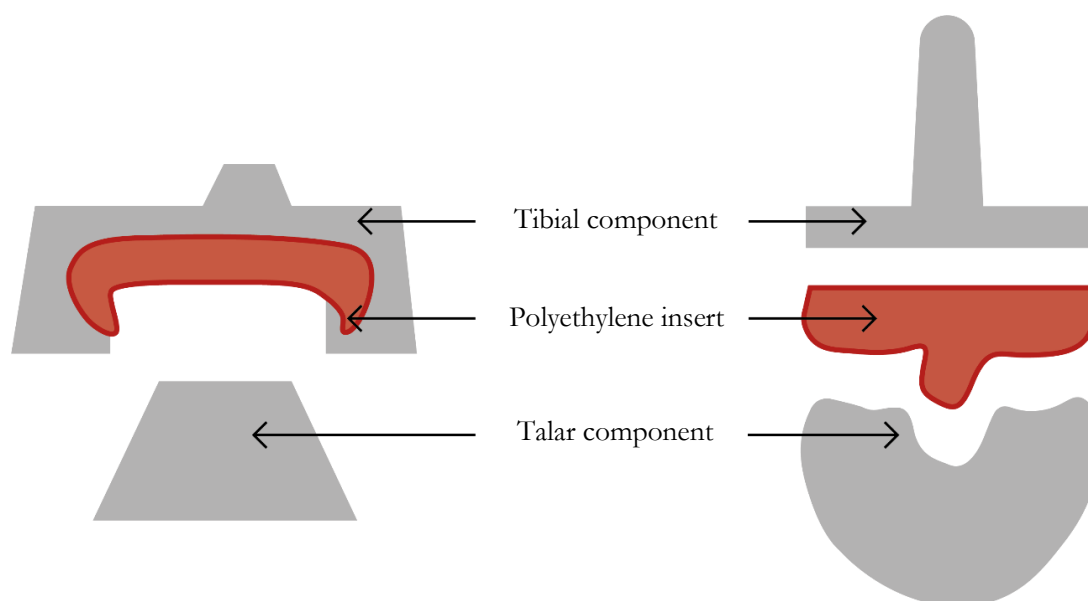


Figure 12. Schematic of a fixed (left) and mobile (right) TAR, consisting of metallic tibial and talar components and an UHMWPE meniscal insert.

#### 1.4.4.2 Survivorship

Even the latest generation of TAR designs are not surgeons' automatic choice of intervention for end-stage ankle OA, mainly due to the surgical procedure being highly complex (Usuelli et al., 2017) and relatively low survivorship compared to both AA and other joint replacements of the lower limb (Haddad et al., 2007; Daniels et al., 2014; Veljkovic et al., 2019; Lawton et al., 2020). A retrospective, cross-sectional cohort study, analysing 238 ankles (88 TAR, 50 arthroscopic AA and 100 open AA) in 229 patients with a mean follow-up of 43.3 months found that the rate of revision was comparable between the treatment groups, but there was a significantly higher re-

operation rate for TAR (Veljkovic et al., 2019). However, the study failed to control for variance in patient demographics between treatment groups and there may have been selection bias, as the patients that received AA do not always have the same indications as the TAR cohort.

Lawton et al. (2020) provided a combined systematic review and meta-analysis of the published literature reporting patient outcomes, complications and revision rate of 4,312 TAA and 1,091 AA procedures. The analysis demonstrated no significant differences in complication rates ( $p = 0.31$ ) or revision rates ( $p = 0.65$ ) between surgical interventions (Lawton et al., 2020). The current literature comparing the survivorship and revision rates of modern TAR and AA techniques is limited by the lack of long-term follow-up studies, which do not support one treatment option over the other for the management of end-stage ankle OA. Ultimately, the selection of implanting either treatment option should be assessed on a case-by-case basis, ensuring an informed discussion is conducted with each patient concerning the surgical interventions goals and potential complications.

#### **1.4.4.3 Complications**

At present there still remains a high level of uncertainty in regard to the factors which cause implant failure and the success of different designs in different patient groups. Aseptic loosening, infection and pain remain the most common failure mechanism in TAR devices (Henricson et al., 2007; Glazebrook et al., 2009; Espinosa et al., 2017). An earlier retrospective study used the Food and Drug Administration (FDA) Manufacturer and User Facility Device Experience (MAUDE) voluntary database, to determine complications reported outside the published literature (Mahmoud et al., 2021). Among the 648 reports available within the database, aseptic loosening (19.3%) and infection (18.2%), were found to be the most common complications.

A total of 339 out of the 7,084 primary TAR procedures reported in the 18<sup>th</sup> NJR annual report indicated that a revision had taken place (NJR, 2021). The NJR Annual Report also identified that aseptic loosening (24.7%), infection (14.5%), and pain (11.0%), were the major indications for first revisions following primary TAR (Figure 13) (NJR, 2021). Aseptic loosening is usually found at the metallic talar component (Tomlinson and Harrison, 2012), and can be accredited to: inadequate fixation or small fixation surfaces (Misgeld et al., 2017); mal-alignment of the hindfoot or implant (Sopher et al., 2017); polyethylene component incongruity (Saito et al., 2019); and osteolytic lesions (Glazebrook et al., 2009). The common management option following loosening of the components is conversion to AA, although revision TAR using modular stemmed components has risen in popularity (Adukia et al., 2020). A previous study identified an 83% survivorship of 117 revision TARs at the six-year follow-up phase, where aseptic loosening had been identified again (Hintermann et al., 2013).

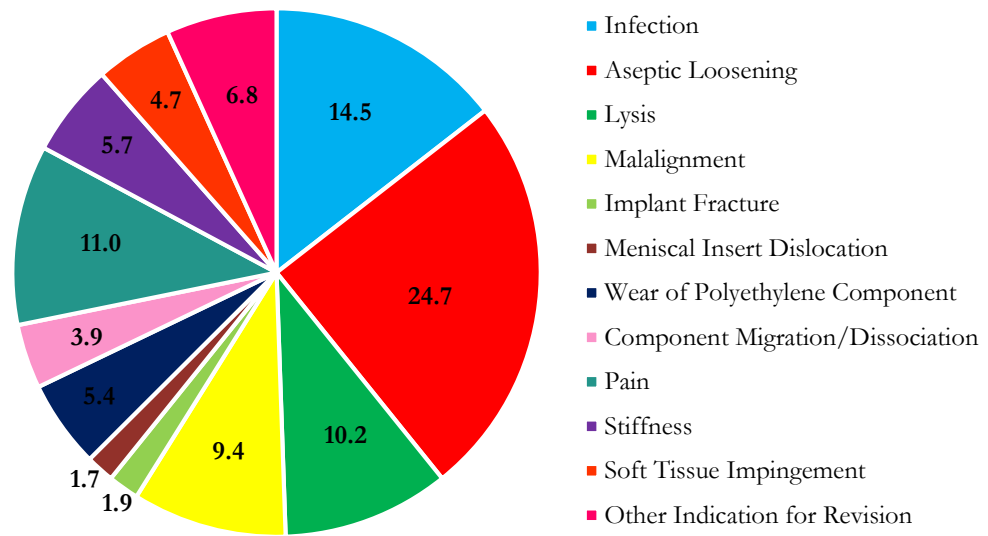


Figure 13. Indications for the first revisions following primary TAR (NJR, 2021).

#### 1.4.5 Biomechanics of Total Ankle Replacements

The first study to assess gait mechanics in TAR patients dates back to Stauffer et al. (1977), which analysed kinetics and kinematics from 9 TAR patients against 5 healthy participants pre-operatively, and after one year post-operatively. The study found that both cadence and sagittal ROM did not significantly improve after one year post-surgery. Demottaz et al. (1979) also completed a gait based study on 21 ankles from 6 different TAR designs against a healthy cohort and found that most patients were unable to walk barefoot after an average follow-up period of 14.7 months (range 3-25). However, both of these earlier studies were limited by selected implants from the first generation of TAR designs, which were all abandoned and removed from the UK market due to the high complication and failure rates (Section 1.4.4.1) (Vickerstaff et al., 2007).

Most of the studies reporting gait changes in second and third generation TAR designs showed post-operative improvements in sagittal plane ROM compared to pre-operative values, but still remained significantly lower when compared to healthy control groups (Dyrby et al., 2004; Choi et al., 2013) or contralateral limbs (Brodsky et al., 2013). Both the studies that used healthy participants as their control failed to match the patient group by body mass index (BMI) or comorbidities, which may have led to the significant difference in sagittal ROM (Dyrby et al., 2004; Choi et al., 2013). Using a contralateral limb as a control is inappropriate, as before and after the surgery, the opposing limb may have exhibited compensatory mechanisms to maintain natural gait. Therefore, the contralateral limb may not truly produce normal ROM values. Other studies have compared different TAR age cohorts (Tenenbaum et al., 2017) and implant designs

(Queen et al., 2017b), with neither study indicating significant differences between cohort or design.

More recent gait based studies using MFM to measure kinematic adaptations following TAR surgery have demonstrated improved pain relief and function after surgery, as supported by better PROMs, increased spatiotemporal parameters (i.e. walking speed), and significant improvements in sagittal ROM of the tibia and hindfoot (Fritz et al., 2021; Deleu et al., 2022). While MFM kinematics were improved in both studies, they remained impaired compared to the healthy control cohort. Most of the studies mentioned above also compared gait mechanics at one-year post-surgery, with the longest follow-up being 3.5 years (Fritz et al., 2021). This meant that each of the studies failed to determine the longer term effect TAR surgery has on patient function and clinical outcome. This is required to truly determine the safety and performance of an implant over the lifetime of the device being *in situ*. Another limiting factor of all the studies mentioned in this section is that they did not directly compare the improved post-operative effects of TAR to other end-stage OA surgical interventions, such as AA. These comparator studies are required to aid surgeons in their selection for the optimal treatment option.

#### **1.4.6 Biomechanical Differences between Arthrodesis and Replacement**

There is much clinical debate surrounding the preferred treatment option for ankle OA, but comparative biomechanical studies remain limited. Most of the comparative gait studies have reported improved spatiotemporal and increased sagittal plane ROM post-operatively in TAR compared with AA patients (Piriou et al., 2008; Hahn et al., 2012; Singer et al., 2013; Flavin et al., 2013; Segal et al., 2018; Sanders et al., 2021). A recent systematic review with meta-analysis comparing treatment options, which included 17 studies with a total of 883 patients, verified this finding (Deleu et al., 2020a). Moderate evidence was found for improved spatiotemporal variables, particularly increased walking speed following TAR, irrespective of implant design. It has been argued that TAR patients retain walking speed by increasing cadence and reducing step duration (Brodsky et al., 2016), while AA patients improve walking speed compared to pre-operative values by increasing their step length, alongside a greater hip ROM in the sagittal plane (Brodsky et al., 2016). The systematic review also demonstrated reasonable evidence that TAR patients were able to conserve existing pre-operative sagittal ROM compared to AA patients (Deleu et al., 2020a). This finding coupled with the improved walking speed, suggests that TAR patients are able to walk and perform ADL more efficiently than AA patients post-surgery. However, neither treatment option was able to successfully attain comparable walking speeds or sagittal plane ROM when compared to healthy participant cohorts (Piriou et al., 2008).

The increased sagittal ROM in TAR patients is also a compounding factor in improving moments and power at the ankle joint. Greater plantarflexion moment and ankle power generation is a strong indicator of an improvement in the ability to propel the foot forward and an increase in strength of the calf muscles (Ingrosso et al., 2009). Hahn et al. (2012) found that TAR patients

produced significantly higher sagittal ROM ( $p = 0.036$ ) and reduced plantarflexor moment during late stance ( $p = 0.042$ ) compared to the AA patient cohort. The improved sagittal ROM (particularly during dorsiflexion) likely lessened the internal passive resistance to peak forefoot forces. The greater sagittal ROM and subsequent angular velocity at toe-off helped maintain power generation, allowing the TAR patients to possess more natural ankle joint function. The increased peak plantar flexor moment found in the AA patients may be caused through greater rigidity of the AJC. The foot was likely to exhibit a longer moment arm, with the centre of pressure extending to the metatarsals during early stance. This may lead to AA patients possessing long-term external dorsiflexion moments across distally located joints of the foot, which may result in the development of adjacent-joint OA (Ling et al., 2015).

The kinematic differences between treatment options in the studies above all measured ankle motion using a rigid, single-segment foot model (SFM), which does not isolate true ankle motion and includes the compensatory movements of adjacent foot joints in the calculation of ankle ROM. A recent study by Deleu et al. (2021b) showed that SFM significantly overestimates sagittal and transverse ROM, while underestimates frontal plane motion in healthy and arthritic participants compared to the MFM. The main disadvantage of SFM is that they do not allow the researcher to differentiate between motion occurring at the hindfoot, midfoot, or forefoot. Therefore, it is difficult to determine from the previous studies where hypermobility or impairments may occur in the joints distal to the ankle, which influence how a patient functions post-surgery (Deleu et al., 2021b).

Only two published studies used MFM to compare gait mechanics between treatment options (Seo et al., 2017; Sanders et al., 2021). Seo et al. (2017) found significantly increased ( $p = 0.004$ ) hindfoot sagittal ROM in the TAR patient cohort ( $15.1^\circ$ ) compared to the AA cohort ( $10.2^\circ$ ). The authors also observed that the range of forefoot sagittal motion was greater in TAR ( $9.3^\circ$  versus  $5.8^\circ$  in AA;  $p = 0.004$ ), as well as significantly higher ( $p = 0.008$ ) maximum ankle power (1.16) compared to AA (0.32). However, sagittal ROM of the hindfoot and forefoot was significantly lower in both TAR and AA patients compared with the control group ( $p = 0.000$ ). Sanders et al. (2021) also found that TAR patients produced significantly greater sagittal ROM compared to AA patients, post-operatively ( $21.1^\circ$  versus  $14.7^\circ$ ,  $p = 0.003$ ). In addition, forefoot-tibia motion ( $25.3 \pm 5.9^\circ$  versus  $18.6 \pm 5.1^\circ$ ,  $p = 0.015$ ) and hindfoot-tibia motion ( $15.4 \pm 3.2^\circ$  versus  $12.2 \pm 2.5^\circ$ ,  $p = 0.022$ ), were significantly higher in the TAR patient cohort. Both studies suggest better intersegmental motion tendency than AA, which would be a more effective treatment for end-stage ankle OA. However, both the MFM are limited by a short follow-up period that was comparable to most of the SFM ankle literature (1 to 3 years post-surgery). With patients developing end-stage ankle OA being generally younger than hip and knee patients, it is critical that studies consider the immediate-to-long-term effects of both surgical interventions.

The majority of the gait studies limited their analysis to the ankle and did not consider the intervention's effect on the lower kinetic chain, which is vitally important to consider since the segments of the lower limb are a linked system (Dubbeldam et al., 2013). In the studies which considered the neighbouring joints following ankle surgery, there was moderate evidence to suggest that TAR patients increased their sagittal ROM at the hip and knee post-operatively (Brodsky et al., 2011; Hahn et al., 2012; Choi et al., 2013; Segal et al., 2018). In contrast, the AA patients exhibited limited post-operative change in knee ROM, but an increase on average of 4.77° in hip ROM (Deleu et al., 2020a). This supports the notion that arthritic patients compensate more at the hip than at the knee during reduced ankle sagittal ROM (Segal et al., 2018). It is now apparent that future gait studies must use MFMs, coupled with 3D lower limb models and intermediate follow-up periods, to avoid erroneous kinematic data and to enhance the understanding of the functional compensatory adaptations occurring at the adjacent foot joints following TAR and AA.

#### **1.4.7 The Bologna-Oxford Ankle**

This thesis focuses on the BOX® ankle, manufactured by MatOrtho Ltd (Leatherhead, UK). The name refers to the collaborative effort between researchers of the Istituto Ortopedico Rizzoli (Bologna, Italy) and Oxford Orthopaedics Engineering Centre (Oxford, UK) and was first implanted in 2003. Since 2010, there have been 796 BOX® ankle procedures, which makes up 11.2% of the overall market share in the UK during this time period (NJR, 2021). The BOX® ankle is a three-component MB implant, with a cobalt-chrome-molybdenum (CoCrMo) alloy component fixed to the body of the talus and the distal part of the tibia, along with an interposed UHMWPE meniscal bearing (Figure 14) (Bianchi et al., 2021). The BOX® ankle was designed specifically to maintain physiological joint mobility amongst the implanted components and retained ankle ligaments (Leardini and O'Connor, 2002). This is achieved through allowing the ligaments to function naturally, controlling passive mobility, thus permitting an adequate ankle ROM (Leardini et al., 2004).

The implant has been shown to achieve full congruity of the articulating surfaces throughout the entire ROM, due to the spherical, convex tibial component and the talar component with a longer radius of curvature in the sagittal plane than the natural talus (Leardini, 2001; Leardini and O'Connor, 2002; Leardini et al., 2004). The conventional UHMWPE insert is bi-concave, which allows full conformity with the metallic articulating surfaces, regardless of joint position during motion (Giannini et al., 2011). The BOX® ankle also possesses hydroxyapatite coating at the bone implant interface (Figure 14), which promotes cementless bone ingrowth and osseointegration (Bianchi et al., 2021).

The BOX® ankle has shown promising clinical outcomes, with an overall survivorship of 97% at a mean follow-up of 58 months (Najefi et al., 2019a) and 6.5 years (Giannini et al., 2017), respectively. The former study found no reports of implant loosening in the radiographs of 75

patients, while the later demonstrated significant improvements in pain and function in 34 consecutive cases of the BOX® ankle. However, a more recent retrospective study evaluating the long-term results with a minimum of ten years follow-up of primary BOX® ankle cases (80 patients) demonstrated a lower survival rate of 66% (Bianchi et al., 2021). Although, the survival patients were found to have good clinical outcomes and satisfaction rates (97%), through the use of the American Orthopaedic Foot and Ankle Society (AOFAS) and Visual Analogue Scale (VAS) scoring systems. Several other studies on different TAR designs have been published with an average follow-up of ten years (Henricson and Carlsson, 2015; Koivu et al., 2017; Di Iorio et al., 2017; Frigg et al., 2017; Palanca et al., 2018; Clough et al., 2019; Krishnapillai et al., 2019). Most of these long-term studies focused on the Scandinavian Total Ankle Replacement (STAR™; Stryker) prostheses, which is another MB device available on the UK market. The cumulative revision rates for this device were found to vary between 63.3-80.6%, which is comparable to the BOX® ankle. This verifies that MB designs possess considerably lower survival rates compared to modern day hip and knee implants.



Figure 14. The three components of the BOX® ankle: tibial component (above), UHMWPE meniscal component (in between), talar component (below). Adapted from the MatOrtho Ltd Operative Technique (MatOrtho Ltd, 2015).

There have been only two previous studies which have focused on the gait mechanics of the BOX® ankle. Ingrosso et al. (2009) showed that patients fitted with the BOX® ankle possessed significantly improved AOFAS outcome scores, spatiotemporal, and sagittal ROM at one-year post-surgery compared to arthritic pre-surgery values. The second study combined both 3D fluoroscopic and gait analysis techniques to assess 20 BOX® ankles during stair climbing at 12 months post-surgery (Cenni et al., 2013). The study detailed comparable kinematics and electromyography patterns between the operated and non-operated ankles (Cenni et al., 2013). Fluoroscopic analysis detailed the consistent and smoothed paths of motion, with sizeable coupled rotations and anterior/posterior (AP) translation of the meniscal bearing, indicating that the BOX® ankle design permits natural motions and translations for the ankle joint (Cenni et al., 2013). The results from both studies suggest the BOX® ankle is capable of improving ankle

motion at a short-term follow-up. Thus, future studies should focus on the longer-term biomechanical performance, to ensure that the BOX® ankle can maintain the promising kinematic adaptations.

## 1.5 Fundamentals of Biotribology

Tribology is described as the discipline of interacting surfaces during movement (Dowson, 2012). When interacting surfaces are part of the body, including joint replacements, the term biotribology is favoured, and encompasses the principles of friction, lubrication and wear (Di Puccio and Mattei, 2015).

### 1.5.1 Friction

Friction has previously been expressed as the resistance preventing the relative movement of two contacting surfaces (Figure 15) (Hall et al., 2001). The resistance between the two surfaces is produced from the need to shear, alongside roughness and ploughing components producing overall frictional force. Friction is calculated using the coefficient of friction ( $f$ ), which is defined as the ratio between the magnitudes of the frictional force ( $T$ ) and the normal force ( $N$ ) at the surface interface (Equation 1.1).

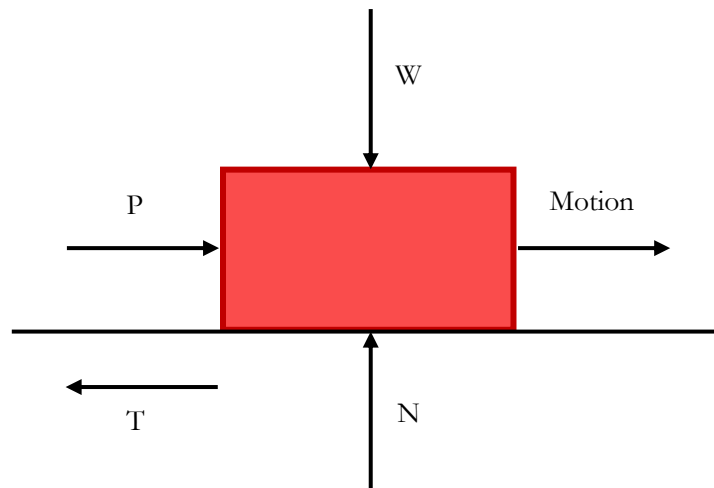


Figure 15. Free body diagram of forces in sliding contact, where the ( $W$ ) is the weight of the body, ( $N$ ) is the normal force exerted by the surface, ( $P$ ) is the horizontal external force, and ( $T$ ) is the frictional force exerted by the surface.

**Equation 1.1:**

$$f = \frac{T}{N} = \frac{T}{N}$$

Equation 1.1 explains the first law of friction, which is that frictional force produced is directly proportional to the normal load (Di Puccio and Mattei, 2015). The second and third laws state that the frictional force is independent of the apparent contact area and of the sliding velocity, respectively.

At the microscopic scale, most polished surfaces are uneven, exhibiting jagged projections termed "asperities" (Figure 16) (Hall et al., 2001). The majority of TARs possess metal-on-polyethylene articulating surfaces, so contact occurs between the asperities of the articulating surfaces, rather than the whole surface. It is thought that friction is the consequence of adhesion and deformation processes. Adhesion is the resistance to separating the articulating surfaces from each other, and deformation at the asperity junctions (Rabinowicz and Tanner, 1966). Adhesive bonds form between the asperities of the two contacting surfaces and energy is needed to break these bonds to allow motion, which is usually known as frictional resistance (Hall et al., 2001). Deformation may occur in TAR when the harder metallic surfaces plough into the softer UHMWPE meniscal insert during motion (Di Puccio and Mattei, 2015).

The subsequent change in surface roughness of the articulating surfaces will affect frictional and wear properties over time, which can be separated into 'run-in' and 'steady-state' phases. After initial implantation of an implant, the 'run-in' wear phase will be exhibited, due to elevated friction associated within sufficient lubrication and wearing of the higher polyethylene asperities (Nečas et al., 2020). Steady-state phase is characterised by a continuously increasing wear rate due to the removal of surface films and higher asperities. The polishing effect during articulation reduces the contact asperity ratio of the surfaces, reducing the frictional force effect and allowing the implant to articulate smoothly for a longer duration (Nečas et al., 2020).

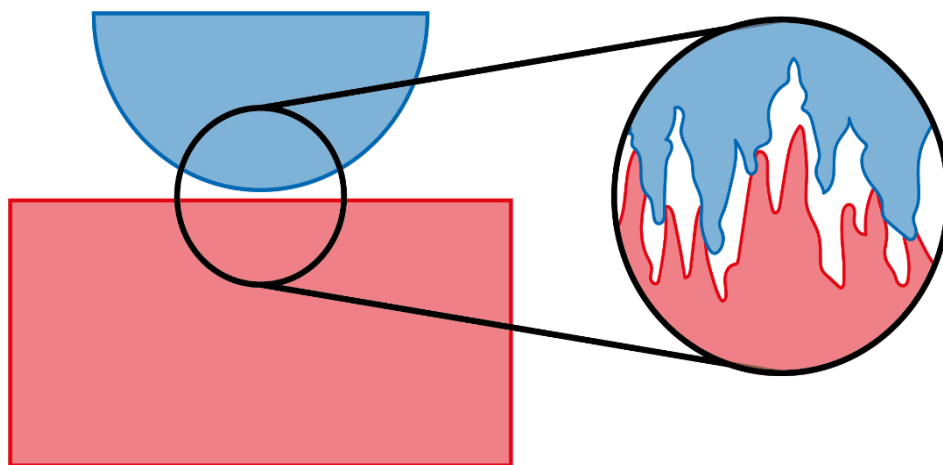


Figure 16. Microscopic detail of a real surface contact, displaying asperities on the articulating surfaces.

### 1.5.2 Lubrication

As friction produces energy dissipation, leading to enduring surface deformation, lubrication can be presented to a system to support mobility through separating and regulating the contacting asperities, thus lowering the associated frictional force (Di Puccio and Mattei, 2015). Lubrication is known to be one of the most efficient approaches of decreasing frictional factor and subsequently delaying the onset of wear debris production (Sagbas, 2016). The lambda ratio is a commonly used to determine the distance in contacting asperities of the articulating surfaces

(Mattei et al., 2011). The ratio is calculated using the minimum film thickness ( $h_{min}$ ) and composite surface roughness of the two surfaces ( $R_{ac}$ ), as shown in Equation 1.2.

**Equation 1.2: Lambda ratio**

$$\lambda = \frac{h_{min}}{R_{ac}}$$

The Stribeck curve is usually used to show the coefficient of friction in relation to the lambda ratio in three distinct lubrication regimes (Figure 17) (Lu et al., 2006). The first regime is ordinarily known as boundary lubrication ( $\lambda < 1$ ), where the lubricant thickness is related to the magnitude of molecules present (Dowson, 2012). Penetration of the lubrication film may occur in this regime, resulting in increased asperity contact and production of wear debris (Dowson, 2012). As the thickness of the lubricant layer increases, fluid film lubrication occurs ( $\lambda \geq 3$ ), which causes the surfaces to be completely separated and protects the articulating surfaces from wear (Stewart, 2010). This lubrication regime can be further separated into hydrodynamic and elastohydrodynamic lubrication (EHL).

During hydrodynamic lubrication regime, the pressure of the lubricant equilibrates the loading, which causes reduced frictional forces and wear (Jin et al., 2006). As the two surfaces slide against each other, the hydrodynamic pressure in the fluid film rises and the fluid film is able to bear the normal load (Stewart, 2010). EHL occurs when the pressure in the fluid film increases and/or the fluid film itself becomes too thin, resulting in the fluid film being unable to bear the normal load and elastic deformation of the bearing surfaces occurs (Dowson, 2012). Despite the elastic deformation, the bearing surfaces remain not in contact. However, with an increase in load, reduction of sliding velocity or the viscosity of the lubricant decreases, the hydrodynamic forces within the lubricant may become insufficient to maintain the thin lubricant layer between the bearing surfaces. This is when boundary lubrication becomes the pre-dominant lubrication phase, resulting in contacting of the surface asperities. The mixed lubrication regime incorporates features from boundary and fluid film lubrication (Figure 17). This regime possesses reduced friction and wear compared to the boundary regime, but higher than fluid film, dependent upon the levels of asperity contact (Jin et al., 2006; Dowson, 2012).

The abscissa in Figure 17 is represented as the Sommerfeld number ( $z$ ), and for a particular geometry is relative to the lubricant viscosity ( $\eta$ ), entraining velocity ( $u$ ), and applied load ( $W$ ) (Equation 1.3).

**Equation 1.3:**

$$z = \frac{\eta u}{W}$$

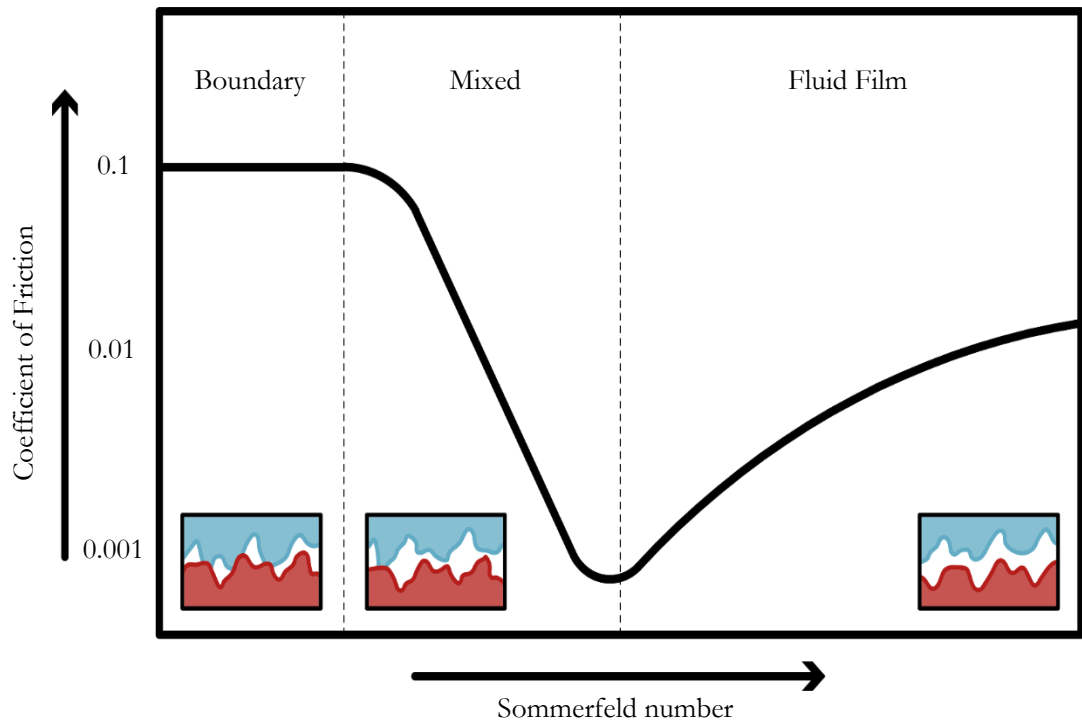


Figure 17. Stribeck curve used to demonstrate the lubrication regime.

Boundary lubrication is indicated by a constant coefficient of friction with an increasing Sommerfeld number, while the fluid film regime is indicated by an increasing friction factor and Sommerfeld number, which is accounted for by the viscous shear in the lubricant (Dowson, 2012). Mixed lubrication has an increased Sommerfeld number compared to boundary lubrication, due to the higher loads being disseminated between the asperity contacts and lubricant film, which reduces the coefficient of friction (Sagbas, 2016).

The pressurisation of the fluid occurs as a result of the relative velocity at the bearing surfaces, with an increase in sliding velocity causing the formation of a thicker lubricant film (Houdková et al., 2017). However, when a fluid thickness becomes much larger than the surface roughness, this can result in internal frictional forces between the fluid layers, causing an additional frictional force to the artificial joint (Shen et al., 2019). Apart from its influence on the formation of a lubricant film, sliding velocity also has been reported to cause a deposition of the proteins on the bearing surfaces (Saikko, 2003). Protein precipitation may alter the lubricant regime, with an increased volume being related to the depletion of the soluble proteins within the lubricant and their ability to maintain boundary lubrication at the bearing surface (Lu and McKellop, 1997). A study by Zhang et al. (2008) demonstrated that sliding velocity had an effect on temperature at the bearing surfaces of an amorphous poly-ether-ether-ketone (PEEK) coating, which could affect the rate of protein adsorption (Lu and McKellop, 1997). Moreover, changes in temperature may affect lubricant viscosity, thus resulting in changes of the lubricant regime (Scholes and Unsworth, 2006). Therefore, it is important to mimic the sliding velocity of new *in vivo* artificial joints when carrying out simulator based studies before clinical applications.

Most TAR devices on the worldwide market are made up from metallic tibial and talar components, divided by a meniscal UHMWPE insert. In this type of artificial joint, the *in vivo* lubrication regime between the metallic and polyethylene surfaces is usually considered to be boundary lubrication. Contacting asperities are unavoidable due to the soft and rough UHMWPE surface (Sagbas, 2016), resulting in wear of the components and generation of polyethylene wear debris particles. The machining of the UHMWPE inserts produces the high surface finish and can only obtain particular resolutions, which causes relatively significant residual surface roughness and results in overall boundary lubrication regime.

The lubricants used during biotribological simulations have a direct influence on the friction and wear characteristics of the joint replacement. It is widely documented that the proteins within the synovial fluid are sensitive to the nanostructure of the articulating surfaces (Shen et al., 2019), causing increased friction through the arrangement of a passive protein layer (Heuberger et al., 2005). Deionised water was previously used during *in vitro* wear studies of hips and knees, however, research identified quantities of material transfer from the soft UHMWPE to the metallic bearing surfaces, indicating the lack of an active protein layer (Cooper et al., 1993). This material transfer has been found to roughen the bearing surfaces, resulting in an increased wear rate (Shen et al., 2019).

A more commonly used lubricant in wear simulations is newborn calf or bovine serum, which when combined with a sodium azide additive, can reproduce the protein concentration of the natural joint capsule (Shen et al., 2019). Using bovine serum has been found to produce no indefinable material transfer from the polymer to the metal bearing surfaces, which symbolises protein adsorption and formation of a boundary layer on the articulating surfaces (Scholes and Unsworth, 2006; Saikko, 2006). Conversely, the protein concentration degrades overtime in the simulator environment, due to the increased heat generated, so there is a restricted duration of time for optimal lubricant, before implant wear rate is affected (Liao et al., 1999). Active protein films at concentrations higher than 10-17g/L are also connected with diminished implant wear (Brown and Clarke, 2006). Therefore, it is important to control the temperature, concentration and volume of the lubricant during wear simulation of joint replacements.

### 1.5.3 Wear

Wear is the surface damage or material loss between contacting asperities of the articulating surfaces (Szeri, 2010). There is no specific correlation to friction, but wear will generally decrease with the introduction of a lubricant (Dowson, 2012). Archard developed the first wear model in 1956 to measure worn volume ( $V$ ) (Equation 1.4), where:  $K$  is (non-dimensional) wear coefficient;  $N$  the normal load;  $s$  the sliding distance; and  $H$  the material hardness (Archard and Hirst, 1956).

**Equation 1.4:**

$$A = KNs/H$$

Several mechanisms of wear have been identified in the literature and will normally occur in combination during motion (Jin et al. 2006). Abrasive wear is due to the action of hard metallic asperities or third-body particles that plough through the softer polymer bearing surface (Di Puccio and Mattei, 2015). Abrasive wear is inversely proportional to surface material hardness and can be reduced with improved surface finish (Wang et al. 1998). Adhesive wear is recognised when material from one bearing surface is transferred or attached onto another during movement (Sagbas, 2016). During continued articulation, the transferred material may loosen and produce third-body wear (Rabinowicz and Tanner, 1966). Adhesive wear is proportional to both load and sliding distance, while inversely proportional to material hardness at the bearing surface (Di Puccio and Mattei, 2015). Surface fatigue is due to the repeated cyclic loading of the polymer asperities, which causes increased localised stresses that surpasses the fatigue strength of the material, resulting in fracture and debris detachment (Jin et al. 2006). Erosive wear is produced during motion when material is lost from the solid surface that is in contact with a fluid containing solid particles (Sagbas, 2016). Finally, corrosive wear is produced by chemical or electrochemical reactions between surface materials, in which metal ions are released and regulate oxidative wear (Jin et al. 2006).

The consequence of wear is not only associated to diminished function and replacing components, but the unfavourable influence on the body due to the production of wear particles (Jin et al., 2006). During loading, wear particles are produced during motion at the articulating surfaces of an implant (Kandahari et al., 2016). As previously mentioned, most TARs are manufactured from metal (tibial and talar components) and UHMWPE (meniscal inserts). Conventional UHMWPE has been associated with producing significant wear debris, which can eventually cause periprosthetic osteolysis (Tipper et al., 2006). It is hypothesised that the magnitude and volume of wear particles will influence the host's immune response, and are a function of implant design, material combinations and stresses applied to the implant (Kandahari et al., 2016). Wear particles produced from conventional UHMWPE generally range from 10nm to 1mm (Tipper et al., 2006). Larger wear particles (>20 µm) stimulate multinucleated giant cell development and may become osteolytic (Ingham and Fisher, 2005). It is the smaller wear particles, in the 0.1–1.0 µm range that are, however, believed to increase biological activity (Tipper et al., 2000; Green et al., 2000; Ingham and Fisher, 2005).

At the cellular level, the UHMWPE wear particles provoke an inflammatory reaction from the neighbouring or permeating osteoclasts, macrophages, and dendritic cells in the surrounding tissue at the bone-implant interface (Figure 18) (Bitar and Parvizi, 2015). Large numbers of macrophages become increasingly activated and produce pro-inflammatory cytokines, such as

tumour necrosis factor- $\alpha$  (TNF- $\alpha$ ) and interleukins, IL-1 $\beta$ , IL-6 and IL-8 (Tipper et al., 2001), which contribute to further inflammation. Cytokine secretion may result in the activation of osteoclasts, which are the cells that resorb bone at the bone-implant interface (Figure 18) (Cobelli et al., 2011). Previous research identified that conventional UHMWPE wear debris measuring 0.24  $\mu\text{m}$ , caused the greatest bone resorption rate and cytokine production in an *in vitro* mouse model (Green et al., 2000). This imbalance in normal bone metabolism can develop into aseptic loosening at the bone-implant interface, and the eventual requirement for revision surgery (Bitar and Parvizi, 2015).

In an attempt to moderate wear particle production, highly cross-linked polyethylene (XLPE) inserts were developed (Oral and Muratoglu, 2011). XLPE goes through a manufacturing process of high-energy irradiation (gamma or electron beam), which causes the carbon-hydrogen chains to break, producing free radicals, which combine with adjacent molecules to establish cross-linking between the polymeric chains (Bracco et al., 2017). The residual free radicals in an oxygen rich environment may initiate oxidative degradation, resulting in polyethylene embrittlement and ultimate failure of the device (McKellop et al., 1999a; Muratoglu and Bragdon, 2016). Therefore, the XLPE is stabilised using thermal treatments (annealed or melted) to eliminate the remaining free radicals (Bracco et al., 2017). The melting of polyethylene at high temperatures increases the removal of the free radicals, but causes microstructural changes, leading to a reduction in ultimate strength and fatigue resistance (Ries and Pruitt, 2005). The annealing method attempts to preserve the mechanical properties, but is not as effective at removing the excess free radicals and causes reduced oxidation stability of the XLPE (Muratoglu and Bragdon, 2016).

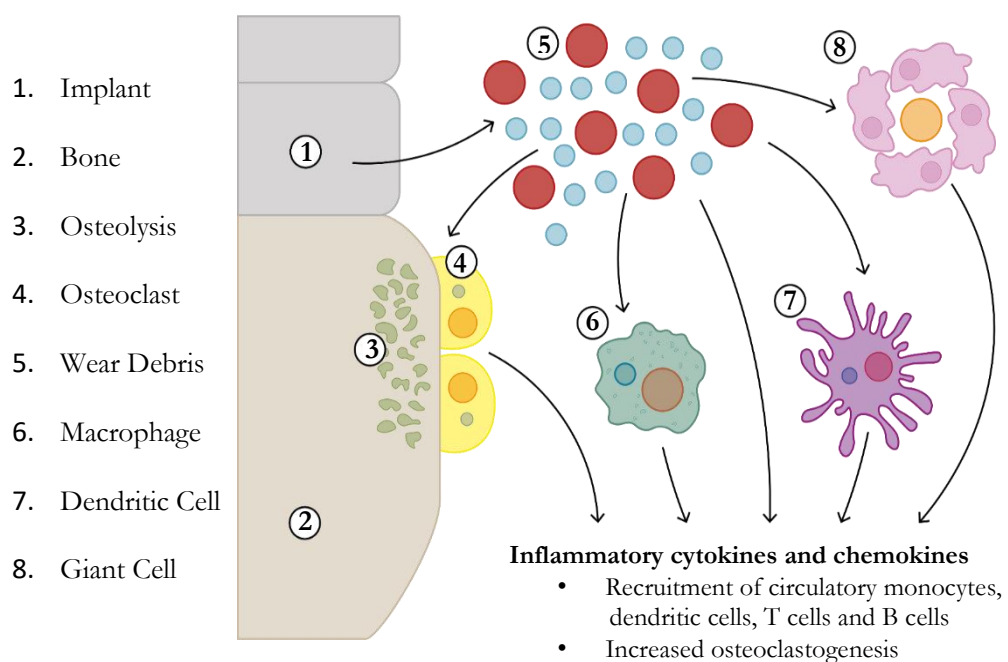


Figure 18. Schematic of periprosthetic inflammation and aseptic osteolysis. Adapted from Cobelli et al. (2011).

The combined effect of irradiation and thermal treatment has shown to improve oxidation resistance and implant wear in XLPE compared to conventional UHMWPE in THR (Kurtz et al., 2011) and TKR (Minoda et al., 2009; Paxton et al., 2015; Meneghini et al., 2016). However, the wear particles produced from XLPE have been reported to be in the smaller, more biologically active range of 0.1–1.0 $\mu$ m (Endo et al., 2001), which may develop into periprosthetic osteolysis and subsequent aseptic loosening. The issue surrounding polyethylene fatigue resistance has also prohibited the widespread adoption of XLPE in TARs, with only two current systems using XLPE (Trabecular Metal Total Ankle; Zimmer Biomet, Warsaw, USA and Cadence Total Ankle System; Integra LifeSciences, Plainsboro, USA). There is limited clinical data supporting the use of XLPE in the ankle. A short-term follow-up study of 55 Trabecular Metal Total Ankles (range: 24.0-39.8 months) found an implant survival rate of 93%, with none of the revisions relating to polyethylene fracture (Barg et al., 2018).

There is also limited published data from wear simulations (Section 1.6.3) and the effects of wear mediated osteolysis in TAR. Yoon et al. (2014) determined that 37 of the 99 TAR radiographs had evidence of osteolysis. Although these osteolytic lesions were relatively inactive, this does raise concerns regarding modern TARs because of their high incidence and potential for later mechanical failure as compared to AA (Yoon et al., 2014). Other studies have shown that MB designs are associated with a significantly higher percentage of cysts (22.1%) when compared to FB (11.5%) implants (Arcangelo et al., 2019). A similar trend has been found at the knee joint, with the finding being attributed to the size of the wear particles produced due to the increased ROM at the joint (Huang et al., 2002; Huang et al., 2007).

## 1.6 Wear Simulation

Hip and knee implants are successful surgical interventions for the long-term management of OA, and this is a result of years developing preclinical experimentation techniques to understand the biotribological performance of such implants (Mujukian et al., 2020). Joint wear simulators are well-known mechanical machines used to mimic the intended use and physiological conditions of the implant *in vivo* (Affatato and Ruggiero, 2020). There are multiple factors that contribute to the wear of a joint replacement. Some parameters can be controlled such as, material pairing, surface finish, and conformity. Meanwhile, other parameters are determined by the patient, for example, loading, joint kinematics, and patient activity levels.

All implant information from the published wear studies on TAR is summarised in Table 1, including: implant model; metallic alloys for the tibial and talar components; and the manufacturing process for the polyethylene insert. The wear simulator information for each study, including: the number of samples; simulator stations; simulator manufacturer; simulator control (force or displacement); lubricant used; polyethylene type; implant design (mobile or fixed); number of cycles run; and reported mean wear rate of each experiment, is summarised in Table 2.

Table 1. Wear simulator study implant, material and manufacturing details.

Study	Implant Design (Manufacturer)	Tibial Component		Talar Component		Polymer Manufacturing
		Alloy	Alloy	Alloy	Alloy	
Bell et al. (2007)*	Mobility (Depuy) Buechel-Pappas (Endotec)	CoCr	CoCr	CoCr	CoCr	1050 GUR UHMWPE: machined from extruded bar, sterilised by gamma irradiation under vacuum in foil. 1050 GUR UHMWPE: machined from extruded bar, sterilized by gas plasma
Affatato et al. (2007)*	BOX (MatOrtho Ltd)	CoCrMo	CoCrMo	CoCrMo	CoCrMo	1020 PUR UHMWPE: compression moulded sheet, sterilized by gamma irradiation (25-35 kGy) in presence of nitrogen
Postak et al. (2008)†	STAR (Stryker)	CoCrMo	CoCrMo	CoCrMo	CoCrMo	UHMWPE: sterilized by gamma irradiation (25 - 29 kGy) in presence of nitrogen
Kincaid et al. (2013)‡	Bicondylar fixed-bearing TAR (Zimmer) Zimmer Trabecular	Ti-6AL-4V	Ti-6AL-4V	CoCrMo	CoCrMo	1050 GUR UHMWPE Prolong®: cross-linked by electron beam irradiation
Bischoff et al. (2015)*	Metal Total Ankle (Zimmer)	Ti-6AL-4V	Ti-6AL-4V	CoCrMo	CoCrMo	UHMWPE: did not report manufacturing characteristics; XLPE: sterilized by gas plasma after electronic beam irradiation (6.5 Mrad) and melt-annealed at 150°
Reinders et al. (2015)*	Hintegra (Integra Life Sciences)	CoCr	CoCr	CoCr	CoCr	UHMWPE: unreported
Smyth et al. (2017)*	Zenith (Corin Group)	TiN	TiN	TiN	TiN	1050 GUR UHMWPE: unreported
Schipper et al. (2018)*	N/A	N/A	N/A	N/A	N/A	UHMWPE: sterilized in ethylene oxide without gamma irradiation; XLPE: sterilized by gas plasma after electronic beam irradiation (6.5 Mrad) and melt-annealed at 150°

CoCr = Cobalt-chrome, CoCrMo = Cobalt-chromium-molybdenum, Ti-6AL-4V = Titanium, TiN = Titanium nitride. \*Peer-reviewed journal article. †Conference proceedings (AAOS 2010). ‡Conference poster presentation (ORS 2013). NA = Not Available.

Table 2. Wear study simulation information.

Study	Implant	Samples	Stations	Simulator Manufacturer	Control	Lubricant	Polyethylene Type	Design	Cycles (Mc)	Wear Rate (mm <sup>3</sup> /Mc)
Bell et al. (2007)	Mobility Buechel-Pappas	3	6	ProSim Knee Wear Simulator (Linked Axes), Simulator Solutions, Stockport, UK	Displacement	Bovine calf serum	UHMWPE	Mobile	5	3.4 ± 10.0
Affatato et al. (2007)	BOX	4	4	Knee Wear Simulator, Shore Western, Los Angeles, CA, USA	Displacement	Deionised water	UHMWPE	Mobile	5	18.6 ± 12.8
Postak et al. (2008)	STAR	5	1	Custom, Single-station Motion Simulator	Displacement	Bovine calf serum	UHMWPE	Mobile	10	5.7 ± 2.1
Kincaid et al. (2013)	Bicondylar fixed-bearing TAR	6	6	KS2-6-1000, Advanced Mechanical Technology, Watertown, MA, USA	Displacement	Bovine calf serum	XLPE	Fixed	2	3.3 ± 0.4
Bischoff et al. (2015)	Zimmer Trabecular Metal Ankle	3	6	KS2-6-1000, Advanced Mechanical Technology, Watertown, MA, USA	Displacement	Bovine calf serum	UHMWPE	Fixed	5	8.0 ± 1.4
Reinders et al. (2015b)	Hintegra	3	6	KS2-6-1000, Advanced Mechanical Technology, Watertown, MA, USA	Force	Bovine calf serum	UHMWPE	Mobile	3	18.2 ± 1.4
Smyth et al. (2017)	Zenith	5	6	ProSim Knee Wear Simulator (Linked Axes), Simulator Solutions, Stockport, UK	Displacement	Bovine calf serum	UHMWPE	Mobile	2	1.2 ± 0.6
									2	25.8 ± 3.1
									2	15.2 ± 2.5
									2	0.4 ± 0.2
									2	13.3 ± 2.5
									2	11.8 ± 3.7
Schipper et al. (2018)	N/A	4	4	Type 3/1-02, Endolab Rosenheim, Germany	Displacement	Bovine calf serum	UHMWPE	Fixed	5	18.0 ± 1.4
							XLPE		5	2.2 ± 0.3

### 1.6.1 Simulator Inputs

The relative numbers of TAR wear simulator studies are limited and presently use a small range of standard test conditions, compared to both THR and TKR studies. There is also a lack of specialised pre-clinical ankle simulators available on the market, meaning that all the studies used knee simulators. This involved inverting the TAR device to accommodate flexion about the constant radius of the talar component, so that internal/external rotation (IER) and AP displacement was applied at the tibial component (Section 2.3.2). The applied load and kinematic motion for each wear simulator study is presented in Table 3.

Table 3. Applied ranges of load and motions in previous ankle wear simulations.

Study	Axial Load (N)	DF (-)/PF (+) (°)	IR (-)/ER (+) (°)	AP Displacement (mm)
Bell et al. (2007)	100 to 3100	-10.0 to +15.0	-2.0 to +8.0	-1.5 to +1.5
Affatato et al. (2007)	100 to 1600 <sup>†</sup>	-10.0 to +20.0	-2.6 to +7.7	0 to +8.45
Postak et al. (2008)	3000	-10.0 to +20.0	-2.0 to +2.0	-2.5 to +2.5
Kincaid et al. (2013)	100 to 3188 <sup>†</sup>	-16.0 to +15.2	-2.0 to +8.0	-1.5 to +1.5
Bischoff et al. (2015)	200 to 3188	-16.0 to +15.2	-2.0 to +8.0	-1.5 to +1.5
Reinders et al. (2015b)*	200 to 1890	-14.9 to +14.9 <sup>‡</sup>	-12.0 to +14.7 <sup>§</sup>	+3.7 to +6.6 <sup>¶</sup>
Smyth et al. (2017)	100 to 3150	-15.0 to +15.0	-2.3 to +8.0	-2 to +7 followed by reduction to -0.9 to +3.1
Schipper et al. (2018)	200 to 3188	-16.0 to +15.2	-2.0 to +8.0	-1.5 to +1.5

AL = Axial Load; DF = Dorsiflexion; PF = Plantarflexion; IR = Internal Rotation; ER = External Rotation; AP Anterior-Posterior. \*Study was run under force control. <sup>†</sup>Study did not specify minimal axial load value. <sup>‡</sup>Study did not specify a degree range. <sup>§</sup>Due to IE torque of -6.1 to +0.3Nm. <sup>¶</sup>Due to AP force of -268 to +129N.

Most wear studies used a peak axial load (AL) ranging from 3000-3188 N, which were based on previous ankle cadaveric models by Stauffer et al. (1977) and Procter and Paul (1982), who predicted maximum loads equivalent to 4.5 to 5 times BW of a 70 kilogram (kg) individual (3150 N) (Section 1.2.6). Two of the studies used significantly lower maximum AL of 1600 N (Affatato et al., 2007) and 1890 N (Reinders et al., 2015b), respectively. The authors from both these studies claimed that this load was more comparable to TAR patients, when compared to the higher loads calculated from healthy cadaveric feet. Conversely to the other authors, Postak et al. (2008) used a static load of 3000 N throughout the range of sinusoidal motion, instead of the more traditional dynamic loading. This method does not truly reflect the varying load that occurs throughout the stance phase of walking, so the wear rate from the study should be dealt with caution. All the studies barring Postak et al. (2008) also used a swing phase load of 100 to 200 N to maintain joint contact, in an attempt to imitate soft tissue tension that occurs in natural gait. The inconsistent loading profiles throughout the studies make it difficult to draw conclusions regarding UHMWPE wear.

Seven of the eight wear studies used comparable tibial IER ROM, ranging from a peak internal rotation of approximately -2° to a maximum external rotation of 8°. This range was selected from a previous gait study by Lamoreux et al. (1971), while the peak external rotation angle of 8° was

determined from a previous study which calculated this value with the use of electro-goniometric exoskeletons (Calderale et al., 1983). Postak et al. (2008) used a much lower maximum external rotation angle ( $2.0^\circ$ ) compared to the other authors, which failed to justify the data this was cited from. All of the studies used displacement control to simulate rotation angles. However, Reinders et al. (2015b) controlled internal and external torque (10.3 to 26.1 Nm) and measured the resulting degrees of rotation ( $-12.0^\circ$  to  $+14.7^\circ$ ).

The greatest variation in simulator input studies is AP displacement, with the ROM between 2.9 and 9.0 mm. Seven of the eight studies did not express the origin of their AP displacement profile, with values being largely limited in the ankle literature. Smyth et al. (2017) defined AP motion using data from Conti et al. (2006), which involved fluoroscopic analysis of 10 TAR patients during weight bearing dynamic gait conditions and resulted in 3.5 mm AP displacement ROM during stance. The studies reviewed can be separated into two cohorts dependent on whether the AP displacement range was small or large. Five studies used a relatively small AP translation, with an overall narrow distribution of 2.9 to 3.0 mm, in an attempt to avoid dislocation during simulation (Bell and Fisher, 2007; Kincaid et al., 2013; Reinders et al., 2015b; Bischoff et al., 2015; Schipper et al., 2018). The remaining three studies used a larger AP translation, ranging from 5.0 to 9.0 mm (Affatato et al., 2007; Postak et al., 2008; Smyth et al., 2017). Smyth et al. (2017) was the only study to define where the AP translation profile was attained and also investigated the effect of varying AP magnitudes (4 mm to 9 mm) on implant wear rate (Section 1.6.3).

All studies also applied a dorsi-/plantarflexion ROM of approximately  $30^\circ$ , which is consistent with previous kinematic cadaveric studies (Section 1.2.5) (Stauffer et al., 1977; Ounpuu, 1990). It is also significant that none of the published simulator studies on TAR controlled medial-lateral (ML) translation or more importantly inversion/eversion. This is likely due to limitations in the experimental set up to kinematic inputs in six degrees of freedom (DoF) or due to the authors wanting to simulate motion at the true ankle joint, without including version occurring about the subtalar complex.

### **1.6.2 Wear Rates and Limitations**

The wear rates for each simulator study are shown in Table 2. The first published TAR wear simulator by Bell and Fisher (2007) found that after 5 million cycles (Mc) and no AP displacement, wear rate was higher in the Buechel–Pappas™ device ( $10.4 \pm 11.8 \text{ mm}^3/\text{Mc}$ ) compared to the Mobility ( $3.4 \pm 10.0 \text{ mm}^3/\text{Mc}$ ). After the inclusion of AP translation (5-6 Mc), mean wear rate significantly increased for both devices (Buechel–Pappas™ =  $16.4 \pm 17.4 \text{ mm}^3/\text{Mc}$ ; and Mobility  $10.4 \pm 14.7 \text{ mm}^3/\text{Mc}$ ). However, the inserts had already been worn and potentially damaged from the previous 5 Mc of kinematic inputs, which may have been the responsible for the subsequent increased wear rate. This does come as a limitation, as this does not truly represent the effects of AP on the wear rates, particularly with AP displacement high variability within the ankle literature. With AP motion only being applied during the final Mc, it

did not allow for the authors to truly determine the effects of this parameter on wear behaviour. There was, however, no significant differences in mean wear rate identified between TAR models before and after the introduction of AP translation. This finding may be influenced by the relatively small sample size in this study ( $n = 3$ ). Small sample size was also apparent in all other studies apart from Kincaid et al. (2013), which was the only study to attain the sample size of 6 implants recommended in the recent ISO 22622:2019. This produced high variability and large confidence limits (CL) in the wear rates measured, making it difficult to draw specific conclusions in TAR wear rates.

Affatato et al. (2007) reported a mean wear rate of  $18.6 \pm 12.8 \text{ mm}^3/\text{Mc}$  (range: 7.5-31.7  $\text{mm}^3/\text{Mc}$ ) for four BOX® ankles, with this being the only study to have examined the wear behaviour of this specific TAR model. The slightly higher wear rate may be associated with the reduced simulator period of 2 Mc. Reinders et al. (2015b) also determined a comparable wear rate of  $18.2 \pm 1.4 \text{ mm}^3/\text{Mc}$  after 3 Mc of force controlled kinematics. The higher wear rate from both these studies compared to the other simulations, could be associated with the inserts transitioning from 'run-in' to 'steady-state' wear, with the wear rate increasing due to the polishing effect at the insert surface interface (Section 1.5.1). All of the other studies attained a minimum simulation of 5 Mc, which is now recommended in the ankle specific ISO 22622:2019. The reduced testing duration, coupled with the use of deionised water as the testing lubricant (Section 1.6.5) are distinctive experimental limitations in this study.

Both Affatato et al. (2007) and Reinders et al. (2015b) applied reduced loads 1600 N and 1890 N respectively, which are equivalent to 2.32 and 2.57 times BW (Section 1.6.1) of a 70kg individual. This reduced load does not appear to have caused significant differences in wear rate compared to most of the other studies which used conventional UHMWPE (Bell and Fisher, 2007; Postak et al., 2008; Smyth et al., 2017; Schipper et al., 2018). This finding supports the notion that wear rate is not proportional to increased loads, due to the relationship being linear between load and contact area (Liu et al., 2011). This was also verified by Schipper et al. (2018), as in their conventional UHMWPE inserts, the wear rate was comparable ( $18.0 \pm 1.4 \text{ mm}^3/\text{Mc}$ ) under a load that was approximately double (3188 N). However, there remains too many differences between the simulator studies mentioned for this to be the only factor.

The relatively high variability in wear rates between samples in Affatato et al. (2007) paper were subsequently related to the differing wear patterns, with two samples displaying multidirectional scratching and burnishing, while another exhibited no apparent signs of wear on the tibial component. The variability in wear patterns may result from mal-positioning of the device during serum changes or damage caused during simulator calibration. These issues could have occurred in the other studies, but was not reported on by the authors for their variability between samples.

During the following year, Postak et al. (2008) used much simpler kinematics to test the wear behaviour of five STAR devices, finding a wear rate of  $5.7 \pm 2.1 \text{ mm}^3/\text{Mc}$ . The substantially lower wear rate and variability between samples in this study compared to the other simulations and designs is likely a combination of the simplified static loading conditions (Section 1.6.1), longer simulator duration (10 Mc 5 Mc) and number of implants used. Smyth et al. concluded that TAR wear rate is greatly reliant on increased tibial IER within the gait profile (Smyth et al., 2017). The study demonstrated that the addition of  $11^\circ$  rotation caused a statistically significant increase in implant wear to  $25.8 \pm 3.1 \text{ mm}^3/\text{Mc}$  (Smyth et al., 2017). Therefore, the smaller rotational ROM used in this study is another significant condition that caused the reduced wear rate compared to the other studies. Conversely, the other studies used more physiologically accurate profiles in an attempt to replicate ankle ROM *in vivo*.

The study by Kincaid et al. (2013) used a higher number of specimens ( $n = 6$ ), which were XLPE and found a comparably reduced wear rate of  $3.3 \pm 0.4 \text{ mm}^3/\text{Mc}$  at 2 Mc. The authors determined that the reduced wear rates compared to previous studies is attributed to both design features and XLPE within the bearing couple (Section 1.6.3). However, this study was an abstract and limited information was available to truly assess their selected methodology. Bischoff et al. (2015) measured the effect of XLPE on implant wear against a conventional UHMWPE semi-constrained Zimmer Trabecular Metal device. Using a similar kinematic profile to that of Bell and Fisher (2007), the study demonstrated that XLPE ( $2.1 \pm 0.3 \text{ mm}^3/\text{Mc}$ ) reduced wear rate significantly compared to the conventional UHMWPE ( $8.0 \pm 1.4 \text{ mm}^3/\text{Mc}$ ) design. The most recent published study also found that the crosslinking process reduced wear rate compared to conventional UHMWPE ( $18.0 \pm 1.4 \text{ mm}^3/\text{Mc}$  and  $2.2 \pm 0.3 \text{ mm}^3/\text{Mc}$ ) after the same simulation period of 5 Mc (Schipper et al., 2018). However, unlike the implants used in Bischoff et al. (2015), the implants were not identical, which created a confounding variable (Schipper et al., 2018). In particular, variation in clearance between implant types may have influenced the wear rate. The locking system on the polyethylene liner was different between implant types, which meant that the conventional UHMWPE system required alteration of its metallic tibial tray to enable to successful removal of the liner. Although this modification did not influence wear or produce back-side wear, this does not represent *in vivo* wear behaviour.

Reinders et al. (2015b) published the only force-controlled TAR simulator study, which produced an overall wear rate of  $18.2 \pm 1.4 \text{ mm}^3/\text{Mc}$ . The slightly higher wear rate was likely due to the increased rotational kinematics applied (as shown by Smyth et al. 2017), alongside the reduced testing duration of 3 Mc, compared to the other wear simulations. The forces and torques were calculated using mathematic models and inverse kinematics from healthy participant gait data, which does not represent the gait mechanics of the TAR patient population (Section 1.4.5). Furthermore, the validity of these modelling techniques is unknown and isn't categorically verified, as no data exists of TAR *in vivo* loading.

The simulation study by Smyth et al. (2017) was the longest in duration (12 Mc), which compared the varying combinations of rotations and displacements at 2 Mc intervals, in order to determine parameter influence on wear rate (Smyth et al., 2017). Unidirectional inputs with no AP displacement produced wear rates of  $1.2 \pm 0.6 \text{ mm}^3/\text{Mc}$ , while the addition of  $11^\circ$  of rotation and 9 mm of AP displacement (ROM), caused a significant increase in the wear rate to  $25.8 \pm 3.1 \text{ mm}^3/\text{Mc}$  (Smyth et al., 2017). However, when changing to a lower AP displacement of 4 mm, there was no significant difference in wear rate (ranging from 11.8 to  $15.2 \text{ mm}^3/\text{Mc}$ ). The reduced 4 mm of AP, coupled with rotation, resulted in a wear rate of  $13.3 \pm 2.5 \text{ mm}^3/\text{Mc}$ . This stage of the study was used to drive some of the simulator studies within this thesis.

A previous THR wear study highlighted that varying simulator designs produce differing wear results when using the same implant design (Affatato et al., 2008). International Organisation for Standardisation (ISO) documentation has been published, providing recommendations for experimental methodology and simulator input parameters, to accurately predict the clinical wear behaviour of THR (ISO 14242-1:2014) and TKR (ISO 14243-3:2014). Only recently, ISO 22622:2019 was published for TAR wear simulations. Thus, the wear studies have not yet utilised the new guidelines and as a result there are a variety of simulator inputs and experimental conditions in the literature. The wear rates can be influenced by many factors such as simulator input profiles, lubrication, temperature, and the centre of rotation specific to each centres protocol. This it makes it difficult to compare wear rates directly, although does provide a useful benchmark for future TAR wear simulations.

### **1.6.3 Conventional versus Cross-linked Polyethylene**

The obvious difference in wear rates in TAR studies is the use of XLPE, which presented mean wear rates, ranging from  $2.1 \pm 0.3$  to  $3.3 \pm 0.4 \text{ mm}^3/\text{Mc}$  (Kincaid et al., 2013; Bischoff et al., 2015; Schipper et al., 2018), which is significantly lower than the mean wear rate (range:  $3.4 \pm 10.0$  to  $25.8 \pm 3.1 \text{ mm}^3/\text{Mc}$ ) from conventional UHMWPE studies (Bell et al., 2007; Affatato et al., 2007; Postak et al., 2008; Reinders et al., 2015b; Smyth et al., 2017). As discussed in Section 1.5.3, the crosslinking process removes free radicals, which have been shown to trigger oxidative degradation and compromises the material properties of the polyethylene insert (Bracco et al., 2017). Assessment of the wear performance in the three studies that compared XLPE and conventional UHMWPE in the same ankle design and simulator parameters also demonstrated a 73.6%, 74.0% and 88.0% reduction in wear when using XLPE (Kincaid et al., 2013; Bischoff et al., 2015; Schipper et al., 2018). However, the varying experimental methodologies and implant designs make it difficult to directly compare XLPE and conventional UHMWPE between studies. Each study failed to determine the effect of XLPE under varying implant and simulator parameters, or address the potential reduction in fatigue resistance of the XLPE due to reduced toughness (Bracco et al., 2017). There are also no MB devices on the market which have selected to use XLPE.

#### 1.6.4 Force versus Displacement Control

Another crucial consideration in designing TAR studies is whether to run the simulator under force or displacement control. Most of the studies mentioned used force control to measure AL, while joint kinematics (dorsi-/plantarflexion; IER; and AP displacement) were run under displacement control. Reinders et al. (2015b) were the only authors to use torsional moments to mimic IER and force control to generate AP displacement. Force controlled simulators attempt to mimic the effects of the passive structures (capsule; soft tissue; and ligaments) on the kinematics at the joint, resulting in a more physiologically relevant wear simulation (Abdelgaied et al., 2017). However, the mean wear rate from Reinders et al. (2015b) study was comparable to the displacement controlled studies using conventional UHMWPE. Further research by Ho et al. (2020) demonstrated that force control simulation in a cadaveric model of 12 feet, produced comparable magnitudes of IER and AP displacement specified by ISO 22622:2019 using displacement control. The study also demonstrated that the implementation of force controlled simulators may present uncertainties in the resultant motion, through imitating the passive structures, making it difficult to reproduce the same experimental conditions when comparing different TAR designs, materials and investigators (Ho et al., 2020). Therefore, the simulator complexities and substantial costings related with force controlled simulations may not be justified in TAR research.

#### 1.6.5 Simulator Lubrication

Seven of the eight wear simulator studies used bovine serum with varying volume, additives and protein concentrations, produced to mimic the synovial fluid of the natural joint capsule (Table 1). Affatato et al. (2007) were the only authors to use deionised water as their testing lubricant, which may have contributed to the higher wear rate ( $18.6 \pm 12.8 \text{ mm}^3/\text{Mc}$ ) after 2 Mc. Water or saline solution was the most commonly used lubricant fluid in the first 15 years of wear simulator studies due to being easily obtained, inexpensive and it did not degrade overtime (Brown and Clarke, 2006). However, simulator studies have shown inconsistent wear rates compared to clinical implant wear (Brown and Clarke, 2006). Using water as a lubricant does not result in a protective adsorbed layer of protein molecules on the bearing surfaces, which is found when using bovine or new born calf serum and provides surface protection during the stance phase of gait (Mavraki and Cann, 2011). This means that boundary lubrication prevails, through the increased load and reduced sliding distance during contact, thus creating a slow speed and high contact pressures. Therefore, in water, there is penetration of the fluid film, causing an increased friction and release of wear particles during articulation between the metallic (hard) and the asperities at the polyethylene (soft) bearing surfaces, resulting in the increased wear rate published in Affatato et al. (2007).

In metal-on-polyethylene THRs studies using water as the testing lubricant, there is prominent signs of polyethylene transfer from the liners to the femoral heads, which is not reported *in vivo*

(Cooper et al., 1993). Besides, the transfer of material could roughen the counterface, resulting in the increased wear rate when using water as the testing lubricant. This finding also demonstrates the lack of an active protein layer, which has been found *in vivo* and *in vitro* studies (Campbell et al., 1995; Wang et al., 1995). Wear particles produced in simulations using water were large flake-like particles, with some being several millimetres across (Wang et al., 1996a). In contrast, serum lubrication produces extremely small wear particles, mostly of submicron size which are rounded or elongated in shape (Wang et al., 1996a). This is similar to wear debris found in retrieved peri-prosthetic tissues removed during revision of THR (Shanbhag et al., 1994) and further highlights the reason why water has been abandoned as a testing lubricant. This was a limitation of the paper by Affatato et al. (2007) and was acknowledged by the authors in their paper.

The rest of the papers used bovine serum as their testing lubricant, which has been shown to replicate the formation of a tribofilm, which transpires naturally in the joint and ultimately produces a realistic wear rate (Brown and Clarke, 2006). Bovine serum has also been shown to eliminate the presence of material transfer from the polyethylene to the metallic components in artificial joints, through the formation of a protein boundary layer (Brown and Clarke, 2006). Low concentrations of proteins in the testing lubricant can have a negative effect on implant wear, while high protein concentrations can result in protein degradation and precipitation that mask the polyethylene wear (Lu and McKellop, 1997). The ratio of albumin to gamma-globulin of bovine serum has also been shown to influence wear rates. An increased albumin/gamma-globulin ratio from 0.8 to 4, the wear rate increased by 50% in UHMWPE acetabular cups after 1 Mc (Wang et al., 2004). Controlling the ratio between 0.82 and 2.0, as well as diluting the bovine serum to 20 mg/mL (to reduce the protein concentration found in raw serum), produced wear rates of UHMWPE similar to that seen clinically. Therefore, the selection of the protein concentration is crucial when using organic serum as the testing lubricant to produce wear rates within the reported clinical range of joint replacements.

### **1.6.6 Fixed versus Mobile Design**

The large variability in experimental methodologies makes it challenging to extract consequential differences between FB and MB designs. Both design types demonstrated comparable wear rates in the studies which used implants containing conventional UHMWPE. This appeared to contrast with data from a previous TKR comparator study, which showed that MB devices exhibited significantly lower wear ( $7.34 \pm 1.81 \text{ mm}^3/\text{Mc}$ ) than a FB design ( $22.12 \pm 6.02 \text{ mm}^3/\text{Mc}$ ). The improved wear resistance was related to the transition of knee rotation into unidirectional motion at the metallic-insert articulating interfaces (McEwen et al., 2001). The unidirectional motion improves wear resistance, due to the UHMWPE expressing strain hardening features with the lamellar crystals being able to rotate and realign along the direction of deformation (McEwen et al., 2001). However, the study by Smyth et al. (2017) demonstrated

that with the addition of rotation and displacement, the wear rate of the MB device increased multi-directional motion on the unconstrained articulating surfaces, resulting in comparable wear rates between implant designs. The influence of cross-shear and multidirectional motion is discussed in much more detail within Chapters 3 and 4, alongside the comparison between FB and MB implant designs.

### **1.6.7 Wear Simulator Summary**

The wear data presented in this section supports the notion that implant wear, independent of implant design, is significantly affected by implant and simulator experimental conditions. Therefore, this thesis will focus on both the effect of varying implant and simulator parameters on the wear behaviour of a MB implant. The development of further simulator studies is essential to enhance their predictive capability, under varying implant and simulator conditions, in order to fully understand the wear behaviour of TAR and subsequently improve overall clinical outcome.

## **1.7 Summary of the Literature Review**

The ankle is a complex joint vulnerable to developing OA, with almost 30,000 patients being referred to specialist ankle surgeons annually and over 1.7 million adults in the UK are diagnosed with OA of the foot and ankle (Goldberg et al., 2012). Trauma is considered the most frequent cause of ankle OA (Thomas and Daniels, 2003), which is commonly referred to as PTOA (Chou et al., 2008). The prevalence of ankle OA may further increase, as being active or taking part in sports, have both being associated with increased risk of repeated ankle sprain or fracture, leading to the onset of PTOA (Hintermann and Ruiz, 2014). Typically, PTOA is associated with a younger population (Barg et al., 2013), so it is essential that treatment options allow successful motion preserving capabilities.

AA remains surgeon's number one choice for treating ankle OA (Gowda and Kumar, 2012), which provides pain relief and well-documented long-term survivorship (Haddad et al., 2007; Kim et al., 2017; Lawton et al., 2020). However, AA leads to altered gait mechanics and mechanical loads that can cause the degeneration of adjacent degeneration (Wu et al., 2000; Coester et al., 2001; Beyaert et al., 2004; Thomas et al., 2006). In the last decade, TAR has increased in popularity as a motion preserving alternative to AA, but limited gait studies exist that directly compare both surgical interventions (Piriou et al., 2008; Hahn et al., 2012; Singer et al., 2013; Flavin et al., 2013; Segal et al., 2018; Stone et al., 2021). The main reported benefit of TAR over AA is the conservation of existing pre-operative sagittal ROM and improved walking speed post-surgery. However, the majority of this research utilised SFM, which do not account for the motion at the adjacent foot joints, resulting in inaccuracies in ankle kinematics (Pothrat et al., 2015). More recent comparator studies have begun using MFM to determine the kinematic effects of the adjacent joints (Seo et al., 2017; Sanders et al., 2021), but are limited by short follow-

up periods post-surgery and neglect the influence TAR has on compensatory mechanisms at the hip and knee joints.

Although TARs seem to have improved gait mechanics and may resolve the issue surrounding adjacent joint degeneration, TAR is not without its own surgical complications. Aseptic loosening has been attributed to wear-mediated osteolysis (Glazebrook et al., 2009), through the production of wear debris and is the main contributor to early device failure (Henricson et al., 2007; Espinosa et al., 2017). Failure of an implant, which is defined by the NJR as removal of primary implant components (revision) is low for both THR and TKR (NJR, 2021) and falls within the Government guidelines (NICE), which stipulate that revisions should not exceed 5% at 10 years. This clinical success contributes to the large numbers of THR and TKR surgeries that are undertaken annually. Although the newer generation of TARs have shown improved survival rates at short-to-intermediate follow-up periods when compared to AA surgery (Veljkovic et al., 2019; Lawton et al., 2020), long-term outcomes of TAR remain unsatisfactory in comparison to THR and TKR. It is proposed that this apparent lack of clinical success is key in the low numbers of TARs implanted, relative to the potential demand.

The development of a successful TAR has been further restricted by limited research undertaken in the field. TAR has not been subject to the same pre-clinical testing and validation requirements as THR and TKR, as it has only recently been given an equivalent medical device classification. The relative numbers of TAR wear simulation studies are severely limited and experimental protocols are widely varied, compared to hip and knee studies (Affatato et al., 2007; Bell and Fisher, 2007; Postak et al., 2008; Kincaid et al., 2013; Bischoff et al., 2015; Reinders et al., 2015b; Smyth et al., 2017; Schipper et al., 2018). Current TAR wear studies have failed to truly recognise the influence of varying implant and simulator parameters on the same implant design. In addition, no published studies have utilised the newly developed ISO 22622:2019 under force or displacement control, which was introduced to reduce the clear experimental variability between research sites.

Investigating both the *in vitro* and *in vivo* behaviour of TARs has highlighted how far behind the curve they are compared to THR and TKR, and has emphasised the need for further investigation. Therefore, the overall aim of this PhD was to determine the biomechanical and wear behaviour of a third generation MB TAR using a combination of gait analysis and experimental simulation methodologies. Enhancement of pre-clinical *in vitro* TAR simulations under varying implant and simulator parameters, coupled with comparing gait mechanics of different surgical interventions is important, in order to inform future device development, in terms of biomechanical and wear performance.

**CHAPTER 2**

**METHOD DEVELOPMENT**

## CHAPTER 2

### METHOD DEVELOPMENT

#### 2.1 Introduction

Pre-clinical tribological simulation is a well-documented methodology used to predict the mechanical and wear behaviour of contemporary designs and materials during prosthesis development (Mattei et al., 2011). *In vitro* wear studies are used to confirm that joint replacements attain acceptable safety and performance measures before being implanted in humans (Ali et al., 2016). Wear simulator studies of THR and TKR are commonly reported in the literature, under a range of experimental conditions, designed to determine the wear behaviour of the implant (Fisher, 2012). Knee wear simulators have also been used effectively in representing ankle kinematics to establish the wear of different TAR designs (Affatato et al., 2007; Bell and Fisher, 2007; Bischoff et al., 2015; Reinders et al., 2015b; Smyth et al., 2017; Schipper et al., 2018). The use of a knee simulator rather than an ankle specific simulator, promotes an increased rate of implementation of the experimental methodology, when compared to the TAR simulation literature. Therefore, this Chapter aimed to outline the simulator methods and experimental conditions employed for each wear study detailed in Chapters 3 and 4, to further understand the influence of varying implant and simulator parameters on TAR wear behaviour.

#### 2.2 Materials

As one of the most implanted MB devices in the UK (NJR, 2021), the BOX® ankle (MatOrtho Ltd, Leatherhead, UK) was used throughout the simulator studies. The three-component MB prosthesis consists of cast cobalt-chrome-molybdenum (CoCrMo) alloy tibial and talar components, separated by an unconstrained low calcium medical grade UHMWPE insert (PUR 1020; MatOrtho Ltd, Leatherhead, UK). The insert was placed in gas-impermeable film packaging, evacuated, and back filled with nitrogen, before being sterilised by gamma irradiation with a Co60 source to 25-35 kGy, giving a sterility assurance level of  $10^{-6}$  (Giannini et al., 2011). The bi-concave meniscal insert was designed to fully conform to the metallic articulating surfaces, regardless of joint position (Giannini et al., 2011).

The distal tibial component has a convex, spherical articulating surface which interacts with the superior, concave spherical insert surface (Giannini et al., 2011). The tibial component also possesses two parallel cylindrical bars running anteroposteriorly on the proximal flat surface, designed to improve osseointegration of the device (Giannini et al., 2011). The radius of curvature of the talar component is larger than that of the natural talus, allowing fibres within the calcaneofibular and tibiocalcaneal ligaments to experience isometric loading during passive joint motion (Leardini et al., 2004). This design feature also provides lateral stabilisation of the ankle through restraining inversion in the neutral or dorsiflexed position (Golanó et al., 2010). For the cementless component-to-bone fixation of the BOX® ankle, both the non-articulating metallic

surfaces are covered with small cast-in balls and coated by plasma spray with a 50-mm-thick layer of hydroxyapatite (Giannini et al., 2011).

A range of implant sizes were chosen for the simulator studies (Table 4), to determine the influence this parameter may have on implant wear (Chapter 3). The thinnest conventional UHMWPE insert (5 mm) was selected for each implant size, to create the highest risk situation. Increasing the thickness of the conventional UHMWPE insert has previously been demonstrated to produce a more uniform distribution of contact pressure (Kakkar and Siddique, 2011) and decrease the von Mises stresses (Martinelli et al., 2017) in TARs. This is consistent with Bartel et al. (1986), who demonstrated that in knee implants, contact stresses increase as the thickness of polyethylene decreases. Maintaining the insert thickness also nullified the effect of varying liner thickness on the implant wear rate. Additional conventional UHMWPE inserts were immersed in the lubricant for the duration of each wear test and used to compensate for moisture uptake (Galvin et al., 2009).

Table 4. Implant size dimensions for the extra small, small and medium BOX® ankle.

	UHMWPE Insert		Talar Component		Tibial Component	
	ML (mm)	AP (mm)	ML (mm)	AP (mm)	ML (mm)	AP (mm)
<b>Medium</b>	26.00	23.20	29.00	38.20	29.00	35.00
<b>Small</b>	24.00	20.50	27.00	33.91	27.00	30.00
<b>Extra Small</b>	20.65	20.50	23.00	31.74	23.00	30.00

\*AP = Anteroposterior length; ML = Mediolateral width

### 2.3 Simulator Methods

A second generation ProSim pneumatic knee simulator (KSpn; Simulation Solutions, Stockport, UK) was used in the initial wear simulation study to determine the influence of implant size on wear behaviour (Chapter 3). The same simulator has successfully been used to determine the wear of varying TKRs designs (Brockett et al., 2012). KSpn consisted of six stations divided across two banks of three (Figure 19), with each station being supplied with its own air for pneumatic control. Each station had six DoF, with four controlled axes of motion (Table 5). The AL, tibial IER and AP displacement were all controlled pneumatically, while flexion/extension (FE) motion was applied electromechanically. The positive directions of these motions within KSpn, are highlighted in Figure 20. The bespoke fixtures fixed the ML displacement (Section 2.3.3), while abduction/adduction was allowed to move passively, due to the simulators inability to actively control this motion.

The studies within Chapters 3 and 4 were undertaken to determine the influence of specific implant and simulator parameters, which resulted in each study being run under displacement control. The implementation of force control simulation, while physiologically more accurate in representing the soft tissue effect on implant wear, may introduce uncertainties in the resulting motions (Reinders et al., 2015b). Using force-controlled simulators has also been found to cause

increased inter-station variability and reduced reproducibility when comparing between TAR designs (Ho et al., 2020). The use of displacement control was therefore selected as the most appropriate option to determine the wear behaviour of the same implant design.



Figure 19. Six station predominately pneumatic driven ProSim Knee Simulator (KSpn; Simulation Solutions, Stockport, UK).

Table 5. ProSim Pneumatic Knee Simulator (KSpn) Simulator Controls.

Simulator Input	Input Type	Simulator Control
Axial Load (AL)	Force	Pneumatic
Flexion/Extension (FE)	Displacement	Electromechanical
Internal/External Rotation (IER)	Displacement	Pneumatic
Anterior/Posterior Displacement (AP)	Displacement	Pneumatic

### 2.3.1 Simulator Inputs

The relevant loading and motion profiles were defined from a recent MB implant wear simulation performed at the University of Leeds (UoL) (Smyth et al., 2017), and will be referred to as the UoL profile (Figure 21). The authors derived each simulator profile using a MATLAB (Mathworks) coding function to interpolate intermediary time points throughout the gait cycle from published gait and simulator studies.

#### 2.3.1.1 Axial Load

A peak AL of 3150 N was selected for the simulation, which was equivalent to 4.5 times BW of a 70kg individual. The peak AL was selected as it laid within the capacity of the simulator and published values (Seireg and Arvikar, 1975; Stauffer et al., 1977; Procter and Paul, 1982; Simonsen et al., 1995; Glitsch and Baumann, 1997; Sharkey and Hamel, 1998). In a more recent study, a swing phase load of 100N was applied, which aimed to replicate the natural soft tissue tension and ensured continued contact between the articulating surfaces of the implant (Smyth et al.,

2017). The AL profile was applied in phase with the FE, tibial IER, and AP displacement kinematic profiles, in relation to the gait cycle (Figure 21).

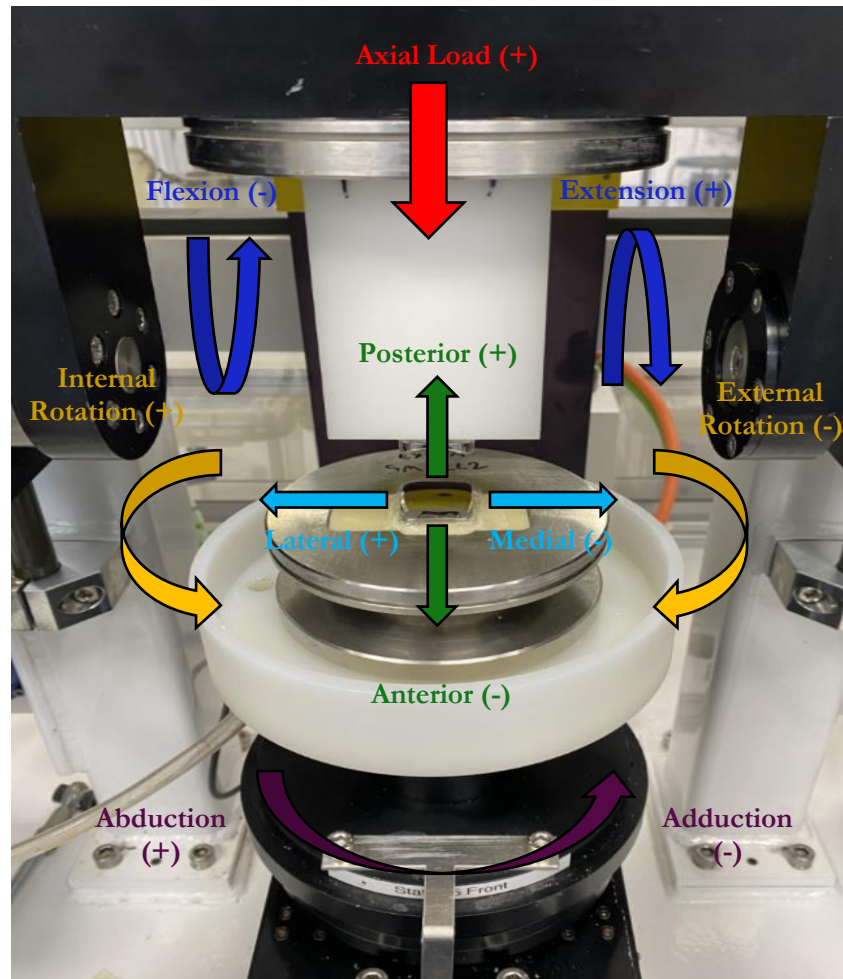


Figure 20. Axes of rotation and translation on a knee simulator for a left ankle.

### 2.3.1.2 Flexion/Extension

The peak values of  $15^{\circ}$  (-) dorsiflexion (flexion within the simulator) and  $15^{\circ}$  (+) plantarflexion (extension within the simulator) were selected (Smyth et al., 2017) (Figure 21). This resulted in  $30^{\circ}$  of sagittal plane motion and fell within the measured ROM from the majority of previous gait and simulator based studies (Stauffer et al., 1977; Ounpuu, 1990; Novacheck, 1998; Rao et al., 2006; Nester et al., 2007; Bell and Fisher, 2007; Piriou et al., 2008; Ingrosso et al., 2009; Flavin et al., 2013).

### 2.3.1.3 Internal/External Rotation

When defining the tibial IER profile, it was important to distinguish between previous studies, which presented motions of the AJC rather than specific talocrural joint articulation. It also ensured the motions were being applied in correspondence to a similar coordinate system measured in the natural ankle (Smyth et al., 2017). The UoL profile produced by Smyth et al. (2017) exhibited  $2.3^{\circ}$  of internal rotation (-) and  $8^{\circ}$  of external rotation (+) (Figure 21), resulting

in a ROM of 10.3°. The tibial IER peak and ROM selected for the simulations corresponded to the earlier ankle literature (Moseley et al., 1996; Smith et al., 2001; Arndt et al., 2004; de Asla et al., 2005; C Nester et al., 2007; Lundgren et al., 2008; Ingrosso et al., 2009).

### 2.3.1.4 Anterior/Posterior Displacement

Smyth et al. (2017) used values at varying data points of the stance phase, taken from the displacement profile for the natural ankle reported by Conti et al. (2006), to define the profile shape. Peak anterior translation of 7 mm (+) and peak posterior translation of 2 mm (-) were selected to represent TAR AP displacement (Figure 21). Peak anterior translation input value was programmed to occur at the same time point in the gait cycle as peak plantarflexion and tibial external rotation (Figure 21). The overall ROM of 9 mm for AP displacement is comparable to that of the limited number of studies measuring AP motion within natural or replaced ankles (Komistek et al., 2000; de Asla et al., 2005; Conti et al., 2006).

In the study by Smyth et al. (2017), different gait conditions (six test stages) were explored every Mc for a total of 12 Mc to determine the influence of kinematics on implant wear. During stage 5, a reduced AP displacement ROM of 4 mm (+3.1 mm peak anterior displacement and -0.9 mm peak posterior displacement) was found not to have a significant impact on volumetric wear rate of a MB implant (Smyth et al., 2017) and was therefore selected for the wear simulations in this thesis.

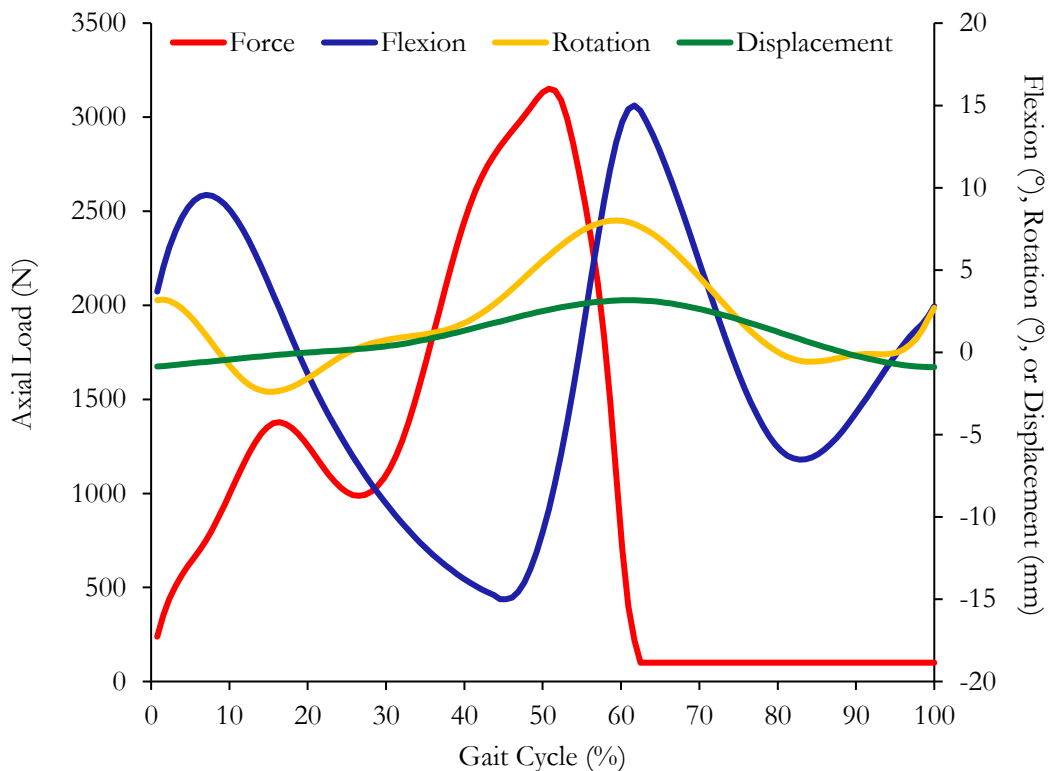


Figure 21. Knee simulator input profiles (UoL) for AL (red), FE (blue), tibial IER (yellow), and AP displacement (green). Adapted from Smyth et al. (2017).

### 2.3.2 Simulator Input Translation

The lack of an ankle-specific simulator meant that each implant had to be inverted in KSpn, so that flexion could be applied about the constant radius of the talar component in the superior position (Figure 22). The tibial component, as given by ISO 14243-3:2014 (wear of TKR under displacement control), remained the tibia, while the femoral component became the talar component of the TAR.

Inverting the TAR within the knee simulator has been extensively used in displacement-controlled TAR publications (Affatato et al., 2007; Bell and Fisher, 2007; Kincaid et al., 2013; Bischoff et al., 2015; Smyth et al., 2017; Schipper et al., 2018). IER is measured as the motion of the foot relative to the tibia, which occurs at the tibial articulation in a TAR (Smyth et al., 2017). As the rotation is applied to the tibial component, the direction of the IER must be reversed. The AP displacement was also applied to the tibial component, driving it in the opposite direction. Moving the tibial component anteriorly enabled the natural posterior motion of the talus. This meant that the displacement profile was deemed anterior when the joint contact lies anterior to the midline of the talus (Smyth et al., 2017). With few gait and simulator studies available which measured AP displacement, the AP profile produced by Smyth et al. (2017) may not fully represent the natural AP motion in the TAR population. However, it is still important to understand the combined effect this parameter may have on implant wear.

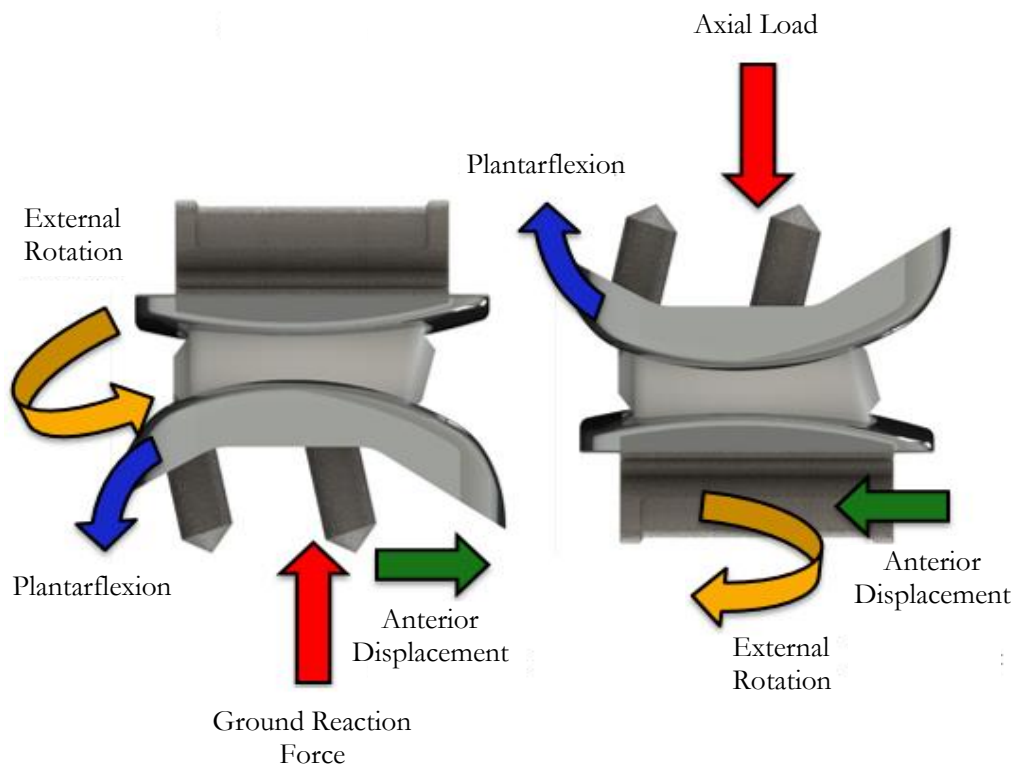


Figure 22. Schematic drawing demonstrating the loads and motions of a left-sided device (left) relative to the inverted simulator positioning (right). Adapted from MatOrtho (2020).

### 2.3.3 Talar Fixtures

Six Delrin fixtures were designed and manufactured for each implant size. Each talar fixture was specifically fabricated to align with the centre of rotations, conform to the structure of the talar component and mimic the surgeon positioning of the implant. The constant radius of the medium, small, and extra small talar components to the bearing surface was 36°, 33° and 31.5°, respectively. To fix the talar components to the manufactured fixture, a 1mm layer of cement had to be accounted for when positioning to the simulator centre of rotation. The centre of rotation was aligned with the flexion cradle, which was fixed at 68mm for each implant size, due to simulator dimensions (Appendix A.1 and ).

### 2.3.4 Component Set-up

The talar components were cemented into the bespoke Delrin talar fixture using Poly (methyl methacrylate) (PMMA). The cavity of the tibial fixture was cemented with PMMA, with the rotation and displacement cradle situated in the neutral position and in line with the talar component (Figure 23). The metallic components were positioned to ensure the insert was central within the TAR and the whole implant aligned neutrally. A bespoke weight was used to hold the position of the tibial component in place whilst the cement cured.

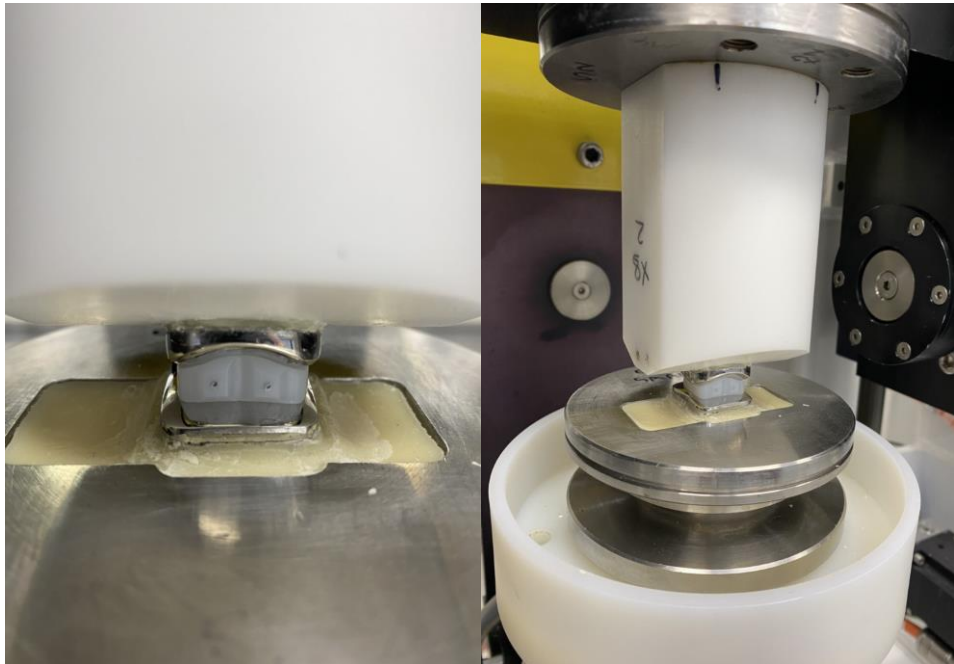


Figure 23. Tibial and talar component setup within ProSim Pneumatic Knee Simulator (KSpn; Simulation Solutions, Stockport, UK).

### 2.3.5 Contact Areas

To verify the central alignment of the articulating surfaces of each TAR, a Microset (Microset 101 FF, Microset Products Ltd, UK) two-part polymer was applied to the metallic surfaces. The insert was set in the centre of the tibial component and the talar component was then lowered to

initiate contact. A load of 1000 N was then applied to determine the contact area of the insert on the metallic surfaces (Figure 24). This process was repeated after every Mc to ensure continued alignment, and the samples were rotated around the simulator stations to compensate for any inter-station variation.



Figure 24. Contact areas of the talar (left), UHMWPE insert (middle), and tibial (right) components, demonstrating central alignment.

### 2.3.6 Calibration

The Institute of Medical and Biological Engineering (iMBE) calibration protocol was followed at the start of each simulator study. The calibration involved applying known AL and displacements to each station, while measuring the Linear Variable Differential Transformer (LVDT) positional output parameters. For each station, AL was calibrated using an externally calibrated load cell, fixed between the FE cradle and an existing Delrin block (Figure 25). A cam box applied a load to the calibrated load cell and the load applied was entered into the simulator. Five loads of increasing value were applied, and a calibration report was produced.

Existing fixtures were used to calibrate the IER and AP displacement through  $5^\circ$  ( $10^\circ$  to  $-10^\circ$ ) and 5 mm ( $-10$  mm to 10 mm) increments, respectively (Figure 25). A digital inclinometer was attached to the flexion cradle used to give an angular measure of FE displacements at  $5^\circ$  increments. The calibration compared the calibrated load cell to the simulator load cell. The calibration scale and offset generated by the simulator was the gradient and y offset of the data, which gave the best line of fit of the simulator load cell to the calibrated load cell. Calibration constants were derived from the known orientations at each motor position. This ensured that the simulator output values gave an accurate representation of the actual loads and displacements. Providing that the new calibration constant inputted was closer to the calibrated load cell reading, the recorded measurements for each of the simulator inputs were recorded directly onto the calibration software of the simulator. An example simulator calibration report for station 1 from one of the wear studies is presented in Appendix B, while the simulator calibration record for each study is presented in Appendix C.

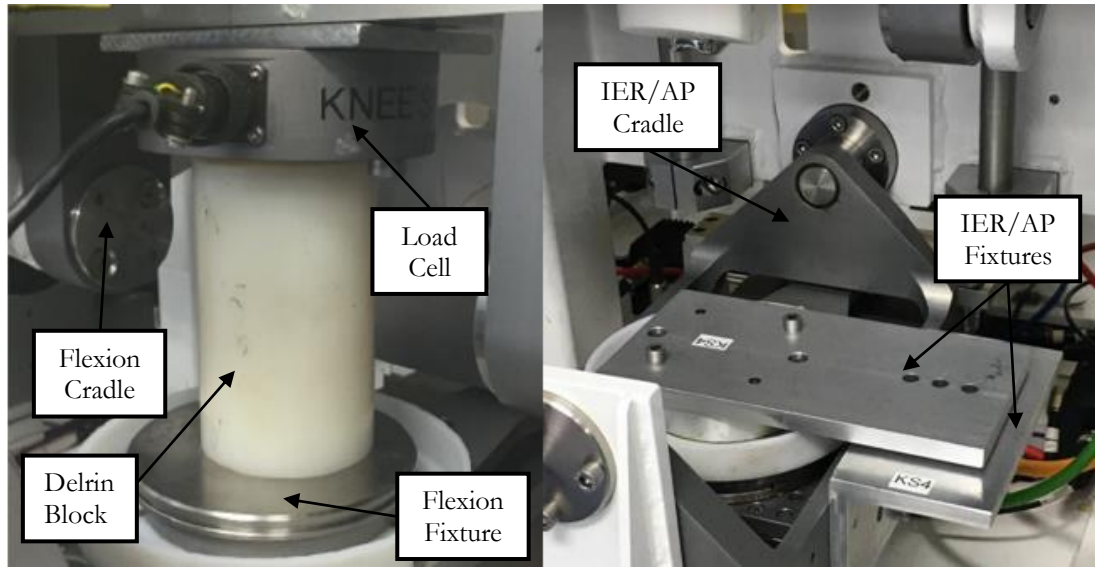


Figure 25. ProSim Pneumatic Knee Simulator (KSpn) load (left) and rotation/displacement (right) calibration set-up.

### 2.3.7 Simulation Preparation

Prior to wear simulation, each conventional UHMWPE meniscal insert was etched on the top corner of the lateral side, to distinguish between individual samples. The inserts were then washed following the American Society for Testing and Materials (ASTM) F1714-96 (2018) guidelines, which involved three stages of cleaning: soapy water; Distel disinfectant (Tristel, UK); and ultrasonic washing. The inserts were then left to dry and placed in a balance room for 48 hours. This allowed the inserts to equilibrate in a controlled environment of constant temperature ( $20^{\circ}\text{C} \pm 1^{\circ}\text{C}$ ) and humidity ( $40\% \pm 5\%$ ) (Smyth et al., 2017). After this rest period, the inserts were weighed using an XP26 Analytical Microbalance (Mettler Toledo, Leicester, UK). The conventional UHMWPE inserts were then immersed in deionised water and stored at room temperature for a minimum of two months prior to the wear simulation, to ensure fluid absorption effects were accounted for (Wang et al., 1998; D’Lima et al., 2001). After the two-month period, the inserts were removed from soak and cleaned, before being left to dry and acclimatise to the conditions of the controlled environment in the balance room for 48 hours.

### 2.3.8 Frequency

The frequency of the simulator was set to mimic natural walking gait, which was approximately 60 steps per minute (Kamali et al., 2010). This corresponds to a frequency of 1Hz and was calibrated by monitoring the frequency of the cycles using a stopwatch for at least 100 seconds after each serum change.

### 2.3.9 Lubrication

To simulate *in vivo* wear conditions, the contacting surfaces of the tibial and talar components were immersed in a fluid test medium to mimic the synovial fluid of the natural joint. The use of distilled water has previously been shown to be insufficient, as it produces varying lubrication

regimes, wear particles and wear patterns in knee tibial inserts (Schwenke et al., 2005). Bovine or new-born calf serum is considered the most clinically relevant lubricant for wear studies of joint replacements and is recommended by the ISO standards for THR (ISO 14242-1:2014/Amd 1:2018), TKR (ISO 14243-3:2014) and TAR (ISO 22622:2019). However, there is no generally accepted levels of protein ratio that has been stipulated for wear simulation, with different laboratories using varying concentrations and compositions of serum.

Each TAR investigated was secured in chambers filled with 450 mL of lubricant, which consisted of 25% (v/v) new-born calf serum (Thermo Fisher Scientific, Paisley, UK) diluted with 0.04% (v/v) sodium azide solution (Severn Biotech Ltd, Kidderminster, UK), to prevent phosphate precipitation and bacterial degradation (Smyth et al., 2017). The resulting lubricant contained between 15.75g/L to 16.00g/L of protein (Appendix D), which has previously been claimed to imitate natural joint lubricant (Saari et al., 1993). The serum was stored in a frozen environment (-20°C) to reduce microbial contamination. The study was conducted at room temperature to reduce the risk of protein deposition and denaturation at increased temperatures, which may have led to potential artefact formation (Cowie et al., 2016).

## **2.4 Gravimetric Measurement Method**

Gravimetric assessment for each wear study was performed on the Mettler Toledo XP26 Analytical Balance (Mettler Toledo, Leicester, UK). This methodology is the most common technique used to quantify volumetric wear of joint replacements and is recommended for use in the ISO standards of THR (ISO 14242-1:2014/Amd 1:2018), TKR (ISO 14243-3:2014) and TAR (ISO 22622:2019). Using this technique, the conventional UHMWPE inserts were weighed before and after each Mc and the difference of the two measurement values was calculated (Sagbas and Durakbasa, 2012).

Before each measurement session, the balance doors were opened and closed repeatedly until the balance gave a reading of 0 mg, which allowed the balance to equilibrate with the room environment. The laboratory temperature (20°C ± 1°C) and humidity (40% ± 5%) was recorded at the start and end of each weighing session; to minimize fluctuations that may influence the measurements (ASTM F2025-06, 2018). The balance was calibrated using a metal control pin of known weight (1.6165 g), ensuring the balance remained stable during weighing. The Mettler Toledo XP26 Analytical Balance had a resolution of 1 µg.

Gloves were worn to place the conventional UHMWPE insert on the balance and left for a minimum of five minutes to allow the balance to settle. The inserts were passed through an active anti-static (internal ioniser), designed to continuously generate both positively and negatively charged ions at the electrodes. These act to neutralise the charges on the insert surface, without creating any disruptive air currents. This process eliminated any electrostatic charge, which can cause drifting measurement readings, longer stabilisation times, and non-repeatability of results.

The inserts were placed centrally in the balance and the weight for each insert was recorded. Each insert was weighed sequentially until five consecutive measurements were within  $\pm 0.005$  mg of each other. The balance was ensured to return and settle at zero after each measurement. A mean of the five weights was determined for each conventional UHMWPE insert and used to calculate the mean volumetric wear.

Volumetric wear was calculated by dividing the weight loss, considering the effect of fluid absorption through the soak controls, by the density of the UHMWPE insert ( $935.5 \text{ kg/m}^3$ ), which lies in the middle of the ISO 5834-2:2019 (Equation 2.1). The net change in mass was used to calculate the mean wear rate for each implant size under different experimental conditions.

Equation 2.1 Volumetric Wear Equation:

$$W_n = W_{an} + S_n$$

$W_n$  = net mass loss

$W_{an}$  = average uncorrected mass loss

$S_n$  = average mass increase for the soak control

## 2.5 Simulation Duration and Serum Changes

The simulator was run in Mc sections and the lubricant was changed every 330,000 cycles to ensure a sustained protein content was present. Each station was washed thoroughly with soapy water and Distel disinfectant, before being dried, wiped using 70% iso-propanol/water, and fixed back into the correct station with newly made serum. The implants were repositioned in different stations after each Mc, to compensate for inter-station variability. The simulator was visually checked every 24 hours to ensure it was functioning properly and was able to reproduce the desired kinematic inputs (Section 2.6).

## 2.6 Loading and Kinematic Performance

KSpn automatically recorded 1 out of every 20,000<sup>th</sup> cycle, with the output kinematics from each station being averaged across the six stations. This gave an overall output profile for the four simulator input parameters. In addition, the differences between the input and output loading and kinematic values were calculated as a percentage of the corresponding maximum demanded value. These differences were then averaged for the six stations and compared to the demand input profile and peak values, within a  $\pm 5\%$  maximum tolerance of the output kinematics. This method was also used to determine the level of loading and kinematic profile variability between the simulator stations during each wear study.

Adequate tuning of the Proportional–Integral–Derivative (PID) control parameters were performed to reduce the differences between simulator kinematic output and input profiles. This process was also carried out to minimise inter-station variability between Mc segments,

particularly where the implants were moved around the stations of the simulator. PID tuning involves five processes: the potential gain value (P); integral gain value (I); differential gain value (D); tuning profile; and scale of the tuning profile.

The potential gain was the value between the applied and desired kinematics. If this was set to high then the desired value would have been overshoot, causing oscillations in the output profiles throughout the gait cycle. Integral gain accounted for past values simulated and integrated them over time, while differential gain involved the best estimate for future trend of the applied input, based on the current rate of change. The tuning profile adjusted the applied input kinematics, which was done at the same point the deviation between profiles occurred. A similar method was used for scaling of the applied profiles to mimic the desired input profile. The tuning process was performed at each serum change and was checked on several occasions during the first 24 hours after.

## **2.7 Surface Roughness Measurements**

A two-dimensional (2D) contacting profilometer (Form Talysurf PGI800; Taylor Hobson, Leicester, UK) was used to assess the surface roughness and associated parameters of the articulating surfaces of the varying implant sizes before and after each wear study (Figure 26). This contact measurement technique has successfully been used in earlier TAR research at the UoL (Bell and Fisher, 2007; Smyth et al., 2017). This method utilised a 2  $\mu\text{m}$  conical tip stylus to take five 2D surface traces in the ML direction on the four articulating surfaces. The stylus was coupled with a transducer, which converted the vertical motion into an electrical signal. The part of the stylus contacting the material was a diamond tip with a carefully manufactured shape, defined in ISO 3274:1996.

A single long trace was used for the tibia and superior insert surfaces, to ensure the full representation of the articulating surfaces. The more curved geometry of the talus and inferior insert meant that a single trace would cause the failure of the Gaussian regression, which was used to extract the waviness profiles. Therefore, each trace for the talar and inferior insert surfaces was segmented into three sections: the medial slope (red), central region (blue), and lateral slope (green) (Figure 27). Five ML traces were spaced across the articulating surface of each TAR (Figure 28). The sample traces used for measuring the surface roughness for the different TAR sizes are shown in Tables 6-9. The medial measurement defines the distance from the most medial point on the articulating surface and the posterior measurement defines the distance from the most posterior point on the articulating surface (for the first trace only).

A Gaussian regression (least squares arc) filter was applied to each of the articulating surfaces (ISO 16610-21:2011). In accordance with ISO 4288:1996 and the Taylor Hobson guidelines, an upper roughness cut-off filter ( $L_c$ ) of 0.25 mm was used for the metal components, whereas a 0.8 mm cut-off was applied to the UHMWPE surfaces (Smyth et al., 2017). The lower cut-off

(Ls) was 0.0025 mm and 0.008 mm for the metallic and UHMWPE insert surfaces, respectively. The cut-off is a filter, which was used to separate the wavelengths of the components. For example, the 0.8 mm cut-off for the metallic components allowed wavelengths below 0.8 mm to be assessed with wavelengths above 0.8mm being reduced in amplitude. A 100:1 bandwidth ratio was selected for both materials, which is the ratio between the Lc cut-off (upper) and Ls cut-off (lower) values. A trace speed of 0.5 mm/s was selected for both material surfaces. Despite later changes in roughness, the parameters remained unchanged to ensure the results were comparable throughout each study.

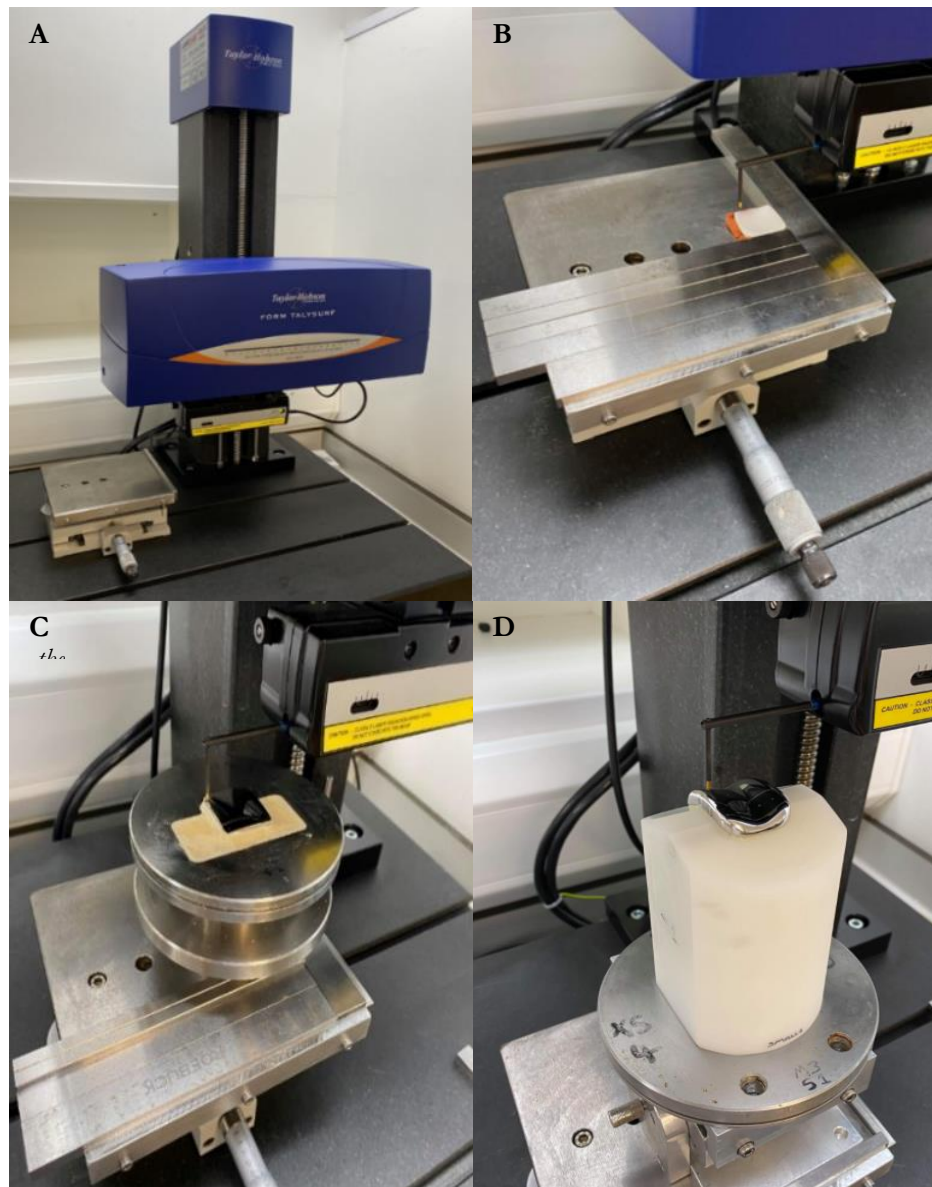


Figure 26. Form Talysurf PGI800 (A) used to measure the surface roughness of the UHMWPE insert (B), tibial (C), and talar (D) articulating surfaces.

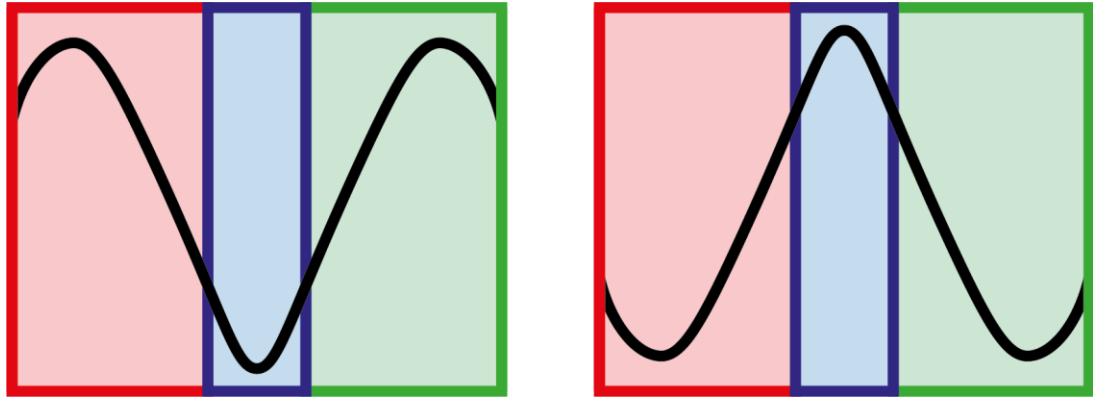


Figure 27. The segmentation process for the talar (left) and superior insert (right) roughness traces.

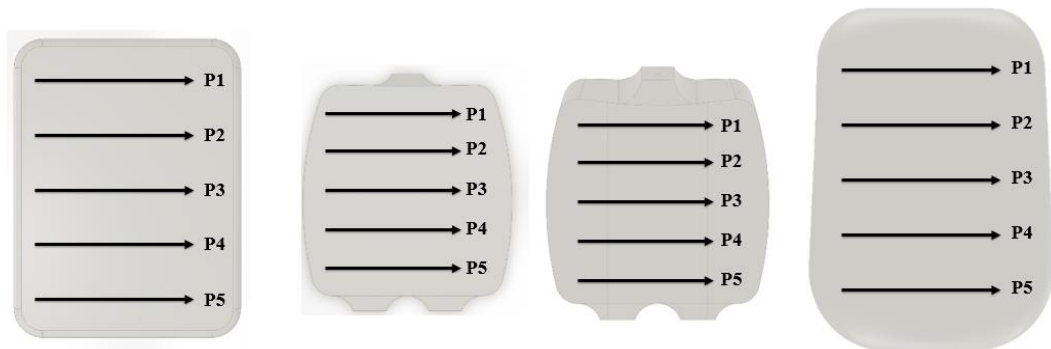


Figure 28. Sample traces of the tibia (A), superior insert (B), inferior insert (C) and talus (D) articulating surfaces of the BOX® ankle.

Table 6. Surface roughness trace information for the tibial component.

	Trace Length (mm)	Trace Space (mm)	Medial (mm)	Posterior (mm)
Medium	25	6	2	6
Small	23	5	2	5
Extra Small	19	5	2	5

Table 7. Surface roughness trace information for the superior insert.

	Trace Length (mm)	Trace Space (mm)	Medial (mm)	Posterior (mm)
Medium	19	4	2	3
Small	18	3	2	4
Extra Small	14	3	2	4

Table 8. Surface roughness trace information for the inferior insert.

	Trace Length (mm)	Trace Space (mm)	Medial (mm)	Posterior (mm)
Medium	23	6	2	8
Small	20	6	2	5.5
Extra Small	18	5	2	5

Table 9. Surface roughness trace information for the talar component.

	Trace Length (mm)	Trace Space (mm)	Medial (mm)	Posterior (mm)
Medium	20	6	2	6
Small	19	3	2	4
Extra Small	15	3	2	4

It is important to measure the surface roughness of each TAR, as previous *in vitro* testing on THR and TKR has demonstrated that conventional UHMWPE wear increases in the presence of counter face scratches perpendicular to the direction of motion, which can lead to subsequent implant failure (Cooper et al., 1991; Jones et al., 2001; Scholes et al., 2012). Therefore, several roughness indices were used to assess the surface topography of the articulating surfaces of each TAR.

The average surface roughness ( $R_a$ ) is the arithmetic average of the absolute values of the profile heights over the evaluation length. The maximum profile peak height ( $R_p$ ) represents the distance between the highest point of the profile and the mean line within the evaluation trace, while the maximum profile valley depth ( $R_v$ ) is the distance between the deepest valley of the given profile and the mean line within the evaluation trace (Figure 29) (Cowie and Jennings, 2021).

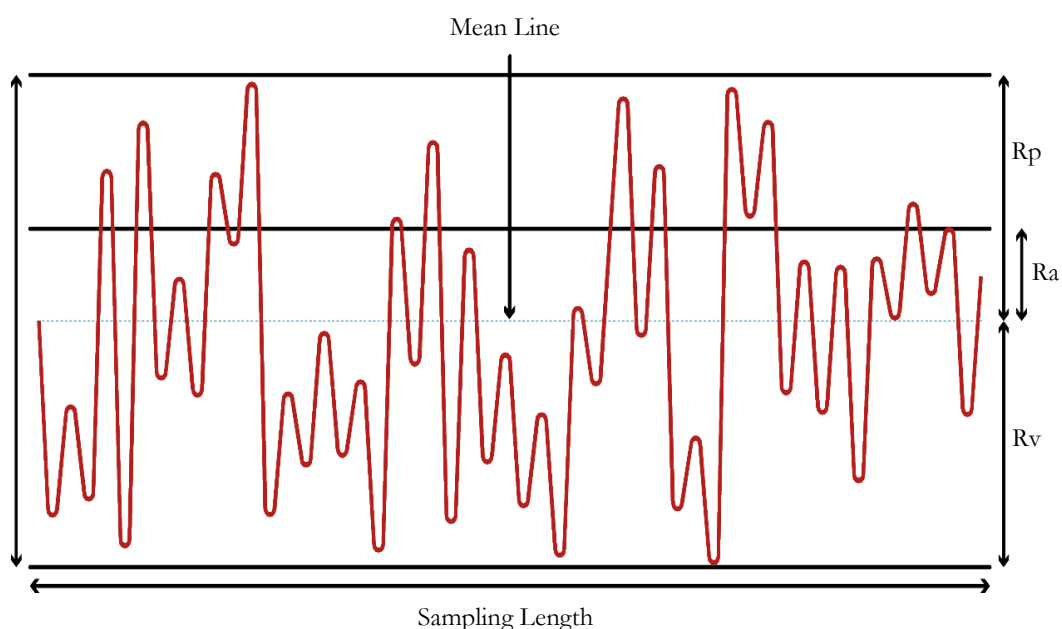


Figure 29. Schematic showing 2D surface roughness parameters of interest for the TAR articulating surfaces. Adapted from Cowie and Jennings (2021).

Skewness ( $R_{sk}$ ) signifies the asymmetry of the profile around the mean line. Pre-dominant profiles at peaks above the mean are reflected in positive skewness, while negative skewness refer to profiles prevalent in deep valleys (Figure 30) (Cheikh et al., 2021). A normally distributed profile has a skewness value of zero. For the metallic components, a higher  $R_p$  or more positive  $R_{sk}$ , is more likely to have poor lubricant retention, due to the lack of deep valleys in which to retain lubricant traces (Figure 30) (Leach, 2010). Surface kurtosis ( $R_{ku}$ ) provides a measure of the peakedness of the profile about the mean evaluation line (Leach, 2010). The  $R_{ku}$  of a perfectly Gaussian surface is 3. A sharp peak dominated surface will have a higher  $R_{ku}$  value and a bumpy surface will possess a low  $R_{ku}$  value (Figure 31).  $R_{ku}$  can be used to predict implant wear behaviour and lubrication retention (Leach, 2010), with a higher  $R_{ku}$  value representing a greater lubricant retention capacity and improved resistance to wear.

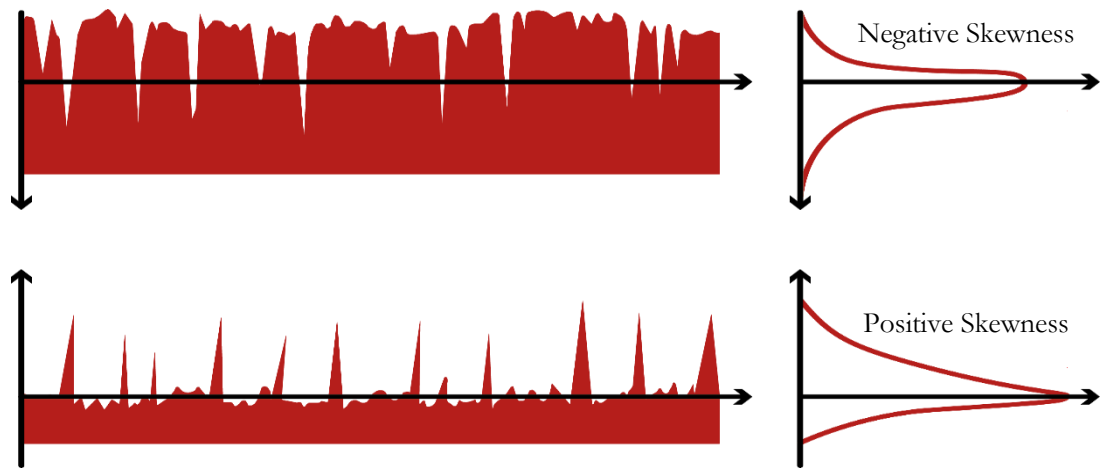


Figure 30. Profiles with negative (top) and positive (bottom) skewness ( $R_{sk}$ ) values. Adapted from Leach (2010).

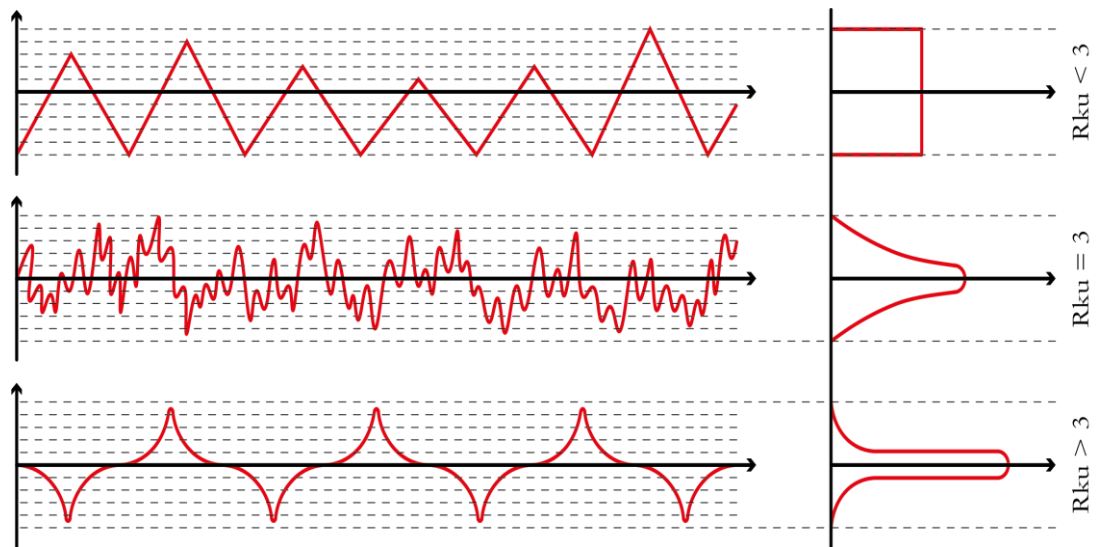


Figure 31. Profiles with low (top) and high (bottom) values of  $R_{ku}$ . Adapted from (Leach, 2010).

## 2.8 Visual Surface Damage Modes

Alongside the contact profilometry, a non-contact Infinite Focus microscope ( Alicona, Austria) was used to determine damage on the superior insert surface. Damage has been defined as the microscopic and visual changes to a surfaces' geometry and is associated with increased wear debris production (McKellop, 2007). The damage modes were defined using the Hood scoring system, which categorises damage seen on the articulating surface into seven visual characteristics on the polyethylene components (Table 10). This historic assessment technique has since been modified and used in several studies comparing wear simulated and retrieved (Affatato et al., 2009; Vaupel et al., 2009a; Stratton-Powell et al., 2016; Cottrino et al., 2016; Currier et al., 2019).

The Alicona InfiniteFocus microscope created the 3D image of the superior insert surface by identifying the optimal focus related to a known distance from the insert (Macdonald, 2014). This was constructed by moving the microscope objectives vertically, relative to the superior insert,

bringing the object in and out of focus. The sensor within the microscope recognised and measured where the object was best in focus (Macdonald, 2014). The process was repeated at chronological lateral positions to process an image of the insert surface. The inserts were fixed with the superior bearing surface facing towards the microscope lens. The lowest available microscope lens (10x magnification) was used to image the full superior insert surface, which helped reduced overall scanning time. The highest available resolution of 20x magnification was used to image damage modes in specific regions on the insert surface.

The Alicona scanning parameters were adopted from an earlier TAR study at the UoL (Stratton-Powell et al., 2018). This meant that a mid-range value for exposure (160  $\mu$ s) and contrast (1.5) was selected for both microscope lenses, with the same parameter values used throughout each wear study. A vertical resolution of 300 nm and lateral resolution of 3.914  $\mu$ m were used to successfully image the superior insert surface without exceeding the data point limit.

Table 10. Retrieval damage modes as described by Hood et al. (1983).

<b>Damage Mode</b>	<b>Visual Description</b>
<b>Burnishing</b>	Removal of machining marks triggered by high pressure articulation and characterised by a polished area and superficial multidirectional surface undulations.
<b>Scratching</b>	Depressed lines initiating material removal. Usually parallel with the direction of articulation in the areas of increased wear.
<b>Surface Deformation</b>	Permanent deviation from the initial shape of the articulating surface, caused by creep and/or cold flow.
<b>Pitting</b>	Irregularly shaped depressions visible in the articulating surface.
<b>Abrasion</b>	Tufts of material appearing after a region was torn from the surface.
<b>Delamination</b>	Subsurface failure typically surrounding an area of avulsed substrate caused by fatigue.
<b>Embedded Particles</b>	Distinct colour or texture, expected to be cement or metal particle embedded in the polyethylene surface.

## 2.9 Retrievals Analysis

After each Mc, all articulating surfaces of the implants were visually inspected and photographed to determine surface damage modes (Section 2.7). The damage modes were compared to the collection of TAR MB retrievals within the retrievals bank at UoL. The use of retrievals is important to inform laboratory based research to ensure that the *in vitro* wear simulation is producing outcomes relevant to the clinical environment. The retrievals were collected from UK hospitals under ethical approval (HRA ethics ref: 09/H1307/60). A Canon 700D SLR Camera with a 100 mm macro lens (Canon Ltd, UK) was used for all surface imaging. The exposure and depth of field functions of the camera were altered to achieve the optimum image quality, showing the most amount of surface damage, for the metallic and polyethylene surfaces. The combination of volumetric wear, surface roughness, and damage mode visualisation is important to understand the tribological behaviour of a TAR.

## **CHAPTER 3**

# **THE EFFECT OF IMPLANT PARAMETERS ON THE WEAR OF A TOTAL ANKLE REPLACEMENT**

## CHAPTER 3

# THE EFFECT OF IMPLANT PARAMETERS ON THE WEAR OF A TOTAL ANKLE REPLACEMENT

### 3.1 Introduction

Polyethylene wear debris, generated through the constant articulation of an implant during its lifetime, has been associated with an immune response, which triggers osteolysis and subsequent implant loosening of the metallic components (Fisher et al., 2010). With the ever increasing survivorship of modern day MB implants, there is a greater risk that wear-mediated osteolysis and ultimate failure of the device will become more prevalent. Although there are several factors affecting polyethylene wear, implant parameters remain an essential factor influencing wear behaviour (Battaglia et al., 2014a). The effect of varying implant parameters on TKR wear has previously been simulated and includes: conformity (Abdelgaied et al., 2014; Brockett et al., 2018); congruency (Koh et al., 2019); material (Essner et al., 2011); polyethylene type (Mohammad et al., 2019); and liner thickness (El-Deen et al., 2006). However, only one wear based study concerning TARs considered the effect of implant parameters (conventional UHMWPE versus XLPE) on the same implant design (Schipper et al., 2018).

TAR's are commercially available in a wide range of different designs, shapes and sizes to fit varying patient anatomies, all with the aim to reduce implant wear (Kretzer et al., 2011). Intra-operatively, surgeons have to select the right choice of implant size to increase the chances of a successful implantation, since both under- and oversizing may have a negative effect on implant survivorship and requirement for revision. As wear is a function of the sliding distance, increased implant size and subsequent contact area has resulted in higher volumetric wear rates in THR, but does have the benefit of reducing the risk of post-operative dislocation when compared to smaller sized devices (Kang et al., 2009).

In knee simulator studies, a larger implant size has been found to produce almost double the cumulative weight loss compared to smaller sized knee implants (Affatato et al., 2013; Battaglia et al., 2014). The authors reported that the larger inserts possessed a wider contact area which underwent more sliding during motion, resulting increased friction and wear. However, due to the lower contact pressure experience by the larger conventional UHMWPE meniscal inserts, there were significantly reduced morphological changes on a molecular scale when compared to the smaller inserts (Affatato et al., 2013). Further research also determined that larger sized knee implants were able to improve the restoration of functional knee rotation, which was not the case with medium and small sized implants (Fekete et al., 2018). The influence of implant size on wear behaviour remains unknown in TAR, with the majority of studies using mid-range bearing sizes. Therefore, the first objective of this Chapter was to determine the influence of two different implant sizes on the wear of a MB device.

The limited testing durations of the pre-clinical simulations in the TAR wear literature also fail to reflect the age of the implant *in vivo* or potential *in vivo* oxidation (Medel et al., 2009). Oxidation of conventional UHMWPE impairs their wear resistance and fatigue strength, resulting in wear-mediated osteolysis and implant failure (MacDonald et al., 2018). It is believed that oxidation of conventional UHMWPE inserts is caused by a chemical reaction cascade between the macromolecules and oxygen (Costa and Bracco, 2016; Pezzotti, 2017). The irradiation processes from sterilisation generate free bonds (radicals) on the molecules that react with the oxygen (Costa and Bracco, 2016). This can lead to a chain scission of the macromolecules, resulting in degradation of the UHMWPE inserts (Schwiesau et al., 2014).

To establish the consequences of the oxidation effect on long-term wear, accelerated artificial ageing protocols, such as the ASTM F2003:2015 and ISO 5834-3:2019, have been run to replicate the oxidation process of UHMWPE *in vivo*. During this process, the conventional UHMWPE is aged at elevated temperatures and oxygen pressure; enabling researchers to simulate worst-case scenarios. The process also allows for the effect of reduced oxidative stability to be determined in a relatively short period of time (i.e. weeks), while shelf-ageing and implantation can take months or years to induce deleterious mechanical changes of the insert. Artificial ageing has been shown to increase the volumetric wear and reduce mechanical properties of conventional UHMWPE in THR (Collier et al., 1996; Merola and Affatato, 2019) and TKR (McKellop et al., 2000; Muratoglu et al., 2004; Dumbleton et al., 2006; Schwiesau et al., 2014). However, the effect of the accelerated artificial ageing process on implant wear and potential mechanical degradation remains unknown in TAR. Thus, this was the second objective of this Chapter. The combination of the two objectives discussed will help to achieve the overall aim of the Chapter, being to investigate the effect of varying implant parameters on the wear of a modern MB device. Improving the understanding of implant parameters on the tribological behaviour of TARs is required to help develop longer lasting future designs.

### 3.2 Materials

As outlined in the in-depth methodology of Chapter 2, six medium and six extra small sized BOX® ankles were used in the implant size comparison study, while six small sized implants were used in the accelerated artificially aged study. The bearing batch and LOT numbers for each implant size are identified in Table 11. Each UHMWPE insert used the minimum thickness available (5mm), which represented a worst-case scenario for implant wear (Section 2.2).

Table 11. Bearing details for the medium, small and extra-small implant sizes.

Implant Size	Tibial	Talar	UHMWPE Insert
Medium	161-140	161-340	161-245
	219563	219938	219822
Small	161-140	161-340	161-245
	228616	228758	228136
Extra Small	161-110	161-310	161-205
	220644	220647	220649

### 3.2.1 The Simulator and Calibration Set-up

#### Implant Size

The KSpn discussed in Section 2.3 was used for the implant size comparison study, consisting of six stations divided across two banks of three, which were supplied with air for pneumatic control. The calibration process for the KSpn is detailed in Section 2.3.6, with the calibration records for the simulator being presented in Appendix C.1 and C.2.

#### Accelerated Artificial Ageing

For this study, an electromechanical knee simulator (KSem; Simulation Solutions, Stockport, UK) was used to measure the wear behaviour of the six artificially aged small sized BOX® ankles. KSem consisted of six stations divided across two banks (Figure 32) and the implants were set up in an inverted position. To facilitate the different implant size, six new delrin fixtures were designed and manufactured to ensure the talar component aligned with the centre of rotation (Appendix A.3). A comparison study analysing the two simulator types in terms of implant wear, topographic changes and kinematic performance, is discussed in Chapter 4.



Figure 32. Three stations of the ProSim electromechanically driven knee simulator (KSem; Simulation Solutions, Stockport, UK).

The calibration process varied between the two simulator types. In order to calibrate the AL channel of the six-axis load cell in KSem, a calibrated load cell was inserted into each station and mounted centrally on the FE rocker (Figure 33A). The abduction/adduction and ML slide was removed and replaced with a steel cap, to protect the top of the load cell. A threaded rod was screwed into the calibrated load cell and the steel-ball bearing on the end of the rod pressed on the pressure plate at each station of KSem (Figure 33A). The threaded rod replaced the delrin

block method used in KSpn (Section 2.3.6). The cam box applied a load to the calibrated load cell and the load was entered into the simulator. A similar method was used to calibrate the FE torque and abduction/adduction torque channels of the six-axis load cell. The process was repeated until five load measurements of increasing value had been applied.

To calibrate simulator AP force, the calibrated load cell was mounted on a right-angled bracket attached to the FE rocker (Figure 33B). Two load springs attached to the load cell sensor were pressed against the internal walls of the u-shaped bracket, attached to the multi-axis load cell (Figure 33B). During AP force calibration, movement in the posterior direction applied a compressive force to the anterior spring attached to the calibrated load sensor, resulting in a negative value. This process was repeated until all five loads had been applied. When the posterior spring was compressed, the force entered into the simulator was positive. It should be noted that both KSpn and KSem were unable to provide AP force feedback under displacement control, but was still calibrated to complete the full calibration report (Appendix C). The ML channel of the six-axis load cell was calibrated in the same way as the AP channel, except the load cell was rotated 90° prior to calibration.

The calibration jig used for calibrating the tibial rotation torque channel of the six-axis load cell is shown in Figure 33C. The calibrated load cell was fixed on the right side of the abduction/adduction rocker and was connected by two load springs, which were wound out to their maximum and adjusted until the calibrated load cell read zero (the zero position). The AP slide moved in a posterior direction, applying tension force to the anterior spring attached to the calibrated load cell sensor, resulting in a clockwise (negative) tibial rotation torque. A positive torque was produced when the AP slide moved in an anterior direction. The process was repeated until five measurements of increasing value had been applied.

The calibration of the AP linear position sensors within the simulator was achieved by scaling the output of the sensor against known positions of the sensor using slip gauges (Figure 33D). The central (zero) position of the AP slide was determined by a 60mm slip gauge positioned between the front edge of the slide and the machined front side of the abduction/adduction carriage (Figure 33D). To begin the calibration, an 80mm slip gauge was positioned in place, which corresponded to an actual position of 20mm. This process was repeated with slip gauges of 70mm, 60mm, 50mm and 40mm, which corresponded with the actual 10mm, 0mm, -10mm and -20mm, respectively. The same digital inclinometer used in the implant size study (Section 2.3.6), was placed on the FE carriage to give an angular readout of the carriage position. An example of the simulator calibration report for station 1 of the KSem, used in the artificially aged study, can be found in Appendix B, while the simulator calibration record for the aged study is detailed in Appendix C.4.

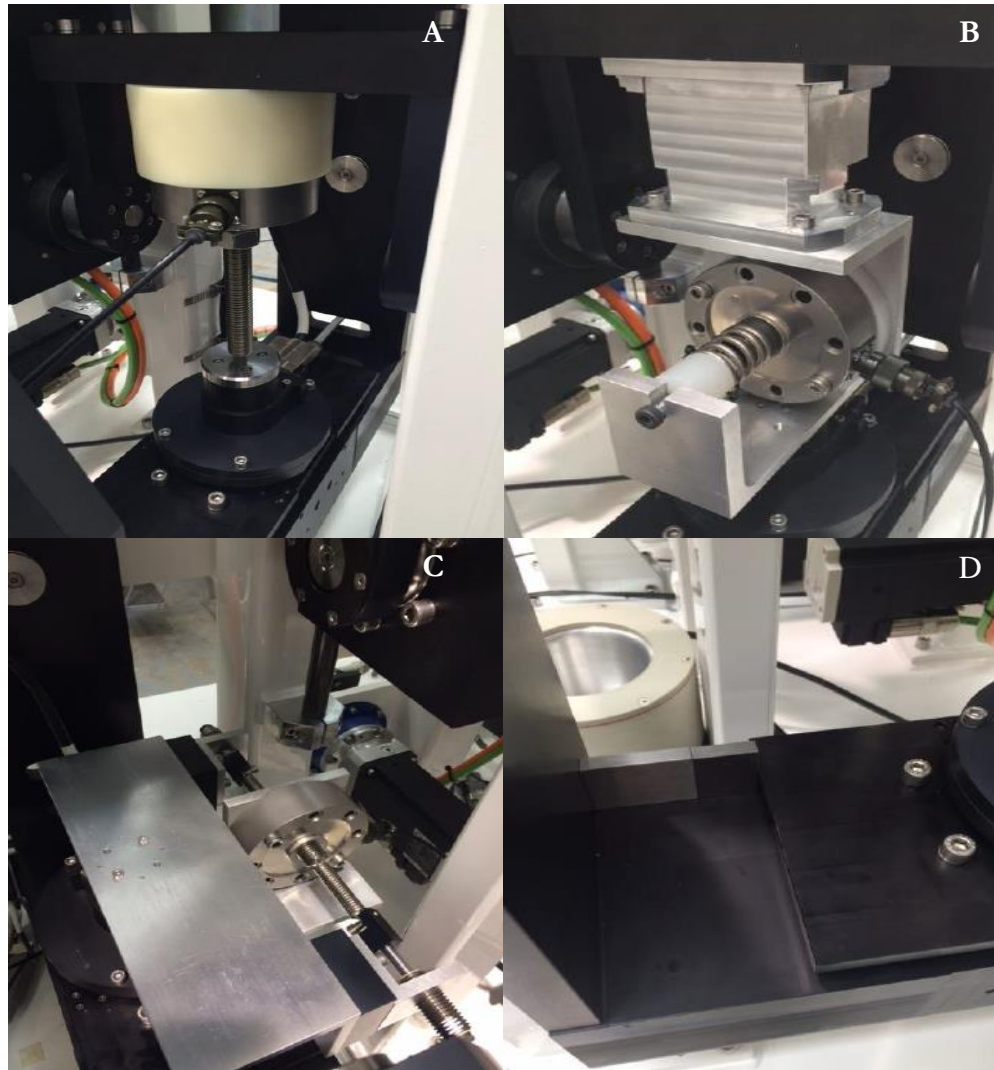


Figure 33. ProSim Electromechanical Knee Simulator (KSem): (A) AL, FE torque and abduction/adduction torque; (B) AP force; (C) tibial rotation torque; and (D) AP linear position.

### 3.2.3 Simulator Inputs

#### Implant Size

At the time of the study, there were no ISO standard guidelines for the wear simulation of a TAR. Therefore, the physiologically relevant loading and motion profiles were defined from a recent TAR wear study performed at the UoL (Smyth et al., 2017) and is referred to as the UoL profile. The description of each input profile is detailed in Section 2.3.1.

#### Accelerated Artificial Ageing

Before this study began, a new ISO standard for studying the wear behaviour of TAR devices under loading and displacement control parameters was introduced (ISO 22622:2019). This study used the recommended kinematic and loading parameters for displacement control from ISO 22622:2019 (Figure 34), but continued to use the same experimental conditions discussed in Chapter 2. This allowed more comparable wear results between implant parameter studies and

to previous work performed at the UoL (Smyth et al., 2017). A study comparing implant wear under ISO 22622:2019 and UoL input profiles is detailed in Chapter 4.

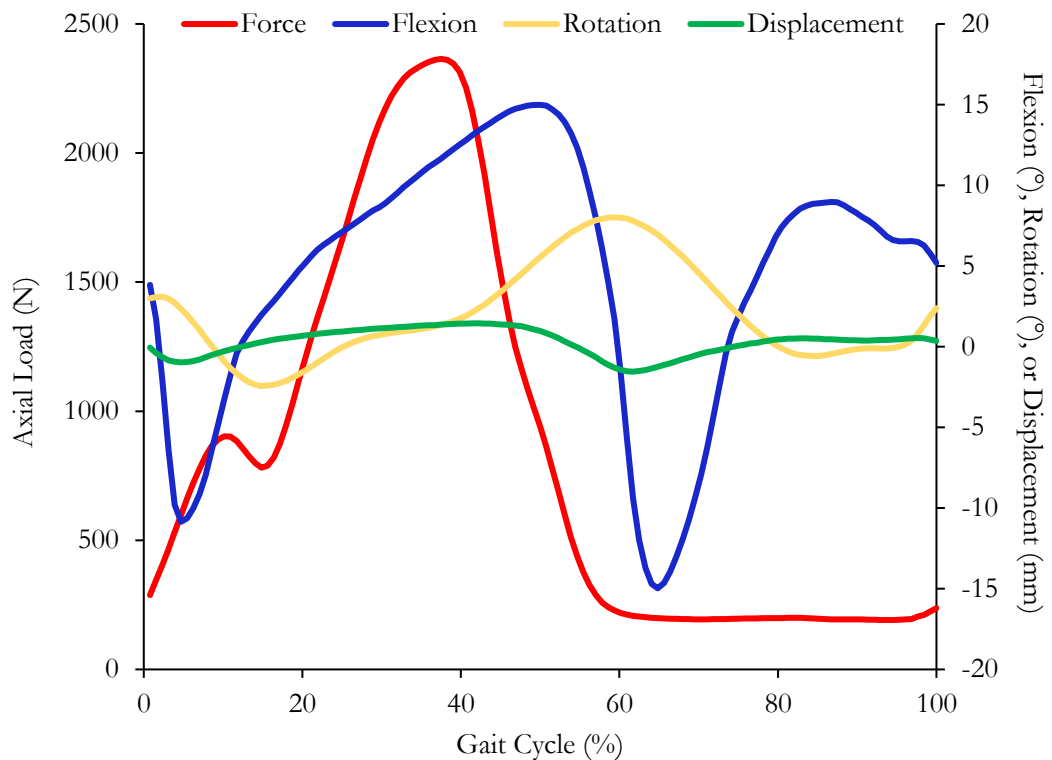


Figure 34. ISO standard input profiles for AL (red), FE angle (blue), tibial IER angle (yellow), and AP displacement (green). Adapted from ISO 22622:2019.

### 3.3 Methods

Chapter 2 provides more detail on the experimental conditions used to determine the wear behaviour of the MB device, independent of implant parameter. The medium ( $n = 6$ ) and extra small ( $n = 6$ ) implants used in the implant size comparison study were run for 5 Mc (two simulations of  $n = 3$  for both implant sizes) in KSpn. Four unloaded soak controls (two of each insert size) were used to negate weight changes due to fluid absorption (Galvin et al., 2009). The small ( $n = 6$ ) artificially aged implants also underwent 5 Mc of the same experimental conditions (Chapter 2) and used one unloaded soak control.

Before the wear simulation of the small sized inserts, the samples underwent the accelerated artificial ageing process as outlined in ASTM F2003:2015 and ISO 5834-3:2019. The inserts were removed from their packaging and positioned in a thermal chamber, in such a way that ensured uniform access of the articulating surfaces to oxygen. The thermal chamber was validated using a calibrated temperature sensor to within  $\pm 1^\circ\text{C}$  of the ageing temperature. A pressure vessel (oxygen bomb) enclosed the inserts and was calibrated to maintain the desired value, when at equilibrium, to an accuracy of  $\pm 7\text{ kPa}$  ( $\pm 1\text{ psi}$ ). The pressure vessel was filled at room temperature and purged with oxygen for a minimum of three times before the initiation of the

ageing experiment. The pressure vessel began at room temperature ( $23 \pm 2^\circ\text{C}$ ) and was raised incrementally ( $1.0^\circ \pm 0.1^\circ\text{C}/\text{min}$ ) to the ageing temperature of  $70 \pm 1^\circ\text{C}$ . The conventional UHMWPE inserts were aged at this constant temperature and pressurised at  $503 \pm 7 \text{ kPa}$  (73 psi, 5 atmospheres) of pure oxygen for  $336 \pm 1 \text{ h}$  (14 days). There were no interruptions during the ageing period, which meant that the pressure vessel remained closed for the 14 day duration.

Both implant parameter studies were run under displacement control with an operating frequency of 1 Hz. The samples were moved between stations at the beginning of each Mc to account for inter-station variability. Contact area checks were performed to ensure similar component positioning across stations (Section 2.3.5). The lubricant consisted of 25% bovine serum supplemented with 0.04% sodium azide to prevent bacterial degradation (Smyth et al., 2017). The protein concentration for the implant study was 16.00g/L (Appendix D.1) and 15.75g/L for the artificial ageing study (Appendix D.3). The serum was replaced approximately every 330,000 cycles to ensure the continued protein concentration was maintained (Section 2.3.9).

Digital images of the superior insert wear imprint on the tibial components were obtained upon completion of the implant size study, using a Kodak DX6490 digital camera. The mean contact wear area, expressed as the percentage cover of the UHMWPE superior insert surface wear imprint over the tibial component surface, was quantified using Image Pro-Plus 3.0 software (Media Cybernetics, Maryland, USA). This technique was used to determine the influence of implant size on contact wear area and subsequent implant wear rate.

As previously mentioned in Section 2.4, implant wear was determined gravimetrically after each Mc. Loading and kinematic output profiles were recorded automatically every 20,000 cycles and averaged across the six stations, giving an overall average output profile of 50 cycles at 1 Mc intervals. Simulator loading and kinematic performance for both implant parameter studies were investigated by comparing the average peak output values for the stations against the peak demanded input values. The differences between the output and input kinematic profiles were calculated as a percentage of the corresponding maximum demanded value and compared to the maximum tolerance of the output kinematics ( $\pm 5\%$ ) (Section 2.6). Both simulators used in the implant parameter studies underwent PID control tuning to reduce inter-station variability and to ensure that each profile was being reproduced to the simulators best ability. Contact surface measurements were taken before and after each simulator study to understand the topographic changes at the bearing surfaces (Section 2.7). The articulating surfaces were visually inspected to determine the extent of damage and modes of wear that were present during wear simulations of the varying TAR sizes (Section 2.8). The damage modes found on the samples that underwent wear simulation were also compared to MB TAR retrievals (Section 2.9).

The mean wear rate and surface roughness parameters were calculated with a 95% CL for both implant parameter studies. A student's (independent) t-test was used to compare the mean wear

rates and topographic changes within the implant size comparison study. A one-way analysis of variance (ANOVA) was used to determine statistical differences in mean wear rates between aged and unaged implants in the accelerated artificially aged study. If statistical significance was shown then a Bonferroni post hoc test was conducted to determine significant differences between the aged and unaged samples. Paired (dependent) t-tests were used to determine statistical differences between run-in and steady-state wear phases within the same device size and also between the pre- and post-mean topographic parameter values for both implant parameter studies. Significance level was accepted at the  $p \leq 0.05$  level and all statistical analysis was conducted using Statistical Package for the Social Sciences (SPSS) version 26.0 (SPSS Inc, Chicago, USA).

### **3.4 Results**

#### **3.4.1 Simulator Loading and Kinematic Performance**

##### **Implant Size**

Figure 35 displays the differences between the mean loading and kinematic output profiles (for all six stations) and the UoL simulator input profiles (Smyth et al., 2017). The four graphs within Figure 36 presents the loading and kinematic output profile variance between each station during the second simulation period of 5 Mc (medium = 3 and extra small = 3).

During the stance phase, each station of KSpn were unable to facilitate the desired peak demand AL of 3150 N (Figure 36A). This resulted in a reduced mean peak AL of  $2542.3 \pm 86.5$  N and was outside of the maximum tolerance ( $\pm 5\%$ ) of the desired peak AL input (-19.2%) (Figure 35A). Each of the six stations of KSpn also overloaded the peak swing phase load of 100 N ( $222.1 \pm 11.0$  N) (Figure 36A), with an oscillating profile throughout. The minimum output load recorded by the simulator was substantially higher than the maximum tolerance of the recommended swing phase load (112.1%). The pneumatic control system of KSpn could also not rapidly respond to the AL loading cycle, which resulted in a small lag when following the AL profile (Figure 36A).

The electromechanically controlled FE cradles for each station were capable of accurately following the input FE angle of  $\pm 15^\circ$  (plantarflexion:  $15.1 \pm 0.0^\circ$ ; dorsiflexion:  $-15.0 \pm 0.0^\circ$ ) (Figures 35B and 36B). The tight CL throughout the gait cycle demonstrated that the six stations behaved similarly and that peak plantarflexion (0.5%) and dorsiflexion (0.0%) were within the maximum output tolerance ( $\pm 5\%$ ). Due to the electromechanical control of FE and thus not being able to control the air supply, it meant that there was no associated phase lag between the desired FE input and output profiles of KSpn.

Station 1 produced a greater peak external rotation angle than the maximum input demand, while the five other stations did not achieve the desired peak value of  $8^\circ$  (Figure 36C). This resulted in a mean peak external rotation of  $7.2 \pm 0.1^\circ$ , with KSpn failing to remain within the maximum output tolerance for external rotation angle (-9.5%) (Figure 35C). There was also a clear phase

lag of around 0.05 seconds between the IER demand profile and simulator IER output profiles from all six stations (Figure 36C).

Each station of KSpn had an apparent phase lag in AP displacement motion and seemed to occur after peak AL rather than being in-phase with the input load (Figure 36D). Three of the simulator stations (2, 5 and 6) produced greater anterior displacement, while the remaining three stations (1, 3 and 4) produced lower peak anterior displacement than the demand input value of 3.1 mm (Figure 36D). This resulted in a mean peak output value of  $3.6 \pm 1.0$  mm and was outside of the maximum output tolerance (10.2%) for peak AP displacement (Figure 35D).

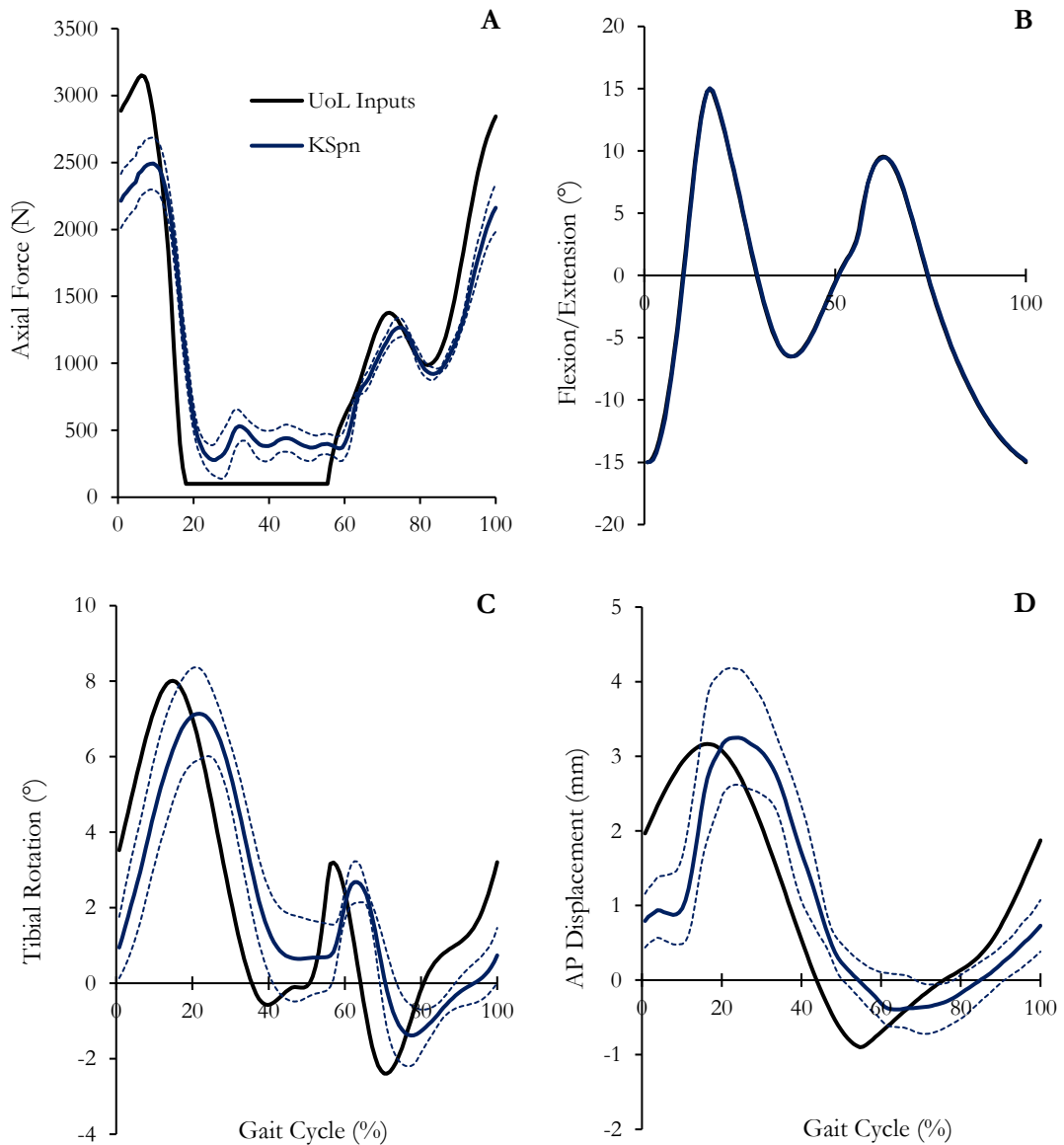


Figure 35. Simulator input (black) and output profiles (blue) (mean  $\pm$  95% CL, n = 6) across all stations for AL (A), FE angle (B), tibial IER angle (C) and AP displacement (D).

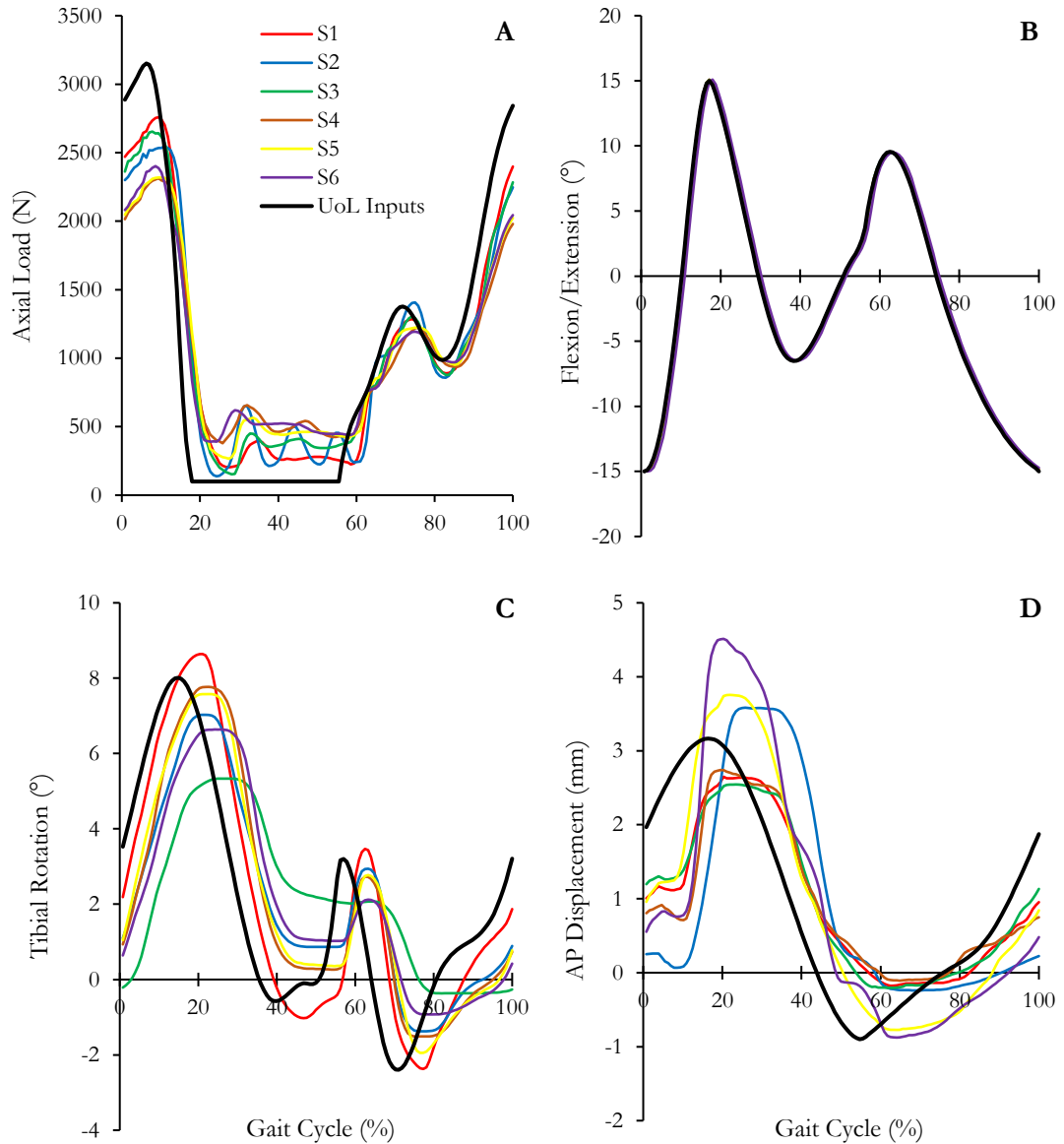


Figure 36. Simulator input (black) and output profiles for each station of KSpn for AL (A), FE angle (B), tibial IER angle (C) and AP displacement (D).

### **Accelerated Artificial Ageing**

During the final serum change between 0-1 Mc, one of the bearing inserts (sample 4 in station 4) was damaged during set-up. The insert dislocated when the load was applied at the station, which was likely due to the insert not being positioned centrally on the tibial bearing surface. This caused metal-on-metal contact, and although the simulator was immediately stopped, the surface damage was significant. Therefore, the sample was removed from the study, leaving a sample of five small sized aged implants.

Figure 37 displays the mean ( $\pm$  95% CL) output loading and kinematic profiles of KSem compared to the simulator inputs defined by ISO 22622:2019. Figure 38 presents the inter-station variability across the six stations in terms of loading and kinematic output profiles, compared against the ISO 22622:2019 desired input profiles. The mean output loading profile from the six

stations of KSem was comparable to the desired input AL and was able to attain the peak AL value during heel-strike ( $2395.5 \pm 5.9$  N compared to 2365.7 N) (Figure 37A). The simulator achieved the recommended peak AL within the maximum output tolerance (1.3%) of  $\pm 5\%$ . The substantial difference between loading input and output profiles occurred during the period of simulation aiming to mimic swing phase load (Figure 37A). Each station produced a slightly lower load ( $120.1 \pm 7.3$  N) compared to the desired minimum load value (191.5 N) (Figure 38A). They also produced an oscillating profile throughout swing and failed to remain within the desired maximum output tolerance of the ISO 22622:2019 loading profile (-37.3%) (Figure 38A).

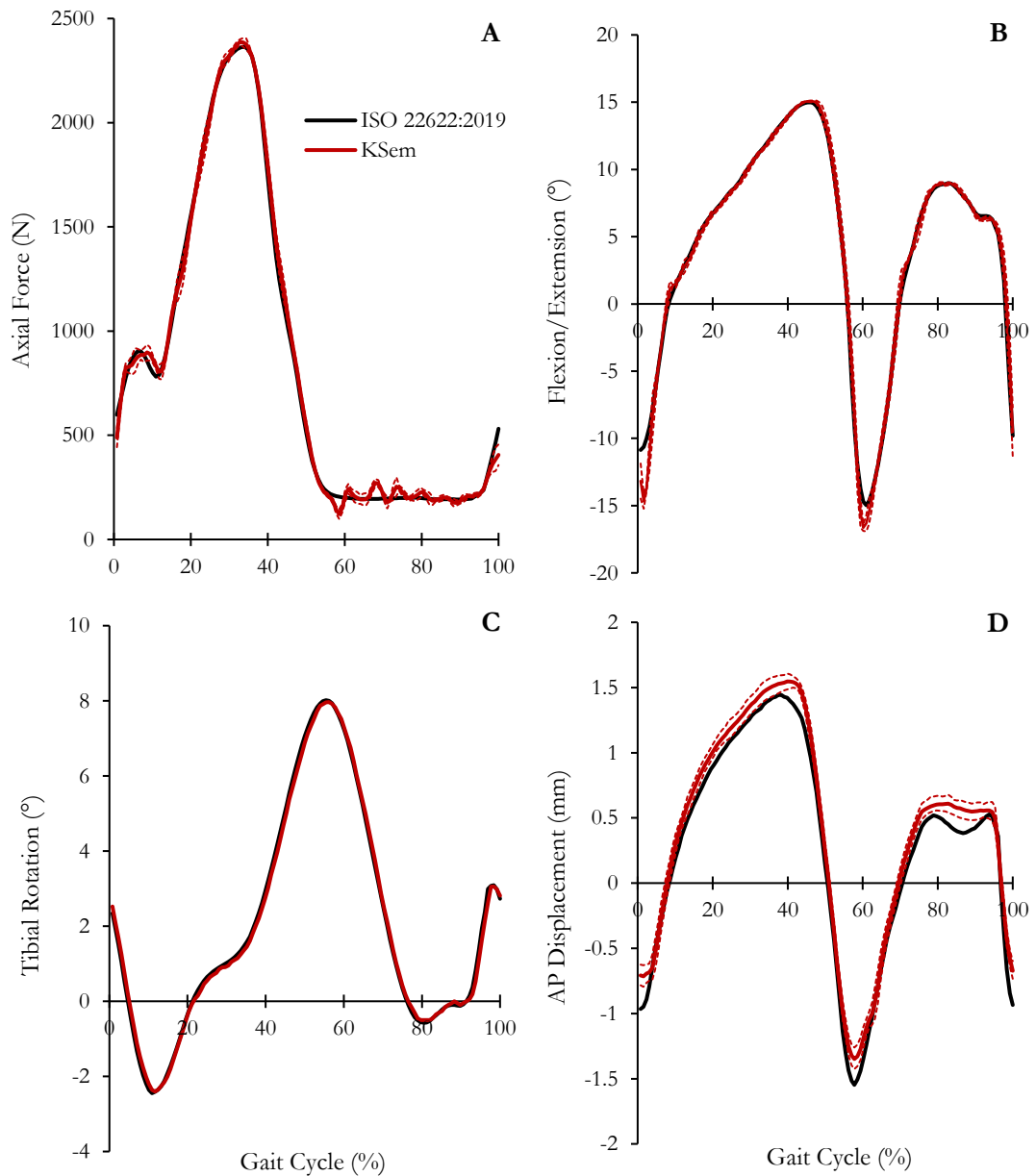


Figure 37. Simulator inputs (black) and average outputs (red) (mean  $\pm$  95% CL,  $n = 5$ ) across all the stations for AL (A), FE angle (B), tibial IER angle (C) and AP displacement (D).

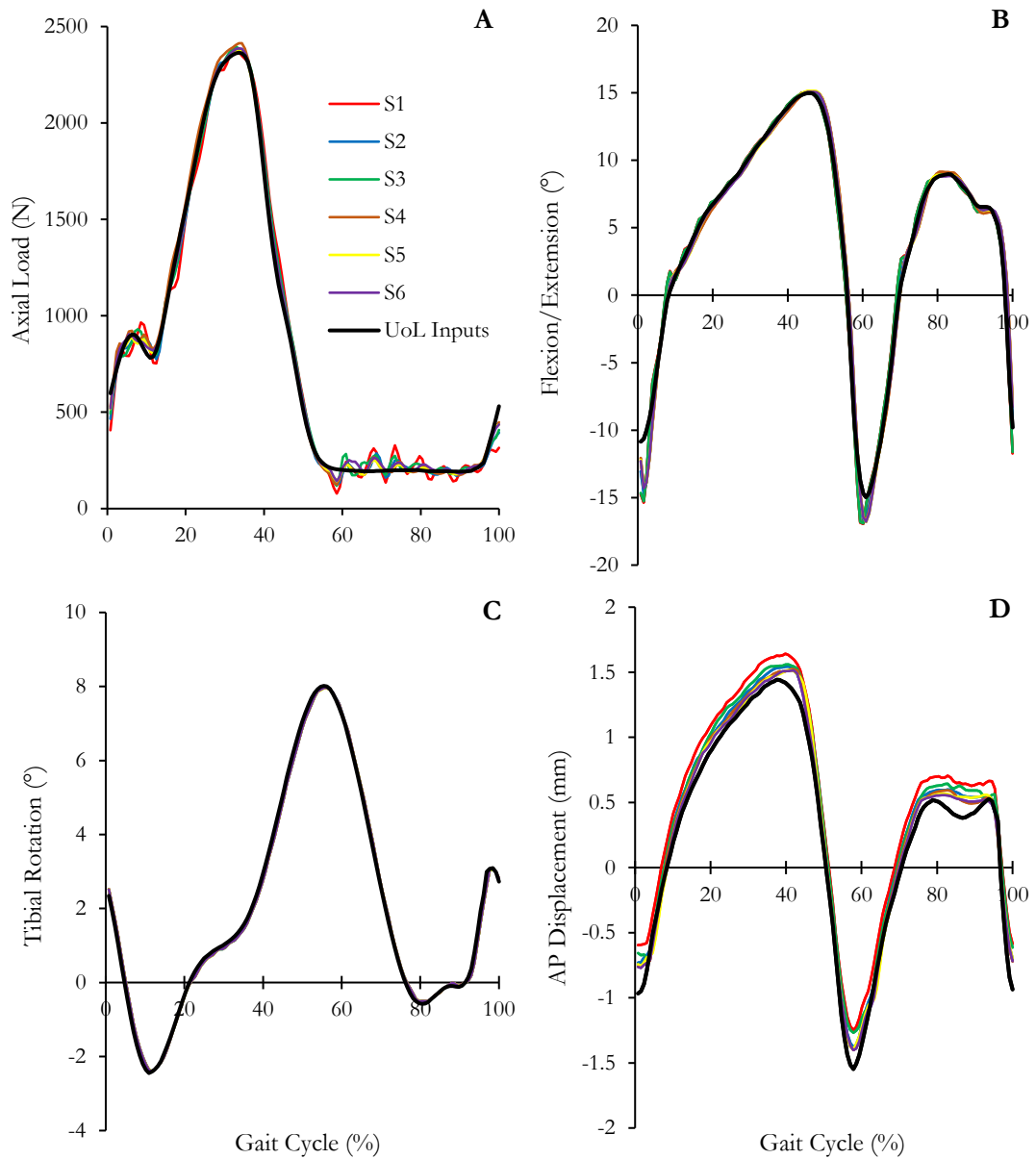


Figure 38. Simulator input (black) and output profiles for each station of KSem for AL (A), FE angle (B), tibial IER angle (C) and AP displacement (D).

Tibial IER was the most closely followed kinematic profile for each station, with limited inter-station variability throughout the 5 Mc (Figure 38C). There was also no apparent phase lag between input and output profiles from any of the stations within KSem. Peak internal ( $8.0 \pm 0.0^\circ$ ) and external ( $-2.4 \pm 0.0^\circ$ ) rotation angles were comparable to the desired input values of  $8.02^\circ$  and  $-2.4^\circ$ , respectively (Figure 37C). Both peak internal ( $-0.7\%$ ) and external ( $-1.8\%$ ) tibial rotation was attained within the maximum output tolerance of the desired peak IER values. Each of the stations of the KSem produced slightly higher anterior translation ( $1.6 \pm 0.0$  mm) than the peak input demand (1.45 mm), resulting in KSem not being within the maximum output tolerance (6.9%) (Figure 38D). Furthermore, all stations failed to attain the desired posterior translation of -1.55 ( $-1.4 \pm 0.1$  mm;  $-11.9\%$ ). Unlike KSpn, there was no apparent phase lag, with peak anterior translation occurring at the same time as peak AL (Figure 37D).

### 3.4.2 Wear Rate Comparison

#### Implant Size

The cumulative and mean wear rates ( $\pm 95\%$  CL) for the medium and extra small sized implants in KSpn are shown in Figures 39 and 40, respectively. Under the same experimental conditions and UoL input profiles (Smyth et al., 2017), there was no statistically significant difference ( $p = 0.872$ ) in the mean wear rate between implant size (medium =  $11.00 \pm 3.06 \text{ mm}^3/\text{Mc}$ ; extra small =  $10.64 \pm 4.61 \text{ mm}^3/\text{Mc}$ ) (Figure 40). The cumulative volumetric wear graph for both implant sizes shows the presence of an initial increased wear period during the first Mc (Figure 39). Therefore, the gravimetric wear measurements were further separated into two wear phases: initial run-in phase (0-1 Mc) and steady-state phase (1-5 Mc).

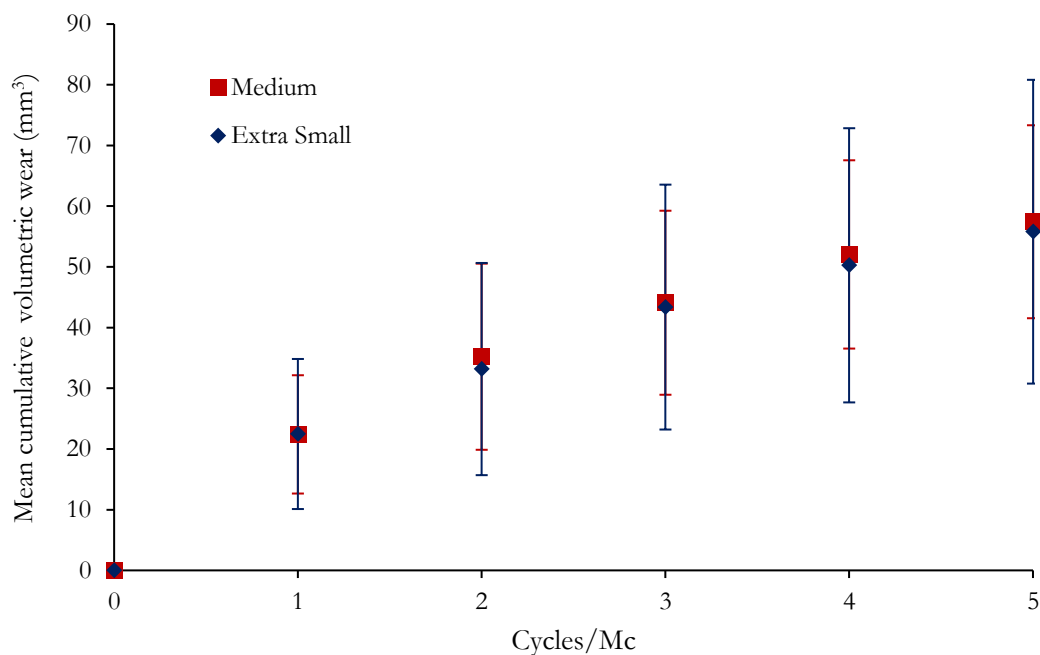


Figure 39. Cumulative mean wear rates ( $\text{mm}^3$ ) with  $\pm 95\%$  CL for the medium (red) and extra small (blue) sized implants after 5 Mc ( $n = 6$  for both implant sizes).

During the run-in wear phase, there was no significant difference ( $p = 0.992$ ) in mean wear rate between implant sizes (medium =  $22.40 \pm 9.74 \text{ mm}^3/\text{Mc}$  and extra small =  $22.47 \pm 12.36 \text{ mm}^3/\text{Mc}$ ) (Figure 40). The high CL found during the run-in wear phase for both medium and extra small implant sizes indicated that there was variation in the wear rates between individual inserts. After the initial run-in phase, the wear rate reduced significantly during the steady-state phase to  $7.21 \pm 2.25 \text{ mm}^3/\text{Mc}$  ( $p = 0.003$ ) and  $6.91 \pm 2.84 \text{ mm}^3/\text{Mc}$  ( $p = 0.010$ ) for the medium and extra small sized implants, respectively (Figure 40). Similar to the run-in wear phase comparison, there was no significant difference ( $p = 0.835$ ) in steady-state wear between the implant sizes. The mean contact wear area, expressed as the UHWMPE superior inserts wear imprint over the overall tibial component surfaces, were also comparable between implant sizes

( $p = 0.225$ ; medium:  $70.09\% \pm 5.57\%$ ; extra small:  $67.22\% \pm 6.54\%$ ), owing to the identical bearing design.

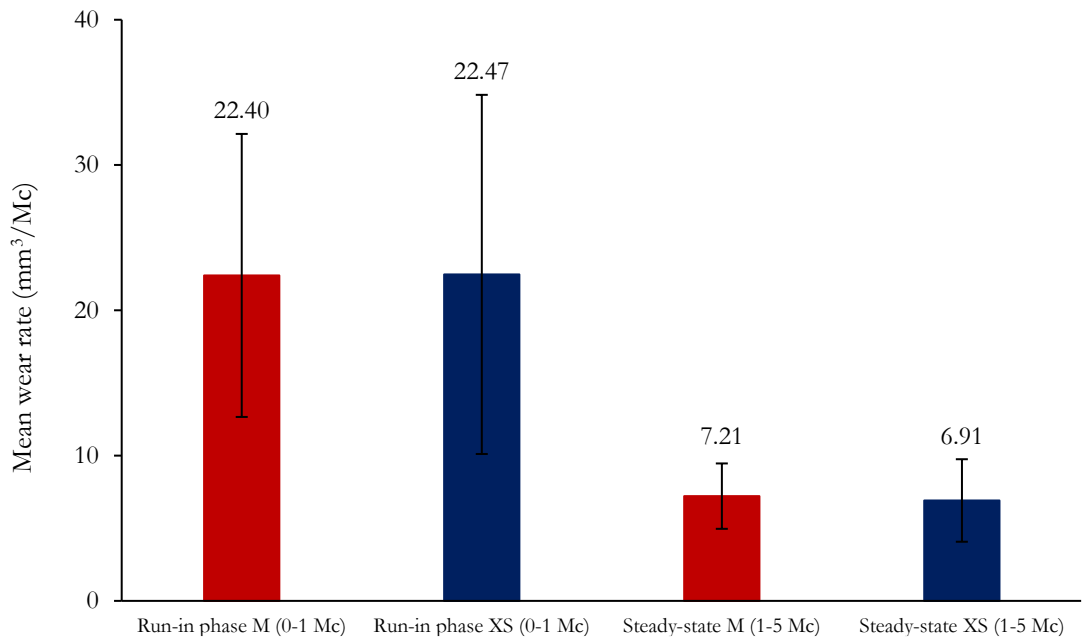


Figure 40. Mean run-in and steady-state wear rate ( $\text{mm}^3/\text{Mc}$ ) with  $\pm 95\%$  CL for the medium (M; red) and extra small (XS; blue) implants after 5 Mc ( $n = 6$  for each implant size).

The inter-station variability and volumetric wear for inserts in the second half of simulation for both implant sizes ( $n = 3$ ) is shown in Figure 41. Station 4 was found to produce a substantially lower initial run-in wear rate ( $8.65 \text{ mm}^3$ ) compared to the other five samples (Figure 41). However, this effect was not sustained throughout the steady-state wear phase.

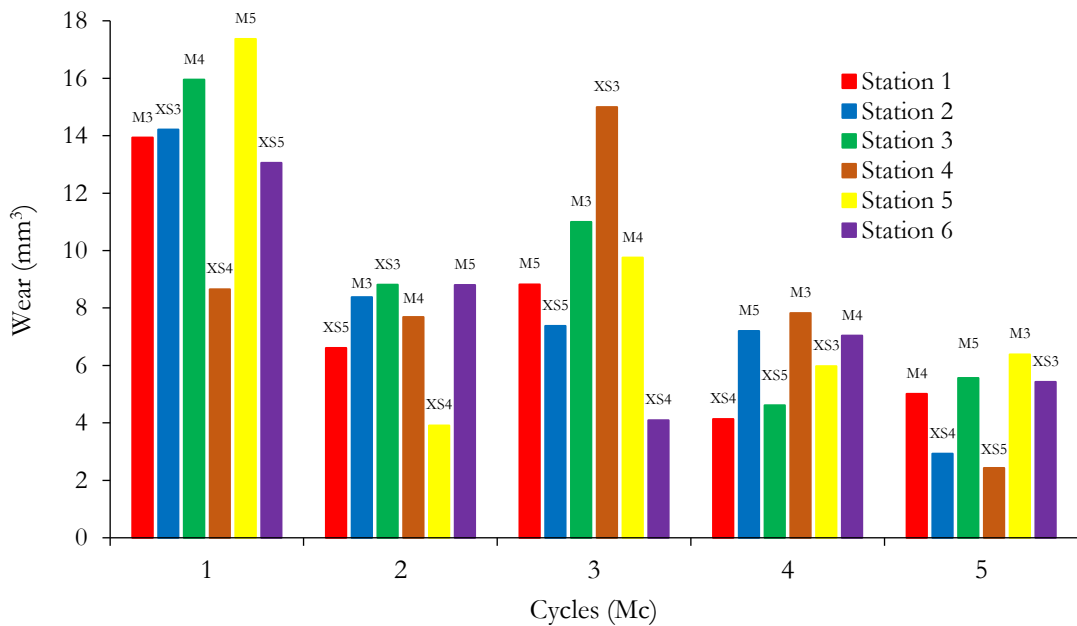


Figure 41. Individual wear rates for the medium (M) and extra small (XS) sized inserts during each Mc ( $n = 6$  for both implant sizes), with the colours representing the station within the pneumatic simulator.

During this phase, sample 3 (extra small) was found to have a considerably higher wear rate (14.99 mm<sup>3</sup>) in station 4 during 2-3 Mc when compared to the other five samples being examined. The wear rate did not remain high and they returned to be comparable with the other samples. Despite station 1 producing a substantially higher peak external rotation angle than the intended input profile, this was not apparent in the individual wear rates across stations.

### **Accelerated Artificial Ageing**

Chapter 4 indicated that there were no statistically significant differences between simulator type and input profiles on wear rates of the MB implant. Therefore, the mean wear rates from the small sized artificially aged implants, which underwent wear simulation in KSem using ISO 22622:2019, were compared against the non-aged medium and extra-small sized implants. As mentioned earlier, these unaged implants were simulated within KSpn under UoL input profiles (Smyth et al., 2017), but both implant parameter studies used the same experimental conditions.

The cumulative and mean wear rates ( $\pm$  95% CL) for the accelerated artificially aged implants are shown in Figures 42 and 43, respectively. Despite the higher overall mean wear rate, there was no statistically significant differences between the small sized artificially aged implants ( $16.98 \pm 5.31$  mm<sup>3</sup>/Mc) and to both the medium ( $11.00 \pm 3.06$  mm<sup>3</sup>/Mc;  $p = 0.071$ ) and extra small ( $10.64 \pm 4.61$  mm<sup>3</sup>/Mc;  $p = 0.053$ ) unaged implants. There was no significant differences in mean run-in wear phase rates between the aged ( $24.86 \pm 5.71$  mm<sup>3</sup>/Mc) and unaged (medium =  $22.40 \pm 9.74$  mm<sup>3</sup>/Mc;  $p = 1.000$  and extra small =  $22.47 \pm 12.36$  mm<sup>3</sup>/Mc;  $p = 1.000$ ) implants. After the initial run-in wear phase, the wear rate significantly reduced ( $p = 0.001$ ) during the steady-state phase to  $12.53 \pm 4.34$  mm<sup>3</sup>/Mc. This finding was also apparent for both unaged implant sizes. The steady-state wear rate was significantly higher than both the unaged medium ( $7.21 \pm 2.25$  mm<sup>3</sup>/Mc;  $p = 0.015$ ) and extra small ( $6.91 \pm 2.84$  mm<sup>3</sup>/Mc;  $p = 0.021$ ) implants.

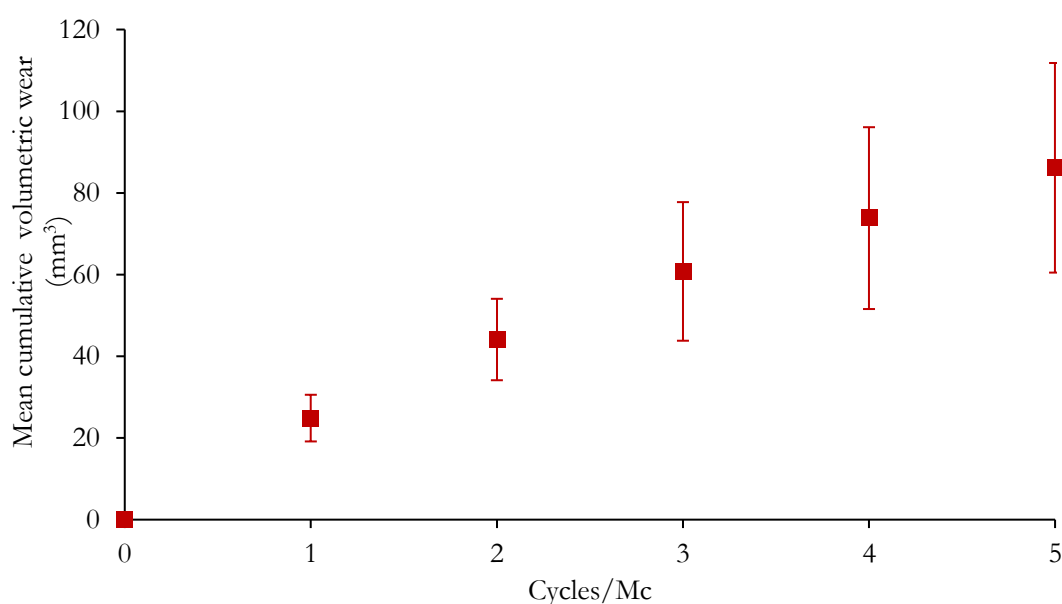


Figure 42. Cumulative mean wear rates (mm<sup>3</sup>) with  $\pm$ 95% CL for the small sized artificially aged implants after 5 Mc (n = 5).

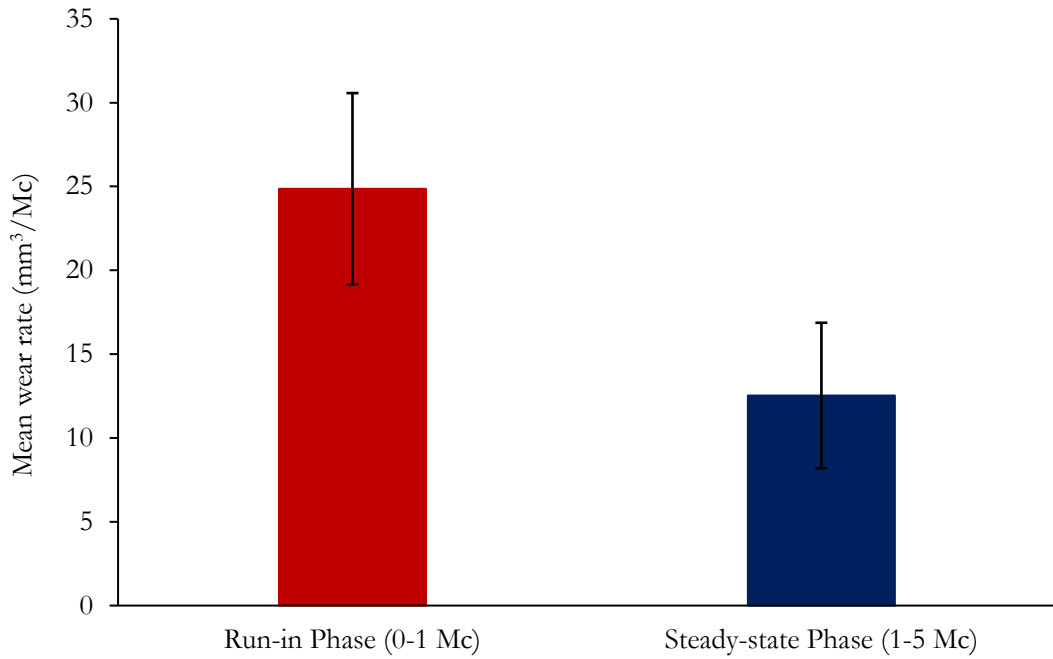


Figure 43. Mean run-in (red) and steady-state (blue) wear rate (mm<sup>3</sup>/Mc) with  $\pm$  95% CL for the small artificially aged implants after 5 Mc (n = 5).

Despite the improved loading and kinematic following in KSem compared to KSpn (Chapter 4), there was still variation in wear rates between individual insert samples (Figure 44). This variation in wear was seen to be substantially higher during the run-in wear phase (Figure 42). Station 1 (31.49 mm<sup>3</sup>) and 3 (26.94 mm<sup>3</sup>) produced noticeably higher wear rates compared to the other specimens, but this effect was not sustained throughout the further Mc's (steady-state wear).

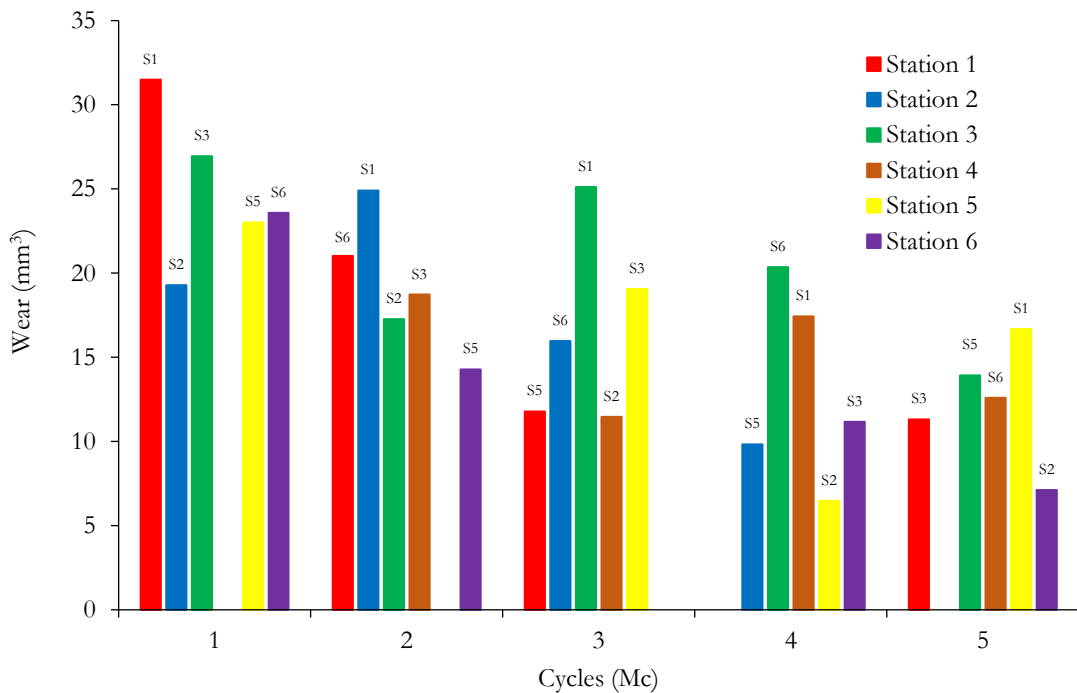


Figure 44. Individual wear rates for the small sized artificially aged inserts during each Mc (n = 5), with the colours representing the station within the pneumatic simulator.

### 3.4.3 Surface Topographic Results

#### Implant Size

The mean ( $\pm$  95% CL) surface topographic parameters for the medium and extra small implants is located in Appendix E.1. Five representative (2D) traces were taken across each of the bearing surfaces before and after wear simulation to determine each of the topographical parameters (Figure 45). The values across the five traces were then averaged to determine the overall topographical change across the bearing surface. The five traces presented in Figure 45 were from one of the medium insert surfaces at 5 Mc, but represent similar output traces for each implant size throughout the simulator studies, independent of artificial ageing, simulator type or simulator inputs.

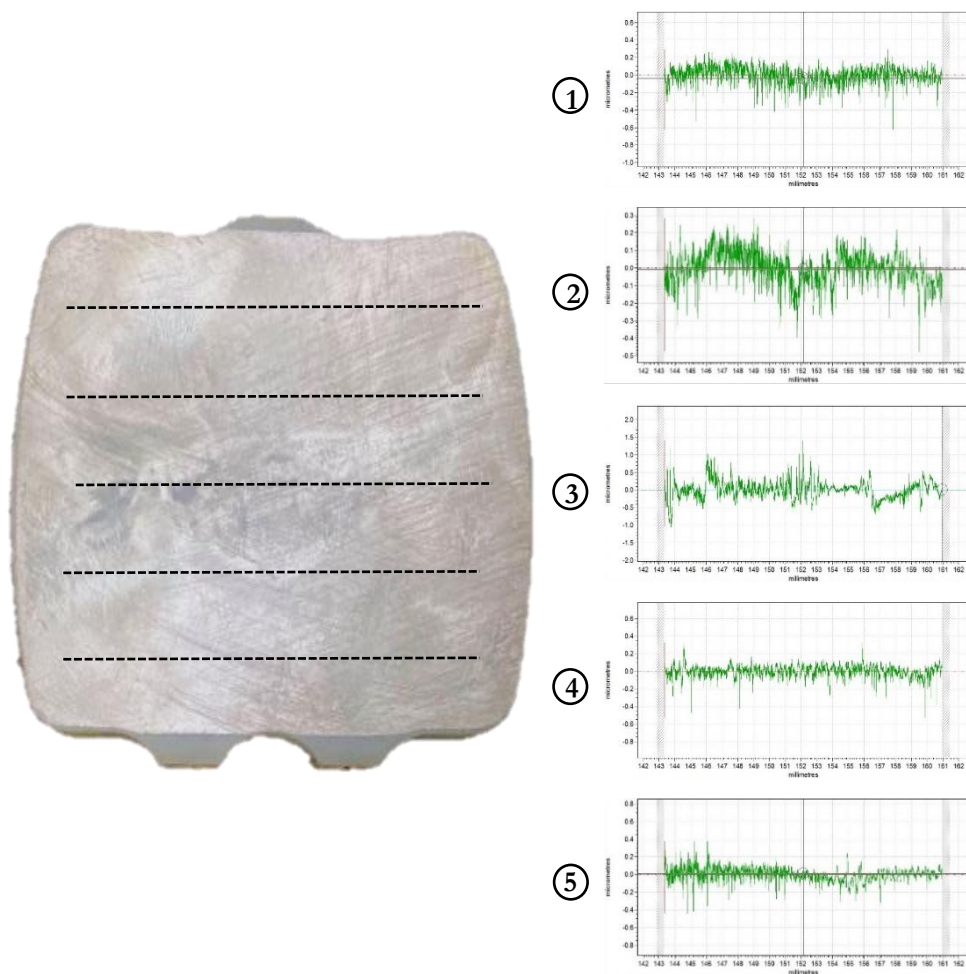


Figure 45. Five representative (two-dimensional) traces across the superior insert bearing surface used to determine the topographical parameters.

Prior to the start of wear simulation, there were no significant differences ( $p \geq 0.05$ ) in topographic parameters of the unworn articulating surfaces between the medium and extra small sized implants. Therefore, the post-simulation topographic mean measurements were compared between implant sizes, as well as comparing between the pre- and post-values.

### ***Average Surface Roughness (Ra)***

In general, roughness of the metallic components increased whereas roughness of the UHMWPE inserts decreased. The most notable change in Ra was seen on the superior insert surface, with a 92.03% ( $p = 0.000$ ) and 88.81% ( $p = 0.000$ ) decrease in Ra for the medium and extra small inserts, respectively. The medial, central and lateral regions of the inferior insert curved surfaces showed significant reductions in Ra for both implant sizes. This reduction in Ra for both insert bearing surfaces indicated that the peaks had flattened, which was likely due to the removal of the machining lines and polishing of the surface (burnishing) during the continued articulation within the wear simulator (Section 3.4.4). There was a significant increase in Ra at the tibial bearing surfaces between the pre- and post-simulation values (medium = 200.00%;  $p = 0.046$  and extra small = 100.00%;  $p = 0.006$ ). The central talar region of the medium inserts (100.00%;  $p = 0.030$ ) and medial talar region of the extra small inserts (50.00%;  $p = 0.036$ ) also exhibited significant differences in Ra after 5 Mc. However, there was no significant differences ( $p \geq 0.05$ ) in Ra for the articulating metallic and polyethylene bearing surfaces between implant sizes after 5 Mc.

### ***Maximum Profile Peak Heights (Rp)***

There were no significant differences ( $p \geq 0.05$ ) in Rp between the bearing surfaces of both implant sizes after 5 Mc. The Rp was found to increase for the metallic components but decrease for the conventional UHMWPE insert surfaces. The superior insert surface possessed the greatest significant reduction in Rp after simulation, with a 91.60% and 89.38% decrease in Rp for the medium ( $p = 0.000$ ) and extra small ( $p = 0.000$ ) inserts, respectively. All three regions of the inferior insert surfaces of both implant sizes also produced significant reductions in Rp. There was a significantly increased Rp value for the tibial articulating surface for the extra small insert between pre- and post-simulation (50.00%;  $p = 0.047$ ). Following a comparable trend to Ra results, the central region from the talar surface of the medium inserts (133.33%;  $p = 0.029$ ) was significantly higher at post-simulation.

### ***Maximum Profile Valley Depth (Rv)***

Comparing the values of the deepest valley on the articulating surfaces, there was no significant differences in Rv between implant sizes ( $p \geq 0.05$ ) before and after wear simulation. The superior insert of both implant sizes demonstrated the highest reduction in Rv, with the medium and extra small inserts exhibited an 87.95% ( $p = 0.000$ ) and 85.29% ( $p = 0.000$ ) significant decrease in Rv. A similar pattern was seen in the inferior insert surfaces of both implant sizes, with a significant decrease in Rv in all three bearing regions. Both tibial articulating surfaces from both implant sizes had significantly higher Rv after 5 Mc (medium = 100.00%;  $p = 0.026$  and extra small = 120.00%;  $p = 0.002$ ), while only the central region of the talar articulating surfaces from the medium sized inserts were significantly higher ( $p = 0.036$ ).

### ***Surface Skewness (Rsk)***

Each articulating surface showed a negative skewness after 5 Mc, with the metallic bearing surfaces demonstrating the greatest change in Rsk. The superior insert surfaces possessed the greatest significant decrease in Rsk for the medium (1200.00%;  $p = 0.026$ ) and extra small (311.11%;  $p = 0.044$ ) insert surfaces. Each of the inferior insert articulating surface regions also had significantly lower ( $p \leq 0.05$ ) values post-simulation for the medium and extra small inserts. Only the tibial articulating surface from the medium sized implants had significantly lower Rsk at 5 Mc compared to the pre-simulation topographic measurement (878.95%;  $p = 0.026$ ). Both central regions of the talar articulating surface from both implant sizes were significantly lower post-simulation ( $p \leq 0.05$ ).

### ***Surface Kurtosis (Rku)***

Each bearing surface had an increased Rku value after 5 Mc, however, there was no significant differences ( $p \geq 0.05$ ) in Rku between the implant sizes. There was a significant increase in Rku at the superior insert surface for the medium ( $p = 0.008$ ) and extra small ( $p = 0.001$ ) implant sizes. The central region of the inferior insert surface was significantly higher in the medium sized implants (66.00%;  $p = 0.006$ ), while the medial (33.59%;  $p = 0.041$ ) and central (110.74%;  $p = 0.010$ ) regions of inferior insert were significantly higher in the extra small implants. Each of the metallic bearing surfaces, apart from the medial region of the talus from the extra small implant, was significantly higher ( $p \leq 0.05$ ) after 5 Mc when compared to the pre-simulation values.

### **Accelerated Artificial Ageing**

The mean ( $\pm 95\%$  CL) surface topographic parameter results for the accelerated artificial aged small sized implants can be found in Appendix E.2.

### ***Average Surface Roughness (Ra)***

Both the metallic bearing surfaces possessed increased Ra, whereas roughness of the inserts decreased. The most notable change in Ra was seen at the superior insert surface, with a 93.10% significant decrease ( $p = 0.000$ ). The medial (60.32%;  $p = 0.000$ ), central (61.98%;  $p = 0.001$ ) and lateral (56.93%;  $p = 0.000$ ) regions of the inferior inserts also demonstrated significant reductions in Ra. Both the tibial (200.00%;  $p = 0.000$ ) and medial region of the talar (33.33%;  $p = 0.011$ ) surfaces produced significantly higher Ra after 5 Mc.

### ***Maximum Profile Peak Heights (Rp)***

The most significant Rp change was located at the superior insert surface, with a 91.67% ( $p = 0.000$ ) decrease. Each region of the inferior insert surface also demonstrated significant reductions in Rp (medial = 74.93%;  $p = 0.011$ , central = 53.56%;  $p = 0.011$ , lateral = 72.27%;  $p = 0.011$ ). The tibial surface presented significantly higher Rp across the articulating surface (28.57%;  $p = 0.017$ ), while each of the talar regions did not significantly change between pre- and post-simulation values ( $p \geq 0.05$ ).

### ***Maximum Profile Valley Depth (Rv)***

The superior insert surface was associated with the most wear, which subsequently led to a significant decrease in Rv (89.78%;  $p = 0.000$ ). There were also significant reductions in Rv for each of the three regions of the inferior insert surfaces (medial = 62.50%;  $p = 0.000$ , central = 28.27%;  $p = 0.024$ , lateral = 62.35%;  $p = 0.000$ ). Both the metallic tibial (120.00%;  $p = 0.026$ ) and lateral region of the talar surface (116.67%;  $p = 0.013$ ) had significantly higher Rv after 5 Mc.

### ***Surface Skewness (Rsk)***

Each articulating surface showed a negative skewness after 5 Mc, with the metallic bearing surfaces demonstrating the greatest change in Rsk. Both the tibial (1035.00%;  $p = 0.026$ ) and central region of the talar (360.71%;  $p = 0.023$ ) articulating surfaces were significantly lower at post-simulation. The medial (220.59%) and lateral (1018.18%) regions of the talar components also showed substantial reductions in Rsk, but due to the high variability and associated CL between samples, these differences were not statistically different to the pre-simulation values ( $p \geq 0.05$ ). This was also the case for the superior insert and medial region of the inferior insert surfaces ( $p \geq 0.05$ ).

### ***Surface Kurtosis (Rku)***

Each articulating surface had an increased Rku value after 5 Mc, with the superior insert surface showing the greatest significant increase post-simulation (908.86%;  $p = 0.005$ ). Both the tibial articulating surface (147.70%;  $p = 0.003$ ) and the central (345.37%;  $p = 0.034$ ) and lateral regions (327.27%;  $p = 0.009$ ) of the talar components produced significantly higher Rku post-simulation.

## **3.4.4 Superior Insert Visual Comparison**

### **Implant Size**

The greatest topographic changes occurred at the superior insert and can be explained by the visual damage seen on the insert surfaces (Figure 46). The continued articulation throughout the 5 Mc, independent of implant size, caused significant polishing and the removal of machining lines, demonstrating strong evidence of burnishing. Each superior insert surface from both implant size samples showed a clear indication of abrasive wear, pitting, material on the surface and multidirectional scratching (Figure 46). The inferior insert surfaces showed comparable visual damage modes, with signs of burnishing and scratching, but not as significant as that seen on the superior surface. This is likely due to the more curved bearing surfaces at the inferior insert and talar surface interface. On both insert surfaces, scratching was primarily orientated in the AP direction, which was consistent with the intended direction of articulation. However, there were clear signs of multi-directional scratching produced by tibial rotation (Figure 47).

Despite the reduced topographic changes measured for both metallic components compared to the conventional UHMWPE insert surfaces, there were still visible changes and damage modes present. On the tibial components there were visible outlines of the UHMWPE contact area on

the cast CoCrMo alloy surface. There were also obvious signs of adhesive wear and multidirectional scratching within the UHMWPE contact area. The talar component possessed more unidirectional scratching aligned in the AP direction for both implant sizes. Scratching perpendicular to the direction of the primary articulation was also identified, demonstrating the uncoupled multidirectional rotational and displacement motions of the MB surfaces.



Figure 46. Photographs of three medium (top) and extra small (bottom) superior insert surfaces after 5 Mc. Machining lines are no longer visible and there are clear signs of abrasive wear, burnishing and scratching.

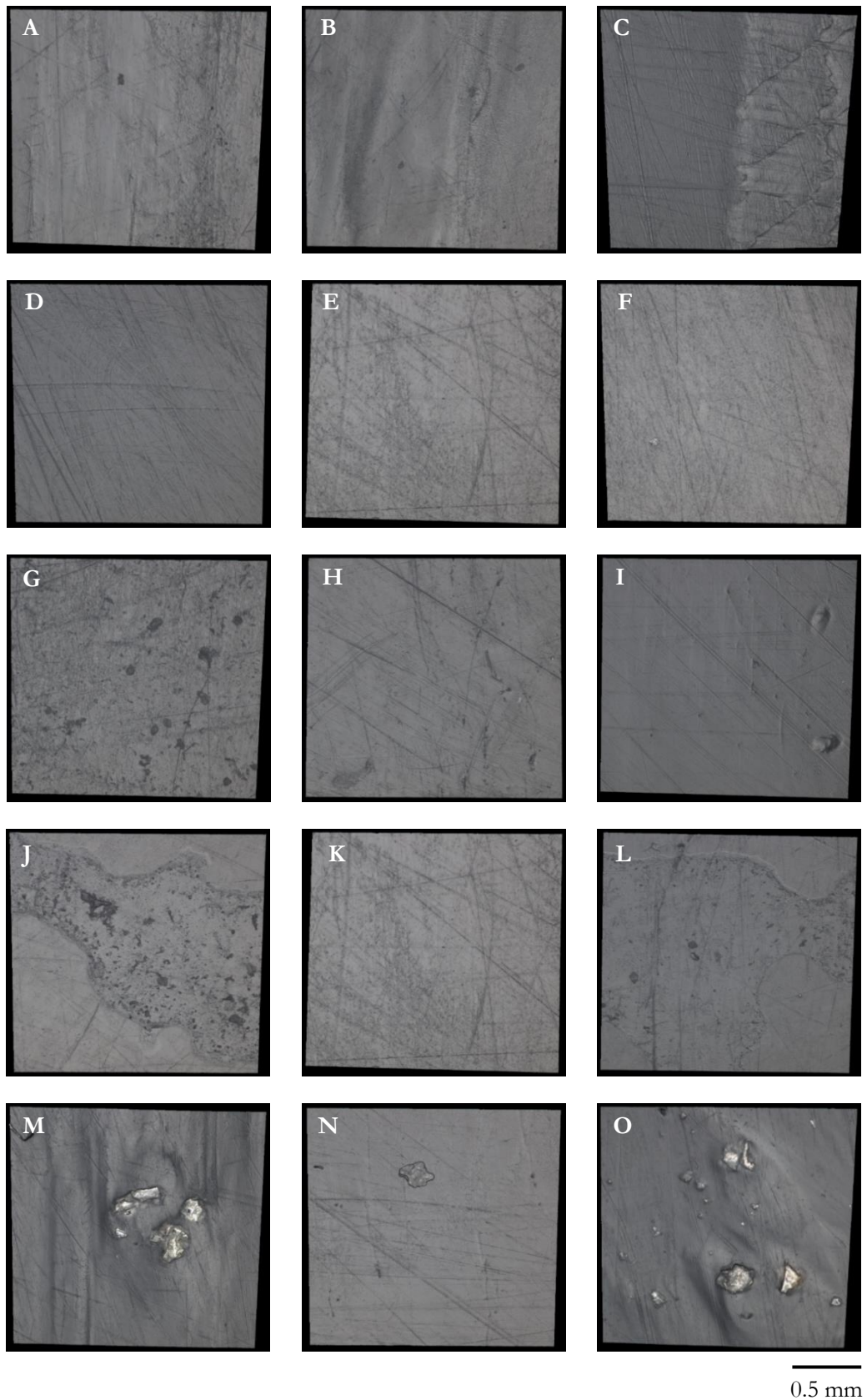


Figure 47. Damage modes on the superior bearing insert surface from both implant sizes after 5 Mc (n = 6 for both implant sizes): A-C = Burnishing; D-F = Scratching; G-I = Pitting; J-L = Abrasive wear; M-O = Material on the surface. Multiple damage modes were captured with the Alicona InfiniteFocus microscope (20x resolution).

### **Accelerated Artificial Ageing**

After 5 Mc of artificially aged wear simulation, burnishing was the predominant damage mode visible on the insert surfaces, particularly at the superior insert, with limited machined lines still intact (Figure 48). There was also obvious signs of abrasive wear, pitting, debris on the surfaces and multidirectional scratching (Figure 49). There was no evidence of crack formation or delamination observed at the end of the simulation, which has been associated with the accelerated artificial ageing process (Figure 49). Similar to the implant size study, there were clear visible outlines of the conventional UHMWPE contact area on the tibial articulating surfaces. Within this contact area, there was evidence of polyethylene transfer and multidirectional scratching. The talar components also displayed fine multidirectional scratching across the bearing surface, which was likely caused by the uncoupled multidirectional rotational and displacement motions of the MB device.

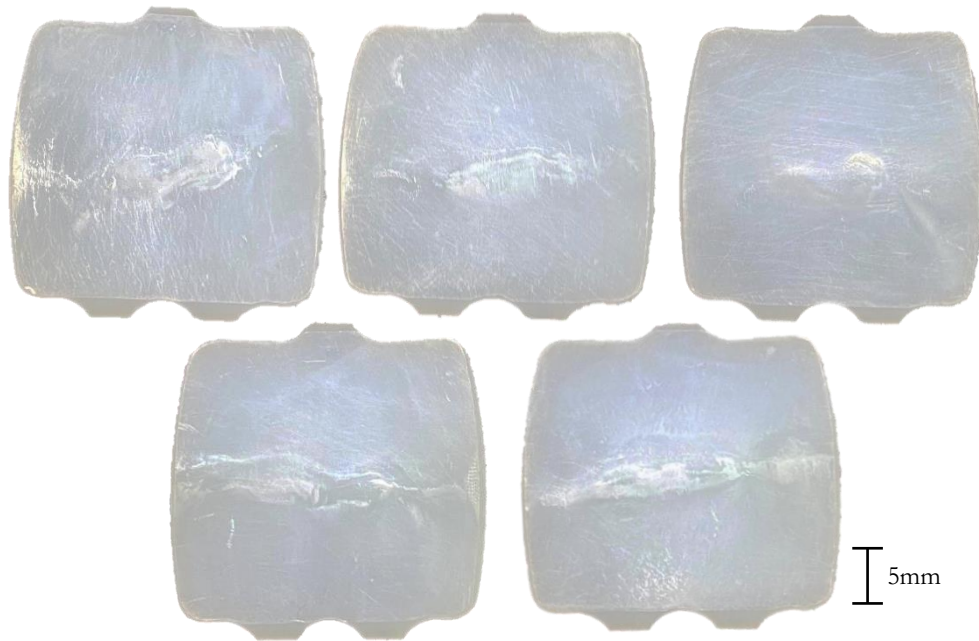


Figure 48. Photographs of the five aged small superior insert surface after 5 Mc. Machining lines are no longer visible and there are clear signs of abrasive wear, burnishing and scratching.

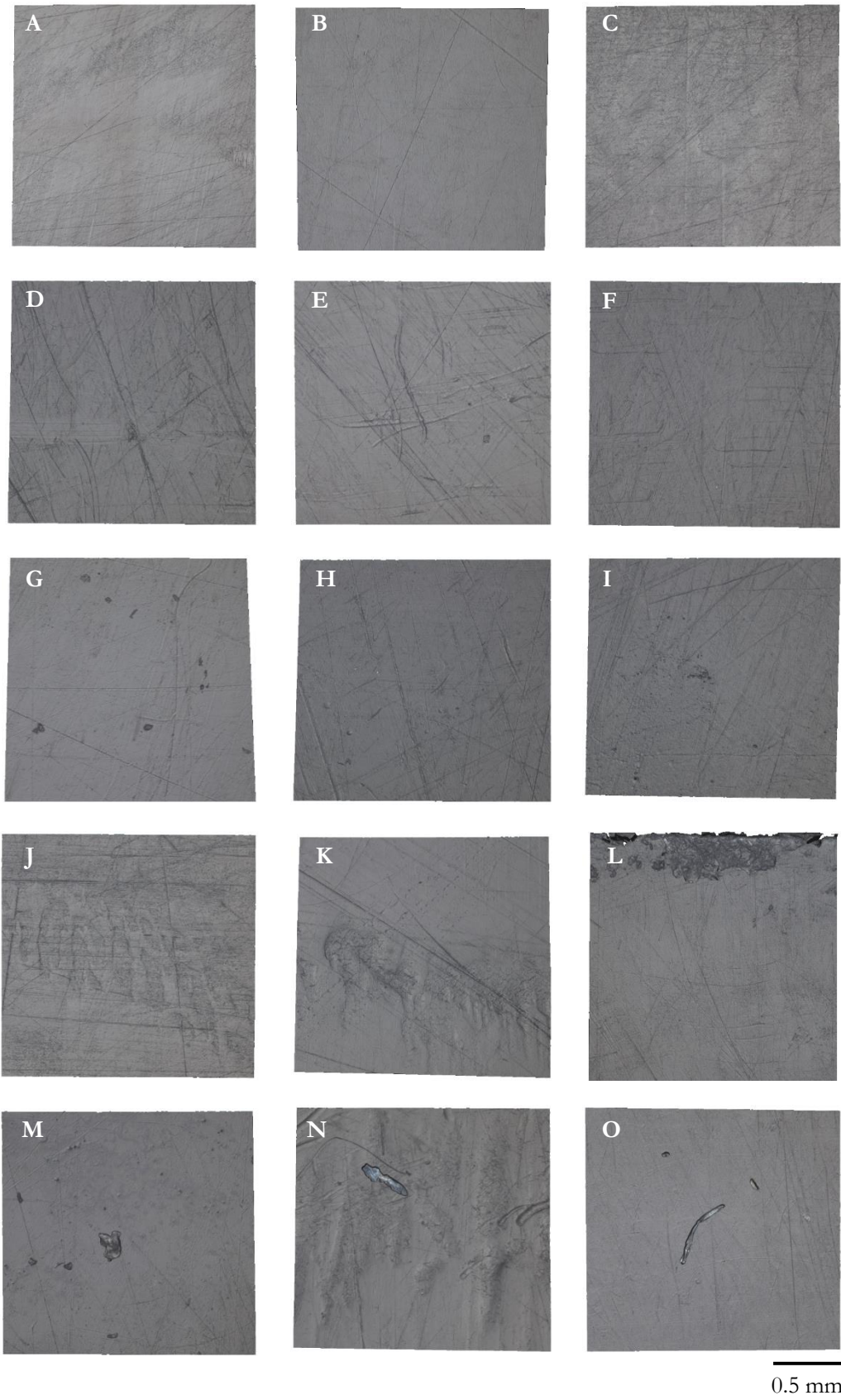


Figure 49. Damage modes on the superior bearing insert surface of the small sized artificially aged implants (n = 5): A-C = Burnishing; D-F = Scratching; G-I = Pitting; J-L = Abrasive wear; M-O = Material on the surface. Multiple damage modes were captured with the Alicona InfiniteFocus microscope (20x resolution).

### 3.5 Discussion

The tribological behaviour of a TAR is deeply influenced by implant parameters, but wear data remains limited. It is thought that the present studies are the first to compare the wear between different sized implants and artificially aged conventional UHMWPE of a third generation MB device.

#### 3.5.1 The Wear Effects of Implant Size

The two sizes (medium and extra small) of commercially available MB implants with the same design features were tested *in vitro*, according to Smyth et al. (2017) kinematic and loading (UoL) profiles under displacement control. The comparable simulator inputs and experimental conditions which were applied to both implant sizes resulted in no significant differences in the mean wear rates, contact wear area and topographic changes after 5 Mc. It is hypothesised that smaller implants are characterised by a smaller contact area. This corresponds to a greater contact pressure on the UHMWPE insert, and it is well known that increased pressure is a precondition to high wear (Plante-Bordeneuve and Freeman, 1993; Pellengahr et al., 2005). According the Archard's Law, the wear volume is proportional to contact load (Lewis, 1964). However, the equation is not able to completely predict UHMWPE wear, since it is also a function of contact area (Mazzucco and Spector, 2003; Galvin et al., 2009). It has since been established that polyethylene wear may need a more complex wear prediction equation, as proposed by the algorithm of Strickland et al. (2012).

Increasing the contact area at the bearing interfaces has been shown to cause increased adhesive and abrasive wear, while reducing the contact area results in higher contact stresses and potentially causing fatigue wear and delamination (Sathasivam et al., 2001). There is well-documented evidence of this phenomenon in THR, with larger femoral heads known to cause increased volumetric wear rates when compared to smaller sized heads, while under the same loading and kinematic input profiles (Kang et al., 2009). This finding has also been found in TKR, with larger mobile knee inserts ( $37.80 \pm 2.80$  mg) producing approximately a two-fold increase in volumetric wear with respect to the smaller inserts ( $19.46 \pm 0.93$  mg) and consequently raised wear rate ( $p = 0.001$ ) after 2 Mc (Affatato et al., 2013).

The reduced wear rate from the smaller THR and TKR sizes is likely a result of the smaller contact area. However, contact area between the implant sizes was not directly measured in the studies mentioned. The current study determined that both implant sizes had comparable mean wear contact areas, which could have been one of the main reasons for the comparable wear rates. Earlier research by Mazzucco and Spector (2003) and Liu et al. (2011) defined proportional relationships between wear and the combined effect of contact area and sliding distance. Moreover, the wear theory by Mazzucco and Spector (2003) proposed that wear relates to the materials and experimental conditions, but was not specific. Liu et al. (2011) elaborated through

suggesting that the wear constant would incorporate cross-shear ratio, while being independent from contact pressure. This wear prediction is more widely accepted than Archard's law for determining implant wear rates (Liu et al., 2011). The idea of wear being unrelated to contact pressure contradicts the historical belief that wear rates increase exponentially with contact stresses. It also disregards the correlation between wear factor and maximum contact stresses, with a decrease in wear factor occurring with increased stresses (Wang, 2001). However, these theories were developed from previous pin-on-disc experiments under constant load and it remains unknown how a changing load will impact these relationships.

The contacting asperities on the conventional UHMWPE at the articulating surfaces deform elastically under constant load (Bucknall et al., 2020). Therefore, the linear relationship between the real contact area and load does not hold for polyethylene bearing surfaces, unlike metallic surfaces (Wang et al., 2003). Consequently, an increase in load does not result in a linear increase in real contact area and wear rate. This finding was further verified by Battaglia et al. (2014) who suggested that volumetric mass loss was comparable between implant sizes when subjected to a load increase of 15% after an additional 2 Mc. Thus, this suggests that the increased load does not affect wear rates alone, supporting the notion that wear rate is not proportional to the load (Liu et al., 2011). This finding further justified the choice to maintain the same load for both implant sizes, despite smaller patients with lower BMI being likely to be implanted with a smaller sized device.

MB implants, like the one used in this study, have been shown to reduce polyethylene stresses compared to FB designs, through the distribution of loads across a larger congruent contact surface and through reducing constraints at the bearing interface (Affatato et al., 2009). The biconcave features of the conventional UHMWPE meniscal insert are fully congruent with the metallic components throughout the ROM, independent of joint position (Reggiani et al., 2006). The increased TAR conformity, yields higher contact wear area on the conventional UHMWPE bearing relative to the overall insert size. Therefore these effects may be reduced. Computational modelling has also verified that changing implant conformity causes varying wear patterns due to the cross-shear ratio at the periphery of the contact area being higher with increased conformity (Abdelgaied et al., 2014). The current study suggests that the combination of the same loading and kinematic input parameters, coupled with the comparable biconcave conformity (implant contact wear area) was the main reason for the comparable wear rates between implant sizes.

Throughout the wear simulation, the substantial changes in surface topography of each of the UHMWPE and metallic components did not appear to influence the wear rate between implant sizes. Under the same loading and kinematic parameters, Smyth et al. (2017) reported similar Ra results (superior insert = 0.08  $\mu\text{m}$ ; inferior insert = 1.26  $\mu\text{m}$ ; tibial = 0.02  $\mu\text{m}$ ; talar = 0.18  $\mu\text{m}$ ) of five MB Zenith TARs after 2 Mc (Stage 5). It should be noted that the same roughness value

can represent surfaces with substantially different surface profiles (Figure 50), and is a limitation when focusing on individual Ra values. For example, a bearing surface with a positively skewed distribution of surface heights may also have the same average Ra across the surface as a negatively skewed distribution, which would have more capability of retaining synovial fluid for the lubricant and improving wear resistance. This is the reason why the wear studies in this thesis did not focus on average Ra value only, unlike previous TAR studies at the UoL (Bell and Fisher, 2007; Smyth et al., 2017).

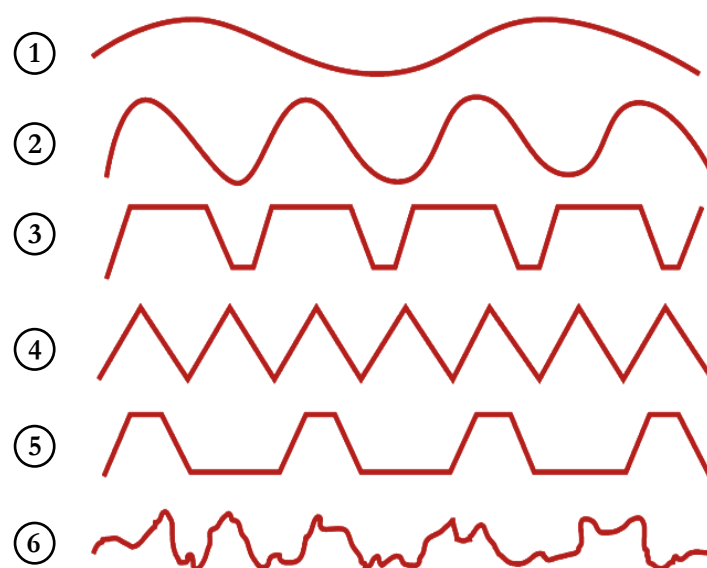


Figure 50. Six hypothetical surface profiles (red lines) with the same surface roughness value but with different surface texture characteristics (e.g. surface or kurtosis).

The high wear rate during the 1 Mc (run-in wear phase) is likely due to the ploughing of the metallic bearing surfaces on the softer polyethylene inserts, commonly referred to as abrasive wear. The larger Ra, positive Rsk and reduced Rku at the beginning of testing on the UHMWPE inserts indicated that the surfaces were full of asperities, due to the machined finish. There must have been a large number of peaks over the trace length and likely caused the lambda ratio to be low ( $\lambda < 1$ ), which is associated with the boundary lubricant regime. In this lubricating regime, the lubricant thickness is directly related to the magnitude of molecules present (Dowson, 2012).

The bovine serum used likely presented a monolayer of protein molecules absorbed at the bearing surfaces, which acted to prevent direct contact between surfaces (Wang et al., 1996a). However, this regime is associated with a reduced thickness of the fluid film, as the pressures of the fluid were unable to maintain normal load and caused penetration of the contacting asperities. This is unavoidable due to the soft and rough UHMWPE sliding across the hard metallic surfaces. During motion, there was an increased load going through the contacting surfaces compared to when stationary. This coupled with the reduction in sliding speed, due to the ploughing of the contacting asperities, resulted in increased contact pressures at the bearing surfaces. Increased asperity contact during load and motion is associated with increased friction (Rabinowicz and

Tanner, 1966) and production of wear debris (Dowson, 2012). The high asperity contact at the start of testing between the bearing surfaces also resulted in clear signs of burnishing and micro-adhesion (Section 3.5.4), which are associated with implants that have undergone high wear (Dowson, 2012). These findings clearly demonstrate that the TAR were associated with a reduced minimum film thickness and high surface roughness, which are key attributes to a boundary lubricant regime.

After the initial ploughing (abrasive wear) of the roughened polyethylene surfaces, full of high contacting asperities, the boundary lubrication likely aided in the reduction in wear rate throughout the 5Mc simulation (Lu and McKellop, 1997). The abrasive wear, which was prominent on all insert samples was likely reduced throughout testing in boundary lubrication, through the shearing of the lubricating (protein) layer at the bearing surfaces, rather than the continued plowing or deformation of the softer surface. The negative Rsk and positive Rku found at the UHMWPE surfaces of both implant sizes at the end of testing indicated that there were fewer peaks above the midline of the roughness profile. This further indicated that the rough surface (machined lines) had been smoothed (burnishing), which resulted in valleys throughout the surface. These sharp valleys associated with high Rku and negative Rsk provide nanoscale reservoirs for lubricant (Etsion, 2009).

A large change in Rsk and Rku was also seen at the metallic surfaces, independent of implant size or artificial ageing (Section 3.5.2). The tibial and talar surfaces were found to have a substantially negative Rsk, coupled with a positive Rku, which follows a similar trend to the conventional UHMWPE insert surfaces. A similar trend was demonstrated in Chapter 4 for medium sized implants tested under varying simulator types and input profiles (Appendix E). By combining both parameters, the surface can be described as a plateau-like smooth surface with deep valleys (Sedlaček et al., 2012). A high value of Rku and more negative Rsk has been found to improve contact conditions through reduced friction and causes a shorter distance to steady-state wear conditions under boundary lubrication, which is associated with reduced wear rates (Chang and Jeng, 2013; Dzierwa, 2017; Dzierwa et al., 2020). This may be explained through the polishing effect at the polyethylene surface through abrasive wear, providing better hydrodynamic properties and consequently lower friction and subsequent wear.

This effect has been highlighted when testing metallic surfaces, with the wear volume of 42CrMo steel surface preparation of a 100Cr6 steel ball being directly related to the skewness parameter (Rsk) during ball-on-disc testing (Dzierwa et al., 2017). In the same study, it was observed that higher values of Rku were related to lower values of volumetric wear. It has also been shown that the deep valleys, associated with a negative Rsk, contain reservoirs that are too small to trap wear particles ranging from 10 to 100  $\mu\text{m}$ , which reduces wear while retaining the lubricant (Sedlaček et al., 2012; Zhu et al., 2020). Based on these findings, the combination of negative Rsk and

positive Rku is advantageous for enhancing the boundary lubrication and reducing the wear in joint replacements (Naylor et al., 2016).

Despite the topographical changes discovered, a limitation was that only two measurement points were taken at the start and end of testing. Future work should consider measuring surface topographical changes throughout the simulation, to determine when the greatest changes in roughness parameters occur. More studies are also required to determine the impact of the same topographical parameters measured in this study have on TAR wear. Other limitations associated with the topographical assessment used in the wear studies throughout this thesis can be found in Section 6.2.1.4

The findings from this implant size comparison study could, in future, help surgeons' intra-operative choice of the optimal TAR size. In fact, the human ankle anatomy displays large variations in size and morphology, with a possible under or oversizing of the implanted device resulting in poor clinical outcomes. Moreover, this may cause pain and reduced ROM at the ankle, which could ultimately lead to the need for revision surgery and significantly impact on patients QoL.

### **3.5.2 The Wear Effects of Accelerated Artificial Ageing**

Under similar simulator input profiles and the same experimental conditions, the small sized, artificially aged inserts did not produce a significantly higher mean wear rate compared to non-aged medium and extra small inserts. The wear results from for all implant sizes in this study, independent of artificial ageing, exhibited biphasic wear. There was a short run-in period of higher wear (0-1 Mc), succeeded by a lower wear steady-state phase (1-5 Mc). This follows similar wear patterns to the other implant and simulator parameter comparison studies mentioned in this thesis, as well as previous TAR simulations at the UoL (Bell and Fisher, 2007; Smyth et al., 2017), which were carried out under equivalent loading and kinematic input parameters. The increased wear rate during the run-in phases for all implant sizes, is likely due to the increased number of surface asperities, resulting from the machined lines on the conventional UHMWPE being worn away (Schmalzried and Callaghan, 1999). The steady-state wear should theoretically remain constant until an external condition is significantly altered (e.g. adverse biomechanics) (Stewart, 2010).

When the wear rate was separated into the two wear phases, there was no difference between the aged and unaged implants in the run-in phase. However, the wear rates between the artificially aged and unaged implants were significantly different during steady-state wear. The implant size comparison study used a different simulator type and simulator inputs profiles when compared to the aged study. Chapter 4 examined the influence of both simulator parameters on implant wear and found no significant differences between simulator type and inputs used. The implant

size comparison study in this Chapter demonstrated that implant size had no effect on overall wear rate.

The higher wear rate of the artificially aged inserts after 5 Mc compared to the unaged inserts, independent of implant size or simulator input conditions. It was hypothesised that the increased wear rate was likely due to greater damage at the bearing surfaces caused by the ageing process. The accelerated artificial ageing process resulted in peak dominant (positive Rsk) and bumpy (lower Rku) bearing insert surface, demonstrating high volume of asperities (Appendix E.2). During the wear study, these asperities were worn down, causing a significant reduction in Ra at the insert bearing surfaces from 0-5 Mc, particularly the superior insert side. However, no apparent differences were found in surface topographical parameters between the aged and unaged implants after 5 Mc. A similar trend was also seen for the visual damage modes identified (Section 3.5.4). It should be noted that the current study failed to statistically compare the influence of the ageing process on surface roughness parameters compared to the aged cohort. This was because the main focus of the study was determine wear rates between aged and unaged inserts, with topographical changes being used to help describe the tribological behaviour at the bearing surfaces. These findings indicate that the differences between the aged and unaged implants, was likely due to the ageing process itself.

The higher wear rate may have been due to the generation of free radicals that oxidise, which lead to mechanical property degradation of the conventional UHMWPE (Schwiesau et al. 2014). Wear of conventional UHMWPE is believed to occur due to plastic deformation of the polymer, with molecular alignment occurring in the direction of the motion being applied to the insert (Wang et al., 1997; McKellop., 1999b; Wang, 2001). This causes the formation of the polyethylene fibrils to be orientated parallel to each other, increasing the strength along the direction of sliding but weakening them in the transverse direction (Bracco et al., 2017). During the multi-directional motion applied to the samples in this study, a multi-directional scratching damage mode was visible on each of the samples (Section 3.5.4). This orientation-softening phenomenon is likely responsible for the detachment of fibrous wear debris from the aged and worn surfaces (McKellop et al., 1995; Tipper et al., 2000), causing increased steady-state wear compared to the unaged samples.

The free radicals formed in the conventional UHMWPE during the irradiation process may have also increased the implants susceptibility to *in vivo* oxidative degeneration, which has been found to significantly affect the physical, chemical and mechanical properties of conventional UHMWPE (Kurtz, 2015; Grupp et al., 2017). Despite the significant difference in steady-state wear between aged and unaged samples, there was no indication of structural failure in any of the aged samples, even with the mechanical and chemical stresses applied during the ageing process.

In the last decade, the use of crosslinking of UHMWPE (XLPE) has been introduced to aid in the reduction of volumetric wear in joint replacements (McKellop et al., 1999a; Glyn-Jones et al., 2008; McCalden et al., 2009). XLPE is formed from higher doses of ionizing radiation, producing more cross-links between the carbon-carbon bonds of the adjacent chains and inhibiting such molecular orientation (McKellop et al., 1999a). Crosslinking aims to slow down the formation of surface fibrils and improves the resistance to wear (Wang et al., 1997; McKellop et al., 1999a). This process also reduces the production of free radicals and the risk of oxidative degradation, which are eradicated by subsequent thermal or chemical treatment (Bracco et al., 2017). Muratoglu et al. (2004) found that XLPE reduced wear rates in tibial inserts of a cruciate retaining TKR when compared to conventional UHMWPE inserts, after undergoing the same ageing process as the current study. Since then, XLPE has been introduced in TARs and wear rates have substantially reduced, ranging from  $2.1 \pm 0.3$  to  $3.3 \pm 0.4$  mm<sup>3</sup>/Mc (Kincaid et al., 2013; Bischoff et al., 2015; Schipper et al., 2018). In contrast, the mean wear rate of conventional UHMWPE, over varying simulation duration, ranges from  $3.4 \pm 10.0$  to as high as  $25.8 \pm 3.1$  mm<sup>3</sup>/Mc (Bell et al., 2007; Affatato et al., 2007; Postak et al., 2008; Reinders et al., 2015b; Smyth et al., 2017).

In more recent literature concerning THR and TKR, vitamin E has been introduced to improve ageing resistance, through reactions with the free bonds and interruption of the oxidation reaction cascade (Lerf et al., 2010; Bracco and Oral, 2011; Turner et al., 2014). Accelerated ageing has been found to have no influence on the wear behaviour in a unidirectional wear test (Wannomae et al., 2010) or knee simulator study applying level walking (Micheli et al., 2012) on XLPE stabilised with vitamin E. However, one disadvantage of crosslinking and associated irradiation methodology is that polymer chain scission may occur after surgery, due to the presence of oxygen in the synovial fluid (Schipper et al., 2018). This can cause polyethylene embrittlement, which reduces fatigue resistance and results in surface cracking or fracture of the XLPE insert (Schipper et al., 2018).

These factors have limited the widespread adoption of vitamin E doped or even standard XLPE in TAR, with only two designs available on the UK market. This point has recently been challenged by Schipper et al. (2019), who found that XLPE had sufficient fatigue strength to withstand 10Mc of loading at 5 times BW (5600N) at the point of peak stresses during the gait cycle in a FB implant. However, further clinical evidence with larger patient and testing cohorts, are required to translate fatigue strength with clinical use of XLPE in MB devices.

The artificial ageing methodology used in this study was limited by the fact it models the effect of real-time ageing gamma-air-sterilised UHMWPE inserts. However, the BOX® ankles were sterilised using gamma irradiation in the presence of nitrogen. This meant that the samples may have benefitted from some degree of crosslinking that occurred from this sterilisation method, which could have improved the wear properties of the conventional UHMWPE (Kurtz et al., 1999). Therefore, the potential crosslinking effect may have been the reason to the comparable

trend in surface roughness changes and wear damage modes presented between the aged unaged samples, independent of implant size (Section 3.5.4). This method of sterilisation avoids contact with oxygen from the air and has sufficient barrier packaging during its shelf life (Lu et al., 2003). Sterilisation in an air environment causes radicals to react readily with oxygen, which triggers a cyclic, auto-sustained process, leading to the formation of oxidation products on the polymer (Bracco et al., 2017). This results in an overall reduction in molecular mass and significant changes to the polyethylene morphology.

As mentioned in Section 3.4.1, one of the components was damaged due to dislocation and was subsequently removed from the study. There would have been some value in continuing to run the sample, as this would have represented a potential real world ‘worst-case’ scenario. The wear rate produced from this sample may have represented patients that had undergone malalignment or early dislocation of their implanted device. However, if the sample was used in the study, this would have had a significant influence on the mean wear rate and would have been more difficult to truly determine the influence of the accelerated artificial ageing process. There are other limitations associated with the pre-clinical wear simulations, such as the selection of input profiles, the simulator type, experimental protocol, gravimetric wear and topographic assessment methods. A detailed review of the limitations associated with the studies mentioned in this Chapter and in Chapter 4 (simulator parameters) can be found in Chapter 6 (Section 6.2).

### **3.5.3 Wear Rate Comparison**

The conventional UHMWPE wear rates from the MB TARs, independent of size (medium:  $11.00 \pm 3.06 \text{ mm}^3/\text{Mc}$  and extra small:  $10.64 \pm 4.61 \text{ mm}^3/\text{Mc}$ ) and ageing process ( $16.98 \pm 5.31 \text{ mm}^3/\text{Mc}$ ), were comparable to the majority of the displacement control wear simulation literature, in which wear rates ranged from  $3.4 \pm 10.0$  to  $25.8 \pm 3.1 \text{ mm}^3/\text{Mc}$  (Affatato et al., 2007; Bell and Fisher, 2007; Smyth et al., 2017; Schipper et al., 2018). The magnitudes of the wear rates presented in the current studies may have a relevant osteolytic potential, but with the limited duration of 5 Mc, this is not sufficient enough to cause osteolysis in such a short period (Reinders et al., 2015b). This suggests that there are other reasons for early implant failure of TARs (Section 6.1.1.).

Both implant (Chapter 3) and simulator (Chapter 4) parameter studies were based on experimental conditions from previous research performed at the UoL (Smyth et al., 2017). The implant size comparison study also used the same simulator input conditions from this study (Stage 5) and produced comparable wear rates with a reduced AP displacement of 4 mm ( $13.3 \pm 2.5 \text{ mm}^3/\text{Mc}$ ). The reduced variance (CL) in the mean wear rate from the current studies and from the published work by Smyth et al. (2017) suggests that the simulator experimental conditions and set-up were comparable between the samples and stations used. This finding also gives confidence in the high repeatability of the test set-up between samples of the six stations. The higher variability in the earlier published studies on MB designs, was likely due to the reduced

sample size, number of cycles (< 5 Mc), number of stations (< 6) and lubricant used. Bell and Fisher (2007) was the first study to simulate TAR wear, with mean wear rates varying from  $3.4 \pm 10.0 \text{ mm}^3/\text{Mc}$  to  $10.4 \pm 11.8 \text{ mm}^3/\text{Mc}$  after 5 Mc for two implant designs (Buechel-Pappas™ and Mobility®). However, the study did not include any AP translation until after 5 Mc, where the wear rates substantially increased in both TAR cohorts (Buechel-Pappas™ =  $16.4 \pm 17.4 \text{ mm}^3/\text{Mc}$ ; and Mobility®  $10.4 \pm 14.7 \text{ mm}^3/\text{Mc}$ ). With AP translation only being applied for the final Mc, it is difficult for the authors to truly state that the wear rates represent the clinical environment. The large variation in the mean wear rates, independent of design or the presence of AP translation was likely due to the small sample size used ( $n = 3$  for both prostheses). The current studies used a minimum of five samples for each testing condition, which is well above the recommended amount of samples in ISO 22622:2019 ( $n = 3$ ).

Only the published work by Affatato et al. (2007) used the same implant model as the one used for all the wear studies in this Chapter. The authors reported the highest mean wear rate of  $18.6 \pm 12.8 \text{ mm}^3/\text{Mc}$  (range:  $7.5\text{-}31.7 \text{ mm}^3/\text{Mc}$ ) in literature of MB designs with a conventional UHMWPE meniscal insert. The study by Affatato et al. (2007) also presented a substantially higher wear rate and variance (CL) compared to the samples from the current studies and the wear rates presented in Chapter 4. This was likely due to the limited number of cycles (2 Mc) performed, limited sample size ( $n = 4$ ) and the use of deionised water as the test lubricant. The study did not have enough time to reach steady-state wear and should have been run until reaching the recommended 5 Mc to see the true effect on the devices. The large variability in data and limited sample sizes from both Bell and Fisher (2007) and Affatato et al. (2007) makes it very difficult to draw any truly meaningful conclusions from their work, in terms of how the wear rates relate to TARs in the biological environment.

Water has been proven to be poor at replicating the lubricant properties experienced *in vivo* compared to bovine serum (Good et al., 1996). For instance, *in vitro* simulator studies for THR have reported wear factors of conventional UHMWPE to be 14 times higher in water than in serum (Derbyshire et al., 1994; Besong, 1999). The wear debris produced when simulated in water appeared as large flake-like particles, which were several millimetres long (Saikko et al., 1993). In contrast, the wear particles produced in serum lubricated testing and *in vivo* are generally submicron in size (Wang et al., 1996a). With water used as a lubricant, material transfer from the soft UHMWPE to the metallic bearing surfaces was also apparent, which means there was a lack of an active protein layer (Cooper et al., 1993). This material transfer has been found to cause significant topographic changes at the articulating surfaces and results in an increase in wear rates (Shen et al., 2019). This is important, as this transfer layer is not seen clinically on explants or in wear simulations using calf or bovine serum as the testing lubricant (Campbell et al., 1995; Wang et al., 1995). It should also be noted that the Affatato et al (2007) study was not recent and the

reasons above which have been discussed has dismissed the use of water as a lubricant in wear simulations of polymetric materials for joint prostheses.

Apart from the use of water as the testing lubricant, the high variance in the wear rate from Affatto et al. (2007) study was also related to the variability in wear patterns found at the bearing surfaces of the four samples. Two of the samples were found to have large regions of multi-directional scratching and burnishing, while the other two samples displayed limited signs of wear damage modes on the tibial bearing surface. This finding may indicate that some of the components had undergone mal-positioning during component set-up or damage may have been sustained during simulator calibration or fixture positioning. However, this was not reported by the authors of this study and the components from the implant parameter studies also showed comparable wear damage modes across the bearing surfaces (Section 3.5.4).

Bischoff et al. (2015) performed a displacement controlled simulation with six FB implants (Zimmer Trabecular Metal) and found a significantly lower mean wear rate of  $8.0 \pm 1.4 \text{ mm}^3/\text{Mc}$  after 5Mc. FB designs have been shown to provide improved stability during articulation without the risk of subluxation of the meniscal insert (Mehta et al., 2010). Therefore, the highly constrained design of the FB device used in Bischoff et al. (2015) may explain the lower wear rate. MB designs, like the one used in the current studies, aim to reduce shear forces through minimal constraints (Gaudot et al., 2014), while separating the motions across two surfaces. This has been shown to reduce wear in mobile TKR, when compared to FB designs (McEwen et al., 2005). However, instead of decoupling the motions, so that only unidirectional motion occurs at each articulating surface, the unconstrained surfaces produce multidirectional rotational and displacement motion as displayed by the multidirectional scratching found on the bearing surfaces (Section 3.5.4). It should be noted that despite the reduced wear rate in the FB implants in Bischoff et al. (2015) study, this type of device is more susceptible to loosening of the tibial component due to greater shear forces found at the bone-implant interface (Valderrabano et al., 2012). Moreover, Queen et al. (2017b) demonstrated that there were no statistically or clinically meaningful differences between FB and MB devices when comparing gait mechanics and PROMs at one-year post-surgery. Longer duration simulator based studies ( $> 5 \text{ Mc}$ ), under a range of varying ADLs, are required to truly determine the difference in wear behaviour between FB and MB designs.

It has previously been highlighted that different hip simulators provide varying wear rates, even when testing the same implants (Saverio Affatato et al., 2008). The wear rates can be influenced by many factors such as kinematic inputs, lubrication, temperature, and the centre of rotation specific to each centres' experimental protocol. Therefore, the differences in simulator protocols/inputs (Chapter 4), type of simulator (Chapter 4) and implant design/materials make it difficult for TAR studies to directly compare individual wear rates. However, each study provides a useful benchmark for future TAR wear simulations.

### 3.5.4 Damage Mode Comparison

The ability to compare the existing components to retrievals was limited to implants collected by the retrieval centre at the School of Mechanical Engineering, UoL. As there were no BOX® ankle retrievals in the UoL collection, the implants were instead compared with retrievals from a previous study at the UoL involving 22 Ankle Evolutive System (AES; Biomet, Valence, France) retrievals (Stratton-Powell et al., 2016). The AES is a second generation MB device with a conventional UHMWPE insert and cobalt chrome metallic components, which are similar to the design of the BOX® ankle. The study also compared the visual damage modes from the aged and unaged implants against previously simulated medium sized Zenith (Corin Group PLC, Cirencester, UK) devices. These devices underwent the same loading and kinematic input profiles (UoL) and comparable experimental conditions to that of the implant size study (Smyth et al., 2017). The Zenith device is a third generation MB design, consisting of titanium nitride metallic components and a conventional UHMWPE meniscal insert.

Visual inspection of each implant, independent of size or ageing, demonstrated extensive damage across most of the bearing surfaces of the metallic and polyethylene components. In agreement with the retrieval (Stratton-Powell et al., 2016) and simulation (Smyth et al., 2017) studies, adhesive wear, burnishing and multidirectional scratching were observed as the pre-dominant damage mode mechanisms (Figure 51). Other studies measuring retrieved BOX® ankle inserts have been displayed clear signs of burnishing and multi-directional scratching conditions on both the upper spherical and the lower anticlastic insert surfaces (Affatato et al. 2009). Pitting was also seen across the meniscal bearing surfaces, which is a result in the release of large volumes of polyethylene debris.

Each of the tibial articulating surfaces, independent of implant size and artificial ageing, had a visible imprint of the superior insert surface (Figure 51). This was likely a result of adhesive wear produced from the constant articulation and highly conforming nature of the BOX® ankle inserts. A comparable imprint was also visible on the previously simulated Zenith implants and AES retrievals, which underwent even greater multidirectional motion and loading (Figure 51). It should be noted that the samples from the UoL based *in vitro* study involving the Zenith implants at the UoL had undergone a greater ROM and for a longer testing duration of 12 Mc (Smyth et al., 2017). The retrieved implants underwent varying loading and motion patterns during a range of ADL (Stratton-Powell et al., 2016). In contrast, the bearing surfaces from the *in vitro* studies underwent loading and kinematic conditions representing overground walking. This finding is apparent in Figure 51, with more prominent, deeper scratching on both the tibial and superior insert surfaces compared to the current study implants.

The simulated components may not fully replicate the more extreme damage modes found in explanted devices. This is due to the presence of third-body wear debris in explanted devices, such as cortical bone, cement or metallic particles, which can amplify abrasive wear (Davidson et

al., 1994). This is likely the reason for the deeper scratching and other damage modes at the tibial articulation on the retrieved TARs, as shown in Figure 51 (Stratton-Powell et al., 2016). Third-body debris has been proven to cause significant increases in wear rates of a TKR (Schroeder et al., 2013). The *in vitro* simulation study used a uni-compartmental FB design doped with either bone or cement particles and was run under ISO 14243-1:2002 for 5 Mc. The bone particles had no effect on the wear rate during the steady-state phase ( $3.0 \pm 1.27 \text{ mm}^3/\text{Mc}$ ), but the introduction of cement particles resulted in a 5.7 times increase in implant wear rate ( $25.0 \pm 16.93 \text{ mm}^3/\text{Mc}$ ) (Schroeder et al., 2013).

Previous retrieval studies on MB (BOX® ankle) (Affatato et al., 2009) and FB (Agility; DePuy, Warsaw, USA) (Vaupel et al., 2009) used scanning electron microscopy (SEM) techniques and demonstrated evidence of burnishing, pitting and multidirectional scratching at the bearing surfaces. Embedded debris was only found in the latter study at the tibial-insert interface, which was potentially a result of micromotion between the cement and implant (Vaupel et al., 2009). MB designs, including the BOX® ankle used in this study, do not use bone cement during implantation, which means that MB devices are not affected by bone cement particles. However, a study by Cottrino et al. (2016) discovered the presence of titanium and cobalt chrome alloy wear particles embedded in the bearing insert surface of six AES implants. Metallic alloys and hydroxyapatite coatings have been identified as third-body wear particles in MB designs, which have been associated with the early onset of wear-mediated osteolysis (van Wijngaarden et al., 2015; Schipper et al., 2017; Najefi et al., 2021; Kim et al., 2021).

Conversely, there was no evidence of imprinted metallic debris within the insert surfaces and therefore may have been remnants from the lubricant, following the cleaning process. It should also be noted that the AES system was removed from the market in 2012 due to the early development of osteolysis, which was likely due to excessive shear stresses at the bone-implant interface, causing the degradation of the fixation surface and release of wear particles (Koivu et al., 2012; Besse et al., 2015). No such wear simulator study featuring third-body wear has been published. Therefore, future work should focus on investigating the effect of these third-body wear mechanisms in newer generations of FB and MB TAR designs, to determine the potential risk of early failure mechanisms.

The *in vitro* simulated inserts from the studies did present material on the surface, but the study was limited by the resolution available on the Alicona InfiniteFocus microscope (20x resolution). Using a high-resolution SEM would have provided greater precision to determine this material. This technique would have allowed the ability to determine any metallic debris embedded in the conventional UHMWPE inserts through abrasive wear. Only one published study has used SEM to determine wear patterns between tested and retrieved superior insert surfaces of MB design (BOX® ankle) (Affatato et al., 2009). The study identified comparable wear patterns between *in vitro* and *in vivo* inserts, but with multidirectional scratching and pitting being more prominent in

the retrieved bearing surfaces. SEM can also be used to highlight the formation of any biotribofilms and can quantify wear debris size and morphology (Stratton-Powell et al., 2022). However, SEM was not available for the current project, but future work should consider imaging the *in vitro* inserts to confirm the damage modes across the entire bearing surface for each of the implant and simulator parameters.

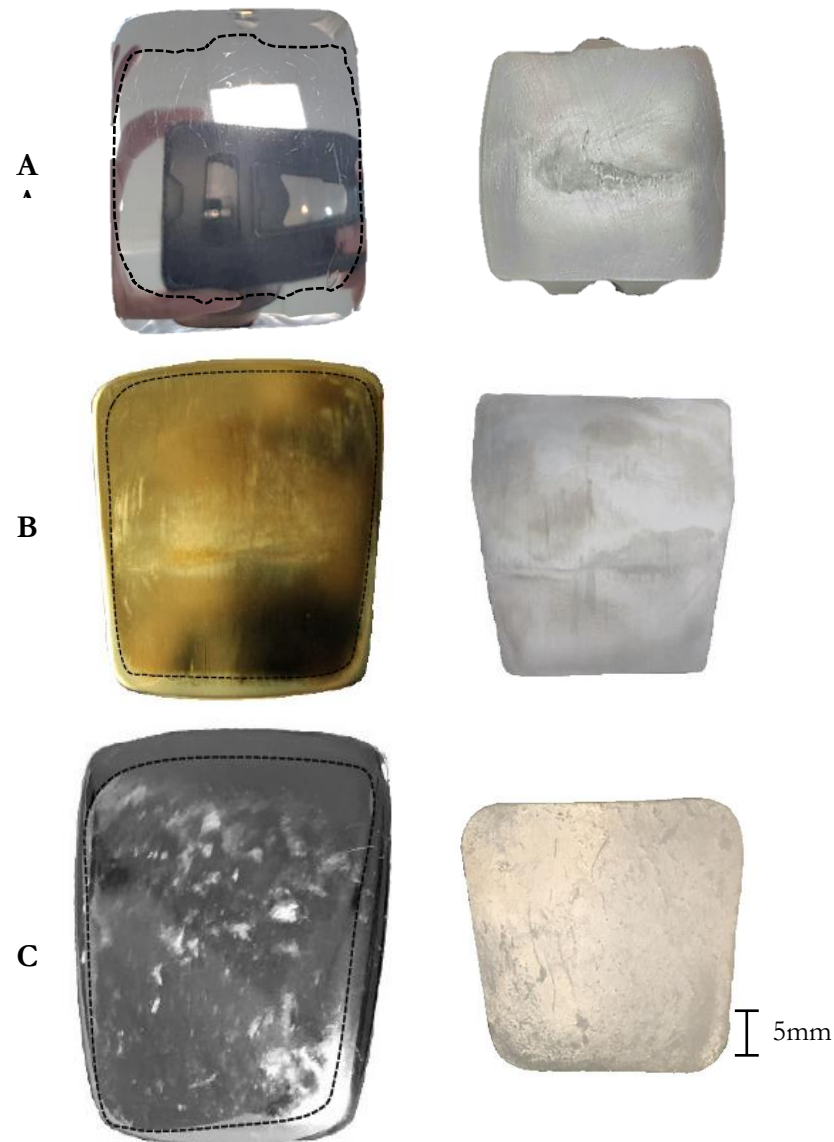


Figure 51. Wear tested surface of the BOX® ankle superior insert and the visual imprint from the conventional UHMWPE articulation on the tibial component (A) compared to that of an *in vitro* Zenith after 12 Mc (B) and Biomet AES retrieval (C). Adapted from Smyth et al. (2017).

Despite the lack of third-body wear, the simulator based studies in this thesis (including the testing reported in Chapter 4) demonstrated that some of the damage modes produced (abrasive wear, burnishing and multidirectional scratching) at the bearing surfaces are also seen in explants, which provided confidence that the simulation was replicating some of the natural environment of a TAR. However, there were no BOX® ankle devices within the explanted collection at the UoL to confirm that these damage modes occur *in vivo* with this specific brand of TAR. It was

possible to compare to the previous study by Affatato et al. (2009), but no details were provided on if the retrieved devices were due to early failure or patient death. This is an important point to consider when comparing simulated and explanted devices as the latter are self-selected in nature, which comes as limitation, as the damage modes may represent failed implants and do not represent the *in vivo* performance of well-functioning prostheses.

The simulator studies in this project were set up to replicate a successful device, with correct alignment, and were not trying to recreate failure, which may have led to more serious damage modes that are more comparable to retrieved devices. This was also apparent in the variability of damage modes discovered, with the controlled conditions of the *in vitro* tested samples providing much less variability in damage modes visualised compared to the retrievals. The increased variability in the retrieved devices used from Stratton-Powell et al. (2016) study was most likely due to the different loading and kinematics through a range of ADLs, individual's weight and number of years implanted. The nature of the displacement controlled simulators used in this project ensured the same loading and kinematic inputs are applied throughout the testing duration, while each of the patients implanted with the AES system will not have the same gait for each step. Furthermore, it could not be determined if each retrieval analysed from Stratton-Powell et al. (2016) represented damage modes from a one-off adverse event such as dislocation or the damage was caused by prolonged wear from repetitive loading. This also makes it not possible to assign a timeline to each wear and damage mode identified. All these factors discussed add to differences in clinical damage modes seen between the simulated and retrieved devices, irrespective of implant design.

### **3.6 Conclusion**

In addition to establishing a wear simulation methodology, this study has furthered the understanding of the effects of implant parameters on the wear of MB devices. Under the same loading and motion conditions, the mean wear rates and topographic changes were unaffected by the different implant size. The evidence from this Chapter could, in the future, help surgeons with their intra-operative choice of the optimal implant parameters for varying patient demographics. There was also a positive indication that accelerated artificial ageing of conventional UHMWPE inserts resulted in increased wear rates over non-aged implants, during the steady-state phase. However, the aged components demonstrated no indication of structural failure or failure under the ISO 22622:2019 kinematic and loading profiles. The wear results from both studies were comparable to those previously published for MB implants, under simulator displacement control. With increasing implant life expectancy *in vivo*, wear rates of this significance may augment the risk of wear debris induced osteolysis and subsequent implant loosening.

## **CHAPTER 4**

# **THE EFFECT OF SIMULATOR PARAMETERS ON THE WEAR OF A TOTAL ANKLE REPLACEMENT**

## CHAPTER 4

### THE EFFECT OF SIMULATOR PARAMETERS ON THE WEAR OF A TOTAL ANKLE REPLACEMENT

#### 4.1 Introduction

Each of the previous TAR *in vitro* wear studies, including the research presented in Chapter 3, have successfully used a variety of mechanical knee simulators to recreate ankle loads and kinematics. Given that ankle specific simulators are not commercially available, the use of a knee simulator allows more institutions and testing facilities to perform wear based studies of the ankle. However, differences in simulator hardware, coupled with varying experimental conditions, make it challenging to compare the wear results between different simulator types.

First generation pneumatically controlled simulators have been used extensively over the past twenty years to determine wear of TKRs under standard gait conditions (McEwen et al., 2001; Barnett et al., 2002; Galvin et al., 2009; Brockett et al., 2012; Abdelgaied et al., 2014; Brockett et al., 2016). The simulators have six DoF, with three of the four axes of motion being pneumatically controlled and FE motion being electromechanically controlled. The lack of fully independent control was however, a limitation with this simulator model (Barnett et al., 2002; McEwen et al., 2005; Brockett et al., 2016). For example, it was difficult to control the air supply with regards to the positioning, accuracy and repeatability of the implants between stations (Barnett et al., 2002). Pneumatic control has also been associated with a lag in output kinematics, meaning that the simulators were unable to rapidly respond to the desired input motions, leading to higher inter-station variability and possible influence on implant wear rate (Brockett et al., 2012).

Modern generation pneumatic simulators, including the one used for the implant size comparison wear study (KSpn) (Chapter 3), possess independent air supply for each station, which allows for station-specific tuning. In theory, this should have improved output kinematic following and reduced inter-station variability, when compared to the first generation pneumatic simulators. In practice, KSpn was able to produce relatively low inter-station variability throughout the UoL input profiles (Smyth et al., 2017) for AL, tibial IER and FE, with the latter being driven electromechanically (Section 3.4.1). However, even when tuning the PID controls of KSpn, there remained large variability in AP displacement output profiles between stations, causing the simulator to produce greater AP displacement than the required input value. KSpn was also unable to attain the maximum output tolerances ( $\pm 5\%$ ) compared to the desired inputs for AL and tibial IER, with a phase lag being present. The electromechanically driven FE cradle was able to achieve the peak FE profile tolerance of the UoL profile, suggesting that other axes of the simulator should be run under electromechanical control, to further reduce inter-station variability and improve loading and kinematic following.

In the last decade, electromechanical knee simulators (KSem), with five fully independently controlled axes of articulation for each station, have been developed to meet the increased demands of joint simulation. The main advantage of KSem over a pneumatic system, is the removal of balancing of the air supply of independent stations and improved ability of the motor to respond rapidly to the variation in load and kinematics (Ali et al., 2016). These improvements should allow the user to produce improved loading and kinematic following of the selected input profiles. Greater accuracy and precision in output load and motion profiles compared to the desired input profiles results in a better representation of implant wear. The first objective of this Chapter was therefore, to determine the wear of a modern MB device using KSem, compared to previous wear data from KSpn (Chapter 3), under the same displacement controlled (UoL) simulator gait inputs and experimental conditions (Smyth et al., 2017).

The simulator type comparison study used the same loading and kinematic input profiles, developed at the UoL (Smyth et al., 2017), to determine the effect of the simulator model on implant wear. More recently, ISO 22622:2019 was published, providing universal input parameters and experiment conditions to determine the wear rates of future TAR devices. However, no published studies have used ISO 22622:2019 to measure implant wear. Thus, the second objective of this Chapter was to determine if the recommended loading and kinematic input profiles in ISO 22622:2019 would produce comparable implant wear rates to the same device simulated under UoL profiles.

The combination of the two objectives discussed above will help to achieve the overall aim of the Chapter, being to investigate the effect of varying simulator parameters on the wear of a modern MB device. Improving the understanding of simulator parameters on the tribological behaviour of MB devices is essential for improving pre-clinical methods, and ultimately future device development.

## 4.2 Materials

Following the non-significant difference found in wear rate between implant sizes in Chapter 3, six medium sized BOX® ankles were selected for use in both simulator parameter studies, with a 5mm insert thickness. The bearing batch and LOT numbers for the six medium-sized samples are shown in Table 12. The same implants were used for both simulator parameter studies, with the first 3 Mc being run under UoL loading and kinematic profiles and the remaining 2 Mc under ISO 22622:2019 profiles.

Table 12. Bearing details for the medium sized implants.

Implant Size	Tibial	Talar	UHMWPE Insert
Medium	161-140	161-340	161-245
	219814	219562	226126

### 4.2.1 The Simulator and Calibration Set-up

The KSem had six fully independent stations, separated across two banks. The implants were inverted, causing rotation and displacement to be applied about the tibial component. Each station of KSem contained a six-axis load cell and displacement sensors for each controlled axis, which permitted the simulator output profiles to be determined and compared to the desired input profiles. Six medium sized delrin fixtures were manufactured to ensure talar alignment in the medium sized components about the simulators centre of rotation (Appendix A.3). The calibration process of KSem is detailed in Chapter 3 (Section 3.2.2) and the calibration record for each station has been documented in Appendix C.3.

### 4.2.2 Simulator Kinetics and Kinematics

The first study condition comparing the effect of simulator type on implant wear was run under UoL profiles (Section 2.3.1), while the second condition compared the effect of the UoL profile against the recently published ISO 22622:2019 recommended profiles. The differences between the loading and kinematic input profiles of UoL and ISO 22622:2019 have been displayed in Figure 52, while the differences in profile peak values are detailed in Table 13.

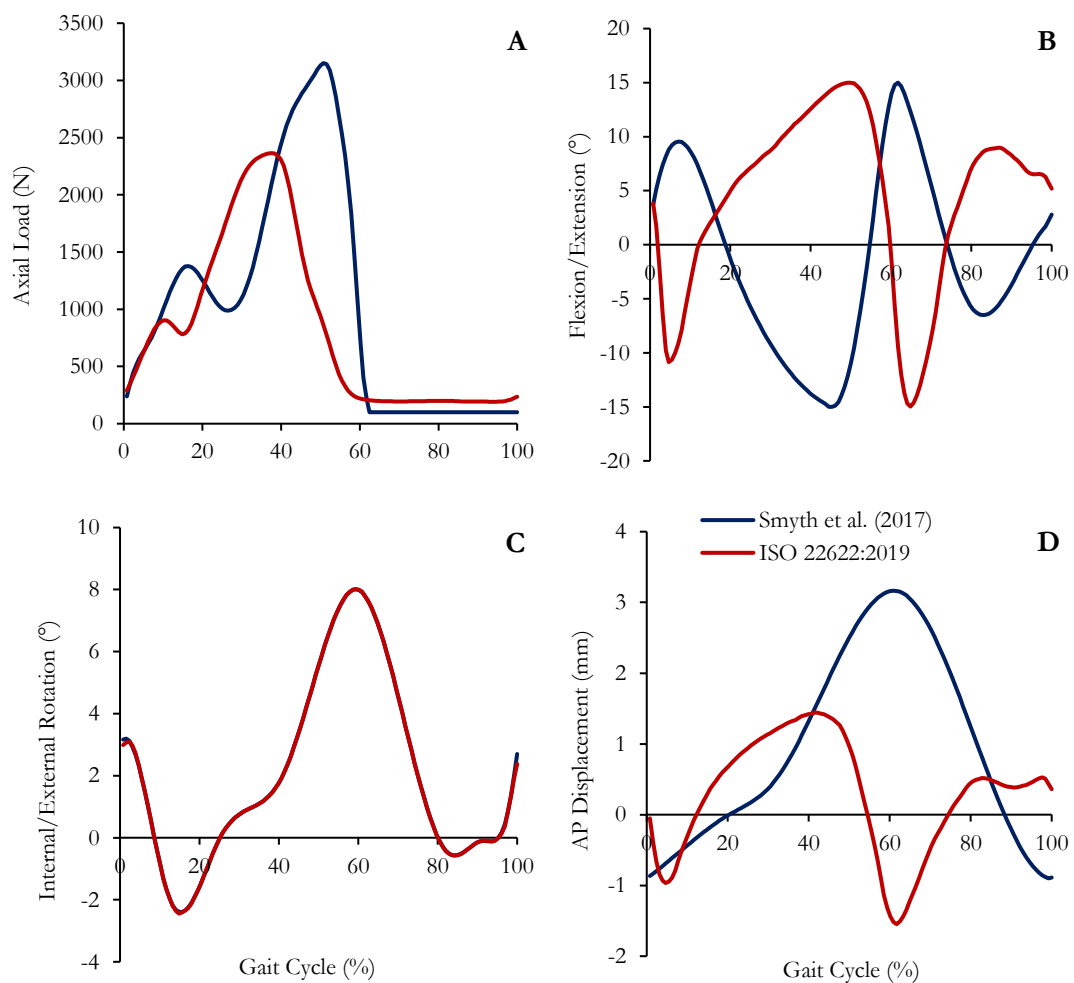


Figure 52. ISO standard input profiles (red) compared to the previously simulated UoL (blue) input profiles for AL (A), FE angle (B), IER angle (C) and AP displacement (D).

Table 13. Comparison of peak inputs from University of Leeds (UoL) and ISO 22622:2019 profiles.

Input	Axial Load (N)	DF/PF (°)	Tibial IER (°)	AP Displacement (mm)
ISO 22622:2019	191.5 to 2365.7	+15.0 to -15.0	-2.45 to +8.02	+1.45 to -1.55
UoL	100 to 3150	-15.0 to +15.0	-2.3 to +8.0	+3.1 to -0.9

Both displacement controlled simulator inputs had similar tibial IER and FE profiles (Figure 53), but a difference in polarity (i.e. direction of application) was apparent in the FE profile. For the ISO 22622:2019 input profile, extension in KSem was used to mimic dorsiflexion (positive) and flexion motion was used to measure plantarflexion (negative), while the UoL FE profile was run in the opposite direction (Figure 53). The ISO 22622:2019 profile also used a reduced peak AL (2365.7 N) and AP displacement ROM (3.0 mm) compared to the UoL profile (3150 N and 4.0 mm, respectively). Figure 54 exhibits the sign conversion alongside the positive directions of the load and motion for a left ankle joint, according to ISO 22622:2019.

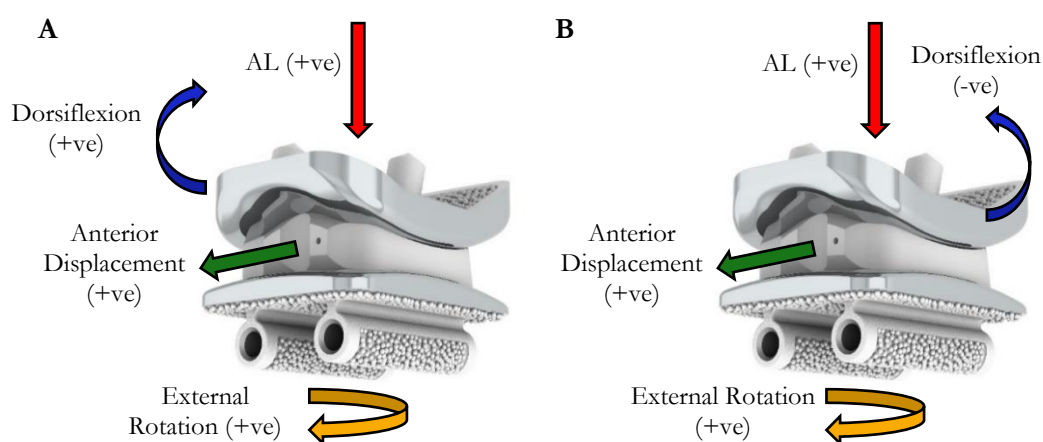


Figure 53. Schematic diagram with sign convention for the loading and kinematic profile directions from ISO 22622:2019 (A) and University of Leeds (Smyth et al., 2017) (B) of a left implant in the inverted position.

### 4.3 Methods

KSem was run for 3 Mc under the UoL profile to compare the effect of simulator type. The same inserts were then run for an additional 2 Mc under ISO 22622:2019 profiles, to investigate the effect of varying simulator inputs on implant wear. The re-use of samples within the same wear simulator study is not an unusual practice, with earlier studies using worn samples throughout their tests to determine the influence of varying kinematic inputs on the wear rates of TKR (McEwen et al., 2005) and TAR (Smyth et al., 2017).

Both studies using KSem applied the same methodological approach and experimental conditions as discussed in Chapters 2 and 3. KSem was run under displacement control with an operating frequency of 1 Hz (Section 2.3.8). The lubricant contained 25% bovine serum diluted

with 0.04% sodium azide solution (Section 2.3.9), resulting in a final protein concentration of 15.75 g/L (Appendix D.2). The serum was replaced every 330,000 cycles to ensure a continued protein content was maintained. After each Mc, the components were moved between stations to determine inter-station variability and contact area checks were performed to ensure similar component positioning across stations (Section 2.3.5).

The mean and independent loading and kinematic output profiles from the six stations of KSem were compared to the desired simulator input requirements. Differences between output and input kinematics were calculated and averaged across the six stations as a percentage of the corresponding maximum demanded. They were then compared to the maximum tolerance of the output kinematics ( $\pm 5\%$ ). Tuning of the PID control parameters of KSem was completed for each station after every serum change and start of a new Mc. This was performed to optimise output profiles compared to the desired input demand and reduce inter-station variability (Section 2.6).

Prior to the start of the wear simulation, the conventional UHMWPE inserts were soaked in deionized water for a minimum of four weeks. Wear was determined gravimetrically at 1 Mc intervals, with an unloaded soak control being used to monitor moisture uptake and weighing conditions. Cumulative volumetric wear was calculated for the independent stations and the mean wear rate was then determined for all six stations of KSem for both simulator type and input conditions (Section 2.4). The wear results from the first 3 Mc in KSem were compared to previous data obtained for the same sized implant in KSpn (Chapter 3). Although the implants were run for 5 Mc in KSpn, the same wear time point of 3 Mc was selected, to allow for a direct comparison of wear rates between the two simulator models.

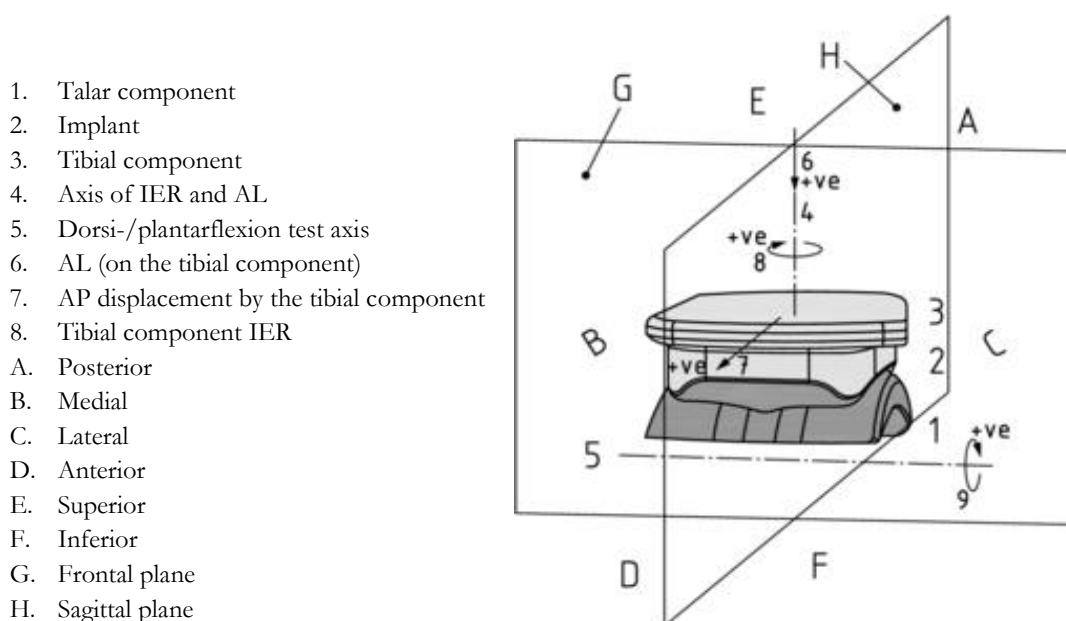


Figure 54. Sign convention and positive directions for the load and motion, shown for a left ankle joint-prosthesis. Adapted from ISO 22622:2019.

The first Mc (0-1) in both implant parameter studies (Chapter 3) was associated with a significantly higher wear rate, which was referred to as the run-in phase. The steady-state wear rate (1-3 Mc) from the simulator type study, under UoL inputs, was compared to the wear rate after an additional 2 Mc of ISO 22622:2019 inputs on the same inserts. A comparison between run-in wear rates (0-1 Mc) would not have been appropriate, as the run-in phase could not be conducted twice on the same implants. This is especially since the first Mc in both implant parameter studies (Chapter 3) was associated with a significantly higher wear rate. This study followed a similar kinematic input comparison study by Smyth et al. (2017), which explored varying input conditions at 2 Mc intervals and determined that changes in surface roughness (Ra) were reduced after the initial 'run-in' period.

2D contact surface measurements were taken on each of the bearing surfaces of the implants, with average surface roughness (Ra), maximum profile peak height (Rp), maximum profile valley depth (Rv), surface skewness (Rsk), and surface kurtosis (Rku) being determined (Section 2.7). This process was performed at the end of the simulator type (3 Mc) and simulator input (5 Mc) studies, which allowed comparisons of the topographic changes between the simulator conditions. During the study on KSpn (Chapter 3), the topographic assessment was performed at the end of the 5 Mc, resulting in roughness changes not being measured at the same time point as the study in KSem (under the same UoL inputs). As the implants in KSpn were exposed to a longer simulation period between measurement points (increased likelihood of continued surface damage), no statistical analysis was performed between the post-simulation measurements. Instead, the pre-and post-simulation contact measurements were compared statistically to determine if the same trend in topographic changes occurred in both simulator types. The topographic changes were also compared statistically between the simulator input conditions.

The superior inserts from both simulator parameter studies were visually inspected and digital images were taken to establish the mode of wear and the extent of damage. Damage modes defined by Hood et al. (1983) (Section 2.8) were visualised using non-contact microscopy. The simulated inserts from both simulator parameter study conditions were also compared to previously simulated devices, as well as a collection of MB implant retrievals within the UoL retrieval bank (Section 2.9).

To compare the mean wear rates (95% CL) between the simulator types and simulator inputs, a student's (independent) t-test was used. Whereas, a paired (dependent) t-test was used to determine the wear rate differences between run-in and steady-state wear phases. Additional paired t-tests were also applied to verify the pre- and post-simulation topographic changes in the simulator type study. Again, a student's t-test was used to determine the difference in topographic changes between simulator input conditions during steady-state wear. Significance level was accepted at the  $p \leq 0.05$  level and all statistical analysis was conducted using SPSS v26.0 (SPSS Inc, Chicago, USA).

## 4.4 Results

### 4.4.1 Simulator Loading and Kinematic Performance

#### Pneumatic vs Electromechanical

During the 2 Mc, one of the bearing inserts (implant 5 in station 6) dislocated during simulator set-up after a serum change, which resulted in metal-on-metal contact between the tibial and talar components and significant deep scratching on both articulating surfaces. The set-up error occurred due to the meniscal insert shifting and not being positioned centrally on the tibial bearing surface. The extent of the surface damage would have had a significant effect on the samples' wear rate, which would have in turn, influenced mean wear rate and subsequent conclusions drawn from the study. The sample was therefore removed from the study, leaving the remaining five implants to undergo the rest of the wear simulations.

In order to understand the differences between the simulator types, the mean (Figure 55) and station specific (Figure 56) simulator loading and kinematic outputs were compared across the gait cycle to the desired UoL input profiles. The mean ( $\pm$  95% CL) peak output AL was  $3158.8 \pm 2.4$  N, which compared well to the desired peak output of 3150 N. In addition, KSem was able to produce the peak AL (0.3%) within the tolerances of the desired input AL ( $\pm$  5%). Despite the attempts to tune and scale the output loading and kinematic profiles through the adjustment of the simulator PID control parameters, KSpn was unable to attain the desired AL demand, producing a substantially lower mean peak value of  $2542.3 \pm 86.5$  N (Figure 55A). The substantially lower AL, which aimed to mimic heel-strike, was outside of the maximum output tolerance for peak AL (-19.3%).

During the swing phase, neither simulator was able to remain within maximum output tolerance ( $\pm$  5%), in relation to the desired swing phase load of 100 N. KSem was unable to attain the desired load, producing a lower output mean load of  $67.0 \pm 5.1$  N, which was out of the maximum output tolerance (-33.0%). Whereas, KSpn produced a larger AL ( $222.1 \pm 11.0$  N) during the swing phase than the desired maximum input, which also resulted in the simulator failing to produce output AL within the tolerance of the peak AL (112.1%). The pneumatic control system of KSpn produced substantial oscillations in the output profiles, while the simulator could not rapidly respond to the input AL cycle. This resulted in a small lag of approximately 0.05 seconds in AL output profile for all stations (Figure 55A).

Figure 56A displays a greater variance in output loading profiles between the six stations in KSpn compared to KSem. This was particularly apparent during the start of each cycle, before attaining peak AL and in the swing load phase. Each station from KSem produced higher AL than the desired peak AL input, while all stations from KSpn produced lower load than the selected input. All six stations from both simulator types produced significant resonance in the output profile during the swing load phase. This deviation from the desired output was more apparent in KSpn,

and was likely the result of the simulators inability to maintain such a low load, particularly when the desired swing load occurred straight after the peak AL. This may also be a limitation of the load cell calibration, particularly during the low loads replicating the swing phase. The FE axis on both simulators was driven electromechanically, therefore it was not unexpected that each simulator performed similarly and were both capable of accurately following the FE angle input profile throughout the gait cycle and attaining the intended peak values for plantarflexion and dorsiflexion ( $\pm 15.0^\circ$ ) (Figure 55B). The mean peak output plantarflexion and dorsiflexion angles were  $15.7 \pm 0.0^\circ$  and  $-15.2 \pm 0.0^\circ$  in KSem, compared to  $15.1 \pm 0.0^\circ$  and  $-15.0 \pm 0.0^\circ$  in KSpn (Figure 55B). Both KSem and KSpn were able to produce outputs within the maximum output tolerance ( $\pm 5\%$ ) for peak plantarflexion (4.9% and 0.5%) and dorsiflexion (1.3% and 0.0%) angles. The tight CL throughout the gait cycle also demonstrated that the variance between stations was negligible in both simulator types (Figure 56B).

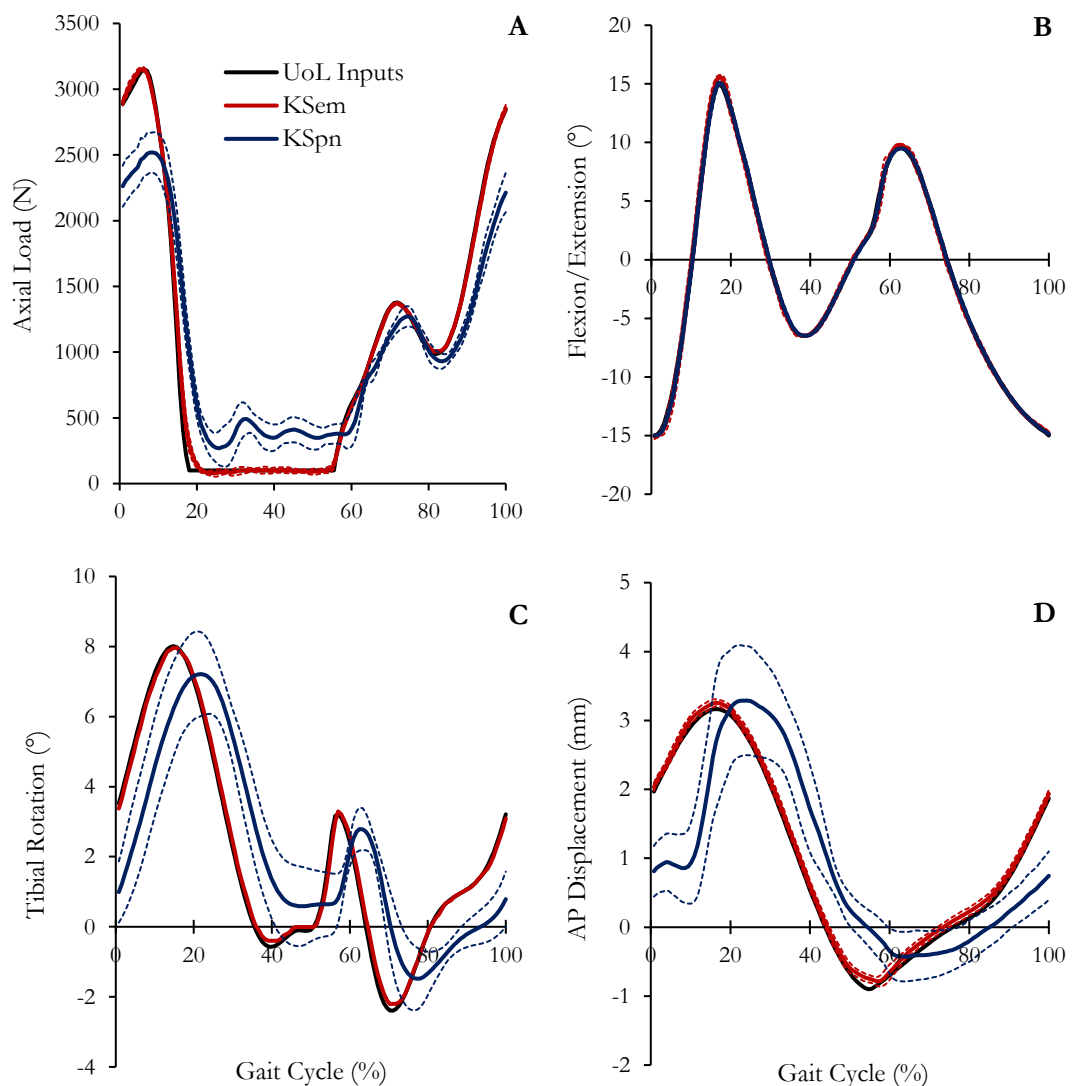


Figure 55. Simulator input (black) and output profiles (red) (mean  $\pm$  95% CL,  $n = 6$ ) across all stations for AL (A), FE angle (B), tibial IER angle (C) and AP displacement (D) from the electromechanical (red) and pneumatic (blue) simulators.

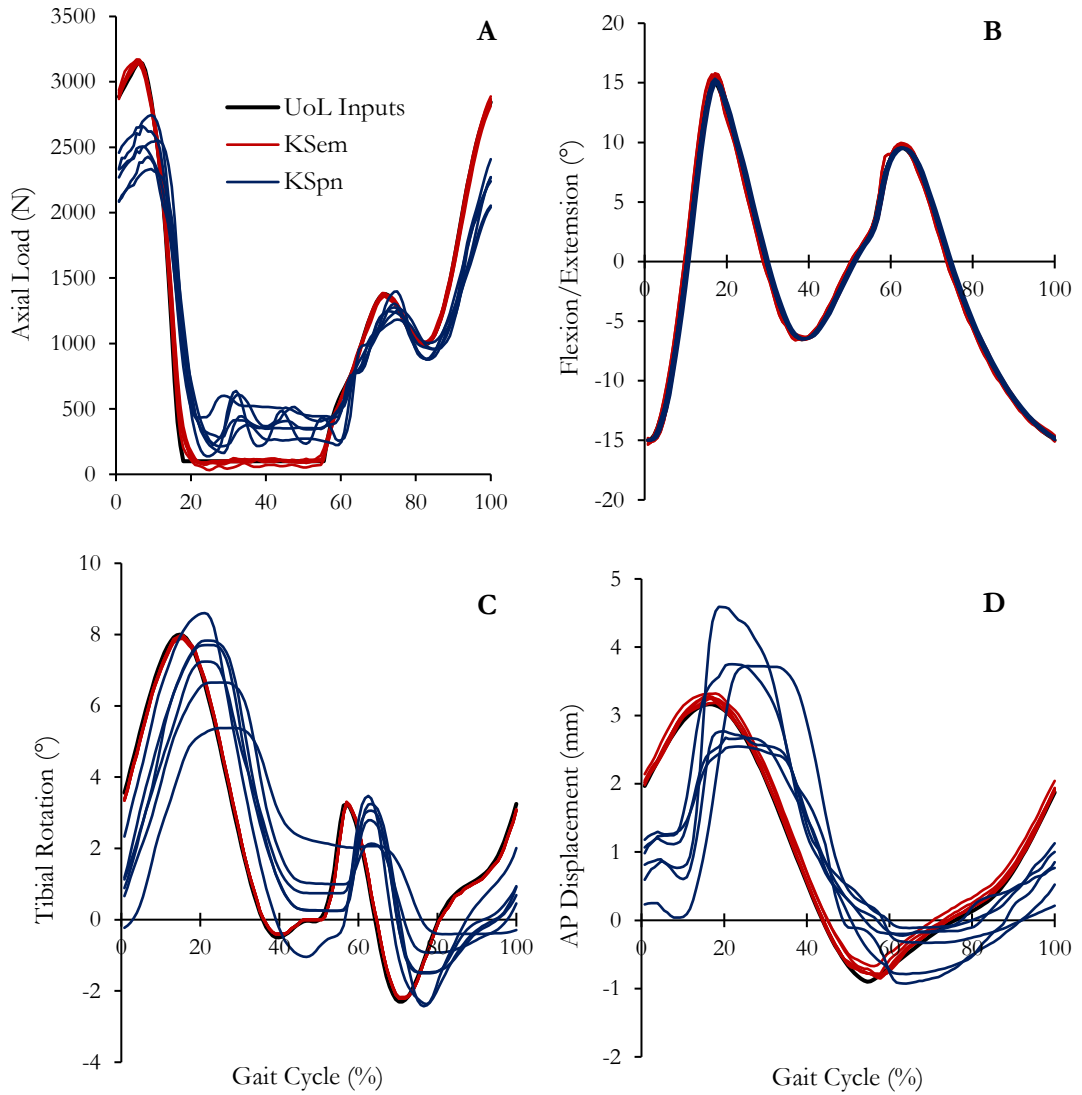


Figure 56. Simulator input (black) and output profiles for each station of KSem (red) and KSpn (blue) for AL (A), FE angle (B), tibial IER angle (C) and AP displacement (D).

The KSem was able to produce a mean peak external rotation angle of  $8.0 \pm 0.0^\circ$ , which was considerably higher than the mean output angle produced by KSpn ( $7.2 \pm 0.1^\circ$ ), and more closely matched the desired external rotation input angle of  $8.0^\circ$  (Figure 56C). This resulted in KSem being within the maximum output tolerance ( $-0.4\%$ ) for peak input external rotation angle, while KSpn was unable to attain external rotation peak angle within the maximum tolerance ( $-9.5\%$ ) of the UoL input profile (Figure 55C). KSem ( $-2.2 \pm 0.0^\circ$ ) was also able to reproduce the peak internal rotation angle ( $-2.3^\circ$ ) more closely than KSpn ( $-1.5 \pm 0.3^\circ$ ). Similarly, KSem remained within the maximum output tolerance for internal rotation ( $-4.0\%$ ), while KSpn produced significantly lower mean peak internal rotation angle outside the output tolerance ( $-32.9\%$ ). The small CL measured for mean peak IER angles in KSem demonstrated that there was insignificant inter-station variability, which was apparent for the rest of the gait cycle (Figure 56C). There was larger variation in rotation profiles in KSpn, with station 1 producing greater external rotation than the desired input demand, with the other five stations being unable to reproduce the peak

external rotation angle of  $8.0^\circ$  (Figure 56C). KSpn caused a phase lag of around 0.05 seconds between the rotation demand and associated output profiles across the six stations (Figure 56C). This lag could be attributed to problems of data logging within KSpn.

Despite the attempts to optimise the kinematic output performance of both simulators through PID tuning, the corresponding mean peak AP displacements achieved by KSem ( $3.3 \pm 0.1$  mm) and KSpn ( $3.6 \pm 1.0$  mm) were slightly higher than the desired UoL peak AP displacement of 3.1 mm (Figure 55D). This resulted in both simulators failing to remain within the maximum output tolerance for peak input AP displacement (KSem = 6.5%; and KSpn = 10.2%). All six stations of KSem produced slightly higher AP displacement than the peak simulator input, but variance between stations was limited (Figure 56D). KSpn produced substantially greater inter-station variability throughout the 3 Mc, with three stations (2, 5 and 6) producing greater mean AP displacement compared to the input demand requested, while the other three stations (1, 3 and 4) maintained a reduced AP motion (Figure 56D). Each station of KSpn also possessed a phase lag, which occurred just after peak AL rather than in phase with it. This lag phase was not apparent in KSem, with peak AP displacement occurring around the same time period as maximum AL during stance.

### **University of Leeds vs ISO Input Profiles**

Figure 57 shows the mean ( $\pm$  95% CL) output profiles from KSem compared to the corresponding ISO 22622:2019 inputs. Figure 58 presents the inter-station variability for each output profile against the desired input. KSem was able to produce a mean peak AL ( $2378.2 \pm 2.9$ ), which was comparable to the desired peak AL (2365.7 N) (Figures 57A). In addition, KSem achieved the recommended ISO 22622:2019 AL peak input (0.5%) within its maximum output tolerance ( $\pm$  5%). Five of the six stations produced slightly greater peak AL, while station 3 tended to underload the device throughout the 2 Mc (Figures 58A). Each station of KSem continued to display oscillations in the output AL profile during the period of low load, which was likely related to load cell calibration during low loads.

KSem was capable of accurately following FE angles throughout the majority of the input gait cycle (Figure 57B). The mean peak output flexion (dorsiflexion) and extension (plantarflexion) angles were  $15.1 \pm 0.0^\circ$  and  $-16.8 \pm 0.0^\circ$ , respectively, compared to the peak input value of  $\pm 15.0^\circ$ . This resulted in the simulator being able to produce a mean peak dorsiflexion angle (0.4%) within the input tolerance ( $\pm$  5%). Each of the stations' output profiles were tuned to replicate the desired input profiles to the simulators best ability. Despite this, all six stations over-shot the required peak plantarflexion angle (Figure 58B) and failed to remain within output tolerance (12.0%). This was likely due to the quick transition between peak dorsiflexion and plantarflexion angles, with the simulator overshooting the latter. This finding was apparent on all six stations, with limited variability between stations, as shown by the negligible CL for peak output angles and throughout the ROM (Figure 58B).

Tibial IER was the most closely followed input profile (Figure 57C), with limited variability between the six stations for the peak values and ROM (Figure 58C). KSem achieved a mean peak external rotation angle of  $8.0 \pm 0.0^\circ$  and internal rotation angle of  $-2.2 \pm 0.0^\circ$ , which compared well to the peak input values of  $8.02^\circ$  and  $-2.45^\circ$ , respectively. The simulator was able to successfully run tibial IER, as both peak internal ( $-4.0\%$ ) and external rotation ( $-0.4\%$ ) output values were within the maximum output tolerance for peak IER ( $\pm 5\%$ ). KSem also continued to produce greater AP displacement ( $1.6 \pm 0.0$  mm) than the desired input (Figure 57D), when running under UoL input profiles (Figure 55D). All six stations produced higher displacement than the intended peak anterior displacement, resulting in KSem not being within the maximum output tolerance (7.4%).

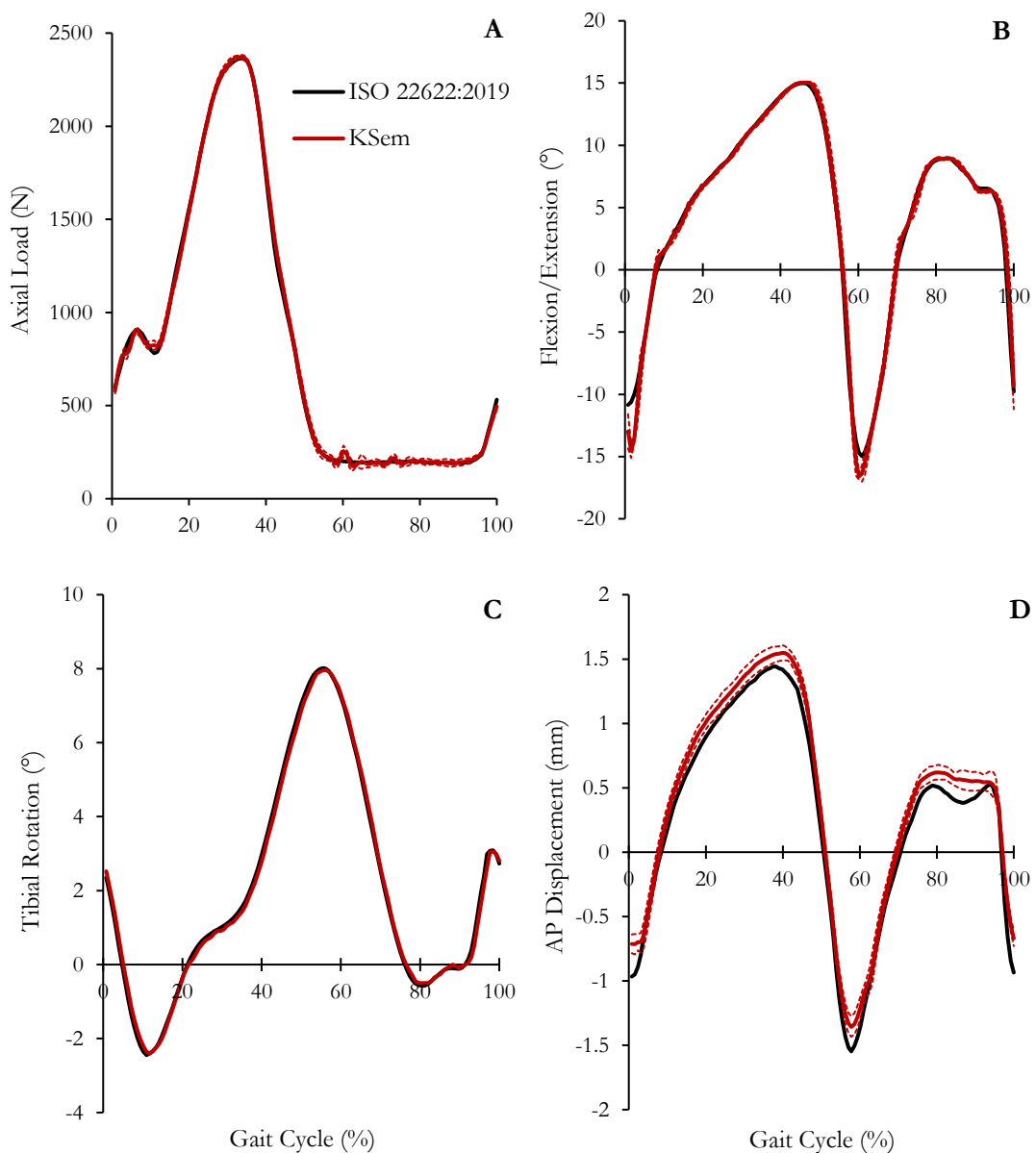


Figure 57. Simulator input (black) and output profiles (red) (mean  $\pm$  95% CL,  $n = 6$ ) across all stations for AL (A), FE angle (B), tibial IER angle (C) and AP displacement (D) for the duration of the simulation (2 Mc).

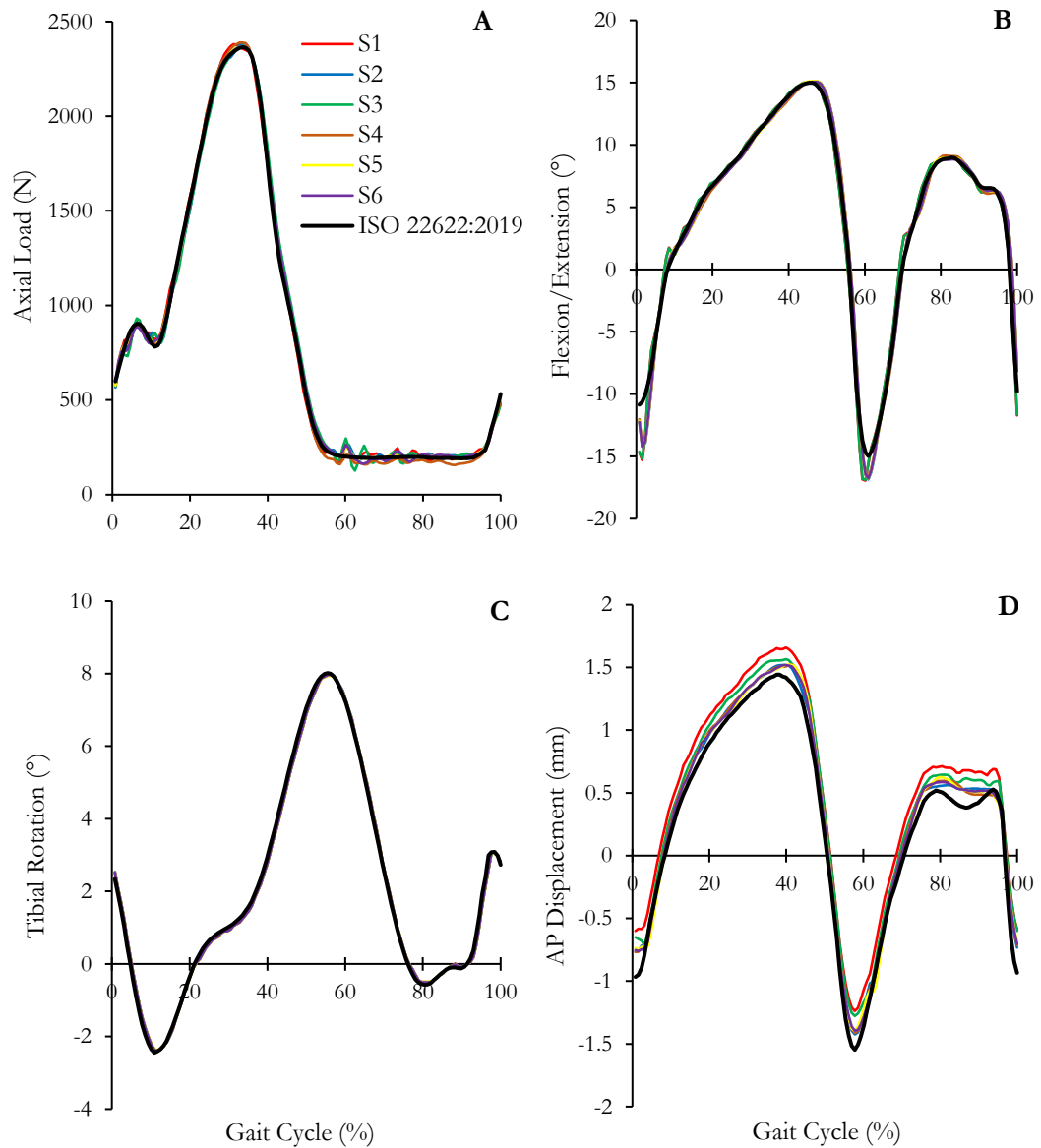


Figure 58. Simulator input (black) and mean output profiles from each of the six stations for AL (A), FE angle (B), tibial IER angle (C) and AP displacement (D) for the duration of the simulation (2 Mc).

#### 4.4.2 Wear Rate Comparison

##### Pneumatic vs Electromechanical

The cumulative and mean wear rates ( $\pm 95\%$  CL) for the medium sized implants in both simulator types are shown in Figures 59 and 60. Despite the closer following of the UoL input profiles in KSem, there was no statistically significant difference ( $p = 0.378$ ) in mean wear rate between simulator types (KSem =  $17.18 \pm 5.46 \text{ mm}^3/\text{Mc}$  and KSpn =  $14.51 \pm 5.27 \text{ mm}^3/\text{Mc}$ ) after 3 Mc.

Similar to the implant parameter studies (Chapter 3), the gravimetric wear measurements were further separated into two wear phases: initial run-in phase (0-1 Mc) and steady-state phase (1-3 Mc). The wear rate during the run-in wear phase in KSem measured  $22.38 \pm 9.41 \text{ mm}^3/\text{Mc}$ ,

which was not significantly different ( $p = 0.997$ ) to the run-in wear rate from KSpn ( $22.40 \pm 9.74$  mm<sup>3</sup>/Mc) (Figure 60). After the initial Mc, the steady-state wear rate reduced significantly to  $9.59 \pm 3.02$  mm<sup>3</sup>/Mc ( $p = 0.007$ ) and  $7.11 \pm 3.12$  mm<sup>3</sup>/Mc ( $p = 0.003$ ) in KSem and KSpn, respectively. However, there was no significant difference ( $p = 0.170$ ) between simulator type during steady-state wear phase.

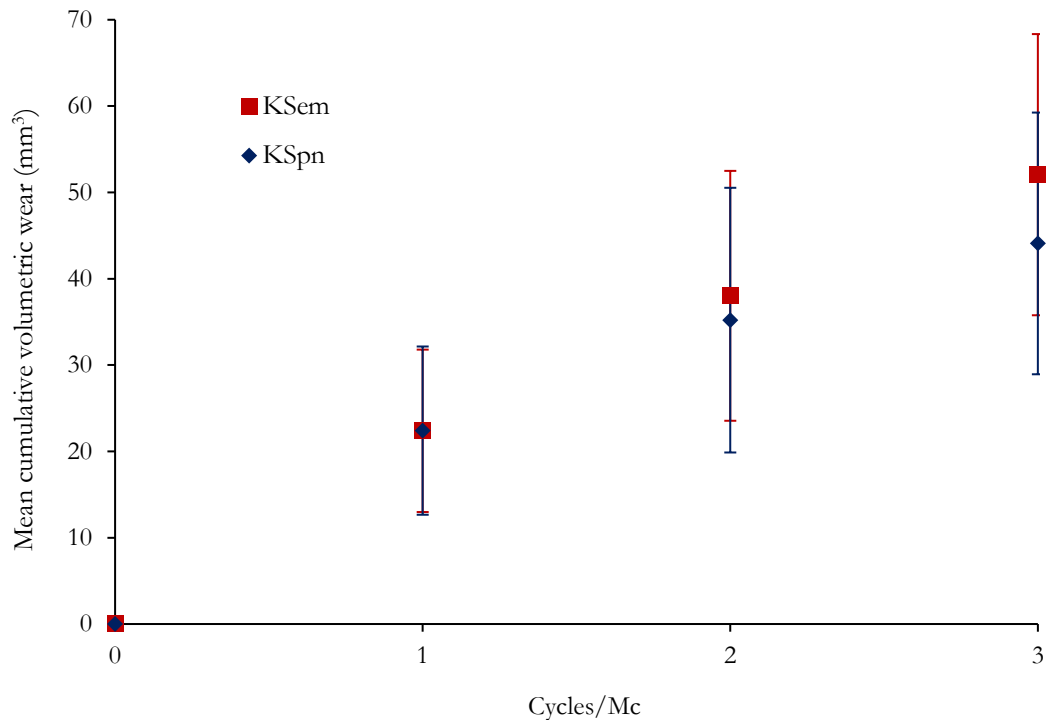


Figure 59. Cumulative mean wear rates (mm<sup>3</sup>) with  $\pm 95\%$  CL for the medium sized implants within the electromechanical (red) and pneumatic (blue) controlled simulators after 3 Mc ( $n = 5$ ).

The large variability ( $\pm 95\%$  CL), evidenced by the error bars in Figure 60, demonstrates that there was some variation in wear rates between individual inserts. This variability was most apparent during the run-in wear phase (Figure 60). As for all the simulator studies in this project, inserts were moved between stations to reduce the effect of inter-station variability, due to the possibility one station may apply higher or lower loads and kinematics than the desired input profiles (Section 4.4.1). The variability in volumetric wear for both the inserts and stations in KSem are shown in Figure 61.

During the run-in wear phase (0-1 Mc), sample 3 ( $29.93$  mm<sup>3</sup>) and 6 ( $29.28$  mm<sup>3</sup>) experienced higher wear rates in stations 3 and 6, respectively (Figure 61). However, this effect was not sustained throughout the further 2 Mc's for each of the stations during the steady-state wear phase. This finding may be a result of the manufacturing tolerance of the insert rather than the specific simulator stations. There were also no noticeable changes between stations, in terms of reproducing tibial rotation, which has previously been shown to have a significant effect on implant wear (Smyth et al., 2017). All the stations produced substantially higher peak

plantarflexion than the desired maximum input, which affected each of the 6 samples throughout the 3 Mc simulation. KSpn showed much higher variability in wear rates between inserts and stations (Section 3.4.2).

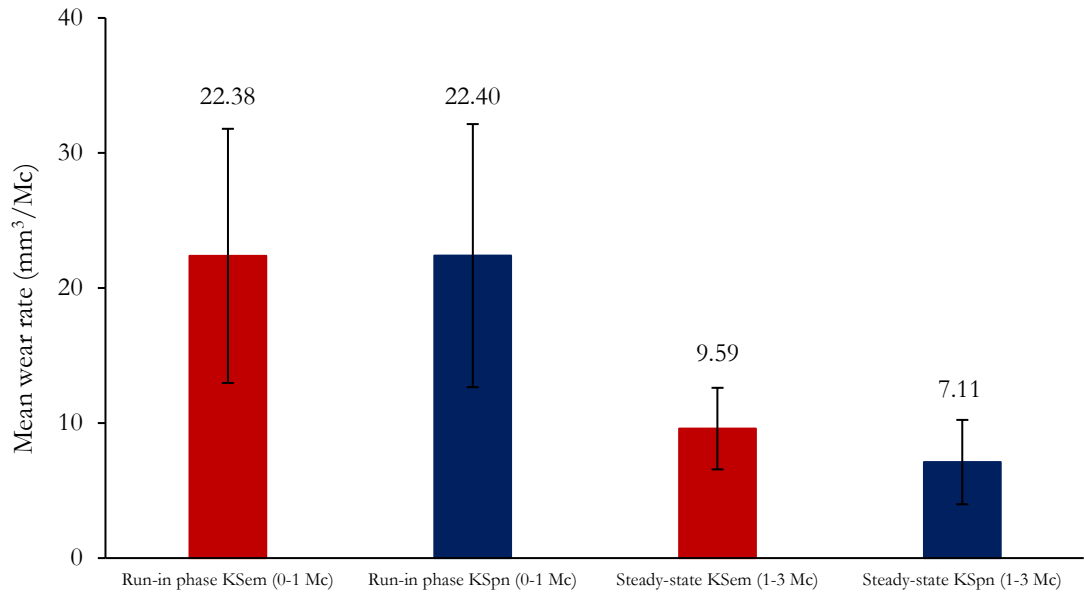


Figure 60. Mean run-in and steady-state wear rate (mm<sup>3</sup>/Mc) with  $\pm$  95% CL for the medium sized implants within the electromechanical (red) and pneumatic (blue) controlled simulators after 3 Mc (n = 5).

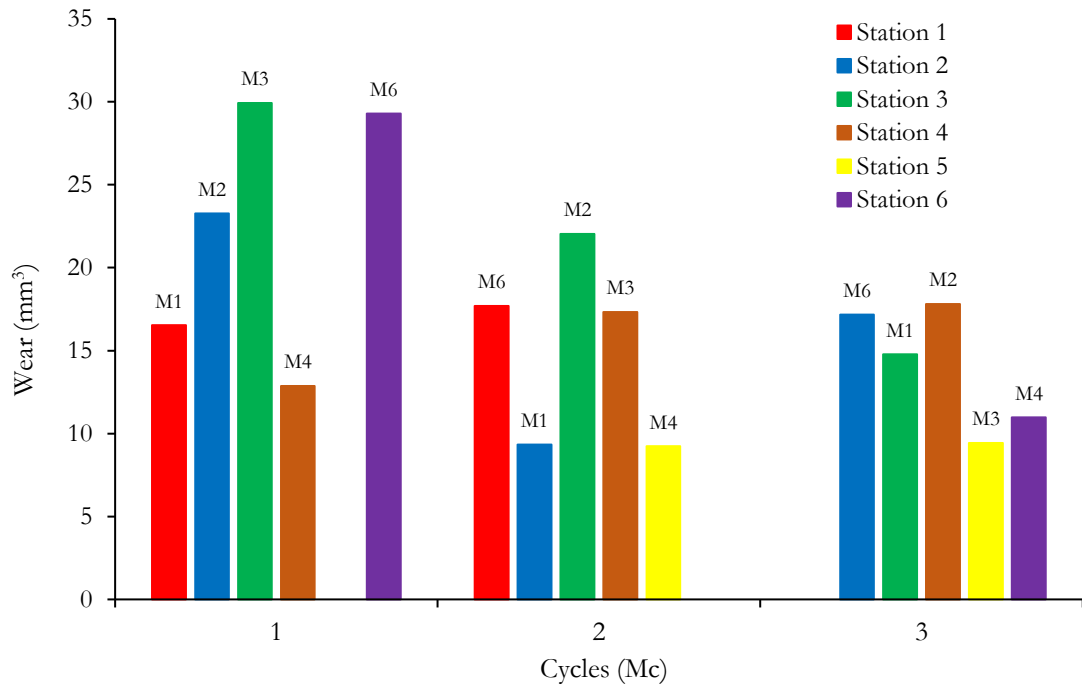


Figure 61. Individual wear rates for the medium sized inserts during each Mc (n = 5), with the colours representing the station within the electromechanical simulator.

### **University of Leeds vs ISO Input Profiles**

Even after the addition of the different simulator inputs on the previously worn components, there was no significant difference ( $p = 0.054$ ) in the mean steady-state wear rate between the ISO 22622:2019 ( $13.07 \pm 3.05 \text{ mm}^3/\text{Mc}$ ) and UoL ( $9.59 \pm 3.02 \text{ mm}^3/\text{Mc}$ ) input profiles after 2 Mc (Figure 62). With regard to the inter-station variability, sample 6 was found to have substantially higher wear rate during the first Mc compared to the other four samples (Figure 63). However, this effect did not remain for the following Mc. This was more than likely due to machining tolerance or potential malalignment of the insert when setting up between serum changes, rather than inter-station variability due to inadequate loading and kinematic capabilities.

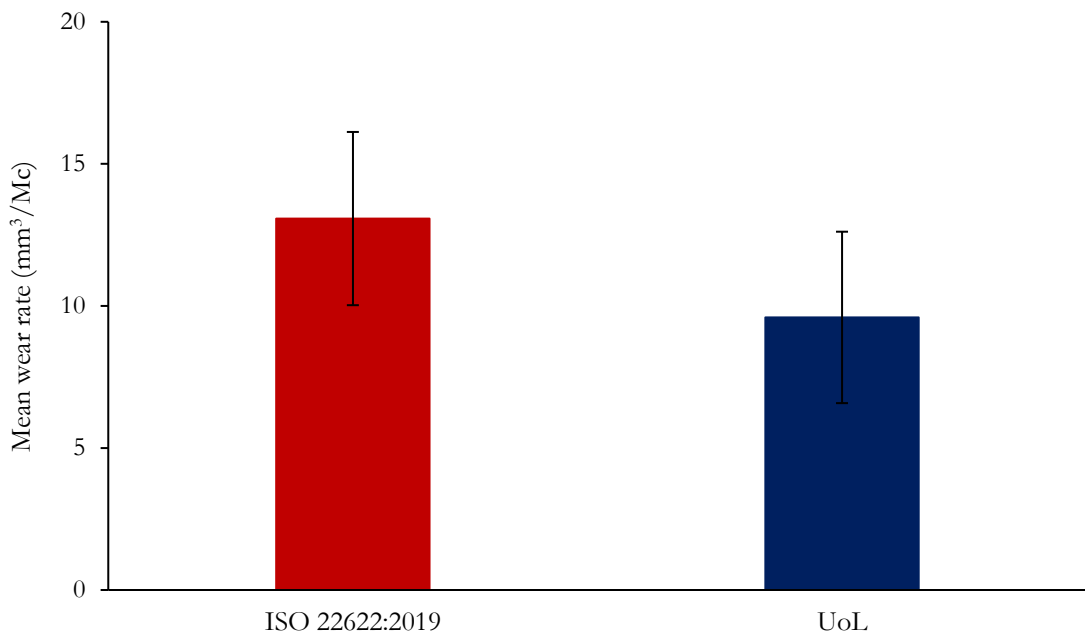


Figure 62. Mean steady-state wear rate ( $\text{mm}^3/\text{Mc}$ ) with  $\pm 95\%$  CL for the medium sized implants simulated under ISO 22622:2019 (red) and University of Leeds (blue) loading and kinematic inputs for 2 Mc ( $n = 5$ ).

### **4.4.3 Surface Topographic Results**

#### **Pneumatic vs Electromechanical**

The mean ( $\pm 95\%$  CL) surface topographic parameters for the medium sized implants in both pneumatic and electromechanical simulators are presented in Appendix E.3. Prior to the start of the wear simulation, there were no statistically significant differences ( $p \geq 0.05$ ) in mean topographic parameters of the unworn bearing surfaces between simulator types. The topographic changes of the implants run under pneumatic control for 5 Mc, can be found in Section 3.4.3.

#### ***Average Surface Roughness (Ra)***

There was a notable reduction in Ra at the bearing surfaces of the conventional UHMWPE, while Ra tended to increase for the different regions of the metallic components. The trends in

topographic changes in Ra between pre- and post-simulation were comparable between simulator types, particularly at the insert bearing surfaces.

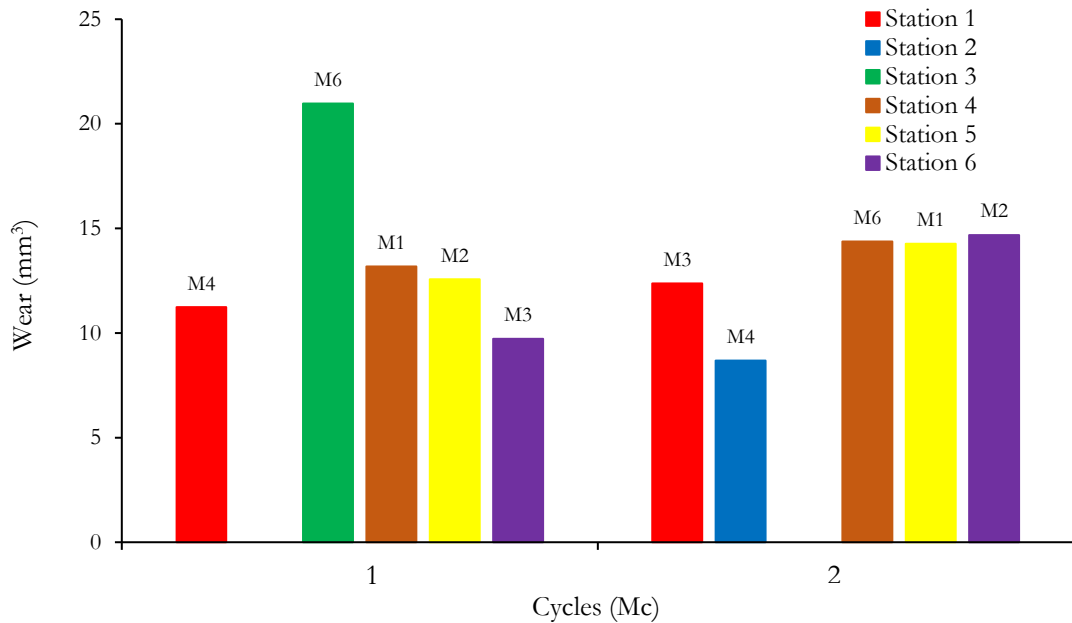


Figure 63. Individual wear rates for the medium sized inserts during each Mc (n = 5), under ISO 22622:2019 loading and kinematic inputs. Each colour represents the specific station within the electromechanical simulator.

The mean medial, central and lateral curved regions of the inferior articulating surfaces of the conventional UHMWPE inserts significantly reduced in Ra by 53.85% ( $p = 0.002$ ), 61.40% ( $p = 0.001$ ) and 55.73% ( $p = 0.000$ ), respectively. The less curved surface of the superior insert had an even greater reduction ( $p = 0.000$ ) in mean Ra (91.87%). The reduction in Ra for both articulating UHMWPE surfaces indicated that the peaks on the surface were flattening, which was likely related to the removal of the machining lines and polishing of the surface, particularly during the run-in wear phase (Section 4.4.4). A significant increase in Ra occurred at both the tibial ( $p = 0.012$ ) and central region of the talar articulating surfaces ( $p = 0.020$ ) between the pre- and post-simulation measurements.

#### ***Maximum Profile Peak Heights (Rp)***

The greatest change in Rp occurred at the superior insert surface, with a significant ( $p = 0.000$ ) reduction of 90.94%. Each region of the curved inferior insert surface demonstrated significantly reduced Rp ( $p = 0.000$ ). The tibial bearing surface showed a significant increase in Rp between topographic measurements ( $p = 0.039$ ), while the medial ( $p = 0.011$ ), central ( $p = 0.005$ ) and lateral ( $p = 0.014$ ) regions of the talar components also indicated significant increases in Rp.

#### ***Maximum Profile Valley Depth (Rv)***

Following a similar topographic change pattern, the superior insert surface was found to have the largest significant ( $p = 0.000$ ) decrease in Rv (87.50%) from pre-to-post wear simulation in

KSem. All three regions of the inferior insert surface also exhibited statistically significant reductions ( $p = 0.000$ ). The medial ( $p = 0.001$ ), central ( $p = 0.016$ ) and lateral ( $p = 0.003$ ) regions of the talar components demonstrated significant increases in Rv, as well as the bearing surface of the tibial component ( $p = 0.043$ ).

### ***Surface Skewness (Rsk)***

Each of the articulating surfaces, independent of material, demonstrated a negative Rsk after 3 Mc. Due to the large variability ( $\pm 95\%$  CL) between the five samples measured, Rsk was not found to be significantly different between pre-and post-simulation ( $p \geq 0.05$ ). The only significant finding was found at the central curved region of the inferior insert surface ( $p = 0.017$ ; 827.27%) after 3 Mc of continued articulation.

### ***Surface Kurtosis (Rku)***

Each articulating surface had an increased Rku value after 3 Mc, with the superior insert surface producing a 717.84% increase in Rku ( $p = 0.005$ ). The medial side of the inferior insert was significantly higher post-simulation ( $p = 0.025$ ), while the central ( $p = 0.119$ ) and lateral ( $p = 0.218$ ) regions did not significantly differ from the unworn surfaces. All the metallic surfaces were also significantly ( $p \leq 0.05$ ) between the pre-and post-simulation measurements.

### **University of Leeds vs ISO Input Profiles**

The medium sized inserts underwent an additional 2 Mc of ISO 22622:2019 loading and kinematic inputs, to determine if there was any significant topographic changes between the two input profiles. The tables displaying the mean ( $\pm 95\%$  CL) surface topographic parameters for each of the articulating surfaces can be found in Appendix E.4.

Following a similar trend to the measured topographical changes under the UoL profile at 3 Mc, the superior insert bearing surface continued to exhibit the greatest reduction in Ra (30.00%), Rp (25.00%) and Rv topographic parameters. Nevertheless, none of these topographic changes at the superior insert surface and other articulating surfaces of the implants were statistically significant ( $p \geq 0.05$ ) between the differing loading and kinematic profiles at 3 Mc and 5 Mc, respectively. Each of the bearing surfaces continued to have a negative Rsk, independent of material and simulator input. The lateral region of the talar articulating surface was found to have a significantly lower ( $p = 0.000$ ) Rsk after the additional 2 Mc of ISO 22622:2019 profiles, when compared to the mean value recorded after 3 Mc under the UoL input profile (400.00%). However, the associated variability for each of the bearing surfaces was relatively high at both topographic measurement points. The medial ( $p = 0.407$ ) and central region ( $p = 0.864$ ) were not significantly different between the input profiles, nor between both articulating surfaces of the conventional UHMWPE. The Rku continued to increase at each of the bearing surfaces, with significant differences being found at the central ( $p = 0.000$ ) and lateral ( $p = 0.041$ ) curved regions of the talar components.

#### 4.4.4 Visual Damage Mode Comparison

##### Pneumatic vs Electromechanical

Figure 64 depicts the visual damage modes found at the superior insert surface after 3 Mc of continued articulation on KSem. The wear damage modes produced by KSpn can be found in Section 3.4.4. Both simulators produced comparable wear damage modes, with significant polishing and the removal of the machining lines on the superior insert surfaces, demonstrating strong evidence of burnishing. There were also obvious signs of abrasive wear, pitting, material on the surface, and multidirectional scratching (Figure 65).

Evidence of burnishing and multidirectional scratching were also found at the inferior bearing surface of the conventional UHMWPE from both simulator types. However, these damage modes could not accurately be imaged on the Alicona system, due to the large curvature of the inserts. There was evidence of polyethylene transfer and multidirectional scratching within the polyethylene contact area on the tibial components, while the talar components displayed fine unidirectional scratching aligned in the AP direction from both simulators. The talar components also showed signs of scratching perpendicular to the direction of primary articulation, caused by the multidirectional rotational and displacement motions at the MB bearing surface.

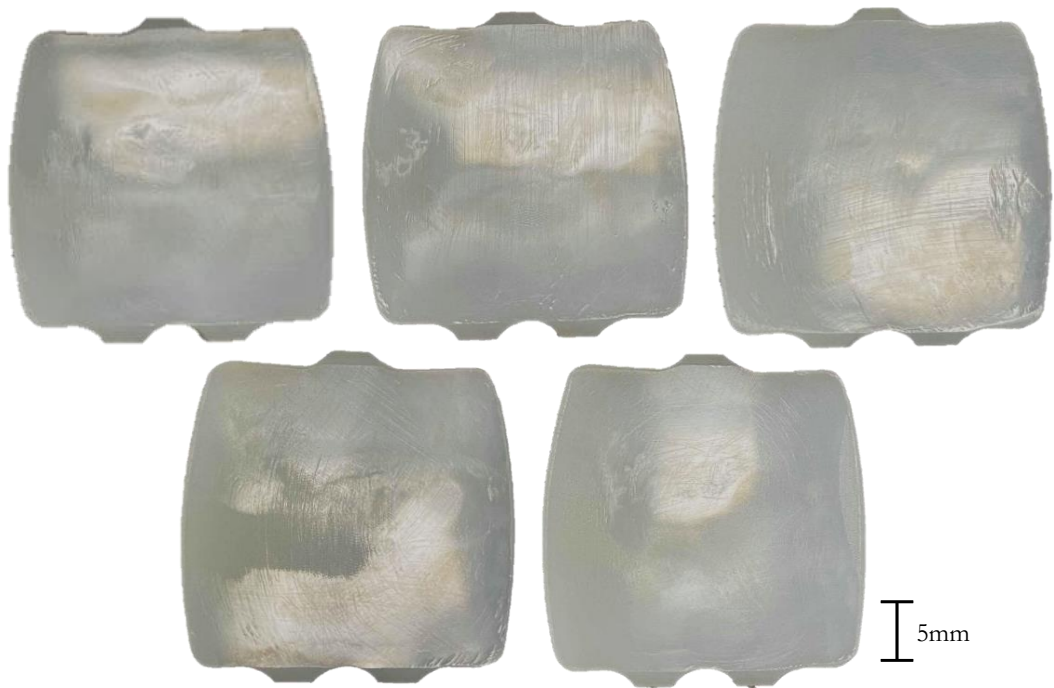


Figure 64. Photographs of five medium sized superior insert surfaces after 3 Mc in the electromechanical simulator (KSem), under University of Leeds (UoL) loading and kinematic input profiles. Machining lines are no longer visible and there are clear signs of abrasive wear, burnishing and multidirectional scratching across the articulating surface.

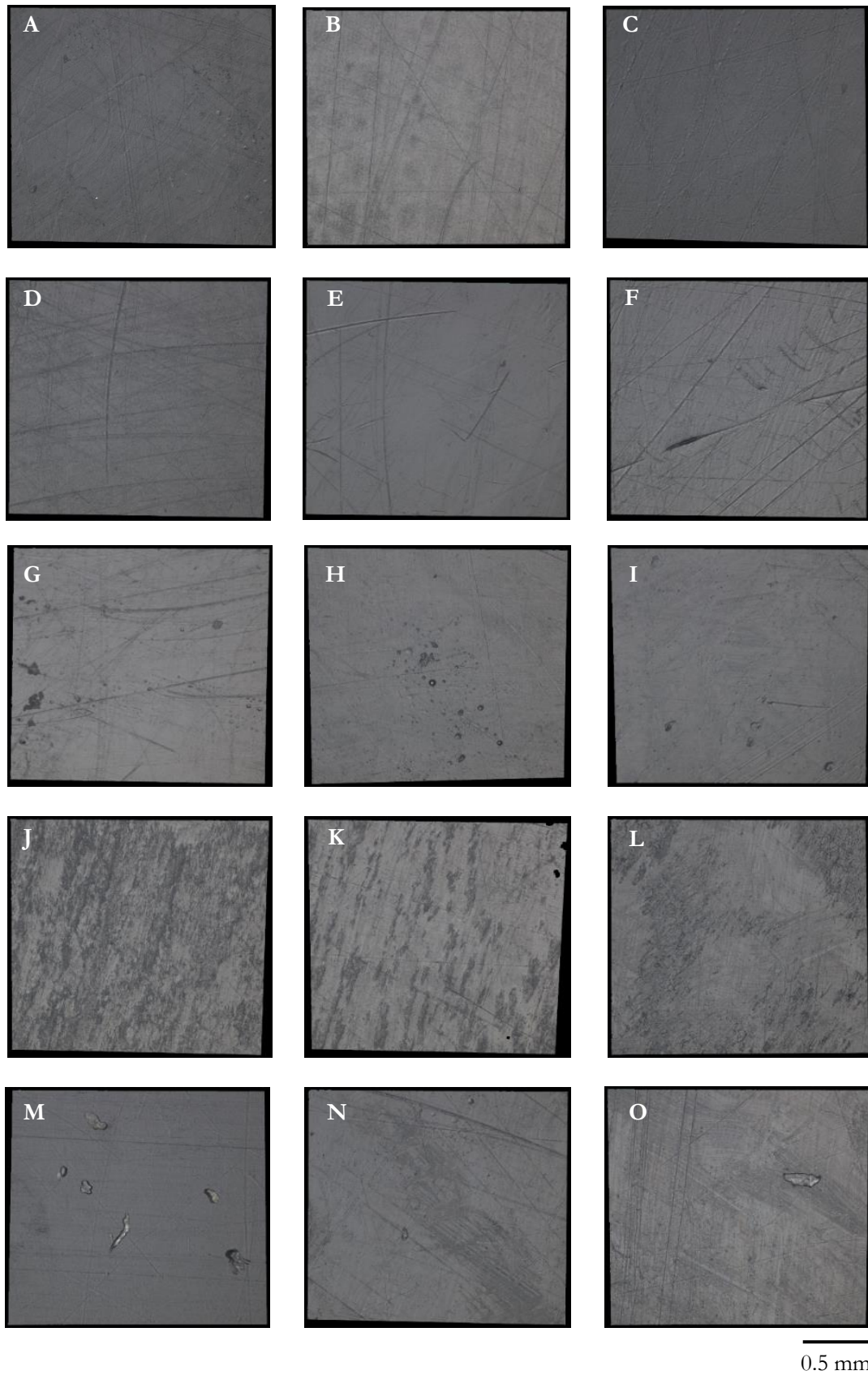


Figure 65. Damage modes on the superior bearing insert surface of the five medium sized implants after 3 Mc (n = 5): A-C = Burnishing; D-F = Scratching; G-I = Pitting; J-L = Abrasive wear; M-O = Material on the surface. Multiple damage modes were captured with the Alicona InfiniteFocus microscope (20x resolution).

### **University of Leeds vs ISO Input Profiles**

The ISO 22622:2019 loading and kinematic profiles produced comparable wear damage modes to the UoL profiles, with continued abrasive wear, burnishing and multidirectional scratching on the superior insert surfaces (Figure 66). The non-contact Infinite Focus microscope (Alicona, Austria) also identified areas of pitting and material transfer on the superior insert samples (Figure 67). The material found on the surface was not defined, but was likely to be proteins from the bovine serum that had adhered to the bearing surface. There was continued evidence of polyethylene transfer and multidirectional scratching within the conventional UHMWPE contact area on the tibial components. The articulating surface of the talar components also displayed multidirectional scratching, due to the mobile nature of the device. Both studies demonstrated similar visual wear damage modes to that seen in the implant parameter studies in Chapter 3 (Section 3.4.4) and to previously simulated and retrieved MB implants (Section 3.5.4).



Figure 66. Photographs of the six medium sized superior insert surfaces after 5 Mc, with the last 2 Mc being run under ISO 22622:2019 loading and kinematic input profiles. Machining lines are no longer visible and there are clear signs of abrasive wear, burnishing and multidirectional scratching across the whole articulating surface (n = 5).

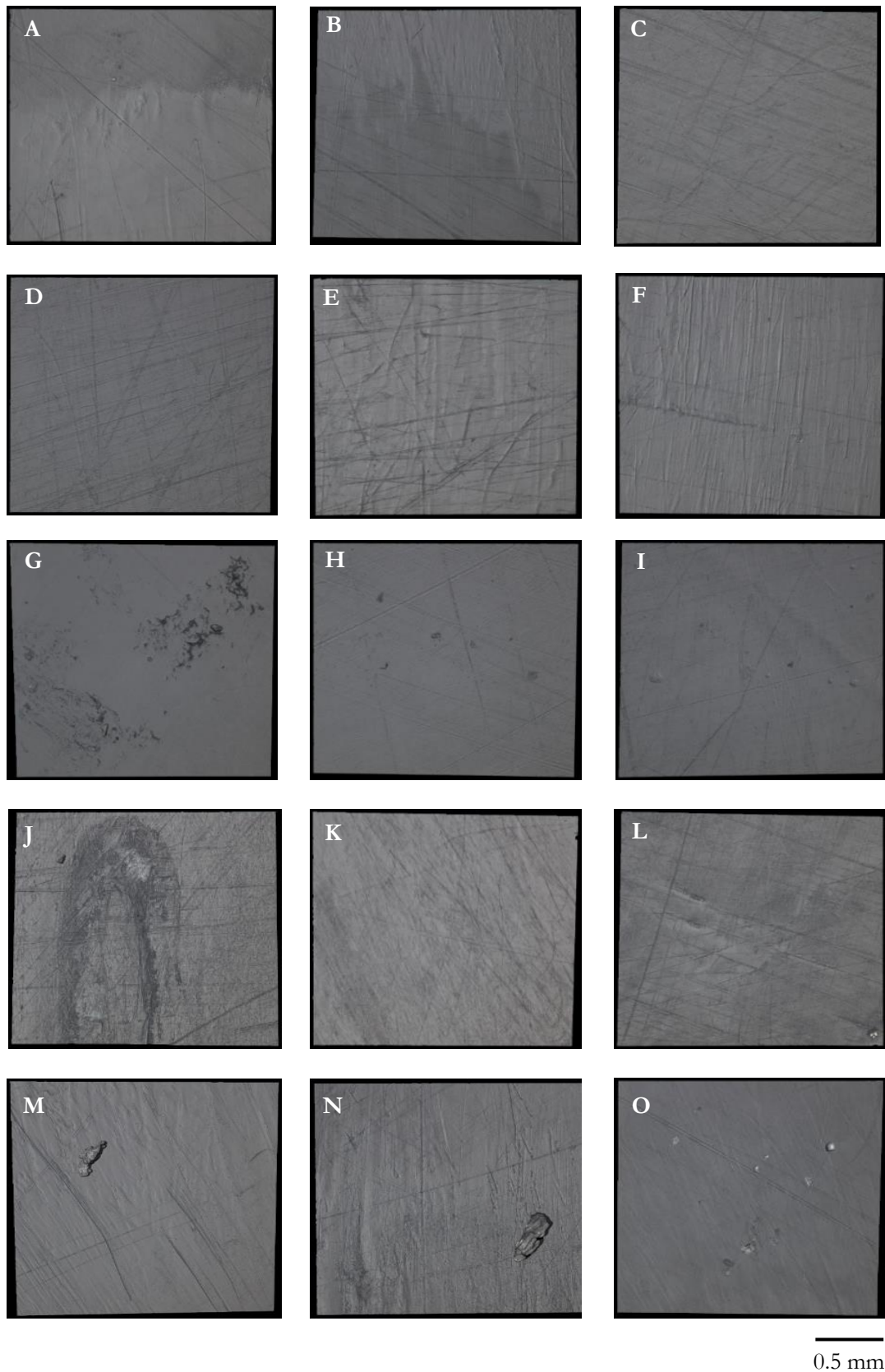


Figure 67. Damage modes on the superior bearing insert surface of the medium sized implants after an additional 2 Mc of ISO 22622:2019 loading and kinematic input profiles (n = 5): A-C = Burnishing; D-F = Scratching; G-I = Pitting; J-L = Abrasive wear; M-O = Material on the surface. Multiple damage modes were captured with the Alicona InfiniteFocus microscope (20x resolution).

## 4.5 Discussion

It is common practice in the orthopaedic industry to validate a change in mechanical simulator through implementing wear simulations under comparable simulator inputs and experimental conditions. This is done to determine if both simulators are capable of producing similar wear rates, while observing each simulators ability to follow the desired loading and kinematic input profiles. The first study condition investigated the effect of two types of commercially available mechanical simulators (KSem and KSpn) on implant wear rate, topographic changes and damage wear mechanisms. Both simulators were run under the same simulator input profiles and experimental conditions developed at the UoL (Smyth et al., 2017). The wear results from the medium sized samples, which underwent testing in KSpn, are documented in the implant size study within Chapter 3. The second study condition used the same inserts within KSem to investigate the influence of the recommended ISO 22622:2019 loading and kinematic inputs on implant wear, as well as comparing the findings to the wear results produced under the UoL input profiles. To date, the present study conditions are the first to compare the wear of a third generation MB device between different simulator types and under the ISO 22622:2019 input profiles.

### 4.5.1 Wear Rate Comparison

Under equivalent input gait conditions, there was no significant differences in mean wear rate between the different simulator types (KSem =  $17.18 \pm 5.46$  mm<sup>3</sup>/Mc and KSpn =  $14.51 \pm 5.27$ mm<sup>3</sup>/Mc) after 3 Mc. The wear rates during the run-in (0-1 Mc) and steady-state (1-3 Mc) wear phases were also comparable between the simulator models. The addition of ISO 22622:2019 input profiles for another 2 Mc did not have significant effect on steady-state wear when compared to UoL input profile condition. The comparable wear rates between simulator type and inputs was likely due to the similar loading and kinematic input profiles used (Section 4.5.2).

Both simulator parameter conditions (type and input profiles) produced comparable wear rates to the same implant design, independent of size and artificial ageing (Chapter 3). The mean wear rates also compared well to the previous ankle wear simulation literature, in which average wear rates ranged from  $3.4 \pm 10.0$  to  $25.8 \pm 3.1$  mm<sup>3</sup>/Mc (Affatato et al., 2007; Bell and Fisher, 2007; Smyth et al., 2017; Schipper et al., 2018). Section 3.5.3 provided a comprehensive review of the comparable wear rates of the MB design between different study conditions analysed within this thesis and of the TAR wear simulation literature. Nevertheless, caution needs to be taken when comparing the wear rates between simulator studies (even between the same implant designs), due to the varying experimental conditions and input profiles used.

Regardless of the comparable wear rates between the UoL and ISO 22622:2019 input profile conditions, the latter now provides researchers with a universal set of recommendations

concerning implant set-up, experimental conditions and input profiles. This will further improve the consistency between wear studies and better allows comparisons between wear rates from different centres. The input comparison study in this Chapter, did however continue to use the experimental conditions developed at the UoL, which were also used in the implant parameter studies (Chapter 3). This removed the effect of varying experimental conditions and simulator type on the volumetric wear rate produced by both simulator inputs.

#### **4.5.2 Simulator Loading and Kinematic Performance**

There were obvious differences between the applied loads and kinematic outputs produced from both simulator types. The slightly lower wear rate found in KSpn was likely caused by the differences in the simulators' ability to follow the desired loading and kinematic input profiles. It should be noted that both simulators underwent PID control parameter tuning at each restart, following a serum change, to reduce inter-station variability and improve the loading and kinematic following of the input conditions (Section 2.6). This meant that the kinematic performance of the simulators were able to reproduce the selected input profiles to the best of their ability.

KSem attained the desired peak AL within  $\pm 0.3\%$  of the desired input AL (3150 N), while the mean peak load from KSpn was substantially lower  $2542.3 \pm 86.5$  N and out of maximum output tolerance ( $-19.3\%$ ). This suggested that KSem possessed improved capability in following the desired loading profile, which were within maximum output tolerances. Despite the reduced peak AL applied by KSpn, the decreased magnitude was equivalent to approximately 3.7 times BW of a 70kg individual. This was closer to previous TAR simulation studies, which applied reduced loads equivalent to 2.57 and 2.32 times BW respectively (Affatato et al., 2007; Reinders et al., 2015b). It was also more comparable to the recommended peak AL of 2365.7 N in ISO 22622:2019, which based its recommended load from Reinders et al. (2015b) force-controlled simulator study. Both Affatato et al. (2007) and Reinders et al. (2015b) argued that the reduced AL corresponded with tibiotalar contact forces found at the implant in TAR patients, while other TAR wear simulator studies used loads based on contact forces of healthy participants or produced in cadaveric models (Stauffer et al., 1977; Procter and Paul, 1982).

The differences in AL between simulator types were not identifiable in the measured wear rates. This finding may support the notion that wear rate is unrelated to the load applied at the implant, as the relationship between load and contact area is not linear (Liu et al. 2011). This finding was also supported in the simulator input study, with no significant differences in wear rates found, despite the lower AL in ISO 22622:2019. It should be noted that contact area was not directly measured in the wear studies, but this wear contact area was determined in samples from KSpn. As the same sized implant model was used in KSem studies (simulator type and inputs), it can be assumed that the wear contact areas are similar. The comparable contact areas may have resulted in similar contact pressures during the stance phase of gait. Increased contact pressures are

known to cause a reduction in wear rate (Baykal et al., 2014), therefore, the higher loads in both KSem and UoL profiles did not result in significantly higher wear rates.

The AL from ISO 22622:2019 (2365.7 N) lies in the middle of the two profiles it was generated from (Reinders et al., 2015b; Smyth et al., 2017). At the time of the former study, there was no *in vivo* loading of TARs, so AL was scaled based on comparisons of the utilised models to *in vivo* loading of THR (Bergmann et al., 1993; Bergmann et al., 2001; Stansfield et al., 2003) and TKR (D'Lima et al., 2008; Mündermann et al., 2008; Kutzner et al., 2017). The AL progression was adapted from previous data on healthy patients (Seireg and Arvikar, 1975), while the peak AL was reduced by 30%, as loading is known to decrease in a replaced joint (Stauffer et al., 1977). This resulted in a peak AL of 2.5 times BW (1890N) (Reinders et al., 2015b), which was substantially lower than the latter study, which used a peak AL of 3.15 kN (4.5 times BW of a 70kg individual) (Smyth et al., 2017). However, the study by Smyth et al. (2017) also predicted maximum loads from cadaveric anthropometric data from healthy individuals (Procter and Paul, 1982). These findings suggest that the ISO 22622:2019 does not take into account the true contact forces at the bearing surface.

More recent studies have begun predicting TAR contact forces through the use of finite element analysis (Yu et al., 2022) and patient-specific musculoskeletal modelling (Zhang et al., 2020). Both studies found peak contact force to be approximately 5.89 and 6.55 times BW, in patients weighing 60.00kg and 80.85 kg, respectively. These loads are considerably higher than those represented in ISO 22622:2019, suggesting that the current standard is under loading the implants. However, both studies are limited to a single patient's data set, as well as the fact that the authors failed to consider the subtalar joint motion into the remodelling of the AJC. The findings from both the computationally driven studies should be used to drive future research into determining the true contact forces found at the AJC in the TAR population. Computational models driven from patient specific data will allow the development of normal and adverse loading conditions through a range of ADL, to then be inputted into a mechanical simulator to run more clinically relevant wear simulations of TARs.

Both simulators drove the FE axis electromechanically and were successful in reproducing the desired FE input profiles throughout the gait cycle, which were within the maximum output tolerances for peak plantarflexion (KSem =  $\pm$  4.9%; and KSpn =  $\pm$  0.5%) and dorsiflexion (KSem =  $\pm$  1.3%; and KSpn =  $\pm$  0.0%) input values, respectively. However, when comparing the inputs between the UoL and ISO 22622:2019 profiles, the direction of application of the FE motion was reversed (Section 4.2.2). This is commonly referred to as the polarity of motions, which is the 'sign convention' within the simulator input profiles. Such differences in polarity may affect the kinematics at the bearing surfaces, alongside the contact mechanics and resultant implant wear of a TAR.

A computational study, which sought to reverse the polarity for tibial rotation and AP, focused on two TKR wear simulation standards (ISO 14243-3:2014 and ISO-14243-3:2004) (Abdelgaied et al., 2022). The change in polarity caused a reduction in contact area and increased contact stresses during the stance phase of gait in ISO 14243-3:2014, resulting in a lower computationally predicted volumetric wear rate (Abdelgaied et al., 2022). However, the effect of reversing the polarity of FE was not determined. It is also recognised that wear rate is dependent on many wear factors, such as sliding distance and cross-shear. The current study used the same implants in the input comparison study, with the FE profile being near identical (i.e. having the same peak and ROM parameters but with different polarities). Coupled with the comparable tibial rotation and similar AP displacement, the sliding distances and cross-shear ratios at the bearing surfaces were comparable and resulted in similar wear rates between the input conditions.

Peak plantarflexion was applied at approximately the same time as the other loading and motion peak inputs, during early stance phase in the UoL profiles. Whereas, in the ISO 22622:2019 profiles, peak dorsiflexion occurred at the same time as peak anterior displacement, with peak AL and external rotation occurring at different time points during stance. The difference in phasing between simulator inputs may have had an influence on the cross-shear velocities and contact mechanics, due to the varying position of the bearing during the different motion profiles. However, this effect was not enough to cause statistically significant differences in implant wear rate.

KSem was able to attain the desired peak tibial IER angles within the maximum output tolerance ( $\pm 5\%$ ), while KSpn was outside the maximum output tolerance for both tibial internal ( $\pm 32.9\%$ ) and external ( $\pm 9.5\%$ ) rotation. Despite the difference between the two output profile angles being marginally small, the reduced tibial IER may have resulted in the lower wear rate in KSpn, particularly during the steady-state wear phase. A previous study comparing fixed TKRs, demonstrated that reducing the magnitude of tibial IER from  $\pm 5^\circ$  to  $\pm 2.5^\circ$  significantly lowered the wear rate from  $9.8 \pm 3.7 \text{ mm}^3/\text{Mc}$  to  $3.9 \pm 2.9 \text{ mm}^3/\text{Mc}$  (McEwen et al., 2005). This finding was substantiated in another FB TKR study, which showed a tenfold reduction in wear in the absence of tibial rotation (Johnson et al., 2001). MB TAR wear rates have also been shown to be highly dependent on the addition of tibial IER, particularly during the steady-state wear phase (Smyth et al., 2017).

It has been indicated that increased tibial rotation causes greater frictional force in the direction transverse to the sliding motion (AP displacement) and multidirectional motion, at the uncoupled metallic-insert articulating surfaces (Bragdon et al., 1996; Wang, 2001). This process resulted in increased shear forces which triggered surface chain orientation to change throughout articulation, while initiating shearing of the polyethylene particles at the surfaces and subsequently resulting in increased implant wear (Bragdon et al., 1996; Wang, 2001). Therefore, the comparable tibial IER in the UoL and ISO 22622:2019 input profiles suggested that the implants continued

to articulate with multidirectional motion at the bearing surfaces, particularly at the tibial-superior insert interface, generating comparable wear rates (Bragdon et al., 1996; Wang, 2001).

Both simulator designs produced slightly higher AP displacement than the desired peak input value and were outside of maximum output tolerance (KSem =  $\pm 6.5\%$ ; and KSpn =  $\pm 10.2\%$ ). The minor differences in the magnitude of AP displacement profiles did not appear to effect implant wear rate. The reduced AP displacement ROM in the ISO 22622:2019 input profile, was also not found to have a significant effect on the overall wear rate when compared to the UoL inputs. An earlier simulator based study on five Zenith (Corin Group PLC., Cirencester, UK) MB devices demonstrated this finding, with the wear rate depending solely on the addition of rotation, with the magnitude of AP displacement having no significant effect on implant wear rate (Smyth et al., 2017). The study by Smyth et al. (2017) demonstrated that an AP displacement of 4 mm produced non-significant difference in implant wear after 2 Mc ( $13.3 \pm 2.5 \text{ mm}^3/\text{Mc}$ ) compared to an increased AP displacement of 9 mm ( $11.8 \pm 3.7 \text{ mm}^3/\text{Mc}$ ) (Figure 68).

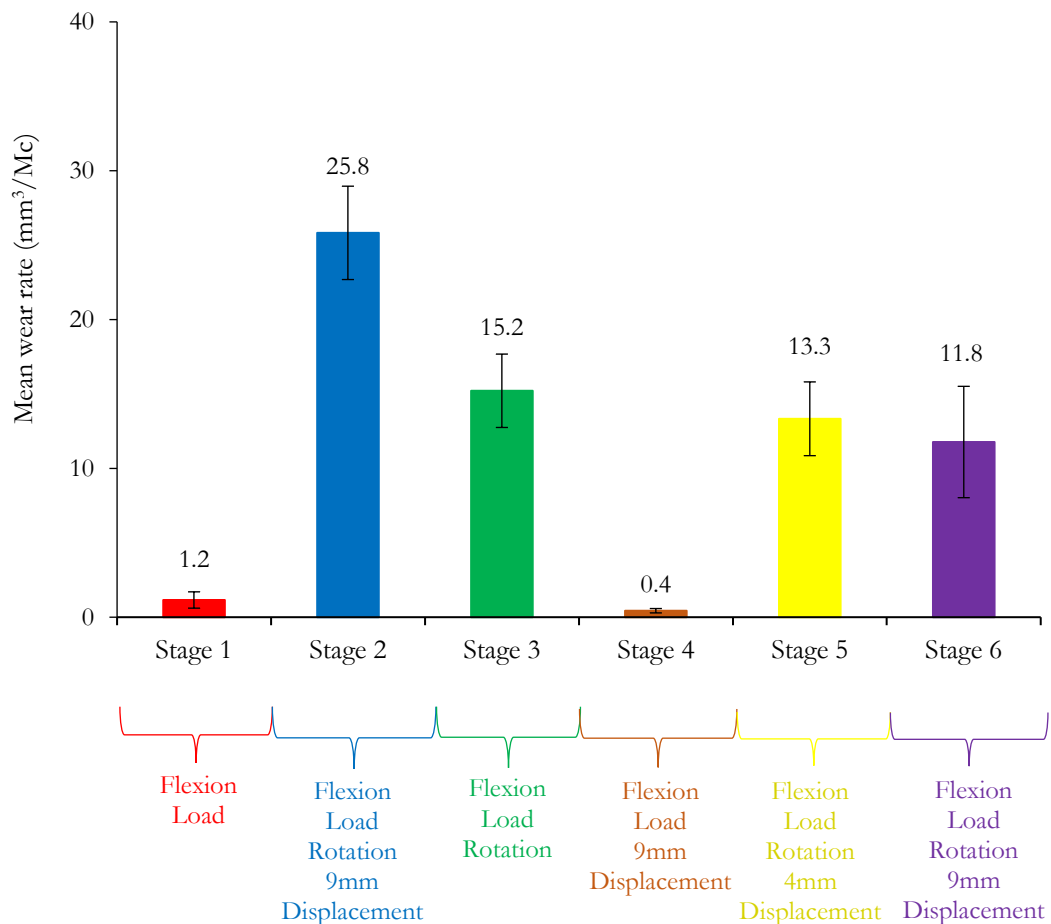


Figure 68. Mean ( $\pm 95\%$  CL) wear rate ( $\text{mm}^3/\text{Mc}$ ) for the Zenith (Corin Group PLC., Cirencester, UK) mid-range implant sizes for the six 2 Mc stages from Smyth et al. (2017) kinematic comparison study ( $n = 5$ ). Adapted from Smyth et al. (2017).

The AP displacement kinematic waveform from Smyth et al. (2017) was taken from the maximum displacement profile reported by Conti et al. (2006). This study calculated the motion through a 3D model-fitting technique which obtained 3D component positions from 2D fluoroscopic images. Conti et al. (2006) determined that in 10 patients implanted with the Agility (DePuy, Warsaw, USA) FB design, the mean AP displacement ROM was 3.5 mm during weight bearing dynamic gait conditions. Therefore, the 9 mm motion used in Smyth et al. (2017) does not represent the true motion occurring in the TAR patient population. These findings support the selection of a lower AP displacement of 4 mm in the wear studies in this thesis.

The reverse has been shown in FB knee implants, with an earlier simulator study highlighting that a reduction in AP motion by almost half caused a significantly lowered wear rate from  $16.0 \pm 4.0 \text{ mm}^3/\text{Mc}$  to  $9.8 \pm 3.7 \text{ mm}^3/\text{Mc}$  (McEwen et al., 2005). This was a result of reducing the sliding distance and surface area of UHMWPE being worn during continued articulation. It was also proposed that the strain hardening effect was responsible for the reduction in wear of the TKR, with motion occurring in the direction of the UHMWPE chains (unidirectional) and thus improving wear resistance (McEwen et al., 2005). This was a result of the decoupling of motion at each surface in a rotating platform knee, so that FE and AP displacement occurred on the top surface and rotation at the backside interface (McEwen et al., 2005). The difference in findings between the wear studies on TKR and TAR may be related to the mobile nature of the ankle devices. Under simulator conditions, rotating platform knee implants are able to split into two uni-directional wear surfaces, whereas the MB ankle does not do this, so it isn't able to address the cross-shear effect in the same way. The MB design also allows for increased sliding distance and subsequent sliding velocity, which has directly been associated with improving the lubrication and reducing the wear effect at the bearing surface interfaces. This could explain the comparable wear rates found between the simulator types and simulator input study conditions.

The AP displacement output profiles suggested that both simulator options were unable to reproduce AP displacement. This was likely due to the simulators being unable to shift between the relatively small peak values in such a short period of time, while also trying to follow the other kinematic profiles. In addition, the motor which drives the motion of KSpn was unable to rapidly respond to the variation in motion profiles compared to the KSem, resulting in a lag phase when following the AP displacement profile. This was also a feature in KSpn, when attempting to follow the AL and tibial IER UoL input profiles. This associated lag phase was not found in KSem, with peak tibial external rotation and anterior displacement occurring around peak AL during early stance phase. The out of phase loading and kinematic following may have resulted in different contact mechanics between simulator types due to the different position of the bearing, which is known to influence wear rates. However, the small lag in following input profiles was not substantial enough to cause a significant difference in implant wear rates between simulator types.

The effect of inter-station variability did not appear to last when the inserts moved into steady-state wear and were more consistent in KSem than KSpn. Moving the implants between stations of the simulators has previously been shown to reduce the impact of inter-station variability on wear results in a TKR (Abdelgaied et al., 2017). That being said, ISO 22622:2019 does not mention whether to move implants between stations periodically nor whether to move them throughout the duration of the wear simulation. The results from this study suggest that future studies should move components between stations to compensate for inter-station variability, as this could have a significant effect on calculated volumetric wear and overall conclusions.

Previously worn components were used in the simulator input comparison study. Although this is not unusual practice (McEwen et al., 2005; Smyth et al., 2017), this meant that the finding demonstrating non-significance, may not have been strictly independent of the changes in loading and motion profiles. It is possible there may have been differences in the machined tolerances and roughness measurements that were not identified in the topographic assessment of the bearing surfaces (Section 4.5.3). It was also difficult to isolate in this study, where the apparent differences in wear rates between inserts stemmed from. In this study, this was particularly problematic during the run-in phase in both simulator types, as the topographic assessment was performed at the end of both simulator parameter studies. However, the differences between insert wear rates was likely a combination of the individual stations' ability to produce the required input profiles, coupled with machining and potential misaligned insert set-up. Further limitations associated with the running of a mechanical simulation can be found in Chapter 6 (Section 6.2). With the above considerations in mind, future studies using unworn implants which follow the recommended experimental conditions and input profiles, are required to truly determine the effect of ISO 22622:2019 on the wear behaviour of a MB the device.

### **4.5.3 Surface Analysis and Damage Modes**

Surface contact measurements were taken to determine if there were differences in roughness and associated topographic parameters, before and after wear simulation. This process can help to determine the regions of the bearing surfaces which underwent the greatest change in physical properties, affecting the film thickness to roughness ratio and the lubrication regime (Sagbas, 2016). The topographic changes of the medium sized implants followed comparable trends between simulator types, despite the additional 2 Mc that each of the samples underwent in KSpn (Chapter 3). There were also no significant differences in the pre-simulation values, with each sample being within the maximum roughness tolerance ( $2\mu\text{m}$ ) specified for the insert surfaces. This finding meant that the post-simulation results were not affected by differences of the unworn surfaces. However, statistical analysis was not performed, as the final surface contact measurements were not taken at the same simulation time point. The surface topographic changes of the implants were also measured at the end of the ISO 22622:2019 input profile

condition, with no apparent differences in roughness parameters within the same worn implants. This was one of the reasons for the comparable wear rates between simulator inputs.

Independent of simulator type and input conditions, the metallic components underwent significant increases in Ra, while the conventional UHMWPE inserts produced significantly reduced Ra, particularly at the superior insert surfaces. This was expected, as asperities were found throughout the pre-worn bearing surfaces, due to the machining of conventional UHMWPE, which likely caused the increased Ra at the pre-test contact measurement. During the run-in wear phase, the soft and rough polyethylene inserts resulted in high asperity contact, which potentially increased micro-adhesion and burnishing wear at the bearing surface. The latter was visually confirmed on each of the superior insert surfaces from both simulator types, through the appearance of a polished bearing surface. Even with the addition of ISO 22622:2019 input profiles, the findings remained similar. The removal of the machined lines (burnishing), due to the continued articulation was associated with the reduced wear rate seen during steady-state wear (Section 4.5.1).

The continued articulation during each simulator parameter condition triggered a reduction in asperity contacts between the metallic and conventional UHMWPE bearing surface, evidenced by the reduced  $R_p$ , negative  $R_{sk}$  and increased  $R_{ku}$  mean parameter values post-simulation. However, as surface topographic changes were only recorded at the end of each simulator condition (3 Mc for the simulator type and 5 Mc for the simulator input), the time of when this change in tribological performance occurred was unknown. The topographic changes suggested that the implants, independent of simulator condition, were likely experiencing a boundary lubricating regime, which has previously been agreed as the predominant mechanism in hard-on-soft bearing joints (Sagbas, 2016). This was also supported by the fact that the lubricant regime was associated with abrasive wear on the softer polyethylene surface, with this wear mechanism being detected on all of the tested inserts.

Despite the differences in the loading and kinematic following (Section 4.5.2), both simulator types produced comparable wear damage modes on each of the articulating surfaces of the MB device. There was strong evidence of adhesive wear, burnishing and multidirectional scratching, particularly on the superior insert surface (Section 4.4.4). Following the additional 2 Mc of ISO 22622:2019 input profiles, the same damage modes remained the obvious wear mechanisms. These findings are consistent with the implant parameter studies (Chapter 3) and the previous work conducted by Smyth et al. (2017), who developed the UoL input profiles used in the simulator type study.

The damage modes of abrasive wear and multidirectional scratching from both simulator parameter studies are also evident on the explanted devices from the UoL retrieval bank. In both in vitro tested and explant samples, the machined lines have been worn away, indicating strong

evidence of burnishing. This shows that both simulator types and inputs were able to produce certain damage modes that are seen *in vivo*. However, certain clinical damage modes such as third-body abrasive wear and delamination were not present in the *in vitro* tested inserts. This means that although the simulator studies, independent of type or input, were able to produce some damage modes seen on retrieved devices, it does not replicate all the clinical damage modes present. The presence of third-body debris (metallic, bone or cement), which likely causes increased wear compared to abrasive wear found on the *in vitro* inserts and may have resulted in the early failure of some of the retrieved samples. A more detailed comparison of the simulated devices in the current thesis to previously simulated and retrieved MB implants, can be found in Section 3.5.4.

#### **4.4 Conclusion**

This study has established that under the same experimental conditions, there tended to be no differences in mean wear rates between simulator type (pneumatic and electromechanical) and simulator inputs (UoL and ISO 22622:2019). However, the output loading and kinematic profiles followed the desired input profiles more closely on KSem compared to KSpn, and were within maximum output tolerances for peak UoL input values, with the exception of peak anterior displacement. KSem also produced greater peak plantarflexion when compared to the maximum output tolerance of the ISO 22622:2019 recommended profile. Nevertheless, the variation in loading and kinematic input following between simulators and input profiles was not sufficient to significantly change the tribological conditions of the MB TAR. The wear results from the current studies were comparable to the previously published literature on MB devices ( $3.4 \pm 10.0$  to  $25.8 \pm 3.1$  mm<sup>3</sup>/Mc) (Bell et al., 2007; Affatato et al., 2007; Postak et al., 2008; Reinders et al., 2015b; Smyth et al., 2017), independent of simulator design and input profiles. This was also the case for topographic changes at each of the bearing surfaces. The similarities in damage modes to previously simulated and retrieval MB devices, offered assurance that both simulator parameters provided reliable TAR wear simulation.

Despite the non-significant difference in wear rate between simulator types, this study recommends the use of KSem, due to the improved accuracy and precision of the output loads and kinematics when compared to the desired input profiles. KSem also has the ability to control abduction/adduction to mimic implant inversion/eversion, which is an important implication for future pre-clinical simulation. Future TAR studies should also utilise the recommended ISO 22622:2019 input profiles, as the current variance in kinematic inputs in the TAR wear literature make it difficult to directly compare wear behaviour. This would allow for a better interpretation of which TAR devices are producing improved wear results, compared to competitor devices on the market.

## **CHAPTER 5**

# **BIOMECHANICAL PERFORMANCE OF ANKLE ARTHRODESIS AND TOTAL ANKLE REPLACEMENTS DURING OVERGROUND WALKING**

## CHAPTER 5

# BIOMECHANICAL PERFORMANCE OF ANKLE ARTHRODESIS AND TOTAL ANKLE REPLACEMENTS DURING OVERGROUND WALKING

### 5.1 Introduction

An increasing body of clinical evidence has demonstrated that patients suffering from end-stage ankle OA have considerable functional impairments of the AJC and lower limb, characterised by a reduced step length, walking speed and mobility, when compared to healthy controls (Queen, 2017a; Deleu et al., 2020a). As noted previously, AA is widely recognised as the gold standard treatment option for end-stage ankle OA and there is a plethora of studies that have demonstrated this surgical intervention is effective in alleviating post-operative pain and recovering patient QoL (Pinsker et al., 2016; Kim et al., 2017; Gaedke et al., 2018). However, concerns over non-union, abnormal force distribution, and gait adaptations that may increase the risk of subsequent adjacent joint degeneration (Wu et al., 2000; Coester et al., 2001; Beyaert et al., 2004; Thomas et al., 2006), has encouraged the use of motion conserving procedures such as TAR (Ling et al., 2015; Sokolowski et al., 2019). Although first generation designs were discarded because of the high revision rates (Bonasia et al., 2010), newer versions have resulted in comparable pain relief to AA, and in some studies, a superior improvement in PROMs and the preservation of ankle ROM (Haddad et al., 2007; Saltzman et al., 2009; Robati et al., 2016; Lawton et al., 2017; Benich et al., 2017).

As TAR becomes a more widely accepted intervention among surgeons treating end-stage ankle OA, understanding the differences in gait mechanics between AA and TAR is a necessity for improving long-term patient outcomes. In the last decade, there have been a number of gait studies which have compared both surgical options (Piriou et al., 2008; Hahn et al., 2012; Singer et al., 2013; Flavin et al., 2013; Segal et al., 2018; Stone et al., 2021). Faster walking speed, increased sagittal plane motion and improved ankle power, were the most reported gait changes postoperatively in TAR patients, when compared with AA patients. A combined systematic review and meta-analysis of seventeen gait studies assessing the AJC function following both surgical interventions, determined moderate evidence of improved walking speed (i.e. mean 0.19 m/s increase in walking speed), sagittal plane ankle kinematics (i.e. mean 3° increase dorsi-/plantarflexion ROM) and kinetic patterns, compared to their pre-operative arthritic condition when using TAR (Deleu et al., 2020a).

The increased sagittal ROM could be attributed to supplementary hypermobility of the distally located foot joints (Deleu et al., 2020a). It is believed that the reduced pain associated with both treatment options post-surgery, may also be due to increased mobility and loading occurring at the adjacent joints of the foot, as a result of the gait adaptations discussed (Deleu et al., 2020a).

However, each of the studies included in the meta-analysis treated the foot as a single, rigid segment, which neglects the influence of the adjacent joints and can lead to significant inaccuracies in ankle joint ROM (Pothrat et al., 2015; Lullini et al., 2020; Deleu et al., 2021b; Fritz et al., 2021). Furthermore, SFM in the TAR patient population have been proven to overestimate post-operative ankle ROM in all three planes of motion, when compared to a MFM (Deleu et al., 2021b).

A recent study using 3D MFM determined compensatory mechanisms at the joints, distal to the AJC, in PTOA patients compared to healthy reference data during overground walking (Deleu et al., 2021b). The hindfoot of PTOA patients was found to be in a more inverted position, which was associated with a more adducted position of the Calcaneus-Midfoot joint. This could be explained by the co-contraction phenomena between the gastrocnemius and tibialis anterior muscles. These muscles act to cause the feet to adduct and invert, providing stability at the AJC from heelstrike to midstance phases of the gait cycle (Deleu et al., 2021b). Other studies have also begun to use MFM in AA (Brodsky et al., 2016; Eerdeken et al., 2020a) and TAR (Lullini et al., 2020; DiLiberto et al., 2021; Fritz et al., 2021; Deleu et al., 2022) patient cohorts. Pain and function were reported to improve following both treatment options, as evidenced by better PROMs, improved spatiotemporal parameters and increased sagittal ROM at the AJC and surrounding joints, compared to pre-operative values. While MFM kinetics and kinematics were improved at the varying follow-up periods, they were not restored to that of healthy controls.

Only two studies have utilised MFM to directly compare both surgical interventions, with each reporting increased intersegmental (hindfoot and forefoot) sagittal ROM (especially during dorsiflexion) and plantarflexion power in TAR patient cohorts, when compared to AA (Seo et al., 2017; Sanders et al., 2021). The recovery of sagittal ROM compared to pre-operative values is usually attributed to improved dorsiflexion at the hindfoot (Seo et al., 2017), while increased plantarflexion power is associated with an improved ability of a patient to propel their feet forward during locomotion (Ingrosso et al., 2009). This is also related to greater strength of the gastrocnemius muscles (Neptune et al., 2001). Additionally, the study by Seo et al. (2017) showed that the AA patient cohort exhibited increased peak plantarflexion motion at the forefoot with this compensatory motion potentially resulting in further adjacent joint OA and the need for further surgical interventions.

From a biomechanical perspective, these gait differences indicate that TAR should be a more effective treatment option for end-stage ankle OA (Seo et al., 2017; Sanders et al., 2021). However, both the MFM gait comparison studies were limited by short post-surgery follow-up periods of one and three-years, respectively (Seo et al., 2017; Sanders et al., 2021). Other studies using MFM to measure gait outcomes of AA (Eerdeken et al., 2020a) and TAR (Deleu et al., 2022) patient populations to pre-operative measurements, were also limited by short-term follow-up periods of just one-year. Despite the associated kinetic and kinematic improvements at the

AJC and intrinsic foot joints, it would be clinically beneficial to determine whether these improvements are maintained at longer-term follow-ups. This is important to determine whether patient cohorts return to even more active lifestyles, resulting in more extensive use of the ankle and surrounding foot joints. A recent intermediate follow-up study using a SFM to measure TAR gait mechanics found that the gait outcomes of interest at 7.6 years were consistent with the initial short-term findings (Brodsky et al., 2021). However, this study failed to determine the influence of adjacent foot joints, which over a longer period of time, may display hypermobility and possess increased loads to compensate for the surgically treated ankle joint (Deleu et al., 2021b).

While these MFM studies have shown significant clinical differences in AA and TAR patient populations, only a small volume of gait based studies have reported the effect on both kinetic and kinematic adaptations at the proximal joints of the lower limb (Brodsky et al., 2011; Hahn et al., 2012; Choi et al., 2013; Tenenbaum et al., 2017; Segal et al., 2018). The earlier studies which considered hip and knee gait mechanics, demonstrated that TAR patients possessed increased sagittal ROM in both joints, whilst AA patients exhibited comparable knee ROM to pre-operative values but improved hip ROM (Brodsky et al., 2011; Hahn et al., 2012; Choi et al., 2013; Tenenbaum et al., 2017; Segal et al., 2018). These findings suggest that arthritic patients compensate more at the hip than at the knee joint during overground walking, when sagittal plane ankle ROM is limited following surgery (Segal et al., 2018). Combining the use of MFM and lower limb models, allows for an improved understanding of the functional compensatory mechanisms of the adjacent foot and proximal joints in patients treated with AA and TAR. Understanding the combined effect of gait mechanics on the patient's ability to walk, will also aid a surgeon's choice in selecting the appropriate treatment option, which will maintain improved biomechanical performance over a longer-lasting period for a patient suffering with end-stage ankle OA.

The aim of this exploratory study was to compare the post-operative kinetic and kinematics of the AJC, alongside other lower limb joints during gait, in patients treated with a TAR or AA at an intermediate follow-up period. The study used a MFM to determine the kinematic adaptations at the intrinsic foot inter-segment angles distal to the affected ankle joint between surgical interventions. The study will be used to determine possible clinically meaningful differences in gait mechanics and reported outcomes between the treatment options, with the key findings from this study being used to drive a much larger, powered gait study at a longer-term follow-up. This would then allow surgeons to truly determine which procedure is clinically superior.

Chapters 3 and 4 established comparable pre-clinical wear behaviour of the MB device in question to other devices on the market, but this does not always correspond to *in vivo* clinical function. Therefore, the gait study in this chapter allowed for the clinical performance of the third-generation MB implant to be determined and compared to AA and other TAR designs.

## 5.2 Methods

This method describes the collection of biomechanical data for nine AA, six ‘mixed’ TAR, and six BOX® ankle patients. A motion capture research laboratory at Chapel Allerton Hospital (CAH; Leeds, UK), was used to collect gait data from the ‘mixed’ TAR and AA patient cohorts. Due to patient availability and location, it was not feasible for the surgical cases to travel to the same research site. Therefore, a second motion capture laboratory (Nottingham Trent University (NTU); Nottingham, UK), was used to collect data from the BOX® ankle patient cohort.

### 5.2.1 Ethics for Data Collection

The study protocol was approved by the National Health Service (NHS) Research Ethics Committee (REC reference: 19/ES/0070) (Appendix F3) and the NHS Health Research Authority (HRA) (Appendix F4). Local ethical approval was also obtained from the Faculty of Mechanical Engineering Ethics Committee, University of Leeds (ethical review number: MEEC 17-037) (Appendix F1) and the College of Science and Technology Ethics Committee, NTU (ethical review number: 640) (Appendix F2).

### 5.2.2 Pilot Study

A pilot study was conducted to determine the repeatability of 3D gait data obtained at both CAH and NTU motion capture laboratories. Eleven healthy participants (8 males/3 female) were assessed at both research sites within a three-month period. The participants mean age ( $p = 0.564$ ), height ( $p = 0.655$ ) weight ( $p = 0.838$ ) and BMI ( $p = 0.929$ ) were not significantly different between the two research sites. For each test session, the same spatiotemporal, kinetic and kinematics parameters measured in the current Chapter were collected during 5 successful overground level walking trials. A single evaluator, which was the same individual in the current study, placed the identical MFM and lower limb marker model (Section 5.2.5) on the participants at both research sites. Biomechanical data was collected at self-selected walking speed and the variability in the gait data was determined by comparing the mean ( $\pm 95\%$  CL) peak and ROM parameters. A non-parametric Wilcoxon signed-rank test was used to measure statistical significant differences in spatiotemporal and gait parameters, with a significance accepted at the ( $p \leq 0.05$ ) level. All statistical analyses was conducted using SPSS version 26.0 (SPSS Inc, Chicago, USA).

The mean ( $\pm 95\%$  CL) kinetic and kinematic waveforms, alongside the tables presenting the gait data at both research sites can be found in Appendix G. The greatest variability in kinematic data was found in the transverse plane of motion at the proximal hip and knee joints. However, there was no statistically significant differences in the peak IER angles and ROM. There was also no significant differences ( $p \leq 0.05$ ) for any of the measured spatiotemporal, kinematic and kinetic data between the two research sites. The pilot study demonstrated that it was possible to collect comparable gait data across two motion capture laboratories. This was likely the case due to the

use of the same examiner, identical anatomical segment definitions for biomechanical models and the fact that experimental conditions were standardised across research sites. Thus, the data collected from the same research sites in the post-operative exploratory gait study could be compared directly. The pilot study was also used to establish the study protocol for the post-operative gait comparative study discussed in this chapter.

### **5.2.3 Gait Laboratory Set-up**

#### **5.2.3.1 Motion Capture Equipment**

Although the precise optoelectronic motion capture system and number of cameras used differed at both research sites, the number and model of force platforms were used from the same manufacturer (Advanced Mechanical Technology Incorporated; AMTI, Watertown, MA). The infrared cameras were used to measure the reflection of the markers, in order to determine their 3D position within the global coordinate system. The force platforms were synchronised to the motion capture system and measured ground reaction force (GRF) during the overground walking trials. The force platforms measured the GRF in three directional components: Fx (mediolateral); Fy (anteroposterior); and Fz (vertical).

#### **Chapel Allerton Hospital**

A ten camera infrared passive marker motion capturing system (Vicon Motion Systems, Oxford, UK), operating at a frequency of 100 Hz, was positioned around the movement space to capture kinematic data. The ten cameras were positioned precisely, allowing markers to be located throughout each trial by at least three cameras within the calibrated movement volume of 5m<sup>3</sup>. This reduced the need for post processing interpolation (Section 5.2.7). Two force platforms (AMTI BP400600, Watertown, MA, USA; dimensions: 400 by 600 mm), sampling at a frequency of 1000 Hz, were arranged in succession to allow simultaneous collection of concurrent operated and non-operated gait events. The force platforms were embedded within the ground and in the centre of an 8 m walkway.

#### **Nottingham Trent University**

A thirteen camera Qualisys Oqus 3D motion capture system (Qualisys™ Medical AB, Goteborg, Sweden), sampling at 100Hz, was aligned to allow for the calibration of the movement volume (5m<sup>3</sup>) (Figure 69). Nine of the thirteen cameras were mounted to a 5m high rail surrounding the gait laboratory (4x700+ Oqus and 7x400 Oqus), with an additional four Oqus 700+ cameras on portable mounts, positioned around the embedded force platforms. Similar to the set-up at CAH, the force platforms were arranged in succession and positioned flush with the ground, in the middle of an 8 m walkway (Figure 69). GRF data was recorded through the use of two force platforms (AMTI BP400600, Watertown, MA, USA; dimensions: 400 by 600 mm), sampling synchronous data at a frequency of 500 Hz. Despite the differences in sampling frequency of the same force plate model between the two sites, the pilot study showed that this did not have an

effect of calculated GRF or moment data (Appendix G). For instance, the pilot study demonstrated no statistically significant differences in GRF at the measured first ( $p = 0.197$ ) and second ( $p = 0.357$ ) peaks.

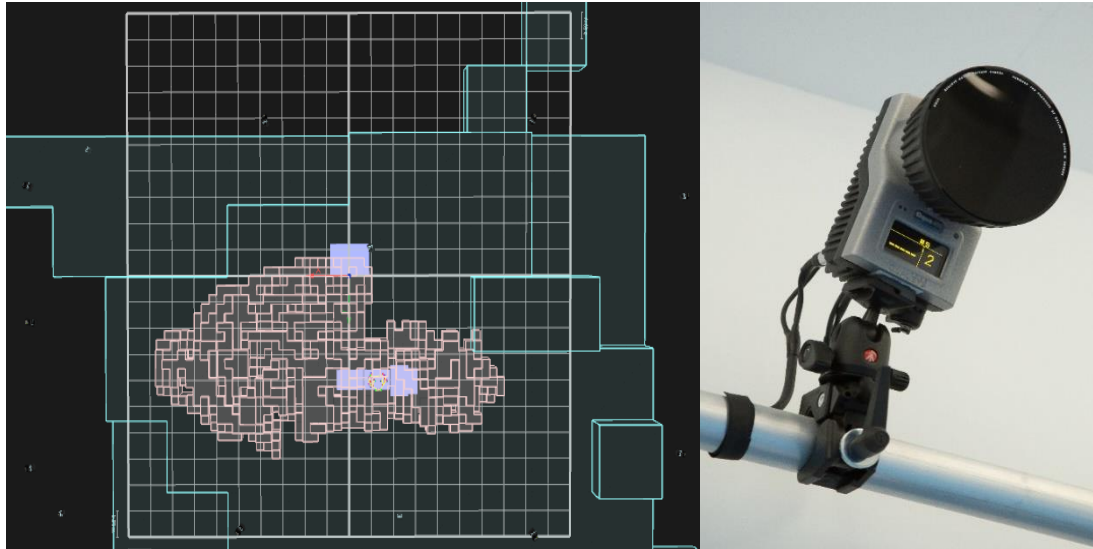


Figure 69. The superior view of the Qualisys Oqus 3D motion capture system (blue area) and the smaller calibrated movement volume (pink area); and the Qualisys Oqus cameras (right) at the NTU gait laboratory. The force platforms (violet rectangles) are positioned in the middle of the movement volume to capture GRF data.

### 5.2.3.2 Calibration of the 3D Volume

#### Chapel Allerton Hospital

Prior to data collection, the 3D movement capture area was calibrated using a Vicon Active Calibration Wand (Vicon MX, Oxford Metrics, UK) (Figure 70). The frame of the active wand constituted of a long and short arm perpendicular to one another, with five pairs of LEDs embedded in the frame (Figure 70). The active wand was placed at the corner of one of the force platforms to establish the global origin. The active wand was then moved through the 3D capture area, until a minimum of one thousand dynamic frames of the wand were captured for each of the ten cameras. The calibration was deemed suitable if the image error for each of cameras was below 0.12 mm. The force platforms were also calibrated (zeroed) before each trial to eradicate any residual force readings that may remain from the previous walking trial.

#### Nottingham Trent University

A different calibration technique was performed at the NTU gait laboratory through the use of an L-shaped reference frame and a T-shaped calibration wand marker (Qualisys™ Medical AB, Goteborg, Sweden) (Figure 71). The reference frame consisted of a long and short arm perpendicular to one another, with four spherical retroreflective markers secured to the frame: one at the corner (origin), one on the short arm (200 mm from the origin), and two along the long arm (550 mm and 770 mm from the origin) (Figure 71). The L-shaped frame was placed at

the corner of the embedded force platforms and used in conjunction with the carbon fibre T-wand, to calibrate the movement volume.



Figure 70. The Vicon Active Wand (Vicon MX, Oxford Metrics, UK) required for the calibration process at CAH.

The calibration wand possessed two mounted markers (751.2 mm apart) and was moved throughout the 3D measurement volume for a duration of 60 seconds. The system was calibrated by analysing the exact position of the markers within the capture volume. The calibration was considered acceptable if the average residual for each camera was below 2 mm and the standard deviation of the reconstructed wand length error was also below 2 mm. Similar to the Vicon System at CAH, the force platforms were zeroed before each trial to prevent the inclusion of forces that may remain from the previous walking trial.



Figure 71. The L-shaped reference structure and T-shaped wand (Qualisys™ Medical AB, Goteborg, Sweden) required for the calibration process at NTU.

### 5.2.3 Participant Information

Twenty-one participants were divided into three groups: nine AA patients, six ‘mixed’ TAR patients and six BOX® ankle patients. The mixed TAR cohort included four participants with a Rebalance® (Zimmer-Biomet, Indiana, USA) prosthesis, one participant with a Mobility® (DePuy, Leeds, UK) prosthesis and one participant with an INFINITY® (Wright Medical

Technology, Memphis, TN) prosthesis. All AA and mixed TAR surgeries were performed at a single institution (CAH), while the BOX® ankle surgeries took place at the Nottingham City Hospital. Basic demographic characteristics of the three patient cohorts are shown in Table 14. There were no statistically significant differences between the three patient cohorts for age ( $p = 0.298$ ), years since surgery ( $p = 0.115$ ), height ( $p = 0.624$ ), weight ( $p = 0.162$ ), and BMI ( $p = 0.081$ ) (Table 14).

Table 14. Participant demographics for the three treatment option cohorts.

	<b>AA</b>	<b>Mixed TAR</b>	<b>BOX®</b>
Age (years)	62.67 ± 15.17	73.33 ± 6.62	71.50 ± 6.66
Sex	7M/2F	5M/1F	3M/3F
Affected Side (R/L)	4R/5L	4R/2L	1R/5L
Years Since Surgery	4.44 ± 2.60	6.83 ± 2.79	5.50 ± 0.55
Height (m)	1.71 ± 0.12	1.71 ± 0.12	1.66 ± 0.11
Weight (kg)	101.43 ± 20.60	82.68 ± 12.46	79.60 ± 11.22
BMI (kg/m <sup>2</sup> )	34.67 ± 6.71	28.33 ± 2.47	28.98 ± 3.57

Strict inclusion and exclusion criteria were applied to ensure that the gait differences could be attributed to the surgical intervention alone. Inclusion criteria ensured that the patients had undergone primary AA or TAR on one ankle; been diagnosed with PTOA or isolated primary OA; an implantation time between 1-10 years post-surgery; were over the age of eighteen; and were healthy and were free from injury or surgery of the foot and lower body for the past six months, before taking part in the study. Exclusion criteria for the study included: (1) the presence of inflammatory joint conditions (i.e. rheumatoid arthritis); (2) history of infection in the operated joint; (3) patients suffering from skeletal immaturity; (4) patients suffering from osteoporosis/any loss of musculature or neuromuscular disease that compromises the operated joint; (5) those who have had AA or TAR surgery on both ankles; (6) those currently pregnant; (7) patients suffering from open ulcerations/significant wound infection; (8) those unable to walk unaided (e.g. without the use of walking stick or frame); and (9) patients who suffer from dizzy spells or fainting episodes.

#### **5.2.4 Patient Reported Outcomes**

Before data collection, each patient completed the Manchester-Oxford Foot Questionnaire (MOxFQ) (Isis Innovation Ltd, Oxford, UK). The MOxFQ is a sixteen item PROMs, which is validated for use in patients, who have received foot and/or ankle corrective surgery (Morley et al., 2013). Responses to each of the sixteen questions consisted of a 5-point Likert scale ranging from no limitation (scoring 0) to maximum limitation (scoring 4) (Muller et al., 2020). Each item was grouped into one of three domains: walking/standing (seven items); pain (five items); and social interaction (four items). The overall domain scores were then calculated by adding the patient responses to each item within each domain and translating to a 0-100 metric, where higher scores signified greater severity (Dawson et al., 2012).

### 5.2.5 Participant Preparation

Participant's height was measured using a stadiometer and weight was determined when the participant stood on one of the force platforms during a static trial. Participants wore skin tight shorts and top, in order to reduce marker movement and allow for more accurate marker positioning. Reflective areas on the participants clothing were covered to prevent the appearance of phantom markers, which could be mistaken for an anatomical marker within the marker set and cause errors during data processing. All overground walking trials were completed barefoot, which was due to the number of markers on the foot and the fact that MFM is not yet considered accurate in shod conditions (Stone et al., 2021).

A single evaluator (the author of this thesis) with five years of experience in motion capture, attached thirty-six super-spherical retro-reflective passive markers (Qualisys™ Medical AB, Goteborg, Sweden), to anatomical landmarks of interest on the feet and lower limbs using double-sided hypoallergenic tape (Figure 72). Three different sized marker sizes were used: (1) 14.0 mm  $\varnothing$  for the pelvis, hip, knee and malleoli; (2) 9.5 mm  $\varnothing$  for the non-operated foot; and (3) 8.0 mm  $\varnothing$  for the operated foot. The anatomical landmarks were identified through palpation in accordance with the Colour Atlas of Skeletal Landmark Definitions (van Sint Jan, 2007).



Figure 72. Anatomical locations of the 36 marker model set in the anterior (left) and posterior (right) view

Retroreflective markers were placed following the Calibrated Anatomical System Technique (CAST) protocol marker set, which is considered to be the gold standard protocol for 3D kinematic analysis (Cappozzo et al., 1995). Other researchers have used the “Newington” model (Davis et al., 1991), on which Vicon’s Plug-in Gait model is based. However, this method relies on the accurate placement of markers on the thigh and shank, which are crucial in determining

the alignment of the knee axis. The “Newington” model outputs are also highly sensitive to marker placement error (Groen et al., 2012).

The CAST model used in this study had clusters of non-colinear tracking markers (four-marker semi-rigid thermoplastic shells) attached to the sacrum, lateral thighs and lateral shanks (Figure 73), which measured segment kinematics in six DoF (Benedetti et al., 1998). The fixed clusters strapped to the lower limb segments also reduced the source of error associated with soft tissue artefacts (STA) (Cappozzo et al., 1997). Both biomechanical models produce equivalent sagittal plane joint angles and kinetics particularly at the ankle, whereas the CAST model displayed significantly lower frontal plane mean error when compared to Plug-in Gait (Ferrari et al., 2008).



Figure 73. Four-marker semi-rigid thermoplastic shell used as tracking markers for the thigh (left) and thigh (right) during kinematic data collection.

The non-operated foot was modelled as a single-segment, whilst the operated foot was analysed using the “Istituti Ortopedici Rizzoli” (IOR) MFM (Figure 74). This foot model was selected due to its well-documented repeatability in the assessment of MFM biomechanics, with a mean inter-trial coefficient of multiple correction of  $>0.820$  (Deschamps et al., 2012a; Deschamps et al., 2012b). The IOR foot model provided 3D kinematic data for intrinsic foot inter-segment angles of the hindfoot, midfoot and forefoot (Leardini et al., 2007; Portinaro et al., 2014). This foot model has also recently been used to determine gait differences in AA (Eerdeken et al., 2020a) and TAR (Lullini et al., 2020) patients. Table 15 displays the full list of anatomical and tracking markers used in the study. A regression model based on the position of pelvic markers was used to determine the hip joint centre (Bell et al., 1989; Bell et al., 1990). Retroreflective markers were placed on the left and right anterior superior iliac spine, and on the right and left posterior superior iliac spine. The knee joint centres were identified by the midpoints between the medial and lateral femoral epicondyles markers, while the ankle joint centres were determined through calculating the midpoints between the medial and lateral malleoli (Cappello et al., 1997).

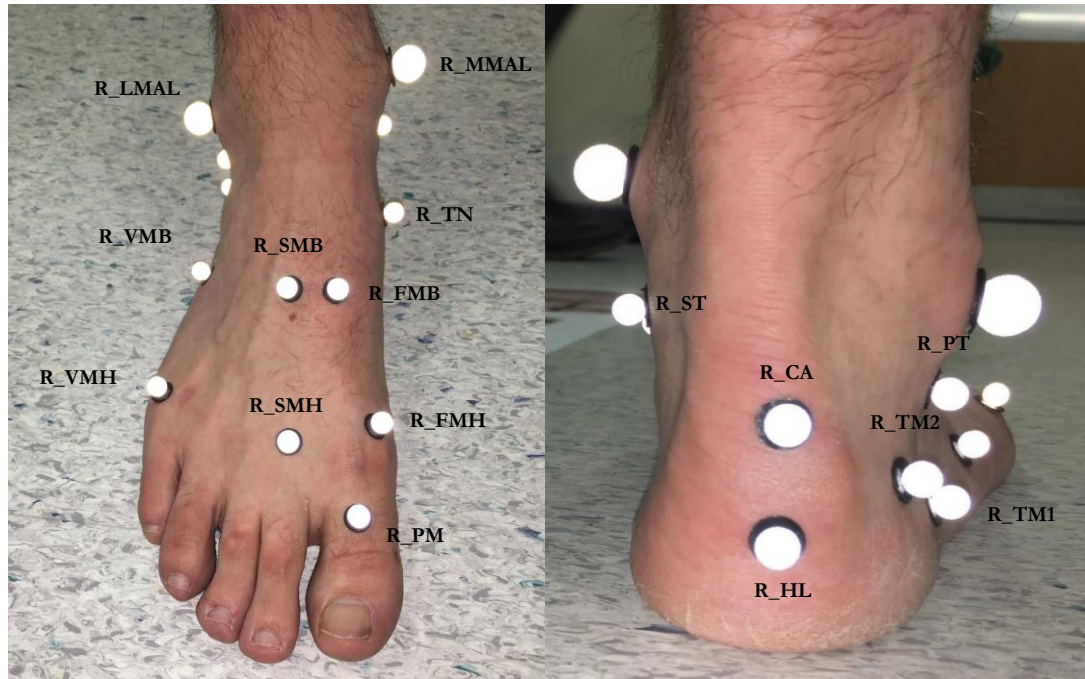


Figure 74. The IOR multi-segment foot model used to measure the kinematic data for the hindfoot, midfoot and forefoot segments.

Table 15. Location of the skin-mounted and tracking markers.

Abbreviation	Anatomical Landmarks
ASIS	Anterior superior iliac spine
PSIS	Posterior superior Iliac Spine
PEL_U	Upper aspect of the sacrum pelvic cluster
PEL_L	Lower aspect of the sacrum pelvic cluster
ILC	Iliac crest
GTR	Most lateral aspect of the femoral head (greater trochanter)
TH1-4	Lateral aspect of the of the thigh (thigh clusters)
LKNEE	Most lateral prominence of the lateral femoral epicondyle
MKNEE	Most medial prominence of the medial femoral epicondyle
SK1-4	Lateral aspect of the shank (shank clusters)
LMAL	Lateral prominence of the lateral malleolus
MMAL	Most medial prominence of the medial malleolus
CA	Upper central ridge of the calcaneus posterior surface i.e. Achilles' tendon attachment
HL	Distal attachment of the Achilles' tendon.
ST	Most medial apex of the sustentaculum tali
PT	Lateral apex of peroneal tubercle
TM1	Extra hindfoot tracking marker
TM2	Extra hindfoot tracking marker
TN	Most medial apex of the tuberosity of the navicular
FMB	Base of the first metatarsal, dorso-medial aspect of the first metatarso-cuneiform joint
FMH	Head of the first metatarsal, dorso-medial aspect of the first metatarso-cuneiform joint
SMB	Base of the second metatarsal, dorso-medial aspect of the second metatarso-phalangeal joint
SMH	Head of the second metatarsal, dorso-medial aspect of the second metatarso-phalangeal joint
VMB	Base of the fifth metatarsal, dorso-lateral aspect of the fifth metatarso-cuboid joint
VMH	Head of the fifth metatarsal, dorso-lateral aspect of the fifth metatarso-phalangeal joint
PM	Most distal and dorsal point of the head of the proximal distal phalanx of the hallux

## 5.2.6 Data Collection

Before walking trials commenced, a static trial was completed to determine the position of the anatomical and tracking marker clusters, with respect to the foot and lower limb joint locations. Participants stepped onto the force platform, then stood still with their feet hip width apart whilst adopting the anatomical position, for approximately five seconds (Figure 75). Once recorded, the visibility of the markers were checked and the participant then performed the walking trials as instructed. If markers moved significantly, dropped off or were not picked up by the infrared cameras, a new static trial was mandated to guarantee the original marker positions were determined.

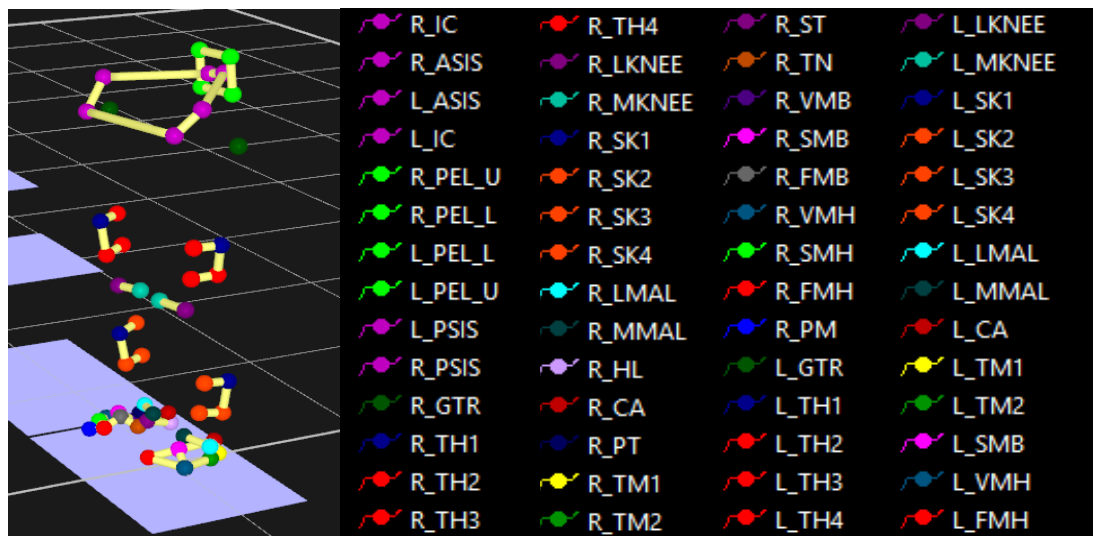


Figure 75. Static trial (left) and the label list for the 36 reflective markers (right) within Qualisys software.

Each participant had a familiarisation period prior to completing five successful overground walking trials at a comfortable self-selected pace. A successful trial was defined as the point at which markers were in view of the cameras and the operated foot landed fully within the boundary of the force platforms, without under- or over-striding (Figure 76). The participants were also asked to look forward during each trial to prevent ‘targeting’ the force platforms, which may cause the participant to adjust their stride patterns in an attempt to maintain full foot contact (Queen et al., 2006).

The walkway was the same length (8 m) at both research sites, allowing a minimum of four steps before the participant stepped onto the force platforms, to accommodate natural walking speed. Black duct tape was placed directly on the floor to indicate the participants starting position. It would have been unnatural for a study of this nature to account for walking speed, as this would in turn, influence lower limb joint kinetics and kinematics between the different patient cohorts. Walking speed and other spatiotemporal changes post-surgery are also crucial indicators of patient function post-surgery. Therefore, controlling walking speed may have masked the effect of this parameter on kinetic and kinematic behaviour. Moreover, increased walking speed on joint

kinetics has been found to have a significant effect when the walking speed exceeds 6 km/h (Eerdeken et al., 2019). However, this speed was not attained by any of the patient cohorts in the current study.



Figure 76. An example of a participant completing a successful trial within the movement area.

## 5.2.7 Data Processing

### Chapel Allerton Hospital

The successful trials were analysed within Vicon Nexus 2.9.2 software (Vicon Motion Systems, Oxford, UK). Each trial included one full gait cycle where the operated foot was in full contact with the force platform. All markers were manually labelled for each static trial, while the dynamic trials were labelled through an auto-labelling function within Vicon Nexus software which recognised the marker location from the static trial. The trajectories from all the markers were manually checked to ensure continuous identification of the retroreflective markers. If incomplete marker trajectories were present (e.g. deletion of frames, blocking or dropping out of markers), a spline fill function was applied which predicted the missing values between marker gaps. Walking trials with gaps missing for more than ten consecutive frames were not filled, with the incomplete trials being discarded.

### Nottingham Trent University

A similar processing technique was used within Qualisys Track Manager 2019.3 software (Qualisys™ Medical AB, Goteborg, Sweden) for labelling a static trial. An automated identification of markers (AIM) model was created and applied to all further successful trials for each participant. Once each trial was checked, they were added to the AIM model, which improved the reconstruction accuracy for use in later trials, as well as condensing the time taken for manual marker identification. The Qualisys software applied a polynomial interpolation to

calculate the line of best fit of the missing marker trajectories for gaps below ten frames. Gap filling was performed on the successful trials, but not on the calibrating or static trials.

### 5.2.8 Data Analysis

Labelled marker coordinates and kinetic data from the successful trials from both motion capture systems were exported to .C3D files and imported to Visual 3D (C-Motion, Germantown, USA) for further analysis. A 3D biomechanical model of the foot and lower limb body segments was created using the six DOF model (C-Motion, Germantown, USA). The linked segments were then used to calculate the kinetics and kinematics of the hip (pelvis and thigh), knee (thigh and shank), and ankle (shank and foot) (Figure 77).

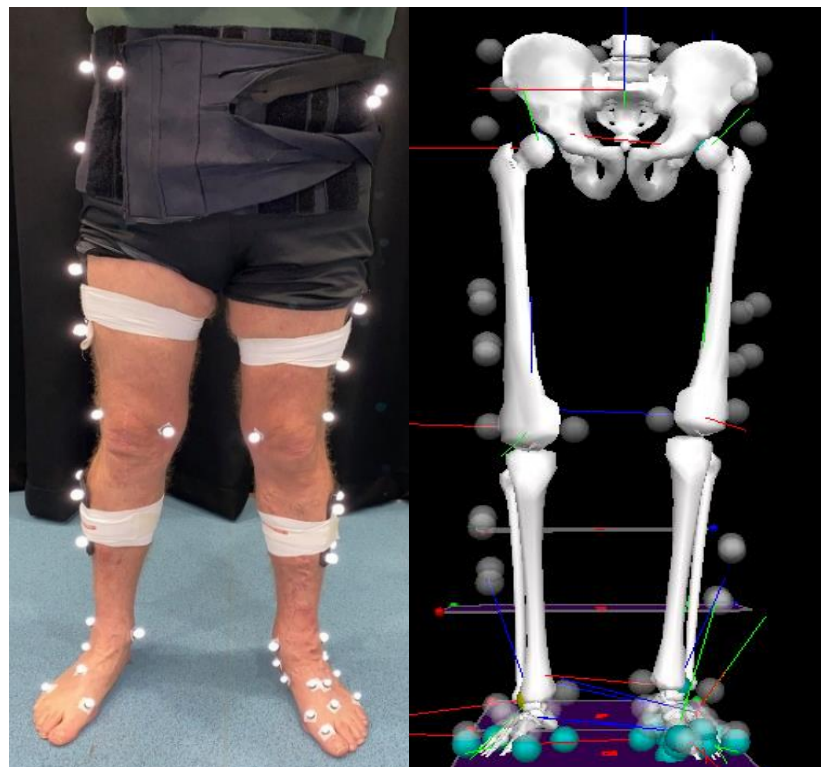


Figure 77. The marker set-up for the static condition (left) and the Visual 3D model created from the body segments.

Ankle joint kinematics for the non-operated foot were derived using a rigid SFM, with the proximal end of the segment being defined as the medial and lateral malleoli and the distal end as the first and fifth metatarsal head markers (Table 15). Markers at the base of the second metatarsal, the Achilles tendon attachment and two at the lateral aspect of the hindfoot, were used to track the single-segment during the walking trials. A limitation of the SFM was that the orientation of the foot segment was at an offset of approximately  $30^\circ$  during plantarflexion, which was not a clinically relevant representation of the ankle joint during walking. To avoid this issue, a virtual foot model was developed for the use in the kinematic computations of the foot segment. The virtual foot was employed to remove the offset and project the segment coordinate system to ensure it was parallel with the floor, regardless of the foot position during the static

trial. The segment coordinate system was rotated (+Z in the AP direction and -Y in the distal to proximal axis) to be consistent with the cardan sequence of all other lower limb segments.

The IOR model further separated the operated foot into four segments (the calcaneus, midfoot metatarsus and hallux). The modelling of the MFM was based on the methods detailed in the 'IORFoot Tutorial Angles' within C-Motion Visual 3D Wiki Documentation (C-Motion, 2018). The IOR model allowed for the 3D joint rotations to be calculated between the foot segments to measure hindfoot, midfoot and forefoot motion. Hindfoot motion was defined as the calcaneus with respect to the shank (i.e. the AJC). Midfoot motion was defined as the midfoot with respect to the calcaneus (i.e. Chopart joint). Forefoot motion was defined as the metatarsus with respect to the midfoot (i.e. Lisfranc joint). A final segment defined the metatarsus with respect to the calcaneus and is here after referred to as forefoot-to-hindfoot segment.

The biomechanical model was built using each participant's static trial and paired with the associated walking trials. The height and weight of each participant was input into the segmental model, which was used for joint moment calculations and kinetic normalisation. A pipeline was then applied to the data, allowing for the creation of complex scripts which automated the calculation and filtered the gait data (Appendix H). The filtering process selectively rejected or attenuated certain frequencies (noise) of the raw signal (Robertson et al., 2013). Kinematic signal generally occurs in high amplitudes at lower frequencies (Winter, 1984), while kinetic data has previously been reported to be more accurate and in less need of filtering (Roewer et al., 2014). Therefore, a fourth order low-pass Butterworth filter, with a cut-off frequency of 6Hz and 25Hz, was added to the pipeline, for the kinematic and kinetic data, respectively (Robertson and Dowling, 2003). The gait events of heel strike and toe-off were determined using thresholds (>20N and <20N) from the vertical GRF (Kristianslund et al., 2012), while the kinematic and kinetic data were both normalised to 100% of the gait and stance phase.

In order to determine overall function for each patient cohort, the spatiotemporal parameters of step length (m), walking speed (m/s) and cadence (steps/min) were calculated. Step length was measured as the distance between the proximal end positions of the contralateral foot at the previous contralateral heel strike, to the proximal end position of the ipsilateral foot at the ipsilateral heel strike (Shendkar et al., 2015). Walking speed was computed using the actual stride length divided by the actual stride time, while cadence was defined as the average number of steps per minute (Shendkar et al., 2015).

Joint angles were computed relative to the proximal segments for the hip, knee and ankle. The kinematics of the hip and knee were calculated according to International Society of Biomechanics (ISB) recommendations (Grood and Suntay, 1983; Wu et al., 2002), using the X-Y-Z cardan sequence of rotations (where X is flexion/extension; Y is abduction/adduction; and Z is internal/external rotation). The SFM rotations were also calculated using the X-Y-Z cardan

sequence of rotations (where X is dorsi-/plantarflexion; Y is eversion/inversion; and Z is abduction/adduction). The kinematics of the IOR foot model were quantified using the Z-X-Y cardan sequence of rotations, where dorsi-/plantarflexion was defined as the rotation about the z-axis (medio-lateral) of the proximal segment, abduction/adduction was defined about the y-axis (vertical) and eversion/inversion was defined as the axis orthogonal to the z- and y-axis (Leardini et al., 2007; Portinaro et al., 2014). Peak angles and ROM for the hip, knee and foot models were extracted for statistical analysis. Joint ROM was calculated as the difference between the peak angles during the gait cycle.

GRF data was normalised to each participant's BW (kg). Two distinct peaks during walking gait were quantified in this study.  $GRF1_{max}$  was calculated as the peak from early to mid-stance and  $GRF2_{max}$  was measured as the peak value from mid-stance to terminal stance (Figure 78). Net internal joint moments of the hip, knee and ankle were calculated during the stance phase using a Newton-Euler inverse dynamic calculation, within Visual 3D software. This calculation involved two equations: force equals mass multiplied by linear acceleration ( $F = m \cdot a$ ); and moment of force equals inertia multiplied by angular acceleration ( $M = I \cdot a$ ). The calculation predicted the necessary turning effect across the lower limb passive tissues and muscle structures, required to complete the overground level walking trials. The resultant internal moments were normalised proportional to participant's BW, ensuring differences between participants were due to individual gait mechanics, rather than weight (Winter, 2009). The joint power at the proximal end of a segment relative to a parent segment was calculated as the product of joint moment and joint angular velocity. Only the power generated at the lower limb joints was measured, as the antigravity muscles (glutei, quadriceps, and plantarflexors) are required during overground walking and may remain a challenge in patients implanted with AA or TAR.

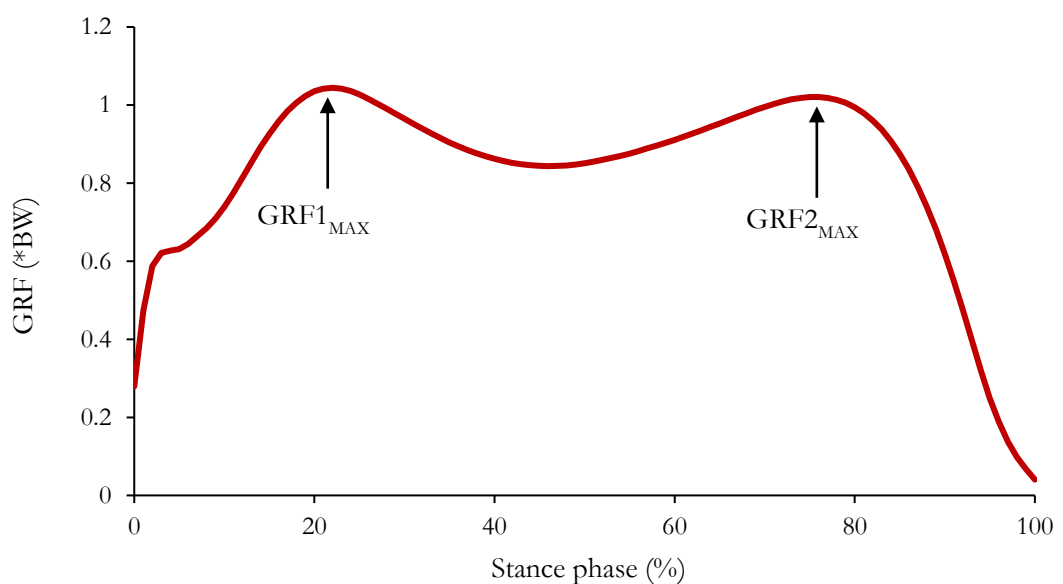


Figure 78. Schematic of the ground reaction force waveform and vertical peaks ( $GRF1_{max}$  and  $GRF2_{max}$ ).

### 5.2.9 Statistical Analysis

This was a post-operative exploratory analysis rather than a hypothesis driven study, which was also limited by small sample sizes in each patient cohort. Thus, formal inferential analysis was deemed inappropriate. Results were instead presented descriptively as mean ( $\pm$  95% CL) peak and ROM of the 3D kinematic and kinetic parameters between patient cohorts. All descriptive statistics analyses were conducted using SPSS version 26.0 (SPSS Inc, Chicago, USA). Absolute mean values were selected as it allowed a direct comparison to the limited published studies comparing both treatment options. This also acted to determine if the patient cohorts from this study produced similar gait mechanic trends to the published literature. However, due to the limited sample size of each of the treatment cohorts, caution must be dealt when extrapolating the results to the larger patient populations.

## 5.3 Results

### 5.3.1 Patient Reported Outcome Measures

Descriptive statistics (mean  $\pm$  95% CL) in relation to the MOxFQ walking/standing, pain and social interaction domains are reported in Table 16. A higher score was associated with a greater severity in the reported outcome. The three patient cohorts demonstrated comparable domain scores for walking/standing, while the mixed TAR cohort presented slightly higher scores in the pain ( $29.17 \pm 29.85$ ) and social interaction ( $30.21 \pm 30.63$ ) when compared to the AA and BOX® ankle patient cohorts (Table 16). However, the large variability ( $\pm$  95% CL) within the respective patient cohorts for each of the MOxFQ domain scores showed that each patient's perception of the surgery was substantially different, particularly in the implant patient groups. This finding was more than likely due to the combination of a small sample size coupled with the patient's interpretation and understanding of their condition. The scores for all three domains of the MOxFQ were summed and converted to a metric from 0 to 100 to create a summary index score (MOxFQ-Index), which was comparable between the surgical interventions (Table 16).

Table 16. Mean ( $\pm$  95% CL) MOxFQ domain scores between the three patient cohorts.

MOxFQ Domain Scores	AA	TAR	BOX®
Walking/Standing	$17.86 \pm 18.12$	$17.86 \pm 23.66$	$18.45 \pm 23.00$
Pain	$22.22 \pm 18.73$	$29.17 \pm 29.85$	$19.17 \pm 22.54$
Social Interaction	$15.28 \pm 18.25$	$30.21 \pm 30.63$	$16.67 \pm 31.38$
MOxFQ Index	$18.06 \pm 18.24$	$19.01 \pm 19.13$	$18.23 \pm 22.80$

### 5.3.2 Spatiotemporal Parameters

Descriptive analysis (mean  $\pm$  95% CL) of the spatiotemporal parameters measured are presented in Table 17. The mixed TAR cohort demonstrated increased walking speed ( $1.17 \pm 0.14$  m/s) compared to the AA ( $0.97 \pm 0.18$  m/s) and BOX® ankle ( $0.90 \pm 0.35$  m/s) patient cohorts (Table 17). A similar trend was also shown for cadence at the operated limb, with the mixed TAR

cohort exhibiting increased cadence ( $108.43 \pm 7.87$  steps/min) when compared to the other treatment options (Table 17). However, the large variance ( $\pm 95\%$  CL) meant that there was unlikely to be substantial differences in walking speed and cadence of the operated limb between surgical interventions. The measured cadence of the non-operated limb and step length were relatively similar between the patient cohorts, with relatively high variance associated with each surgical intervention (Table 17).

Table 17. Mean ( $\pm 95\%$  CL) spatiotemporal gait parameters for the three patient cohorts.

<b>Spatiotemporal Parameters</b>	<b>AA</b>	<b>TAR</b>	<b>BOX®</b>
Walking Speed (m/s)	$0.97 \pm 0.18$	$1.17 \pm 0.14$	$0.90 \pm 0.35$
Step Length (m) - OL	$0.61 \pm 0.08$	$0.66 \pm 0.08$	$0.53 \pm 0.16$
Step Length (m) - NOL	$0.56 \pm 0.09$	$0.64 \pm 0.01$	$0.52 \pm 0.18$
Cadence (steps/min) - OL	$93.58 \pm 7.67$	$108.43 \pm 7.87$	$100.89 \pm 17.44$
Cadence (steps/min) - NOL	$97.86 \pm 6.00$	$105.34 \pm 7.45$	$103.05 \pm 15.12$

\*OL = Operated Limb; NOL = Non-operated Limb

### 5.3.3 Hip Kinematics

Figure 79 presents the mean ( $\pm 95\%$  CL) sagittal, frontal and transverse hip kinematics during the gait cycle. The sagittal plane kinematic waveform followed a similar trend for all three patient cohorts throughout the gait cycle (Figure 79A). However, the BOX® ankle patient cohort tended to exhibit increased peak hip flexion angle ( $32.97 \pm 16.22^\circ$ ) compared to both the AA ( $24.98 \pm 10.18^\circ$ ) and mixed TAR cohort ( $23.29 \pm 6.10^\circ$ ) (Table 18). The BOX® ankle patients also possessed a reduced peak hip extension angle ( $-1.86 \pm 19.79^\circ$ ) when compared to AA ( $-11.80 \pm 9.15^\circ$ ) and mixed TAR ( $-14.73 \pm 8.23^\circ$ ) patient cohorts (Table 18). The relatively large CL in the measured peak parameters for the BOX® ankle patients meant that there was large variability in hip sagittal plane motion. Despite the associated offset in the BOX® ankle patient cohort, the sagittal ROM was comparable between the three patient cohorts (Table 18).

Table 18. Mean ( $\pm 95\%$  CL) hip kinematics for the three patient cohorts.

<b>Hip Kinematics (°)</b>	<b>AA</b>	<b>TAR</b>	<b>BOX®</b>
Peak Hip Flexion	$24.98 \pm 10.18$	$23.29 \pm 6.10$	$32.97 \pm 16.22$
Peak Hip Extension	$-11.80 \pm 9.15$	$-14.73 \pm 8.23$	$-1.86 \pm 19.79$
Sagittal Hip ROM	$36.78 \pm 4.42$	$38.03 \pm 2.79$	$34.83 \pm 8.38$
Peak Hip Adduction	$8.97 \pm 5.77$	$10.31 \pm 5.56$	$10.03 \pm 3.71$
Peak Hip Abduction	$-3.29 \pm 4.88$	$-1.78 \pm 5.87$	$1.14 \pm 4.15$
Frontal Hip ROM	$12.27 \pm 2.45$	$12.10 \pm 2.92$	$8.90 \pm 3.59$
Peak Hip Internal Rotation	$-3.25 \pm 9.29$	$-1.02 \pm 9.09$	$9.64 \pm 11.28$
Peak Hip External Rotation	$-15.80 \pm 9.19$	$-12.09 \pm 6.34$	$-2.18 \pm 12.83$
Transverse Hip ROM	$12.55 \pm 1.78$	$11.07 \pm 3.54$	$11.82 \pm 4.10$

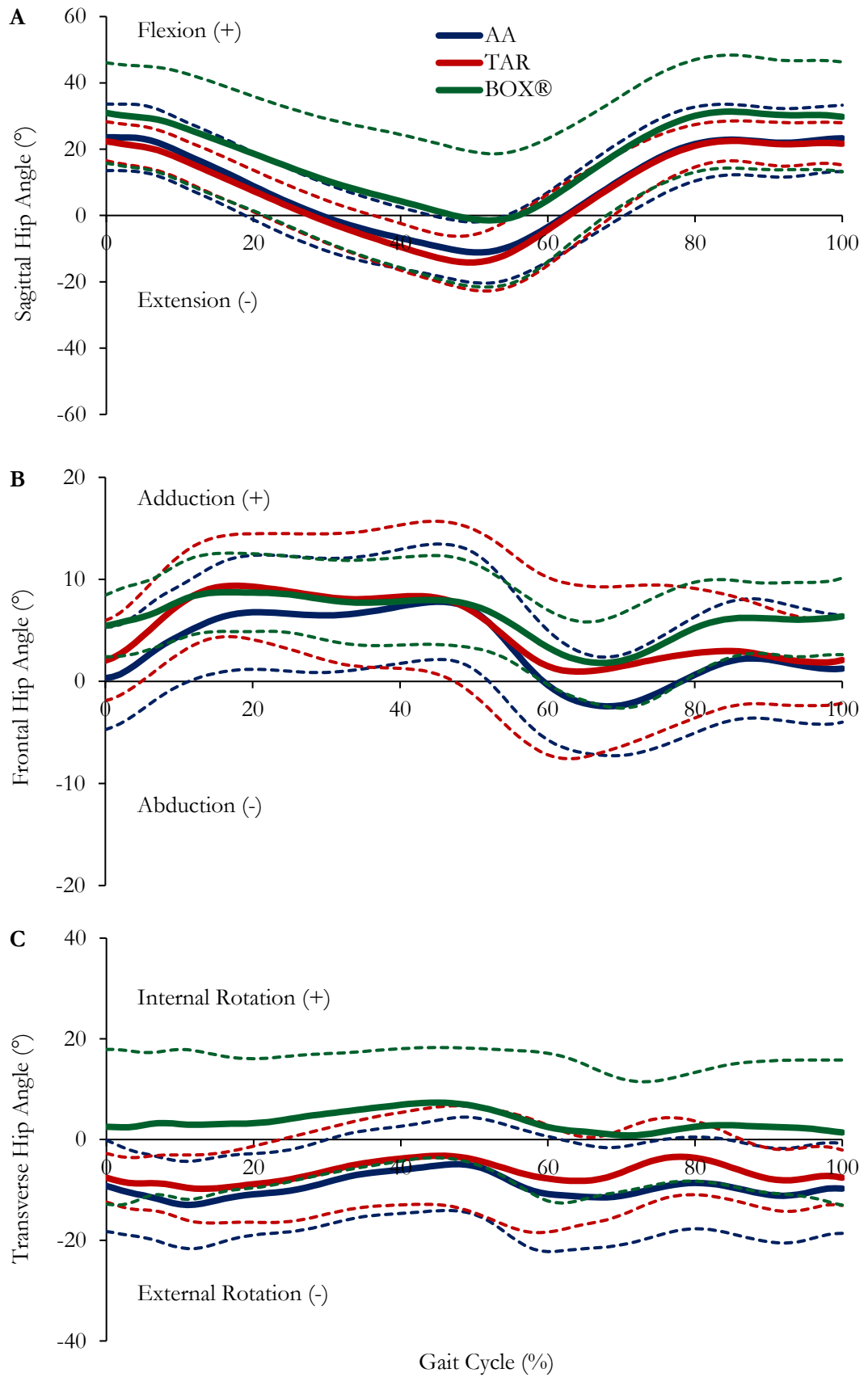


Figure 79. Mean ( $\pm$  95% CL) hip flexion (+)/extension (-) (A), adduction (+)/abduction (-) (B) and internal (+)/external (-) rotation (C) kinematic waveforms during the gait cycle, in patients with AA (blue), TAR (red) and BOX® ankle (green).

During initial contact, the BOX® ankle patients tended to be in a more adducted position compared to both other patient cohorts (Figure 79B). This finding caused the BOX® ankle patients to remain in an adducted position throughout the gait cycle. The AA and TAR cohorts tended to display abduction motion during toe-off (Figure 79B). The mean ( $\pm$  95% CL) frontal plane kinematics were however, similar between the three patient cohorts (Table 18). In the transverse plane, the BOX® ankle cohort were the only patient group which produced a peak internal rotation at the hip joint, while the two other cohorts remained externally rotated throughout the gait cycle (Figure 79C). The high variability in transverse hip rotation angles, demonstrated by the large CL in Figure 79C, meant that transverse plane ROM was comparable between the patient cohorts (Table 18).

### 5.3.4 Knee Kinematics

Mean ( $\pm$  95% CL) sagittal, frontal and transverse plane kinematic waveforms during the gait cycle are presented in Figure 80. The sagittal plane kinematic waveform for the knee joint followed a similar pattern throughout the entire gait cycle (Figure 80A). Peak sagittal knee flexion and extension were comparable and occurred during the same time point in the gait cycle between treatment options (Table 19). This also resulted in similar sagittal knee ROM between the patient cohorts at the intermediate follow-up period (Table 19). In the frontal plane of motion, no substantial differences were detected between cohorts for peak adduction, abduction and ROM.

Both the mixed TAR and BOX® ankle cohorts remained adducted throughout the gait cycle, while the AA patients tended to reach peak knee abduction during the swing phase (Figure 80B). The mean transverse plane waveform for the BOX® ankle cohort suggested that the patients remained externally rotated throughout the gait cycle (Figure 80C). There was increased variability within each patient cohort for knee IER, as demonstrated by the high CL in Figure 80C. Despite the large variation within the patient cohorts, there tended to be only small differences in mean peak IER and ROM (Table 19).

Table 19. Mean ( $\pm$  95% CL) knee kinematics for the three patient cohorts.

<b>Knee Kinematics (°)</b>	<b>AA</b>	<b>TAR</b>	<b>BOX®</b>
Peak Knee Flexion	61.86 $\pm$ 4.18	62.26 $\pm$ 5.70	60.40 $\pm$ 7.25
Peak Knee Extension	4.23 $\pm$ 5.47	4.48 $\pm$ 3.81	6.66 $\pm$ 9.56
Sagittal Knee ROM	57.63 $\pm$ 3.54	57.78 $\pm$ 4.71	53.75 $\pm$ 9.10
Peak Knee Adduction	9.09 $\pm$ 5.14	8.21 $\pm$ 2.12	8.70 $\pm$ 3.69
Peak Knee Abduction	-2.62 $\pm$ 6.77	0.03 $\pm$ 2.78	0.97 $\pm$ 4.01
Frontal Knee ROM	11.71 $\pm$ 2.62	8.18 $\pm$ 2.92	7.73 $\pm$ 1.04
Peak Knee Internal Rotation	1.07 $\pm$ 4.56	1.72 $\pm$ 7.71	-1.67 $\pm$ 8.02
Peak Knee External Rotation	-13.16 $\pm$ 5.39	-13.10 $\pm$ 4.12	-18.23 $\pm$ 10.75
Transverse Knee ROM	14.23 $\pm$ 2.23	14.82 $\pm$ 5.46	16.56 $\pm$ 5.30

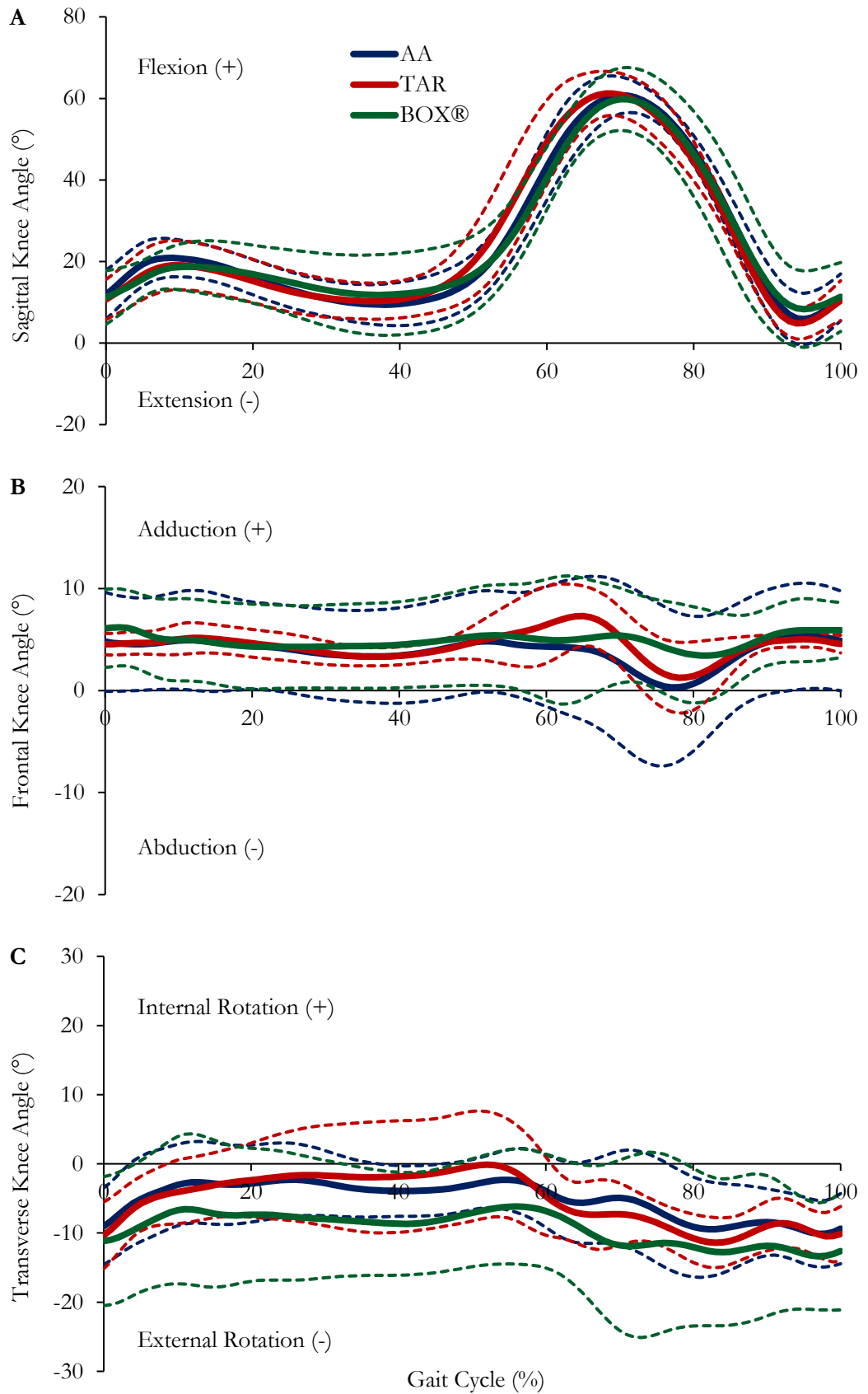


Figure 80. Mean ( $\pm$  95% CL) knee flexion (+)/extension (-) (A), adduction (+)/abduction (-) (B) and internal (+)/external (-) rotation (C) kinematic waveforms during the gait cycle, in patients with AA (blue), TAR (red) and BOX® ankle (green).

### 5.3.5 Single-segment Foot Model Kinematics

Figure 81 depicts the mean ( $\pm$  95% CL) sagittal, frontal and transverse kinematics waveforms of the ankle throughout the gait cycle, measured with the SFM. Both implant patient cohorts exhibited higher sagittal plane ROM (mixed TAR =  $20.11 \pm 8.83^\circ$  and BOX® ankle:  $13.56 \pm 4.10^\circ$ ) compared to AA patients ( $13.10 \pm 1.96^\circ$ ) (Table 20). However, the patient cohorts demonstrated comparable mean peak dorsiflexion and plantarflexion in the sagittal plane. The patient cohorts displayed similar frontal plane kinematic waveforms throughout the gait cycle (Figure 81B), resulting in similar peak and ROM values (Table 20).

The greatest variance between patient cohorts occurred in the transverse plane of motion (Figure 81C), which followed a similar pattern to both the hip (Figure 79C) and knee (Figure 80C) joints. The AA and TAR cohorts displayed corresponding kinematic waveforms in the transverse plane, while the BOX® ankle patients tended to have a more abducted ankle throughout the gait cycle (Figure 81C). However, the total transverse ROM measured was comparable between all three treatment cohorts.

Table 20. Mean ( $\pm$  95% CL) single-segment foot kinematics for the three patient cohorts.

Single-segment Ankle Kinematics (°)	AA	TAR	BOX®
Peak Ankle Dorsiflexion	$12.71 \pm 1.78$	$15.45 \pm 4.37$	$15.99 \pm 3.98$
Peak Ankle Plantarflexion	$-0.40 \pm 1.70$	$-4.66 \pm 6.11$	$-1.91 \pm 6.66$
Sagittal Ankle ROM	$13.10 \pm 1.96$	$20.11 \pm 8.83$	$17.90 \pm 3.67$
Peak Ankle Eversion	$2.26 \pm 1.74$	$2.59 \pm 2.09$	$0.77 \pm 4.41$
Peak Ankle Inversion	$-6.90 \pm 3.34$	$-8.29 \pm 2.09$	$-10.98 \pm 4.31$
Frontal Ankle ROM	$9.17 \pm 2.56$	$10.88 \pm 2.84$	$11.75 \pm 3.28$
Peak Adduction	$-0.76 \pm 7.34$	$0.63 \pm 7.67$	$-6.69 \pm 7.16$
Peak Abduction	$-9.48 \pm 6.34$	$-9.25 \pm 5.46$	$-15.28 \pm 7.88$
Transverse Ankle ROM	$8.72 \pm 2.23$	$9.88 \pm 3.99$	$8.59 \pm 2.29$

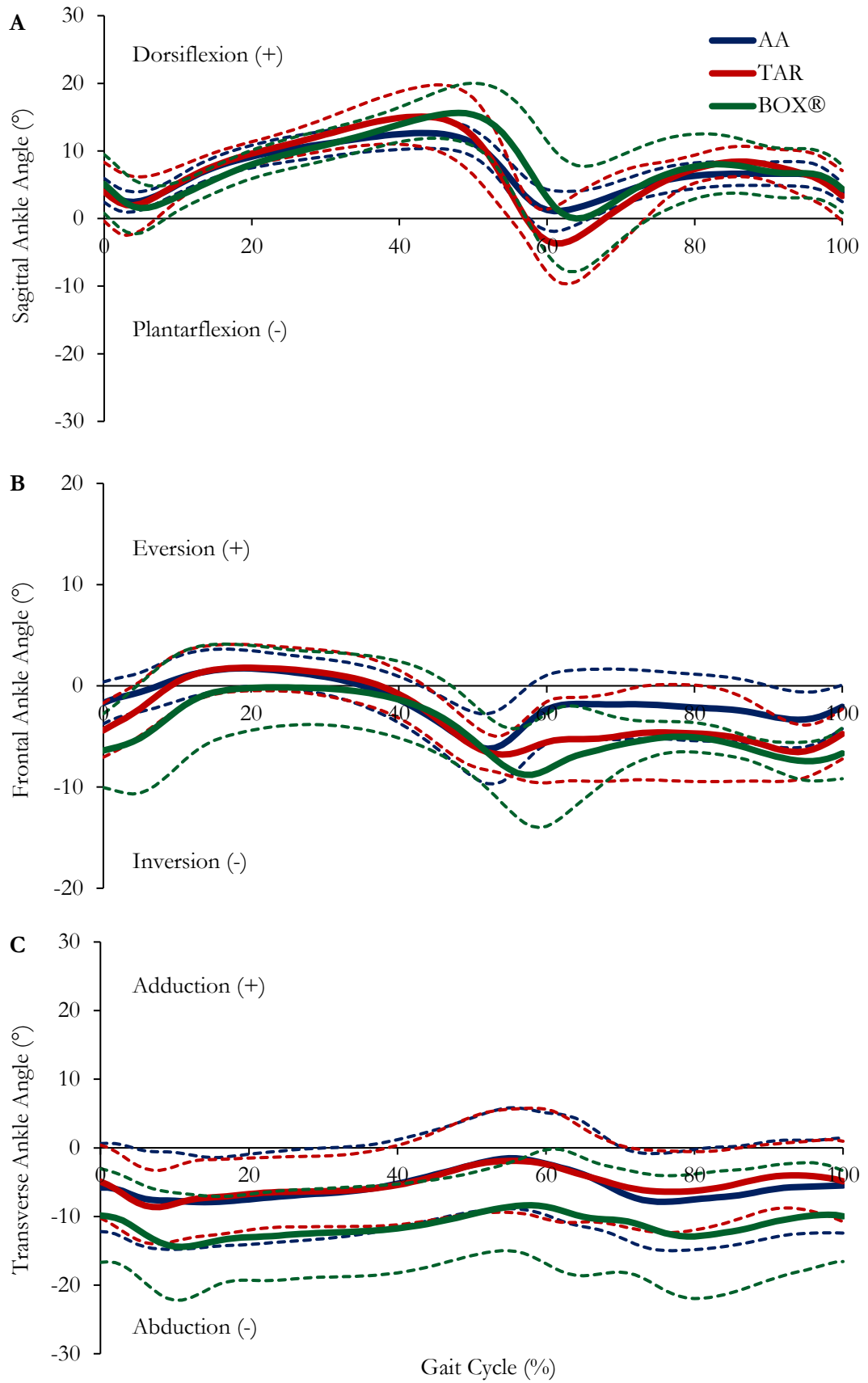


Figure 81. Mean ( $\pm$  95% CL) single-segment ankle dorsiflexion (+)/plantarflexion (-) (A), eversion (+)/inversion (-) (B) and adduction (+)/abduction (-) (C) kinematic waveforms during the gait cycle, in patients with AA (blue), TAR (red) and BOX® ankle (green).

### 5.3.6 Multi-segment Foot Model Kinematics

#### 5.3.6.1 Hindfoot (Segment) Kinematics

The sagittal plane kinematic waveform of the hindfoot segment followed a similar pattern for all three treatment options (Figure 82A). The BOX® ankle patient cohort demonstrated increased peak dorsiflexion and reduced plantarflexion motion (Table 21), but this may have resulted from the patients possessing greater dorsiflexion of the hindfoot segment at initial contact. The mixed TAR cohort demonstrated the greatest peak plantarflexion angle during toe-off, but the large CL suggests that there was likely no substantial differences between the patient cohorts for peak plantarflexion at the hindfoot. The descriptive statistics highlighted increased sagittal ROM in both implant cohorts (mixed TAR:  $15.08 \pm 5.73$  and BOX® ankle:  $13.56 \pm 4.10$ ) compared to AA patients ( $9.21 \pm 1.73^\circ$ ) (Table 21). The hindfoot segment also exhibited reduced sagittal ROM parameters compared to the SFM (Table 21), which also accounted for the corresponding motion at the midfoot and forefoot segments.

The kinematic waveform of the hindfoot segment in the frontal (Figure 82B) and transverse (Figure 82C) planes of motion compared well with that of the SFM. In the frontal plane, all patients remained in an inverted position throughout the gait cycle (Figure 82B). During initial contact, the BOX® ankle patient cohort tended to be in a more inverted position compared to both other patient cohorts, which may have resulted in the increased peak inversion angle at around toe-off (Figure 82B). The BOX® ankle patient cohort was also associated with having a greater frontal plane ROM ( $8.61 \pm 1.97^\circ$ ) compared to the AA patients ( $5.15 \pm 1.61^\circ$ ) (Table 21). The transverse plane kinematic waveform and selected parameters appeared to be comparable between the patient cohorts at the intermediate follow-up period post-surgery (Table 21).

Table 21. Mean ( $\pm$  95% CL) hindfoot kinematics for the three patient cohorts.

<b>Hindfoot Segment Kinematics (°)</b>	<b>AA</b>	<b>TAR</b>	<b>BOX®</b>
Peak Dorsiflexion	$7.26 \pm 5.08$	$8.09 \pm 4.28$	$13.42 \pm 8.28$
Peak Plantarflexion	$-1.95 \pm 4.51$	$-6.99 \pm 7.41$	$-0.14 \pm 9.52$
Sagittal Hindfoot ROM	$9.21 \pm 1.73$	$15.08 \pm 5.73$	$13.56 \pm 4.10$
Minimum Inversion	$-5.92 \pm 5.07$	$-4.01 \pm 7.03$	$-8.24 \pm 6.95$
Peak Inversion	$-11.06 \pm 6.12$	$-11.32 \pm 7.00$	$-16.85 \pm 6.71$
Frontal Hindfoot ROM	$5.15 \pm 1.61$	$7.31 \pm 2.55$	$8.61 \pm 1.97$
Peak Adduction	$5.03 \pm 6.68$	$4.07 \pm 8.31$	$1.65 \pm 10.31$
Peak Abduction	$-3.21 \pm 6.59$	$-4.28 \pm 7.45$	$-6.93 \pm 10.68$
Transverse Hindfoot ROM	$8.24 \pm 1.31$	$8.34 \pm 2.68$	$8.58 \pm 1.67$

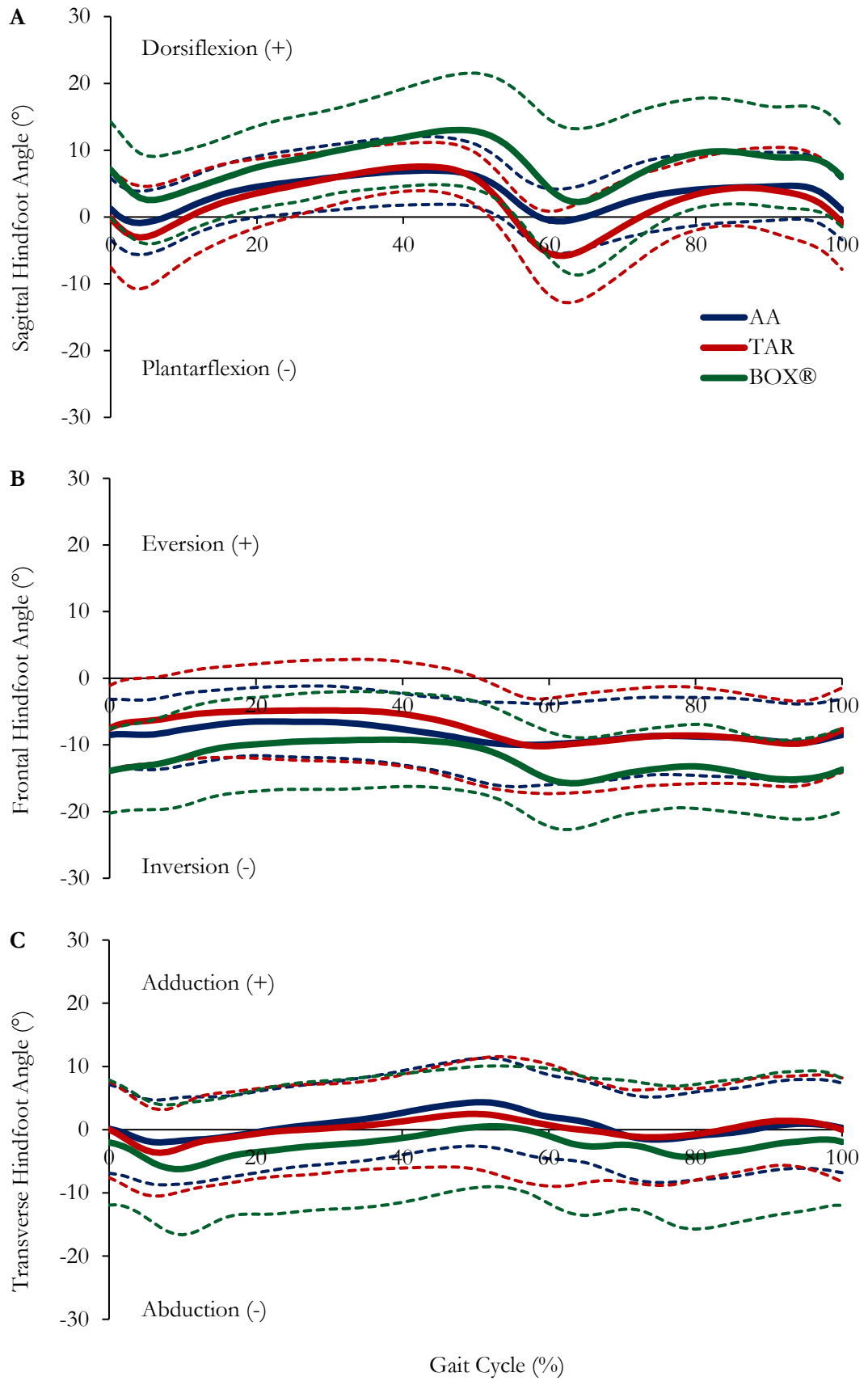


Figure 82. Mean ( $\pm$  95% CL) hindfoot segment dorsiflexion (+)/plantarflexion (-) (A), eversion (+)/inversion (-) (B) and adduction (+)/abduction (-) (C) kinematic waveforms during the gait cycle, in patients with AA (blue), TAR (red) and BOX® ankle (green).

### 5.3.6.2 Midfoot (Segment) Kinematics

Figure 83 shows the mean ( $\pm$  95% CL) sagittal, frontal and transverse midfoot segment kinematics during the gait cycle. With respect to the sagittal plane, all three patient cohorts remained in dorsiflexion (Figure 83A), so peak and minimum dorsiflexion was reported (Table 22). The AA patient cohort tended to exhibit greater peak dorsiflexion ( $41.32 \pm 7.32^\circ$ ) and minimum dorsiflexion ( $33.47 \pm 7.07^\circ$ ) angles compared to both implant cohorts (Table 22), but the large CL between within each patient cohort suggests that caution must be taken when extrapolating this result to larger patient populations. Despite these differences in peak parameter values, mean sagittal plane ROM was similar between the three patient cohorts (Table 22).

A small ROM occurred in the frontal and transverse planes of motion, independent of the surgical intervention (Table 22). The mean frontal plane kinematic waveforms suggested that each patient cohort remained in inversion during the gait cycle (Figure 83B), resulting in the minimum inversion value being compared instead of peak eversion. Frontal plane peak and ROM variables were comparable between all three patient cohorts (Table 22). In the transverse plane, the BOX<sup>®</sup> ankle cohort remained adducted, while the AA cohort remained in an abducted position throughout the gait cycle (Figure 83C). This finding resulted in substantially different mean peak adduction angles between the BOX<sup>®</sup> ankle ( $6.03 \pm 7.81^\circ$ ) and AA ( $-1.41 \pm 7.61^\circ$ ) patient cohorts. However, mean transverse plane ROM was similar between each of the patient cohorts.

Table 22. Mean ( $\pm$  95% CL) midfoot kinematics for the three patient cohorts.

<b>Midfoot Segment Kinematics (°)</b>	<b>AA</b>	<b>TAR</b>	<b>BOX<sup>®</sup></b>
Peak Dorsiflexion	$41.32 \pm 7.32$	$36.06 \pm 9.71$	$38.26 \pm 7.45$
Minimum Dorsiflexion	$33.47 \pm 7.07$	$25.75 \pm 9.94$	$28.70 \pm 7.15$
Sagittal Midfoot ROM	$7.86 \pm 1.79$	$10.31 \pm 6.04$	$9.56 \pm 2.48$
Minimum Inversion	$-3.35 \pm 5.05$	$-5.34 \pm 7.48$	$-0.71 \pm 4.02$
Peak Inversion	$-7.22 \pm 4.60$	$-10.49 \pm 5.81$	$-5.36 \pm 4.53$
Frontal Midfoot ROM	$3.86 \pm 1.05$	$5.16 \pm 2.13$	$4.65 \pm 1.52$
Peak Adduction	$-1.41 \pm 7.61$	$2.01 \pm 10.44$	$6.03 \pm 7.81$
Peak Abduction	$-3.74 \pm 7.67$	$-1.47 \pm 9.50$	$3.00 \pm 7.45$
Transverse Midfoot ROM	$2.33 \pm 0.76$	$3.47 \pm 1.23$	$3.02 \pm 0.99$

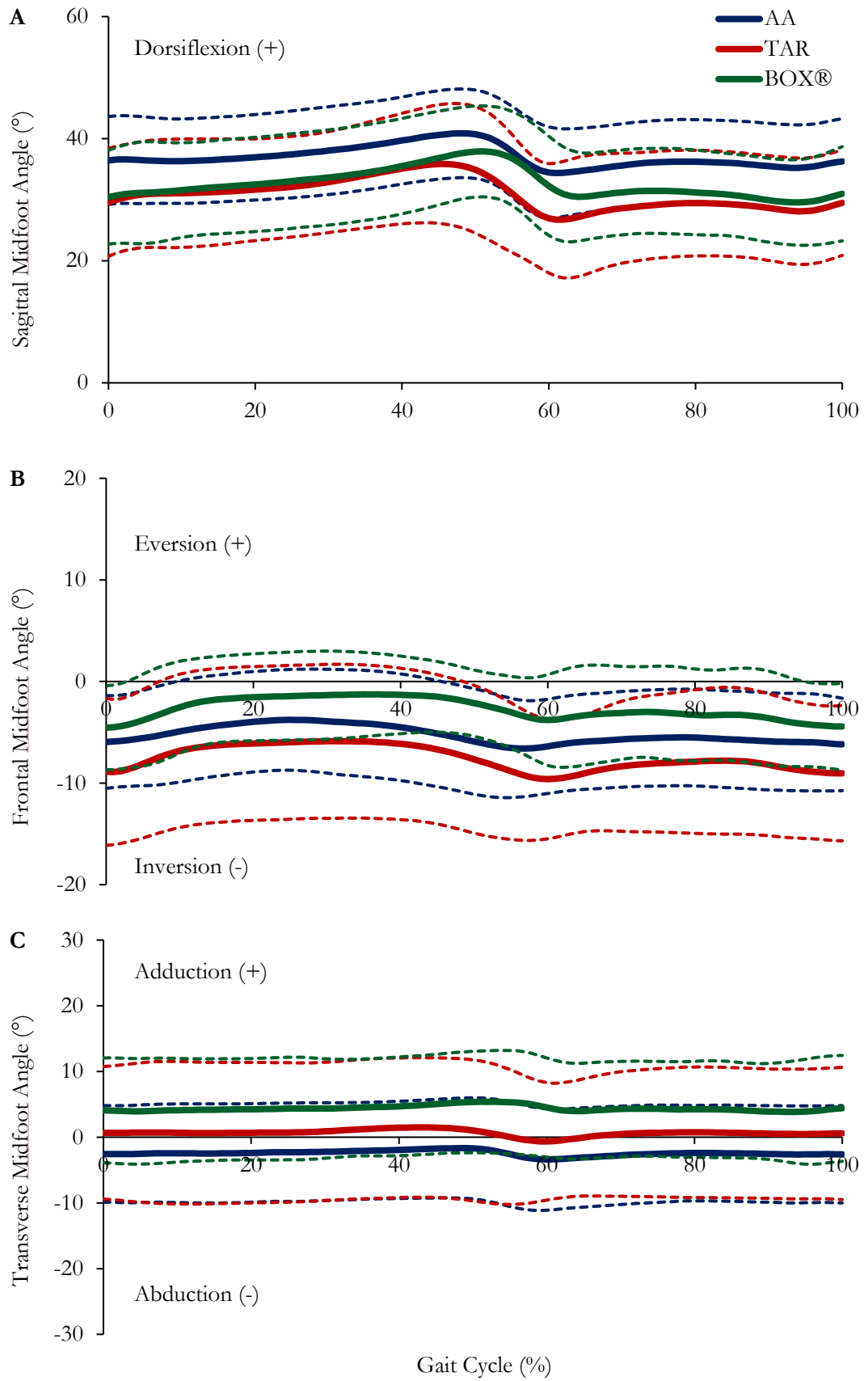


Figure 83. Mean ( $\pm$  95% CL) midfoot segment dorsiflexion (+) (A), eversion (+)/inversion (-) (B) and adduction (+)/abduction (-) (C) kinematic waveforms during the gait cycle, in patients with AA (blue), TAR (red) and BOX® ankle (green).

### 5.3.6.3 Forefoot (Segment) Kinematics

Mean ( $\pm$  95% CL) sagittal, frontal and transverse plane kinematic waveforms of the forefoot segment are presented in Figure 84. As expected, small ROM was observed in all three planes of motion throughout the gait cycle (Table 23). All three patient cohorts remained in a plantarflexed position during the overground walking trials (Figure 84A), which meant that minimum plantarflexion was compared instead of peak dorsiflexion (Table 23). Peak plantarflexion tended to be higher in AA patients ( $-82.52 \pm 7.16^\circ$ ) compared to both the mixed TAR ( $-69.78 \pm 6.67^\circ$ ) and BOX® ankle ( $-75.53 \pm 6.12^\circ$ ) patients (Table 23). Despite this difference, sagittal plane ROM was similar for all three patient cohorts and followed a similar pattern to that observed at the midfoot.

The frontal plane kinematics of the forefoot indicated that all three patient cohorts remained inverted throughout the gait cycle (Figure 84B). This resulted in minimum inversion being reported instead of peak eversion at the forefoot segment (Table 23). Both peak values and frontal plane ROM were comparable between the patient cohorts (Table 23). In the transverse plane, the forefoot segment remained adducted in the AA and mixed TAR patients, whilst the BOX® ankle patients were shown to abduct for the duration of the gait cycle (Figure 84C). Regardless of this, the transverse ROM was similar for each patient cohort (Table 23).

Table 23. Mean ( $\pm$  95% CL) forefoot kinematics for the three patient cohorts.

Forefoot Segment Kinematics ( $^\circ$ )	AA	TAR	BOX®
Minimum Plantarflexion	$-74.81 \pm 6.51$	$-64.53 \pm 7.88$	$-67.66 \pm 6.36$
Peak Plantarflexion	$-82.52 \pm 7.16$	$-69.78 \pm 6.67$	$-75.53 \pm 6.12$
Sagittal Forefoot ROM	$7.72 \pm 1.83$	$5.25 \pm 3.95$	$7.87 \pm 2.17$
Minimum Inversion	$-13.07 \pm 3.77$	$-9.65 \pm 8.60$	$-5.52 \pm 5.47$
Peak Inversion	$-17.72 \pm 3.57$	$-15.87 \pm 8.66$	$-11.06 \pm 5.35$
Frontal Forefoot ROM	$4.65 \pm 0.94$	$6.22 \pm 1.25$	$5.54 \pm 1.49$
Peak Adduction	$5.62 \pm 9.16$	$4.92 \pm 8.90$	$-0.60 \pm 6.56$
Peak Abduction	$2.57 \pm 9.55$	$1.20 \pm 9.35$	$-4.28 \pm 7.20$
Transverse Forefoot ROM	$3.05 \pm 1.07$	$3.72 \pm 0.82$	$3.68 \pm 0.96$

### 5.3.6.4 Forefoot-to-Hindfoot (Segment) Kinematics

Figure 85 evidences the mean ( $\pm$  95% CL) sagittal, frontal and transverse forefoot-to-hindfoot segment kinematics throughout the gait cycle. In the sagittal plane, all three patient cohorts remained in plantarflexion during the entire gait cycle (Figure 85A). Therefore, minimum plantarflexion was reported instead of peak dorsiflexion, which followed a similar trend to the forefoot. The kinematic waveforms from all three patient cohorts were relatively similar during the gait cycle and resulted in comparable peak and sagittal ROM values (Table 24).

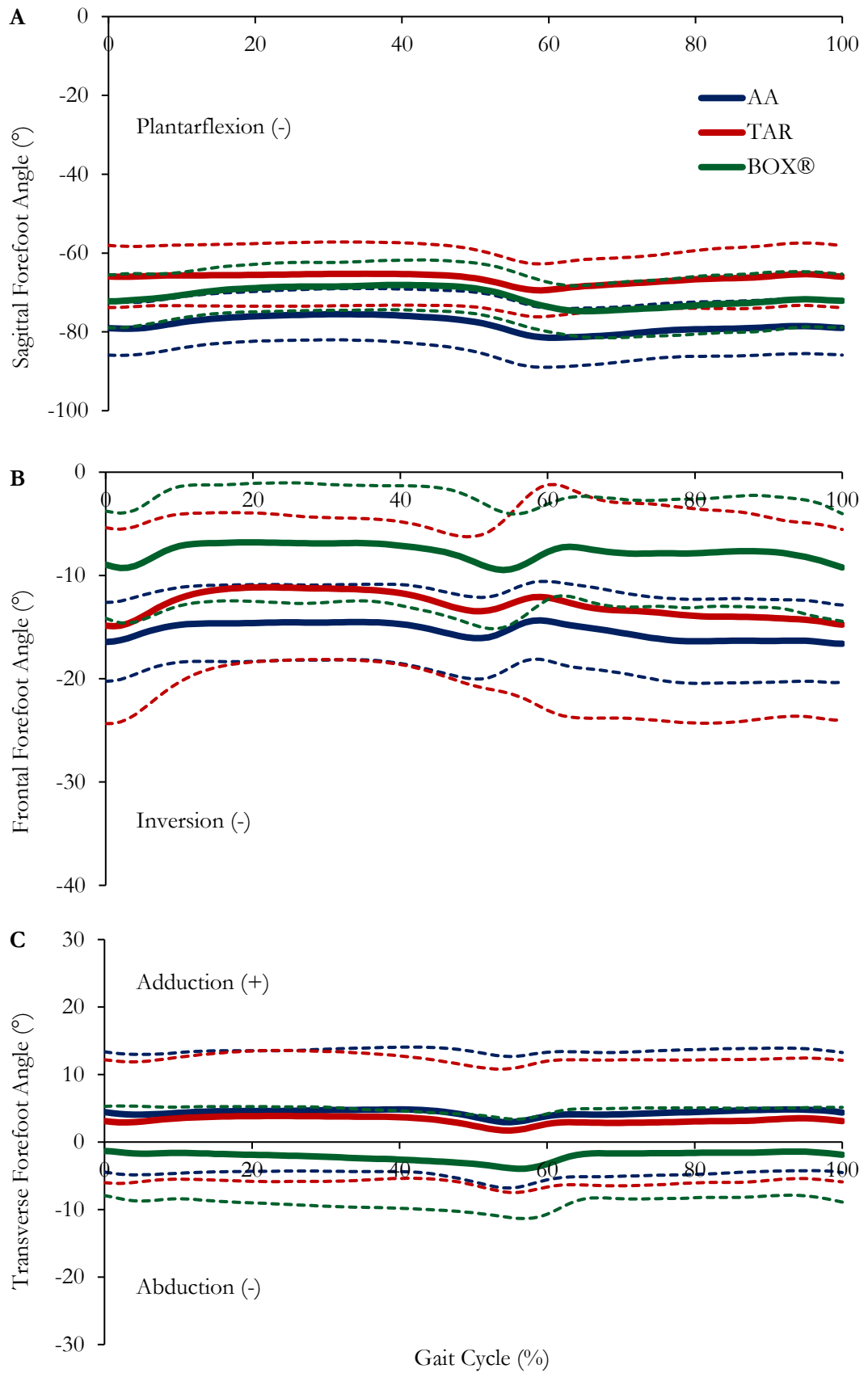


Figure 84. Mean ( $\pm$  95% CL) forefoot segment plantarflexion (-) (A), inversion (-) (B) and adduction (+)/abduction (-) (C) kinematic waveforms during the gait cycle, in patients with AA (blue), TAR (red) and BOX® ankle (green).

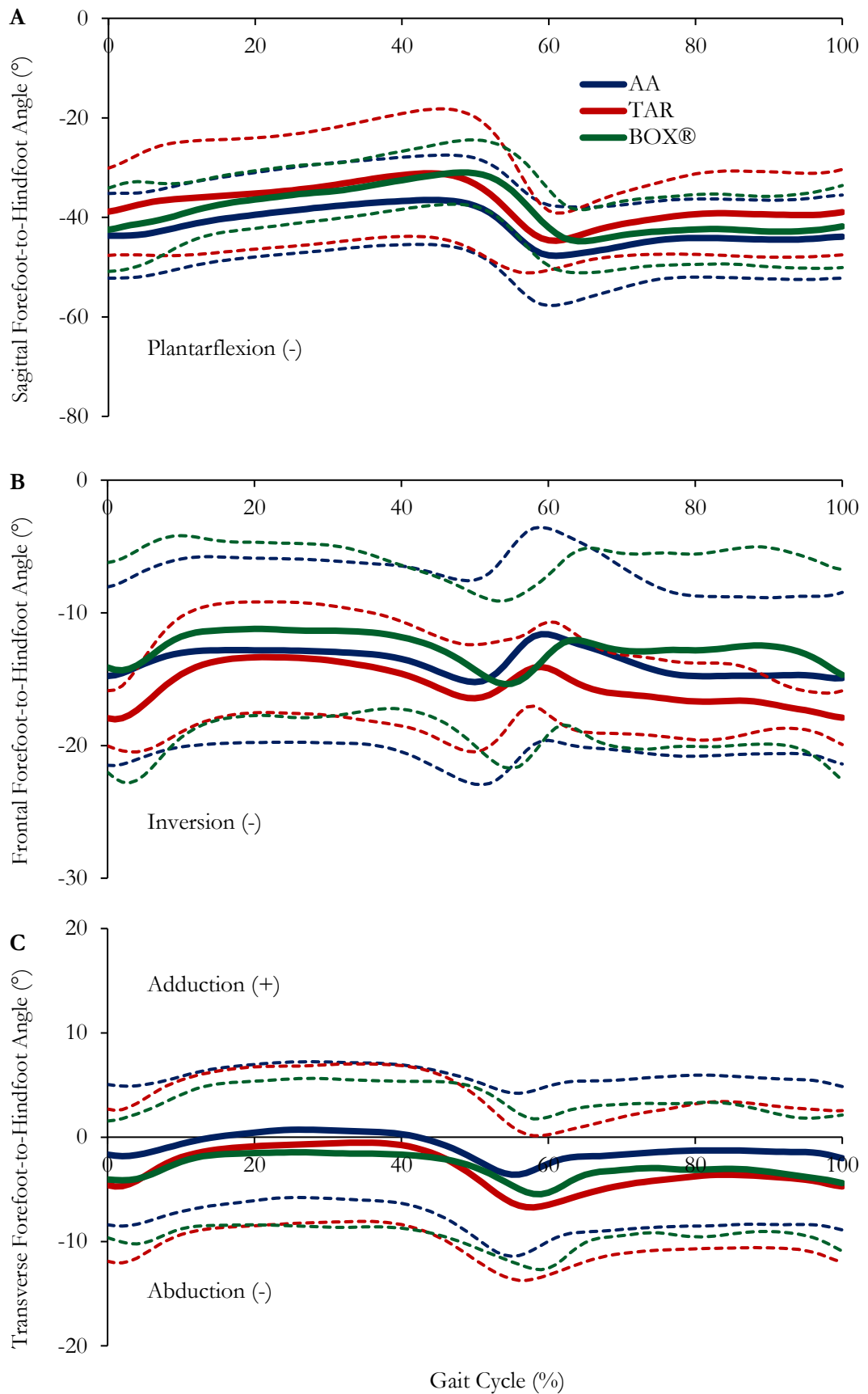


Figure 85. Mean ( $\pm$  95% CL) forefoot-to-hindfoot segment plantarflexion (-) (A), inversion (-) (B) and adduction (+)/abduction (-) (C) kinematic waveforms during the gait cycle, in patients with AA (blue), TAR (red) and BOX® ankle (green).

All three patient cohorts remained in an inverted position throughout gait (Figure 85B), which meant that minimum inversion was recorded instead of peak eversion value (Table 24). The mean values for each of the gait parameters measured in the frontal plane were similar between the patient cohorts (Table 24). This finding was also apparent in the transverse plane, with limited differences found between peak and ROM values for the patient cohorts (Table 24). The BOX® ankle cohort remained in an abducted position during the gait cycle, whilst the AA and mixed TAR cohorts produced both abduction and adduction motions (Figure 85C).

Table 24. Mean ( $\pm$  95% CL) forefoot-to-hindfoot kinematics for the three patient cohorts.

Forefoot-to-Hindfoot Segment Kinematics (°)	AA	TAR	BOX®
Minimum Plantarflexion	-35.39 $\pm$ 9.08	-30.86 $\pm$ 12.55	-30.68 $\pm$ 6.45
Peak Plantarflexion	-49.19 $\pm$ 9.03	-45.79 $\pm$ 6.73	-46.03 $\pm$ 7.48
Sagittal Forefoot-to-Hindfoot ROM	13.80 $\pm$ 3.10	14.93 $\pm$ 8.92	15.35 $\pm$ 3.68
Minimum Inversion	-10.23 $\pm$ 7.73	-11.29 $\pm$ 2.74	-9.39 $\pm$ 5.73
Peak Inversion	-16.88 $\pm$ 6.76	-19.19 $\pm$ 2.21	-17.43 $\pm$ 7.19
Frontal Forefoot-to-Hindfoot ROM	6.66 $\pm$ 1.74	7.90 $\pm$ 2.16	8.04 $\pm$ 2.54
Peak External Rotation	1.38 $\pm$ 6.56	0.03 $\pm$ 7.53	-0.77 $\pm$ 6.99
Peak Internal Rotation	-4.43 $\pm$ 7.54	-7.85 $\pm$ 6.86	-6.59 $\pm$ 6.48
Transverse Forefoot-to-Hindfoot ROM	5.81 $\pm$ 2.07	7.88 $\pm$ 3.33	5.82 $\pm$ 1.74

### 5.3.7 Ground Reaction Forces

The vertical GRF profiles for the three patient cohorts are presented in Figure 86, with each following a typical loading pattern of the stance phase during overground level walking. The vertical GRF profile for the BOX® ankle cohort demonstrated reduced force generation up to GRF1<sub>max</sub> compared to the other patient cohorts (Figure 86). However, there was no substantial differences between the patient cohorts for mean peak vertical GRF from early to mid-stance (GRF1<sub>max</sub>) and from midstance to terminal stance (GRF2<sub>max</sub>) (Table 25).

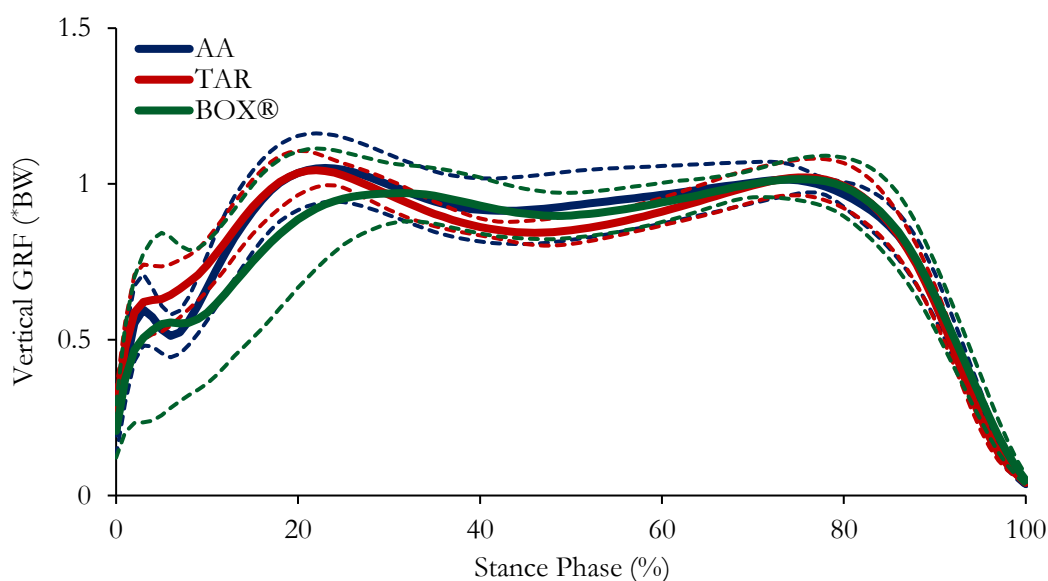


Figure 86. Mean ( $\pm$  95% CL) vertical GRF during the stance phase, in patients with AA (blue), TAR (red) and BOX® ankle (green).

Table 25. Mean ( $\pm$  95% CL) peak vertical ground reaction force for the three patient cohorts.

Vertical GRF (BW)	AA	TAR	BOX®
GRF1 <sub>max</sub>	1.07 $\pm$ 0.01	1.08 $\pm$ 0.01	1.09 $\pm$ 0.04
GRF2 <sub>max</sub>	1.11 $\pm$ 0.07	1.07 $\pm$ 0.03	1.05 $\pm$ 0.04

### 5.3.8 Joint Moments

#### 5.3.8.1 Hip Moments

Sagittal hip moment demonstrated comparable waveform patterns throughout stance for all three patient cohorts (Figure 87A). The BOX® ankle cohort appeared to show reduced mean peak hip flexion moment during late stance (Table 26), however the large variability within each patient cohort likely meant that there was no substantial difference in peak flexion moment between them.

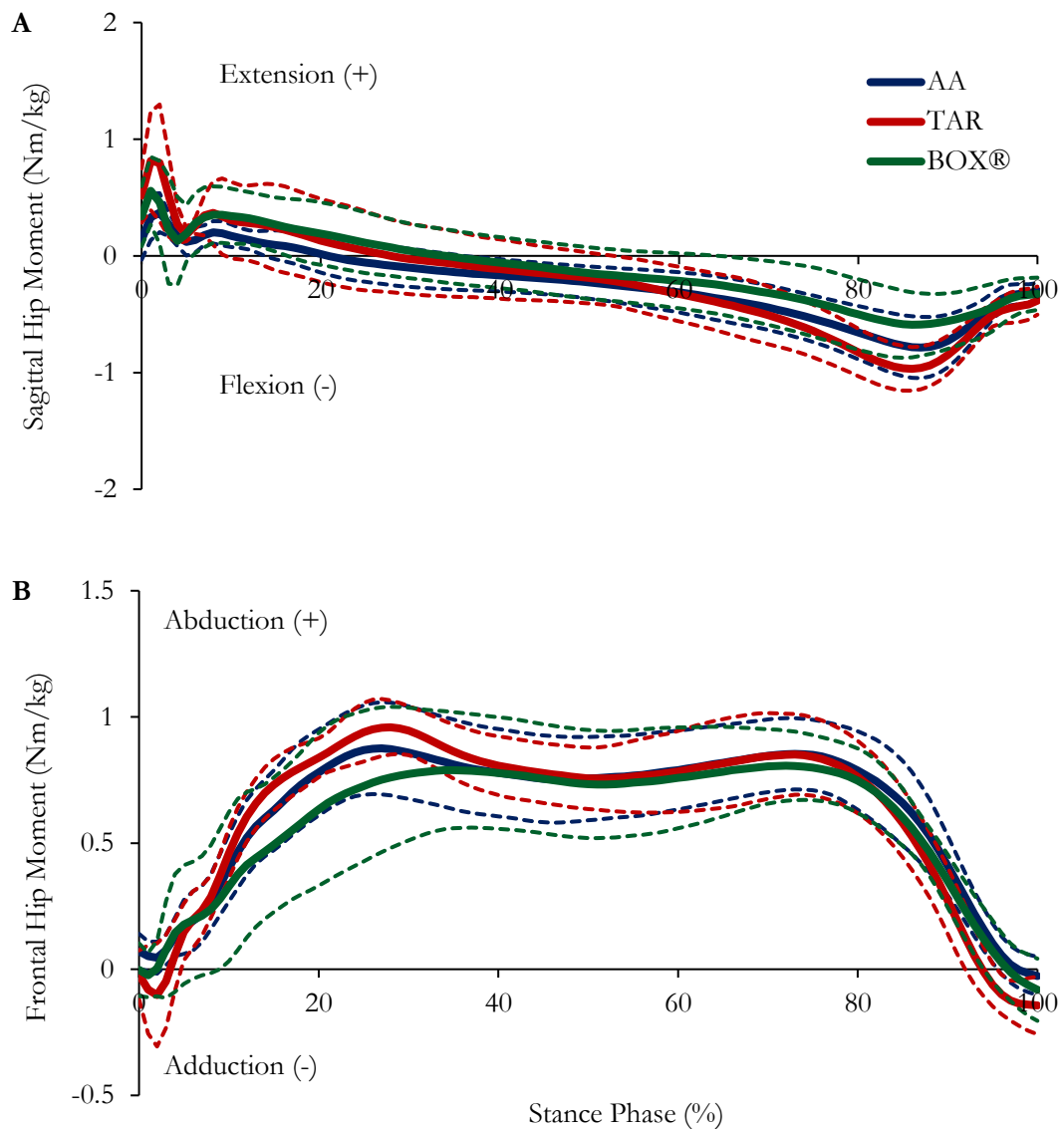


Figure 87. Mean ( $\pm$  95% CL) sagittal (A) and frontal (B) hip internal moments during the stance phase, in patients with AA (blue), TAR (red) and BOX® ankle (green).

The BOX® ankle cohort also produced a lower abduction moment at the beginning of the stance phase compared to both other treatment options (Figure 87B). Small differences were found between mean peak abduction values for the three patient cohorts (Table 26). Similar to most of the kinematic parameters measured, the BOX® ankle cohort was associated with the most variance in hip moment within the patient group (Table 26).

### 5.3.8.2 Knee Moments

Figure 88 presents the mean ( $\pm$  95% CL) knee moments in the sagittal and frontal planes during the stance phase for each patient cohort. The BOX® ankle cohort produced a lower mean peak knee extension moment ( $0.55 \pm 0.12$  Nm/kg) compared to the AA ( $0.82 \pm 0.18$  Nm/kg) and mixed TAR ( $0.68 \pm 0.15$  Nm/kg) patient cohorts (Table 26).

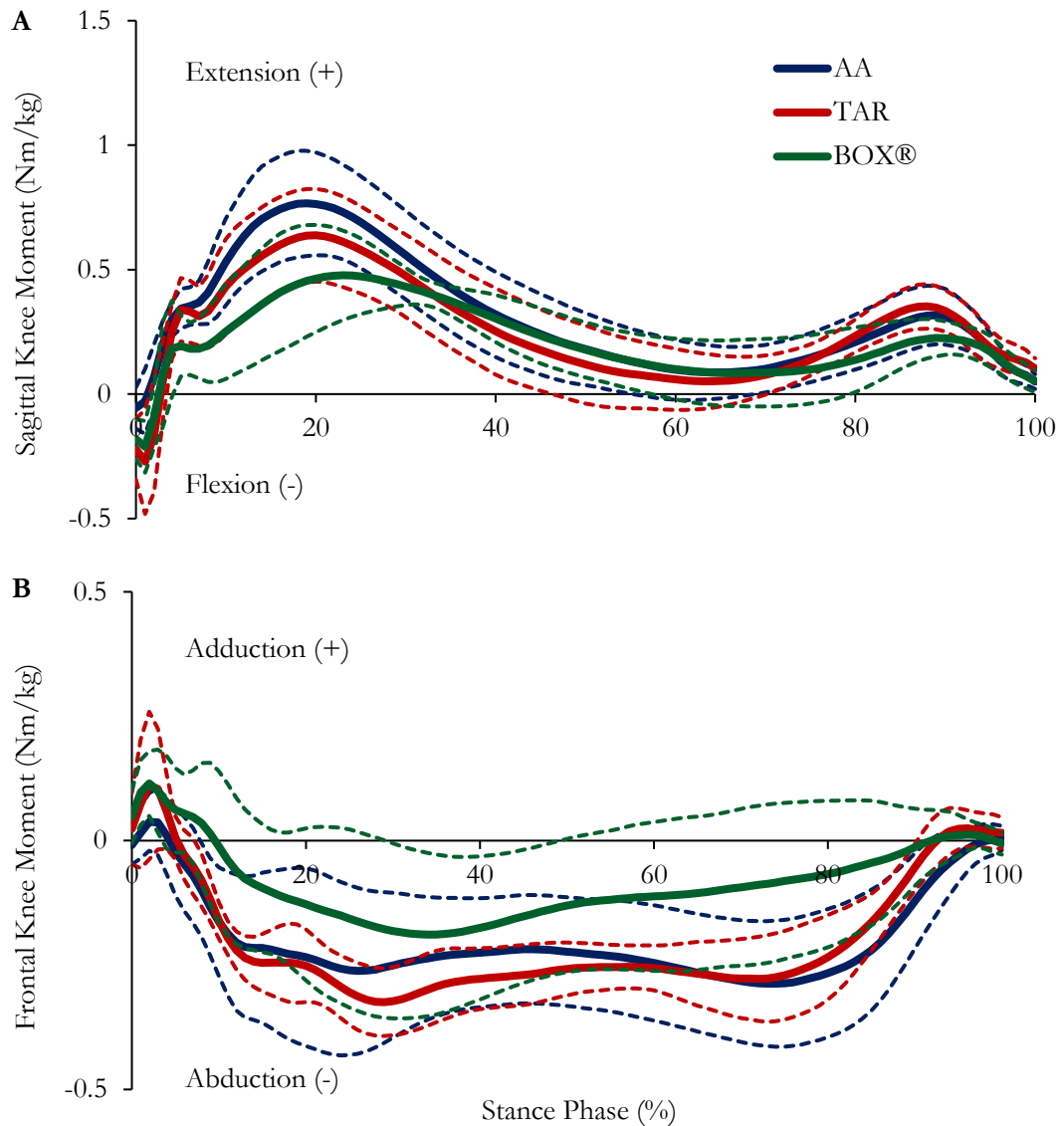


Figure 88. Mean ( $\pm$  95% CL) sagittal (A) and frontal (B) knee internal moments during the stance phase, in patients with AA (blue), TAR (red) and BOX® ankle (green).

In the frontal plane of motion, knee internal abduction moment tended to be lower in the BOX® ankle cohort compared to the other patient cohorts throughout the stance phase (Figure 88B). However, mean peak abduction moment was relatively comparable, likely due to the high variability ( $\pm$  95% CL) within each patient cohort (Table 26).

### 5.3.8.3 Ankle Moments

Figure 89 displays the mean ( $\pm$  95% CL) sagittal and frontal plane ankle moments during the stance phase for overground walking. All three patient cohorts followed a similar waveform for sagittal plane ankle moment (Figure 89A). The mixed TAR cohort possessed substantially higher mean peak internal plantarflexion moment ( $1.36 \pm 0.17$  Nm/kg) compared with the AA ( $1.15 \pm 0.13$  Nm/kg) and BOX® ankle patients ( $1.13 \pm 0.12$  Nm/kg) (Table 26).

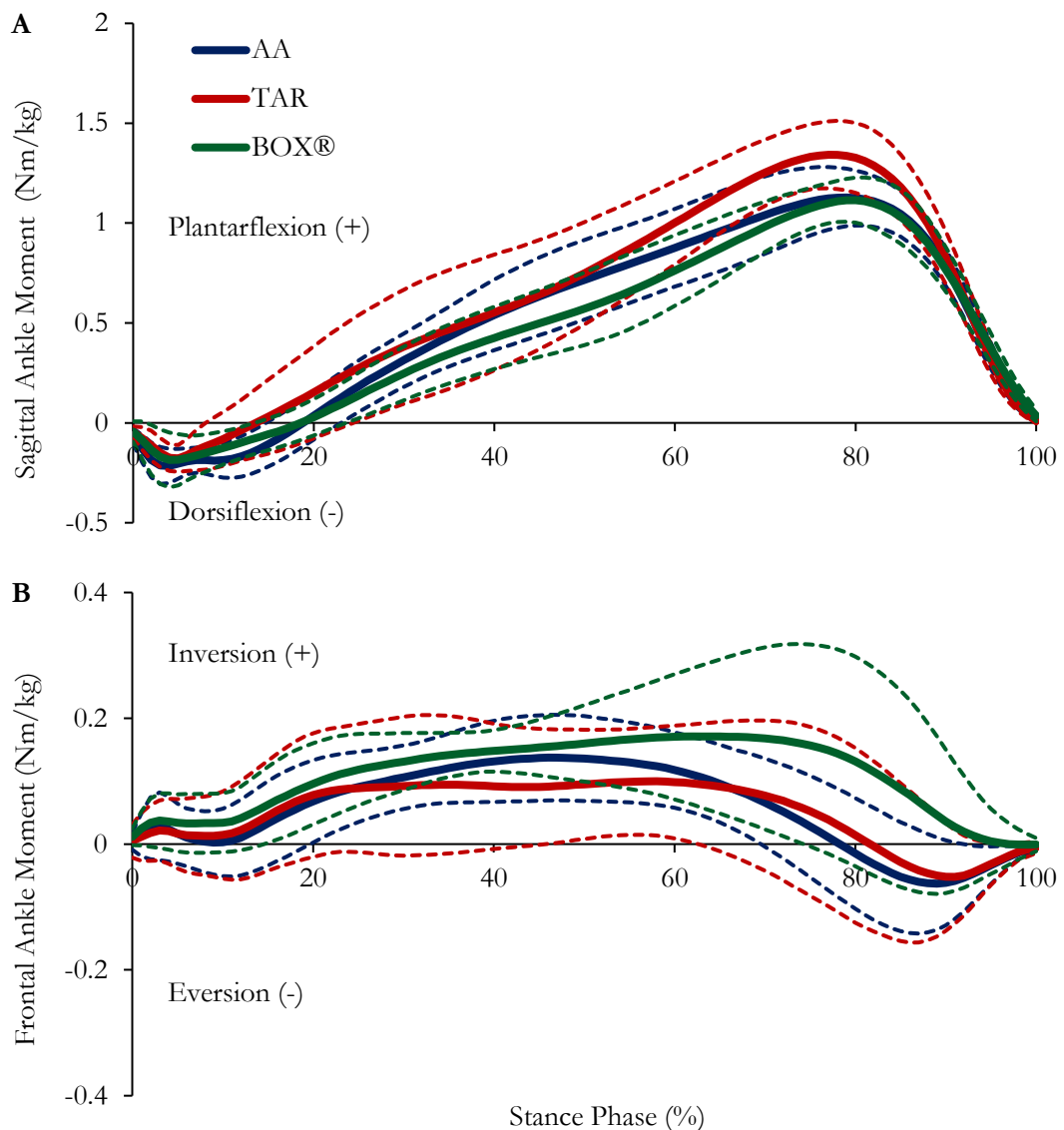


Figure 89. Mean ( $\pm$  95% CL) sagittal (A) and frontal (B) ankle internal moments during the stance phase, in patients with AA (blue), TAR (red) and BOX® ankle (green).

The BOX® ankle patients were associated with higher inversion moment throughout the majority of the stance phase (Figure 89B), which resulted in a slightly higher mean peak inversion moment ( $0.22 \pm 0.10$  Nm/kg) compared to AA ( $0.16 \pm 0.06$  Nm/kg) and mixed TAR ( $0.16 \pm 0.10$  Nm/kg) patient cohorts (Table 26). That being said, the relatively high variability within each patient cohort meant that peak inversion moment values were not substantially different.

Table 26. Mean ( $\pm$  95% CL) peak internal joint moments in the sagittal and frontal plane for the three patient cohorts.

<b>Peak Joint Moments (Nm/kg)</b>	<b>AA</b>	<b>TAR</b>	<b>BOX®</b>
Hip Flexion	$-0.81 \pm 0.25$	$-0.98 \pm 0.18$	$-0.64 \pm 0.21$
Hip Abduction	$0.99 \pm 0.14$	$1.00 \pm 0.11$	$0.91 \pm 0.21$
Knee Extension	$0.82 \pm 0.18$	$0.68 \pm 0.15$	$0.55 \pm 0.12$
Knee Abduction	$-0.36 \pm 0.14$	$-0.37 \pm 0.04$	$-0.23 \pm 0.16$
Ankle Plantarflexion	$1.15 \pm 0.13$	$1.36 \pm 0.17$	$1.13 \pm 0.12$
Ankle Inversion	$0.16 \pm 0.06$	$0.16 \pm 0.10$	$0.22 \pm 0.10$

### 5.3.9 Joint Power

The generated sagittal plane power of the hip, knee and ankle during the stance phase are shown in Figure 90, with the mean peak generated power for each joint presented in Table 27. The sagittal plane waveform for hip moment demonstrated that the mixed TAR cohort ( $1.33 \pm 0.34$  W/kg) exhibited substantially higher generated power compared to the AA ( $0.75 \pm 0.23$  W/kg) and BOX® ankle ( $0.87 \pm 0.42$  W/kg) patient cohorts (Table 27). However, the large variability within the BOX® ankle patient group meant that it may not be as different, as presented in Figure 90A.

All three patient cohorts exhibited similar waveforms for knee joint power throughout the stance phase of the overground walking trials (Figure 90B). This finding resulted in comparable mean peak knee generated power in the sagittal plane between the three patient cohorts (Table 27). There was however, substantial differences in sagittal ankle joint power waveforms, particularly at peak generation (Figure 90C). Mean peak generated ankle power was greater in the mixed TAR cohort ( $2.59 \pm 1.21$  W/kg) than the AA ( $1.28 \pm 0.42$  W/kg) and BOX® ankle ( $1.37 \pm 0.63$  W/kg) patient cohorts (Table 27).

Table 27. Mean ( $\pm$  95% CL) peak joint generated power for the three patient cohorts.

<b>Peak Generated Power (W/kg)</b>	<b>AA</b>	<b>TAR</b>	<b>BOX®</b>
Hip	$0.75 \pm 0.23$	$1.33 \pm 0.34$	$0.87 \pm 0.42$
Knee	$0.60 \pm 0.17$	$0.70 \pm 0.41$	$0.46 \pm 0.47$
Ankle	$1.28 \pm 0.42$	$2.59 \pm 1.21$	$1.37 \pm 0.63$

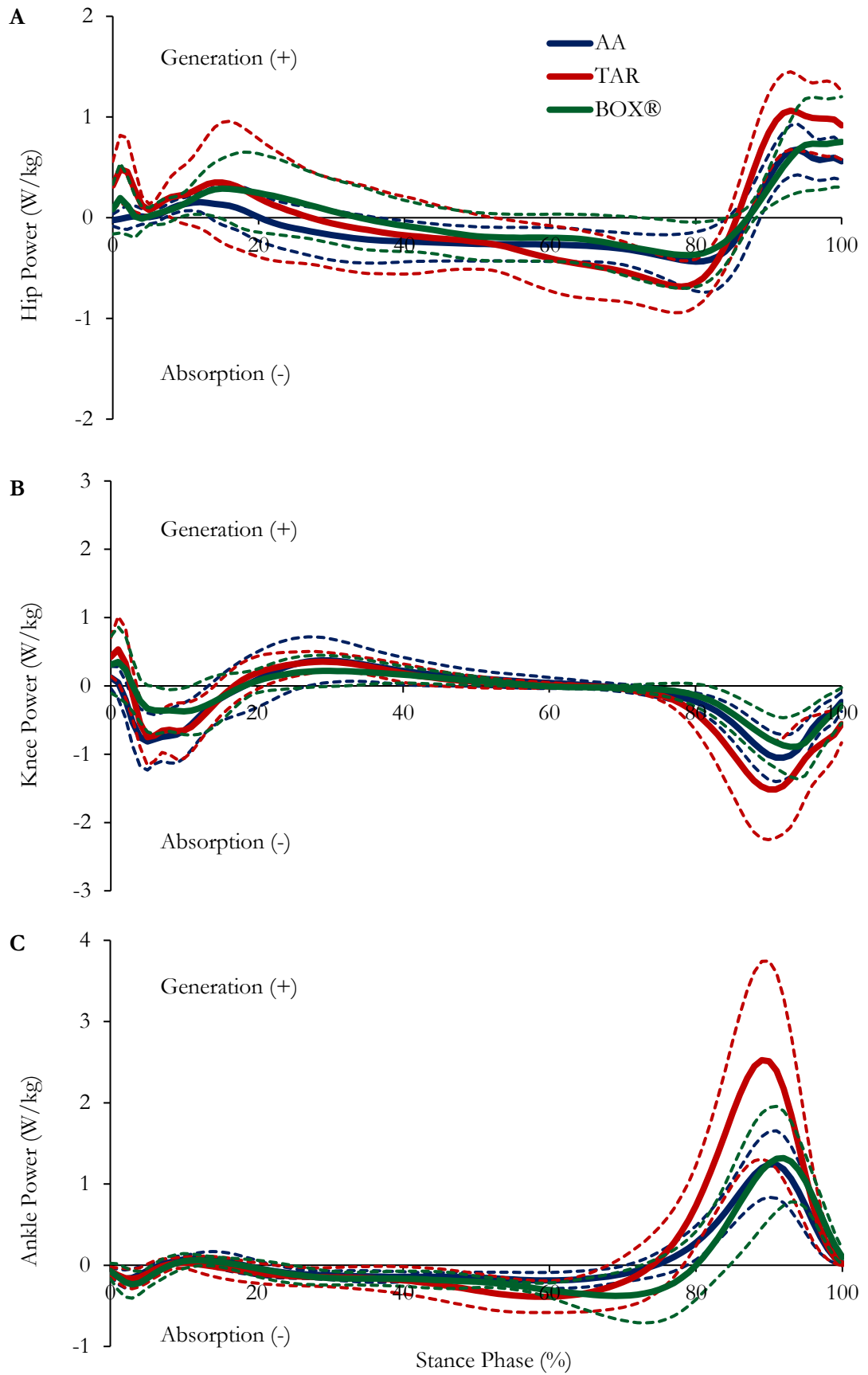


Figure 90. Mean ( $\pm$  95% CL) sagittal hip (A), knee (B) and ankle (C) joint power during the stance phase, in patients with AA (blue), TAR (red) and BOX® ankle (green).

## 5.4 Discussion

Both AA and TAR surgical procedures are used to treat end-stage ankle OA, which have both been found to improve pain-free function, clinical outcomes and QoL (Lawton et al., 2020; Kohring et al., 2020; Goldberg et al., 2022). AA remains the gold standard surgical strategy in patients with end-stage ankle OA (Goldberg et al., 2022). However, it has been postulated that the fusion process may lead to altered mechanical load and maladaptive motion at the foot joints distal to the AJC (Tenenbaum et al., 2017), which results in adjacent joint degeneration, functional impairments and the requirement for future surgical interventions (Pinsker et al., 2016). This has amplified the need for motion conserving alternatives such as TAR, which have the potential to maintain pre-operative ankle ROM and protect the distal joints of the foot (Deleu et al., 2022).

There have been several studies which have investigated the biomechanical effects of both surgical techniques during overground walking, with confounding gait outcomes (Piriou et al., 2008; Hahn et al., 2012; Singer et al., 2013; Flavin et al., 2013; Segal et al., 2018; Stone et al., 2021). Each of the above studies mentioned, were limited by relatively short follow-up period's post-surgery (maximum three years) and the use of a SFM or basic MFM, which fail to measure the potential compensatory mechanisms in the distally located joints of the foot. Only two studies in the published literature have exploited a MFM, which directly compared the effects of AA and TAR on gait mechanics, with both studies demonstrating improved motion across the foot segments in TAR patients compared to AA (Seo et al., 2017; Sanders et al., 2021).

However, both the gait based MFM comparison studies failed to report the effect of the two surgical interventions on lower limb joint kinetics and kinematics, at an intermediate follow-up duration post-surgery (Seo et al., 2017; Sanders et al., 2021). Therefore, the current post-operative exploratory study was designed to compare the gait mechanics and functional reported outcomes of differing TAR models and AA with respect to the lower limbs and distal foot segments at an intermediate post-operative follow-up, during overground walking. The combined kinematic and kinetic evaluation allowed for an enhanced functional understanding of the compensatory adjustments of the distal foot and proximal lower limb joints following AA and TAR surgeries.

The main findings from the study suggested relatively comparable kinematic and kinetic gait parameters between AA and TAR patient cohorts at the intermediate follow-up post-surgery. There were however, a small number of biomechanical differences observed between the surgical interventions: (1) increased hindfoot motion in the both implant cohorts when compared to AA; (2) greater peak sagittal plane angles in the distal foot segments in AA patients; and (3) higher hip and ankle generated power in the mixed TAR patient cohort. From a biomechanical perspective, these gait differences suggested that TAR may be a more effective treatment option for end-stage ankle OA at an intermediate follow-up period post-surgery.

### 5.4.1 Multi-segment Foot Model Kinematics

Kinematic analysis of each foot segment was measured with an established and validated skin marker based MFM, commonly referred to as IOR (Leardini et al., 2007; Portinaro et al., 2014; Caravaggi et al., 2015). The IOR foot model allowed for tracking of the hindfoot, midfoot and forefoot segments, which was used to estimate the individual motions at the AJC (hindfoot), Chopart (midfoot) and Lisfranc (forefoot) joints (Uselli et al., 2021). The MFM was also used to measure the motion of the forefoot with respect to the hindfoot. This method enabled the study to determine which joints of the foot-ankle system provided the functional ROM necessary to maintain gait post-surgery.

There were some potential differences in gait mechanics at the hindfoot segment between the three patient cohorts. The BOX® ankle patients tended to have an increased mean peak dorsiflexion compared to both other treatment options, but produced a lower peak plantarflexion angle, similar to which was measured in the AA cohort during walking. This finding was likely a result of the patients being in a more dorsiflexed position during initial contact compared to the other two patient cohorts. It should also be noted that the BOX® ankle patient cohort was associated with higher variability (a wider  $\pm$  95% CL) at the peak sagittal parameters and throughout the ROM during overground walking. This finding may suggest that patients implanted with BOX® ankle present have variable hindfoot motion or that the mechanical outcome is less predictable compared to other implant designs or AA surgery. However, a gait based study with a much larger patient population is required to further substantiate this finding. The peak plantarflexion angle at the hindfoot segment was shown to have large variance in both TAR groups, suggesting that the difference in this parameter was likely to be negligible. In spite of the associated variance in hindfoot kinematics, the study ultimately supported the notion that recovery of patient biomechanics usually occurs through ankle dorsiflexion in TAR patients, while the comparable plantarflexion between patient groups implied that compensation of plantarflexion occurred in the distal foot segments.

The relatively high intra-subject variability at the hindfoot segment within each patient cohort can also be seen in other kinetic and kinematic measurements of the foot segments and proximally located joints of the foot. This largely comes down to the small sample sizes in each patient cohort. However, there are also some inherent limitations which are associated with traditional motion capture techniques, such as STA and segment definition. This is particularly apparent when analysing small complex anatomical segment biomechanics. A more detailed review of the technical limitations associated with the current study, which should be considered when considering the biomechanical differences between surgical interventions, can be found in Chapter 6 (Section 6.2.2).

The main kinematic difference found at the hindfoot segment was the greater sagittal ROM in both TAR groups, when compared to the AA patient cohort. The sagittal ROM of the hindfoot

segment in both the mixed TAR ( $15.08 \pm 5.73^\circ$ ) and BOX® ankle ( $13.56 \pm 4.10^\circ$ ) compared well to the ROM ( $15.10 \pm 3.30^\circ$ ) measured in an earlier gait study of seventeen MB devices at one year post-surgery (Seo et al., 2017). Other studies using MFM to measure hindfoot motion in FB devices demonstrated improved hindfoot motion, particularly during the loading response phase of stance when compared to pre-operative values (Fritz et al., 2021; Deleu et al., 2022). The loading response is characterised by the transfer of BW onto the forward limb, which uses the calcaneus as a ‘rocker mechanism’ during motion (Deleu et al., 2022). This suggests that the increased sagittal ROM in both implant cohorts may be due to patients no longer being fearful of landing properly at their ankle joint during overground walking. Although pre-intervention mechanics are affected by the arthritic condition, which likely caused the significant differences between pre-and post-surgery hindfoot kinematics, as noted in the previous studies. The MFM literature has also shown that hindfoot ROM is often not fully restored after surgery and is significantly lower than in healthy control participants, particularly during midstance and swing phase of gait (Fritz et al., 2021; Deleu et al., 2022).

The primary cause of the reduced hindfoot motion in the AA patients when compared to the implant groups, is that the tibiotalar joint is fused, resulting in a significantly stiffer joint during overground walking. Despite the reduced sagittal hindfoot ROM in the AA patient cohort, the kinematic waveform was comparable to the most recent MFM based gait study measuring AA function at one-year post-surgery (Eerdeken et al., 2020a). Using the same MFM, the authors demonstrated no significant differences between pre- and post-operative measurement points in the absolute ROM of any of the foot segments, particularly at the hindfoot segment (Eerdeken et al., 2020a). It is therefore reasonable to suggest that the main purpose of AA surgery is to relieve pain at the AJC without compromising pre-operative gait mechanics. It is worth noting that the IOR foot model used to measure the kinematic differences of the foot segments was unable to differentiate between the motions of the tibiotalar and subtalar joints at the AJC. An *in vivo* based study measuring hindfoot motion determined that the subtalar joint contributes up to  $8.8^\circ$  of sagittal plane ROM during walking (Lundgren et al., 2008). Therefore, the measured motion at the hindfoot segment may potentially be solely attributed to one of these joints.

In the frontal plane, hindfoot segment ROM was found to be greater in the BOX® ankle patients ( $8.61 \pm 1.97^\circ$ ) compared to the AA ( $5.15 \pm 1.61^\circ$ ) patients. This finding was likely due to the design of the BOX® ankle, which is designed to possess ligament-compatible shapes of the articulating surfaces and allows for complete congruence between the bearing surfaces during ROM (Giannini et al., 2011). The tibial component has a spherical convex shape, while the talar component possesses an upper anticlasic shape (i.e. convex in the sagittal and concave in the frontal planes) and a longer radius of curvature in the sagittal plane than the natural talus. This promotes increased ROM at the replaced joint (Leardini et al., 1999; Leardini and O’Connor, 2002). More importantly, the meniscal insert matches the shape of the metallic articulating

surfaces, allowing the ankle joint to maintain significant contact area and full congruity during pronation (Ingrosso et al., 2009). This in theory, allows the ligaments to remain isometric and rotate about their origins and insertion points without stretching or slacking.

One of the only studies using MFM to compare the gait mechanics of AA and TAR demonstrated no statistical significant differences in hindfoot frontal plane motion (Seo et al., 2017). This finding was consistent with the relatively comparable frontal plane hindfoot ROM found between the mixed TAR and AA cohorts. This is likely the case due to the similar MB design used by Seo et al. (2017) (Hintegra; Integra LifeSciences, Plainsboro, NJ). Another recent study concerning a newly designed FB implant (Cadence; Smith & Nephew, London, UK) also found no difference in frontal plane hindfoot kinematics between TAR and pre-operative values (Deleu et al., 2022). This was likely due to each implant possessing a non-anatomical flat tibial component, coupled with a flat surface on the superior insert surface of the UHMWPE insert. This limits the natural eversion/inversion motion, compared to the more anatomical and congruent bearing surface between the UHMWPE insert and tibial component of the BOX® ankle.

At the midfoot segment, both implant patient cohorts were associated with slightly greater sagittal and frontal plane ROM compared to AA patients. This finding, coupled with the substantially greater hindfoot motion, highlights that at an intermediate follow-up period, TAR patients tended to have improved foot and ankle function, compared to AA patients. Deleu et al. (2022) also established that patients implanted with a FB implant produced increased motion at the midfoot during loading response, at one-year post-surgery compared to pre-operative measurements. Improved midfoot function is a good indicator of reduced joint pain as the midfoot joints control the longitudinal arch deformation during loading (Deleu et al., 2020b). However, the extent to which the changes in kinematics of the midfoot, alongside other segments of the foot are attributable to pain reduction and contribute to a functioning ankle during locomotion, cannot be determined from this study.

Greater peak dorsiflexion angle was also found in the AA patient cohort compared to both TAR groups. This corresponds with a number of earlier studies, which found increased midfoot dorsiflexion during the second rocker phase of gait cycle in AA patients (Mazur et al., 1979; Wu et al., 2000; Sealey et al., 2009). In the radiographic assessment of 48 patients following AA at one-year post-surgery, Sealey et al. (2009) found that the increased dorsiflexion at the midfoot appeared to cause impingement at the posterior facet of the subtalar joint, which may be the reason for the increased incidence of subtalar OA following AA. However, the large variability between patient groups in the current study meant that the peak dorsiflexion angle was likely not significant and caution must be considered when extrapolating this result to the larger patient populations.

With regard to the forefoot segment, peak plantarflexion was substantially larger in the AA patient cohort compared to both TAR patient groups. Whereas, minimum dorsiflexion appeared to be greater, although not substantially higher, in both TAR groups. This finding was also supported when modelling the forefoot-to-hindfoot segment (representing the windlass mechanism), with a trend towards the AA patients producing greater peak plantarflexion angle, while both TAR patient cohorts produced slightly greater dorsiflexion. The current study displayed similar results to another comparator gait study by Seo et al. (2017), which indicated dorsiflexion being significantly higher in TAR patients at the forefoot segment, while plantarflexion was higher for the AA patients. In addition, Pedowitz et al. (2016) demonstrated increased sagittal motion of the distal joints of the foot after AA surgery compared to TAR. Although the study reported the increased motion of the adjacent joints when the ankle was fixed in a static position during a radiographic assessment, which does not demonstrate this effect during dynamic movement.

This hypermobility at the distally located foot segments in the AA cohort, particularly at the forefoot, was likely a result of the loss of motion at the hindfoot. This increased function may come at the cost of altered internal loading at the distally located foot joints (Beyaert et al., 2004; Barton et al., 2011). Greater peak pressure has been found in the subtalar, talonavicular, and calcaneocuboid joints following AA surgery (Wayne et al., 1997; Jung et al., 2007; Suckel et al., 2007), which is thought to cause significant degenerative changes, with increased incidence of OA at the adjacent foot joints (Coester et al., 2001; Ling et al., 2015). The hypermobility within the forefoot segment may lie within the passive supportive entities, such as the ligaments, leading to overuse and gradually contributing to further foot deformities. However, other studies have identified the presence of OA in the adjacent foot joints before AA surgery was performed (Winson et al., 2005; Sheridan et al., 2006). Therefore, a causal relationship has not definitively been confirmed in the published literature (Bruening et al., 2016).

In a computational model designed to understand the biomechanical effects of AA, the talonavicular joint was found to undertake a peak contact pressure of up to 2.14 MPa during the second peak instant post-surgery (Wang et al., 2015). This increased contact stress overtime at the articular surfaces is believed to be a predominant factor of OA (Buckwalter and Martin, 2006). The *in silico* models also demonstrated increased von Mises stresses at the second (52 MPa) and third (34 MPa) metatarsal bones at the second-peak instant in AA compared to healthy controls (Wang et al., 2015). The metatarsals are relative thin and have longer geometries than other bones of the foot, which aid in load transfer, making them more susceptible to bone fractures and is one of the most common complaints following AA surgery (Weatherall et al., 2013). As von Mises stress is considered a predictor of bony stress fracture (Keyak and Rossi, 2000), it can be postulated that AA patients may be more susceptible to stress fractures at the forefoot bones. The current study was limited to kinematic measurements across the foot segments, but the

hypermobility alongside potentially increased stresses at the forefoot joints, means that surgeons should be aware of these risks when operating on end-stage ankle OA patients.

The hypermobility may cause the AJC to less effectively lock the Chopart joint during the heel rise phase, reducing the required ROM at the hindfoot (Flavin et al., 2013). This finding is contradictory to the most recent post-operative gait study of AA (Eerdeken et al., 2020a), which found no significant differences in kinematics at the midfoot or forefoot segments when compared to pre-operative data. The study, however, was limited to a short follow-up period of one-year post-surgery, suggesting that AA patients suffer from hypo-mobility at distal foot joints due to pre-operative disuse. The current study indicates that over a longer follow-up period, the AA patients began to compensate at the distally located foot joints, causing greater peak kinematic values and increased likelihood of subsequent OA. However, this effect is small when compared to the associated variability in the kinematics measured within the small sample sizes for each patient cohort. It also remains unclear if the kinematic differences of the foot segments were related to the pre-operative condition and compensatory strategies arising from ankle OA, anatomical variations, alterations in ligamentous tension, tibiotalar alignment or arthrogenic muscle inhibition (von Tschärner and Valderrabano, 2010; Deleu et al., 2022).

The use of a MFM has indicated that TAR has the potential to improve ROM in most of the foot segments measured, whilst greater peak dorsiflexion angle in the midfoot segment and plantarflexion angle in the forefoot segment in the AA patients, may act as a compensatory mechanism to maintain comparable spatiotemporal (Section 5.4.6) and PROMs (Section 5.4.7) parameters to the TAR cohorts. However, the small sample size for each of the patient cohorts and subsequent large variability in kinematic data makes it difficult to be able to fully confirm these findings. A much larger study, as described in Section 6.1.2, would need to be performed to determine if the results from the current study represent the true patient population for each treatment option. The current study also failed to collect pre-operative data, due to the time constraints of the study duration, with the study focused on obtaining data at an intermediate follow-up. This meant that, even with the trend to support improved ROM in TAR patients compared to AA, the study is unable to determine which treatment option had the greatest improvement post-surgery. The TAR patients may already have possessed increased ROM pre-surgery, or improvement substantially at a short-term follow-up. This makes it difficult to determine from the current study if TAR did produce improved ROM compared to AA patients. Even with the potentially improved ROM, the early failure modes (Section 6.1.1) associated with TAR, surgeons are still reluctant to select this treatment option and prefer the 'safer option' in AA.

Future studies could benefit from the use of biplane fluoroscopic analysis combined with motion capture studies, to analyse further the hypermobility occurring at the distal joints of the foot following both surgical interventions. This measurement technique better represents individual

bone motion through the registration of volumetric computed tomography (CT) data and images obtained *in vivo* by two fluoroscopes (Lenz et al., 2020). A previous dual fluoroscopic imaging study demonstrated increased plantarflexion motion at the subtalar joint during overground walking in AA patients (Lenz et al., 2020), which could explain the increased rate of subsequent subtalar OA that occurs after AA surgery (Fuchs et al., 2003). The same authors repeated a similar study in TAR patients and demonstrated no significant kinematic compensation at the subtalar joint, which corresponds with the results from the current study and the relatively low frequency of future OA following TAR procedures (Lenz et al., 2022).

#### **5.4.2 Single-segment Foot Model Kinematics**

The SFM kinematic data suggested that the sagittal plane ROM tended to be higher in both the mixed TAR ( $20.11 \pm 8.83^\circ$ ) and BOX® ankle ( $17.90 \pm 3.67^\circ$ ) patient cohorts, when compared to the AA ( $13.10 \pm 1.96^\circ$ ) patient group. Despite the differences in experimental set-up (e.g. laboratories) and implant design or AA technique, the sagittal ROM was similar to previous gait based studies (Piriou et al., 2008; Hahn et al., 2012; Singer et al., 2013; Flavin et al., 2013; Segal et al., 2018). In each of the previous studies, post-operative sagittal ROM ranged between  $13.5^\circ$  to  $18.1^\circ$  in TAR patients and  $10.0^\circ$  to  $16.2^\circ$  in AA patients. Most of the studies above reported greater sagittal ROM in TAR compared to AA patients (Piriou et al., 2008; Hahn et al., 2012; Flavin et al., 2013). However, there were differences in regard to where the increased ROM was accounted for, with some studies reporting significantly higher dorsiflexion in their TAR cohorts compared to AA (Singer et al., 2013; Flavin et al., 2013), and another reporting significantly greater plantarflexion motion in TAR patients (Hahn et al., 2012).

There seemed to be an apparent difference in peak adduction and abduction angles in the BOX® ankle cohort compared to both other treatment options, with the ankle remaining in an abducted position. A similar trend was also observed in the MFM for the different foot segments, but to a much lesser extent (Section 5.4.1). However, the overall ROM across the different foot segments and in the SFM remained comparable to the AA and mixed TAR cohort. This suggested that there was an apparent offset in the data. As proven by the pilot study (Appendix G), it was possible to get repeatable data across the same gait laboratories used in the current study. The same marker model and testing methodology was also used between sites.

It is likely that the increased variability in the frontal and transverse planes of the BOX® ankle cohort may be attributed to differences in marker placement between the sites. The patients are of a much larger BMI than the participants used in the pilot study, making it difficult to accurately place the markers at the anatomical landmarks. With such a small sample, the misplacement of markers of one patient will have a substantial influence on calculated joint kinematics, particularly in planes of smaller motion (transverse plane). However, this would have been the same at the CAH site used to collect data for the AA and mixed TAR cohorts. There were differences in the optoelectronic marker system, calibration procedure and laboratory set-up (e.g. number of

cameras used) between the two research sites which have both been shown to influence the repeatability of gait data (Di Marco et al., 2016; Kaufman et al., 2016). Again, the pilot study seemed to suggest that these differences did not affect the repeatability of the data in the same individuals between the two research sites. It is clear from this finding that a much larger patient cohort is required to fully confirm if this difference in peak values are true in the BOX® ankle cohort or it is due to differences in the set-up and systems used between research sites. The future study should be performed at the same testing site to remove the confounding factors associated with collecting data at different laboratories.

Each of the previous gait studies using SFM did not report motion in the frontal or transverse planes due to the complex nature of movement at the AJC and the high variability found between individuals. This was particularly apparent in the transverse plane in the current study, with all three cohorts presenting high variability ( $<5^\circ$ ). The transverse plane is associated with a reduced amount of motion compared to the sagittal and frontal plane, which was evidenced with this study. Therefore, with the small sample size and variability, one patient's dataset could have influenced the calculated peak angles, which may have also accounted for the difference in peak values in the transverse plane of the BOX® ankle group.

In addition to the relatively small sample sizes and corresponding large variations within the patient populations in the current and previous gait based studies, the differences in ankle kinematic results may also be attributed to the marker location on the foot. In the study by Hahn et al. (2012), only one marker was placed on the distal second metatarsal joint dorsum, while Flavin et al. (2013) and Singer et al. (2013) utilised basic MFM which positioned additional markers at the calcaneus and forefoot. However, neither study focused on the midfoot or forefoot segment kinematics intervention, so the contribution of these distal segments remained unknown and were therefore treated as a single-segment.

The major concern with modelling the foot as a single-segment is its inability to measure the motion occurring intrinsically in the distally located foot joints (Zelik and Honert, 2018). The results from the current study showed that the choice of foot model had a significant effect on ROM, with the SFM overestimating the sagittal and frontal plane ROM when compared to the MFM hindfoot segment. Conversely, transverse ROM was found to be similar between the two foot modelling techniques. A similar clinical difference was established by Deleu et al. (2021b), who demonstrated that SFM overestimated sagittal plane motion. This could lead to an overestimation of ankle joint kinematics, resulting in the amplification of ankle joint power (Zelik and Honert, 2018). The findings in the current study emphasise the clinical need of using MFM when assessing the outcome of surgical interventions, particularly when monitoring the potential compensatory mechanisms in the distally located foot joints.

### 5.4.3 Ankle Moment and Power

In addition to the kinematic differences, analysing the impact of kinetic parameters helped to interpret the ankle joint function. The mixed TAR cohort appeared to produce a slightly higher peak plantarflexion moment during stance when compared to the other patient cohorts. Increased plantarflexion moment is widely accepted as a good indicator of a patients' ability to propel their foot forward and the subsequent strength of the calf muscles (Ingrosso et al., 2009). This is also verified by the greater ROM associated at the hindfoot segment, along with slightly quicker walking speed. However, Seo et al. (2017) demonstrated that despite the improved motion at the hindfoot and forefoot segments, peak plantarflexion moment was comparable between AA and TAR patient groups. The current study also contradicts the work by Hahn et al. (2012), who found that AA patients exhibited increased plantarflexor moment (from  $0.71 \pm 0.22$  Nm/kg to  $0.80 \pm 0.19$  Nm/kg) at one-year post-surgery compared to pre-operative values, while TAR patients produced a reduced moment (from  $0.84 \pm 0.29$  Nm/kg to  $0.71 \pm 0.32$  Nm/kg). The authors suggested that the reason for the increased moment in the AA cohort was due to the talus being fixed to the tibia, with its moment being a combined effect of both ankle joint bones (Hahn et al., 2012). Without the associated pain in the ankle, the resulting increased ankle plantarflexor moment found in the AA group would likely not cause the patient discomfort, as it would have pre-surgery.

Ankle joint power was calculated by multiplying the internal joint moment by the joint angular velocity. Since the ankle joint velocity was relatively comparable between each patient cohort, the greater ankle joint moment in the mixed TAR patient cohort was likely the reason for the increased ankle power generated ( $2.59 \pm 1.21$  W/kg) when compared to both the BOX® ankle ( $1.37 \pm 0.62$  W/kg) and AA ( $1.28 \pm 0.42$  W/kg) patient groups. Whilst the BOX® ankle cohort appeared to have a lower ankle power than the mixed TAR cohort, the relatively large variance in both implant groups and in the kinematics parameters measured, meant that it was difficult to truly determine a difference.

There was a more apparent difference between the mixed TAR and AA patient cohorts. This finding was of great importance as the plantarflexor leg muscles (soleus and gastrocnemius) significantly influence the progression of the body forward during walking (Neptune et al., 2001). The greater power generated in the TAR cohort may be due to the conservation of the Achilles tendon, which provides the connection between the soleus and gastrocnemius muscles to the calcaneus and is functionally involved in plantarflexion motion (Maquirriain, 2011). The study by Seo et al. (2017) also demonstrated that TAR patients ( $1.16 \pm 0.47$  W/kg) produced significantly greater generated ankle power compared to an AA patient cohort ( $0.32 \pm 0.07$  W/kg). However, the study highlighted that neither surgical intervention was able to replicate ankle power found in healthy controls, with the AA and TAR patient groups attaining 10.3% and 37.4% of the control group ankle generated power, respectively. This apparent reduction in plantarflexor

power, was likely due to preoperative atrophy of the plantarflexion muscle complex in the arthritic patients (DiLiberto et al., 2021). It should be noted however that the control group in Seo et al. (2017) was not aged-matched, which likely influenced the significant differences between patient and control cohorts.

The current study was not designed to determine the degree to which the changes in muscle function, leading to the increased ankle power generation, are attributable to the improved biomechanical function. Therefore, further studies should assess the potential mechanisms of ankle power generation in both types of surgical intervention. This could be addressed through changing the implant design to improve hindfoot sagittal plane stability during late stance, to improve ankle power. Alternatively, the effect of long term consequences of ankle OA on ankle plantarflexor weakness could be investigated through focusing on post-operative rehabilitation protocols to improve the strength of the muscles surrounding the ankle joint.

The TAR patients in this study tended to generate greater rotational forces and power during level walking compared to AA patients. This may translate into an enhanced ability to perform a variety of ADL and subsequently improved QoL. Additional research is therefore required to assess differences in patients undergoing both surgical interventions when performing tasks that better mimic ADL at an intermediate period post-surgery. Recent efforts have also led to the development of 3D kinetic foot models, which have been used to quantify the biomechanical functioning of the different foot segments (Deschamps et al., 2012a; Eerdeken et al., 2019). This modelling technique has been used alongside the IOR foot model to determine the kinetic behaviour of the adjacent foot joints in AA patients (Eerdeken et al., 2020a). An inverse dynamic analysis program (Matlab; MathWorks, Natick, MA, USA) computed joint moments and power, using Newton–Euler equations of the distally located foot joints. The study demonstrated that the kinetic parameters of the distally located foot joints did not significantly differ at one-year post surgery, compared to pre-operative values (Eerdeken et al., 2020a). However, this technique is not without limitations in terms of its repeatability, the mathematical estimations made and the force measurement technology used, which has prevented its widespread adoption and use within clinical analysis.

#### **5.4.4 Proximal Joint Kinetics and Kinematics**

Another aim of the study was to determine the kinematic and kinetic changes after each surgical intervention at the proximally located joints. The results from this study identified an overall increase in hip power between the mixed TAR ( $1.33 \pm 0.34$  W/Kg) and AA ( $0.75 \pm 0.23$  W/Kg) patient groups. Whilst the BOX® ankle cohort also exhibited reduced peak hip power ( $0.87 \pm 0.42$  W/kg), the large variance in this cohort meant that it was difficult to determine if this patient cohort truly produced lower hip power compared to the mixed TAR cohort. This patient group did however, generate increased hip power compared to the AA patient group. The greater hip power suggested that the TAR patients were able to retain improved functioning of the

surrounding soft tissues of the hip, which was essential for maintaining smooth and efficient forward motion during walking (Queen et al., 2019). The measured knee moments and power were more comparable between the three patient cohorts.

This finding has also been associated with the re-distribution of propulsive power from the deficient ankle joint (Franz, 2016; Fickey et al., 2018). This distal to proximal redistribution of load and subsequent generated power at the hip joint, may result in further implications for both fall risk and implant loading, which are required for bone adaption and potential implant success (Kerrigan et al., 2000; Zerahm and Kofoed, 2004; So et al., 2021). However, the TAR patients in this study possessed higher ankle power, so were less likely to suffer from this, compared to AA patients. This study highlights the importance of continuing to study the effect of treatment of end-stage ankle OA on proximal joint kinetics in larger cohorts of patients at a longer follow-up period. This will help determine how both surgical interventions may affect the incidence and progression of hip and knee OA.

The current study demonstrated that surgical intervention did not have a substantial effect on hip or knee ROM. A similar finding was determined by Seo et al., (2017), who found no significant differences between AA and TAR patients at the proximal joints. The motion at the hip and knee joints are relatively greater than the motion at the hindfoot. Therefore, the effect of the ankle operation on the hip and knee kinematics was considered to be relatively small at this intermediate follow-up period. Conversely, other research has determined that hip ROM was larger in AA, whereas knee ROM was larger in TAR patients (Hahn et al., 2012). This finding corresponds with a more recent meta-analysis which suggested AA patients showed no post-operative change in knee ROM, but a pooled average increase of  $4.77^\circ$  in hip ROM (Deleu et al., 2020a). This suggests that patients suffering from end-stage ankle OA compensate more at the hip than at the knee for reduced ankle ROM (Segal et al., 2018).

One of the main differences at the proximal joints was that the BOX® ankle patients exhibited an apparent offset in the sagittal plane motion at the hip joint, which resulted in a greater peak hip flexion angle and reduced hip extension angle, when compared to the other patient groups. There was also an apparent difference in the transverse plane of motion, with the BOX® ankle patients producing increased peak internal rotation and reduced peak external rotation angle, when compared to the other treatment options. However, each of the reported mean values were associated with large variance, so caution must be dealt when trying to draw clinically meaningful differences at the proximal joints.

One of the reasons for the differences may have been due to the differences in gender between the patient cohorts. The BOX® ankle cohort had a greater number (50%) of female patients in the cohort compared to the other patient cohorts. Women have been shown to exhibit greater active hip internal rotation than men (Simoneau et al., 1998), which may explain, in part, the

larger Q-angle (Woodland and Francis, 1992). However, the offset was unlikely due to patient related factors, but potential systemic error associated with the calibration process during the static trials (Benedetti et al., 2013; Di Marco et al., 2016), alongside the small sample size within each patient cohort. It is worth considering that the pilot study, which contained a greater number of participants ( $n = 11$ ), did not find statistical significant differences in hip motion across the three planes between the two motion capture laboratories (Appendix G). Moreover, despite the associated kinematic offset, the overall hip joint ROM was comparable between the patient cohorts.

It should be noted that a number of patients from the current study were also implanted with a THR or TKR (AA: one patient with bilateral hip surgery and one patient with their knee replaced; mixed TAR: one patient with bilateral TKR surgery and one patient with their hip replaced; BOX® ankle: three patients with replaced knees with one having bilateral surgery). This was likely the reason for the large variability in patient kinetic and kinematics at the proximal joints, particularly for measured knee generated power in the TAR patient group and hip peak angles in the sagittal and transverse planes. Not surprisingly, TKR surgery has been found to have a significant effect on gait mechanics at the knee (McClelland et al., 2007; Rahman et al., 2015), consistently demonstrating reduced total ROM and flexion during stance. It has also been shown the TKR surgery can have an even greater biomechanical change at the hip joint. A study by Saari et al. (2005) demonstrated that their patients flexed their hip more than their control group. The TKR patients also extended their hip less than the control group, but no differences were found for hip abduction/adduction motion. These compensatory mechanisms at the hip joint may explain the gait differences in the BOX® ankle cohort.

The influence of THR and TKR in some of the patients in each cohort acted as a confounding factor to determine the biomechanical differences after TAR, particularly with the small sample sizes. However, removing patients from the study who were implanted with THR or TKR would result in the remaining patient cohorts not representing the true patient populations. This limitation stands true for the previous gait studies mentioned above, which examined the effect of both treatment options on proximal joint kinetic and kinematics. The variability in reported motion of the proximal joints following AA and TAR surgical interventions was likely due to the relatively small sample sizes, biomechanical models and patient populations used. Therefore, any significant kinematic differences found at the hip and knee joints must be dealt with caution and studies which a much larger patient population is needed to determine clinical differences between the two treatment options.

#### **5.4.5 Ground Reaction Forces**

The vertical GRF results indicated that each treatment options produced comparable peak values ( $GRF1_{MAX}$  and  $GRF2_{MAX}$ ). This finding contradicts research by Piriou et al. (2008), who suggested that TAR patients have a vertical GRF pattern similar to healthy individuals, when

compared to AA patients. The authors attributed the finding to the restoration of the “rocker mechanisms” of the foot in the TAR patients, which permitted the smooth progression of GRF across the foot (Piriou et al. 2008). This notion has been linked to an efficient gait and possible protection of the adjacent foot joints (Deleu et al., 2022). It should be noted however, that the study by Piriou et al. (2008) compared vertical GRF at one-year post-surgery, while the results from this study presented intermediate follow-up changes in GRF between treatment options. Thus, these findings tends to suggest that TAR patients may be able to return to normal loading of the joint quicker than AA patients. Conversely, at the intermediate follow-up in this study, the AA patients seemed to produce comparable vertical GRF to TAR patients. This may have been due to the compensatory mechanisms found at the midfoot and forefoot in the AA cohort (Section 5.4.1), which was likely the reason for similar gait and loading patterns to the TAR groups.

Despite the non-significant findings in peak GRF between the treatment options, the BOX® ankle cohort seemed to have a different loading response (5-20%) of the stance phase. This may be related to the BOX® ankle cohort having more fear placing load through their operated foot (Piriou et al., 2008), causing a reduction in the GRF during initial contact with the force platform. However, each of the patient cohorts was associated with large variance during this stage of loading, particularly the BOX® ankle participants. The small sample meant that if one patient had substantially reduced loading at heel strike, this would subsequently have a large impact on the average GRF waveform. It should also be noted that both implant cohorts tended to present improved hindfoot motion throughout gait, which is supportive of patients not being fearful of landing on their ankle during the walking trials. This finding has been reported in recent literature of FB designs when compared to pre-operative values (Fritz et al., 2021; Deleu et al., 2022). Thus, supporting the notion that the large variability in vertical GRF likely caused the shift in the waveform of the BOX® ankle cohort. The large variance in kinetic data within the patient cohorts makes it difficult to determine if these values are truly reflective of the larger patient population. Therefore, a study with much larger patient numbers is required to see if patients implanted with this third generation MB device demonstrate the same loading responses during stance. This finding was also likely heightened due to the barefoot conditions, a potential confounding factor in this study (Section 6.2.2.2), as patients who are less confident in walking would usually wear shoes with a lot more cushioning.

#### **5.4.6 Spatiotemporal Outcomes**

The mixed TAR patient cohort tended to have a faster walking speed and increased cadence of the operated limb, when compared to the AA patient cohort (Piriou et al., 2008; Flavin et al., 2013; Seo et al., 2017). The increased walking speeds has been attributed to different strategies implemented by each surgical group (Queen, 2017a). TAR patients improve their walking speed through increasing their cadence and reducing their step duration, while AA patients possess

increased step length accompanied by increased hip ROM (Brodsky et al., 2016). However, the current study demonstrated relatively large variance within the respective patient cohorts, alongside comparable step length in both the operated and non-operated limbs. This finding further indicates that each surgical intervention was able to provide a sense of stability and reduced joint pain (Section 5.4.7), while walking post-surgery (Queen et al., 2012; Deleu et al., 2021a; Deleu et al., 2022). The relatively large variability ( $\pm$  95% CL) within patient cohorts, particularly in the BOX® ankle cohort, was likely due to patient specific compensatory walking patterns that develop following surgery. This finding was also verified by the large variance within patient cohorts for all PROMs measurements (Section 5.4.7), which suggested each patient has a different perception on how well their device is performing.

The current study allowed patients to walk at their own speed, due to it being unnatural for the study to account for walking speed. It has also been shown to influence lower limb joint kinetics and kinematics (Kalron et al., 2017). Eerdekens et al. (2020a) demonstrated that walking speed that exceeding 6 km/h caused a significant increase in joint kinetic measurements. However, this speed was not attained by any of the patient cohorts during overground walking trials which meant that the gait data presented was truly representative of each patient cohort.

#### **5.4.7 Patient Reported Outcome Measures**

The MOxFQ walking/standing domain score is considered the most sensitive to determine improvement in foot and ankle conditions (Dawson et al., 2012; Morley et al., 2013). In this study, there was no substantial differences in the walking/standing outcome score between the patient cohorts. This is a similar finding to a recent multi-centre, open label randomised control trial (RCT) comparing AA (36.8) and TAR (30.4) walking/standing domain scores of the MOxFQ, at a shorter follow-up period of one-year (Goldberg et al., 2022). The current study also showed no significant differences between patient cohorts for pain, social interaction and the MOxFQ summary index scores.

The mean domain scores of the BOX® ankle patient group can be compared to the only other study to measure PROMs with the same TAR design (Najefi et al., 2019b). Najefi et al. demonstrated improvements in MOxFQ for pain ( $43.8 \pm 20.2$ ,  $p < 0.001$ ), standing and walking ( $55.6 \pm 19.8$ ,  $p < 0.001$ ) and social activities ( $45.0 \pm 26.9$ ,  $p < 0.02$ ) at a mean follow-up of 58 months. The MOxFQ scores in each domain of the current study suggested that each intervention was capable of successfully alleviating ankle joint pain and improving ankle function, when compared to the pre-operative scores evidenced in Najefi et al. (2019) and Goldberg et al. (2022) clinical outcome studies. However, the combined effect of the limited sample size and subjectivity of reported outcomes, such as differences in patient's perception of their treatment or misunderstanding of a question. This makes it difficult to truly detect any potentially clinically meaningful outcomes. It also highlights the perception of a patient's pain and functional ability will vary, particularly in small sample populations.

#### 5.4.8 Implant Design

The current study aimed to determine whether the third generation MB design (BOX® ankle) produced improved functional outcomes and PROMs, compared to a mixed TAR cohort of predominately second generation MB designs. The design of the BOX® ankle was manufactured with respect to the ligament mechanics at the AJC, through the mobile meniscal UHMWPE bearing (Cenni et al., 2013). This feature aims to ensure correct ligament tension throughout ROM (Lullini et al., 2020). Despite this, the study suggested that these design features did not result in substantially improved gait mechanics and PROMs of the foot and lower limb at an intermediate follow-up period, compared to other TAR designs.

Only a small number of studies have directly compared the gait mechanics of different implant designs. Queen et al. conducted several studies assessing gait mechanics following TAR, utilising many prosthesis including the STAR™ (Stryker), INBONE® (Wright Medical Group), and Salto Talaris® (Tornier, SA) (Queen et al., 2012; Queen et al., 2014; Queen et al., 2017b). In 2012, the authors compared the results of 23 INBONE® and 28 Salto Talaris® implants, which demonstrated that the only differences were greater single-limb stance time in the Salto Talaris® and greater double-limb stance time in the INBONE® system (Queen et al., 2012). The latest study by the same authors revealed no statistically or clinically meaningful difference between 20 FB (Salto Talaris®) and 20 MB (STAR™) implants (Queen et al., 2017b). More recently, the functional outcome of a two-component FB device (Zimmer Trabecular Metal) was compared to the BOX® ankle (three-component), with both designs showing improved clinical outcomes and minimal gait differences at a minimum of two-years follow-up (Lullini et al., 2020). The study also suggested that ankle ROM in the sagittal plane was 50% less in both patient cohorts compared to a control group (Lullini et al., 2020). However, the control group used in the study was considerably younger than both implant design patient cohorts and was likely the reason for the significantly different kinetic and kinematic parameters measured.

Each of the postoperative gait studies comparing implant designs are limited by short-term follow-up post-surgery. Therefore, the differences found are likely natural gait variability or patients not being fully recovered from the surgical procedure itself, within the small cohort sizes (Deleu et al., 2020a). Another limitation of the above studies, which has been considered in the current study was the use of SFM's, which did not allow the authors to determine the influence of implant design on adjacent joint kinematics. However, even with the inclusion of a MFM, no significant differences were found between the implant designs at each of the foot segments measured. A RCT with a larger patient population, alongside defined sub groups of TAR patients and devices, would need to be performed to confirm this finding. The results from the current study do not indicate the superiority of one device over another, suggesting that the choice of selecting the device to implant should be based on the surgical approach and other patient-specific factors.

## 5.5 Conclusion

The exploratory gait comparison of AA and TAR demonstrated relatively few differences between the measured kinematic and kinetic gait parameters at the intermediate follow-up post-surgery. However, there were some potentially meaningful differences found at the hindfoot and distally located joints of the foot, which may indicate compensatory mechanisms being implemented by the AA cohort to maintain comparable gait patterns to the TAR cohorts. This hypermobility of the neighbouring joints overtime, may increase the risk of developing adjacent joint OA and the subsequent need for future surgery. TAR cohorts produced increased sagittal hindfoot ROM, ankle moment and power, which was likely a result of improved activation of the surrounding muscles to propel the foot and lower body forward during overground level walking. All three patient cohorts produced comparable knee kinetics and kinematics, while greater hip power was found in the mixed TAR cohort and likely resulted in improved functional performance during overground walking.

In addition, the study emphasises the clinical relevance of the use of MFM in biomechanical studies of AA and TAR patient populations, when assessing the outcome of a therapeutic intervention, with SFM overestimating the motion at the ankle joint. The data from the current study may also help inform surgeon decision making, when considering the effect of end-stage ankle OA surgical interventions on the adjacent joints of the foot and the proximal joints of the lower limb. However, the small sample size and large variance within each patient cohort makes it difficult to make foundational statements about which treatment option improves biomechanical function more effectively. A much larger study, preferably a RCT, is required to fully confirm the indications and trends from the current work. This study should also focus on analysing a range of different ADLs, to determine the full ROM a patient will apply to the joint on a day-to-day basis. This is essential to truly establish whether future generations of TAR technologies can improve gait mechanics and subsequent QoL over AA.

## **CHAPTER 6**

# **OVERALL DISCUSSIONS, CONCLUSIONS AND FUTURE WORK**

## CHAPTER 6

### OVERALL DISCUSSIONS, CONCLUSIONS AND FUTURE WORK

#### 6.1 Overall Discussion

The main surgical interventions for end-stage ankle OA are AA and TAR (Goldberg et al., 2009), which have been associated with improvements in pain-free function and QoL (Lawton et al., 2020). However, long-term complications have been reported for both surgical interventions. AA has been associated with abnormal gait mechanics (Thomas et al., 2006; Brodsky et al., 2016) and the subsequent development of adjacent joint OA (Coester et al., 2001; Fuchs et al., 2003), while TAR long-term survivorship remains unsatisfactory in comparison to AA (Maffulli et al., 2017) and that of hip and knee implants (Bonnin et al., 2011; Koivu et al., 2017; Palanca et al., 2018). Previous gait based studies, comparing the two surgical techniques, are also limited by relatively short follow-up periods post-surgery, with many failing to determine the compensatory mechanisms that may be present at the distally located joints of the foot or proximal lower limb joints.

The success of modern day hip and knee replacements is a result of decades of design and development, alongside the standardisation of preclinical wear testing to improve survivorship rates and patient functional outcomes (Mujukian et al., 2020). TARs have not been exposed to the equivalent pre-clinical testing requirements and only recently has an ISO standard (ISO 22622:2019), with set kinematic and loading parameter profiles been published. This explains the varying *in vitro* experimental methodologies and conditions used in limited TAR wear studies to date, when compared to hip and knee replacement simulations (Affatato et al., 2007; Bell and Fisher, 2007; Postak et al., 2008; Kincaid et al., 2013; Bischoff et al., 2015; Reinders et al., 2015b; Smyth et al., 2017; Schipper et al., 2018). The majority of earlier studies also failed to determine the influence of implant or simulator parameters on wear rates, rather focusing on specific implant designs' wear performance.

The main aim of this project was to understand the biomechanical and wear behaviour of a third generation MB device, in current clinical use, using a combination of gait analysis and experimental simulation methodologies. This overarching aim was addressed through the series of objectives detailed in Chapters 3-5. The objectives included the investigation of *in vitro* TAR wear behaviour of varying implant and simulator parameters. The *in vivo* behaviour of the same MB device was then determined, through an exploratory post-operative gait study comparing AA and TAR function at an intermediate follow-up period. The current chapter provides an executive summary of each of these objectives and the fulfilment of the overall PhD aim.

### 6.1.1 Wear Effects of Implant and Simulator Parameters

The implant parameter study was further separated into two objectives, which aimed to determine the influence of implant size and accelerated artificial ageing on implant wear rate. The implant size study compared the wear rates, topographic changes and damage wear modes of a medium and extra small sized MB device. The knee simulator was pneumatically controlled (KSpn) and was run under displacement control using the same experimental conditions and UoL simulator inputs. Despite the greater surface area that the medium sized implants had for multidirectional articulation to occur, there was no significant difference in implant wear rate or topographical changes after 5 Mc, when compared to the extra small sized implants ( $n = 6$ ). This finding does not correspond with earlier studies focused on size differences in the hip (Kang et al., 2009) and knee (Affatato et al., 2013). This was likely a result of the comparable wear contact areas between the implant sizes and subsequent cross-shear, which occurred at the uncoupled bearing surfaces, between the tibial component and superior insert.

Both implant sizes produced comparable wear damage modes of abrasive wear, burnishing and multidirectional scratching, to that which are seen on retrieved devices (Affatato et al., 2009; Vaupel et al., 2009b; Krause et al., 2011; Brunner et al., 2013). The same damage modes were also found in each of the implant and simulator parameter studies within this thesis. However, other wear modes such as embedded particles (third-body wear) or excessive UHMWPE wear/delamination which are clinically identified, were not observed on any of the testing samples, independent of implant or simulator parameter differences. The incapability of mechanical wear simulation to replicate all relevant damage modes which are seen clinically, represents a general limitation in this field.

The implant parameter study demonstrated that the conventional UHMWPE meniscal inserts, which had undergone the accelerated artificial ageing process (ASTM F2003:2015 and ISO 5834-3:2019), produced significantly higher wear rates during the steady-state phase, when compared to unaged inserts. However, there were no signs that of structural failure or fracture, likely due to oxidative degradation on any of the five small sized aged samples. This may be due to the BOX® ankles being sterilised using gamma irradiation in the presence of nitrogen. The implants may have benefited from some degree of crosslinking, which has been shown to improve the wear resistance properties compared to conventional UHMWPE (Muratoglu et al., 2001). It is well known that increased cross-link density produces greater multidirectional sliding wear resistance and reduced release of wear particles during continued articulation (Kurtz et al., 1999; Wang, 2001). There is a known trade off amongst fatigue crack propagation resistance, wear resistance and oxidative stability in polyethylene bearing inserts (Atwood et al., 2011). Re-melting procedures of UHMWPE has been found to cause improved wear resistance and oxidative stability, but resulted in poor resistance to fatigue crack propagation. Increased cross-linking combined with annealing procedures produced good resistance to wear and fatigue crack

propagation, but can cause the insert to be susceptible to oxidation (Atwood et al., 2011). Resistance to fatigue crack propagation has also been correlated with larger lamellar cross-sectional area, suggesting more lamellae may require increased energy for cracks to form or travel through (Atwood et al., 2011).

It should be noted that the study performed was not a fatigue test and used normal loading conditions of the natural ankle during walking, which are well within normal fatigue strength limits of the conventional UHMWPE inserts. Running the implants for longer testing durations or under malalignment, would likely cause increased contact stresses at the insert bearing surfaces with reduced mechanical properties following artificial ageing. Only one previous study has developed a method to determine the fatigue strength of a FB implant (Bischoff et al. 2019), which found that XLPE had sufficient fatigue strength to withstand 10 Mc of loading inputs at more than five time BW at the points in the gait cycle exhibiting peak stresses. Moreover, future studies should use fatigue testing on MB devices, under adverse loading conditions collected from patient specific data, to truly determine the effect ageing or shelf life has on the risk of structural failure due to oxidative degradation. These simulations should run for longer periods than traditional wear simulations, in order to replicate the longer-lasting devices currently on the market and to confirm the clinical applicability of these pre-clinical results.

The simulator parameter study was further separated into two objectives, which aimed to determine the influence of simulator type and simulator inputs on implant wear rate. Both electromechanical (KSem) and pneumatic (KSpn) controlled mechanical simulators produced comparable wear rates and topographical changes, which were not significantly different from one another. This finding corresponded with earlier studies which compared the difference in the same two simulator types on implant wear in hips (Ali et al., 2016) and knees (Abdelgaied et al., 2017). However, the output loading and kinematic profiles followed the desired input profiles (UoL) more closely on KSem, which was also shown in the previous studies between tested hip and knee implants (Ali et al., 2016; Abdelgaied et al., 2017). In addition, KSem remained within tolerance of the UoL input profiles, apart from during peak anterior displacement. Although this motion was relatively small compared to the other kinematic conditions and has previously been found to have no effect on implant wear in a similar MB device (Smyth et al., 2017).

The newer generation of KSem, with fully independent control, can also be used for a much greater range of loading and kinematic conditions which were tested in the current wear studies on TAR. This will be particularly important in future studies, which must begin to simulate inversion-eversion motion through the abduction-adduction cradle. Inversion and eversion are involved in the motions of supination and pronation of the foot, which are primary movements that enable the foot to adapt to different terrains (Nigg, 2001), aid in shock absorption and transition to a rigid lever during forward propulsion (Sarrafian, 1993).

The second study condition compared the differences in wear rate of the same implant under UoL and ISO 22622:2019 loading and kinematic input profiles. The different combinations of gait inputs applied caused no significant differences in wear rate. This was likely due to the relatively similar profiles, particularly for tibial IER, which has been found to have the most significant influence on knee (McEwen et al., 2005) and ankle (Smyth et al., 2017) wear rates. Both simulator input profiles produced comparable multidirectional motion at the bearing interfaces, causing the surface chain orientation to change. This resulted in shearing of the conventional UHMWPE, which released wear particles from the surface and caused greater wear rates (Bragdon et al., 1996; Wang, 2001). The study also supports the notion that the reduced AP displacement found in the ISO 22622:2019 input profile had no effect on wear rate (Smyth et al., 2017). Despite the comparable wear rates between input profiles, ISO 22622:2019 provides researchers with a universal set of experimental conditions and inputs, which will allow researchers at different sites to directly compare wear rates from different implant designs. However, the research performed in Chapter 5 clearly shows that both these input profiles overestimate FE and tibial IER, which likely means that both simulator input conditions overestimated implant wear.

The comparable wear rates produced in each of the implant and simulator parameter studies are in a similar range to previous displacement controlled TAR testing on conventional UHMWPE ( $3.4 \pm 10.0$  to  $25.8 \pm 3.1$  mm<sup>3</sup>/Mc) (Affatato et al., 2007; Bell and Fisher, 2007; Smyth et al., 2017). The wear rates for the MB device were also comparable to that of THR (10 to 80 mm<sup>3</sup>/Mc) (Clarke and Gustafson, 2000; Affatato et al., 2008; Shen et al., 2011; Zietz et al., 2013) and TKR (2 to 20 mm<sup>3</sup>/Mc) (D'Lima et al., 2001; Schwenke et al., 2005; Brandt et al., 2012; Schwiesau et al., 2013b), after 5 Mc, which used similar conventional UHMWPE as their insert material. However, metal-on-metal (Chan et al., 1999; Goldsmith et al., 2000) and ceramic-on-ceramic (Al-Hajjar et al., 2010) bearing implants have been shown to produce considerably lower wear rates, so the comparison in wear rate is only comparable to metal-on-polyethylene devices. The similar wear rates in metal-on-polyethylene implants of the lower body corresponds with the similar TAR survivorship rates found in THR and TKR at 5 years (range, 90.4–96.0%). Although TAR have been found to have considerably lower survival rates at longer-term follow up of 10-15 years (range, 63.6–73.0%) (Koivu et al., 2017; Palanca et al., 2018; Clough et al., 2018).

Predicted Kaplan-Meier cumulative revision rates (95% confidence intervals) in the NJR (2021) demonstrated that both hip (4.28%; 4.23-4.33%) and knee (4.13%; 4.08-4.17%) replacements were below the current NICE recommended threshold of 5% at ten years (NICE: Total hip replacement and resurfacing arthroplasty for end-stage arthritis of the hip. Technology appraisal guidance [TA304]). However, the estimated cumulative revision rate for TAR was 8.52% (7.55-9.60%) at 10 years follow-up, which does not fall within the NICE recommended threshold. It should be noted that prior to 2014, the revision threshold recommended by NICE for THR was

10% at ten years (NICE: Guidance on the Selection of Prostheses for Primary Total Hip Replacement. Technology appraisal guidance [TA2]). The change in NICE guidelines stemmed from the improved revision rates for the newer hip devices on the market and this threshold should be considered with TAR, since there is a reduced amount of devices implanted on the market. The reduced survivorship in TAR has resulted in the total number of procedures (7,084) being substantially lower when compared to hip (1,251,164) and knee (1,357,077) replacements (NJR, 2021). This is likely due to the surgeon's reluctance and lack of confidence to implant devices with a higher risk of failure. Another reason for the reduced number of primary cases is the reduced clinical burden. The majority of ankle OA is associated with previous trauma, whereas the primary cause of hip and knee OA is idiopathic. The combined effect of increased revision rates and reduced surgical uptake means that until longer lasting TAR designs are developed, they will remain less widely used compared to hip and knee implants.

A major cause of the low survival rates in TAR is aseptic loosening, cited as the cause of revision in 24.7% of primary cases (NJR, 2021), which has been associated with wear-mediated osteolysis (Schipper et al., 2017). This issue, which is often reported by clinicians with no root cause, has resulted in the early discontinuation of several TAR devices with less than 10 years follow-up post-surgery (Besse et al., 2015). Clinical follow-up studies have also shown the presence of wear-associated complications such as synovitis (Brunner et al., 2013) and bone cyst formation (Besse, 2015; Najefi et al., 2021; Kim et al., 2021). Yet, the relationship between wear and the impact on loosening remains unclear. It has previously been found that wear rates between 5 to 20mm<sup>3</sup>/Mc may be sufficient in achieving an adequate 'osteolytic-free' lifetime in TKR (Fisher et al., 2004). However, this also relies on size and dose dependent wear particles. TKR have been shown to produce a greater concentration of wear particles in the 1.0–10 µm size range, which are related to lower biological activity and subsequent lower osteolytic potential (Tipper et al., 2006).

UHMWPE wear particles from a TAR have been shown to be comparable in size to TKR wear particles (Kobayashi et al., 2004), whilst morphological assessment determined rounder particles with a lower aspect ratio for TAR (Schröder et al., 2013; Reinders et al., 2014). However, the differences in particle morphology has been attributed to differences in the biomechanical environments (Kobayashi et al., 2004). There has only been one wear simulator based study which examined the wear particles produced by TARs (Reinders et al., 2015b). The authors demonstrated that *in vitro* generated wear particles ( $0.23 \pm 0.14 \mu\text{m}$ ) were within the biologically relevant size range ( $\sim 0.2\text{--}0.8 \mu\text{m}$ ) associated with localized bone resorption or osteolysis (Green et al., 2000; Ormsby et al., 2019), as well as finding that there was no relevant size difference to *in vivo* UHMWPE wear particles (Reinders et al., 2015b). Whilst *in vitro* wear characteristics suggests that TAR may have a relevant osteolytic potential, the wear rates observed in the wear studies presented in this thesis are certainly not sufficient to cause osteolysis in such a short

period. More research is therefore required to determine the effect on wear-mediated osteolytic immune response at a longer-term follow-up in the current generation of MB designs.

Although this thesis focused on the influence of primary bearing wear on implant performance, this is generally not considered the main reason for the short-term TAR performance (Besse et al., 2015). As discussed, the wear results from the *in vitro* studies in this thesis, which aimed to mimic up to the first five years of the implants lifetime *in situ*, demonstrated relatively low primary bearing wear rates and were comparable to previously published studies on different TAR designs (Affatato et al., 2007; Bell and Fisher, 2007; Smyth et al., 2017). However, the latest NJR annual report showcased that the device in question of this thesis (BOX® ankle) possessed a higher estimated cumulative revision rate (95% confidence interval) at 10 years follow-up (11.43%; 8.55-15.20%) compared to the mobility (11.10% 9.32-13.20%), Salto (7.66%; 4.23-13.66%) and Zenith (8.31%; 6.53-10.55%) devices (NJR, 2021). However, it should be noted that each of these estimated revision rates were calculated from a patient population of less than 250 cases remaining at risk at the given time point. Therefore, caution must be taken when making definitive conclusions from relative small patient populations, in comparison to hip and knee implants. Nevertheless, this suggests that there must be other reasons for the high incidences of early revision cases, particularly for the BOX® ankle patients.

A more consistent concern in the orthopaedic community is the presence of wear debris produced by other wear modes, often found at the bone-implant interface. The prominent hypothesised TAR failure modes reported in the literature include: implant malalignment (van Hoogstraten et al., 2022); fixation coating delamination (Besse et al., 2009; Singh et al., 2016); fluid pressure related to micromotion (Yoon et al., 2014) or the incidence of pre-existing cysts (Najefi et al., 2021). This combination of mechanical and biological factors are likely the reason for the lower survivorship after 10 years for TAR, when compared to AA or other lower limb implants.

Correct positioning during TAR surgery is known to be difficult, which is related to the reduced surgical access, large volume of surrounding soft tissues and smaller contact surfaces, resulting in an increased risk of malalignment. Incorrect alignment may also arise when a surgeon fails to correct natural varus/valgus malalignment, and has been associated with a high incidence of early implant failure (Haskell and Mann, 2004; Hobson et al., 2009). It has been predicted that as many as 45% of TAR patients may have been implanted with some form of malalignment (Uselli et al., 2017). Effective alignment is considered to be instrumental for long-term implant survivorship, particularly through allowing for the optimal transmission of forces. This is essential at the ankle joint, with its contact area approximately three times smaller than that of the hip and knee joints. The ankle joint also experiences substantially higher peak forces (Vickerstaff et al., 2007), which have been measured at approximately 6-times BW compared to 2.5- and 4-times BW in the hip and knee, respectively (Anderson and Pandey, 2001). The combined effect of a

smaller contact area and increased forces, alongside misaligned components may result in higher contact stresses at the AJC (Anderson and Pandey, 2001). Other studies have reported a causal relationship between the progression of degenerative lesions and post-surgery deformity at the AJC, which includes constrained inversion-eversion ROM and alignment issues (Wang et al., 2018; Morasiewicz et al., 2019).

Computational models of varying TAR designs have been developed and demonstrated that TAR malalignment of greater than  $5^\circ$  inversion can result in the polyethylene inserts reaching their yield stress, leading to an increased production of wear particles and loosening long before predicted implant survivorship (Espinosa et al., 2010). A more recent computational analysis found that a  $10^\circ$  of valgus malalignment at the tibial component caused the greatest contact pressure of 177 MPa compared to 98.4 MPa in the neutral position at the tibial bone-implant interface (van Hoogstraten et al., 2022). These increased contact pressure exceeds the ultimate yield point of trabecular bone. This finding, coupled with the fact that the metallic alloys used at the tibial and talar components of TAR designs are substantially stiffer than the surrounding cortical and trabecular bone, results in the transmission of force from the implant to the bone and producing peak stresses at the bone-implant interface (Sopher et al., 2017). Continued high stress peaks at the ankle can contribute to permanent bone damage and reduced implant fixation (Morgan et al., 2018). Furthermore, tibial bone strains alter upon malalignment of the device, causing localised overloading (edge loading) and stress shielding, contributing to implant loosening and eventual requirement for early revision surgery (Mondal and Ghosh, 2019).

Despite these known early failure modes, there is a lack of experimental validation on the effect of malalignment. One simulator based study at the UoL found that component lift off was highly prevalent under lower swing phase loads (100-300N), which resulted in edge loading and localised peak pressures occurring at the insert edges (Smyth et al., 2018). The study also suggested that when the inserts of three MB TARs were placed in  $10^\circ$  of coronal malalignment, the inserts produced a peak pressure of 16-18 MPa, which is a similar yield stress of conventional UHMWPE (Smyth et al., 2018). This follows a similar pattern to the computationally based studies and suggests that malalignment causes increased wear and potential polyethylene failure. A significant limitation with this study was the use of a Tekscan sensor to measure contact pressure across varying coronal angles of malalignment. This technique could only be used on the flat-on-flat interface between the superior insert surface and tibial component, while failing to measure contact pressures between the inferior insert surface and talar component, which the two computational modelling studies were able to quantify (Espinosa et al., 2010; van Hoogstraten et al., 2022). However, a limitation of both computational modelling studies is the fact that both focused on measuring post-operative cases, where no bony ingrowth between the implant and bone interfaces had taken place. After such bonding occurs through the process known as osseointegration, the stresses found at the ankle may be reduced. This suggests that the data

presented from both studies represents early failure modes and again highlighting fixation being a critical factor in early TAR failure.

All MB implants rely on cementless fixation by bone ingrowth, which requires low relative micromotion of 20-50  $\mu\text{m}$  between the implant and the bone in the post-surgery (Jasty et al., 1997). Previous research has shown that implant design has a significant impact on micromotion. Sopher et al. (2017) utilised finite element analyses to determine bone-implant relative micromotion in three different implant designs: central stem; dual-cylinder stem; and a keel. The greatest amount of micromotion was found in implants possessing central stems, while the keel designed implants (which is more similar to the design of the implant used in this thesis) had the smallest (Sopher et al., 2017). McInnes et al. (2014) also found that the largest micromotion occurred at the same point as the greatest applied torque. However, it is worth noting that both studies used axial loads (Sopher et al., 2017) or a combination of an AL with moments around the anatomic axes of the foot (McInnes et al., 2014), which do not represent the complex and dynamic loaded that occurs at the ankle during ADLs.

To address these shortcomings, González et al. (2021) used a combination of experimental testing, musculoskeletal modelling and finite element analysis, to demonstrate that peak micromotion under static peak AL alone was between 2 to 79 times smaller than measured peak micromotion during overground walking. The inclusion of combined multiaxial forces and moments resulted in micromotion of up to 30 times than that measured in Sopher et al. (2017) for stem design implants. The study, however, used line-to-line contact between the fixation geometries and the bones, which did not consider the effect of press-fit or gaps at the interface. The study by Sopher et al. (2017) showcased a gap between the implant and bone during malalignment conditions, which led to a higher amount of micromotion. Therefore, future computational studies should assess the effect of a gap at the bone-implant interface and its influence on localised loading due to the reduced contact area of the implant. Another limitation with all the studies mentioned is that they are all computationally driven and not validated by experiments. However, there is substantial difficulties in experimentally growing bone and being able to replicate fixation at the bone-implant interface. Incremental improvements in experimental testing and implant design will further reduce the risk of micromotion at the bone-implant interface, while enhancing bone-implant fixation and initial stability, to prevent long-term implant loosening (McInnes et al., 2014).

The larger axial loading forces on the ankle have been associated with increased rates of osteolytic cysts in TARs, due to the lower numbers of surrounding muscles at the ankle providing additional support (Lee et al., 2013). Moreover, hip and knee implants attempt to cover the resected bone surfaces with cement or with the device itself, while in most TAR designs, the subchondral bone located at the metallic components are uncovered and are exposed to the intra-articular fluid (Arcangelo et al., 2019). This could lead to fluid circulation and cyst formation (Fahlgren et al.,

2010), due to increased pressure of the intra-articular synovial fluid in the smaller joint space compared to that of the hip and knee (Rodriguez et al., 2010). The wear debris may also get trapped in these joint spaces, which will influence the osteolytic potential. It is hoped with the improvement of future generation of designs, the incidence of early cyst formation will reduce, or will at least delay the onset of wear-mediated osteolysis or implant loosening.

The MB device in the in vitro wear studies (BOX® ankle) was coated in hydroxyapatite coating which aids in the osseointegration process (Botterill and Khatkar, 2022). However, the disintegration of these fixation surfaces during continued articulation has been found to produce an array of sub-micron particles, while also been associated with causing extensive osteolysis (Singh et al., 2016). Elemental analysis of peri-prosthetic tissues in 71 patients undergoing revision surgery following failed TAR, found elevated levels of calcium phosphate, cobalt chromium, iron, molybdenum, nickel and titanium in patients with peri-prosthetic cysts when compared to patients without ballooning osteolysis (Singh et al., 2016). High concentrations of calcium ( $>0.5$  g/g) were associated with a 297-fold increased risk of ballooning osteolysis (Singh et al., 2016). However, the authors noted the difficulty in mass spectrometry and elemental composition being able to differentiate the origin of the wear debris, as this may have been produced by the hydroxyapatite coating or bone around the implant.

The metallic particles found in the retrieved devices may have originated from the bearing surfaces due to a number of wear modes such as fatigue failure, third-body wear, extensive abrasive wear or fixation surface delamination. Fixation surface wear has previously been identified in hip and knee explants using a novel wear particle isolation method (Stratton-Powell et al., 2022). Submicron-sized cobalt chromium alloy and titanium wear particles are said to cause an increased risk to developing aseptic loosening (Yao et al., 2017). In a metal-on-metal THR articulation, cobalt chromium alloy particles tended to be in the nanometre size range (Brown et al., 2007a), while particles generated at the fixation surface tended to be larger in size (Maloney et al., 1995). These differences may be attributed to varying mechanisms of wear, with the former being attributed to fretting and the latter relating to abrasive wear (Brown et al., 2007b). The combination of wear particles suggests that the early failure of these devices may be due in part to the multifaceted biological cascade that occurs following particle release and the accumulation of these particles within the small joint space over time. Further research is still required to determine the implications of these particle characteristics on biological activity at the bone-implant interface. The effect of these particles should also be accounted for during validation clinically relevant wear simulator testing and biological response studies during the design and development of TAR devices.

In other replacement joints of the lower limb, there is a large range of case numbers necessary to achieve consistently improved alignment and reduced patient complications (Usuelli et al., 2017). When a high volume orthopaedic surgeon is implanting a new hip or knee prostheses, a total of

40 (Seng et al., 2009) and 25 (King et al., 2007) cases are required before stabilisation of resection accuracy and reduced operative time, respectively. The location of the AJC makes the surgical procedure highly complex, resulting in the increased failure rate at the short-term compared to hip and knee implants. Multiple investigations have demonstrated that the survival rates of TAR increases substantially with increased surgical experience, identifying the presence of a significant learning curve in various TAR designs and models (Clement et al., 2013; Lee et al., 2013; Roukis and Simonson, 2015; Usuelli et al., 2017). Schimmel et al. (2014) compared the first and last consecutive 50 cases by a single surgeon using the STAR™ (Stryker) implant. The last 50 patients demonstrated reduced perioperative complications and operating time, alongside improved sagittal alignment (Schimmel et al., 2014). Another study focusing on the survivorship of the Depuy Mobility® device demonstrated a reduced incidence of perioperative complication from the first 30 patients to the second 30 patients (36.7% vs 16.7%,  $p = 0.08$ ) (Lee et al., 2013). However, the majority of studies mentioned have shown that the best surgical outcomes have typically been authored by individual who may have designed or have a financial interest in the implant being examined (Maccario et al., 2021).

Usuelli et al. (2017) determined a significant learning curve for surgical time (16<sup>th</sup> patient), PROMs (13<sup>th</sup> to 21<sup>st</sup> patient), alpha and gamma radiographic joint angles (18<sup>th</sup> and 15<sup>th</sup> patient respectively) and complication rates (39<sup>th</sup> patient), with a single surgeon who did not develop the device in question. This suggests that most clinical and radiological outcomes stabilise after a surgeon has implanted 28 cases. However, this study is also limited to a retrospective, single surgeon, single-implant and single-centre design, which may limit the generalisability of the learning curve data (Usuelli et al., 2017). This is because surgeons have different levels of technical ability and experiences with certain devices, which will affect their individual learning curve. Greater restriction on patient selection is therefore required for at least the first 20-50 TAR cases, in order to prevent the continued early failure of TAR devices when compared to hip and knee devices.

Taking into consideration the complexity of the surgical procedure for TARs, coupled with the increased load bearing nature of the talocrural joint, there is no surprise that patient indications for TAR surgery are highly limited. The ideal candidate for a TAR is an individual who is generally over the age of 50 years, who is less than 250 pounds, has no hindfoot deformity, has a lower physical demand, has failed to respond to other non-invasive treatments, and has severe pain secondary to ankle OA (van der Plaats and Haverkamp, 2017). The contraindications, which have been discussed within this section, which are associated with the short-to-mid-term failure of TAR, has likely contributed to AA remaining the preferred surgical intervention for the majority of orthopaedic surgeons (Ferguson et al., 2019). With the younger and more active patient populations with ankle OA compared to the knee and hip, TAR should be more widely available. However, the limited confidence and volume of early failure modes, makes fewer surgeons willing

to update such devices compared to AA, as well as other artificial implants of the lower limb. If devices continue to fail early in the 'ideal' patient demographic, this will likely lead to catastrophic failure in patients outside this bracket. These reasons identify why TAR remains much further behind the success curve compared to modern day hip and knee designs.

One of the many design improvements in hip and knee devices was the introduction of XLPE and vitamin E doped polyethylene, which has been clinically shown to improve oxidation resistance and reduce implant wear (Minoda et al., 2009; Affatato et al., 2012; Paxton et al., 2015; Meneghini et al., 2016). This has led to significantly reduced prevalence of wear-mediated osteolysis, risk of subsequent loosening at bone-implant interface and overall implant survivorship (Lachiewicz et al., 2016; Rames et al., 2021). However, XLPE has been associated with polymer chain scission and increased embrittlement, which can reduce fatigue properties and result in early fracture and ultimate failure of the implant (Akagi et al., 2006; Sakellariou et al., 2013). This known risk, coupled with the combination of increased loading and small bearing surfaces in the ankle, has limited the number of companies manufacturing TAR implants with a XLPE meniscal bearing, with only two designs available on the UK market in 2022. This is despite the significantly lower wear rates found in XLPE tested devices ( $2.1 \pm 0.3$  to  $3.3 \pm 0.4$  mm<sup>3</sup>/Mc) (Kincaid et al., 2013; Bischoff et al., 2015; Schipper et al., 2018) compared to conventional UHMWPE ( $3.4 \pm 10.0$  to  $25.8 \pm 3.1$  mm<sup>3</sup>/Mc) (Bell et al., 2007; Affatato et al., 2007; Postak et al., 2008; Reinders et al., 2015b; Smyth et al., 2017).

Morphometric and biological trends in wear simulator studies, using equivalent circle diameter computed methodologies, have demonstrated that XLPE wear particles produced in a TAR were smaller than those produced by conventional UHMWPE (Bischoff et al., 2015; Schipper et al., 2018). Both studies found that the wear particles generated from both polyethylene types were smaller than those reported in hip and knees. However, the clinical impact of the different sized wear particles is not yet known. It has also been shown that XLPE in a TAR device, possessed enough fatigue strength to withstand 10 Mc of loading at 5 times body weight (5600 N), with no signs of gross fracture at the bearing surfaces or locking mechanism (Bischoff et al., 2019). Further research is warranted to determine if TAR with XLPE used as its meniscal bearing can exhibit the beneficial wear properties found in hip and knee implants, without the increased risk of bearing fracture.

It is hoped that the newer generation of TARs are able to provide improved long-term survivorships which are comparable to hip and knee implants, whilst also falling within the NICE technology appraisal guidance (5% or less revision rate at 10 years post-surgery). More research is also required to understand the biomechanical function of newer TAR designs, particularly with AA remaining the preferred surgeon choice for the treatment of end-stage ankle OA (Section 6.1.2). Pre-clinical wear simulation driven by inputs generated from the biomechanical assessment of TAR patients (Chapter 5), will result in a greater understanding of *in vivo* wear

performance. This will help to improve future TAR designs which last longer in younger and more active patients. However, the development of longer lasting devices increases the likelihood of the patient suffering from wear-mediated osteolysis and aseptic loosening at the bone-implant interface.

### **6.1.2 Biomechanical Effects of Ankle Arthrodesis and Total Ankle Replacement**

Chapter 5 explored the post-operative differences in the kinetic and kinematics of the varying foot segments and proximal joints of the lower limb during overground walking, in patients implanted with AA and TAR, at an intermediate follow-up period. A third patient cohort was included in the study, who were all being implanted with the same design (BOX® ankle), which was the same prosthesis used in the wear simulation studies (Chapters 3 and 4). This was performed to determine if the third-generation MB device was able to perform as well clinically, as was found during pre-clinical simulator testing.

The patients implanted with TAR tended to have substantially greater ROM at the hindfoot segment, which corresponds with the previously published literature comparing AA and TAR (Piriou et al., 2008; Hahn et al., 2012; Flavin et al., 2013; Seo et al., 2017; Segal et al., 2018; Sanders et al., 2021). This finding is likely the result of the fusing of the AJC in AA patients, which caused the hypermobility found at the distally located foot segments, compensating for the reduced hindfoot motion. The increased sagittal ROM at the hindfoot in the TAR group may also be explained by the fact that the TAR patients may be more confident to land properly on their foot during the loading phase of gait when performing overground walking. Another important trend in the kinematics at the hindfoot segment was the greater ROM in the frontal plane in the BOX® ankle cohort when compared to both other patient cohorts. This may be a result of the design of the device, since the MB device in question preserves ligament isometry, which helps maintain natural ROM during motion (Lullini et al., 2020). This finding may also relate to the improved transmission of forces between the hindfoot and forefoot, supported by the restrained mechanism at the subtalar joint, which functions to absorb the load after initial contact and provides a rigid lever for propulsion during walking (Henricson et al., 2007).

Peak dorsiflexion at the midfoot segment and peak plantarflexion angle at the forefoot segment was considerably higher within the AA patients compared to TAR cohorts. This kinematic compensatory mechanism was likely a result of the reduced hindfoot motion remaining from the surgical procedure itself. This compensatory mechanism was also found to produce comparable PROMs and spatiotemporal results between the AA and TAR cohorts, which suggest an improved stability and reduced joint pain while walking at the intermediate follow-up period (Queen et al., 2012; Deleu et al., 2022). The TAR patients produced a greater minimum dorsiflexion angle as all groups remained in plantarflexion throughout the gait cycle. These findings correspond with Seo et al. (2017), with the study implying that TAR patients exhibited greater dorsiflexion in a comparable forefoot segment, whilst plantarflexion angle was

significantly greater in AA patients. Dorsiflexion is considered a good indicator of improved foot function post-surgery (Eerdeken et al., 2020a), while the higher plantarflexion in the AA patients is likely compensating for the loss of hindfoot motion and could further result in joint degeneration and need for subsequent surgical intervention.

Although the study identified varying kinematic behaviour at the AJC and distally located foot segments, the extent to which the changes in foot segment angles are attributed to pain relief, cannot be fully determined in the current study. This was also the case with alterations in patients' gait and the extent to which this will improve ankle function. It should be noted that across all kinematics parameters measured at the foot segments, the time-series graphs demonstrated that the greatest variance within and between patient cohorts, was in the transverse plane of motion. However, this is not as clinically meaningful when compared to differences in sagittal and frontal plane motion. This is due to the small amount of motion which occurs and is the reason why many researchers do not report the results. These motions were still important to measure, given they still form part of each foot segment ROM. Further studies may be required to determine subtle differences in this plane of motion.

The increased ankle plantarflexor moment found in the mixed TAR cohort, compared to the other treatment groups, represents an indicator of improved foot function and its ability to propel forward during walking (Ingrosso et al., 2009). This may also indicate that this cohort improved the strength of their plantarflexor leg muscles (soleus and gastrocnemius) when performing the walking task. In addition, the higher ankle power in the mixed TAR cohort may be related to the conservation of the Achilles tendon, coupled with the apparent functioning of the plantarflexor muscle groups and kinematics. The increased ankle power in the mixed TAR cohort resulted in increased hip extensor generated power during walking, which indicates proximal redistribution occurs more at the hip than at the knee in TAR patients. However, the large variability in all three patient cohorts resulted in comparable kinematics in all three planes of motion at both the hip and knee joints, respectively. This finding aligns with Seo et al. (2017), who identified no statistically significant differences in hip and knee kinematics. The authors attributed this to the relatively small changes in motions at the foot segments, which did not result in significant functional differences at the proximal joints through the lower limb kinematic chain. The gait study presented in this thesis supports the notion that both surgical procedures had negligible effect on proximal joint kinematics.

The current study implied that the third generation MB design did not result in any substantial changes to patient gait mechanics or reported outcomes, when compared to patients implanted with mostly second-generation mobile designs. The improved hindfoot frontal plane motion within the BOX® ankle cohort was nullified by the reduced ankle plantarflexion moment and associated power, compared to the mixed TAR cohort. However, the latter was likely due to the relatively high patient variation in both study groups. Both TAR cohorts presented large

variability, for the majority of the PROMs and gait parameters measured, suggesting that biomechanical performance appears to be more specific to AA surgery. Although as a whole, both groups showed improved functional outcomes to AA. The comparable finding is well supported in the ankle literature which has previously compared gait mechanics of varying designs (Queen et al., 2012; Queen et al., 2014; Queen et al., 2017b; Lullini et al., 2020).

Gait outcome comparisons between the three patient cohorts identified potentially clinically meaningful observations, which warrant further exploration in subsequent larger scaled prospective studies, to determine whether the current findings of local mechanical differences between the treatment groups are transferrable to the larger patient populations. This should be in a form of multi-centre trial involving a much greater sample size of patients, to avoid both surgeon and research site bias. The larger scaled study should also include pre-operative information, so that patient population matched data and true improvement of each surgery can be determined. This is a limitation of the current study and is discussed in Section 6.2.

There is a current RCT (TARVA) comparing AA and TAR to determine which treatment option offers better pain free function and QoL, fewer complications and better value for money. The TARVA trial is estimated to finish in 2029 and has published short-term data after one-year (Goldberg et al., 2022). However, the study only reports PROMs information and ROM collected using a goniometer. Future studies should look at similar outcomes mentioned in the TARVA RCT, but use similar gait analysis techniques used in the current study, to fully determine the long-term effect of each treatment option on gait mechanics of the two treatment options. This should also be performed under a range of varying ADL, which would represent the patients' movements on a day-to-day basis, rather than just measuring overground walking. From the results of this exploratory study, the null hypothesis of the larger study would be that TAR improves ROM at the hindfoot, while AA causes increased peak motions at the midfoot and forefoot segments. Until such a study takes place, there is no clear evidence as to which procedure is clinically superior.

### **6.1.3 Biomechanical versus Wear Performance**

The mean gait derived kinematics from the BOX® ankle patient cohort (Chapter 5) are substantially lower the ISO 22622:2019 recommended input profiles, which was used in some of the wear studies reported in this thesis. Reduced hindfoot dorsi-/plantarflexion (equivalent to FE in the simulator) and reduced adduction/abduction (equivalent to tibial IER in the simulator) motion in the sagittal and transverse planes can be found in the BOX® ankle patient input profiles, when compared against the input profiles from ISO 22622:2019. This is presented in Figure 91, where the patient data was interpolated from 101 time series measurements of the gait cycle to the required 128 data points of the mechanical simulator input profile. Mean peak and ROM parameters for flexion and rotation of the derived input profiles from ISO 22622:2019 and BOX® ankle patient data are displayed in Table 28. The offset in FE and tibial IER kinematic

waveforms (Figure 91) of the patient specific data compared with ISO 22622:2019 profiles was likely due to the hindfoot segment being used instead of the full foot segment, which removed the effects of the midfoot and forefoot segments.

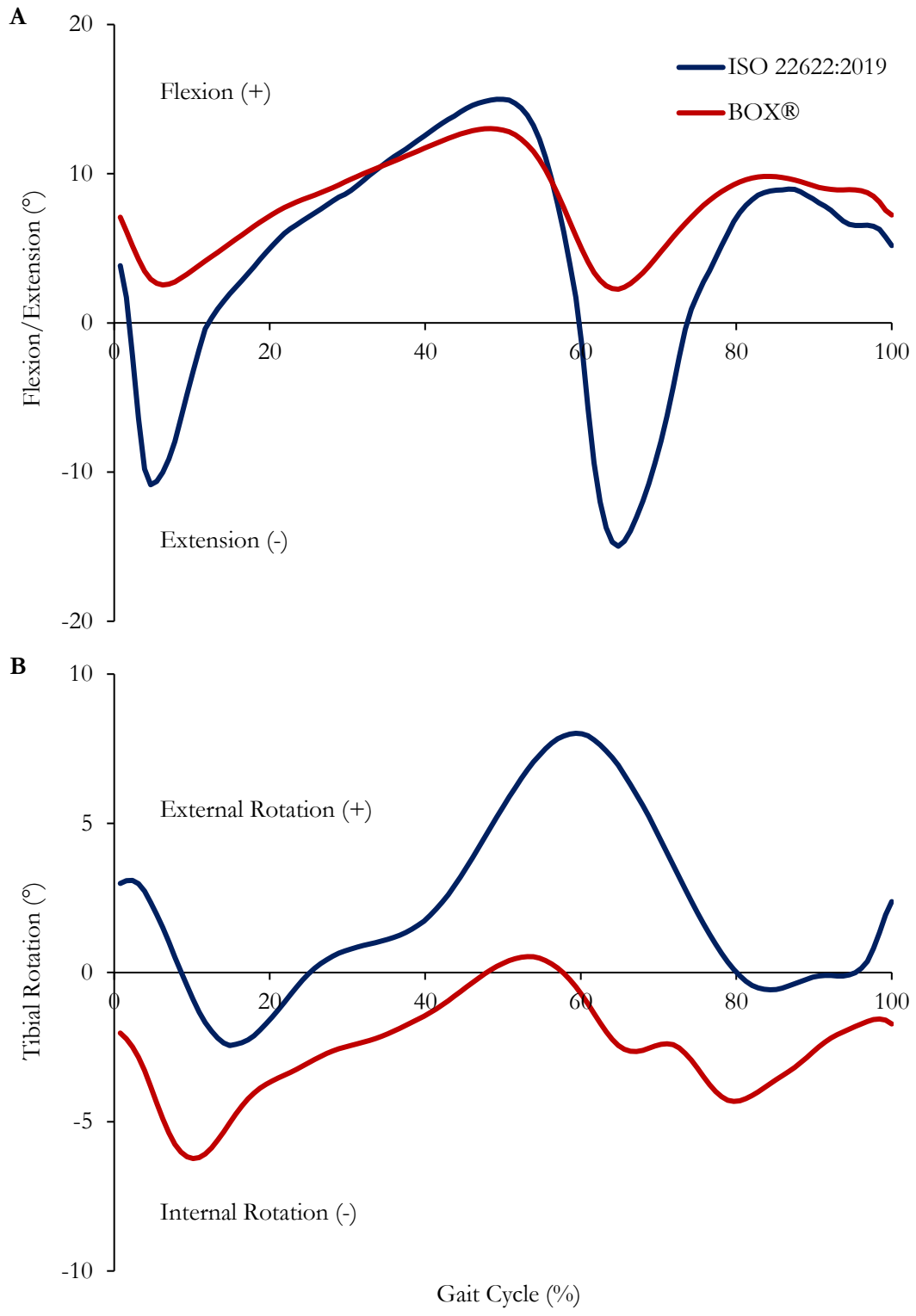


Figure 91. Current pre-clinical testing recommended flexion (+)/extension (-) (A) and tibial rotation (B) input profiles from the ISO 22622:2019 (blue) compared to the mean kinematic waveforms from the BOX® ankle patient cohort (red).

Table 28. Comparison of peak and ROM parameters for flexion/extension and tibial rotation input from ISO 22622:2019 and patient specific profiles.

<b>Simulator Peak and ROM Inputs</b>	<b>ISO 22622:2019</b>	<b>BOX® ankle</b>
Peak Flexion (Dorsiflexion)	15.00	13.42
Peak Extension (Plantarflexion)	-15.00	-0.14
Sagittal plane ROM	30.00	13.56
Peak External Rotation (Adduction)	8.02	1.65
Peak Internal Rotation (Abduction)	-2.45	-6.93
Transverse plane ROM	10.47	8.58

The FE profile ROM is nearly 50% less in patient driven kinematic waveform compared to the ISO 22622:2019, while the tibial IER ROM is approximately 2° less. The reduced multidirectional motion that would occur under the patient specific kinematic profiles would likely lead to reduced cross-shear ratio and subsequent reduced wear rate, under similar experimental conditions. An increase in tibial rotation, coupled with comparable loading and flexion profiles has been found to cause greater wear rates in a MB device (Zenith, Corin Group PLC) (Smyth et al., 2017), which is of a similar design to the BOX® ankle. The multidirectional motion causes shear forces which change the orientation of the polyethylene fibrils. This resulted in shearing of the polyethylene particles from the insert bearing surfaces, generating wear and increased risk of wear-mediated osteolysis (Bragdon et al., 1996; Wang, 2001). Conversely, by applying higher kinematics closer to that seen in healthy individuals (Appendix G), the simulator inputs used in each of the wear studies provided more demanding wear conditions to investigate implant and simulator parameters.

It should be noted that Figure 91 displays the mean hindfoot segment motion of only six patients implanted with the BOX® ankle. The variability in this patient group was considerable, which could have added to the offset in data between the two input profiles. This means that certain patients may fall closer in line with the ISO input profiles than others, implying that the difference may not be as substantial. The small sample size and large variability associated with the BOX® ankle cohort means that a much larger (powered) study is required to truly determine if there are clinically meaningful kinematic differences between patient driven and ISO 22622:2019 profiles. However, with the ISO standard using historic data from healthy patients, it is clear that this larger scaled study must go ahead to help shape an ISO standard driven by patient specific data, from a variety of implant designs and materials. This also brings into question whether standards should be created for specific patient demographics or implant designs, as its clear from even the small sample gait study (Chapter 5), differences exist in certain kinematic parameters between varying implant designs.

Despite AP displacement not being defined in the BOX® ankle patient cohort due to limitations in the marker-based motion capture technology used in Chapter 5, changes in applied AP displacement has been proven to not have a significant effect on overall implant wear rate (Smyth

et al., 2017). The vertical GRF recorded in the TAR cohort would need to be inputted into a musculoskeletal model to determine the contact forces at the ankle joint, to then be used as the AL input profile in the simulator. However, further research is required to develop such a model of the ankle joint, which can accurately calculate the contact forces. A review of the limitations and future work associated with the wear and biomechanical studies can be found in Section 6.2 and Section 6.4, respectively.

An alternative to displacement control simulation is load control, which use a combination of AP force and axial torque profiles, allowing components to translate and rotate based on the simulated physiological constraints, such as ligamentous laxity characteristics (DesJardins et al., 2007; Reinders et al., 2015b). FE is displacement controlled and AL is load controlled in both simulator concepts. Alongside patient driven gait data, force controlled simulations have the ability to generate more accurate clinically relevant motions of TAR patients (Reinders et al., 2015b). Conversely, the force-controlled conditions are associated with more variables, as the effect of ligaments and muscles are included within the calculation of simulator kinematics, and are therefore more difficult to implement. Ho et al. (2020) reinforced this finding that the implementation of force controlled simulators may present uncertainties in the resultant motion, through imitating the passive structures, making it difficult to reproduce the same experimental conditions between different TAR designs, materials and investigators (Ho et al., 2020). This may also result in more variation in the motion between the simulator stations, leading to greater inter-station variability.

In two identical sets of posterior cruciate retaining TKR which were tested under displacement and force control, the samples tested under force control ( $20.9 \pm 4.2$  mg/Mc) showed more than double ( $p = 0.034$ ) the wear of those tested under displacement control ( $9.2 \pm 0.9$  mg/Mc) (Schwenke et al., 2009). All three samples of the displacement control group developed similar wear rates, indicated by the small variance (standard deviation), while the load control group possessed substantially higher variability. The authors reported that the higher wear rate and variability observed under force control might have been due differences in the time domain throughout the simulated gait cycle (Schwenke et al., 2009). The tibial component was found to rotate much earlier under force control, which caused cross-shear to occur under the full compressive load of the third peak load (i.e. 800–2400 N during 25–45% of gait). In contrast, the displacement controlled samples went into internal rotation at a later stage of the stance phase (after the third peak force), and compression was reduced to swing phase loads. These differences in cross-shear and contact mechanics likely resulted in the higher volumetric wear.

If the current wear simulations were run under force control, the accuracy of following the intended profiles would have been more impacted in KSpn, likely due to the stiffness of the stations and variation in control of air supply. KSpn also suffered from an apparent lag phase during tibial rotation (Section 3.4.1), which under force control, may be more apparent and result

in changes to cross-shear motion. This will have likely had a significant impact on the measured wear rates, under the varying implant and simulator conditions. Therefore, to answer the aims of the wear based studies, the use of displacement control was deemed the more appropriate option to determine differences in volumetric wear.

To conclude, under the patient mechanics, the reduced ROM in the sagittal and transverse planes of the TAR compared to the recommended input profiles. This would likely result in lower wear rates compared to the ones measured in each of the simulator based studies within this thesis and from earlier literature. The international standard (ISO 22622:2019) would therefore need to be updated to replicate TAR patient-specific data, as it currently produces greater kinematic motion, particularly during FE, than the ROM evident in patients implanted with a TAR. It should be noted that the mean patient profile is generated from only a small sample size ( $n = 6$ ), so caution must be taken when extrapolating to the larger patient population implanted with the same device. A larger patient population, which consider a greater range of activities, is required to fully determine the gait mechanics. The outputs of this should be used as simulator inputs, in order to truly determine TAR wear behaviour. Furthermore, there was large variability found in each of the surgical intervention cohorts in Chapter 5, particularly in the BOX® ankle patient group. This variability should be considered in future wear simulation studies, through the combination of ‘normal’ and ‘adverse’ loading and kinematic conditions.

#### **6.1.4 Target Product Profile for Future Wear Simulator Studies**

A Target Product Profile (TPP), also commonly referred to as a Quality Target Product Profile, summarises the necessary characteristics of an innovative product to address an unmet clinical need (Cocco et al., 2020). TPPs represent the concept of ‘beginning with the goal in mind’, which establish the key features and performance specifications in advance to ensure that the new device meets the specific clinical requirement. TPPs should be seen as ‘living’ documents and can be updated as further relevant information becomes available (Cocco et al., 2020). Through the development and implementation of the wear simulator and gait based studies in this project, a TPP has been developed for future mechanical wear simulations of TAR (Table 29). The TPP contains the key features and the minimum acceptable/ideal results required to determine the wear of the chosen implant design. The ideal (future testing) mechanical simulator parameters are discussed in further in Section 6.4.

Table 29. A Target Product Profile for future wear simulations of a TAR.

Key Features	Minimum Acceptable	Ideal (Future Testing)
<b>Intended Function</b>	Joint wear simulator developed to simulate the loads and motions of ankle joint to determine the tribological behaviour of a TAR <i>in vivo</i>	
<b>Target Population</b>	Patients implanted with a TAR	
<b>Target User</b>	Bioengineers	
<b>Target User Setting</b>	University and Industry Medical Laboratories	
<b>Simulator Type</b>	Electromechanical or AMTI Multi-axis wear-testing machines	The development of an ankle specific wear simulator, without having to run the implants inverted
<b>Simulator Format</b>	Displacement or Force controlled	Force controlled simulation used to mimic the soft tissues surrounding the AJC, driven through musculoskeletal or computational models based from patient specific data. This method also allows to control AP and ML forces.
<b>Test Specimen</b>	Selected FB or MB implant design (consisting of the tibial, talar and meniscal insert)	
<b>Degrees of Freedom Controlled</b>	4	6. More research is required around the simulation of inversion/eversion, to truly mimic pronation/supination of the ankle
<b>Simulator Duration</b>	5 Mc	10 Mc or more, to demonstrate the long-term tribological behaviour of the tested implant
<b>Number of Samples/Stations</b>	6	12, which would account for a repeat of selected study
<b>Calibration</b>	After every 5 Mc	After each Mc, to ensure correct following and motions produced by each station
<b>Sample Alignment</b>	Microset applied to the metallic surfaces to verify central alignment of the device	Microset to determine initial alignment. Tekscan sensor to determine contact forces at stages throughout the gait cycle (input profile) to measure contact pressure for different alignments
<b>Simulator Input Profiles</b>	ISO 22622:2019	Patient (implant) specific data and contact loads driven from gait analysis large datasets and musculoskeletal models (based from the gait data). Inputs should also be developed for both normal and adverse conditions
<b>Activity Profiles</b>	Overground Walking	ADLs (e.g. stair climbing, uneven walking), which are run in a singular profile, to better mimic the day-to-day of a patient
<b>Soak Controls</b>	Loaded or unloaded	Loaded is the preferred option
<b>Testing Lubricant</b>	Bovine or new-born calf serum	Synovial fluid or lubricant which better replicates the natural lubricant and does not suffer from precipitation effects
<b>pH Levels</b>	Routine monitoring of the pH of the fluid test medium should be undertaken	
<b>Temperature</b>	Temperature control system, capable of maintaining the temperature of the fluid test medium at 37 °C ± 2 °C	
<b>Reproducibility</b>	Simulator output profiles should remain within ± 5% of the desired input profile throughout the gait cycle	
<b>Data Output</b>	Volumetric wear: gravimetric Topographical assessment:	Volumetric wear: µCT or CMM Topographical assessment: non-contacting (areal surface topographical parameters)

## **6.2 Limitations**

This thesis has presented a thorough investigation into the biomechanical and wear performance of a MB TAR. There are however, a number of limitations that must be considered when examining the results from the simulator and gait based studies. This section also discusses alternative techniques which could have been employed and the reasoning behind the methodologies of choice for the studies in question.

### **6.2.1 Pre-clinical Wear Simulation**

#### **6.2.1.1 Simulator**

There was not a universal ankle specific wear simulator available on the market. Therefore, in order to compare against previous TAR wear studies, all experiments were performed in two types of commercially available mechanical wear knee simulators. The tibial components were cemented into a metallic tibial fixture, which has also been used in previous TKR wear simulator studies (McEwen et al., 2015; Brockett et al., 2016). However, the components of the MB TAR had to be inverted to allow the IER profile to be applied to the tibial component, while the flexion profile was applied about the constant radius of the talar component. Although this is a standard procedure in previous displacement controlled TAR simulations (Affatato et al., 2013; Bell and Fisher 2007; Smyth et al., 2017), the inverted position of the devices may have had an influence on implant biomechanics.

Inverting the natural or replaced hip joint with respect to the anatomical position, is an accepted methodology in friction (Groves et al., 2017) and wear simulation (Affatato et al., 2008) studies. Hip implants oriented in the inverted position have been demonstrated to distribute test lubricant more evenly during motion, while subsequently reducing the temperature at the bearing surface (Affatato et al., 2008). Conversely, this effect may cause a slower rate of protein denaturation and a reduction in precipitation, causing increased wear rate as a result of a smaller protein film (Lu and McKellop, 1997). This has also been linked to entrapped wear debris within the taper connection of a hip replacement (Wight et al., 2021). These concerns were less relevant in the simulated TAR, due to the mobile nature of the bearing surfaces of the selected device design.

During the implant size study, there were issues with controlling the airflow and tuning of the pneumatic system on KSpn over the prolonged simulation period. This also resulted in an apparent lag phase across all six stations in the loading, rotation and displacement output profiles. This difference between the UoL input and output loading and kinematic profiles were not apparent in the individual wear rates for stations after the initial run-in wear stage. There were also no noticeable changes in the visual damage modes at the implant articulating surfaces. The simulator was checked a number of times every day and was always corrected (PID tuning) within 24 hours to minimise the ongoing issue. Despite the improved ability to tune the output loads and kinematics under displacement control, it was also found that KSem was unable to remain

within the maximum output tolerances of both the UoL and ISO 22622:2019 input profiles. This finding was particularly apparent for AP displacement, with both simulator designs over-shooting the maximum anterior displacement input value. However, Smyth et al. (2017) demonstrated that increasing AP displacement did not have an effect on overall wear rate of a MB TAR and the studies from this thesis also suggested the same

### **6.2.1.2 Experimental Protocol**

Implant and simulator parameter studies were carried out using one design of MB TARs. The influence of the varying testing conditions may affect other TAR designs differently. Again, caution must be taken when comparing wear rates between different studies which use a variety of experimental conditions and implant designs. Both implant parameter wear simulations were also run for a period of 5Mc, which is the recommended simulator duration as per ISO 22622:2019. However, previous pedometer measurements have revealed that active knee replacement patients walked 3.5 times the number of steps per day, compared to simulator recommended durations (Schmalzried et al., 1998). TAR patients will undergo a wider range of loads and motions during a variety of ADLs, when compared to the cyclic walking motion which is simulated. Therefore, future simulations should be carried out over a longer testing duration under a variety of loads, kinematics and ADLs (Section 6.4).

At the end of each Mc, samples were moved between stations to account for the effect of inter-station variability. There was a potential that one station within each simulator used could have caused higher wear, but this was consistently disproven and no definitive pattern was discovered for wear across the six stations. This finding could have led to subsequent studies of this project abandoning the idea of moving samples between stations. Moving samples between stations may have also caused an increased risk of component malalignment, particularly with the frequency (every Mc). Malalignment is known to have a significant negative effect on contact mechanics, causing a loss of joint congruency, reduction of contact area, increased focal stresses, edge loading and potential risk of dislocation and polyethylene cracking (Uselli et al., 2017). This risk was heightened within the implant size study, through having to adjust stations between different sized samples. However, this confounding factor was reduced with the use of a Microset (Microset 101 FF, Microset Products Ltd, UK) to ensure continued alignment throughout the wear studies.

There were reported differences between stations in terms of kinematic following, particularly in KSpn (Section 3.4.1). This was likely due to the requirement to control the airflow and tuning (PID control parameters) between stations. Despite controlling these factors, some of the stations of KSpn remained stiffer and were unable to fully reproduce the desired loading and kinematic input conditions. The moving of components acted as a precaution of this effect having an influence on mean wear rates. More importantly, the wear studies set out to determine variation within condition changes instead of specific samples. Therefore, by moving samples

across each station, this limited the impact of the specific simulator stations instead of confounding it.

Digital images of the inserts at completion of the implant size study were obtained and manual tracing of the superior insert imprint on the tibial bearing surface was performed to calculate the percentage of the contact wear area on ImageJ software. A similar method was used by Brockett et al. (2012) who calculated the wear scar area as a percentage of the overall superior insert surface of a TKR using Image Pro Plus (Media Cybernetics, USA) software. This was performed to acknowledge that both implant sizes have comparable contact wear area during the simulated walking conditions. There are more advanced methodologies available to calculate the contact area including pressure sensors, such as Tekscan (Boston, USA), which have been used to measure the contact pressures and area in both natural tissue and joint replacements under static and dynamic loading conditions (Wilharm et al., 2013; Bedi et al., 2013; Wang et al., 2014). However, this type of pressure sensor can only be used at a flat bearing interface, which the BOX® ankle does not possess. The sensors are also highly sensitive to increased loads and adding a layer in between the bearing surfaces, could have effected implant wear rate.

The lubricant used was 25% bovine serum, diluted with 0.04% sodium azide solution to retard bacterial growth. This is the most commonly used protein lubricant concentration in artificial joint studies (Wang et al., 2004; Galvin et al., 2007) and has been found to provide clinically relevant wear rates and wear debris (Wang et al., 1996a; Bigsby et al. 1997; Besong et al. 1999). A hip simulator study comparing the influence of distilled water and bovine serum on conventional UHMWPE wear found that the use of bovine serum resulted in wear particles of a similar size to those found *in vivo* (Wang et al. 1996a). There was also no evidence of a transfer film on the femoral head, which follows a similar pattern on retrieval hip implants (Wang et al. 1996a). However, when distilled water was used, there were significantly larger wear particles and a transfer film on the femoral heads, which have been found on hip explants (Couto et al., 2020).

Bovine serum degrades over time and needs to be changed regularly. During a serum change, there is a possibility that the wear particles were removed from the testing environment. Replacing the lubricant is critical for *in vitro* studies to maintain the protein content. However, the main issue surrounding this lubricant choice is the raised levels of precipitated proteins (Lu and McKellop, 1997; Liao et al., 2003). The increase in proteins can cause a significant drop in wear rate due to the denaturalisation and remaining insoluble proteins that form an unphysiological protective layer at the bearing surface (Ghosh et al., 2015). The protein concentration within the test lubricant did contain a similar volume found in the natural joint capsule (Saari et al., 1993) (Appendix D) and the bearing surfaces visually presented comparable UHMWPE adhesive wear and other damage modes to previously simulated (Smyth et al., 2017) and retrieved TAR cohorts.

The lubricant temperature was not measured during each of the wear simulations. The constant articulation of the bearing surfaces, combined with the enclosed capsule where the serum is contained, likely caused temperatures to be higher than room temperature. Increased temperatures have also been found to cause higher wear rates in metal-on-UHMWPE hips (Tateiwa et al., 2006) and knees (Cowie et al., 2019) in protein rich bovine serum. This finding may be due to the effect of excessive precipitation, which causes the gradual depletion of the soluble proteins within the lubricant and effects their ability to promote boundary lubrication at the bearing surface (Lu and McKellop, 1997). This may lead to accelerated adhesive wear and subsequently increased implant wear rate. A previous wear test of TARs at the UoL determined the average capsule temperature of bovine serum to be approximately 30°C, through the use of a calibrated thermocouple (Smyth et al., 2017). This was significantly lower than the recommended lubricant temperature of  $37^{\circ} \pm 2^{\circ} \text{C}$  in ISO 22622:2019, which is reflective of core body temperature. However, Palmieri et al. (2006) measured the natural ankle surface temperature to be  $29.6 \pm 3.0^{\circ} \text{C}$  compared to the core temperature of  $36.4 \pm 1.4^{\circ} \text{C}$ . This suggests that performing TAR wear simulations at room temperature was deemed appropriate, in order to maintain serum temperature similar to that of *in vivo*.

A final limitation with the experimental protocol was that each of the simulator studies performed had a sample size of five or six, which may lessen the effectiveness and power of the study. Caution must be taken when extrapolating the data from each simulator study to demonstrate the wear behaviour MB implants. However, the samples used in the study were machined within specific tolerances for both the metallic and polyethylene components, resulting in reduced variance compared to natural bearing wear simulations, which would require much greater samples to confirm potential meaningful findings. It should be noted that the number of samples selected in the simulator studies were comparable to the previously published literature (ranging from 3-6), which were used to determine differences in wear rates between varying implant materials (Kincaid et al., 2013; Bischoff et al., 2015; Schipper et al., 2018) and kinematic conditions (Bell and Fisher, 2007; Smyth et al., 2017). The pneumatic and electromechanical simulators were also limited to six stations, meaning that the maximum number of samples were used in each of the simulator based studies.

ISO 22622:2019 recommends a minimum of three test specimens to represent the wear of a specific implant design, so the studies reported in this thesis comply well with the standard. It is also important to consider that the effects of implant and simulator parameters were performing using a single design of MB TAR, and the influence of the varying conditions may differ with difference TAR designs. Therefore, future work is required to verify the findings on the specific TAR design selected in this thesis, as well as using the same methodological approach on other implant designs, to allow for comparison of implant wear rates and topographical changes.

### 6.2.1.3 Gravimetric Wear Assessment

The study relied on the gravimetric assessment for quantifying volumetric wear, which is the most commonly used method to determine wear loss in artificial joint simulations (Shen et al., 2019). UHMWPE is a porous structure, which will readily absorb the lubricant surrounding it during simulation, which in turn, increases the mass of the measured components. The effect of serum absorption was accounted for through the use of unloaded soak controls for each simulation study. Due to the availability from the manufacturer, the accelerated artificially aged and simulator parameter study conditions only had one unloaded control, while the implant size study had two for each size. This may have posed an issue due to the variability in fluid uptake of the conventional UHMWPE, which are susceptible to temperature as a result of fluid absorption. Before each insert was weighed, they went through a standard cleaning and drying process, which also helped eliminate the influence of fluid uptake and contamination at the bearing surfaces (Aurora et al., 2006; Hu et al., 2014). However, the embedded particles and protein layers produced during motion may be removed in the cleaning processes (Shen et al., 2019).

The unloaded controls were placed in the simulator alongside the test samples to maintain consistent experimental conditions. However, as the inserts were not placed under load, this method may not have fully accounted for fluid uptake. Early studies reported that conventional UHMWPE pins placed under dynamic loading possessed significantly higher fluid uptake compared to those soaked under static and no loads (Schwenke et al., 2006). This has also been reported in knee replacements, with the mean correction from loaded soak controls measuring  $1.65 \pm 0.88$  mg/Mc compared to the lower correction of  $0.89 \pm 0.85$  mg/Mc for the unloaded soak controls (Haider, 2016). Conversely, both cases resulted in an increased net wear rate from the apparent gravimetric measurements, with significance of these volumes being dependent on the wear rate of the knee replacement samples themselves (Haider, 2016). The large variability associated in the loading output profiles produced in KSpn would have affected loaded control samples significantly, causing greater variation between the samples compared to unloaded samples.

Differences in applied load of as little as 6%, has previously been found to cause a significant change in fluid uptake of loaded conventional UHMWPE liners (Yao et al., 2001). Smaller loads between stations may have increased the volume of fluid being pumped into the liners over each cycle, affecting wear measurements. As the process of correcting for fluid absorption for the unloaded soak control inserts was constant across the simulation studies, this method was considered to be reliable enough to compare between implant and parameter conditions. Another limitation with gravimetric measurements is the potential presence of embedded metallic particles within the polyethylene components. These particles may cause an increase in mass of the polyethylene inserts, resulting in an inaccurate evaluation of the wear volume.

A final limitation associated with gravimetric assessment is the assumption in the volumetric wear calculation of the polyethylene density. The material density of the specific device used in this study (BOX® ankle) was unobtainable, therefore a UHMWPE density of 935.5 kg/m<sup>3</sup>, which was in the middle of the density recommended in ISO 5834-2:2019 was selected. This was also the same value used by Smyth et al. (2017) in a previous wear simulator study on another third generation MB device. The volumetric wear calculation also assumed that the density of the conventional UHMWPE remained uniformly distributed, which is unlikely to be the case. In newer designs, such as vitamin E infused UHMWPE used in the Rebalance® (Zimmer-Biomet, Indiana, USA), the material density will be different to that of known characteristics of conventional UHMWPE. This has triggered the development of other volumetric measurements to determine implant wear.

Coordinate Measuring Machines (CMM) offers the opportunity for calculating linear and volumetric wear, wear scar distribution and creep for individual components through the use of a contact probing (Kop and Swarts, 2007; Blunt et al., 2008). The probe takes sequential coordinates across the entire surface of an implants bearing surface, with the denser the population of points, the increased accuracy of the wear scar being characterised (Bills et al., 2005). Unlike gravimetric assessments, this method is not affected by the fluid absorption of the polyethylene inserts. This technique has successfully been used to measure the volumetric wear of THR (Bills et al., 2012; Uddin et al., 2016; Hua and Li, 2020) and TKR (Muratoglu et al., 2003; Bills et al., 2005; Blunt et al., 2008). However, only one study to date has used this method, but was used to compare surface deviations and damage modes of three explanted BOX® ankle bearing inserts (Affatato et al., 2009). The linear penetration of the superior insert surface was between 0.025 to 0.091 mm compared to a computational model of the same component (Affatato et al., 2009).

Another technique which has grown interest in the last decade in the measurement of volumetric wear is micro computed tomography ( $\mu$ CT). This method had been used in earlier studies focused on meniscal inserts of TKR (Teeter et al., 2011a; Teeter et al., 2014). Teeter et al. (2011a) compared unworn TKR inserts using gravimetric and  $\mu$ CT to determine volumetric wear loss. The study demonstrated no statistical significant difference between the two measurement methods (0.04%). This technique has also been used on acetabular liners in THR (Teeter et al., 2010; Affatato et al., 2017), spinal disks replacements (Vicars et al., 2009) and glenoid components of total shoulder replacements (Day et al., 2012).

The main advantage of both methods is the ability to measure the actual density of the polyethylene component (Teeter et al., 2017), which gravimetric assessments used in this study could only estimate.  $\mu$ CT analysis also provides spatial information of volumetric wear loss, which can be related to component alignment and specific locations where damage modes were identified. Conversely, gravimetric analysis can only measure non-specific volume loss of the selected component. However,  $\mu$ CT has not yet been used to measure volumetric changes in

TAR. Since gravimetric analysis relies on a reference measurement, it is not possible to use this technique when examining the wear of retrieved samples. This is an important factor, as analysing the wear of retrieved devices (which have not failed) is required to fully determine if the simulator generated wear rates are comparable to what is seen clinically. However, no study to date has determined the volumetric wear of ex vivo TARs. Future analysis of both *in vitro* and retrieved implants could benefit from using both these techniques over gravimetric measurements, to provide quantitative measures of volumetric wear. Nevertheless, each technique is not without limitations.

The clamping and probing forces during CMM measurements may induce deformations to the polyethylene components of joint replacements, which may not be visible when comparing the volumetric wear with and without reference (Jiang et al., 2018). This needs to be accounted for as an uncertain contribution, similar to the effect of contacting profilometry when assessing topographical changes (Section 6.2.1.4). Spinelli et al. (2009) also found that CMM measurements tended to overestimate the volumetric wear compared to gravimetric assessments, which highlighted the significance of the choice of the “time scale for creep evaluation”.

When measuring using  $\mu$ CT, metal artefacts may be present in certain TAR models. The polyethylene component of the STAR™ (Stryker) contains radiopaque markers used to identify liner displacement or fracture (Lin et al., 2022). This may create erroneous data points within the  $\mu$ CT imaging, which would require post-processing and may be difficult to remove. In an ideal situation, the radiopaque markers would be removed before measurements would be taken, but this may result in damaging the bearing insert. This may not have been an issue in the device used in this project, but would possibly limited the comparison of volumetric wear between implant designs using this technique. The use of  $\mu$ CT technology is known to be highly dependent on the resolution selected (Teeter et al., 2011a) and requires a threshold to be determined for volumetric analysis (Jiang et al., 2018). It has previously been reported that  $\mu$ CT caused an increased measured volumetric wear compared to gravimetric analysis (Jiang et al., 2018), which was related to errors in thresholding and in the scanner, causing a reduced intensity of the image (Kinzel et al., 2004). The measurement time cost for both CMM and  $\mu$ CT is considerably longer than gravimetric analysis, which can take up to 40-90 minutes per scan (Jiang et al., 2018).

The significant limitation with both techniques is the requirement to define the pre-worn reference surface, in order to determine volumetric material loss (Vicars et al., 2009). This may be in the form of computational models or in this projects case, the pre-worn samples from the *in vitro* simulator studies of the same component. This may not represent the geometrical differences produced during the manufacturing process as there can be variances in geometry of new unused UHMWPE bearing inserts of different manufacturing lots and design tolerances (Teeter et al., 2013). Average manufacturing variance of six TKR inserts has been found to be as much as  $15 \pm 59 \mu\text{m}$  (Teeter et al., 2011b).

THR possess spherical femoral heads and acetabulum cups that have a defined radius within a defined tolerance. This allows the original reference pre-worn surface to be estimated relatively easily (Lord et al., 2015). In the fully conforming MB device used in the studies, the inferior and superior surfaces are both articulating with the metallic surfaces, meaning that there is no unworn datum on the surface to compare pre-and post-simulation measurements. The polyethylene inserts will have also undergone creep deformation, which are known to attain a steady-state after one Mc (Estok et al., 2005). Another issue with using this technique with TAR, is their free form geometry, which means that the implants have no rotational symmetry. TAR components possess multiple radii in both anterior/posterior and medial/lateral directions, with multiple centres of rotation. This results in a reduction in reference planes, increasing the difficulty to calibrate the process (Charlton and Blunt, 2008). All of these issues associated with both techniques mean that determining reference surfaces for use in assessing non-homogenous groups of TAR is not easily achieved.

It should be noted that all previous TAR simulator based studies relied on gravimetric measurements to determine volumetric loss (Affatato et al. 2007; Bell et al. 2007; Postak et al. 2008; Bischoff et al. 2015; Reinders et al. 2015b; Smyth et al., 2017; Schipper et al., 2018). Therefore, by using the same method, it allowed for a more reliable comparison between wear based studies. The study also ensured that the combination of volumetric wear, surface topography and damage mode visualisation were included, to better understand the tribological behaviour of a MB implant.

#### **6.2.1.4 Surface Topographic Assessment**

Surface roughness parameters were measured at the beginning (0 Mc) and end (3-5 Mc) of each wear simulation study. This allowed for the determination of substantial roughness changes at the bearing surface at the two measurement points. Without the time constraints on the project, roughness measurements would have been taken after every Mc to determine the change in surface topography throughout the testing duration. This would have been particularly of interest between 0-1 Mc, as this signifies the run-in wear phase of the implants, where higher wear rates were observed compared to steady-state (1-5 Mc). An increased number of measurement points would have improved the limited understanding of topographical changes of a MB device and future work should consider this moving forward.

A contacting profilometer was used to measure surface topographical changes at each of the articulating surfaces of the MB device. This contacting method is the most commonly used technique in the ankle literature (Bell and Fisher, 2007; Smyth et al., 2017). The two previous studies only measured surface roughness (Ra), which cannot be used to fully define topography of a surface (Leach, 2010). This is because the same roughness value can represent surfaces with substantially different surface profiles, which will likely have varying skewed distribution and impact on implant wear. Therefore, the current wear studies considered a number of topographical parameters, including skewness (Rsk) and kurtosis (Rku), which provided a

measure of the shape of the profile and indication of valleys in the surface for lubricant retention, respectively. However, both these measurements are less mathematically stable than the other roughness parameters used in this study. They use 3rd and 4th order differentiations in defining equations, which can result in errors in the calculation of these parameters and may also be the reason for the wider CL and variability between results.

With the use of a contacting stylus profilometer, there are limitations associated with the damage that is caused to the polyethylene bearing surfaces (De Groot, 2017). Despite only millinewton forces travelling through the diamond stylus, these forces are concentrated at the tip diameter, which generated enough contact stresses that caused fine scratching, perpendicular to the measurement surface (Leach and Hart, 2002). This was different to the multidirectional scratching observed at the bearing surfaces and in the opposite direction to AP related linear scratching seen on the talar components. This meant that the minor damage was not mistaken in damage mode comparison between bearing surfaces under different simulator conditions. A further limitation of the contacting stylus methodology was the potential for the tip to 'lift-off' as it moves across the surface as a result of the scanning velocity being too high (Pawlus and Śmieszek, 2005; Mathia et al., 2011). To counteract this, a slow trace speed of 0.5 mm/s was used for each bearing surface material and had previously been used in TAR research with no reports of 'lift-off' occurring on the bearing surfaces (Smyth et al., 2017). The conical shape of the stylus tip may have also prevented the tip from being able to distinguish the peaks or troughs accurately and there is always an element of smoothing of the measurement data that occurs (De Groot, 2017).

The major assumption with this contacting method is that the entire surface topography of the bearing surface was assumed to be the same as the five representative traces that were measured. This is an unrealistic assumption for a component that has undergone damage. The roughness parameters calculated from the single line traces are also highly dependent on the direction and orientation of the sweep. One way to reduce this sampling error and provide an improved approximation of the overall surface roughness of the bearing surfaces would be to map the entire surface using digital stitching of the measurement results. However, this technique was not possible with the technology available for use within this thesis.

Optical profilometer (microscope based) techniques have been developed to measure areal surface roughness parameters. This method used interferometry to construct or destruct superposition of light waves between the reference beam and a second beam, which is reflected from the bearing surface being studied (Hocken et al., 2005). This technique has the advantage of higher acquisition speed, improved resolution and removes the risk of surface damage, which is associated with the stylus instrument (De Groot, 2017). The non-contact Infinite Focus microscope (Alicona, Austria) was only used in the simulator based studies to determine the damage modes on the superior insert bearing surface. This technique could have been used to

determine the roughness parameters across the whole bearing surface, as well as specific areas where the greatest signs of damage modes were imaged, providing an improved discretisation of the data. Previous studies have used this technique to measure wear characteristics of retrieved (Liza et al., 2011) and wear simulated (Holland et al., 2018) TKR inserts, with the latter suggesting that both wear simulated and retrieved implants display similar characteristics of surface topography across the bearing surface. However, there are still limitations with this technique which limits its use in joint replacement, but particularly for TAR.

Quantitative light microscopes have been found to overestimate surface roughness parameters, primarily due to the diffraction and dispersion effect, which causes variances between the surface height measurements (Lehmann et al., 2014). The polyethylene bearing surfaces are opaque and have limited reflectivity, which causes material absorption and results in reduced quality of signal obtained. The metallic surfaces are highly reflective, making it difficult to focus on certain areas on the surface and the production of large bright spots of missing scanned data due to dispersion of the light. This makes it challenging to measure roughness of joint replacement bearing surfaces. Optical metrology techniques are also limited by the ability to accurately measure curved surfaces (Gao et al., 2008). The InfiniteFocus microscope used in the wear simulator studies could measure surface height information for slopes up to 20°. This would have been sufficient to characterise the superior bearing insert surface, but would have failed to measure the inferior bearing insert surface as the curves are too steep for this non-contacting profilometer to measure.

A final limitation of non-contact techniques is the high computing power to process data generated from larger surface areas (De Groot, 2017). The lowest available microscope lens (10x magnification) was used to image the full superior insert surface, but to improve the roughness measurements which could be obtained, a higher resolution (20-50x magnification) should be used. However, would mean that the scanning time would substantially increase and would still involve the stitching of multiple datasets. This was not feasible in the current project timescale. Therefore, despite the limitations of the stylus based measurements in this study, until vast improvements are made in optical methods, this methodology will remain the researcher choice for determining implant surface roughness parameters.

Regardless of the associated limitations within the wear simulator studies, the methodology developed in the similar based studies provided a good approximation for the clinical wear rates of the MB device, under a range of implant and simulator conditions. Such estimations can be used to predict the risk associated with wear mediated osteolysis and subsequent adverse immune reactions, leading to the loosening of the implant and early failure.

## 6.2.2 Gait Analysis

### 6.2.2.1 Participant Population

The sample size used in this study contained 21 patients separated into three patient cohorts (9 AA; 6 mixed TAR; and 6 BOX® ankle). This relatively small sample mirrors most gait studies comparing AA and TAR, which range between 5 and 17 participants per group (Piriou et al., 2008; Hahn et al., 2012; Flavin et al., 2013; Singer et al., 2013; Seo et al., 2017; Segal et al., 2018; Sanders et al., 2021). The small sample size may therefore represent groups of unique individual results, rather than a closely assembled group which all acted in a comparable manner. Each of the patient groups were self-selected, which was most apparent in the mixed TAR cohort. This patient cohort was made up of three different implant designs (4 = Rebalance®; 1 = Mobility®; 1 = INFINITY®), which questions the information gained from analysis of samples of  $n = 1$ . It should be noted that this group was used as a comparator against the BOX® ankle and a much larger population is required to truly determine the gait mechanics of these three implant types. The study was limited by the volume of TAR patients available at both research sites, particularly during the COVID-19 pandemic, which also resulted in the small sample sizes. In the ideal situation, the gait study would have used a comparison TAR cohort implanted with the same device.

The small sample sizes led to large variability among the patient populations in most of the outcome measures of interest, particularly in the BOX® ankle cohort. This suggests that the surgical intervention is patient dependent and impacts the recipient in varying ways. This was also supported by the large variance in PROMs information. Thus, caution must be taken when extrapolating results, as they may not be representative of larger patient populations. These reasons also why this study explored trends between the patient cohorts and highlighted the areas of differences that warrant further explanation and investigation. Larger scale studies, which are appropriately powered, would identify further improvements in surgical interventions more accurately.

The BOX® ankle patient cohort was even more limited by the number of patients that met the inclusion criteria, coupled with patients being unable to participate in the study due to COVID-19 restrictions. A number of the patients who took part in the study were also implanted with either a hip or knee replacement, which is likely one reason for the large variability within and between patient cohorts. However, removing patients from the study that had received other lower limb joint replacements would mean result in study did not representing the true patient population.

Within the gait study, there was no inclusion of a healthy control group, to examine the differences between surgical interventions and healthy participants. Instead, the aim was to compare how each patient cohort's gait mechanics differed at an intermediate implantation period. Whilst the study could have compared this data to the results from the pilot study

(Appendix G), which used the same experimental protocol, this participant population were not age or weight matched. This would likely have led to a high volume of significant differences in gait outcomes. Preoperative gait analysis was also not included in this study. The presence of a pre-operative would have provided information on the pre-existing gait differences between the patient cohorts and to what extent the surgical intervention had on patient biomechanics during overground walking. However, pre-operative data in these patient populations would present gait deficiencies associated with end-stage ankle OA, which has been reported in the previous literature and out the scope of this project (Valderrabano et al., 2007; Horisberger et al., 2009). Additionally, the significant time constraints on the project did not allow for pre-operative patient data to be collected. The exclusion criteria also restricted patients being included within one-year post-surgery. These patient populations were likely to still be affected by the surgical procedure, which could mask the true biomechanical ability, which can be measured in patients at an intermediate follow-up.

The non-randomisation of the allotted treatment option is another limitation. However, randomisation was not ethically possible in the patients within this study, since the surgical intervention was chosen based on the recommended indications and surgeon choice, combined with the fact this was a retrospective study. The absence of randomisation may bias the functional outcome and gait parameter results when comparing between patient cohorts. The study did not aim to compare the superiority of each surgical option over the other, rather the purpose was to understand the effect on adjacent and proximal joint gait mechanics after treatments. The findings of the study should be used to drive a larger RCT, which would enable the discovery of smaller significant differences between treatment options.

#### **6.2.2.2 Data Collection**

The first limitation associated with the data collection method was the inability of the IOR foot model to separately segment the subtalar joint. Fluoroscopic assessment, used to measure joint motion, was unavailable at both research sites, while bone-pin based models were unethical to use in the patient populations. Due to the highly invasive nature of bone-pin markers, skin-mounted markers were placed to represent the underlying anatomical bony landmarks of the segment of interest. Marker locations can be detected with sub-millimetre accuracy (Topley and Richards, 2020; Cunningham and Brooks, 2022) and were used to determine the location and orientation of the lower limb body segments, in order to calculate joint position and angles (Miranda et al., 2013). However, the relative motion between a marker and its corresponding bone represents an artefact, commonly referred to as a STA (Cappozzo et al., 1997; Camomilla et al., 2017).

STAs are regarded as the most critical source of error in human motion analyses, affecting the accuracy of the derived kinematic measurements (Leardini et al., 2005). STAs are influenced by the presence of skin viscoelasticity, muscle contractions, and shifting of subcutaneous masses

(Leardini et al., 2005). This can lead to errors in the estimation of joint centres, marker location, skeletal segment positioning and joint kinematics (Arndt et al., 2004; C. Nester et al., 2007). A previous study found joint centre translational and rotational errors as high as 0.3 mm and 0.44°, respectively (Miranda et al., 2011).

As the distances between markers of the foot are small, any form of displacement can result in relatively large angular errors compared to markers spaced further apart (Schallig et al., 2021b). Previous literature has demonstrated that STAs of foot markers are variable across participants and marker location, but have a greater potential to significantly influence measured kinematics (Reinschmidt et al., 1997; Tranberg and Karlsson, 1998; Okita et al., 2009; Chen et al., 2011; Birch and Deschamps, 2011; Schallig et al., 2021b). STA has been reported to cause angular errors to be as much as 2.45°, 3.57° and 4.28° in dorsi-/plantarflexion, inversion/eversion and IER angles, respectively (Kessler et al., 2019). It should be considered however, that STA will have affected each patient cohort kinematics similarly, allowing for comparative analysis. The study also filtered the kinematic data, which has been proven to help reduce some of the associated soft tissue error (Peters et al., 2010). However, without using bone mounted markers, this error cannot be eliminated (Benoit et al., 2006) and STA will continue to limit studies using marker-based methods.

There is a rapidly growing interest in the use of markerless motion capture, which utilises standard video and deep learning-based software to record and identify movement without markers (Wade et al., 2022). This process removes the errors associated with STA, which are inherent in marker-based methods, as well as decreasing data collection and processing time (Moro et al., 2022). Furthermore, markerless methods enable clinicians to collect data while patients are wearing their normal clothing, instead of patients being asked to wear tight-fitting clothing, which may influence their gait (Wade et al., 2022). This could allow systems to be set up in a patients' home setting or communal areas in care homes, facilitating data collection of an increased number of patients in one day, in an environment less likely to alter their gait (Robles-García et al., 2015). However, markerless motion capture has not been taken up by the majority of the biomechanical industry, primarily due to inaccuracy surrounding the detection of joint centre locations (Harsted et al., 2019) and the fact that it requires greater understanding of computational and programming algorithms.

The potential error associated with STA affected the lower limb angle, moment and power data, but was reduced through accurate marker placement by a single evaluator. Consistent and accurate marker positioning is critical to obtaining reliable and meaningful joint kinematics (Della Croce et al., 2005), particularly in MFM, where repeatability between evaluators and days is primarily subject to variability of marker placement (Carson et al., 2001). This variability has been reported to be around 5 mm, with outliers up to 13 mm between evaluators (Bishop et al., 2013; Deschamps et al., 2014). More recently, marker placement sensitivity for the IOR foot model

was determined in a range of foot sizes (Schallig et al., 2021a). The authors found that the most sensitive value (calculated through linear regressions) occurred at the base of the second metatarsal and that foot size had a small effect on 40% of sensitivity values (Schallig et al., 2021a). Other studies have demonstrated that the IOR foot model is highly repeatable, with a variability of approximately 2-3° offsets across walking trials (Caravaggi et al., 2011; Deschamps et al., 2012a; Mahaffey et al., 2013). Therefore, the current study used a single evaluator with 5 years' experience in gait analysis of the lower limb to measure all patient populations.

All overground walking trials were performed under barefoot conditions. In the elderly population (65+), which the majority of the patients within the study were, approximately 20-30% habitually walk barefoot or in socks within their homes (Bates et al., 1999), due to reasons of convenience and comfort (Menant et al., 2008). Most of the other activities the patients would perform outside of their home will involve the use of footwear. There have been a number of studies that have compared the effect of barefoot and shod conditions on gait mechanics, with the former being associated with decreased walking speed (Moreno-Hernández et al., 2010), stride length (Lythgo et al., 2009), and hip and knee joint moments (Keenan et al., 2011), while increasing cadence (Wolf et al., 2008), knee flexion (Zhang et al., 2013) and ankle plantarflexion angles (Oeffinger et al., 1999). The above changes in gait mechanics coincide with a more cautious gait and suggests that walking barefoot is associated with a greater balance threat than shod conditions (Tsai and Lin, 2013). This means that the differences observed in the gait study may be different when patients wear their own footwear.

Studies that have previously examined the influence of footwear on foot and lower limb function either introduce an unfamiliar footwear to participants, or compares the foot functions of participants with different footwear use history, with both study types likely causing alterations to patient gait patterns. The barefoot condition also removes the influence of cushioning in footwear, which has been associated with having the greatest influence on knee and foot kinematics (Zhang et al., 2013), which may have masked the differences between the patient cohorts.

Another reason for the study being performed in barefoot was that there would have been certain movement of the foot within any shod condition selected, thus questionable as to whether retroreflective markers positioned on the shoe directly, provide comparable results to those markers placed on the foot itself. Modifying the shoes, via cutting holes directly into the shoe itself, may have allowed the exact positioning of the markers onto the patients skin (Sinclair et al., 2013). Cutting holes into the footwear in order to directly attach markers to the skin would compromise the structural integrity of the upper material of the footwear, resulting in changes to the properties of the footwear. This method has previously been used to examine the effect of footwear on MFM kinematics (Shultz et al., 2011; Bishop et al., 2013), with the optimum size of material removed without disrupting footwear integrity to be 25 mm. However, these

modifications mean that the footwear used in the earlier studies are not representative of sports trainers, work or office footwear. Further research is required investigate the effect of MFM in a range of footwear types. Another limitation to cutting holes in the shoe is that the position of these holes may change between participants, therefore not measuring the correct anatomical positions.

A significant drawback with marker-based motion capture used in the study, was the requirement of a controlled environment which the patient groups had to attend, in order to collect reliable 3D data (Buckley et al., 2019). There is a potential that the patients altered their usual gait patterns due to having markers placed on their body, alongside their awareness of being under observation (Robles-García et al., 2015). However, the patients were given plenty of time to adjust to the motion capture facility and a number of practice trials were performed before any data was collected.

### **6.2.2.3 Data Analysis**

Due to the relatively small sample sizes in all three patient cohorts, only descriptive statistics in the form of mean and CL of peak and ROM parameters were determined for all three planes of motion. Other studies of similar cohort sizes have used multiple parametric and non-parametric tests, with additional adjustments in the form of post-hoc corrections, to determine significant differences between the chosen parameters. However, the number of biomechanical parameters compared in this study would result in the need for an inappropriately large number of post-hoc corrections, which would result in interpretation error and increased likelihood of a false positive result. Therefore, the results of some of the previous comparison gait studies, which performed multiple tests, should be treated with caution. Further studies are required to validate the post-operative exploratory findings in larger patient populations. These should focus on hypothesis driven studies, which limit adjustments and testing.

## **6.3 Overall Conclusions**

The aim of this research was to use experimental simulation and gait analysis methodologies to further understand the biomechanical (*in vivo*) and wear (*in vitro*) behaviour of a MB TAR. This aim and the subsequent research objectives have been realised through the presentation of the results and discussions in the preceding chapters of this thesis. This work has contributed to the growing body of knowledge within the field of TAR, with the following set of conclusions providing insights from the results of the studies performed.

### **6.3.1 Wear Effects of Implant Parameters**

- Under the same loading and motion conditions, the mean wear rates, contact wear area and topographical changes were unaffected by the different implant sizes, which may be of interest during intra-operative selection of an implant for varying patient anatomies

- There was a positive indication in which the accelerated artificial ageing process caused increased wear rate compared to non-aged implants during the steady-state phase. However, none of the conventional UHMWPE inserts were found to fracture or present signs of structural failure
- The wear rates from the MB device, independent of implant sizes and artificial ageing, seemed to be comparable to previous TAR wear studies using conventional UHMWPE under displacement control
- The simulation produced certain wear damage modes that were similar to those observed in retrieved prostheses, with abrasive wear, burnishing and multi-directional scratching being the pre-dominant wear mechanisms

### **6.3.2 Wear Effects of Simulator Parameters**

- In the simulator type study, discrepancies were found in the ability of each of the simulator designs to follow the UoL gait input profiles, with KSem appearing to produce more comparable loading and kinematic outputs, when compared to KSpn. However the differences in loading magnitudes and kinematic outputs appeared to have no significant effect on the measured wear rates between simulator types
- Assessment of the topographical and visual damage changes tended to support the findings that both simulator designs yielded comparable wear results under the same experimental conditions and simulator input profiles
- Despite the comparable wear and topographical results, the use of KSem is preferable in future pre-clinical simulations, due to the improved capability of replicating varying input profiles, which will be more important when assessing different ADLs and input conditions
- The change in loading and kinematic input profiles to the recommended ISO 22622:2019 after 3 Mc under UoL conditions, were not sufficient to significantly change the tribological conditions of the MB TAR
- There is a great need for further investigation using the latest ISO 22622:2019 input profiles and experimental conditions to enhance the understanding of implant wear, which will allow for direct comparison between wear studies with more controlled comparable parameters
- The wear rates produced from both simulator parameter conditions were comparable to the TAR wear literature, while some of the observed damage modes were similar to previously simulated and retrieval MB devices

### **6.3.3 Biomechanical Effects of Ankle Arthrodesis and Total Ankle Replacement**

- Despite the small PROMs, spatiotemporal and functional differences between the patient cohorts at an intermediate follow-up, the trends in increased hindfoot motion and peak ankle joint power in TAR patients indicates that this surgical intervention may be favoured for

treating end-stage arthritic patients. A much larger, powered study must be performed to truly determine the biomechanical differences reported in this study

- The MB implant (BOX® ankle) used in both wear simulator studies tended to show improved sagittal and frontal plane hindfoot motion compared to AA patients, which was likely a result of the ligament conserving design of the device
- Hypermobility of the midfoot and forefoot segments found in the AA patients may act as a compensatory mechanism to the reduced motion at the fused AJC, which could result in subsequent arthritic conditions and further requirement for surgery, but larger patient cohorts are required to confirm the gait differences in this study
- The gait outcomes from this study demonstrated that alterations in foot inter-segment angles are not limited to the operated ankle joint, but also affect the distally located foot joints. This finding has further highlighted the clinical significance of MFM when evaluating the functional outcomes of AA and TAR patient populations and should be considered by surgeons when selecting which treatment option to implant
- SFM seemed to overestimate the ROM in the sagittal and frontal planes of motion when compared to the MFM hindfoot segment within the three patient cohorts
- The substantially higher peak generated power at the hip joint found in the TAR cohort suggested that these patient populations were able to retain improved functioning of the surrounding soft tissues, which likely aided patient ability to perform the overground walking trials. However, there were minor differences in proximal joint kinematics between the patient cohorts
- Both peak and ROM values in all three planes of motion were relatively comparable between patients implanted with different TAR designs, suggesting no substantial advantage of one TAR design over another
- The sagittal ROM for dorsi-/plantarflexion of the hindfoot, which was used to measure the ankle joint, was considerably lower in the BOX® ankle cohort compared to the recommended FE input profile used by both Smyth et al. (2017) and ISO 22622:2019. Hindfoot motion in the transverse plane was also lower in the BOX® ankle cohort than the recommended simulator input profiles for tibial rotation (ankle IER at the tibial component)
- The reduced ROM produced by the BOX® ankle cohort, when compared to the ISO 22622:2019 recommended input profiles, would likely result in lower wear rates, independent of implant and simulator parameters. Further research using patient population data is required to truly understand the biomechanical and wear performance of a TAR

#### **6.4 Directions of Future Research**

This thesis has made several noteworthy contributions to understanding the biomechanical and wear behaviour of a MB device. However, the results from this thesis have raised additional research questions, for which additional investigation would be beneficial. There is some

difficulty in drawing potential meaningful conclusions from previous simulator studies due to the varying experimental conditions, simulator designs, and kinematic input profiles.

This thesis introduced the use of the recently developed ISO accredited displacement wear standard (ISO 22622:2019). This set of universal experimental and input conditions will allow more compare wear rates between different research institutions and testing laboratories. However, the loading and kinematic profiles were derived from a panel of experts in the field, which use an idealised smooth curve from average input profiles taken from dated literature from healthy participant information. Thus, it is questionable how relative the profiles are to a patient implanted with a TAR. Future studies should not just rely on the recommended by ISO 22622:2019 input profiles, but rather use them as guidelines to find the ideal input profiles. The gait study (Chapter 5) demonstrated variation in kinematic outcomes across the gait cycle for different TAR designs and to the simulator input profiles used (UoL and ISO 22622:2019). This emphasises the need to run clinically relevant simulations through using patient loading and kinematic outputs.

The wear simulator studies from this thesis produced wear rates ranging from  $9.59 \pm 3.02$  to  $17.18 \pm 5.46$  mm<sup>3</sup>/Mc, which are similar to previous displacement controlled TAR testing on conventional UHMWPE ( $3.4 \pm 10.0$  to  $25.8 \pm 3.1$  mm<sup>3</sup>/Mc) (Affatato et al., 2007; Bell and Fisher, 2007; Smyth et al., 2017). However, the both the studies from this thesis and previously published work used loading and kinematic profiles driven from healthy individuals. Therefore, it cannot be claimed that the wear rates produced are clinically relevant and this remains unknown from the current literature. Future studies are needed to develop a wear simulation under loading and kinematic profiles driven from TAR patients using gait analysis techniques. This would then allow for clinically relevant wear rates to be produced for specific implant designs or patient populations, instead of relying on a 'one profile fits all' approach, which is currently recommended in ISO 22622:2019 input profiles.

Future studies should include the presence of third-body wear particles, produced from cortical bone, cement (in FB designs) or metallic/hydroxyapatite coatings. All three of third-body debris have been associated with an implants increased risk of early onset of wear-mediated osteolysis (van Wijngaarden et al., 2015; Schipper et al., 2017; Najefi et al., 2021; Kim et al., 2021). This would allow for researchers to determine the influence of third-body wear mechanisms in TAR.

Another limitation of the ISO 22622:2019 testing standard is that it assumes the peak AL, which aims to mimic the contact forces at the AJC, to be only 2365.7 N. Even the peak AL found in the UoL is marginally higher at 3150 N, approximately 4.5 times BW of a 70kg individual (Smyth et al., 2017). Although the simulator input study found no significant difference in wear rates between both profiles, a larger AL may have resulted in a different outcome. The BOX® ankle cohort had an average weight ( $\pm$  95% CL) of  $79.60 \pm 11.22$  kg, which equates to an AL of 3903.05

N to 5464.27 N (5-7 times BW) during the stance phase of walking. Therefore, it is essential that future studies also consider an individual's BMI when developing patient specific wear simulations to truly determine clinically relevant TAR wear rates.

Patients undergoing surgical interventions for end-stage ankle OA are typically younger and more active than patients suffering with hip or knee OA (Saltzman et al., 2005; Thien et al., 2014), meaning that the demands being placed on the implants are greater. Future pre-clinical evaluations should further reflect the wider range of conditions experienced during daily life, as opposed to placing reliance on the latest ISO 22622:2019 input profiles, based on data collected during walking from healthy individuals. Wear simulations should be also run for an increased number of cycles to simulate the longer life expectancy of newer generation of implants, alongside increased frequency of different activities these patients will perform with their implant device. Furthermore, wear simulator capabilities are constantly improving, enabling researchers to simulate a variety of ADL's and to test conditions beyond standard overground walking. In the last decade there has been a number of publications which have simulated ADLs including: stair ascent; stair descent; jogging; sit-to-stand from a chair; and cycling (Schwiesau et al., 2013a; Wimmer et al., 2015; Reinders et al., 2015a; Abdel-Jaber et al., 2016). However, no published studies have examined the influence of different ADLs on TAR wear.

Future work is therefore require to collect a variety of ADLs using the similar gait analysis techniques discussed in this thesis, as well as implementing them into a wear simulator for longer testing durations, in order to fully determine the tribological behaviour of a TAR for the lifetime of the device. Preferably, the developed ADLs for TAR would include programmed sequential stages, to simulate an entire typical day living for the patient population, based from data collected from the patients when performing each motor task. These simulations should also be combined with strenuous and rest periods, to further mimic the motion and loading that occurs *in vivo*. The inclusion of resting periods during level walking has been found to increase wear rates in hip replacement patients (Hadley et al., 2013), although this effect caused no significant difference for knee replacement patients (Kretzer et al., 2009). The exploitation of these complete protocols would further refine pre-clinical wear evaluations to improve the understanding of *in vivo* tribological phenomena of TAR.

Current simulators may be limited by the capacity of the machine and would have to be physically reconfigured (if possible) to run the deleterious loading and kinematic patterns from real world ADL data. The simulator is limited to 128 data points, with the gait cycle being interpolated into the simulator inputs. During ADLs with greater ROM or more complex motion paths, this may come as a problem, particularly when going from one maximum to minimum loads or kinematics in a short period of time. This problem was seen during the simulated overground walking trials in the current project, with both simulator types under or overshooting the load or kinematics desired input values. Overtime, this would likely have an influence on simulated wear rates, or

during deleterious motions of varying ADLs, an increased risk of dislocation of device, particularly with the small bearing surface of a TAR. In a previous study simulating the influence of different ADLs on a TKR, the simulator produced a smaller peak AL compared to the desired input values (ISO 14243-3:2014) during the squat motor task (Abdel-Jaber et al., 2016). The authors concluded that the reason for the simulator to underload the implants was due to the wide ranges of FE and AP translations, which required high hydraulics absorption in the simulator circuits and valves. Therefore, the development of mechanical simulators which will be able to perform these loads and motion for variety of ADLs is essential. The development of such methods will be crucial in the ongoing development of TAR, and in enhancing clinical performance, through understanding the envelope of TAR performance.

Experimental wear testing is also associated with high costs, limited accessibility to a simulator and is time consuming, due to the large number of low frequency gait cycles that are required to be run (Knight et al., 2007). For each implant or simulator parameter study run in this project, it took up to 4 months to obtain data for six samples. This means it would take up to nearly a year to generate comparative data under the same testing conditions. This would be even longer when attempting to simulate real world ADLs over the lifetime of the device. The limitations associated with mechanical simulations to run more adverse or complex motions has led researchers to turn their attention to computational alternatives. This technique has been extensively used for pre-clinical simulation of TKR (Barbour et al., 1995; Fregly et al., 2005; Abdelgaied et al., 2014; Brockett et al., 2016), but remains limited to TAR. The computational wear prediction of a TKR using a finite element analysis technique demonstrated good agreement between predicted and experimentally wear rates, with 0.94 coefficient of determination of the computational model (Abdelgaied et al., 2018). The *in silico* model could also be used to explain the differences in experimental wear trends through cross-shear, contact area and contact stress distributions between different kinematics throughout the gait cycle (Abdelgaied et al., 2018).

*In silico* wear modelling provides researchers options to explore a broader envelope of load and kinematic conditions, while being able to run multiple and parallel simulations to validate key findings, which are missed during physical simulation. This technique can be used to simulate hypothetical scenarios which do not appear in published datasets, while measuring the effect of adverse conditions such as edge loading, surgical differences and malalignment, which would be difficult to run in current mechanical simulators. Computational models of TAR would allow the researcher to pinpoint the crucial loading and kinematic conditions, which would help to develop a more comprehensive physical simulation to measure wear of joint replacements. This technique lets the user focus on the sensitivity of the outcomes, in order to correct inputs used to drive the computational model. This cannot be achieved in a mechanical simulator and would also help better design future physical simulators.

With the increased pressures on manufacturers from the Medical Device Regulation (EU) 2017/745 to demonstrate the long-term safety and performance of their medical devices, *in silico* modelling is of greater significance, as it speeds up the process of getting this required data than mechanical simulations. However, further development of computational models are required to be able to fully predict the changes found experimentally, such as plastic deformation of polyethylene material and the contribution of lubrication and its effect of the lubrication regime during motion. It is clear that the future of pre-clinical simulation requires the combination of computational and mechanical simulation to predict *in vivo* wear behaviour in TAR. These tests can help a manufacturer optimise and improve different designs before large-scale manufacturing and implantation, as well as adhering to regulatory requirements.

Future studies should look to incorporate *in vivo* loads and motion waveforms in TAR for varying ADLs. Real world hip contact forces measured through instrumented implants are different to the loading profiles of ISO 14242-1:2014, during overground walking (Bergmann et al., 2016) and when performing ADL's (Fabry et al., 2013). However, this technique is inherently invasive and only a relatively small number of patients have been implanted with an instrumented prosthesis. Therefore, the data may not represent the larger population. A recent standard guide for TKR loading profiles has been developed (ASTM F3141), which includes *in vivo* data for a number of ADLs obtained from Orthoload studies performed at the Julius Wolff Institute, Charite Universitätsmedizin Berlin. Musculoskeletal modelling provides an alternative technique in regard to the estimation of non-invasive joint contact forces and kinematics, providing a better representation of loading variability observed in the wider patient population (Zhang et al., 2015; De Pieri et al., 2018; Weinhandl and Bennett, 2019; Lunn et al., 2020). This method has recently been passed through a wear model of a hip replacement, which was developed in Matlab® for the prediction of volumetric and linear wear rates (Mattei et al., 2021). However, further development of an advanced musculoskeletal foot model is required in order to better predict TAR wear behaviour. Larger gait studies, which measure a range of ADLs and different patient characteristics (e.g. BMI) should be conducted, which can be used as inputs to the simulator.

Alongside the use of musculoskeletal modelling for TAR specific contact forces, the development of more complex virtual soft tissue simulations under force control, will improve the simulated effect of ligamentous and soft tissue restrain structures on implant kinematics. These computationally predicted kinematics could then be used as displacement control inputs. This would be particularly important when developing specific implant design or size inputs. In a force controlled simulation, these soft tissue structures can also be inputted through the force and torque actuators of the simulator, and the ligaments can be orientated in 3D. To further improve the mechanical simulation of the soft tissues acting on the AJC, AMTI multi-axial wear-testing machines should be used. This type of mechanical simulator was not available for the current project and provides improved force control functionality through the virtual soft tissue control,

which uses an advanced software model to mimic the constraining influence of the soft tissues surrounding joints. This would allow an improved simulation of the ankle to fully replicate the natural physical environment.

The gait based study is one of the only studies to directly compare the kinematic differences of AA and TAR procedures on the joints distal to the ankle. Recent studies have begun to develop MFM kinetic models alongside the kinematic models, to provide additional information regarding the overall biomechanical functioning in the AJC and distal foot joints (Deschamps et al., 2017; Eerdeken et al., 2020a; Eerdeken et al., 2020b). A greater number of validation studies are required for this methodology to be adopted by the wider research community. Moreover, future work should combine both kinetic and kinematics at a comparable intermediate to long-term follow-up post-surgery to fully establish the compensatory mechanisms occurring in the adjacent joints of the foot.

The gait comparison study was limited by the sample size in each patient cohort. To be confident in the gait outcomes presented, larger scale studies with increased patient populations in the form of a RCT, are required to validate the findings from this thesis. In addition, a larger RCT would further determine smaller significant differences between the patient groups. These RCT should also begin to compare variation in kinematics across the whole time-series and not just the peak values. This can be achieved through one-dimensional statistical parametric mapping to determine differences between surgical interventions (Pataky, 2010). This technique also permits hypothesis testing and vector kinematic trajectory to be included, with random corrections concurrently accounting for temporal correlation and vector covariance (Pataky et al., 2013).

Due to the constraints of PhD sponsorship, the simulator studies only used one MB TAR design. With the recent market trend in the UK favouring towards FB designs, adapting the experimental protocol for these implant designs, under the same conditions and input profiles, would allow improved wear and topographical comparisons between the two design options. With the improvements in optical (non-contact) measurements, future studies may also transition away from contacting stylus methodologies to analyse surface wear of the bearing surfaces in TAR. This would allow measurements to be performed quickly and accurately, while removing the risk of damaging the components. However, these techniques need to overcome their inability to accurately measure more curved surfaces, as seen on the device of choice in this study.

Despite the limitations associated with gravimetric assessment, this has been the preferred methodology for measuring TAR wear in the previous TAR literature and hence the reason for this being used in the simulator studies for more comparable results. Future studies could benefit from using CMM or  $\mu$ CT to quantify volumetric wear, which both remove the assumption of UHMWPE density. However, these techniques are not without limitations, as discussed in Section 6.2. The simulator studies also demonstrated that under each parameter change, certain

wear damage modes were comparable to the collection of retrieved MB devices. The comparison to the volumetric wear of retrieved implants, which cannot be assessed using gravimetric methods, is essential for the continued development of TAR. Further investigation into retrieved devices will provide a platform to understand other failure mechanisms, with potential wear patterns associated with TAR being identified. This will help the further development of suitable adverse device conditions to be run on the mechanical simulators, to replicate failure conditions and ultimately improve patient outcomes. The combined advancements in gait analysis modelling, pre-clinical wear simulation and retrieval comparison will ultimately improve the clinical outcome of patients implanted with a TAR.

## REFERENCE LIST

- Abdel-Jaber, S., Belvedere, C., Mattia, J.S. De, Leardini, A. and Affatato, S. 2016. A new protocol for wear testing of total knee prostheses from real joint kinematic data: Towards a scenario of realistic simulations of daily living activities. *Journal of Biomechanics*. **49**(13), pp.2925–2931.
- Abdelgaied, A., Brockett, C.L., Liu, F., Jennings, L.M., Jin, Z. and Fisher, J. 2014. The effect of insert conformity and material on total knee replacement wear. *Proceedings of the Institution of Mechanical Engineers, Part H: Journal of Engineering in Medicine*. **228**(1), pp.98–106.
- Abdelgaied, A., Fisher, J. and Jennings, L.M. 2017. A comparison between electromechanical and pneumatic-controlled knee simulators for the investigation of wear of total knee replacements. *Journal of Engineering in Medicine*. **231**(7), pp.643–651.
- Abdelgaied, A., Fisher, J. and Jennings, L.M. 2018. A comprehensive combined experimental and computational framework for pre-clinical wear simulation of total knee replacements. *Journal of the Mechanical Behavior of Biomedical Materials*. **78**, pp.282–291.
- Abdelgaied, A., Fisher, J. and Jennings, L.M. 2022. Understanding the differences in wear testing method standards for total knee replacement. *Journal of the Mechanical Behavior of Biomedical Materials*. **132**(105258), pp.1–10.
- Adams, S.B., Setton, L.A., Bell, R.D., Easley, M.E., Huebner, J.L., Stabler, T., Kraus, V.B., Leimer, E.M., Olson, S.A. and Nettles, D.L. 2015. Inflammatory cytokines and matrix metalloproteinases in the synovial fluid after intra-articular ankle fracture. *Foot and Ankle International*. **36**(11), pp.1264–1271.
- Adukia, V., Mangwani, J., Issac, R., Hussain, S. and Parker, L. 2020. Current concepts in the management of ankle arthritis. *Journal of clinical orthopaedics and trauma*. **11**(3), pp.388–398.
- Affatato, S., Bracco, P., Costa, L., Villa, T., Quaglini, V. and Toni, A. 2012. In vitro wear performance of standard, crosslinked, and vitamin-E-blended UHMWPE. *Journal of Biomedical Materials Research Part A*. **100A**(3), pp.554–560.
- Affatato, S., Grillini, L., Battaglia, S., Taddei, P., Modena, E. and Sudanese, A. 2013. Does knee implant size affect wear variability? *Tribology International*. **66**, pp.174–181.
- Affatato, S., Leardini, A., Leardini, W., Giannini, S. and Viceconti, M. 2007. Meniscal wear at a three-component total ankle prosthesis by a knee joint simulator. *Journal of Biomechanics*. **40**(8), pp.1871–1876.
- Affatato, Saverio, Leardini, W., Rocchi, M., Toni, A. and Viceconti, M. 2008. Investigation on wear of knee prostheses under fixed kinematic conditions. *Artificial Organs*. **32**(1), pp.13–18.

- Affatato, S. and Ruggiero, A. 2020. A perspective on biotribology in arthroplasty: From in vitro toward the accurate in silico wear prediction. *Applied Sciences*. **10**(18), pp.1–11.
- Affatato, S., Spinelli, M., Zavalloni, M., Mazzega-Fabbro, C. and Viceconti, M. 2008. Tribology and total hip joint replacement: Current concepts in mechanical simulation. *Medical Engineering and Physics*. **30**(10), pp.1305–1317.
- Affatato, S., Taddei, P., Leardini, A., Giannini, S., Spinelli, M. and Viceconti, M. 2009. Wear behaviour in total ankle replacement: A comparison between an in vitro simulation and retrieved prostheses. *Clinical Biomechanics*. **24**(8), pp.661–669.
- Affatato, S., Valigi, M.C. and Logozzo, S. 2017. Wear Distribution Detection of Knee Joint Prostheses by Means of 3D Optical Scanners. *Materials*. **10**(4), pp.1–11.
- Agel, J., Coetzee, J.C., Sangeorzan, B.J. and Roberts, M.M. 2005. Functional limitations of patients with end-stage ankle arthrosis. *Foot & ankle international*. **26**(7), pp.537–539.
- Akagi, M., Asano, T., Clarke, I.C., Niiyama, N., Kyomoto, M., Nakamura, T. and Hamanishi, C. 2006. Wear and toughness of crosslinked polyethylene for total knee replacements: A study using a simulator and small-punch testing. *Journal of Orthopaedic Research*. **24**(10), pp.2021–2027.
- Al-Hajjar, M., Leslie, I.J., Tipper, J., Williams, S., Fisher, J. and Jennings, L.M. 2010. Effect of cup inclination angle during microseparation and rim loading on the wear of BIOLOX® delta ceramic-on-ceramic total hip replacement. *Journal of Biomedical Materials Research Part B: Applied Biomaterials*. **95B**(2), pp.263–268.
- Ali, M., Al-Hajjar, M., Partridge, S., Williams, S., Fisher, J. and Jennings, L.M. 2016. Influence of hip joint simulator design and mechanics on the wear and creep of metal-on-polyethylene bearings. *Journal of Engineering in Medicine*. **230**(5), pp.389–397.
- Anderson, F.C. and Pandy, M.G. 2001. Static and dynamic optimization solutions for gait are practically equivalent. *Journal of Biomechanics*. **34**(2), pp.153–161.
- Andriacchi, T.P. and Alexander, E.J. 2000. Studies of human locomotion: past, present and future. *Journal of Biomechanics*. **33**(10), pp.1217–1224.
- Archangelo, J., Guerra-Pinto, F., Pinto, A., Grenho, A., Navarro, A. and Martin Oliva, X. 2019. Peri-prosthetic bone cysts after total ankle replacement. A systematic review and meta-analysis. *Foot and Ankle Surgery*. **25**(2), pp.96–105.
- Archard, J. and Hirst, W. 1956. The wear of metals under unlubricated conditions. *Proceedings of the Royal Society of London. Series A. Mathematical and Physical Sciences*. **236**(1206), pp.397–410.
- Arndt, A., Westblad, P., Winson, I., Hashimoto, T. and Lundberg, A. 2004. Ankle and Subtalar

- Kinematics Measured with Intracortical Pins during the Stance Phase of Walking. *Foot & Ankle International*. **25**(5), pp.357–364.
- de Asla, R.J., Wan, L., Rubash, H.E. and Li, G. 2005. Six DOF In Vivo Kinematics of the Ankle Joint Complex: Application of a Combined Dual-Orthogonal Fluoroscopic and Magnetic Resonance Imaging Technique. *Journal of Orthopaedic Research*. **24**(5), pp.1019–1027.
- ASTM F1714 - 96 2018. *Standard Guide for Gravimetric Wear Assessment of Prosthetic Hip Designs in Simulator Devices*.
- ASTM F2025-06 2018. *Standard Practice for Gravimetric Measurement of Polymeric Components for Wear Assessment*.
- Atwood, S.A., Van Citters, D.W., Patten, E.W., Furmanski, J., Ries, M.D. and Pruitt, L.A. 2011. Tradeoffs amongst fatigue, wear, and oxidation resistance of cross-linked ultra-high molecular weight polyethylene. *Journal of the Mechanical Behavior of Biomedical Materials*. **4**(7), pp.1033–1045.
- Aurora, A., DesJardins, J.D., Joseph, P.F. and LaBerge, M. 2006. Effect of lubricant composition on the fatigue properties of ultra-high molecular weight polyethylene for total knee replacement. *Proceedings of the Institution of Mechanical Engineers, Part H: Journal of Engineering in Medicine*. **220**(4), pp.541–551.
- Barbour, P.S.M., Barton, D.C. and Fisher, J. 1995. The influence of contact stress on the wear of UHMWPE for total replacement hip prostheses. *Wear*. **181–183**, pp.250–257.
- Barg, A., Bettin, C.C., Burstein, A.H., Saltzman, C.L. and Gililland, J. 2018. Early clinical and radiographic outcomes of trabecular metal total ankle replacement using a Trans fibular approach. *Journal of Bone and Joint Surgery - American Volume*. **100**(6), pp.505–515.
- Barg, A., Pagenstert, G.I., Hügler, T., Gloyer, M., Wiewiorski, M., Henninger, H.B. and Valderrabano, V. 2013. Ankle osteoarthritis: Etiology, diagnostics, and classification. *Foot and Ankle Clinics*. **18**(3), pp.412–426.
- Barg, A., Wimmer, M.D., Wiewiorski, M., Wirtz, D.C., Pagenstert, G.I. and Valderrabano, V. 2015. Total ankle replacement. *Deutsches Ärzteblatt international*. **112**(11), pp.177–84.
- Barnett, C.H. and Napier, J.R. 1952. The axis of rotation at the ankle joint in man. Its influence upon the form of the talus and the mobility of the fibula. *Journal of Anatomy*. **86**(1), pp.1–9.
- Barnett, P.I., McEwen, H.M.J., Auger, D.D., Stone, M.H., Ingham, E. and Fisher, J. 2002. Investigation of wear of knee prostheses in a new displacement/force-controlled simulator. *Proceedings of the Institution of Mechanical Engineers, Part H: Journal of Engineering in Medicine*. **216**(1), pp.51–61.

- Bartel, D., Bicknell, V.L. and Wright, T.M. 1986. The effect of conformity, thickness, and material on stresses in ultra-high molecular weight components for total joint replacement. *The Journal of Bone & Joint Surgery*. **68**(7), pp.1041–1051.
- Barton, T., Lintz, F. and Winson, I. 2011. Biomechanical changes associated with the osteoarthritic, arthrodesed, and prosthetic ankle joint. *Foot and Ankle Surgery*. **17**(2), pp.52–57.
- Bates, C.J., Prentice, A., Cole, T.J., Van Der Pols, J.C., Doyle, W., Finch, S., Smithers, G. and Clarke, P.C. 1999. Micronutrients: highlights and research challenges from the 1994–5 National Diet and Nutrition Survey of people aged 65 years and over. *British Journal of Nutrition*. **82**(1), pp.7–15.
- Battaglia, S., Taddei, P., Castiello, E., Tozzi, S., Sudanese, A. and Affatato, S. 2014. Combined effect of the body mass index and implant size on the wear of retrieved total knee prostheses. *Journal of the Mechanical Behavior of Biomedical Materials*. **38**, pp.69–77.
- Battaglia, S., Taddei, P., Tozzi, S., Sudanese, A. and Affatato, S. 2014. Toward the interpretation of the combined effect of size and body weight on the tribological performance of total knee prostheses. *International Orthopaedics*. **38**(6), pp.1183–1190.
- Baykal, D., Siskey, R.S., Haider, H., Saikko, V., Ahlroos, T. and Kurtz, S.M. 2014. Advances in tribological testing of artificial joint biomaterials using multidirectional pin-on-disk testers. *Journal of the Mechanical Behavior of Biomedical Materials*. **31**, pp.117–134.
- Bedi, A., Chen, T., Santner, T.J., El-Amin, S., Kelly, N.H., Warren, R.F. and Maher, S.A. 2013. Changes in dynamic medial tibiofemoral contact mechanics and kinematics after injury of the anterior cruciate ligament: A cadaveric model. *Proceedings of the Institution of Mechanical Engineers, Part H: Journal of Engineering in Medicine*. **227**(9), pp.1027–1037.
- Bell, A.L., Brand, R.A. and Pedersen, D.R. 1989. Prediction of hip joint centre location from external landmarks. *Human Movement Science*. **8**(1), pp.3–16.
- Bell, A.L., Pedersen, D.R. and Brand, R.A. 1990. A comparison of the accuracy of several hip center location prediction methods. *Journal of Biomechanics*. **23**(6), pp.617–621.
- Bell, C.J. and Fisher, J. 2007. Simulation of polyethylene wear in ankle joint prostheses. *Journal of Biomedical Materials Research Part B: Applied Biomaterials*. **81B**(1), pp.162–167.
- Benedetti, M.G., Catani, F., Leardini, A., Pignotti, E. and Giannini, S. 1998. Data management in gait analysis for clinical applications. *Clinical Biomechanics*. **13**(3), pp.204–215.
- Benedetti, M.G., Merlo, A. and Leardini, A. 2013. Inter-laboratory consistency of gait analysis measurements. *Gait and Posture*. **38**(4), pp.934–939.

- Benich, M.R., Ledoux, W.R., Orendurff, M.S., Shofer, J.B., Hansen, S.T., Davitt, J., Anderson, J.G., Bohay, D., Coetzee, J.C., Maskill, J., Brage, M., Houghton, M. and Sangeorzan, B.J. 2017. Comparison of Treatment Outcomes of Arthrodesis and Two Generations of Ankle Replacement Implants. *Journal of Bone and Joint Surgery - American Volume*. **99**(21), pp.1792–1800.
- Benoit, D.L., Ramsey, D.K., Lamontagne, M., Xu, L., Wretenberg, P. and Renström, P. 2006. Effect of skin movement artifact on knee kinematics during gait and cutting motions measured in vivo. *Gait & Posture*. **24**(2), pp.152–164.
- Bergmann, G., Bender, A., Dymke, J., Duda, G. and Damm, P. 2016. Standardized loads acting in hip implants. *PLoS ONE*. **11**(5), pp.1–23.
- Bergmann, G., Deuretzbacher, G., Heller, M., Graichen, F., Rohlmann, A., Strauss, J. and Duda, G.N. 2001. Hip contact forces and gait patterns from routine activities. *Journal of Biomechanics*. **34**, pp.859–871.
- Bergmann, G., Graichen, F. and Rohlmann, A. 1993. Hip joint loading during walking and running, measured in two patients. *Journal of Biomechanics*. **26**(8), pp.969–990.
- Besong, A.A. 1999. The influence of lubricant on the morphology of ultra-high molecular weight polyethylene wear debris generated in laboratory tests. *Proceedings of the Institution of Mechanical Engineers, Part H: Journal of Engineering in Medicine*. **213**(2), pp.155–158.
- Besse, J.L. 2015. Osteolytic cysts with total ankle replacement: Frequency and causes? *Foot and Ankle Surgery*. **21**(2), pp.75–76.
- Beyaert, C., Sirveaux, F., Paysant, J., Molé, D. and André, J.M. 2004. The effect of tibio-talar arthrodesis on foot kinematics and ground reaction force progression during walking. *Gait & Posture*. **20**(1), pp.84–91.
- Bhatia, M. 2014. Ankle arthritis: Review and current concepts. *Journal of Arthroscopy and Joint Surgery*. **1**, pp.19–26.
- Bianchi, A., Martinelli, N., Caboni, E., Raggi, G., Manfroni, F. and Sansone, V. 2021. Long-term follow-up of Bologna-Oxford (BOX) total ankle arthroplasty. *International Orthopaedics*. **45**(5), pp.1223–1231.
- Bills, P., Brown, L., Jiang, X. and Blunt, L. 2005. A metrology solution for the orthopaedic industry. *Journal of Physics: Conference Series*. **13**(1), pp.316–319.
- Bills, P.J., Racasan, R., Underwood, R.J., Cann, P., Skinner, J., Hart, A.J., Jiang, X. and Blunt, L. 2012. Volumetric wear assessment of retrieved metal-on-metal hip prostheses and the impact of measurement uncertainty. *Wear*. **274–275**, pp.212–219.

- Birch, I. and Deschamps, K. 2011. Quantification of Skin Marker Movement at the Malleoli and Talar Heads. *Journal of the American Podiatric Medical Association*. **101**(6), pp.497–504.
- Bischoff, J., Fryman, J.C., Parcell, J. and Orozco Villaseñor, D.A. 2015. Influence of crosslinking on the wear performance of polyethylene within total ankle arthroplasty. *Foot and Ankle International*. **36**(4), pp.369–376.
- Bischoff, J.E., Dharia, M.A., Hertzler, J.S. and Schipper, O.N. 2019. Evaluation of Total Ankle Arthroplasty Using Highly Crosslinked Ultrahigh-Molecular-Weight Polyethylene Subjected to Physiological Loading. *Foot & ankle international*. **40**(8), pp.880–887.
- Bishop, C., Paul, G. and Thewlis, D. 2013. The reliability, accuracy and minimal detectable difference of a multi-segment kinematic model of the foot–shoe complex. *Gait & Posture*. **37**(4), pp.552–557.
- Bitar, D. and Parvizi, J. 2015. Biological response to prosthetic debris. *World Journal of Orthopedics*. **6**(2), pp.172–189.
- Blackwood, C.B., Yuen, T.J., Sangeorzan, B.J. and Ledoux, W.R. 2005. The midtarsal joint locking mechanism. *Foot & ankle international*. **26**(12), pp.1074–1080.
- Bloch, B., Srinivasan, S. and Mangwani, J. 2015. Current Concepts in the Management of Ankle Osteoarthritis: A Systematic Review. *The Journal of Foot & Ankle Surgery*. **54**, pp.932–939.
- Bluman, E.M., Chiodo, C.P. and Smith, J.T. 2018. Ankle Arthritis *In: Principles of Orthopedic Practice for Primary Care Providers*. Cham: Springer International Publishing, pp.331–338.
- Blunt, L.A., Bills, P.J., Jiang, X.Q. and Chakrabarty, G. 2008. Improvement in the assessment of wear of total knee replacements using coordinate-measuring machine techniques. *Proceedings of the Institution of Mechanical Engineers, Part H: Journal of Engineering in Medicine*. **222**(3), pp.309–318.
- Bonasia, D.E., Dettoni, F., Femino, J.E., Phisitkul, P., Germano, M. and Amendola, A. 2010. Total ankle replacement: why, when and how? *The Iowa orthopaedic journal*. **30**, pp.119–30.
- Bonnin, M., Gaudot, F., Laurent, J.R., Ellis, S., Colombier, J.A. and Judet, T. 2011. The salto total ankle arthroplasty: Survivorship and analysis of failures at 7 to 11 years. *Clinical Orthopaedics and Related Research*. **469**(1), pp.225–236.
- Bracco, P., Bellare, A., Bistolfi, A. and Affatato, S. 2017. Ultra-High Molecular Weight Polyethylene: Influence of the Chemical, Physical and Mechanical Properties on the Wear Behavior. A Review. *Materials*. **10**(7), pp.1–22.
- Bracco, P. and Oral, E. 2011. Vitamin E-stabilized UHMWPE for total joint implants: A review. *Clinical Orthopaedics and Related Research*. **469**(8), pp.2286–2293.

- Brandt, J.M., Charron, K., Zhao, L., MacDonald, S.J. and Medley, J.B. 2012. Calf serum constituent fractions influence polyethylene wear and microbial growth in knee simulator testing. *Proceedings of the Institution of Mechanical Engineers, Part H: Journal of Engineering in Medicine*. **226**(6), pp.427–440.
- Brockett, C.L., Abdelgaied, A., Haythornthwaite, T., Hardaker, C., Fisher, J. and Jennings, L.M. 2016. The influence of simulator input conditions on the wear of total knee replacements: An experimental and computational study. *Proceedings of the Institution of Mechanical Engineers, Part H: Journal of Engineering in Medicine*. **230**(5), pp.429–439.
- Brockett, C.L., Carbone, S., Fisher, J. and Jennings, L.M. 2018. Influence of conformity on the wear of total knee replacement: An experimental study. *Proceedings of the Institution of Mechanical Engineers, Part H: Journal of Engineering in Medicine*. **232**(2), pp.127–134.
- Brockett, C.L., Jennings, L.M., Hardaker, C. and Fisher, J. 2012. Wear of moderately cross-linked polyethylene in fixed-bearing total knee replacements. *Proceedings of the Institution of Mechanical Engineers, Part H: Journal of Engineering in Medicine*. **226**(7), pp.529–535.
- Brodsky, J.W., Coleman, S.C., Smith, S., Polo, F.E. and Tenenbaum, S. 2013. Hindfoot Motion Following STAR Total Ankle Arthroplasty. *Foot & Ankle International*. **34**(11), pp.1479–1485.
- Brodsky, J.W., Kane, J.M., Coleman, S., Bariteau, J. and Tenenbaum, S. 2016. Abnormalities of gait caused by ankle arthritis are improved by ankle arthrodesis. *Bone and Joint Journal*. **98-B**(10), pp.1369–1375.
- Brodsky, J.W., Polo, F.E., Coleman, S.C. and Bruck, N. 2011. Changes in Gait Following the Scandinavian Total Ankle Replacement. *The Journal of Bone & Joint Surgery*. **93**(20), pp.1890–1896.
- Brodsky, J.W., Scott, D.J., Ford, S., Coleman, S. and Daoud, Y. 2021. Functional Outcomes of Total Ankle Arthroplasty at a Mean Follow-up of 7.6 Years: A Prospective, 3-Dimensional Gait Analysis. *The Journal of bone and joint surgery. American volume*. **103**(6), pp.477–482.
- Brown, C., Williams, S., Tipper, J.L., Fisher, J. and Ingham, E. 2007a. Characterisation of wear particles produced by metal on metal and ceramic on metal hip prostheses under standard and microseparation simulation. *Journal of Materials Science: Materials in Medicine*. **18**(5), pp.819–827.
- Brown, L., Zhang, H., Blunt, L. and Barrans, S. 2007b. Reproduction of fretting wear at the stem-cement interface in total hip replacement. *Proceedings of the Institution of Mechanical Engineers, Part H: Journal of Engineering in Medicine*. **221**(8), pp.963–971.
- Brown, S.S. and Clarke, I.C. 2006. A review of lubrication conditions for wear simulation in

- artificial hip replacements. *Tribology Transactions*. **49**(1), pp.72–78.
- Brunner, S., Barg, A., Knupp, M., Zwicky, L., Kapron, A.L., Valderrabano, V. and Hintermann, B. 2013. The scandinavian total ankle replacement long-term, eleven to fifteen-year, survivorship analysis of the prosthesis in seventy-two consecutive patients. *Journal of Bone and Joint Surgery - Series A*. **95**(8), pp.711–718.
- Buckley, C., Alcock, L., McArdle, R., Ur Rehman, R.Z., Del Din, S., Mazzà, C., Yarnall, A.J. and Rochester, L. 2019. The role of movement analysis in diagnosing and monitoring neurodegenerative conditions: Insights from gait and postural control. *Brain Sciences*. **9**(2), p.34.
- Bucknall, C., Altstädt, V., Auhl, D., Buckley, P., Dijkstra, D., Galeski, A., Gögelein, C., Handge, U.A., He, J., Liu, C.Y., Michler, G., Piorkowska, E., Slouf, M., Vittorias, I. and Wu, J.J. 2020. Structure, processing and performance of ultra-high molecular weight polyethylene (IUPAC Technical Report). Part 3: Deformation, wear and fracture. *Pure and Applied Chemistry*. **92**(9), pp.1503–1519.
- Buckwalter, J.A. and Martin, J.A. 2006. Osteoarthritis. *Advanced Drug Delivery Reviews*. **58**(2), pp.150–167.
- Buckwalter, J.A., Saltzman, C. and Brown, T. 2004. The impact of osteoarthritis: Implications for research. *Clinical Orthopaedics and Related Research*. **427**(Suppl), pp.S6-15.
- Burdett, R.G. 1982. Forces predicted at the ankle during running. *Medicine and Science in Sports and Exercise*. **14**(4), pp.308–316.
- C-Motion 2018. IORFoot Tutorial Angles. Available from: [https://www.c-motion.com/v3dwiki/index.php?title=IORFoot\\_Tutorial\\_Angles](https://www.c-motion.com/v3dwiki/index.php?title=IORFoot_Tutorial_Angles).
- Calderale, P.M., Garro, A., Barbiero, R., Fasolio, G. and Pipino, F. 1983. Biomechanical Design of the Total Ankle Prosthesis. *Engineering in Medicine*. **12**(2), pp.69–80.
- Calhoun, J.H., Li, F., Ledbetter, B.R. and Viegas, S.F. 1994. A Comprehensive Study of Pressure Distribution in the Ankle Joint with Inversion and Eversion. *Foot & Ankle International*. **15**(3), pp.125–133.
- Camomilla, V., Bonci, T. and Cappozzo, A. 2017. Soft tissue displacement over pelvic anatomical landmarks during 3-D hip movements. *Journal of Biomechanics*. **62**, pp.14–20.
- Campbell, P., Ma, S., Yeom, B., McKellop, H., Schmalzried, T.P. and Amstutz, H.C. 1995. Isolation of predominantly submicron- sized UHMWPE wear particles from periprosthetic tissues. *Journal of Biomedical Materials Research*. **29**(1), pp.127–131.
- Cappello, A., Cappozzo, A., La Palombara, P.F., Lucchetti, L. and Leardini, A. 1997. Multiple

- anatomical landmark calibration for optimal bone pose estimation. *Human Movement Science*. **16**(2–3), pp.259–274.
- Cappozzo, A., Cappello, A., Croce, U.D. and Pensalfini, F. 1997. Surface-marker cluster design criteria for 3-d bone movement reconstruction. *IEEE Transactions on Biomedical Engineering*. **44**(12), pp.1165–1174.
- Cappozzo, A., Catani, F., Della Croce, U. and Leardini, A. 1995. Position and orientation in space of bones during movement: anatomical frame definition and determination. *Clinical Biomechanics*. **10**(4), pp.171–178.
- Caravaggi, P., Benedetti, M.G., Berti, L. and Leardini, A. 2011. Repeatability of a multi-segment foot protocol in adult subjects. *Gait and Posture*. **33**(1), pp.133–135.
- Caravaggi, P., Lullini, G., Leardini, A., Berti, L., Vannini, F. and Giannini, S. 2015. Functional and clinical evaluation at 5-year follow-up of a three-component prosthesis and osteochondral allograft transplantation for total ankle replacement. *Clinical Biomechanics*. **30**(1), pp.59–65.
- Carson, M.C., Harrington, M.E., Thompson, N., O'Connor, J.J. and Theologis, T.N. 2001. Kinematic analysis of a multi-segment foot model for research and clinical applications: A repeatability analysis. *Journal of Biomechanics*. **34**(10), pp.1299–1307.
- Castagnini, F., Pellegrini, C., Perazzo, L., Vannini, F. and Buda, R. 2016. Joint sparing treatments in early ankle osteoarthritis: current procedures and future perspectives. *Journal of Experimental Orthopaedics*. **3**(1), pp.1–7.
- Cenni, F., Leardini, A., Pieri, M., Berti, L., Belvedere, C., Romagnoli, M. and Giannini, S. 2013. Functional performance of a total ankle replacement: Thorough assessment by combining gait and fluoroscopic analyses. *Clinical Biomechanics*. **28**(1), pp.79–87.
- Chan, F.W., Bobyn, J.D., Medley, J.B., Krygier, J.J. and Tanzer, M. 1999. Wear and lubrication of metal-on-metal hip implants *In: Clinical Orthopaedics and Related Research*. Lippincott Williams and Wilkins, pp.10–24.
- Chang, L. and Jeng, Y.R. 2013. Effects of negative skewness of surface roughness on the contact and lubrication of nominally flat metallic surfaces. *Proceedings of the Institution of Mechanical Engineers, Part J: Journal of Engineering Tribology*. **227**(6), pp.559–569.
- Charlton, P. and Blunt, L. 2008. Surface and form metrology of polished 'freeform' biological surfaces. *Wear*. **264**(5–6), pp.394–399.
- Cheikh, E., Ba, T., Dumont, M.R., Sérgio Martins, P., Martins Drumond, R., Martins Da Cruz, P. and Ferreira Vieira, V. 2021. Investigation of the effects of skewness R<sub>sk</sub> and kurtosis

- R ku on tribological behavior in a pin-on-disc test of surfaces machined by conventional milling and turning processes. *Materials Research*. **24**(2), p.20200435.
- Chen, J., Siegler, S. and Schneck, C.D. 1988. The three-dimensional kinematics and flexibility characteristics of the human ankle and subtalar joint--Part I. *Journal of biomechanical engineering*. **110**(4), pp.374–85.
- Chen, S.J., Mukul, M. and Chou, L.S. 2011. Soft-tissue movement at the foot during the stance phase of walking. *Journal of the American Podiatric Medical Association*. **101**(1), pp.25–34.
- Chiari, L., Della Croce, U., Leardini, A. and Cappozzo, A. 2005. Human movement analysis using stereophotogrammetry. Part 2: Instrumental errors. *Gait and Posture*. **21**(2), pp.197–211.
- Choi, J.H., Coleman, S.C., Tenenbaum, S., Polo, F.E. and Brodsky, J.W. 2013. Prospective Study of the Effect on Gait of a Two-Component Total Ankle Replacement. *Foot & Ankle International*. **34**(11), pp.1472–1478.
- Chou, L.B., Coughlin, M.T., Hansen, S., Haskell, A., Lundeen, G., Saltzman, C.L. and Mann, R. a 2008. Osteoarthritis of the ankle: the role of arthroplasty. *The Journal of the American Academy of Orthopaedic Surgeons*. **16**(5), pp.249–259.
- Clarke, I.C. and Gustafson, A. 2000. Clinical and hip simulator comparisons of ceramic-on-polyethylene and metal-on-polyethylene wear. *Clinical Orthopaedics and Related Research*. **379**, pp.34–40.
- Clement, R.C., Krynetskiy, E. and Parekh, S.G. 2013. The Total Ankle Arthroplasty Learning Curve With Third-Generation Implants: A Single Surgeon's Experience. *Foot and Ankle Specialist*. **6**(4), pp.263–270.
- Clough, T., Bodo, K., Majeed, H., Davenport, J. and Karski, M. 2019. Survivorship and long-term outcome of a consecutive series of 200 Scandinavian Total Ankle Replacement (STAR) implants. *Bone and Joint Journal*. **101B**(1), pp.47–54.
- Clough, T.M., Alvi, F. and Majeed, H. 2018. Total ankle arthroplasty: what are the risks? *The Bone & Joint Journal*. **100-B**(10), pp.1352–1358.
- Cobelli, N., Scharf, B., Crisi, G.M., Hardin, J. and Santambrogio, L. 2011. Mediators of the inflammatory response to joint replacement devices. *Nat. Rev. Rheumatol*. **7**, pp.600–608.
- Cocco, P., Ayaz-Shah, A., Messenger, M.P., West, R.M. and Shinkins, B. 2020. Target Product Profiles for medical tests: A systematic review of current methods. *BMC Medicine*. **18**(1), pp.1–12.
- Coester, L.M., Saltzman, C.L., Leupold, J. and Pontarelli, W. 2001. Long-Term Results Following Ankle Arthrodesis for Post-Traumatic Arthritis. *Journal of Bone and Joint Surgery - American*

*Volume. 83(2), p.219.*

- Coetzee, J.C., Petersen, D. and Stone, R.M. 2017. Comparison of Three Total Ankle Replacement Systems Done at a Single Facility. *Foot & Ankle Specialist. 10(1)*, pp.20–25.
- Collier, J.P., Sperling, D.K., Currier, J.H., Sutula, L.C., Saum, K.A. and Mayor, M.B. 1996. Impact of gamma sterilization on clinical performance of polyethylene in the knee. *The Journal of arthroplasty. 11(4)*, pp.377–389.
- Conti, S., Lalonde, K.-A. and Martin, R. 2006. Kinematic Analysis of the Agility Total Ankle during Gait. *Foot & Ankle International. 27(11)*, pp.980–984.
- Cooper, J.R., Dowson, D. and Fisher, J. 1993. The effect of transfer film and surface roughness on the wear of lubricated ultra-high molecular weight polyethylene. *Clinical Materials. 14(4)*, pp.295–302.
- Cooper, J.R., Dowson, D., Fisher, J. and Jobbins, B. 1991. Ceramic bearing surfaces in total artificial joints: Resistance to third body wear damage from bone cement particles. *Journal of Medical Engineering and Technology. 15(2)*, pp.63–67.
- Costa, L. and Bracco, P. 2016. Mechanisms of Cross-Linking, Oxidative Degradation, and Stabilization of UHMWPE. *UHMWPE Biomaterials Handbook: Ultra High Molecular Weight Polyethylene in Total Joint Replacement and Medical Devices: Third Edition.*, pp.467–487.
- Cottino, U., Collo, G., Morino, L., Cosentino, A., Gallina, V., Deregibus, M. and Tellini, A. 2012. Arthroscopic ankle arthrodesis: A review. *Current Reviews in Musculoskeletal Medicine. 5(2)*, pp.151–155.
- Cottrino, S., Fabrègue, D., Cowie, A.P., Besse, J.L., Tadier, S., Gremillard, L. and Hartmann, D.J. 2016. Wear study of Total Ankle Replacement explants by microstructural analysis. *Journal of the Mechanical Behavior of Biomedical Materials. 61*, pp.1–11.
- Couto, M., Vasconcelos, D.P., Sousa, D.M., Sousa, B., Conceição, F., Neto, E., Lamghari, M. and Alves, C.J. 2020. The Mechanisms Underlying the Biological Response to Wear Debris in Periprosthetic Inflammation. *Frontiers in Materials. 7*, pp.1–13.
- Cowie, R.M., Briscoe, A., Fisher, J. and Jennings, L.M. 2016. PEEK-OPTIMA as an alternative to cobalt chrome in the femoral component of total knee replacement: A preliminary study. *J Engineering in Medicine. 230(11)*, pp.1008–1015.
- Cowie, R.M., Briscoe, A., Fisher, J. and Jennings, L.M. 2019. Wear and Friction of UHMWPE-on-PEEK OPTIMA™. *Journal of the Mechanical Behavior of Biomedical Materials. 89*, pp.65–71.
- Cowie, R.M. and Jennings, L.M. 2021. Third body damage and wear in arthroplasty bearing materials: A review of laboratory methods. *Biomaterials and Biosystems. 4*, pp.1–11.

- Della Croce, U., Leardini, A., Chiari, L. and Cappozzo, A. 2005. Human movement analysis using stereophotogrammetry: Part 4: assessment of anatomical landmark misplacement and its effects on joint kinematics. *Gait & Posture*. **21**(2), pp.226–237.
- Cunningham, B.W. and Brooks, D.M. 2022. Comparative Analysis of Optoelectronic Accuracy in the Laboratory Setting Versus Clinical Operative Environment: A Systematic Review. *Global Spine Journal*. **12**(2), pp.59S-74S.
- Currier, B.H., Hecht, P.J., Nunley, J.A., Mayor, M.B., Currier, J.H. and Van Citters, D.W. 2019. Analysis of Failed Ankle Arthroplasty Components. *Foot & ankle international*. **40**(2), pp.131–138.
- D’Lima, D.D., Hermida, J.C., Chen, P.C. and Colwell, C.W. 2001. Polyethylene wear and variations in knee kinematics. *Clinical Orthopaedics and Related Research*. (392), pp.124–130.
- D’Lima, D.D., Steklov, N., Patil, S. and Colwell, C.W. 2008. The Mark Coventry Award: In Vivo Knee Forces During Recreation and Exercise After Knee Arthroplasty. *Clinical Orthopaedics and Related Research*. **466**(11), p.2605.
- Daniels, T.R., Younger, A.S.E., Penner, M., Wing, K., Dryden, P.J., Wong, H. and Glazebrook, M. 2014. Intermediate-Term Results of Total Ankle Replacement and Ankle Arthrodesis. *Journal of Bone and Joint Surgery*. **96**, pp.135–142.
- Davidson, J.A., Poggie, R.A. and Mishra, A.K. 1994. Abrasive wear of ceramic, metal, and ultrahigh polyethylene bearing surfaces from third-body bone, pmma bone cement, and titanium debris. *Bio-Medical Materials and Engineering*. **4**(3), pp.213–229.
- Davis, R.B., Öunpuu, S., Tyburski, D. and Gage, J.R. 1991. A gait analysis data collection and reduction technique. *Human Movement Science*. **10**(5), pp.575–587.
- Dawson, J., Boller, I., Doll, H., Lavis, G., Sharp, R., Cooke, P., Jenkinson, C. and Dawson, J. 2012. Responsiveness of the Manchester-Oxford foot questionnaire (MOXFQ) compared with AOFAS, SF-36 and EQ-5D assessments following foot or ankle surgery. *Journal of Bone & Joint Surgery, British Volume*. **94**(2), pp.215–236.
- Day, J.S., MacDonald, D.W., Olsen, M., Getz, C., Williams, G.R. and Kurtz, S.M. 2012. Polyethylene wear in retrieved reverse total shoulder components. *Journal of Shoulder and Elbow Surgery*. **21**(5), pp.667–674.
- Deleu, P.-A., Naaim, A., Chèze, L., Dumas, R., Devos Bevernage, B., Birch, I., Besse, J.-L. and Leemrijse, T. 2022. Changes in ankle and foot kinematic after fixed-bearing total ankle replacement. *Journal of Biomechanics*. **136**, pp.1–8.
- Deleu, P.A., Besse, J.L., Naaim, A., Leemrijse, T., Birch, I., Devos Bevernage, B. and Chèze, L.

- 2020a. Change in gait biomechanics after total ankle replacement and ankle arthrodesis: a systematic review and meta-analysis. *Clinical Biomechanics*. **73**, pp.213–225.
- Deleu, P.A., Chèze, L., Dumas, R., Besse, J.L., Leemrijse, T., Devos Bevernage, B., Birch, I. and Naaim, A. 2020b. Intrinsic foot joints adapt a stabilized-resistive configuration during the stance phase. *Journal of Foot and Ankle Research*. **13**(13), pp.1–12.
- Deleu, P.A., Leemrijse, T., Chèze, L., Naaim, A., Dumas, R., Devos Bevernage, B., Birch, I. and Besse, J.L. 2021a. Post-sprain versus post-fracture post-traumatic ankle osteoarthritis: Impact on foot and ankle kinematics and kinetics. *Gait and Posture*. **86**, pp.278–286.
- Deleu, P.A., Naaim, A., Leemrijse, T., Dumas, R., Devos Bevernage, B., Besse, J.L., Crevoisier, X. and Chèze, L. 2021b. Impact of foot modeling on the quantification of the effect of total ankle replacement: A pilot study. *Gait and Posture*. **84**, pp.308–314.
- Demetracopoulos, C.A., Adams, S.B., Queen, R.M., Deorio, J.K., Nunley, J.A. and Easley, M.E. 2015. Effect of Age on Outcomes in Total Ankle Arthroplasty. *Foot and Ankle International*. **36**(8), pp.871–880.
- Demetracopoulos, C.A., Sturnick, D.R., Ellis, S.J., Deland, J.T. and Baxter, J.R. 2016. Adjacent Joint Kinematics after Ankle Arthrodesis in Cadaveric Gait Simulation. *Foot and Ankle Orthopaedics*. **1**(1), p.2016.
- Demottaz, J.D., Mazur, J.M., Thomas, W.H., Sledge, C.B. and Simon, S.R. 1979. Clinical study of total ankle replacement with gait analysis. A preliminary report. *The Journal of bone and joint surgery. American volume*. **61**(7), pp.976–88.
- Derbyshire, B., Fisher, J., Dowson, D., Hardaker, C. and Brummitt, K. 1994. Comparative study of the wear of UHMWPE with zirconia ceramic and stainless steel femoral heads in artificial hip joints. *Medical Engineering and Physics*. **16**(3), pp.229–236.
- Deschamps, K., Roosen, P., Birch, I., Dingenen, B., Bruyninckx, H., Desloovere, K., Aertbelien, E. and Staes, F. 2014. A Novel Device for Standardizing Marker Placement at the Calcaneus. *Journal of the American Podiatric Medical Association*. **104**(1), pp.43–49.
- Deschamps, K., Staes, F., Bruyninckx, H., Busschots, E., Jaspers, E., Atre, A. and Desloovere, K. 2012a. Repeatability in the assessment of multi-segment foot kinematics. *Gait and Posture*. **35**(2), pp.255–260.
- Deschamps, K., Staes, F., Bruyninckx, H., Busschots, E., Matricali, G.A., Spaepen, P., Meyer, C. and Desloovere, K. 2012b. Repeatability of a 3D multi-segment foot model protocol in presence of foot deformities. *Gait & Posture*. **36**(3), pp.635–638.
- Deschamps, K., Staes, F., Peerlinck, K., Van Geet, C., Hermans, C., Matricali, G.A. and Lobet,

- S. 2017. 3D Multi-segment foot kinematics in children: A developmental study in typically developing boys. *Gait & Posture*. **52**, pp.40–44.
- DesJardins, J.D., Banks, S.A., Benson, L.C., Pace, T. and LaBerge, M. 2007. A direct comparison of patient and force-controlled simulator total knee replacement kinematics. *Journal of Biomechanics*. **40**(15), pp.3458–3466.
- DiLiberto, F.E., Haddad, S.L., Miller, S.A. and Vora, A.M. 2021. Midfoot Function Before and After Total Ankle Arthroplasty. *Foot and Ankle International*. **42**(7), pp.910–918.
- Donatelli, R. 1985. Normal biomechanics of the foot and ankle. *Journal of Orthopaedic and Sports Physical Therapy*. **7**(3), pp.91–95.
- Donatelli, R. 1995. *The biomechanics of the foot and ankle* 2nd ed. (R. Donatelli, ed.). F.A. Davis.
- Donell, S. 2019. Subchondral bone remodelling in osteoarthritis. *EFORT Open Reviews*. **4**(6), p.221.
- Dowson, D. 2012. Bio-tribology. *Faraday Discussions*. **156**, pp.9–30.
- Dubbeldam, R., Nester, C., Nene, A. V., Hermens, H.J. and Buurke, J.H. 2013. Kinematic coupling relationships exist between non-adjacent segments of the foot and ankle of healthy subjects. *Gait and Posture*. **37**(2), pp.159–164.
- Dumbleton, J.H., D’Antonio, J.A., Manley, M.T., Capello, W.N. and Wang, A. 2006. The basis for a second-generation highly cross-linked UHMWPE. *Clinical Orthopaedics and Related Research*. **453**, pp.265–271.
- Dyrby, C., Chou, L.B., Andriacchi, T.P. and Mann, R.A. 2004. Functional Evaluation of the Scandinavian Total Ankle Replacement. *Foot & Ankle International*. **25**(6), pp.377–381.
- Dzierwa, A. 2017. Influence of surface preparation on surface topography and tribological behaviours. *Archives of Civil and Mechanical Engineering*. **17**(3), pp.502–510.
- Dzierwa, A., Pawlus, P. and Zelasko, W. 2020. The influence of disc surface topography after vapor blasting on wear of sliding pairs under dry sliding conditions. *Coatings*. **10**(2), pp.1–13.
- Easley, M.E., Vertullo, C.J., Urban, W.C. and Nunley, J.A. 2002. Total ankle arthroplasty. *The Journal of the American Academy of Orthopaedic Surgeons*. **10**(3), pp.157–167.
- Ebraheim, N.A., Taser, F., Shafiq, Q. and Yeasting, R.A. 2006. Anatomical evaluation and clinical importance of the tibiofibular syndesmosis ligaments. *Surgical and Radiologic Anatomy*. **28**(2), pp.142–149.
- Edington, C., Frederick, E.C. and Cavanagh, P.R. 1990. *Rearfoot Motion in Distance Running*. Human

Kinetics, Champaign, IL.

- Eerdeken, M., Deschamps, K. and Staes, F. 2019. The impact of walking speed on the kinetic behaviour of different foot joints. *Gait and Posture*. **68**, pp.375–381.
- Eerdeken, M., Deschamps, K., Wuite, S. and Matricali, G. 2020. The biomechanical behavior of distal foot joints in patients with isolated, end-stage tibiotalar osteoarthritis is not altered following tibiotalar fusion. *Journal of Clinical Medicine*. **9**(8), pp.1–12.
- Eerdeken, M., Staes, F., Matricali, G.A. and Deschamps, K. 2020. Clinical Applicability of an Existing Proportionality Scheme in Three-Segment Kinetic Foot Models. *Annals of Biomedical Engineering*. **48**(1), pp.247–257.
- Eerdeken, M., Staes, F., Matricali, G.A., Wuite, S., Peerlinck, K. and Deschamps, K. 2019. Quantifying clinical misinterpretations associated to one-segment kinetic foot modelling in both a healthy and patient population. *Clinical Biomechanics*. **67**, pp.160–165.
- El-Deen, M., García-Fiñana, M. and Jin, Z.M. 2006. Effect of ultra-high molecular weight polyethylene thickness on contact mechanics in total knee replacement. *Proceedings of the Institution of Mechanical Engineers, Part H: Journal of Engineering in Medicine*. **220**(7), pp.733–742.
- Endo, M.M., Barbour, P.S.M., Barton, D.C., Fisher, J., Tipper, J.L., Ingham, E. and Stone, M.H. 2001. Comparative wear and wear debris under three different counterface conditions of crosslinked and non- crosslinked ultra high molecular weight polyethylene. *Bio-Medical Materials and Engineering*. **11**(1), pp.23–35.
- Espinosa, N., Klammer, G. and Wirth, S.H. 2017. Osteolysis in Total Ankle Replacement: How Does It Work? *Foot and Ankle Clinics*. **22**(2), pp.267–275.
- Espinosa, N., Walti, M., Favre, P. and Snedeker, J.G. 2010. Misalignment of total ankle components can induce high joint contact pressures. *Journal of Bone and Joint Surgery*. **92**(5), pp.1179–1187.
- Essner, A., Herrera, L., Hughes, P. and Kester, M. 2011. The influence of material and design on total knee replacement wear. *The journal of knee surgery*. **24**(1), pp.9–17.
- Estok, D.M., Bragdon, C.R., Plank, G.R., Huang, A., Muratoglu, O.K. and Harris, W.H. 2005. The measurement of creep in ultrahigh molecular weight polyethylene: a comparison of conventional versus highly cross-linked polyethylene. *The Journal of arthroplasty*. **20**(2), pp.239–43.
- Etsion, I. 2009. State of the Art in Laser Surface Texturing. *Advanced Tribology*., pp.761–762.
- Fabry, C., Herrmann, S., Kaehler, M., Klinkenberg, E.D., Woernle, C. and Bader, R. 2013. Generation of physiological parameter sets for hip joint motions and loads during daily life

- activities for application in wear simulators of the artificial hip joint. *Medical Engineering & Physics*. **35**(1), pp.131–139.
- Fahlgren, A., Bostrom, M.P., Yang, X., Johansson, L., Edlund, U., Agholme, F. and Aspenberg, P. 2010. Fluid pressure and flow as a cause of bone resorption. *Acta Orthopaedica*. **81**(4), pp.508–516.
- Fekete, G., Sun, D., Liu, G., Gu, Y.D., Balassa, G.P., Bíró, I., Neis, P.D. and Jánosi, E. 2018. Preliminary results of size and slide-roll effect on the kinematics of total knee replacements. *Acta Polytechnica Hungarica*. **15**(6), pp.143–153.
- Ferguson, Z., Anugraha, A., Janghir, N. and Pillai, A. 2019. Ankle arthrodesis: A long term review of the literature. *Journal of Orthopaedics*. **16**(5), pp.430–433.
- Ferrari, A., Benedetti, M.G., Pavan, E., Frigo, C., Bettinelli, D., Rabuffetti, M., Crenna, P. and Leardini, A. 2008. Quantitative comparison of five current protocols in gait analysis. *Gait and Posture*. **28**(2), pp.207–216.
- Fickey, S.N., Browne, M.G. and Franz, J.R. 2018. Biomechanical effects of augmented ankle power output during human walking. *Journal of Experimental Biology*. **221**(22), pp.1–24.
- Fisher, J. 2012. A stratified approach to pre-clinical tribological evaluation of joint replacements representing a wider range of clinical conditions advancing beyond the current standard. *Faraday Discussions*. **156**(0), pp.59–68.
- Fisher, J., Jennings, L.M., Galvin, A.L., Jin, Z.M., Stone, M.H. and Ingham, E. 2010. 2009 Knee society presidential guest lecture: Polyethylene wear in total knees. *Clinical Orthopaedics and Related Research*. **468**(1), pp.12–18.
- Fisher, J., McEwen, H.M.J., Tipper, J.L., Galvin, A.L., Ingram, J., Kamali, A., Stone, M.H. and Ingham, E. 2004. Wear, debris, and biologic activity of cross-linked polyethylene in the knee: Benefits and potential concerns. *Clinical Orthopaedics and Related Research*. **428**, pp.114–119.
- Flavin, R., Coleman, S.C., Tenenbaum, S. and Brodsky, J.W. 2013. Comparison of gait after total ankle arthroplasty and ankle arthrodesis. *Foot and Ankle International*. **34**(10), pp.1340–1348.
- Franz, J.R. 2016. The Age-Associated Reduction in Propulsive Power Generation in Walking. *Exercise and Sport Sciences Reviews*. **44**(4), pp.129–136.
- Fregly, B.J., Sawyer, W.G., Harman, M.K. and Banks, S.A. 2005. Computational wear prediction of a total knee replacement from in vivo kinematics. *Journal of Biomechanics*. **38**(2), pp.305–314.
- Frigg, A., Germann, U., Huber, M. and Horisberger, M. 2017. Survival of the Scandinavian total

- ankle replacement (STAR): results of ten to nineteen years follow-up. *International Orthopaedics*. **41**(10), pp.2075–2082.
- Fritz, J.M., Canseco, K., Konop, K.A., Kruger, K.M., Tarima, S., Long, J.T., Law, B.C., Kraus, J.C., King, D.M. and Harris, G.F. 2021. Multi-segment foot kinematics during gait following ankle arthroplasty. *Journal of Orthopaedic Research*. **40**(3), pp.685–694.
- Fuchs, S, Sandmann, C., Skwara, a and Chylarecki, C. 2003. Quality of life 20 years after arthrodesis of the ankle. A study of adjacent joints. *The Journal of bone and joint surgery. British volume*. **85**(7), pp.994–998.
- Fuentes-Sanz, A., Moya-Angeler, J., López-Oliva, F. and Forriol, F. 2012. Clinical Outcome and Gait Analysis of Ankle Arthrodesis. *Foot & Ankle International*. **33**(10), pp.819–827.
- Gaedke, I.E., Wiebking, U., O’loughlin, P.F., Krettek, C. and Gaulke, R. 2018. Clinical and radiological mid- to long-term outcomes following ankle fusion. *In Vivo*. **32**(6), pp.1463–1471.
- Galvin, A.L., Kang, L., Udofia, I., Jennings, L.M., McEwen, H.M.J., Jin, Z. and Fisher, J. 2009. Effect of conformity and contact stress on wear in fixed-bearing total knee prostheses. *Journal of Biomechanics*. **42**(12), pp.1898–1902.
- Galvin, A.L., Tipper, J.L., Jennings, L.M., Stone, M.H., Jin, Z.M., Ingham, E. and Fisher, J. 2007. Wear and biological activity of highly crosslinked polyethylene in the hip under low serum protein concentrations. *Proceedings of the Institution of Mechanical Engineers, Part H: Journal of Engineering in Medicine*. **221**(1), pp.1–10.
- Gao, F., Leach, R.K., Petzing, J. and Coupland, J.M. 2008. Surface measurement errors using commercial scanning white light interferometers. *Measurement Science and Technology*. **19**(1), pp.1–13.
- Ghosh, S., Choudhury, D., Roy, T., Moradi, A., Masjuki, H.H. and Pinguang-Murphy, B. 2015. Tribological performance of the biological components of synovial fluid in artificial joint implants. *Science and Technology of Advanced Materials*. **16**(4), pp.1–12.
- Giannini, S. 2013. The Box Ankle Replacement: Results at a Minimum Follow-up of 5 Years. *Orthopedic & Muscular System*. **2**(3), pp.1–4.
- Giannini, S., Romagnoli, M., Barbadoro, P., Marcheggiani Muccioli, G.M., Cadossi, M., Grassi, A. and Zaffagnini, S. 2017. Results at a minimum follow-up of 5 years of a ligaments-compatible total ankle replacement design. *Foot and Ankle Surgery*. **23**(2), pp.116–121.
- Giannini, S., Romagnoli, M., O’connor, J.J., Catani, F., Nogarin, L., Magnan, B., Malerba, F., Massari, L., Guelfi, M., Milano, L., Volpe, A., Rebecato, A. and Leardini, A. 2011. Early

- Clinical Results of the BOX Ankle Replacement Are Satisfactory: A Multicenter Feasibility Study of 158 Ankles. *Journal of Foot and Ankle Surgery*. **50**(6), pp.641–647.
- Glazebrook, M., Daniels, T., Younger, A., Foote, C.J., Penner, M., Wing, K., Lau, J., Leighton, R. and Dunbar, M. 2008. Comparison of health-related quality of life between patients with end-stage ankle and hip arthrosis. *Journal of Bone and Joint Surgery - Series A*. **90**(3), pp.499–505.
- Glazebrook, M.A., Ganapathy, V., Bridge, M.A., Stone, J.W. and Allard, J.P. 2009. Evidence-Based Indications for Ankle Arthroscopy. *Arthroscopy - Journal of Arthroscopic and Related Surgery*. **25**(12), pp.1478–1490.
- Glitsch, U. and Baumann, W. 1997. The three-dimensional determination of internal loads in the lower extremity. *Journal of Biomechanics*. **30**(11–12), pp.1123–1131.
- Glyn-Jones, S., Isaac, S., Hauptfleisch, J., McLardy-Smith, P., Murray, D.W. and Gill, H.S. 2008. Does Highly Cross-Linked Polyethylene Wear Less Than Conventional Polyethylene in Total Hip Arthroplasty?: A Double-Blind, Randomized, and Controlled Trial Using Roentgen Stereophotogrammetric Analysis. *The Journal of Arthroplasty*. **23**(3), pp.337–343.
- Golanó, P., Vega, J., de Leeuw, P.A.J., Malagelada, F., Manzanares, M.C., Götzens, V. and van Dijk, C.N. 2010. Anatomy of the ankle ligaments: A pictorial essay. *Knee Surgery, Sports Traumatology, Arthroscopy*. **18**(5), pp.557–569.
- Goldberg, A.J., Chowdhury, K., Bordea, E., Hauptmannova, I., Blackstone, J., Brooking, D., Deane, E.L., Bendall, S., Bing, A., Blundell, C., Dhar, S., Molloy, A., Milner, S., Karski, M., Cooke, P., Halliwell, P., Townshend, D., Skene, S.S., Doré, C.J. and Group, T.S. 2022. Total Ankle Replacement Versus Arthrodesis for End-Stage Ankle Osteoarthritis : A Randomized Controlled Trial. *Annals of Internal Medicine*.
- Goldberg, A.J., MacGregor, A., Dawson, J., Singh, D., Cullen, N., Sharp, R.J. and Cooke, P.H. 2012. The demand incidence of symptomatic ankle osteoarthritis presenting to foot & ankle surgeons in the United Kingdom. *Foot*. **22**(3), pp.163–166.
- Goldberg, A.J., Sharp, R.J. and Cooke, P. 2009. Ankle replacement: Current practice of foot & ankle surgeons in the United Kingdom. *Foot and Ankle International*. **30**(10), pp.950–954.
- Goldsmith, A.A.J., Dowson, D., Isaac, G.H. and Lancaster, J.G. 2000. A comparative joint simulator study of the wear of metal-on-metal and alternative material combinations in hip replacements. *Proceedings of the Institution of Mechanical Engineers, Part H: Journal of Engineering in Medicine*. **214**(1), pp.39–47.
- González, F.J.Q., Steineman, B.D., Sturnick, D.R., Deland, J.T., Demetracopoulos, C.A. and Wright, T.M. 2021. Biomechanical evaluation of total ankle arthroplasty. Part II: Influence

- of loading and fixation design on tibial bone–implant interaction. *Journal of Orthopaedic Research*. **39**(1), pp.103–111.
- Good, V.D., Clarke, I.C. and Anissian, L. 1996. Water and bovine serum lubrication compared in simulator PTFE/CoCr wear model. *Journal of Biomedical Materials Research*. **33**(4), pp.275–283.
- Gorton, G.E., Hebert, D.A. and Gannotti, M.E. 2009. Assessment of the kinematic variability among 12 motion analysis laboratories. *Gait and Posture*. **29**(3), pp.398–402.
- Gougoulias, N.E., Khanna, A. and Maffulli, N. 2008. History and evolution in total ankle arthroplasty. *British Medical Bulletin*. **89**(1), pp.111–151.
- Gowda, B. and Kumar, Jm. 2012. Outcome of ankle arthrodesis in posttraumatic arthritis. *Indian Journal of Orthopaedics*. **46**(3), pp.317–320.
- Green, T.R., Fisher, J., Matthews, J.B., Stone, M.H. and Ingham, E. 2000. Effect of size and dose on bone resorption activity of macrophages byin vitro clinically relevant ultra high molecular weight polyethylene particles. *Journal of Biomedical Materials Research*. **53**(5), pp.490–497.
- Greisberg, J., Assal, M., Flueckiger, G. and Hansen, S.T. 2004. Takedown of Ankle Fusion and Conversion to Total Ankle Replacement. *Clinical Orthopaedics and Related Research*. **424**, pp.80–88.
- Grimston, S.K., Nigg, B.M., Hanley, D.A. and Engsberg, J.R. 1993. Differences in Ankle Joint Complex Range of Motion as a Function of Age. *Foot & Ankle*. **14**(4), pp.215–222.
- Groen, B.E., Geurts, M., Nienhuis, B. and Duysens, J. 2012. Sensitivity of the OLGA and VCM models to erroneous marker placement: Effects on 3D-gait kinematics. *Gait and Posture*. **35**(3), pp.517–521.
- Grood, E.S. and Suntay, W.J. 1983. A Joint Coordinate System for the Clinical Description of Three-Dimensional Motions: Application to the Knee. *Journal of Biomedical Engineering*. **105**(2), pp.136–144.
- De Groot, P. 2017. Interference Microscopy for Surface Structure Analysis *In: T. Yoshizawa, ed. Handbook of Optical Metrology*. CRC Press Taylor & Francis Group, pp.791–828.
- Groves, D., Fisher, J. and Williams, S. 2017. An in vitro simulation method for the tribological assessment of complete natural hip joints A. A. Espinoza Orías, ed. *PLoS ONE*. **12**(9), pp.1–15.
- Grupp, T.M., Fritz, B., Kutzner, I., Schilling, C., Bergmann, G. and Schwiesau, J. 2017. Vitamin E stabilised polyethylene for total knee arthroplasty evaluated under highly demanding

activities wear simulation. *Acta Biomaterialia*. **48**, pp.415–422.

- Haddad, S.L., Coetzee, J.C., Estok, R., Fahrbach, K., Banel, D. and Nalysnyk, L. 2007. Intermediate and Long-Term Outcomes of Total Ankle Arthroplasty and Ankle Arthrodesis A Systematic Review of the Literature. *The Journal of Bone and Joint Surgery (American)*. **89**(9), pp.1899–1905.
- Hadley, M., Hardaker, C., Williams, S., Jin, Z., Isaac, G. and Fisher, J. 2013. Development of a stop-dwell-start (SDS) protocol for in vitro wear testing of metal-on-metal total hip replacements *In: ASTM Special Technical Publication*. ASTM International, pp.271–291.
- Hahn, M.E., Wright, E.S., Segal, A.D., Orendurff, M.S., Ledoux, W.R. and Sangeorzan, B.J. 2012. Comparative Gait Analysis of Ankle Arthrodesis and Arthroplasty: Initial Findings of a Prospective Study. *Foot & Ankle International*. **33**(4), pp.282–289.
- Haider, H. 2016. Tribological Assessment of UHMWPE in the Knee *In: S. Kurtz, ed. UHMWPE Biomaterials Handbook - Ultra-High Molecular Weight Polyethylene in Total Joint Replacement and Medical Devices*. Elsevier, pp.599–634.
- Hall, R.M., Bankes, M.J.K. and Blunn, G. 2001. Biotribology for joint replacement. *Current Orthopaedics*. **15**(4), pp.281–290.
- Hamill, J., Knutzen, K. and Derrick, T.R. 2021. *Biomechanical Basis of Human Movement* 5th ed. Wolters Kluwer Health.
- Harsted, S., Holsgaard-Larsen, A., Hestbæk, L., Boyle, E. and Lauridsen, H.H. 2019. Concurrent validity of lower extremity kinematics and jump characteristics captured in pre-school children by a markerless 3D motion capture system. *Chiropractic and Manual Therapies*. **27**(1), pp.1–16.
- Haskell, A. and Mann, R.A. 2004. Ankle arthroplasty with preoperative coronal plane deformity: Short-term results. *Clinical Orthopaedics and Related Research*. **424**, pp.98–103.
- Hendrickx, R.P.M., Stufkens, S.A.S., de Bruijn, E.E., Sierevelt, I.N., van Dijk, C.N. and Kerkhoffs, G.M.M.J. 2011. Medium- to Long-Term Outcome of Ankle Arthrodesis. *Foot & Ankle International*. **32**(10), pp.940–947.
- Henricson, A. and Carlsson, Å. 2015. Survival analysis of the single- and double-coated STAR ankle up to 20 years: Long-term follow-up of 324 cases from the Swedish ankle registry. *Foot and Ankle International*. **36**(10), pp.1156–1160.
- Henricson, A., Skoog, A. and Carlsson, Å. 2007. The Swedish Ankle Arthroplasty Register: An analysis of 531 arthroplasties between 1993 and 2005. *Acta orthopaedica*. **78**(5), pp.569–574.
- Hertel, J. 2002. Functional Anatomy, Pathomechanics, and Pathophysiology of Lateral Ankle

- Instability. *Journal of Athletic Training*. **37**(4), pp.364–375.
- Heuberger, M.P., Widmer, M.R., Zobeley, E., Glockshuber, R. and Spencer, N.D. 2005. Protein-mediated boundary lubrication in arthroplasty. *Biomaterials*. **26**(10), pp.1165–1173.
- Hicks, J.H. 1954. The mechanics of the foot. *Journal of Anatomy*. **88**(1), pp.25–30.
- Hintermann, B. 2005. *Total Ankle Arthroplasty: Historical overview, current concepts, and future perspectives* 1st ed. Springer.
- Hintermann, B. and Ruiz, R. 2014. Ankle arthritis and the treatment with ankle replacement. *Revista Médica Clínica Las Condes*. **25**, pp.812–823.
- Hintermann, B., Zwicky, L., Knupp, M., Henninger, H.B. and Barg, A. 2013. HINTEGRA revision arthroplasty for failed total ankle prostheses. *Journal of Bone and Joint Surgery - Series A*. **95**(13), pp.1166–1174.
- Ho, N.C., McCarty, C.P., Park, S.H., Williams, J.R., Gilmartin, N.F., Ebrahimzadeh, E. and Sangiorgio, S.N. 2020. Is load control necessary to produce physiological AP displacement and axial rotation in wear testing of TAR? *Journal of Orthopaedic Research*. **39**(4), pp.797–805.
- Hobson, S.A., Karantana, A. and Dhar, S. 2009. Total ankle replacement in patients with significant pre-operative deformity of the hindfoot. *Journal of Bone and Joint Surgery - Series B*. **91**(4), pp.481–486.
- Hocken, R.J., Chakraborty, N. and Brown, C. 2005. Optical metrology of surfaces. *CIRP Annals - Manufacturing Technology*. **54**(2), pp.169–183.
- Holland, M., Fleming, L., Walton, K., Cerquiglini, A., Hothi, H., Hart, A., Skinner, J. and Bills, P. 2018. Characterisation of wear areas on UHMWPE total knee replacement prostheses through study of their areal surface topographical parameters. *Surface Topography: Metrology and Properties*. **6**(3), pp.1–13.
- van Hoogstraten, S.W.G., Hermus, J., Loenen, A.C.Y., Arts, J.J. and van Rietbergen, B. 2022. Malalignment of the total ankle replacement increases peak contact stresses on the bone-implant interface: a finite element analysis. *BMC Musculoskeletal Disorders*. **23**(1), pp.1–9.
- Horisberger, M., Hintermann, B. and Valderrabano, V. 2009. Alterations of plantar pressure distribution in posttraumatic end-stage ankle osteoarthritis. *Clinical Biomechanics*. **24**(3), pp.303–307.
- Houdková, Šperka, P., Repka, M., Martan, J. and Moskal, D. 2017. Shifted laser surface texturing for bearings applications. *Journal of Physics: Conference Series*. **843**(1), pp.1–10.
- Hu, P., Liu, R., Liu, J., McRae, G., Yao, M.X. and Collier, R. 2014. Advanced Stellite alloys with

- improved metal-on-metal bearing for hip implants. *Materials and Design*. **60**, pp.424–432.
- Hua, X. and Li, J. 2020. CMM-based method for assessing the volume change of retrieved polyethylene cups in MoP total hip replacements. *Biosurface and Biotribology*. **6**(2), pp.37–42.
- Huang, C.H., Ho, F.Y., Ma, H.M., Yang, C.T., Liao, J.J., Kao, H.C., Young, T.H. and Cheng, C.K. 2002. Particle size and morphology of UHMWPE wear debris in failed total knee arthroplasties—a comparison between mobile bearing and fixed bearing knees. *Journal of Orthopaedic Research*. **20**(5), pp.1038–1041.
- Huang, C.H., Liao, J.J. and Cheng, C.K. 2007. Fixed or mobile-bearing total knee arthroplasty. *Journal of Orthopaedic Surgery and Research*. **2**(1), pp.1–8.
- Huang, Y.-C., Harbst, K., Kotajarvi, B., Hansen, D., Koff, M.F., Kitaoka, H.B. and Kaufman, K.R. 2006. Effects of Ankle-Foot Orthoses on Ankle and Foot Kinematics in Patient With Ankle Osteoarthritis. *Archives of Physical Medicine and Rehabilitation*. **87**(5), pp.710–716.
- Hügler, T., Geurts, J., Nüesch, C., Müller-Gerbl, M. and Valderrabano, V. 2012. Aging and osteoarthritis: An inevitable encounter? *Journal of Aging Research*. **2012**, pp.1–7.
- Ianuzzi, A. and Mkandawire, C. 2016. Applications of UHMWPE in Total Ankle Replacements. *UHMWPE Biomaterials Handbook: Ultra High Molecular Weight Polyethylene in Total Joint Replacement and Medical Devices: Third Edition.*, pp.197–216.
- Ingham, E. and Fisher, J. 2005. The role of macrophages in osteolysis of total joint replacement. *Biomaterials*. **26**(11), pp.1271–1286.
- Ingrosso, S., Benedetti, M.G., Leardini, A., Casanelli, S., Sforza, T. and Giannini, S. 2009. GAIT analysis in patients operated with a novel total ankle prosthesis. *Gait and Posture*. **30**(2), pp.132–137.
- Inman, V.T. 1976. *The Joints of the Ankle* 1st ed. Baltimore: Williams & Wilkins.
- Di Iorio, A., Viste, A., Fessy, M.H. and Besse, J.L. 2017. The AES total ankle arthroplasty analysis of failures and survivorship at ten years. *International Orthopaedics*. **41**(12), pp.2525–2533.
- ISO 14242-1:2014/Amd 1: 2018. *Implants for surgery — Wear of total hip-joint prostheses — Part 1: Loading and displacement parameters for wear-testing machines and corresponding environmental conditions for test.*
- ISO 14243-1: 2002. *Implants for surgery — Wear of total knee-joint prostheses — Part 1: Loading and displacement parameters for wear-testing machines with load control and corresponding environmental conditions for test.*
- ISO 14243-3: 2014. *Implants for surgery — Wear of total knee-joint prostheses — Part 3: Loading and*

*displacement parameters for wear-testing machines with displacement control and corresponding environmental conditions for test.*

ISO 16610-21: 2011. *Geometrical product specifications (GPS) — Filtration — Part 21: Linear profile filters: Gaussian filters.*

ISO 22622: 2019. *Implants for surgery — Wear of total ankle-joint prostheses — Loading load or displacement control and for wear-testing machines with and displacement parameters corresponding environmental conditions for test.*

ISO 3274: 1996. *Geometrical Product Specifications (GPS) — Surface texture: Profile method — Nominal characteristics of contact (stylus) instruments.*

ISO 4288: 1996. *Geometrical Product Specifications (GPS) — Surface texture: Profile method — Rules and procedures for the assessment of surface texture.*

ISO 5834-2: 2019. *Implants for surgery — Ultra-high-molecular-weight polyethylene — Part 2: Moulded forms.*

Iwasa, K., Kanzaki, N., Fujishiro, T., Hayashi, S., Hashimoto, S., Kuroda, R. and Kurosaka, M. 2014. Arthroscopic ankle arthrodesis for treating osteoarthritis in a patient with kashin-beck disease. *Case Reports in Medicine*. **2014**, pp.1–5.

Jastifer, J.R. and Gustafson, P.A. 2014. The subtalar joint: Biomechanics and functional representations in the literature. *Foot*. **24**(4), pp.203–209.

Jasty, M., Bragdon, C., Burke, D., O'Connor, D., Lowenstein, J. and Harris, W.H. 1997. In Vivo Skeletal Responses to Porous-Surfaced Implants Subjected to Small Induced Motions. *The Journal of Bone & Joint Surgery*. **79**(5), pp.707–714.

Jiang, W., Ji, C., Jin, Z. and Dai, Y. 2018. CMM-based volumetric assessment methodology for polyethylene tibial knee inserts in total knee replacement. *Applied Bionics and Biomechanics*. **2018**, pp.1–6.

Jin, Z.M., Stone, M., Ingham, E. and Fisher, J. 2006. (v) Biotribology. *Current Orthopaedics*. **20**, pp.32–40.

Johnson, T.S., Laurent, M.P., Yao, J.Q. and Gilbertson, L.N. 2001. The effect of displacement control input parameters on tibiofemoral prosthetic knee wear. *Wear*. **250–251**(Part 1), pp.222–226.

Jones, C. V., Williams, I.R., Auger, D.D., Walsh, W., Barton, D.C., Stone, M.H. and Fisher, J. 2001. Quantification of third body damage to the tibial counterface in mobile bearing knees. *Proceedings of the Institution of Mechanical Engineers, Part H: Journal of Engineering in Medicine*. **215**(2), pp.171–179.

- Jordan, R.W., Chahal, G.S. and Chapman, A. 2014. Is end-stage ankle arthrosis best managed with total ankle replacement or arthrodesis? A systematic review. *Advances in orthopedics*. **2014**, pp.1–9.
- Julious, S.A. 2005. Sample size of 12 per group rule of thumb for a pilot study. *Pharmaceutical Statistics*. **4**(4), pp.287–291.
- Jung, H.-G., Parks, B.G., Nguyen, A. and Schon, L.C. 2007. Effect of Tibiotalar Joint Arthrodesis on Adjacent Tarsal Joint Pressure in a Cadaver Model. *Foot & Ankle International*. **28**(1), pp.103–108.
- Kadaba, M.P., Ramakrishnan, H.K., Wootten, M.E., Gainey, J., Gorton, G. and Cochran, G.V.B. 1989. Repeatability of kinematic, kinetic, and electromyographic data in normal adult gait. *Journal of Orthopaedic Research*. **7**(6), pp.849–860.
- Kakkar, R. and Siddique, M.S. 2011. Stresses in the ankle joint and total ankle replacement design. *Foot and Ankle Surgery*. **17**(2), pp.58–63.
- Kalron, A., Menascu, S., Dolev, M. and Givon, U. 2017. The walking speed reserve in low disabled people with multiple sclerosis: Does it provide greater insight in detecting mobility deficits and risk of falling than preferred and fast walking speeds? *Multiple Sclerosis and Related Disorders*. **17**, pp.202–206.
- Kamali, A., Hussain, A., Li, C., Pamu, J., Daniel, J., Ziaee, H., W McMinn, D.J., Manager Hussain, R.A., Engineer Li, T.C., Scientist Pamu, M.J., Associate, T., Student, E. and Scientist Daniel, B.J. 2010. Tribological performance of various CoCr microstructures in metal-on-metal bearings. *Journal of Bone & Joint Surgery, British Volume*. **92**(5), pp.717–725.
- Kandahari, A.M., Yang, X., Laroche, K.A., Dighe, A.S., Pan, D. and Cui, Q. 2016. A review of UHMWPE wear-induced osteolysis: The role for early detection of the immune response. *Bone Research*. **4**, pp.1–13.
- Kang, L., Galvin, A.L., Fisher, J. and Jin, Z. 2009. Enhanced computational prediction of polyethylene wear in hip joints by incorporating cross-shear and contact pressure in addition to load and sliding distance: Effect of head diameter. *Journal of Biomechanics*. **42**(7), pp.912–918.
- Kaufman, K., Miller, E., Kingsbury, T., Russell Esposito, E., Wolf, E., Wilken, J. and Wyatt, M. 2016. Reliability of 3D gait data across multiple laboratories. *Gait and Posture*. **49**, pp.375–381.
- Keenan, G.S., Franz, J.R., Dicharry, J., Croce, U. Della and Kerrigan, D.C. 2011. Lower limb joint kinetics in walking: The role of industry recommended footwear. *Gait and Posture*. **33**(3), pp.350–355.

- Kerrigan, D.C., Lee, L.W., Nieto, T.J., Markman, J.D., Collins, J.J. and Riley, P.O. 2000. Kinetic alterations independent of walking speed in elderly fallers. *Archives of Physical Medicine and Rehabilitation*. **81**(6), pp.730–735.
- Kessler, S.E., Rainbow, M.J., Lichtwark, G.A., Cresswell, A.G., D’andrea, S.E., Konow, N. and Kelly, L.A. 2019. A direct comparison of biplanar videoradiography and optical motion capture for foot and ankle kinematics. *Frontiers in Bioengineering and Biotechnology*. **7**, pp.1–10.
- Keyak, J.H. and Rossi, S.A. 2000. Prediction of femoral fracture load using finite element models: An examination of stress- and strain-based failure theories. *Journal of Biomechanics*. **33**(2), pp.209–214.
- Kim, Hyun Jung, Suh, D.H., Yang, J.H., Lee, J.W., Kim, Hak Jun, Ahn, H.S., Han, S.W. and Choi, G.W. 2017. Total ankle arthroplasty versus ankle arthrodesis for the treatment of end-stage ankle arthritis: a meta-analysis of comparative studies. *International Orthopaedics*. **41**(1), pp.101–109.
- Kim, S., Jang, J., Choi, J.H., Yang, H.M., Chun, H.J., Lee, G.W., Lee, K.B. and Lim, D. 2021. Volume and distribution of periprosthetic bone cysts in the distal tibia and talus before early revision of total ankle arthroplasty. *Applied Sciences (Switzerland)*. **11**(16), pp.1–11.
- Kimizuka, M., Kurosawa, H. and Fukubayashi, T. 1980. Archives of Orthopaedic and Traumatic Surgery Load-bearing Pattern of the Ankle Joint Contact Area and Pressure Distribution. *Arch Orthop Traumat Surg*. **96**, pp.45–49.
- Kincaid, B., Gillard, D., Wentorf, F., Popoola, O. and Bischoff, J. 2013. Gravimetric Wear Testing of a Fixed-Bearing Bicondylar Total Ankle Replacement *In: ORS 2013 Annual Meeting* [Online]. Available from: <https://www.ors.org/Transactions/59/PS1--054/1161.html>.
- King, J., Stamper, D.L., Schaad, D.C. and Leopold, S.S. 2007. Minimally Invasive Total Knee Arthroplasty Compared with Traditional Total Knee Arthroplasty. *The Journal of Bone and Joint Surgery-American Volume*. **89**(7), pp.1497–1503.
- Kinzel, V., Scaddan, M., Bradley, B. and Shakespeare, D. 2004. Varus/valgus alignment of the femur in total knee arthroplasty. Can accuracy be improved by pre-operative CT scanning? *Knee*. **11**(3), pp.197–201.
- Kleipool, R.P. and Blankevoort, L. 2010. The relation between geometry and function of the ankle joint complex: A biomechanical review. *Knee Surgery, Sports Traumatology, Arthroscopy*. **18**(5), pp.618–627.
- Knight, L.A., Pal, S., Coleman, J.C., Bronson, F., Haider, H., Levine, D.L., Taylor, M. and Rullkoetter, P.J. 2007. Comparison of long-term numerical and experimental total knee

- replacement wear during simulated gait loading. *Journal of Biomechanics*. **40**(7), pp.1550–1558.
- Kobayashi, A., Minoda, Y., Kadoya, Y., Ohashi, H., Takaoka, K. and Saltzman, C.L. 2004. Ankle arthroplasties generate wear particles similar to knee arthroplasties. *Clinical Orthopaedics and Related Research*. **424**, pp.69–72.
- Koh, Y.G., Park, K.M., Lee, H.Y. and Kang, K.T. 2019. Influence of tibiofemoral congruency design on the wear of patient-specific unicompartmental knee arthroplasty using finite element analysis. *Bone and Joint Research*. **8**(3), pp.156–164.
- Kohring, J.M., Houck, J.R., Oh, I., Flemister, A.S., Ketz, J.P. and Baumhauer, J.F. 2020. Pattern of recovery and outcomes of patient reported physical function and pain interference after ankle fusion: a retrospective cohort study. *Journal of Patient-Reported Outcomes*. **4**(1), pp.1–8.
- Koivu, H., Kohonen, I., Mattila, K., Loyttyneimi, E. and Tiusanen, H. 2017. Long-term Results of Scandinavian Total Ankle Replacement. *Foot & Ankle International*. **38**(7), pp.723–731.
- Komistek, R.D., Stiehl, J.B., Buechel, F.F., Northcut, E.J. and Hajner, M.E. 2000. A Determination of Ankle Kinematics Using Fluoroscopy. *Foot & Ankle International*. **21**(4), pp.343–350.
- Kop, A.M. and Swarts, E. 2007. Quantification of polyethylene degradation in mobile bearing knees: A retrieval analysis of the Anterior-Posterior-Glide (APG) and Rotating Platform (RP) Low Contact Stress (LCS) knee. *Acta Orthopaedica*. **78**(3), pp.364–370.
- Krähenbühl, N., Tschuck, M., Bolliger, L., Hintermann, B. and Knupp, M. 2016. Orientation of the Subtalar Joint. *Foot & Ankle International*. **37**(1), pp.109–114.
- Krähenbühl, N., Zwicky, L., Bolliger, L., Schädelin, S., Hintermann, B. and Knupp, M. 2017. Mid- to Long-term Results of Supramalleolar Osteotomy. *Foot & Ankle International*. **38**(2), pp.124–132.
- Krause, F.G., Windolf, M., Bora, B., Penner, M.J., Wing, K.J. and Younger, A.S.E. 2011. Impact of complications in total ankle replacement and ankle arthrodesis analyzed with a validated outcome measurement. *Journal of Bone and Joint Surgery - Series A*. **93**(9), pp.830–839.
- Kretzer, J., Jakubowitz, E., Hofmann, K., Heisel, C. and Lietz, E. 2009. Influence of resting periods on polyethylene wear in a knee simulator study. *Medical science monitor : international medical journal of experimental and clinical research*. **15**(11), pp.143–146.
- Kretzer, J.P., Jakubowitz, E., Reinders, J., Lietz, E., Moradi, B., Hofmann, K. and Sonntag, R. 2011. Wear analysis of unicondylar mobile bearing and fixed bearing knee systems: A knee simulator study. *Acta Biomaterialia*. **7**(2), pp.710–715.
- Krishnapillai, S., Joling, B., Sierevelt, I.N., Kerkhoffs, G.M.M.J., Haverkamp, D. and

- Hoornenborg, D. 2019. Long-term Follow-up Results of Buechel-Pappas Ankle Arthroplasty. *Foot and Ankle International*. **40**(5), pp.553–561.
- Kristianslund, E., Krosshaug, T. and Van den Bogert, A. 2012. Effect of low pass filtering on joint moments from inverse dynamics: implications for injury prevention. *Journal of biomechanics*. **45**(4), pp.666–671.
- Kurtz, S.M. 2015. UHMWPE Biomaterials Handbook: Ultra High Molecular Weight Polyethylene in Total Joint Replacement and Medical Devices: Third Edition. *UHMWPE Biomaterials Handbook: Ultra High Molecular Weight Polyethylene in Total Joint Replacement and Medical Devices: Third Edition.*, pp.1–815.
- Kurtz, S.M., Gawel, H.A. and Patel, J.D. 2011. History and Systematic Review of Wear and Osteolysis Outcomes for First-generation Highly Crosslinked Polyethylene. *Clinical Orthopaedics and Related Research*. **469**(8), pp.2262–2277.
- Kurtz, S.M., Muratoglu, O.K., Evans, M. and Edidin, A.A. 1999. Advances in the processing, sterilization, and crosslinking of ultra-high molecular weight polyethylene for total joint arthroplasty. *Biomaterials*. **20**(18), pp.1659–1688.
- Kutzner, I., Bender, A., Dymke, J., Duda, G., Von Roth, P. and Bergmann, G. 2017. Mediolateral force distribution at the knee joint shifts across activities and is driven by tibiofemoral alignment. *Bone and Joint Journal*. **99B**(6), pp.779–787.
- Lachiewicz, P.F. 1994. Total ankle arthroplasty: Indications, techniques, and results. *Orthopaedic Review*. **23**(4), pp.315–320.
- Lachiewicz, P.F., Soileau, E.S. and Martell, J.M. 2016. Wear and Osteolysis of Highly Crosslinked Polyethylene at 10 to 14 Years: The Effect of Femoral Head Size. *Clinical Orthopaedics and Related Research*. **474**(2), pp.365–371.
- Lawton, C.D., Butler, B.A., Dekker, R.G., Prescott, A. and Kadakia, A.R. 2017. Total ankle arthroplasty versus ankle arthrodesis-a comparison of outcomes over the last decade. *Journal of Orthopaedic Surgery and Research*. **12**(1), pp.1–19.
- Lawton, C.D., Prescott, A., Butler, B.A., Awender, J.F., Selley, R.S., Dekker II, R.G., Balderama, E.S. and Kadakia, A.R. 2020. Modern total ankle arthroplasty versus ankle arthrodesis: A systematic review and meta-analysis. *Orthopedic Reviews*. **12**(3), pp.1–13.
- Leach, R. and Hart, A. 2002. *A comparison of stylus and optical methods for measuring 2D surface texture*. Teddington, Middlesex.
- Leach, R.K. 2010. Surface topography characterization *In: Fundamental Principles of Engineering Nanometrology*. William Andrew Publishing, pp.211–262.

- Leardini, A. 2001. Geometry and mechanics of the human ankle complex and ankle prosthesis design. *Clinical biomechanics (Bristol, Avon)*. **16**(8), pp.706–9.
- Leardini, A., Benedetti, M.G., Berti, L., Bettinelli, D., Nativo, R. and Giannini, S. 2007. Rear-foot, mid-foot and fore-foot motion during the stance phase of gait. *Gait and Posture*. **25**(3), pp.453–462.
- Leardini, A., Chiari, A., Della Croce, U. and Cappozzo, A. 2005. Human movement analysis using stereophotogrammetry: Part 3. Soft tissue artifact assessment and compensation. *Gait & Posture*. **21**(2), pp.212–225.
- Leardini, A. and O'Connor, J.J. 2002. A model for lever-arm length calculation of the flexor and extensor muscles at the ankle. *Gait & posture*. **15**(3), pp.220–9.
- Leardini, A., O'Connor, J.J., Catani, F. and Giannini, S. 2004. Mobility of the Human Ankle and the Design of Total Ankle Replacement. *Clinical Orthopaedics and Related Research*. **424**(424), pp.39–46.
- Lee, A.Y., Ha, A.S., Petscavage, J.M. and Chew, F.S. 2013. Total ankle arthroplasty: A radiographic outcome study. *American Journal of Roentgenology*. **200**(6), pp.1310–1316.
- Lee, K.T., Lee, Y.K., Young, K.W., Kim, J.B. and Seo, Y.S. 2013. Perioperative complications and learning curve of the mobility total ankle system. *Foot and Ankle International*. **34**(2), pp.210–214.
- Lehmann, P., Kühnhold, P. and Xie, W. 2014. Reduction of chromatic aberration influences in vertical scanning white-light interferometry. *Measurement Science and Technology*. **25**(6), pp.1–9.
- Leigh, R.J., Pohl, M.B. and Ferber, R. 2014. Does tester experience influence the reliability with which 3D gait kinematics are collected in healthy adults? *Physical Therapy in Sport*. **15**(2), pp.112–116.
- Lenz, A.L., Lisonbee, R.J., Peterson, A.C., Roach, K.E., Foreman, K.B., Barg, A. and Anderson, A.E. 2022. Total Ankle Replacement Provides Symmetrical Postoperative Kinematics: A Biplane Fluoroscopy Imaging Study. *Foot and Ankle International*. **43**(6), pp.818–829.
- Lenz, A.L., Nichols, J.A., Roach, K.E., Foreman, K.B., Barg, A., Saltzman, C.L. and Anderson, A.E. 2020. Compensatory Motion of the Subtalar Joint Following Tibiotalar Arthrodesis: An in Vivo Dual-Fluoroscopy Imaging Study. *The Journal of bone and joint surgery. American volume*. **102**(7), pp.600–608.
- Lerf, R., Zurbrügg, D. and Delfosse, D. 2010. Use of vitamin E to protect cross-linked UHMWPE from oxidation. *Biomaterials*. **31**(13), pp.3643–3648.

- Leszko, F., Komistek, R.D., Mahfouz, M.R., Ratron, Y.A., Judet, T., Bonnin, M., Colombier, J.A. and Lin, S.S. 2008. In vivo kinematics of the salto total ankle prosthesis. *Foot and Ankle International*. **29**(11), pp.1117–1125.
- Levine, D., Richards, J. and Whittle, M. 2012. *Whittle's gait analysis* 5th ed. Churchill Livingstone/Elsevier.
- Lewis, G. 1994. The Ankle Joint Prosthetic Replacement: Clinical Performance and Research Challenges. *Foot & Ankle International*. **15**(9), pp.471–476.
- Lewis R B 1964. Predicting the wear of sliding plastic surfaces. *Mechanical Engineering*. **86**(10), pp.32–35.
- Liao, Y.S., Benya, P.D. and McKellop, H.A. 1999. Effect of protein lubrication on the wear properties of materials for prosthetic joints. *Journal of Biomedical Materials Research*. **48**(4), pp.465–473.
- Liao, Y.S., McKellop, H., Lu, Z., Campbell, P. and Benya, P. 2003. The effect of frictional heating and forced cooling on the serum lubricant and wear of UHMW polyethylene cups against cobalt–chromium and zirconia balls. *Biomaterials*. **24**(18), pp.3047–3059.
- Lin, J., Sofka, C.M., Demetracopoulos, C.A. and Potter, H.G. 2022. The Utility of Isotropic 3D Magnetic Resonance Imaging in Assessing Painful Total Ankle Replacements. *Foot and Ankle Orthopaedics*. **7**(2), pp.1–10.
- Ling, J.S., Smyth, N.A., Fraser, E.J., Hogan, M. V, Seaworth, C.M., Ross, K.A. and Kennedy, J.G. 2015. Investigating the Relationship Between Ankle Arthrodesis and Adjacent-Joint Arthritis in the Hindfoot. *The Journal of Bone and Joint Surgery-American Volume*. **97**(6), pp.513–519.
- Liu, F., Galvin, A., Jin, Z. and Fisher, J. 2011. A New Formulation for the Prediction of Polyethylene Wear in Artificial Hip Joints. *Proceedings of the Institution of Mechanical Engineers, Part H: Journal of Engineering in Medicine*. **225**(1), pp.16–24.
- Liza, S., Haseeb, A.S.M.A., Abbas, A.A. and Masjuki, H.H. 2011. Failure analysis of retrieved UHMWPE tibial insert in total knee replacement. *Engineering Failure Analysis*. **18**(6), pp.1415–1423.
- Lord, G. and Marotte, J.H. 1973. Total ankle prosthesis. Technic and 1st results. Apropos of 12 cases. *Revue de chirurgie orthopedique et reparatrice de l'appareil moteur*. **59**(2), pp.139–51.
- Lord, J., Langton, D., Nargol, A., Meek, R.M. and Joyce, T. 2015. The Tribology of Explanted Hip Resurfacings Following Early Fracture of the Femur. *Journal of Functional Biomaterials*. **6**(4), pp.1021–1035.

- Lu, S., Orr, J.F. and Buchanan, F.J. 2003. The influence of inert packaging on the shelf ageing of gamma-irradiation sterilised ultra-high molecular weight polyethylene. *Biomaterials*. **24**(1), pp.139–145.
- Lu, X., Khonsari, M.M. and Gelinck, E.R.M. 2006. The Stribeck Curve: Experimental Results and Theoretical Prediction. *Journal of Tribology*. **128**(4), pp.789–794.
- Lu, Z. and McKellop, H. 1997. Frictional heating of bearing materials tested in a hip joint wear simulator. *Proceedings of the Institution of Mechanical Engineers, Part H: Journal of Engineering in Medicine*. **211**(1), pp.101–108.
- Lullini, G., Caravaggi, P., Leardini, A., Ortolani, M., Mazzotti, A., Giannini, S. and Berti, L. 2020. Retrospective comparison between a two- and three-component ankle arthroplasty: clinical and functional evaluation via gait analysis. *Clinical Biomechanics*. **80**, pp.1–6.
- Lundberg, Arne, Goldie, I., Kalin, B. and Selvik, G. 1989. Kinematics of the Ankle/Foot Complex: Plantarflexion and Dorsiflexion. *Foot & Ankle International*. **9**(4), pp.194–200.
- Lundberg, A., Svensson, O.K., Nemeth, G. and Selvik, G. 1989. The axis of rotation of the ankle joint. *Journal of Bone & Joint Surgery, British Volume*. **71-B**(1), pp.94–99.
- Lundgren, P., Nester, C., Liu, A., Arndt, A., Jones, R., Stacoff, A., Wolf, P. and Lundberg, A. 2008. Invasive in vivo measurement of rear-, mid- and forefoot motion during walking. *Gait and Posture*. **28**(1), pp.93–100.
- Lunn, D.E., De Pieri, E., Chapman, G.J., Lund, M.E., Redmond, A.C. and Ferguson, S.J. 2020. Current Preclinical Testing of New Hip Arthroplasty Technologies Does Not Reflect Real-World Loadings: Capturing Patient-Specific and Activity-Related Variation in Hip Contact Forces. *Journal of Arthroplasty*. **35**(3), pp.877–885.
- Lynch, A.F., Bourne, R.B. and Rorabeck, C.H. 1988. The long-term results of ankle arthrodesis. *Journal of Bone and Joint Surgery - Series B*. **70**(1), pp.113–116.
- Lynch, S.A. and Renström, P.A. 1999. Treatment of acute lateral ankle ligament rupture in the athlete. Conservative versus surgical treatment. *Sports medicine*. **27**(1), pp.61–71.
- Lythgo, N., Wilson, C. and Galea, M. 2009. Basic gait and symmetry measures for primary school-aged children and young adults whilst walking barefoot and with shoes. *Gait and Posture*. **30**(4), pp.502–506.
- Maccario, C., Tan, E.W., Di Silvestri, C.A., Indino, C., Kang, H.P. and Uselli, F.G. 2021. Learning curve assessment for total ankle replacement using the transfibular approach. *Foot and Ankle Surgery*. **27**(2), pp.129–137.
- Macdonald, D.A. 2014. The application of focus variation microscopy for lithic use-wear

- quantification. *Journal of Archaeological Science*. **48**(1), pp.26–33.
- MacDonald, D.W., Higgs, G.B., Chen, A.F., Malkani, A.L., Mont, M.A. and Kurtz, S.M. 2018. Oxidation, Damage Mechanisms, and Reasons for Revision of Sequentially Annealed Highly Crosslinked Polyethylene in Total Knee Arthroplasty. *The Journal of Arthroplasty*. **33**(4), pp.1235–1241.
- Maffulli, N., Longo, U.G., Locher, J., Romeo, G., Salvatore, G. and Denaro, V. 2017. Outcome of ankle arthrodesis and ankle prosthesis: a review of the current status. *British Medical Bulletin*. **124**, pp.91–112.
- Mahaffey, R., Morrison, S.C., Drechsler, W.I. and Cramp, M.C. 2013. Evaluation of multi-segmental kinematic modelling in the paediatric foot using three concurrent foot models. *Journal of Foot and Ankle Research*. **6**(43), pp.1–11.
- Mahmoud, K., Metikala, S., O'Connor, K.M. and Farber, D.C. 2021. Adverse events related to total ankle replacement devices: an analysis of reports to the United States Food and Drug Administration. *International Orthopaedics*. **45**(9), pp.2307–2312.
- Maloney, W.J., Smith, R.L., Schmalzried, T.P., Chiba, J., Huene, D. and Rubash, H. 1995. Isolation and characterization of wear particles generated in patients who have had failure of a hip arthroplasty without cement. *Journal of Bone and Joint Surgery*. **77**(9), pp.1301–1310.
- Maquirriain, J. 2011. Achilles tendon rupture: Avoiding tendon lengthening during surgical repair and rehabilitation. *Yale Journal of Biology and Medicine*. **84**(3), pp.289–300.
- Di Marco, R., Rossi, S., Racic, V., Cappa, P. and Mazzà, C. 2016. Concurrent repeatability and reproducibility analyses of four marker placement protocols for the foot-ankle complex. *Journal of Biomechanics*. **49**(14), pp.3168–3176.
- Martin, L., Stewart, G.W., Stephen and Conti, F. 2007. Posttraumatic Ankle Arthritis: An Update on Conservative and Surgical Management. *Journal of Orthopaedic and Sports Physical Therapy*. **37**(5), pp.253–259.
- Martinelli, N., Baretta, S., Pagano, J., Bianchi, A., Villa, T., Casaroli, G. and Galbusera, F. 2017. Contact stresses, pressure and area in a fixed-bearing total ankle replacement: A finite element analysis. *BMC Musculoskeletal Disorders*. **18**(493), pp.1–9.
- Mathia, T.G., Pawlus, P. and Wiczorowski, M. 2011. Recent trends in surface metrology. *Wear*. **271**(3–4), pp.494–508.
- MatOrtho Ltd 2015. BOX Total Ankle Replacement Operative Technique. . **926**, p.36. [Accessed 12 October 2021]. Available from: [https://www.matortho.com/wp-content/uploads/2018/06/MO\\_BOX\\_Ankle\\_OPTEC\\_ML\\_300\\_008\\_L\\_iss2.pdf](https://www.matortho.com/wp-content/uploads/2018/06/MO_BOX_Ankle_OPTEC_ML_300_008_L_iss2.pdf).

- Mattei, L., Di Puccio, F., Piccigallo, B. and Ciulli, E. 2011. Lubrication and wear modelling of artificial hip joints: A review. *Tribology International*. **44**(5), pp.532–549.
- Mattei, L., Tomasi, M., Artoni, A., Ciulli, E. and Di Puccio, F. 2021. Combination of musculoskeletal and wear models to investigate the effect of daily living activities on wear of hip prostheses. *Proceedings of the Institution of Mechanical Engineers, Part J: Journal of Engineering Tribology*. **235**(12), pp.2675–2687.
- Mavraki, A. and Cann, P.M. 2011. Lubricating film thickness measurements with bovine serum. *Tribology International*. **44**(5), pp.550–556.
- Mazur, J.M., Schwartz, E. and Simon, S.R. 1979. Ankle arthrodesis. Long-term follow-up with gait analysis. *The Journal of Bone & Joint Surgery*. **61**(7), pp.964–975.
- Mazzucco, D. and Spector, M. 2003. Effects of contact area and stress on the volumetric wear of ultrahigh molecular weight polyethylene. *Wear*. **254**(5–6), pp.514–522.
- McCalden, R.W., MacDonald, S.J., Rorabeck, C.H., Bourne, R.B., Chess, D.G. and Charron, K.D. 2009. Wear rate of highly cross-linked polyethylene in total hip arthroplasty: A randomized controlled trial. *Journal of Bone and Joint Surgery - Series A*. **91**(4), pp.773–782.
- McClelland, J.A., Webster, K.E. and Feller, J.A. 2007. Gait analysis of patients following total knee replacement: A systematic review. *Knee*. **14**(4), pp.253–263.
- McEwen, H.M.J., Barnett, P.I., Bell, C.J., Farrar, R., Auger, D.D., Stone, M.H. and Fisher, J. 2005. The influence of design, materials and kinematics on the in vitro wear of total knee replacements. *Journal of Biomechanics*. **38**(2), pp.357–365.
- McEwen, H.M.J., Fisher, J., Goldsmith, A.A.J., Auger, D.D., Hardaker, C. and Stone, M.H. 2001. Wear of fixed bearing and rotating platform mobile bearing knees subjected to high levels of internal and external tibial rotation. *Journal of Materials Science: Materials in Medicine*. **12**(10–12), pp.1049–1052.
- McInnes, K.A., Younger, A.S.E. and Oxland, T.R. 2014. Initial instability in total ankle replacement: A cadaveric biomechanical investigation of the star and agility prostheses. *Journal of Bone and Joint Surgery - American Volume*. **96**(17), pp.e147-148.
- McKellop, H., Shen, F., Lu, B., Campbell, P. and Salovey, R. 1999a. Development of an extremely wear-resistant ultra high molecular weight polyethylene for total hip replacements. *Journal of Orthopaedic Research*. **17**(2), pp.157–167.
- McKellop, H., Shen, F.W., DiMaio, W. and Lancaster, J.G. 1999b. Wear of gamma-crosslinked polyethylene acetabular cups against roughened femoral balls. *Clinical Orthopaedics and Related Research*. **369**, pp.73–82.

- McKellop, H., Shen, F.W., Lu, B., Campbell, P. and Salovey, R. 2000. Effect of sterilization method and other modifications on the wear resistance of acetabular cups made of ultra-high molecular weight polyethylene. A hip-simulator study. *The Journal of bone and joint surgery. American volume.* **82**(12), pp.1708–1725.
- McKellop, H.A. 2007. The lexicon of polyethylene wear in artificial joints. *Biomaterials.* **28**(34), pp.5049–5057.
- McKellop, H.A., Campbell, P., Park, S.H., Schmalzried, T.P., Grigoris, P., Amstutz, H.C. and Sarmiento, A. 1995. The origin of submicron polyethylene wear debris in total hip arthroplasty *In: Clinical Orthopaedics and Related Research* [Online]. Springer Science and Business Media, LLC, pp.3–20. [Accessed 29 April 2022]. Available from: <https://europepmc.org/article/med/7634588>.
- McPoil, T.G. and Knecht, H.G. 1985. Biomechanics of the foot in walking: a function approach. *The Journal of orthopaedic and sports physical therapy.* **7**(2), pp.69–72.
- Medel, F.J., Kurtz, S.M., Hozack, W.J., Parvizi, J., Purtill, J.J., Sharkey, P.F., MacDonald, D., Kraay, M.J., Goldberg, V. and Rimnac, C.M. 2009. Gamma Inert Sterilization: A Solution to Polyethylene Oxidation? *The Journal of Bone and Joint Surgery. American volume.* **91**(4), p.839.
- Mehta, S.K., Donley, B.G., Jockel, J.R., Slovenkai, M.P., Casillas, M.M., Berberian, W.S. and Lin, S.S. 2010. The salto talaris total ankle arthroplasty system: A review and report of early results. *Seminars in Arthroplasty.* **21**(4), pp.282–287.
- Meldrum, D., Shouldice, C., Conroy, R., Jones, K. and Forward, M. 2014. Test-retest reliability of three dimensional gait analysis: Including a novel approach to visualising agreement of gait cycle waveforms with Bland and Altman plots. *Gait and Posture.* **39**(1), pp.265–271.
- Menant, J.C., Steele, J.R., Menz, H.B., Munro, B.J. and Lord, S.R. 2008. Optimizing footwear for older people at risk of falls. *Faculty of Health and Behavioural Sciences - Papers (Archive).* **45**(8), pp.1167–1182.
- Meneghini, R.M., Ireland, P.H. and Bhowmik-Stoker, M. 2016. Multicenter Study of Highly Cross-linked vs Conventional Polyethylene in Total Knee Arthroplasty. *The Journal of Arthroplasty.* **31**(4), pp.809–814.
- Merola, M. and Affatato, S. 2019. Materials for hip prostheses: A review of wear and loading considerations. *Materials.* **12**(3), pp.1–36.
- Michael, J.M., Golshani, A., Gargac, S. and Goswami, T. 2008. Biomechanics of the ankle joint and clinical outcomes of total ankle replacement. *Journal of the Mechanical Behavior of Biomedical Materials.* **1**(4), pp.276–294.

- Micheli, B.R., Wannomae, K.K., Lozynsky, A.J., Christensen, S.D. and Muratoglu, O.K. 2012. Knee simulator wear of vitamin E stabilized irradiated ultrahigh molecular weight polyethylene. *The Journal of arthroplasty*. **27**(1), pp.95–104.
- Minoda, Y., Aihara, M., Sakawa, A., Fukuoka, S., Hayakawa, K., Tomita, M., Umeda, N. and Ohzono, K. 2009. Comparison between highly cross-linked and conventional polyethylene in total knee arthroplasty. *The Knee*. **16**(5), pp.348–351.
- Miranda, D.L., Rainbow, M.J., Crisco, J.J. and Fleming, B.C. 2013. Kinematic differences between optical motion capture and biplanar videoradiography during a jump-cut maneuver. *Journal of Biomechanics*. **46**(3), pp.567–573.
- Miranda, D.L., Schwartz, J.B., Loomis, A.C., Brainerd, E.L., Fleming, B.C. and Crisco, J.J. 2011. Static and Dynamic Error of a Biplanar Videoradiography System Using Marker-Based and Markerless Tracking Techniques. *Journal of Biomechanical Engineering*. **133**(12), pp.121002-1-121002–8.
- Misgeld, B.J.E., Zhang, T., Lüken, M.J. and Leonhardt, S. 2017. Model-based estimation of ankle joint stiffness. *Sensors (Switzerland)*. **17**(4), pp.1–26.
- Mohammad, H.R., Campi, S., Kennedy, J.A., Judge, A., Murray, D.W. and Mellon, S.J. 2019. Long-term in vivo wear of different bearing types used for the oxford Unicompartmental Knee Replacement. *Bone and Joint Research*. **8**(11), pp.535–543.
- Mondal, S. and Ghosh, R. 2019. Effects of implant orientation and implant material on tibia bone strain, implant–bone micromotion, contact pressure, and wear depth due to total ankle replacement. *Proceedings of the Institution of Mechanical Engineers, Part H: Journal of Engineering in Medicine*. **233**(3), pp.318–331.
- Morasiewicz, P., Dejnek, M., Orzechowski, W., Urbański, W., Kulej, M., Dragan, S.L., Dragan, S.F. and Pawik, Ł. 2019. Clinical evaluation of ankle arthrodesis with Ilizarov fixation and internal fixation. *BMC Musculoskeletal Disorders*. **20**(1), pp.1–8.
- Moreno-Hernández, A., Rodríguez-Reyes, G., Quiñones-Urióstegui, I., Núñez-Carrera, L. and Pérez-SanPablo, A.I. 2010. Temporal and spatial gait parameters analysis in non-pathological Mexican children. *Gait and Posture*. **32**(1), pp.78–81.
- Morgan, E.F., Unnikrisnan, G.U. and Hussein, A.I. 2018. Bone Mechanical Properties in Healthy and Diseased States. *Annual Review of Biomedical Engineering*. **20**, pp.119–143.
- Morley, D., Jenkinson, C., Doll, H., Lavis, G., Sharp, R., Cooke, P. and Dawson, J. 2013. The Manchester–Oxford Foot Questionnaire (MOXFQ). *Bone & Joint Research*. **2**(4), pp.66–69.
- Moro, M., Marchesi, G., Hesse, F., Odone, F. and Casadio, M. 2022. Markerless vs. Marker-Based

- Gait Analysis: A Proof of Concept Study. *Sensors*. **22**(5), pp.1–15.
- Moseley, L., Smith, R., Hunt, A. and Gant, R. 1996. Three-dimensional kinematics of the rearfoot during the stance phase of walking in normal young adult males. *Clinical Biomechanics*. **11**(1), pp.39–45.
- Mujukian, A., Ho, N.C., Day, M.J., Ebrahimzadeh, E. and Sangiorgio, S.N. 2020. A Systematic Review of Unsystematic Total Ankle Replacement Wear Evaluations. *Journal of Bone and Joint Surgery Reviews*. **8**(3), pp.1–11.
- Muller, P., Skene, S.S., Chowdhury, K., Cro, S., Goldberg, A.J., Doré, C.J., Bendall, S., Bing, A., Blundell, C., Brown, R., Butcher, C., Butler, M., Clough, T., Cooke, P., Cullen, N., Davenport, J., Davies, M., Dhar, S., Goldberg, A., Halliwell, P., Harries, B., Hepple, S., Kakwani, R., Karski, M., Loveday, D., Makwana, N., Milner, S., Mishra, V., Molloy, A., Murty, A., Raglan, M., Rogers, B., Rogers, M., Siddique, M., Singh, D., Smith, R., Thomas, R., Torres, P., Townshend, D., Welck, M. and Winson, I. 2020. A randomised, multi-centre trial of total ankle replacement versus ankle arthrodesis in the treatment of patients with end stage ankle osteoarthritis (TARVA): Statistical analysis plan. *Trials*. **21**(1), pp.1–9.
- Mündermann, A., Dyrby, C.O., D’Lima, D.D., Colwell, C.W. and Andriacchi, T.P. 2008. In vivo knee loading characteristics during activities of daily living as measured by an instrumented total knee replacement. *Journal of Orthopaedic Research*. **26**(9), pp.1167–1172.
- Muratoglu, O.K. and Bragdon, C.R. 2016. Highly Cross-Linked and Melted UHMWPE. *UHMWPE Biomaterials Handbook*., pp.264–273.
- Muratoglu, O.K., Bragdon, C.R., Jasty, M., O’Connor, D.O., Von Knoch, R.S. and Harris, W.H. 2004. Knee-simulator testing of conventional and cross-linked polyethylene tibial inserts. *Journal of Arthroplasty*. **19**(7), pp.887–897.
- Muratoglu, O.K., Bragdon, C.R., O, D.O., Jasty, M. and Harris, W.H. 2001. A Novel Method of Cross-Linking Ultra-High-Molecular-Weight Polyethylene to Improve Wear, Reduce Oxidation, and Retain Mechanical Properties. *The Journal of Arthroplasty*. **16**(2), pp.149–160.
- Muratoglu, O.K., Perinchief, R.S., Bragdon, C.R., O’Connor, D.O., Konrad, R. and Harris, W.H. 2003. Metrology to quantify wear and creep of polyethylene tibial knee inserts *In: Clinical Orthopaedics and Related Research*., pp.155–164.
- Murray, C., Marshall, M., Rathod, T., Bowen, C.J., Menz, H.B. and Roddy, E. 2018. Population prevalence and distribution of ankle pain and symptomatic radiographic ankle osteoarthritis in community dwelling older adults: A systematic review and cross-sectional study. *PLoS ONE*. **13**(4), pp.1–23.
- Najefi, A., Malhotra, K., Chan, O., Cullen, N. and Goldberg, A. 2019a. The Bologna-Oxford

- ankle replacement: a case series of clinical and radiological outcomes. *International Orthopaedics*. **43**(10), pp.2333–2339.
- Najefi, A., Malhotra, K., Chan, O., Cullen, N. and Goldberg, A. 2019b. The Bologna-Oxford ankle replacement: a case series of clinical and radiological outcomes. *International orthopaedics*. **43**(10), pp.2333–2339.
- Najefi, A.A., Ghani, Y. and Goldberg, A.J. 2021. Bone Cysts and Osteolysis in Ankle Replacement. *Foot and Ankle International*. **42**(1), pp.55–61.
- Naylor, A., Talwalkar, S., Trail, I. and Joyce, T. 2016. Evaluating the Surface Topography of Pyrolytic Carbon Finger Prostheses through Measurement of Various Roughness Parameters. *Journal of Functional Biomaterials*. **7**(2), pp.1–10.
- Nečas, D., Usami, H., Niimi, T., Sawae, Y., Křupka, I. and Hartl, M. 2020. Running-in friction of hip joint replacements can be significantly reduced: The effect of surface-textured acetabular cup. *Friction*. **8**(6), pp.1137–1152.
- Neptune, R.R., Kautz, S.A. and Zajac, F.E. 2001. Contributions of the individual ankle plantar flexors to support, forward progression and swing initiation during walking. *Journal of Biomechanics*. **34**(11), pp.1387–1398.
- Nester, C, Jones, R.K., Liu, A., Howard, D., Lundberg, A., Arndt, A., Lundgren, P., Stacoff, A. and Wolf, P. 2007. Foot kinematics during walking measured using bone and surface mounted markers. *Journal of Biomechanics*. **40**(15), pp.3412–3423.
- Nester, C., Jones, R.K., Liu, A., Howard, D., Lundberg, A., Arndt, A., Lundgren, P., Stacoff, A. and Wolf, P. 2007. Foot kinematics during walking measured using bone and surface mounted markers. *Journal of Biomechanics*. **40**(15), pp.3412–3423.
- Nigg, B.M. 2001. The role of impact forces and foot pronation: A new paradigm. *Clinical Journal of Sport Medicine*. **11**(1), pp.2–9.
- Nihal, A., Gellman, R.E., Embil, J.M. and Trepman, E. 2008. Ankle arthrodesis. *Foot and Ankle Surgery*. **14**(1), pp.1–10.
- NJR 2021. National Joint Registry 18th Annual Report. *National Joint Registry | 18th Annual Report*. [Online]. Available from: [www.njrcentre.org.uk](http://www.njrcentre.org.uk).
- Noonan, K.J., Halliday, S., Browne, R., O'Brien, S., Kayes, K. and Feinberg, J. 2003. Interobserver Variability of Gait Analysis in Patients With Cerebral Palsy. *Journal of Pediatric Orthopaedics*. **23**(3), pp.279–287.
- Nordin, M. and Frankel, V.H. 2021. *Basic Biomechanics of the Musculoskeletal System* 5th ed. Wolters Kluwer Health.

- Norvell, D.C., Ledoux, W.R., Shofer, J.B., Hansen, S.T., Davitt, J., Anderson, J.G., Bohay, D., Coetzee, J.C., Maskill, J., Brage, M., Houghton, M. and Sangeorzan, B.J. 2019. Effectiveness and Safety of Ankle Arthrodesis Versus Arthroplasty: A Prospective Multicenter Study. *The Journal of Bone and Joint Surgery. American Volume*. **101**(16), p.1485.
- Novacheck, T.F. 1998. The biomechanics of running. *Gait and Posture*. **7**, pp.77–95.
- Oeffinger, D., Brauch, B., Cranfill, S., Hisle, C., Wynn, C., Hicks, R. and Augsburg, S. 1999. Comparison of gait with and without shoes in children. *Gait and Posture*. **9**(2), pp.95–100.
- Okita, N., Meyers, S.A., Challis, J.H. and Sharkey, N.A. 2009. An objective evaluation of a segmented foot model. *Gait & Posture*. **30**(1), pp.27–34.
- Oral, E. and Muratoglu, O.K. 2011. Vitamin E diffused, highly crosslinked UHMWPE: a review. *International Orthopaedics*. **35**(2), p.215.
- Ormsby, R.T., Solomon, L.B., Yang, D., Crotti, T.N., Haynes, D.R., Findlay, D.M. and Atkins, G.J. 2019. Osteocytes respond to particles of clinically-relevant conventional and cross-linked polyethylene and metal alloys by up-regulation of resorptive and inflammatory pathways. *Acta Biomaterialia*. **87**, pp.296–306.
- Ounpuu, S. 1990. The biomechanics of running: a kinematic and kinetic analysis. *Instructional course lectures*. **39**, pp.305–318.
- Palanca, A., Mann, R.A., Mann, J.A. and Haskell, A. 2018. Scandinavian Total Ankle Replacement: 15-Year Follow-up. *Foot and Ankle International*. **39**(2), pp.135–142.
- Pataky, T.C. 2010. Generalized n-dimensional biomechanical field analysis using statistical parametric mapping. *Journal of Biomechanics*. **43**(10), pp.1976–1982.
- Pataky, T.C., Robinson, M.A. and Vanrenterghem, J. 2013. Vector field statistical analysis of kinematic and force trajectories. *Journal of Biomechanics*. **46**(14), pp.2394–2401.
- Pawlus, P. and Śmieszek, M. 2005. The influence of stylus flight on change of surface topography parameters. *Precision Engineering*. **29**(3), pp.272–280.
- Paxton, E.W., Inacio, M.C.S., Kurtz, S., Love, R., Cafri, G. and Namba, R.S. 2015. Is There a Difference in Total Knee Arthroplasty Risk of Revision in Highly Crosslinked versus Conventional Polyethylene? *Clinical Orthopaedics and Related Research*. **473**(3), p.999.
- Pellengahr, C., Müller, P.E., Dürr, H.R., Maier, M., Birkenmaier, C., Mazoochian, F., Pfahler, M., Troillier, H., Lienemann, A. and Jansson, V. 2005. The Influence of the Implant Size on the Outcome of Unconstrained Total Knee Arthroplasty. *Acta Chirurgica Belgica*. **105**(5), pp.508–510.

- Perry, J. and Burnfield, J. 2010. *Gait Analysis, Normal and Pathological Function*. 2nd ed. Slack Firm.
- Peters, A., Galna, B., Sangeux, M., Morris, M. and Baker, R. 2010. Quantification of soft tissue artifact in lower limb human motion analysis: A systematic review. *Gait and Posture*. **31**(1), pp.1–8.
- Pezzotti, G. 2017. Raman spectroscopy of biomedical polyethylenes. *Acta Biomaterialia*. **55**, pp.28–99.
- Pham, T.M., Erichsen, J.L., Kowal, J.M., Overgaard, S. and Schmal, H. 2021. Elevation of pro-inflammatory cytokine levels following intra-articular fractures—a systematic review. *Cells*. **10**(4), pp.1–9.
- De Pieri, E., Lund, M.E., Gopalakrishnan, A., Rasmussen, K.P., Lunn, D.E. and Ferguson, S.J. 2018. Refining muscle geometry and wrapping in the TLEM 2 model for improved hip contact force prediction. *PLoS ONE*. **13**(9), pp.1–19.
- Pinsker, E., Inrig, T., Daniels, T.R., Warmington, K. and Beaton, D.E. 2016. Symptom Resolution and Patient-Perceived Recovery Following Ankle Arthroplasty and Arthrodesis. *Foot & ankle international*. **37**(12), pp.1269–1276.
- Piriou, P., Paul, C., Mark, M., Jean-Noel, C., Delphine, P. and Thierry, J. 2008. Ankle Replacement versus Arthrodesis: A Comparative Gait Analysis Study. *Foot & Ankle International*. **29**(1), pp.3–9.
- Van Der Plaats, L.W. and Haverkamp, D. 2017. Patient selection for total ankle arthroplasty. *Orthopedic Research and Reviews*. **9**, pp.63–73.
- Plante-Bordeneuve, P. and Freeman, M.A.R. 1993. Tibial high-density polyethylene wear in conforming tibiofemoral prostheses. *Journal of Bone and Joint Surgery - Series B*. **75**(4), pp.630–636.
- Portinaro, N., Leardini, A., Panou, A., Monzani, V. and Caravaggi, P. 2014. Modifying the Rizzoli foot model to improve the diagnosis of pes-planus: application to kinematics of feet in teenagers. *Journal of Foot and Ankle Research*. **7**(1), pp.1–14.
- Postak, P.D., Rosca, M. and Greenwald, A.S. 2008. *Evaluation of the STAR Total Ankle Replacement: An Evolution in Design*. AAOS.
- Pothrat, C., Authier, G., Viehweger, E., Berton, E. and Rao, G. 2015. One- and multi-segment foot models lead to opposite results on ankle joint kinematics during gait: Implications for clinical assessment. *Clinical Biomechanics*. **30**(5), pp.493–499.
- Procter, P. and Paul, J.P. 1982. Ankle joint biomechanics. *Journal of Biomechanics*. **15**(9), pp.627–634.

- Di Puccio, F. and Mattei, L. 2015. Biotribology of artificial hip joints. *World Journal of Orthopaedics*. **6**(1), pp.77–94.
- Queen, R. 2017a. Directing clinical care using lower extremity biomechanics in patients with ankle osteoarthritis and ankle arthroplasty. *Journal of Orthopaedic Research*. **35**(11), pp.2345–2355.
- Queen, R., Franck, C.T., Schmitt, D. and Adams, S.B. 2017b. Are There Differences in Gait Mechanics in Patients With A Fixed Versus Mobile Bearing Total Ankle Arthroplasty? A Randomized Trial. *Clinical Orthopaedics and Related Research*. **475**(10), pp.1–8.
- Queen, R.M., De Biassio, J.C., Butler, R.J., DeOrio, J.K., Easley, M.E. and Nunley, J.A. 2012. Changes in pain, function, and gait mechanics two years following total ankle arthroplasty performed with two modern fixed-bearing prostheses. *Foot and Ankle International*. **33**(7), pp.535–542.
- Queen, R.M., Butler, R.J., Adams, S.B., Deorio, J.K., Easley, M.E. and Nunley, J.A. 2014. Bilateral differences in gait mechanics following total ankle replacement: A two year longitudinal study. *Clinical biomechanics (Bristol, Avon)*. **29**(4), pp.418–422.
- Queen, R.M., Campbell, J.C. and Schmitt, D. 2019. Gait Analysis Reveals that Total Hip Arthroplasty Increases Power Production in the Hip during Level Walking and Stair Climbing. *Clinical Orthopaedics and Related Research*. **477**(8), pp.1839–1847.
- Queen, R.M., Gross, M.T. and Liu, H.Y. 2006. Repeatability of lower extremity kinetics and kinematics for standardized and self-selected running speeds. *Gait and Posture*. **23**(3), pp.282–287.
- Rabinowicz, E. and Tanner, R.I. 1966. Friction and Wear of Materials. *Journal of Applied Mechanics*. **33**(2), pp.479–479.
- Rahman, J., Tang, Q., Monda, M., Miles, J. and McCarthy, I. 2015. Gait assessment as a functional outcome measure in total knee arthroplasty: A cross-sectional study. *BMC Musculoskeletal Disorders*. **16**(1), pp.1–9.
- Rames, R.D., Hillen, T.J., Pashos, G.E., Maloney, W.J. and Clohisy, J.C. 2021. Incidence and Characteristics of Osteolysis in HXLPE THA at 16-Year Follow up in Patients 50 Years and Less. *Journal of Arthroplasty*. **36**(2), pp.641–646.
- Rao, S.R., Saltzman, C.L., Wilken, J. and Yak, H.J. 2006. Increased passive ankle stiffness and reduced dorsiflexion range of motion in individuals with diabetes mellitus. *Foot and Ankle International*. **27**(8), pp.617–622.
- Reggiani, B., Leardini, A., Corazza, F. and Taylor, M. 2006. Finite element analysis of a total ankle

- replacement during the stance phase of gait. *Journal of Biomechanics*. **39**(8), pp.1435–1443.
- Reinders, J., Sonntag, R. and Kretzer, J.P. 2014. How do gait frequency and serum-replacement interval affect polyethylene wear in knee-wear simulator tests? *Journal of Materials Science: Materials in Medicine* 2014 25:11. **25**(11), pp.2463–2469.
- Reinders, J., Sonntag, R., Vot, L., Gibney, C., Nowack, M. and Kretzer, J.P. 2015a. Wear testing of moderate activities of daily living using in vivo measured knee joint loading. *PLoS ONE*. **10**(3), pp.1–14.
- Reinders, J., Von Stillfried, F., Altan, E., Sonntag, R., Heitzmann, D.W.W. and Kretzer, J.P. 2015b. Force-controlled dynamic wear testing of total ankle replacements. *Acta Biomaterialia*. **12**(C), pp.332–340.
- Reinschmidt, C., Van Den Bogert, A.J., Murphy, N., Lundberg, A. and Nigg, B.M. 1997. Tibiocalcaneal motion during running, measured with external and bone markers. *Clinical Biomechanics*. **12**(1), pp.8–16.
- Ries, M.D. and Pruitt, L. 2005. Effect of cross-linking on the microstructure and mechanical properties of ultra-high molecular weight polyethylene. *Clinical Orthopaedics and Related Research*. **440**, pp.149–156.
- Robati, S., Salih, A., Ghosh, K. and Vinayakam, P. 2016. The Scandinavian Total Ankle Replacement and the ideal biomechanical requirements of ankle replacements. *Journal of Orthopaedics*. **13**(1), pp.48–51.
- Robertson, D.G.E. and Dowling, J.J. 2003. Design and responses of Butterworth and critically damped digital filters. *Journal of Electromyography and Kinesiology*. **13**(6), pp.569–573.
- Robertson, G., Caldwell, G., Hamill, J., Kamen, G. and Whittlesey, S. 2013. *Research Methods in Biomechanics* 2nd ed. Human Kinetics.
- Robles-García, V., Corral-Bergantiños, Y., Espinosa, N., Jácome, M.A., García-Sancho, C., Cudeiro, J. and Arias, P. 2015. Spatiotemporal gait patterns during overt and covert evaluation in patients with Parkinson's disease and healthy subjects: Is there a Hawthorne effect? *Journal of Applied Biomechanics*. **31**(3), pp.189–194.
- Rodriguez, D., Bevernage, B.D., Maldague, P., Deleu, P.A., Tribak, K. and Leemrijse, T. 2010. Medium term follow-up of the AES ankle prosthesis: High rate of asymptomatic osteolysis. *Foot and Ankle Surgery*. **16**(2), pp.54–60.
- Roewer, B.D., Ford, K.R., Myer, G.D. and Hewett, T.E. 2014. The 'impact' of force filtering cut-off frequency on the peak knee abduction moment during landing: Artefact or 'artifiction'. *British Journal of Sports Medicine*. **48**(6), pp.464–468.

- Roislén, J., Skare, Opheim, A. and Rennie, L. 2012. Evaluating the properties of the coefficient of multiple correlation (CMC) for kinematic gait data. *Journal of Biomechanics*. **45**(11), pp.2014–2018.
- Roukis, T.S. and Simonson, D.C. 2015. Incidence of Complications During Initial Experience with Revision of the Agility and Agility LP Total Ankle Replacement Systems: A Single Surgeon's Learning Curve Experience. *undefined*. **32**(4), pp.569–593.
- Saari, H., Santavirta, S., Nordström, D., Paavolainen, P. and Konttinen, Y.T. 1993. Hyaluronate in total hip replacement. *The Journal of Rheumatology*. **20**(1), pp.87–90.
- Saari, T., Tranberg, R., Zügner, R., Uvehammer, J. and Kärrholm, J. 2005. Changed gait pattern in patients with total knee arthroplasty but minimal influence of tibial insert design: Gait analysis during level walking in 39 TKR patients and 18 healthy controls. *Acta Orthopaedica*. **76**(2), pp.253–260.
- Sagbas, B. 2016. Biotribology of Artificial Hip Joints *In: Advances in Tribology*. IntechOpen.
- Sagbas, B. and Numan Durakbasa, M. 2012. Measurement of wear in orthopedic prosthesis. *Acta Physica Polonica A*. **121**(1), pp.131–134.
- Saikko, V. 2006. Effect of contact pressure on wear and friction of ultra-high molecular weight polyethylene in multidirectional sliding. *Proceedings of the Institution of Mechanical Engineers, Part H: Journal of Engineering in Medicine*. **220**(7), pp.723–731.
- Saikko, V. 2003. Effect of lubricant protein concentration on the wear of ultra-high molecular weight polyethylene sliding against a CoCr counterface. *Journal of Tribology*. **125**(3), pp.638–642.
- Saikko, V.O., Paavolainen, P.O. and Slätis, P. 1993. Wear of the polyethylene acetabular cup: Metallic and ceramic heads compared in a hip simulator. *Acta Orthopaedica*. **64**(4), pp.391–402.
- Saito, G.H., Sanders, A.E., O'Malley, M.J., Deland, J.T., Ellis, S.J. and Demetracopoulos, C.A. 2019. Accuracy of patient-specific instrumentation in total ankle arthroplasty: A comparative study. *Foot and Ankle Surgery*. **25**(3), pp.383–389.
- Sakellariou, V.I., Sculco, P., Poultsides, L., Wright, T. and Sculco, T.P. 2013. Highly Cross-Linked Polyethylene May Not Have an Advantage in Total Knee Arthroplasty. *HSS Journal*. **9**(3), p.264.
- Saltzman, C.L., Mann, R.A., Ahrens, J.E., Amendola, A., Anderson, R.B., Berlet, G.C., Brodsky, J.W., Chou, L.B., Clanton, T.O., Deland, J.T., DeOrio, J.K., Horton, G.A., Lee, T.H., Mann, J.A., Nunley, J.A., Thordarson, D.B., Walling, A.K., Wapner, K.L. and Coughlin, M.J. 2009.

- Prospective Controlled Trial of STAR Total Ankle Replacement versus Ankle Fusion: Initial Results. *Foot & Ankle International*. **30**(7), pp.579–596.
- Saltzman, C.L., Salamon, M.L., Blanchard, G.M., Huff, T., Hayes, A., Buckwalter, J. a and Amendola, A. 2005. Epidemiology of ankle arthritis: report of a consecutive series of 639 patients from a tertiary orthopaedic center. *The Iowa orthopaedic journal*. **25**, pp.44–6.
- Saltzman, C.L., Zimmerman, M.B., O'Rourke, M., Brown, T.D., Buckwalter, J.A. and Johnston, R. 2006. Impact of comorbidities on the measurement of health in patients with ankle osteoarthritis. *Journal of Bone and Joint Surgery - Series A*. **88**(11), pp.2366–2372.
- Saltzman, C.L., Zimmerman, M.B., O' Rourke, M., Brown, T.D., Buckwalter, J.A. and Johnston, R. 2006. Impact of Comorbidities on the Measurement of Health in Patients with Ankle Osteoarthritis. *The Journal of Bone & Joint Surgery*. **88**(11), pp.2366–2372.
- Sammarco, G. and Hockenbury, R. 2012. Biomechanics of the foot and ankle *In: M. Nordin and V. H. (Victor H. Frankel, eds. Basic Biomechanics of the Musculoskeletal System*. Philadelphia: Lippincott Williams & Wilkins, pp.222–255.
- Sanders, A.E., Kraszewski, A.P., Ellis, S.J., Queen, R., Backus, S.I., Hillstrom, H. and Demetracopoulos, C.A. 2021. Differences in Gait and Stair Ascent After Total Ankle Arthroplasty and Ankle Arthrodesis. *Foot & ankle international*. **42**(3), pp.347–355.
- Sarraffian, S.K. 1993. Biomechanics of the subtalar joint complex. *Clinical orthopaedics and related research*. **290**, pp.17–26.
- Sathasivam, S., Walker, P.S., Campbell, P.A. and Rayner, K. 2001. The effect of contact area on wear in relation to fixed bearing and mobile bearing knee replacements. *Journal of Biomedical Materials Research*. **58**(3), pp.282–290.
- Scalona, E., Di Marco, R., Castelli, E., Desloovere, K., Van Der Krogt, M., Cappa, P. and Rossi, S. 2019. Inter-laboratory and inter-operator reproducibility in gait analysis measurements in pediatric subjects. *International Biomechanics*. **6**(1), pp.19–33.
- Schallig, W., van den Noort, J.C., Maas, M., Harlaar, J. and van der Krogt, M.M. 2021a. Marker placement sensitivity of the Oxford and Rizzoli foot models in adults and children. *Journal of Biomechanics*. **126**, pp.1–7.
- Schallig, W., Streekstra, G.J., Hulshof, C.M., Kleipool, R.P., Dobbe, J.G.G., Maas, M., Harlaar, J., van der Krogt, M.M. and van den Noort, J.C. 2021b. The influence of soft tissue artifacts on multi-segment foot kinematics. *Journal of Biomechanics*. **120**, pp.1–8.
- Schimmel, J.J.P., Walschot, L.H.B. and Louwerens, J.W.K. 2014. Comparison of the short-term results of the first and last 50 scandinavian total ankle replacements: Assessment of the

- learning curve in a consecutive series. *Foot and Ankle International*. **35**(4), pp.326–333.
- Schipper, O.N., Dharia, M.A., Hertzler, J.S. and Bischoff, J.E. 2019. Fatigue Strength of Highly Crosslinked Polyethylene in Total Ankle Arthroplasty *In: AOFAS Annual Meeting 2019*, p.1.
- Schipper, O.N., Haddad, S.L., Fullam, S., Pourzal, R. and Wimmer, M.A. 2018. Wear Characteristics of Conventional Ultrahigh-Molecular-Weight Polyethylene Versus Highly Cross-Linked Polyethylene in Total Ankle Arthroplasty. *Foot & Ankle International*. **39**(11), pp.1335–1344.
- Schipper, O.N., Haddad, S.L., Pytel, P. and Zhou, Y. 2017. Histological Analysis of Early Osteolysis in Total Ankle Arthroplasty. *Foot and Ankle International*. **38**(4), pp.351–359.
- Schmalzried, T.P. and Callaghan, J.J. 1999. Wear in total hip and knee replacements. *Journal of Bone and Joint Surgery - Series A*. **81**(1), pp.115–136.
- Schmalzried, T.P., Szuszczewicz, E.S., Northfield, M.R., Akizuki, K.H., Frankel, R.E., Belcher, G. and Amstutz, H.C. 1998. Quantitative assessment of walking activity after total hip or knee replacement. *Journal of Bone and Joint Surgery - Series A*. **80**(1), pp.54–59.
- Scholes, S.C., Kennard, E., Gangadharan, R., Weir, D., Holland, J., Deehan, D. and Joyce, T.J. 2012. Topographical analysis of the femoral components of ex vivo total knee replacements. *Journal of Materials Science: Materials in Medicine* 24:2. **24**(2), pp.547–554.
- Scholes, S.C. and Unsworth, A. 2006. The effects of proteins on the friction and lubrication of artificial joints. *Proceedings of the Institution of Mechanical Engineers, Part H: Journal of Engineering in Medicine*. **220**(6), pp.687–693.
- Schröder, C., Reinders, J., Zietz, C., Utzschneider, S., Bader, R. and Kretzer, J.P. 2013. Characterization of polyethylene wear particle: The impact of methodology. *Acta Biomaterialia*. **9**(12), pp.9485–9491.
- Schroeder, C., Grupp, T.M., Fritz, B., Schilling, C., Chevalier, Y., Utzschneider, S. and Jansson, V. 2013. The influence of third-body particles on wear rate in unicondylar knee arthroplasty: A wear simulator study with bone and cement debris. *Journal of Materials Science: Materials in Medicine*. **24**(5), pp.1319–1325.
- Schwartz, M.H., Trost, J.P. and Wervey, R.A. 2004. Measurement and management of errors in quantitative gait data. *Gait & Posture*. **20**(2), pp.196–203.
- Schwenke, T., Kaddick, C., Schneider, E. and Wimmer, M.A. 2005. Fluid composition impacts standardized testing protocols in ultrahigh molecular weight polyethylene knee wear testing. *Proceedings of the Institution of Mechanical Engineers, Part H: Journal of Engineering in Medicine*. **219**(6), pp.457–464.

- Schwenke, T., Orozco, D., Schneider, E. and Wimmer, M.A. 2009. Differences in wear between load and displacement control tested total knee replacements. *Wear*. **267**(5–8), pp.757–762.
- Schwenke, T., Schneider, E. and Wimmer, M.A. 2006. Load profile and fluid composition influence the soak behavior of UHMWPE implants. *Journal of ASTM International*. **3**(8), pp.1–5.
- Schwiesau, J., Fritz, B., Kutzner, I., Bergmann, G. and Grupp, T.M. 2014. CR TKA UHMWPE wear tested after artificial aging of the vitamin e treated gliding component by simulating daily patient activities. *BioMed Research International*. **2014**(4), pp.1–4.
- Schwiesau, J., Schilling, C., Kaddick, C., Utzschneider, S., Jansson, V., Fritz, B., Blömer, W. and Grupp, T.M. 2013a. Definition and evaluation of testing scenarios for knee wear simulation under conditions of highly demanding daily activities. *Medical Engineering and Physics*. **35**(5), pp.591–600.
- Schwiesau, J., Schilling, C., Utzschneider, S., Jansson, V., Fritz, B., Blömer, W. and Grupp, T.M. 2013b. Knee wear simulation under conditions of highly demanding daily activities - Influence on an unicompartmental fixed bearing knee design. *Medical Engineering and Physics*. **35**(8), pp.1204–1211.
- Sealey, R.J., Myerson, M.S., Molloy, A., Gamba, C., Jeng, C. and Kalesan, B. 2009. Roger Mann Award 2008: Sagittal Plane Motion of the Hindfoot Following Ankle Arthrodesis: A Prospective Analysis. *Foot & Ankle International*. **30**(3), pp.187–196.
- Sedlaček, M., Podgornik, B. and Vižintin, J. 2012. Correlation between standard roughness parameters skewness and kurtosis and tribological behaviour of contact surfaces. *Tribology International*. **48**, pp.102–112.
- Segal, A.D., Cyr, K.M., Stender, C.J., Whittaker, E.C., Hahn, M.E., Orendurff, M.S., Ledoux, W.R. and Sangeorzan, B.J. 2018. A three-year prospective comparative gait study between patients with ankle arthrodesis and arthroplasty. *Clinical Biomechanics*. **54**, pp.42–53.
- Seireg, A. and Arvikar, R.J. 1975. The prediction of muscular load sharing and joint forces in the lower extremities during walking. *Journal of Biomechanics*. **8**(2), pp.89–102.
- Seng, B.E., Berend, K.R., Ajluni, A.F. and Lombardi, A. V. 2009. Anterior-Supine Minimally Invasive Total Hip Arthroplasty: Defining the Learning Curve. *Orthopedic Clinics of North America*. **40**(3), pp.343–350.
- Seo, S.G., Kim, E.J., Lee, D.J., Bae, K.J., Lee, K.M. and Lee, D.Y. 2017. Comparison of Multisegmental Foot and Ankle Motion Between Total Ankle Replacement and Ankle Arthrodesis in Adults. *Foot and Ankle International*. **38**(9), pp.1035–1044.

- Shanbhag, A.S., Jacobs, J.J., Glant, T.T., Gilbert, J.L., Black, J. and Galante, J.O. 1994. Composition and morphology of wear debris in failed uncemented total hip replacement. *Journal of Bone and Joint Surgery - Series B*. **76**(1), pp.60–67.
- Sharkey, N.A. and Hamel, A.J. 1998. A dynamic cadaver model of the stance phase of gait: Performance characteristics and kinetic validation. *Clinical Biomechanics*. **13**(6), pp.420–433.
- Sheehan, F.T., Seisler, A.R. and Siegel, K.L. 2007. In Vivo Talocrural and Subtalar Kinematics: A Non-invasive 3D Dynamic MRI Study. *Foot & Ankle International*. **28**(3), pp.323–335.
- Shen, F.W., Lu, Z. and McKellop, H.A. 2011. Wear versus thickness and other features of 5-mrad crosslinked UHMWPE acetabular liners. *Clinical Orthopaedics and Related Research*. **469**(2), pp.395–404.
- Shen, G., Zhang, J.-F., Fang, F.-Z., Shen, G., Zhang, J.-F. and Fang, F.-Z. 2019. In vitro evaluation of artificial joints: a comprehensive review. *Advances in Manufacturing*. **7**(1), pp.1–14.
- Shendkar, C. V., Lenka, P.K., Biswas, A., Kumar, R. and Mahadevappa, M. 2015. Therapeutic effects of functional electrical stimulation on gait, motor recovery, and motor cortex in stroke survivors. *Hong Kong Physiotherapy Journal*. **33**(1), pp.10–20.
- Shepherd, D.E.T. and Seedhom, B.B. 1999. Thickness of human articular cartilage in joints of the lower limb. *Annals of the Rheumatic Diseases*. **58**(1), pp.27–34.
- Sheridan, B.D., Robinson, D.E., Hubble, M.J.W. and Winson, I.G. 2006. Ankle arthrodesis and its relationship to ipsilateral arthritis of the hind- and mid-foot. *Journal of Bone and Joint Surgery - Series B*. **88**(2), pp.206–207.
- Shultz, R., Kedgley, A.E. and Jenkyn, T.R. 2011. Quantifying skin motion artifact error of the hindfoot and forefoot marker clusters with the optical tracking of a multi-segment foot model using single-plane fluoroscopy. *Gait & Posture*. **34**(1), pp.44–48.
- Siegler, S., Toy, J., Seale, D. and Pedowitz, D. 2014. The Clinical Biomechanics Award 2013 -- presented by the International Society of Biomechanics: New observations on the morphology of the talar dome and its relationship to ankle kinematics. *Clinical biomechanics (Bristol, Avon)*. **29**(1), pp.1–6.
- Simoneau, G.G., Hoenig, K.J., Lepley, J.E. and Papanek, P.E. 1998. Influence of hip position and gender on active hip internal and external rotation. *Journal of Orthopaedic and Sports Physical Therapy*. **28**(3), pp.158–164.
- Simonsen, E.B., Dyhre-Poulsen, P., Voigt, M., Aagaard, P., Sjogaard, G. and Bojsen-Moller, F. 1995. Bone-on-bone forces during loaded and unloaded walking. *Acta Anatomica*. **152**(2),

pp.133–142.

- Singer, S., Klejman, S., Pinsker, E., Houck, J. and Daniels, T. 2013. Ankle arthroplasty and ankle arthrodesis: gait analysis compared with normal controls. *The Journal of bone and joint surgery. American volume.* **95**(24), e191(1-10).
- van Sint Jan, S. 2007. *Color Atlas of Skeletal Landmark* 1st ed. Edinburgh: Churchill Livingstone.
- Smith, S.L., Dowson, D. and Goldsmith, A.A.J. 2001. The effect of femoral head diameter upon lubrication and wear of metal-on-metal total hip replacements. *Proceedings of the Institution of Mechanical Engineers, Part H: Journal of Engineering in Medicine.* **215**(2), pp.161–170.
- Smyth, A., Fisher, J., Suner, S. and Brockett, C. 2017. Influence of kinematics on the wear of a total ankle replacement. *Journal of Biomechanics.* **53**, pp.105–110.
- Smyth, A., Fisher, J., Suner, S. and Brockett, C. 2018. Malalignment Biomechanics for a Total Ankle Replacement *In: Orthopaedic Proceedings.* London: Bone & Joint Publishing.
- Snedeker, J.G. and Wirth, S.H. 2012. Biomechanics of the Normal and Arthritic Ankle Joint. *Foot and Ankle Clinics.* **17**(4), pp.517–528.
- So, E., Rushing, C.J., Prissel, M.A. and Berlet, G.C. 2021. Bone Mineral Density Testing in Patients Undergoing Total Ankle Arthroplasty: Should We Pay More Attention to the Bone Quality? *Journal of Foot and Ankle Surgery.* **60**(2), pp.224–227.
- Sokolowski, M., Krähenbühl, N., Wang, C., Zwicky, L., Schweizer, C., Horn Lang, T. and Hintermann, B. 2019. Secondary Subtalar Joint Osteoarthritis Following Total Ankle Replacement. *Foot and Ankle International.* **40**(10), pp.1122–1128.
- Sopher, R.S., Amis, A.A., Calder, J.D. and Jeffers, J.R.T. 2017. Total ankle replacement design and positioning affect implant-bone micromotion and bone strains. *Medical Engineering and Physics.* **42**, pp.80–90.
- Spinelli, M., Carmignato, S., Affatato, S. and Viceconti, M. 2009. CMM-based procedure for polyethylene non-congruous unicompartamental knee prosthesis wear assessment. *Wear.* **267**(5–8), pp.753–756.
- Stansfield, B.W., Nicol, A.C., Paul, J.P., Kelly, I.G., Graichen, F. and Bergmann, G. 2003. Direct comparison of calculated hip joint contact forces with those measured using instrumented implants. An evaluation of a three-dimensional mathematical model of the lower limb. *Journal of Biomechanics.* **36**(7), pp.929–936.
- Stauffer, R.N., Chao, E.Y. and Brewster, R.C. 1977. Force and motion analysis of the normal, diseased, and prosthetic ankle joint. *Clinical orthopaedics and related research.* (127), pp.189–196.

- Stewart, T.D. 2010. Tribology of artificial joints. *Orthopaedics and Trauma*. **24**(6), pp.435–440.
- Stone, A.E., Shofer, J.B., Stender, C.J., Whittaker, E.C., Hahn, M.E., Sangeorzan, B.J. and Ledoux, W.R. 2021. Ankle Fusion and Replacement Gait Similar Post- surgery, But Still Exhibit Differences Versus Controls Regardless of Footwear. *Journal of Orthopaedic Research*. **39**(11), pp.2506–2518.
- Stratton-Powell, A., Tipper, J., Williams, S., Redmond, A. and Brockett, C. 2016. A retrieval analysis of 22 AES total ankle replacement explants. *Foot and Ankle Surgery*. **22**(2), pp.88–89.
- Stratton-Powell, A., Tipper, J.L., Williams, S., Redmond, A. and Brockett, C.L. 2018. Edge Loading in Explanted Total Ankle Replacements: A Polyethylene Insert Form and Volume Analysis *In: Orthopaedic Proceedings*.
- Stratton-Powell, A.A., Williams, S., Tipper, J.L., Redmond, A.C. and Brockett, C.L. 2022. Mixed material wear particle isolation from periprosthetic tissue surrounding total joint replacements. *Journal of Biomedical Materials Research - Part B Applied Biomaterials*.
- Strickland, M.A., Dressler, M.R. and Taylor, M. 2012. Predicting implant UHMWPE wear in-silico: A robust, adaptable computational-numerical framework for future theoretical models. *Wear*. **274–275**, pp.100–108.
- Suckel, A., Muller, O., Herberts, T. and Wulker, N. 2007. Changes in Chopart joint load following tibiotalar arthrodesis: In vitro analysis of 8 cadaver specimen in a dynamic model. *BMC Musculoskeletal Disorders*. **8**(80), pp.1–14.
- Sutherland, D.H. 2002. The evolution of clinical gait analysis: Part II kinematics. *Gait and Posture*. **16**(2), pp.159–179.
- Szeri, A.Z. 2010. *Fluid Film Lubrication* 2nd ed. Cambridge University Press.
- Takakura, Y., Tanaka, Y., Kumai, T. and Tamai, S. 1995. Low tibial osteotomy for osteoarthritis of the ankle. Results of a new operation in 18 patients. *Journal of Bone and Joint Surgery - Series B*. **77**(1), pp.50–54.
- Tateiwa, T., Clarke, I.C., Shirasu, H., Masaoka, T., Shishido, T. and Yamamoto, K. 2006. Effect of low protein concentration lubricants in hip simulators. *Journal of Orthopaedic Science*. **11**(2), pp.204–211.
- Teeter, M.G., Howard, J.L., McCalden, R.W. and Naudie, D.D. 2017. Comparison of articular and backside polyethylene wear in mobile bearing unicompartmental knee replacement. *Knee*. **24**(2), pp.429–433.
- Teeter, M.G., Milner, J.S., MacDonald, S.J. and Naudie, D.D.R. 2013. Manufacturing lot affects

polyethylene tibial insert volume, thickness, and surface geometry. *Proceedings of the Institution of Mechanical Engineers, Part H: Journal of Engineering in Medicine*. **227**(8), pp.884–889.

- Teeter, M.G., Milner, J.S., Naudie, D.D.R. and MacDonald, S.J. 2014. Surface extraction can provide a reference for micro-CT analysis of retrieved total knee implants. *Knee*. **21**(4), pp.801–805.
- Teeter, Matthew G, Naudie, D.D., McErlain, D.D., Brandt, J.M., Yuan, X., MacDonald, S.J. and Holdsworth, D.W. 2011a. In Vitro Quantification of Wear in Tibial Inserts Using Microcomputed Tomography. *Clinical Orthopaedics and Related Research*. **469**(1), pp.107–112.
- Teeter, M.G., Naudie, D.D.R., Charron, K.D. and Holdsworth, D.W. 2010. Three-Dimensional Surface Deviation Maps for Analysis of Retrieved Polyethylene Acetabular Liners Using Micro-Computed Tomography. *Journal of Arthroplasty*. **25**(2), pp.330–332.
- Teeter, Matthew G., Naudie, D.D.R., Milner, J.S. and Holdsworth, D.W. 2011b. Determination of Reference Geometry for Polyethylene Tibial Insert Wear Analysis. *Journal of Arthroplasty*. **26**(3), pp.497–503.
- Tenenbaum, S., Bariteau, J., Coleman, S. and Brodsky, J. 2017. Functional and clinical outcomes of total ankle arthroplasty in elderly compared to younger patients. *Foot and Ankle Surgery*. **23**(2), pp.102–107.
- Thien, T.M., Chatziagorou, G., Garellick, G., Furnes, O., Havelin, L.I., Mäkelä, K., Overgaard, S., Pedersen, A., Eskelinen, A., Pulkkinen, P. and Kärrholm, J. 2014. Periprosthetic femoral fracture within two years after total hip replacement: Analysis of 437,629 operations in the nordic arthroplasty register association database. *Journal of Bone and Joint Surgery - American Volume*. **96**(19), e167(1)-e167(7).
- Thomas, R., Daniels, T.R. and Parker, K. 2006. Gait analysis and functional outcomes following ankle arthrodesis for isolated ankle arthritis. *Journal of Bone and Joint Surgery - Series A*. **88**(3), pp.526–535.
- Thomas, R.H. and Daniels, T.R. 2003. Ankle arthritis. *The Journal of bone and joint surgery. American volume*. **85-A**(5), pp.923–36.
- Tipper, J.L., Firkins, P.J., Besong, A.A., Barbour, P.S.M., Nevelos, J., Stone, M.H., Ingham, E. and Fisher, J. 2001. Characterisation of wear debris from UHMWPE on zirconia ceramic, metal-on-metal and alumina ceramic-on-ceramic hip prostheses generated in a physiological anatomical hip joint simulator. *Wear*. **250–251**(1–12), pp.120–128.
- Tipper, J.L., Galvin, A.L., Williams, S., McEwen, H.M.J., Stone, M.H., Ingham, E. and Fisher, J. 2006. Isolation and characterization of UHMWPE wear particles down to ten nanometers in size from in vitro hip and knee joint simulators. *Journal of Biomedical Materials Research Part*

A. **78A**(3), pp.473–480.

- Tipper, J.L., Ingham, E., Hailey, J.L., Besong, A.A., Fisher, J., Wroblewski, B.M. and Stone, M.H. 2000. Quantitative analysis of polyethylene wear debris, wear rate and head damage in retrieved Charnley hip prostheses. *Journal of materials science. Materials in medicine.* **11**(2), pp.117–24.
- Tochigi, Y., Rudert, M.J., Brown, T.D., McIff, T.E. and Saltzman, C.L. 2005. The effect of accuracy of implantation on range of movement of the Scandinavian Total Ankle Replacement. *The Journal of bone and joint surgery. British volume.* **87**(5), pp.736–740.
- Tomlinson, M. and Harrison, M. 2012. The New Zealand Joint Registry: Report of 11-Year Data for Ankle Arthroplasty. *Foot and Ankle Clinics.* **17**(4), pp.719–723.
- Topley, M. and Richards, J.G. 2020. A comparison of currently available optoelectronic motion capture systems. *Journal of Biomechanics.* **106**, pp.1–5.
- Tranberg, R. and Karlsson, D. 1998. The relative skin movement of the foot: a 2-D roentgen photogrammetry study. *Clinical Biomechanics.* **13**(1), pp.71–76.
- Trouillier, H., Hänsel, L., Schaff, P., Rosemeyer, B. and Refior, H.J. 2002. Long-term results after ankle arthrodesis: Clinical, radiological, gait analytical aspects. *Foot and Ankle International.* **23**(12), pp.1081–1090.
- Tsai, Y.J. and Lin, S.I. 2013. Older adults adopted more cautious gait patterns when walking in socks than barefoot. *Gait and Posture.* **37**(1), pp.88–92.
- von Tscharnner, V. and Valderrabano, V. 2010. Classification of multi muscle activation patterns of osteoarthritis patients during level walking. *Journal of Electromyography and Kinesiology.* **20**(4), pp.676–683.
- Turner, A., Okubo, Y., Teramura, S., Niwa, Y., Ibaraki, K., Kawasaki, T., Hamada, D., Uetsuki, K. and Tomita, N. 2014. The antioxidant and non-antioxidant contributions of vitamin E in vitamin E blended ultra-high molecular weight polyethylene for total knee replacement. *Journal of the Mechanical Behavior of Biomedical Materials.* **31**, pp.21–30.
- Uddin, M.S., Mak, C.Y.E. and Callary, S.A. 2016. Evaluating hip implant wear measurements by CMM technique. *Wear.* **364–365**, pp.193–200.
- Usuelli, F.G., Indino, C., Leardini, A., Manzi, L., Ortolani, M. and Caravaggi, P. 2021. Range of motion of foot joints following total ankle replacement and subtalar fusion. *Foot and Ankle Surgery.* **27**(2), pp.150–155.
- Usuelli, F.G., Maccario, C., Pantalone, A., Serra, N. and Tan, E.W. 2017. Identifying the learning curve for total ankle replacement using a mobile bearing prosthesis. *Foot and Ankle Surgery.*

23(2), pp.76–83.

- Valderrabano, V., Hintermann, B., Nigg, B.M., Stefanyshyn, D. and Stergiou, P. 2003. Kinematic Changes After Fusion and Total Replacement of the Ankle Part 1: Range of Motion. *Foot & Ankle International*. **24**(12), pp.881–887.
- Valderrabano, V., Nigg, B.M., von Tscharnner, V., Stefanyshyn, D.J., Goepfert, B. and Hintermann, B. 2007. Gait analysis in ankle osteoarthritis and total ankle replacement. *Clinical Biomechanics*. **22**(8), pp.894–904.
- Valderrabano, V., Pagenstert, G.I., Müller, A.M., Paul, J., Henninger, H.B. and Barg, A. 2012. Mobile- and Fixed-Bearing Total Ankle Prostheses. Is There Really a Difference? *Foot and Ankle Clinics*. **17**(4), pp.565–585.
- Vaupel, Z., Baker, E.A., Baker, K.C., Kurdziel, M.D. and Fortin, P.T. 2009a. Analysis of retrieved Agility™ total ankle arthroplasty systems. *Foot and Ankle International*. **30**(9), pp.815–823.
- Vaupel, Z., Baker, E.A., Baker, K.C., Kurdziel, M.D. and Fortin, P.T. 2009b. Analysis of retrieved Agility™ total ankle arthroplasty systems. *Foot and Ankle International*. **30**(9), pp.815–823.
- Veljkovic, A.N., Daniels, T.R., Glazebrook, M.A., Dryden, P.J., Penner, M.J., Wing, K.J. and Younger, A.S.E. 2019. Outcomes of Total Ankle Replacement, Arthroscopic Ankle Arthrodesis, and Open Ankle Arthrodesis for Isolated Non-Deformed End-Stage Ankle Arthritis. *Journal of Bone and Joint Surgery - American Volume*. **101**(17), pp.1523–1529.
- Vicars, R., Fisher, J. and Hall, R.M. 2009. The accuracy and precision of a micro computer tomography volumetric measurement technique for the analysis of in-vitro tested total disc replacements. *Proceedings of the Institution of Mechanical Engineers, Part H: Journal of Engineering in Medicine*. **223**(3), pp.383–388.
- Vickerstaff, J.A., Miles, A.W. and Cunningham, J.L. 2007. A brief history of total ankle replacement and a review of the current status. *Medical Engineering & Physics*. **29**(10), pp.1056–64.
- Wade, L., Needham, L., McGuigan, P. and Bilzon, J. 2022. Applications and limitations of current markerless motion capture methods for clinical gait biomechanics. *PeerJ*. **10**, pp.1–32.
- Wagner, U.A., Sangeorzan, B.J., Harrington, R.M. and Tencer, A.F. 1992. Contact characteristics of the subtalar joint: Load distribution between the anterior and posterior facets. *Journal of Orthopaedic Research*. **10**(4), pp.535–543.
- Wang, A. 2001. A unified theory of wear for ultra-high molecular weight polyethylene in multi-directional sliding. *Wear*. **248**(1–2), pp.38–47.
- Wang, A., Essner, A., Polineni, V.K., Stark, C. and Dumbleton, J.H. 1998. Lubrication and wear

- of ultra-high molecular weight polyethylene in total joint replacements. *Tribology International*. **31**(1–3), pp.17–33.
- Wang, A., Essner, A. and Schmidig, G. 2004. The Effects of Lubricant Composition on in Vitro Wear Testing of Polymeric Acetabular Components. *Journal of Biomedical Materials Research - Part B Applied Biomaterials*. **68**(1), pp.45–52.
- Wang, A., Essner, A., Stark, C. and Dumbleton, J.H. 1996a. Comparison of the size and morphology of UHMWPE wear debris produced by a hip joint simulator under serum and water lubricated conditions. *Biomaterials*. **17**(9), pp.865–871.
- Wang, A., Sun, D.C., Stark, C. and Dumbleton, J.H. 1995. Wear mechanisms of UHMWPE in total joint replacements. *Wear*. **181–183**, pp.241–249.
- Wang, A., Sun, D.C., Yau, S.S., Edwards, B., Sokol, M., Essner, A., Polineni, V.K., Stark, C. and Dumbleton, J.H. 1997. Orientation softening in the deformation and wear of ultra-high molecular weight polyethylene. *Wear*. **203–204**, pp.230–241.
- Wang, H., Chen, T., Koff, M.F., Hutchinson, I.D., Gilbert, S., Choi, D., Warren, R.F., Rodeo, S.A. and Maher, S.A. 2014. Image based weighted center of proximity versus directly measured knee contact location during simulated gait. *Journal of Biomechanics*. **47**(10), pp.2483–2489.
- Wang, Q., Whittle, M., Cunningham, J. and Kenwright, J. 1996b. Fibula and its ligaments in load transmission and ankle joint stability. *Clinical orthopaedics and related research*. (330), pp.261–270.
- Wang, Y., Li, Z., Wong, D.W.C., Cheng, C.K. and Zhang, M. 2018. Finite element analysis of biomechanical effects of total ankle arthroplasty on the foot. *Journal of Orthopaedic Translation*. **12**, pp.55–65.
- Wang, Y., Li, Z., Wong, D.W.C. and Zhang, M. 2015. Effects of ankle arthrodesis on biomechanical performance of the entire foot. *PLoS ONE*. **10**(7), pp.1–22.
- Wannomae, K.K., Christensen, S.D., Micheli, B.R., Rowell, S.L., Schroeder, D.W. and Muratoglu, O.K. 2010. Delamination and adhesive wear behavior of  $\alpha$ -tocopherol-stabilized irradiated ultrahigh-molecular-weight polyethylene. *Journal of Arthroplasty*. **25**(4), pp.635–643.
- Watanabe, K., Kitaoka, H.B., Berglund, L.J., Zhao, K.D., Kaufman, K.R. and An, K.N. 2012. The role of ankle ligaments and articular geometry in stabilizing the ankle. *Clinical Biomechanics*. **27**(2), pp.189–195.
- Waugh, T.R., Evanski, P.M. and McMaster, W.C. 1976. Irvine ankle arthroplasty. Prosthetic design and surgical technique. *Clinical Orthopaedics and Related Research*. **114**, pp.180–184.

- Wayne, J.S., Lawhorn, K.W., Davis, K.E., Prakash, K. and Adelaar, R.S. 1997. The effect of tibiotalar fixation on foot biomechanics. *Foot and Ankle International*. **18**(12), pp.792–795.
- Weatherall, J.M., Chapman, C.B. and Shapiro, S.L. 2013. Postoperative second metatarsal fractures associated with suture-button implant in hallux valgus surgery. *Foot and Ankle International*. **34**(1), pp.104–110.
- Weinhandl, J.T. and Bennett, H.J. 2019. Musculoskeletal model choice influences hip joint load estimations during gait. *Journal of Biomechanics*. **91**, pp.124–132.
- Whittle, M.W. 1996. Clinical gait analysis: A review. *Human Movement Science*. **15**(3), pp.369–387.
- Wight, C.M., Whyne, C.M., Bogoch, E.R., Zdero, R., Chapman, R.M., van Citters, D.W., Walsh, W.R. and Schemitsch, E. 2021. Effect of head size and rotation on tapecorrosion in a hip simulator. *Bone and Joint Open*. **2**(11), pp.1004–1016.
- van Wijngaarden, R., van der Plaat, L., Nieuwe Weme, R.A., Doets, H.C., Westerga, J. and Haverkamp, D. 2015. Etiopathogenesis of osteolytic cysts associated with total ankle arthroplasty, A histological study. *Foot and Ankle Surgery*. **21**(2), pp.132–136.
- Wilharm, A., Hurschler, C., Dermitas, T. and Bohnsack, M. 2013. Use of Tekscan K-scan sensors for retropatellar pressure measurement avoiding errors during implantation and the effects of shear forces on the measurement precision. *BioMed Research International*. **2013**, pp.1–7.
- Wimmer, M.A., Nechtow, W., Schwenke, T. and Moio, K.C. 2015. Knee Flexion and daily activities in patients following total knee replacement: A comparison with ISO standard 14243. *BioMed Research International*. **2015**, pp.1–7.
- Windolf, M., Götzen, N. and Morlock, M. 2008. Systematic accuracy and precision analysis of video motion capturing systems-exemplified on the Vicon-460 system. *Journal of Biomechanics*. **41**(12), pp.2776–2780.
- Winston, I.G., Robinson, D.E. and Allen, P.E. 2005. Arthroscopic ankle arthrodesis. *Journal of Bone and Joint Surgery - Series B*. **87**(3), pp.343–347.
- Winter, D.A. 2009. *Biomechanics and Motor Control of Human Movement* 4th ed. (I. John Wiley & Sons, ed.).
- Winter, D.A. 1984. Kinematic and kinetic patterns in human gait: Variability and compensating effects. *Human Movement Science*. **3**(1–2), pp.51–76.
- Wolf, S., Simon, J., Patikas, D., Schuster, W., Armbrust, P. and Döderlein, L. 2008. Foot motion in children shoes-A comparison of barefoot walking with shod walking in conventional and flexible shoes. *Gait and Posture*. **27**(1), pp.51–59.

- Woodland, L.H. and Francis, R.S. 1992. Parameters and comparisons of the quadriceps angle of college-aged men and women in the supine and standing positions. *American Journal of Sports Medicine*. **20**(2), pp.208–211.
- Wu, G., Siegler, S., Allard, P., Kirtley, C., Leardini, A., D, R., Whittle, M., D'Lima, D.D., Cristofolini, L., Witte, H., Schmid, O. and Stokes, I. 2002. ISB recommendation on definitions of joint coordinate system of various joints for the reporting of human joint motion--part I: ankle, hip, and spine. International Society of Biomechanics. *Journal of biomechanics*. **35**(4), pp.543–548.
- Wu, W.L., Su, F.C., Cheng, Y.M., Huang, P.J., Chou, Y.L. and Chou, C.K. 2000. Gait analysis after ankle arthrodesis. *Gait and Posture*. **11**(1), pp.54–61.
- Xu, Y., Zhu, Y. and Xu, X. yang 2017. Ankle joint distraction arthroplasty for severe ankle arthritis. *BMC Musculoskeletal Disorders*. **18**(1), p.96.
- Yao, J.J., Lewallen, E.A., Trousdale, W.H., Xu, W., Thaler, R., Salib, C.G., Reina, N., Abdel, M.P., Lewallen, D.G. and Van Wijnen, A.J. 2017. Local Cellular Responses to Titanium Dioxide from Orthopedic Implants. *BioResearch Open Access*. **6**(1), p.94.
- Yao, J.Q., Laurent, M.P., Gilbertson, L.N. and Crowninshield, R.D. 2001. The effect of minimum load on the fluid uptake and wear of highly crosslinked UHMWPE total hip acetabular components. *Wear*. **250–251**(Part 1), pp.140–144.
- Yoo, H.J., Park, H.S., Lee, D.O., Kim, S.H., Park, G.Y., Cho, T.J. and Lee, D.Y. 2022. Comparison of the kinematics, repeatability, and reproducibility of five different multi-segment foot models. *Journal of Foot and Ankle Research*. **15**(1), pp.1–10.
- Yoon, H.S., Lee, J., Choi, W.J. and Lee, J.W. 2014. Periprosthetic osteolysis after total ankle arthroplasty. *Foot and Ankle International*. **35**(1), pp.14–21.
- Yu, J., Zhao, D., Chen, W.M., Chu, P., Wang, S., Zhang, C., Huang, J., Wang, X. and Ma, X. 2022. Finite element stress analysis of the bearing component and bone resected surfaces for total ankle replacement with different implant material combinations. *BMC Musculoskeletal Disorders*. **23**(1), pp.1–11.
- Zelik, K.E. and Honert, E.C. 2018. Ankle and foot power in gait analysis: Implications for science, technology and clinical assessment. *Journal of Biomechanics*. **75**, pp.1–12.
- Zerahn, B. and Kofoed, H. 2004. Bone mineral density, gait analysis, and patient satisfaction, before and after ankle arthroplasty. *Foot and Ankle International*. **25**(4), pp.208–214.
- Zhang, G., Zhang, C., Nardin, P., Li, W.Y., Liao, H. and Coddet, C. 2008. Effects of sliding velocity and applied load on the tribological mechanism of amorphous poly-ether-ether-

ketone (PEEK). *Tribology International*. **41**(2), pp.79–86.

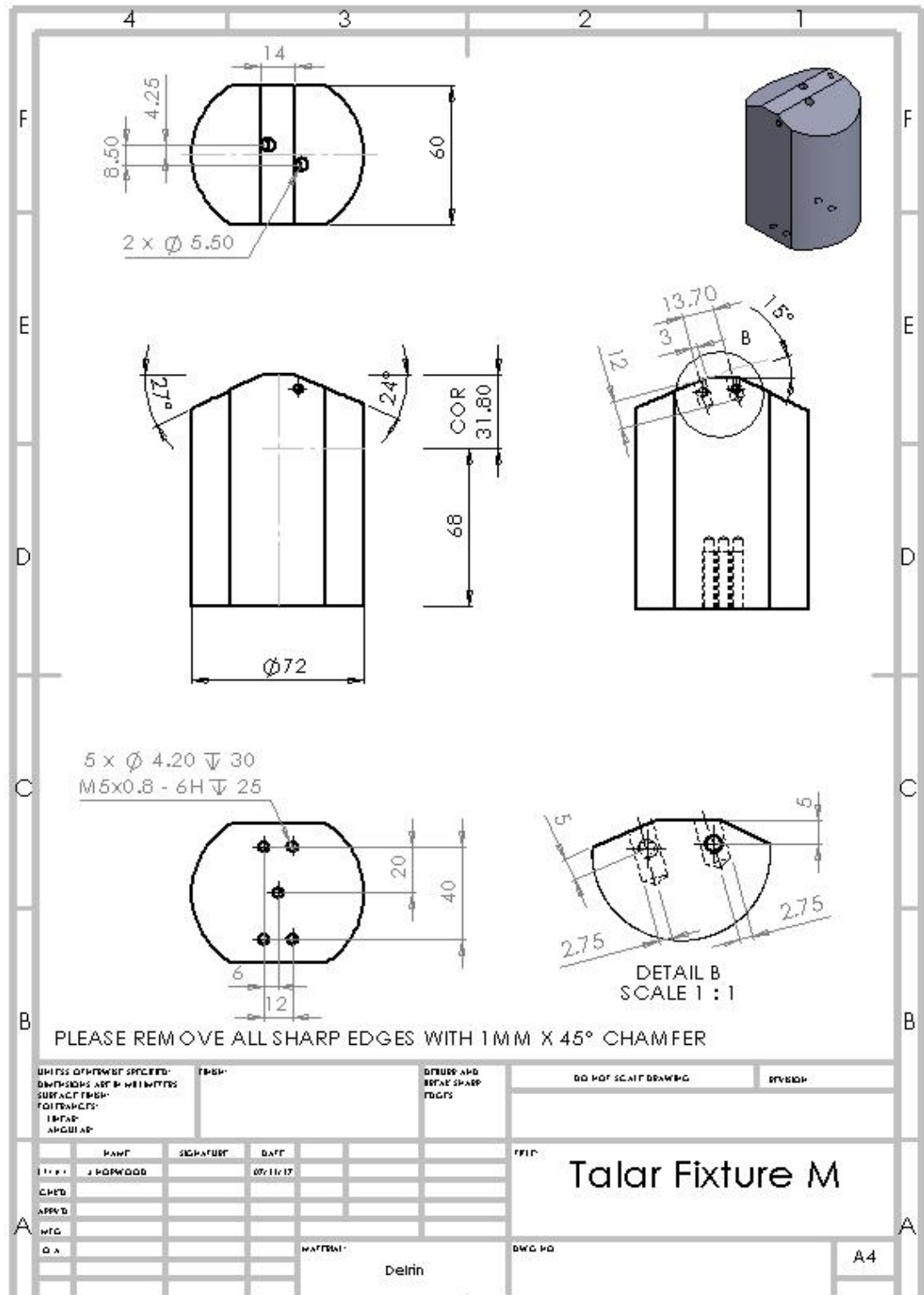
- Zhang, X., Chen, Z., Wang, L., Yang, W., Li, D. and Jin, Z. 2015. Prediction of hip joint load and translation using musculoskeletal modelling with force-dependent kinematics and experimental validation. *Proceedings of the Institution of Mechanical Engineers, Part H: Journal of Engineering in Medicine*. **229**(7), pp.477–490.
- Zhang, X., Paquette, M.R. and Zhang, S. 2013. A comparison of gait biomechanics of flip-flops, sandals, barefoot and shoes. *Journal of Foot and Ankle Research*. **6**(1), pp.1–8.
- Zhang, Y., Chen, Z., Zhao, H., Liang, X., Sun, C. and Jin, Z. 2020. Musculoskeletal modeling of total ankle arthroplasty using force-dependent kinematics for predicting in vivo joint mechanics. *Proceedings of the Institution of Mechanical Engineers, Part H: Journal of Engineering in Medicine*. **234**(2), pp.210–222.
- Zhu, Z., Lou, S. and Majewski, C. 2020. Characterisation and correlation of areal surface texture with processing parameters and porosity of High Speed Sintered parts. *Additive Manufacturing*. **36**.
- Zietz, C., Fabry, C., Middelborg, L., Fulda, G., Mittelmeier, W. and Bader, R. 2013. Wear testing and particle characterisation of sequentially crosslinked polyethylene acetabular liners using different femoral head sizes. *Journal of Materials Science: Materials in Medicine*. **24**(8), pp.2057–2065.
- Zwipp, H. and Randt, T. 1994. Ankle Joint Biomechanics. *Foot and Ankle Surgery*. **1**(1), pp.21–27.

**APPENDIX A**

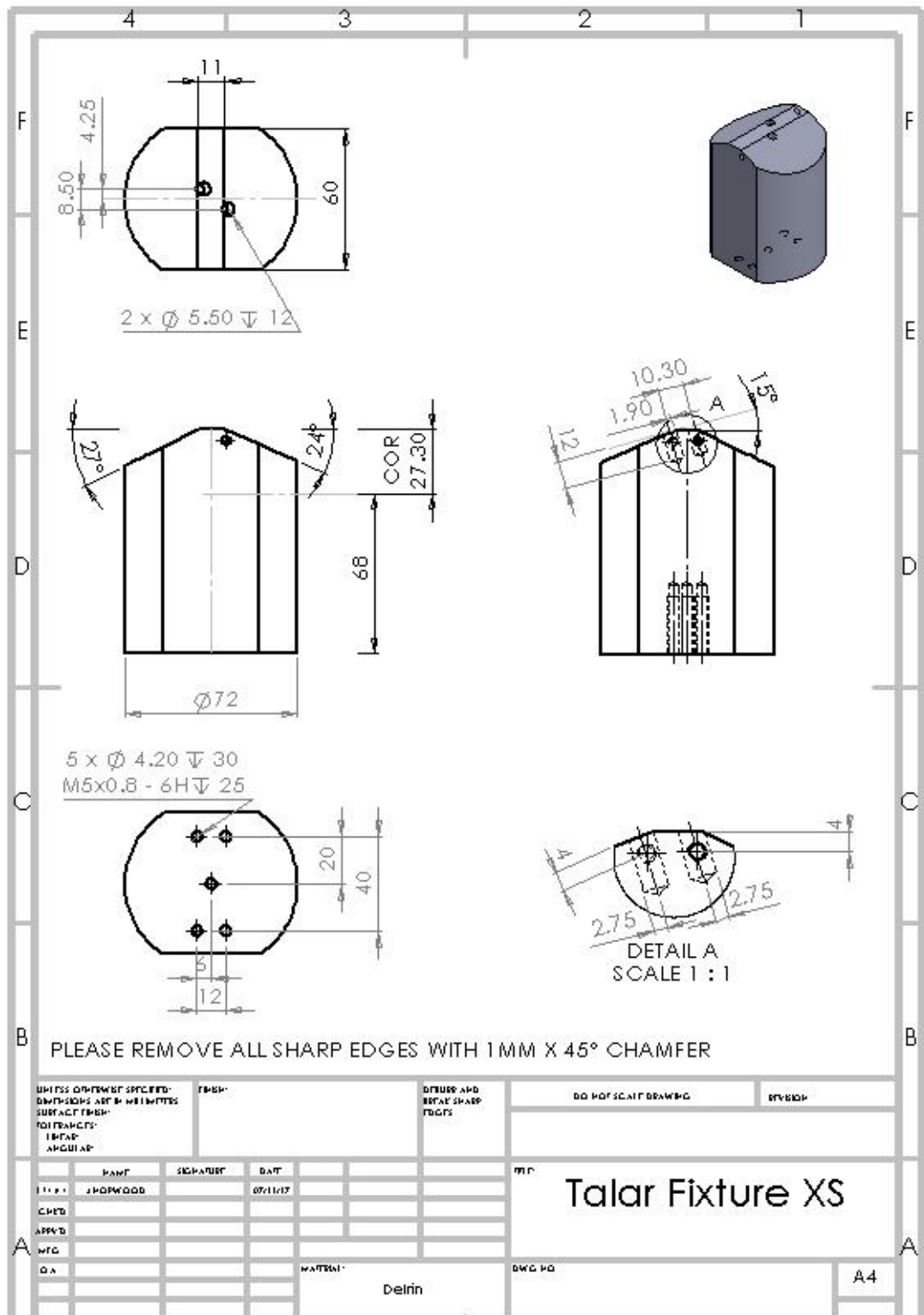
**ENGINEERING DRAWINGS**

## APPENDIX A: ENGINEERING DRAWINGS

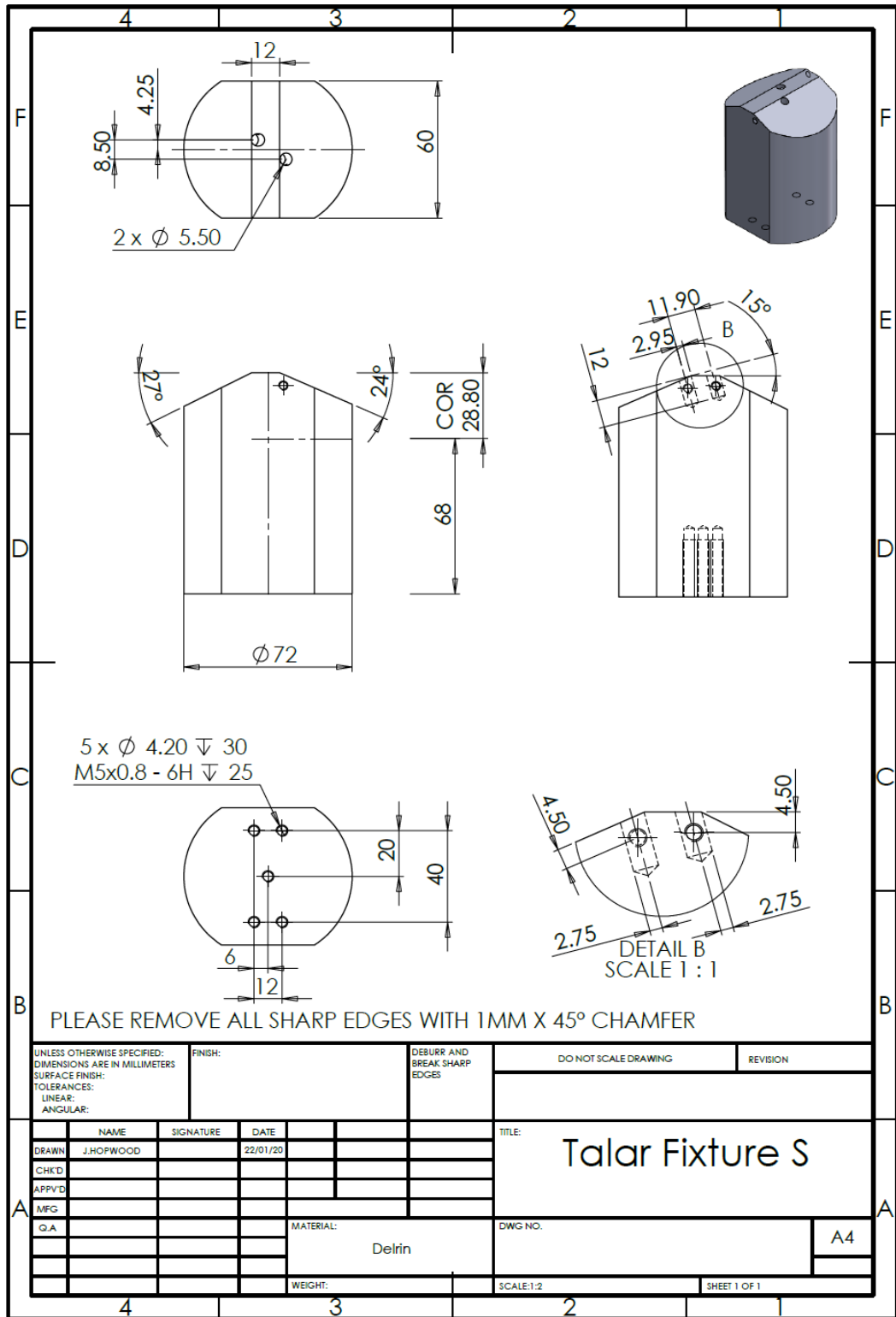
### A.1 ProSim Pneumatic Knee Simulator (KSpn) Medium Sized Delrin Fixture



A.2 ProSim Pneumatic Knee Simulator (KSpn) Extra Small Sized Delrin Fixture



A.3 ProSim Electromechanical Knee Simulator (KSem) Small Sized Delrin Fixture



## **APPENDIX B**

### **EXAMPLE SIMULATOR CALIBRATION REPORT (STATION 1)**

## APPENDIX B: EXAMPLE SIMULATOR CALIBRATION REPORT (STATION 1)

### B.1 Axial Force

Load calibration report for station 1 Axial Force.  
Thursday, 13 August, 2020 at 11:17:20.

No user comments were entered.

ADC Calibration:

Using newly calculated calibration parameters:

Demand Load	Actual Load	ADC	Calib Load	Deviation	% Error
250.0	551.0	14467	549.2	-1.843	-0.33
750.0	1742.0	29677	1745.1	3.068	0.18
1500.0	3540.0	52516	3540.9	0.865	0.02
2250.0	3542.0	52521	3541.2	-0.758	-0.02
3000.0	3543.0	52527	3541.7	-1.333	-0.04

Calibration constants: Scale = 0.078627, Offset = -588.380554

Using existing calibration parameters:

Demand Load	Actual Load	ADC	Calib Load	Deviation	% Error
250.0	551.0	14467	253.9	-297.050	-53.91
750.0	1742.0	29677	752.9	-989.063	-56.78
1500.0	3540.0	52516	1502.2	-2037.777	-57.56
2250.0	3542.0	52521	1502.4	-2039.620	-57.58
3000.0	3543.0	52527	1502.6	-2040.443	-57.59

Calibration constants: Scale = 0.032807, Offset = -220.681625

Demand Calibration:

Demand Load	Actual Load	Deviation	% Error
250.0	551.0	-301.000	-54.63
750.0	1742.0	-992.000	-56.95
1500.0	3540.0	-2040.000	-57.63
2250.0	3542.0	-1292.000	-36.48
3000.0	3543.0	-543.000	-15.33

Calibration constants: Scale = 1.573408, Offset = 222.569580

## B.2 Anterior-Posterior Force

Anterior-Posterior Force calibration report for station 1.  
Thursday, 13 August, 2020 at 14:02:00.

No user comments were entered.

Positive axis, scale = -0.020483, offset = 61.180614.

Demand	Actual	ADC	Calibrated	Calib %Err	Normalised	Combi Cal.	Combi %Err
-12.0	-363.00	20548	-359.72	-0.90	-	-	-
-6.0	-144.00	10091	-145.54	1.07	-	-	-
0.0	16.00	2394	12.14	-24.10	-	-	-
6.0	158.00	-4672	156.89	-0.70	-	-	-
12.0	362.00	-14843	365.22	0.89	-	-	-

Combined calibration constants only from Positive axis, scale = -0.020483, offset = 61.180614.

## B.3 Medial-Lateral Force

Medial-Lateral Force calibration report for station 1.  
Thursday, 13 August, 2020 at 14:12:37.

No user comments were entered.

Positive axis, scale = -0.029391, offset = 46.399181.

Demand	Actual	ADC	Calibrated	Calib %Err	Normalised	Combi Cal.	Combi %Err
-12.0	-354.00	13653	-354.89	0.25	-	-	-
-6.0	-140.00	6346	-140.13	0.10	-	-	-
0.0	2.00	1422	4.58	129.08	-	-	-
6.0	171.00	-4199	169.83	-0.68	-	-	-
12.0	380.00	-11337	379.61	-0.10	-	-	-

Combined calibration constants only from Positive axis, scale = -0.029391, offset = 46.399181.

## B.4 Tibial Rotation Torque Calibration Report For Station 1

Tibial Rotation Torque calibration report for station 1.  
Thursday, 13 August, 2020 at 15:23:21.

No user comments were entered.

Positive axis, scale = 0.000426, offset = -2.415000.

Demand	Actual	ADC	Calibrated	Calib %Err	Normalised	Combi Cal.	Combi %Err
-12.0	-6.88	-10797	-7.02	2.11	-	-	-
-6.0	-5.13	-5909	-4.94	-3.70	-	-	-
0.0	-0.38	4660	-0.43	-	-	-	-
6.0	2.88	12500	2.92	1.42	-	-	-
12.0	6.75	21412	6.72	-0.49	-	-	-

Combined calibration constants only from Positive axis, scale = 0.000426, offset = -2.415000.

## B.5 Flexion-Extension Torque (+)

Flexion-Extension Torque calibration report for station 1.  
Thursday, 13 August, 2020 at 12:28:12.

No user comments were entered.

Positive axis, scale = 0.003828, offset = 0.907940.

Demand	Actual	ADC	Calibrated	Calib %Err	Normalised	Combi Cal.	Combi %Err
60.0	6.68	1525	6.75	1.09	5.84	4.67	-20.05
65.0	12.10	2905	12.03	-0.60	11.12	10.49	-5.68
70.0	17.63	4361	17.60	-0.13	16.69	16.63	-0.37
75.0	23.05	5778	23.03	-0.11	22.12	22.61	2.23
80.0	28.58	7240	28.62	0.16	27.71	28.78	3.84

Negative axis, scale = 0.004495, offset = 0.273928.

Demand	Actual	ADC	Calibrated	Calib %Err	Normalised	Combi Cal.	Combi %Err
60.0	-18.02	-4077	-18.05	0.16	-18.33	-18.97	3.50
65.0	-23.50	-5282	-23.47	-0.13	-23.74	-24.05	1.30
70.0	-29.43	-6606	-29.42	-0.01	-29.70	-29.64	-0.19
75.0	-35.33	-7918	-35.32	-0.02	-35.59	-35.17	-1.18
80.0	-41.15	-9219	-41.17	0.04	-41.44	-40.66	-1.88

Combined axes, scale = 0.004219, offset = -1.767712.

## B.6 Flexion-Extension Torque (-)

Flexion-Extension Torque calibration report for station 1.  
Thursday, 13 August, 2020 at 12:35:25.

No user comments were entered.

Negative axis, scale = 0.004320, offset = 1.357604.

Demand	Actual	ADC	Calibrated	Calib %Err	Normalised	Combi Cal.	Combi %Err
60.0	-7.03	-1947	-7.05	0.41	-8.41	-9.01	7.17
65.0	-12.35	-3171	-12.34	-0.05	-13.70	-14.00	2.18
70.0	-17.80	-4433	-17.80	-0.02	-19.15	-19.14	-0.07
75.0	-23.40	-5711	-23.32	-0.36	-24.67	-24.34	-1.34
80.0	-29.05	-7053	-29.12	0.22	-30.47	-29.81	-2.18

Positive axis, scale = 0.003828, offset = 0.907940.

Demand	Actual	ADC	Calibrated	Calib %Err	Normalised	Combi Cal.	Combi %Err
60.0	6.68	1525	6.75	1.10	5.84	5.13	-12.22
65.0	12.10	2905	12.03	-0.59	11.12	10.74	-3.39
70.0	17.63	4361	17.60	-0.12	16.70	16.67	-0.13
75.0	23.05	5778	23.03	-0.10	22.12	22.44	1.46
80.0	28.58	7240	28.62	0.17	27.72	28.40	2.46

Combined axes, scale = 0.004072, offset = -1.085776.

## B.7 Abduction-Adduction Torque (+)

Abduction-Adduction Torque calibration report for station 1.  
Thursday, 13 August, 2020 at 12:42:46.

No user comments were entered.

Positive axis, scale = -0.003541, offset = 2.790940.

Demand	Actual	ADC	Calibrated	Calib %Err	Normalised	Combi Cal.	Combi %Err
60.0	6.63	-1095	6.67	0.70	3.88	2.55	-34.32
65.0	11.90	-2564	11.87	-0.23	9.08	8.36	-8.00
70.0	17.40	-4114	17.36	-0.22	14.57	14.48	-0.61
75.0	22.77	-5636	22.75	-0.10	19.96	20.50	2.70
80.0	28.27	-7208	28.32	0.15	25.53	26.71	4.65

Negative axis, scale = -0.004191, offset = 3.837848.

Demand	Actual	ADC	Calibrated	Calib %Err	Normalised	Combi Cal.	Combi %Err
60.0	-17.63	5123	-17.64	0.06	-21.47	-22.04	2.63
65.0	-23.10	6424	-23.09	-0.06	-26.92	-27.18	0.95
70.0	-29.02	7842	-29.03	0.01	-32.87	-32.79	-0.25
75.0	-34.95	9257	-34.96	0.02	-38.80	-38.38	-1.07
80.0	-40.78	10645	-40.78	0.00	-44.61	-43.87	-1.67

Combined axes, scale = -0.003953, offset = -1.783037.

## B.8 Abduction-Adduction Torque (-)

Abduction-Adduction Torque calibration report for station 1.  
Thursday, 13 August, 2020 at 12:44:20.

No user comments were entered.

Negative axis, scale = -0.004034, offset = 3.540346.

Demand	Actual	ADC	Calibrated	Calib %Err	Normalised	Combi Cal.	Combi %Err
60.0	-7.13	2666	-7.21	1.24	-10.75	-11.31	5.17
65.0	-12.55	3980	-12.52	-0.27	-16.06	-16.32	1.63
70.0	-18.00	5311	-17.88	-0.65	-21.42	-21.39	-0.16
75.0	-23.52	6708	-23.52	-0.04	-27.06	-26.71	-1.28
80.0	-29.13	8116	-29.20	0.25	-32.74	-32.07	-2.02

Positive axis, scale = -0.003541, offset = 2.790940.

Demand	Actual	ADC	Calibrated	Calib %Err	Normalised	Combi Cal.	Combi %Err
60.0	6.63	-1095	6.67	0.70	3.88	3.02	-22.11
65.0	11.90	-2564	11.87	-0.23	9.08	8.62	-5.11
70.0	17.40	-4114	17.36	-0.22	14.57	14.52	-0.33
75.0	22.77	-5636	22.75	-0.10	19.96	20.32	1.81
80.0	28.27	-7208	28.32	0.15	25.53	26.31	3.07

Combined axes, scale = -0.003810, offset = -1.152315.

## B.9 Anterior-Posterior Displacement

Displacement ADC calibration report for station 1 Anterior-Posterior Displacement  
Thursday, 13 August, 2020 at 11:36:25.

No user comments were entered.

ADC Calibration:

Using newly calculated calibration parameters:

Actual Disp	ADC	Calib Disp	Deviation	% Error
19.750	20375	19.750	-0.0002	-0.00
10.000	9469	10.004	0.0042	0.04
-0.200	-1957	-0.207	-0.0075	3.74
-10.300	-13248	-10.297	0.0031	-0.03
-20.000	-24106	-20.000	0.0004	-0.00

Calibration constants: Scale = 0.000894, Offset = 1.542041

Using existing calibration parameters:

Actual Disp	ADC	Calib Disp	Deviation	% Error
19.750	20375	19.742	-0.0080	-0.04
10.000	9469	9.997	-0.0027	-0.03
-0.200	-1957	-0.213	-0.0134	6.69
-10.300	-13248	-10.302	-0.0018	0.02
-20.000	-24106	-20.004	-0.0036	0.02

Calibration constants: Scale = 0.000894, Offset = 1.535975

Displacement demand calibration report for station 1 Anterior-Posterior.

No user comments were entered.

Demand Calibration:

Demand Disp	Actual Disp	Deviation
-12.00	-11.96	-0.036
-9.33	-9.30	-0.032
-6.67	-6.65	-0.021
-4.00	-3.98	-0.020
-1.33	-1.33	-0.002
1.33	1.33	0.001
4.00	4.02	-0.023
6.67	6.70	-0.036
9.33	9.34	-0.006
12.00	12.00	-0.003

Calibration constants: Scale = 0.990740, Offset = 1.145025

**APPENDIX C**

**SIMULATOR CALIBRATION RECORD**

## APPENDIX C: SIMULATOR CALIBRATION RECORD

### C.1 Calibration Record for ProSim Pneumatic Knee Simulator (KSpn) – Implant Size Study (Test 1)

#### Calibration Record Single Knee Simulator 4

Calibration performed by: **James Hopwood**      Date: **19/04/2018**      Load cell S/N: **26700 LCB-002**      Calibration date: **19/04/2018**

Station	AF Load		AP Force	TR Displacement	AP Displacement	FE Displacement
	Unit/ADC:	Offset:				
1	Load cell	0.07001	N/A	0.00137061	-0.00085110005	N/A
		31.257225				
	Valve	13.818566		-2.1	0.27	
		-261.47798				
2	Load cell	0.097952	N/A	0.001382743363	-0.000923641942	N/A
		-174.180607				
	Valve	14.274543		-0.8	0.8	
		136.718572				
3	Load cell	0.076352	N/A	0.001466705779	-0.0008554319932	N/A
		33.703003				
	Valve	14.354042		-8.58	-0.32	
		-656.89732				

### Calibration Record Single Knee Simulator 4

Calibration performed by: James Hopwood      Date: 19/04/2018      Load cell S/N: 26700 LCB-002      Calibration date: 19/04/2018

Station	AF Load		AP Force	TR Displacement	AP Displacement	FE Displacement
	Load cell	Valve				
4	Unit/ADC:	0.114364	N/A	Unit/ADC: 0.001378851882	-0.0009162963302	N/A
	Offset:	-207.630523				
	Unit/ADC:	13.655744		Offset: -0.26	3.34	
	Offset:	-46.032624				
5	Unit/ADC:	0.087548	N/A	Unit/ADC: 0.001378851882	-0.0008439530762	N/A
	Offset:	-182.555584				
	Unit/ADC:	13.704134		Offset: -0.18	3.4	
	Offset:	-459.503797				
6	Unit/ADC:	0.074212	N/A	Unit/ADC: 0.001378851882	-0.0008362952122	N/A
	Offset:	-40.221272				
	Unit/ADC:	13.977137		Offset: 0.09	0.02	
	Offset:	-315.515643				

C.2 Calibration Record for ProSim Pneumatic Knee Simulator (KSpn) –  
Implant Size Study (Test 2)

**Calibration Record Single Knee Simulator 4**

Calibration performed by: James Hopwood Date: 21/11/2018 Load cell S/N: 26700 LCB-002 Calibration date: 21/11/2018

Station	AF Load		AP Force	TR Displacement		AP Displacement	FE Displacement
	Load cell	Valve		Unit/ADC:	Offset:		
1	Load cell	0.072019	N/A	0.001370614035	N/A	-0.00087546509	N/A
		37.72896					
	Valve	13.543718		-0.88		-0.25	
		-186.200806					
2	Load cell	0.097556	N/A	0.001376651982	N/A	-0.00086734254	N/A
		-115.382727					
	Valve	14.131551		-0.09		0.92	
		-203.236318					
3	Load cell	0.094514	N/A	0.001382743363	N/A	-0.00087466107	N/A
		26.356297					
	Valve	13.677769		-9.2		0.25	
		-31.543277					

### Calibration Record Single Knee Simulator 4

Calibration performed by: James Hopwood    Date: 21/11/2018    Load cell S/N: 26700 LCB-002    Calibration date: 21/11/2018

Station	AF Load		AP Force	TR Displacement	AP Displacement	FE Displacement
	Load cell	Valve				
4	Unit/ADC:	0.142858	N/A	Unit/ADC: 0.001376651982	-0.00085781686	N/A
	Offset:	-574.549005				
	Unit/ADC:	13.820014				
	Offset:	-227.825897				
5	Unit/ADC:	0.110517	N/A	Unit/ADC: 0.001382743363	-0.00085840594	N/A
	Offset:	-218.845896				
	Unit/ADC:	14.166791				
	Offset:	-444.359525				
6	Unit/ADC:	0.072413	N/A	Unit/ADC: 0.001376651982	-0.00086805556	N/A
	Offset:	-23.89358				
	Unit/ADC:	13.75202				
	Offset:	-192.436791				

C.3 Calibration Record for ProSim Electromechanical Knee Simulator (KSem)  
 – Simulator Type and ISO Standard Studies

Date: 08/07/19

Calibration performed by: James Hopwood

Calibration Record Knee Simulator KS6

Calibrated load cell S/N: LCB-002 Cell 16018051

Date calibrated: 01/07/19

Station No.	Six Axes Load Cell								Anterior/ Posterior Displacement position	Anterior/ Posterior motor position	Abduction/ Adduction Angle
	Axial Force	Anterior/ Posterior Force	Medial/ Lateral Force	Tibial Rotation Torque	Flexion/ Extension Torque	Abduction/ Adduction Torque					
1	Scale:	0.078777	-0.020583	-0.028651	0.000443	(+) 0.003807 (-) -0.004164	(+) -0.003828 (-) -0.003781	0.000894	0.989833	N/A	
	Offset:	-415.791016	49.777500	57.986599	0.707124	(+) -2.172788 (-) 0.460620	(+) -3.536229 (-) -3.167444	1.535975	1.162637	N/A	
2	Scale:	0.076447	-0.019420	-0.024855	0.000462	(+) 0.004058 (-) 0.004338	(+) -0.003465 (-) -0.003846	0.000865	1.020500	N/A	
	Offset:	-378.363220	-0.842166	6.385694	-0.919546	(+) -1.140410 (-) -3.345934	(+) -1.038396 (-) -4.803123	1.095159	1.435167	N/A	
3	Scale:	0.078454	-0.019258	-0.023200	0.000488	(+) 0.003807 (-) 0.004180	(+) -0.003616 (-) -0.003659	0.000884	1.002007	N/A	
	Offset:	-433.024445	23.874105	50.760223	3.478830	(+) 0.072408 (-) -3.366006	(+) -0.203171 (-) -0.945808	0.975590	1.730427	N/A	
4	Scale:	0.085232	-0.026673	-0.028617	0.000501	(+) 0.002078 (-) 0.002043	(+) -0.001930 (-) -0.001892	0.000881	1.003173	N/A	
	Offset:	-283.573517	53.908047	41.286804	-3.873492	(+) -2.632269 (-) -2.089728	(+) -3.443437 (-) -2.795391	1.763365	0.708263	N/A	
5	Scale:	0.077040	-0.018002	-0.022234	0.000458	(+) 0.003860 (-) 0.004296	(+) -0.003737 (-) -0.004120	0.000892	0.990392	N/A	
	Offset:	-491.529755	48.521877	22.020266	-0.922282	(+) 0.132014 (-) -4.114158	(+) -0.031346 (-) -3.819947	2.024769	0.882044	N/A	
6	Scale:	-0.019742	-0.020583	-0.024108	0.000490	(+) 0.003863 (-) 0.004282	(+) -0.003573 (-) -0.003973	0.000886	0.995172	N/A	
	Offset:	56.677612	49.777500	69.755676	4.457240	(+) 0.274784 (-) -3.196664	(+) -1.437961 (-) -5.181913	1.292691	1.397992	N/A	

C.4 Calibration Record for ProSim Electromechanical Knee Simulator (KSem)  
 – Accelerated Artificially Aged Study

Date: 11/09/20

Calibration performed by: James Hopwood

Calibration Record Knee Simulator KS6

Calibrated load cell S/N: LCB-002 Cell 17087285

Date calibrated: 11/09/20

Station No.	Six Axes Load Cell								Anterior/ Posterior Displacement position	Anterior/ Posterior motor position	Abduction/ Adduction Angle
	Axial Force	Anterior/ Posterior Force	Medial/ Lateral Force	Tibial Rotation Torque	Flexion/ Extension Torque	Abduction/ Adduction Torque					
1	Scale:	0.078627	-0.020483	-0.029391	0.000426	(+) 0.004219 (-) 0.004072	(+) -0.003810 (-) -0.003781	0.000894	0.990740	N/A	
	Offset:	-588.380554	61.180614	46.399181	-2.415000	(+) -1.767712 (-) -1.085776	(+) -1.152315 (-) -3.167444	1.542041	1.145025	N/A	
2	Scale:	0.076576	-0.019656	-0.024374	0.000487	(+) 0.004525 (-) 0.004492	(+) -0.004050 (-) -0.003846	0.000867	1.020131	N/A	
	Offset:	-335.301025	-16.900040	3.754563	-1.957469	(+) -0.618048 (-) -0.577600	(+) -0.887059 (-) -4.803123	1.064963	1.457202	N/A	
3	Scale:	0.078029	-0.020315	-0.023925	0.000512	(+) 0.004526 (-) 0.004546	(+) -0.003445 (-) -0.000893	0.000884	1.001284	N/A	
	Offset:	-451.196716	-3.617741	22.046936	-1.934437	(+) -0.058590 (-) 0.109327	(+) -2.270416 (-) -0.945808	0.968438	1.729090	N/A	
4	Scale:	0.085246	-0.027097	-0.029116	0.000593	(+) 0.004175 (-) 0.002043	(+) -0.001955 (-) -0.001863	0.000881	1.005024	N/A	
	Offset:	-302.130280	8.267974	12.642922	-1.329452	(+) 2.648385 (-) -2.089728	(+) -1.829616 (-) -1.017803	1.732273	0.735129	N/A	
5	Scale:	0.076868	-0.018230	-0.022526	0.000417	(+) 0.004571 (-) 0.004256	(+) -0.004269 (-) -0.003982	0.000891	0.991902	N/A	
	Offset:	-489.206055	62.454876	28.468410	-2.594578	(+) -1.881787 (-) -0.840009	(+) 0.031346 (-) -1.367196	1.997707	0.903139	N/A	
6	Scale:	0.078454	-0.019757	-0.024437	0.000481	(+) 0.004583 (-) 0.004415	(+) -0.004446 (-) -0.004103	0.000886	0.994808	N/A	
	Offset:	-293.203827	-2.239730	46.388554	6.655794	(+) -1.267663 (-) -0.699397	(+) -2.040082 (-) -0.880856	1.301584	1.376928	N/A	

## **APPENDIX D**

# **SERUM CERTIFICATE OF ANALYSIS**

## APPENDIX D: SERUM CERTIFICATE OF ANALYSIS

### D.1 Serum Protein Concentration for the Implant Size Study (Test 1)

PURCHASED 320 BOTTLES  
FROM LOT N°: 1703862 (Below)  
OCT 2019  
RESERVE N°: 3972465


Customer/Code: GIBCO    GIBCONZ

**Certificate of Analysis**

Newborn Calf Serum  
Performance, Mycoplasma,  
Virus and Endotoxin tested

Catalog Number: 16010  
**Lot Number: 1703862**  
 Storage Temperature: -5 to -20C  
 Country of Origin: NZ  
 Expiration Date: 2019-08

For in vitro diagnostic use.  
Sterile filtered (0.22 um)

TEST	SPECIFICATION	RESULT	UNITS
<sup>1</sup> Electrophoretic Pattern	Normal	Normal	
<sup>2</sup> Endotoxin Testing	Check & Record	<0.500	EU/mL
<sup>3</sup> Hemoglobin	Check & Record	17.0	mg%
<sup>4</sup> Mycoplasma, Supplemental (H-Stain)	Negative	Negative	
<sup>5</sup> Mycoplasma Testing	Negative	Negative	
<sup>6</sup> Osmolality	>=275 to <=310	286	mOsm/kg
<sup>7</sup> pH	>=7.1 to <=7.7	7.4	
<sup>8</sup> Sterility Testing	Negative	Negative	
<sup>9</sup> Total Protein	>=5.5 to <=8.0	6.4	g/dL
<sup>10</sup> Vero Assay	Check & Record	95	%
<sup>11</sup> VT - Bluetongue Virus FA	Negative	Negative	
<sup>12</sup> VT - Bovine Adenovirus FA	Negative	Negative	
<sup>13</sup> VT - Bovine Parvovirus FA	Negative	Negative	
<sup>14</sup> VT - BRSV Fluorescent Antibody	Negative	Negative	
<sup>15</sup> VT - BVDV Fluorescent Antibody	Negative	Negative	
<sup>16</sup> VT - Cytopathogenic Agents	Negative	Negative	
<sup>17</sup> VT - Hemadsorbing Agents	Negative	Negative	
<sup>18</sup> VT - Rabies Virus FA	Negative	Negative	

D.2 Serum Protein Concentration for the Implant Size (Test 2), Simulator Type and ISO Standard Studies



Customer/Code: GIBCO GIBCONZ

Certificate of Analysis

Newborn Calf Serum  
Performance, Mycoplasma,  
Virus and Endotoxin tested

Catalog Number: 16010

Lot Number: 1827308

Storage Temperature: -5 to -20C

Country of Origin: NZ

Expiration Date: 2020-08

For in vitro diagnostic use.

Sterile filtered (0.22 um)

TEST	SPECIFICATION	RESULT	UNITS
<sup>1</sup> Electrophoretic Pattern	Normal	Normal	
<sup>2</sup> Endotoxin Testing	Check & Record	<0.500	EU/mL
<sup>3</sup> Hemoglobin	Check & Record	18.8	mg%
<sup>4</sup> Mycoplasma, Supplemental (H-Stain)	Negative	Negative	
<sup>5</sup> Mycoplasma Testing	Negative	Negative	
<sup>6</sup> Osmolality	>=275 to <=310	297	mOsm/kg
<sup>7</sup> pH	>=7.1 to <=7.7	7.2	
<sup>8</sup> Sterility Testing	Negative	Negative	
<sup>9</sup> Total Protein	>=5.5 to <=8.0	6.3	g/dL
<sup>10</sup> Vero Assay	Check & Record	106	%
<sup>11</sup> VT - Bluetongue Virus FA	Negative	Negative	
<sup>12</sup> VT - Bovine Adenovirus FA	Negative	Negative	
<sup>13</sup> VT - Bovine Parvovirus FA	Negative	Negative	
<sup>14</sup> VT - BRSV Fluorescent Antibody	Negative	Negative	
<sup>15</sup> VT - BVDV Fluorescent Antibody	Negative	Negative	
<sup>16</sup> VT - Cytopathogenic Agents	Negative	Negative	
<sup>17</sup> VT - Hemadsorbing Agents	Negative	Negative	
<sup>18</sup> VT - Rabies Virus FA	Negative	Negative	

### D.3 Serum Protein Concentration for the Accelerated Artificially Aged Study



Customer/Code: GIBCO GIBCONZ

## Certificate of Analysis

**Newborn Calf Serum**  
Performance, Mycoplasma,  
Virus and Endotoxin tested

**Catalog Number:** 16010  
**Lot Number:** 2043354  
**Storage Temperature:** <= -10C  
**Country of Origin:** NZ  
**Expiration Date:** 2022-10

For research use or further manufacturing use only. Serum and blood proteins are not for direct administration into humans or animals.

Sterile filtered (0.22 um)

TEST	SPECIFICATION	RESULT	UNITS
<sup>1</sup> Electrophoretic Pattern	Normal	Normal	
<sup>2</sup> Endotoxin Testing	Check & Record	<0.500	EU/mL
<sup>3</sup> Hemoglobin	Check & Record	13.4	mg%
<sup>4</sup> Mycoplasma, Supplemental (H-Stain)	Negative	Negative	
<sup>5</sup> Mycoplasma Testing	Negative	Negative	
<sup>6</sup> Osmolality	>=275 to <=310	296	mOsm/kg
<sup>7</sup> pH	>=7.1 to <=7.7	7.3	
<sup>8</sup> Sterility Testing	Negative	Negative	
<sup>9</sup> Total Protein	>=5.5 to <=8.0	6.3	g/dL
<sup>10</sup> Vero Assay	Check & Record	118	%
<sup>11</sup> VT - Bluetongue Virus FA	Negative	Negative	
<sup>12</sup> VT - Bovine Adenovirus FA	Negative	Negative	
<sup>13</sup> VT - Bovine Parvovirus FA	Negative	Negative	
<sup>14</sup> VT - BRSV Fluorescent Antibody	Negative	Negative	
<sup>15</sup> VT - BVDV Fluorescent Antibody	Negative	Negative	
<sup>16</sup> VT - Cytopathogenic Agents	Negative	Negative	
<sup>17</sup> VT - Hemadsorbing Agents	Negative	Negative	
<sup>18</sup> VT - Rabies Virus FA	Negative	Negative	

**APPENDIX E**

**SURFACE TOPOGRAPHIC  
MEASUREMENTS FOR EACH WEAR  
SIMULATOR STUDY**

## APPENDIX E: SURFACE TOPOGRAPHIC MEASUREMENTS FOR EACH WEAR SIMULATOR STUDY

### E.1 Implant Size

Table 30. Mean ( $\pm$  95% CL) average surface roughness (Ra) measurements for each articulating surface of the medium (M) and extra small (XS) sized implants alongside the percentage change between the measurement stages (n = 6 for each implant size).

	Ra ( $\mu\text{m}$ )	Pre-Test			5 Mc		
		Medial	Central	Lateral	Medial	Central	Lateral
<b>M</b>	Talar	0.08 $\pm$ 0.01	0.05 $\pm$ 0.01	0.08 $\pm$ 0.01	0.09 $\pm$ 0.05 (12.50%)	0.10 $\pm$ 0.05*	0.11 $\pm$ 0.04 (37.50%)
	Inferior Insert	1.41 $\pm$ 0.39	1.26 $\pm$ 0.41	1.44 $\pm$ 0.37	0.68 $\pm$ 0.11* (-51.77%)	0.56 $\pm$ 0.28* (-55.56%)	0.84 $\pm$ 0.09* (-41.67%)
	Superior Insert		1.38 $\pm$ 0.79			0.11 $\pm$ 0.19* (-92.03%)	
	Tibial		0.01 $\pm$ 0.01			0.03 $\pm$ 0.02* (200.00%)	
<b>XS</b>	Talar	0.08 $\pm$ 0.01	0.04 $\pm$ 0.02	0.09 $\pm$ 0.01	0.12 $\pm$ 0.14* (50.00%)	0.08 $\pm$ 0.06 (100.00%)	0.14 $\pm$ 0.07 (55.56%)
	Inferior Insert	1.27 $\pm$ 0.51	1.15 $\pm$ 0.46	1.36 $\pm$ 0.54	0.77 $\pm$ 0.13* (-39.37%)	0.32 $\pm$ 0.19* (-72.17%)	0.69 $\pm$ 0.22* (-49.26%)
	Superior Insert		1.43 $\pm$ 0.37			0.16 $\pm$ 0.05 (-88.81%)	
	Tibial		0.02 $\pm$ 0.02			0.04 $\pm$ 0.01* (100.00%)	

\*Indicates statistically significant difference between pre- and post-simulation topographic measurements within the same implant size ( $p \leq 0.05$ ).

Table 31. Mean ( $\pm$  95% CL) maximum profile peak heights (Rp) measurements for each articulating surface of the medium (M) and extra small (XS) sized implants alongside the percentage change between the measurement stages (n = 6 for each implant size).

	Rp ( $\mu\text{m}$ )	Pre-Test			5 Mc		
		Medial	Central	Lateral	Medial	Central	Lateral
<b>M</b>	Talar	0.08 $\pm$ 0.02	0.09 $\pm$ 0.02	0.09 $\pm$ 0.01	0.15 $\pm$ 0.10 (87.50%)	0.21 $\pm$ 0.11* (133.33%)	0.18 $\pm$ 0.11 (100.00%)
	Inferior Insert	3.55 $\pm$ 1.15	3.46 $\pm$ 1.19	3.68 $\pm$ 0.91	1.37 $\pm$ 0.36* (-61.41%)	1.36 $\pm$ 0.80* (-60.69%)	1.44 $\pm$ 0.35* (-60.89%)
	Superior Insert		3.57 $\pm$ 2.13			0.30 $\pm$ 0.43* (-91.60%)	
	Tibial		0.06 $\pm$ 0.06			0.08 $\pm$ 0.03 (33.33%)	
<b>XS</b>	Talar	0.09 $\pm$ 0.02	0.10 $\pm$ 0.02	0.10 $\pm$ 0.01	0.17 $\pm$ 0.18 (88.89%)	0.19 $\pm$ 0.15 (90.00%)	0.21 $\pm$ 0.17 (110.00%)
	Inferior Insert	2.97 $\pm$ 1.19	3.11 $\pm$ 1.27	3.25 $\pm$ 1.31	1.04 $\pm$ 0.47* (-64.98%)	0.75 $\pm$ 0.44* (-75.88%)	1.30 $\pm$ 0.32* (-60.00%)
	Superior Insert		3.86 $\pm$ 1.08			0.41 $\pm$ 0.14* (-89.38%)	
	Tibial		0.06 $\pm$ 0.08			0.09 $\pm$ 0.03* (50.00%)	

\*Indicates statistically significant difference between pre- and post-simulation topographic measurements within the same implant size ( $p \leq 0.05$ ).

Table 32. Mean ( $\pm$  95% CL) maximum profile valley depth (Rv) measurements for each articulating surface of the medium (M) and extra small (XS) sized implants alongside the percentage change between the measurement stages (n = 6 for each implant size).

	Rv ( $\mu\text{m}$ )	Pre-Test			5 Mc		
		Medial	Central	Lateral	Medial	Central	Lateral
<b>M</b>	Talar	0.12 $\pm$ 0.02	0.11 $\pm$ 0.01	0.11 $\pm$ 0.02	0.24 $\pm$ 0.15 (100.00%)	0.29 $\pm$ 0.17* (163.64%)	0.31 $\pm$ 0.22 (181.82%)
	Inferior Insert	2.85 $\pm$ 1.03	2.80 $\pm$ 0.89	3.04 $\pm$ 1.01	1.49 $\pm$ 0.38* (-47.72%)	1.46 $\pm$ 0.74* (-47.86%)	1.75 $\pm$ 0.29* (-42.43%)
	Superior Insert		3.07 $\pm$ 1.63			0.37 $\pm$ 0.47* (-87.95%)	
	Tibial		0.05 $\pm$ 0.03			0.10 $\pm$ 0.04* (100.00%)	
<b>XS</b>	Talar	0.13 $\pm$ 0.03	0.13 $\pm$ 0.03	0.11 $\pm$ 0.01	0.23 $\pm$ 0.24 (76.92%)	0.29 $\pm$ 0.23 (123.08%)	0.32 $\pm$ 0.29 (190.91%)
	Inferior Insert	2.41 $\pm$ 0.96	2.53 $\pm$ 1.05	2.71 $\pm$ 1.09	1.21 $\pm$ 0.60* (-49.79%)	0.97 $\pm$ 0.51* (-61.66%)	1.20 $\pm$ 0.65* (-55.72%)
	Superior Insert		3.33 $\pm$ 0.85			0.49 $\pm$ 0.18* (-85.29%)	
	Tibial		0.05 $\pm$ 0.07			0.11 $\pm$ 0.03* (120.00%)	

\*Indicates statistically significant difference between pre- and post-simulation topographic measurements within the same implant size ( $p \leq 0.05$ ).

Table 33. Mean ( $\pm$  95% CL) surface skewness (Rsk) measurements for each articulating surface of the medium (M) and extra small (XS) sized implants alongside the percentage change between the measurement stages (n = 6 for each implant size).

	Rsk ( $\mu\text{m}$ )	Pre-Test			5 Mc		
		Medial	Central	Lateral	Medial	Central	Lateral
<b>M</b>	Talar	0.23 $\pm$ 0.24	-0.50 $\pm$ 0.23	0.02 $\pm$ 0.46	-0.88 $\pm$ 0.88* (-482.61%)	-1.43 $\pm$ 0.91* (-186.00%)	-1.31 $\pm$ 1.34 (6650.00%)
	Inferior Insert	0.17 $\pm$ 0.08	0.15 $\pm$ 0.07	0.14 $\pm$ 0.09	-0.24 $\pm$ 0.15* (-241.18%)	-0.19 $\pm$ 0.15* (-226.67%)	-0.14 $\pm$ 0.35* (-200.00%)
	Superior Insert		0.06 $\pm$ 0.25			-0.66 $\pm$ 0.44* (-1200.00%)	
	Tibial		0.19 $\pm$ 4.30			-1.48 $\pm$ 0.97* (-878.95%)	
<b>XS</b>	Talar	0.23 $\pm$ 0.09	-0.31 $\pm$ 0.36	0.28 $\pm$ 0.22	-0.40 $\pm$ 0.88 (-273.91%)	-2.03 $\pm$ 1.03* (-554.84%)	-0.88 $\pm$ 1.15 (-414.29%)
	Inferior Insert	0.14 $\pm$ 0.10	0.10 $\pm$ 0.13	0.10 $\pm$ 0.10	-0.31 $\pm$ 0.08* (-321.43%)	-0.26 $\pm$ 0.17* (360.00%)	-0.30 $\pm$ 0.41* (-400.00%)
	Superior Insert		0.09 $\pm$ 0.13			-0.19 $\pm$ 0.75* (-311.11%)	
	Tibial		0.39 $\pm$ 3.88			-0.99 $\pm$ 0.86 (-353.85%)	

\*Indicates statistically significant difference between pre- and post-simulation topographic measurements within the same implant size ( $p \leq 0.05$ ).

Table 34. Mean ( $\pm$  95% CL) surface kurtosis (Rku) measurements for each articulating surface of the medium (M) and extra small (XS) sized implants alongside the percentage change between the measurement stages ( $n = 6$  for each implant size).

	Rku ( $\mu\text{m}$ )	Pre-Test			5 Mc		
		Medial	Central	Lateral	Medial	Central	Lateral
<b>M</b>	Talar	4.08 $\pm$ 1.28	5.47 $\pm$ 2.27	4.08 $\pm$ 0.31	11.63 $\pm$ 6.99* (185.05%)	18.22 $\pm$ 5.52* (233.09%)	16.87 $\pm$ 8.62* (313.48%)
	Inferior Insert	2.54 $\pm$ 0.14	2.50 $\pm$ 0.14	2.73 $\pm$ 0.18	4.59 $\pm$ 2.57 (80.71%)	4.15 $\pm$ 0.94* (66.00%)	4.64 $\pm$ 2.26 (69.96%)
	Superior Insert		2.46 $\pm$ 0.31			9.71 $\pm$ 4.47* (294.72%)	
	Tibial		13.04 $\pm$ 8.15			25.10 $\pm$ 4.46* (92.48%)	
<b>XS</b>	Talar	3.20 $\pm$ 0.97	6.15 $\pm$ 1.40	3.00 $\pm$ 1.48	7.24 $\pm$ 4.63 (126.25%)	17.28 $\pm$ 8.20* (180.98%)	10.05 $\pm$ 4.27* (235.00%)
	Inferior Insert	2.59 $\pm$ 1.04	2.42 $\pm$ 0.97	2.61 $\pm$ 1.05	3.46 $\pm$ 0.81* (33.59%)	5.10 $\pm$ 1.75* (110.74%)	3.91 $\pm$ 1.91 (49.81%)
	Superior Insert		2.49 $\pm$ 0.33			9.13 $\pm$ 2.39* (266.67%)	
	Tibial		10.23 $\pm$ 17.93			27.97 $\pm$ 4.39* (173.41%)	

\*Indicates statistically significant difference between pre- and post-simulation topographic measurements within the same implant size ( $p \leq 0.05$ ).

## E.2 Accelerated Artificial Ageing

Table 35. Mean ( $\pm$  95% CL) average surface roughness (Ra) measurements for each articulating surface of the small sized artificially aged implants alongside the percentage change between the measurement stages ( $n = 5$ ).

Ra ( $\mu\text{m}$ )	Pre-Test			5 Mc		
	Medial	Central	Lateral	Medial	Central	Lateral
Talar	0.06 $\pm$ 0.01	0.03 $\pm$ 0.00	0.05 $\pm$ 0.00	0.08 $\pm$ 0.01* (33.33%)	0.03 $\pm$ 0.01 (0.00%)	0.06 $\pm$ 0.01 (20.00%)
Inferior Insert	1.26 $\pm$ 0.08	1.21 $\pm$ 0.10	1.37 $\pm$ 0.11	0.50 $\pm$ 0.01* (-60.32%)	0.46 $\pm$ 0.17* (-61.98%)	0.59 $\pm$ 0.16* (-56.93%)
Superior Insert		1.45 $\pm$ 0.11			0.10 $\pm$ 0.02* (-93.10%)	
Tibial		0.01 $\pm$ 0.00			0.03 $\pm$ 0.01* (200.00%)	

\*Indicates statistically significant difference between topographic measurements ( $p \leq 0.05$ ).

Table 36. Mean ( $\pm$  95% CL) maximum profile peak heights (Rp) measurements for each articulating surface of the small sized artificially aged implants alongside the percentage change between the measurement stages ( $n = 5$ ).

Rp ( $\mu\text{m}$ )	Pre-Test			5 Mc		
	Medial	Central	Lateral	Medial	Central	Lateral
Talar	0.09 $\pm$ 0.01	0.08 $\pm$ 0.01	0.09 $\pm$ 0.01	0.11 $\pm$ 0.04 (22.22%)	0.09 $\pm$ 0.04 (12.50%)	0.06 $\pm$ 0.01 (-33.33%)
Inferior Insert	3.47 $\pm$ 0.19	2.67 $\pm$ 0.25	3.57 $\pm$ 0.21	0.87 $\pm$ 0.08* (-74.93%)	1.24 $\pm$ 0.42* (-53.56%)	0.99 $\pm$ 0.51* (-72.27%)
Superior Insert		3.72 $\pm$ 0.23			0.31 $\pm$ 0.10* (-91.67%)	
Tibial		0.07 $\pm$ 0.01			0.09 $\pm$ 0.02* (28.57%)	

\*Indicates statistically significant difference between topographic measurements ( $p \leq 0.05$ ).

Table 37. Mean ( $\pm$  95% CL) maximum profile valley depth (Rv) measurements for each articulating surface of the small sized artificially aged implants alongside the percentage change between the measurement stages (n = 5).

Rv ( $\mu\text{m}$ )	Pre-Test			5 Mc		
	Medial	Central	Lateral	Medial	Central	Lateral
Talar	0.07 $\pm$ 0.00	0.05 $\pm$ 0.02	0.06 $\pm$ 0.01	0.13 $\pm$ 0.07 (85.71%)	0.08 $\pm$ 0.05 (60.00%)	0.13 $\pm$ 0.05* (116.67%)
Inferior Insert	3.04 $\pm$ 0.16	2.37 $\pm$ 0.22	3.24 $\pm$ 0.17	1.14 $\pm$ 0.13* (-62.50%)	1.70 $\pm$ 0.91* (-28.27%)	1.22 $\pm$ 0.36* (-62.35%)
Superior Insert		3.23 $\pm$ 0.32			0.33 $\pm$ 0.03* (-89.78%)	
Tibial		0.05 $\pm$ 0.01			0.11 $\pm$ 0.03* (120.00%)	

\*Indicates statistically significant difference between topographic measurements ( $p \leq 0.05$ ).

Table 38. Mean ( $\pm$  95% CL) surface skewness (Rsk) measurements for each articulating surface of the small sized artificially aged implants alongside the percentage change between the measurement stages (n = 5).

Rsk ( $\mu\text{m}$ )	Pre-Test			5 Mc		
	Medial	Central	Lateral	Medial	Central	Lateral
Talar	0.34 $\pm$ 0.14	0.28 $\pm$ 0.39	0.11 $\pm$ 0.20	-0.41 $\pm$ 0.95 (-220.59%)	-0.73 $\pm$ 0.79* (-360.71%)	-1.01 $\pm$ 1.43 (-1018.18%)
Inferior Insert	0.14 $\pm$ 0.08	0.13 $\pm$ 0.08	0.09 $\pm$ 0.04	-0.21 $\pm$ 0.49 (-250.00%)	-1.03 $\pm$ 0.89* (-892.31%)	-0.04 $\pm$ 0.09* (-144.44%)
Superior Insert		0.13 $\pm$ 0.15			-0.21 $\pm$ 1.58 (-261.54%)	
Tibial		-0.20 $\pm$ 1.71			-2.27 $\pm$ 0.41* (-1035.00%)	

\*Indicates statistically significant difference between topographic measurements ( $p \leq 0.05$ ).

Table 39. Mean ( $\pm$  95% CL) surface kurtosis (Rku) measurements for each articulating surface of the small sized artificially aged implants alongside the percentage change between the measurement stages (n = 5).

Rku ( $\mu\text{m}$ )	Pre-Test			5 Mc		
	Medial	Central	Lateral	Medial	Central	Lateral
Talar	3.06 $\pm$ 0.68	3.13 $\pm$ 0.86	3.52 $\pm$ 1.03	13.69 $\pm$ 11.64 (347.39%)	13.94 $\pm$ 10.07* (345.37%)	15.04 $\pm$ 6.54* (327.27%)
Inferior Insert	2.60 $\pm$ 0.14	2.06 $\pm$ 0.09	2.63 $\pm$ 0.20	4.80 $\pm$ 3.06 (84.62%)	7.30 $\pm$ 5.16 (254.37%)	3.29 $\pm$ 0.83 (25.10%)
Superior Insert		2.37 $\pm$ 0.08			23.91 $\pm$ 10.52* (908.86%)	
Tibial		16.31 $\pm$ 4.59			40.40 $\pm$ 13.84* (147.70%)	

\*Indicates statistically significant difference between topographic measurements ( $p \leq 0.05$ ).

### E.3 Simulator Type

Table 40. Mean ( $\pm$  95% CL) average surface roughness (Ra) measurements for each articulating surface of the medium sized implants alongside the percentage change between the measurement stages (n = 5).

Ra ( $\mu\text{m}$ )	Pre-Test			3 Mc (UoL)		
	Medial	Central	Lateral	Medial	Central	Lateral
Talar	0.07 $\pm$ 0.00	0.04 $\pm$ 0.00	0.07 $\pm$ 0.00	0.07 $\pm$ 0.01 (0.00%)	0.06 $\pm$ 0.01* (50.00%)	0.08 $\pm$ 0.01 (14.29%)
Inferior Insert	1.17 $\pm$ 0.05	1.14 $\pm$ 0.06	1.31 $\pm$ 0.07	0.54 $\pm$ 0.16* (-53.85%)	0.44 $\pm$ 0.11* (-61.40%)	0.58 $\pm$ 0.11* (-55.73%)
Superior Insert		1.23 $\pm$ 0.02			0.10 $\pm$ 0.04* (-91.87%)	
Tibial		0.01 $\pm$ 0.00			0.02 $\pm$ 0.01* (100.00%)	

\*Indicates statistically significant difference between pre- and post-simulation topographic measurements ( $p \leq 0.05$ ).

Table 41. Mean ( $\pm$  95% CL) maximum profile peak heights (Rp) measurements for each articulating surface of the medium sized implants alongside the percentage change between the measurement stages (n = 5).

Rp ( $\mu\text{m}$ )	Pre-Test			3 Mc (UoL)		
	Medial	Central	Lateral	Medial	Central	Lateral
Talar	0.08 $\pm$ 0.01	0.09 $\pm$ 0.01	0.08 $\pm$ 0.01	0.17 $\pm$ 0.05* (112.50%)	0.19 $\pm$ 0.06* (111.11%)	0.19 $\pm$ 0.06* (137.50%)
Inferior Insert	3.12 $\pm$ 0.10	2.83 $\pm$ 0.14	3.51 $\pm$ 0.12	1.05 $\pm$ 0.36* (-66.35%)	0.92 $\pm$ 0.29* (-67.49%)	1.04 $\pm$ 0.27* (-70.37%)
Superior Insert		3.09 $\pm$ 0.58			0.28 $\pm$ 0.13* (-90.94%)	
Tibial		0.05 $\pm$ 0.00			0.08 $\pm$ 0.02* (60.00%)	

\*Indicates statistically significant difference between pre- and post-simulation topographic measurements ( $p \leq 0.05$ ).

Table 42. Mean ( $\pm$  95% CL) maximum profile valley depth (Rv) measurements for each articulating surface of the medium sized implants alongside the percentage change between the measurement stages (n = 5).

Rv ( $\mu\text{m}$ )	Pre-Test			3 Mc (UoL)		
	Medial	Central	Lateral	Medial	Central	Lateral
Talar	0.11 $\pm$ 0.02	0.093 $\pm$ 0.01	0.098 $\pm$ 0.01	0.18 $\pm$ 0.01* (63.64%)	0.14 $\pm$ 0.05* (55.56%)	0.21 $\pm$ 0.04* (133.33%)
Inferior Insert	2.67 $\pm$ 0.13	2.83 $\pm$ 0.14	3.03 $\pm$ 0.11	1.30 $\pm$ 0.40* (-51.31%)	1.19 $\pm$ 0.20* (-57.95%)	1.34 $\pm$ 0.37* (-55.78%)
Superior Insert		2.80 $\pm$ 0.36			0.35 $\pm$ 0.16* (-87.50%)	
Tibial		0.05 $\pm$ 0.00			0.09 $\pm$ 0.03 (80.00%)*	

\*Indicates statistically significant difference between pre- and post-simulation topographic measurements ( $p \leq 0.05$ ).

Table 43. Mean ( $\pm$  95% CL) surface skewness (Rsk) measurements for each articulating surface of the medium sized implants alongside the percentage change between the measurement stages (n = 5).

Rsk ( $\mu\text{m}$ )	Pre-Test			3 Mc (UoL)		
	Medial	Central	Lateral	Medial	Central	Lateral
Talar	-0.05 $\pm$ 0.23	-0.29 $\pm$ 0.08	-0.12 $\pm$ 0.16	-0.10 $\pm$ 0.33 (-100.00%)	-0.43 $\pm$ 0.53 (-115.00%)	-0.35 $\pm$ 0.32 (-250.00%)
Inferior Insert	0.17 $\pm$ 0.03	0.11 $\pm$ 0.03	0.17 $\pm$ 0.06	-0.26 $\pm$ 0.77 (-217.65%)	-0.80 $\pm$ 0.67* (-827.27%)	-0.33 $\pm$ 0.93 (-276.47%)
Superior Insert		-0.02 $\pm$ 0.01			-0.46 $\pm$ 1.20 (-2200.00%)	
Tibial		0.33 $\pm$ 0.71			-0.86 $\pm$ 1.38 (-360.61%)	

\*Indicates statistically significant difference between pre- and post-simulation topographic measurements ( $p \leq 0.05$ ).

Table 44. Mean ( $\pm$  95% CL) surface kurtosis (Rku) measurements for each articulating surface of the medium sized implants alongside the percentage change between the measurement stages (n = 5).

Rku ( $\mu\text{m}$ )	Pre-Test			3 Mc (UoL)		
	Medial	Central	Lateral	Medial	Central	Lateral
Talar	3.79 $\pm$ 1.83	4.11 $\pm$ 0.88	3.61 $\pm$ 1.17	12.51 $\pm$ 4.71* (229.82%)	7.87 $\pm$ 3.86* (91.48%)	9.82 $\pm$ 5.92* (172.02%)
Inferior Insert	2.69 $\pm$ 0.13	2.58 $\pm$ 0.07	2.85 $\pm$ 0.21	5.92 $\pm$ 2.17* (120.07%)	8.92 $\pm$ 8.76 (245.74%)	8.35 $\pm$ 8.79 (192.98%)
Superior Insert		2.41 $\pm$ 0.07			19.71 $\pm$ 7.48* (717.84%)	
Tibial		14.72 $\pm$ 0.77			33.93 $\pm$ 15.55* (130.50%)	

\*Indicates statistically significant difference between pre- and post-simulation topographic measurements ( $p \leq 0.05$ ).

#### E.4 Simulator Inputs

Table 45. Mean ( $\pm$  95% CL) average surface roughness (Ra) measurements for each articulating surface of the medium sized implants alongside the percentage change between the measurement stages (n = 5).

Ra ( $\mu\text{m}$ )	UoL (0-3 Mc)			ISO 22622:2019 (3-5 Mc)		
	Medial	Central	Lateral	Medial	Central	Lateral
Talar	0.07 $\pm$ 0.01	0.06 $\pm$ 0.01	0.08 $\pm$ 0.01	0.08 $\pm$ 0.02 (14.29%)	0.07 $\pm$ 0.02 (16.67%)	0.09 $\pm$ 0.03 (12.50%)
Inferior Insert	0.54 $\pm$ 0.16	0.44 $\pm$ 0.11	0.58 $\pm$ 0.11	0.46 $\pm$ 0.08 (-14.81%)	0.43 $\pm$ 0.07 (-2.27%)	0.52 $\pm$ 0.12 (-10.34%)
Superior Insert		0.10 $\pm$ 0.04			0.07 $\pm$ 0.02 (-30.00%)	
Tibial		0.02 $\pm$ 0.01			0.03 $\pm$ 0.01 (50.00%)	

Table 46. Mean ( $\pm$  95% CL) maximum profile peak heights ( $R_p$ ) measurements for each articulating surface of the medium sized implants alongside the percentage change between measurement stages after 2 Mc of ISO 22622:2019 loading and kinematic input profiles.

$R_p$ ( $\mu\text{m}$ )	UoL (0-3 Mc)			ISO 22622:2019 (3-5 Mc)		
	Medial	Central	Lateral	Medial	Central	Lateral
Talar	0.17 $\pm$ 0.05	0.19 $\pm$ 0.06	0.19 $\pm$ 0.06	0.15 $\pm$ 0.05 (-11.76%)	0.20 $\pm$ 0.05 (-5.26%)	0.20 $\pm$ 0.08 (-5.26%)
Inferior Insert	1.05 $\pm$ 0.36	0.92 $\pm$ 0.29	1.04 $\pm$ 0.27	0.90 $\pm$ 0.17 (-14.29%)	0.82 $\pm$ 0.18 (-10.87%)	1.03 $\pm$ 0.27 (-0.96%)
Superior Insert		0.28 $\pm$ 0.13			0.21 $\pm$ 0.06 (-25.00%)	
Tibial		0.08 $\pm$ 0.02			0.08 $\pm$ 0.02 (0.00%)	

Table 47. Mean ( $\pm$  95% CL) maximum profile valley depth ( $R_v$ ) measurements for each articulating surface of the medium sized implants after 2 Mc of ISO 22622:2019 loading and kinematic input profiles.

$R_v$ ( $\mu\text{m}$ )	UoL (0-3 Mc)			ISO 22622:2019 (3-5 Mc)		
	Medial	Central	Lateral	Medial	Central	Lateral
Talar	0.18 $\pm$ 0.01	0.14 $\pm$ 0.05	0.21 $\pm$ 0.04	0.22 $\pm$ 0.07 (22.22%)	0.17 $\pm$ 0.11 (21.43%)	0.31 $\pm$ 0.17 (47.62%)
Inferior Insert	1.30 $\pm$ 0.40	1.19 $\pm$ 0.20	1.34 $\pm$ 0.37	1.22 $\pm$ 0.23 (-6.15%)	1.12 $\pm$ 0.25 (-5.88%)	1.28 $\pm$ 0.29 (-4.48%)
Superior Insert		0.35 $\pm$ 0.16			0.26 $\pm$ 0.09 (-25.71%)	
Tibial		0.09 $\pm$ 0.03			0.10 $\pm$ 0.02 (11.11%)	

Table 48. Mean ( $\pm$  95% CL) surface skewness ( $R_{sk}$ ) measurements for each articulating surface of the medium sized implants after 2 Mc of ISO 22622:2019 loading and kinematic input profiles.

$R_{sk}$ ( $\mu\text{m}$ )	UoL (0-3 Mc)			ISO 22622:2019 (3-5 Mc)		
	Medial	Central	Lateral	Medial	Central	Lateral
Talar	-0.10 $\pm$ 0.33	-0.43 $\pm$ 0.53	-0.35 $\pm$ 0.32	-0.30 $\pm$ 0.41 (-200.00%)	0.34 $\pm$ 2.41 (185.00%)	-1.50 $\pm$ 0.30* (-400.00%)
Inferior Insert	-0.26 $\pm$ 0.77	-0.80 $\pm$ 0.67	-0.33 $\pm$ 0.93	-0.63 $\pm$ 0.58 (-200.00%)	-0.55 $\pm$ 0.30 (37.50%)	-0.10 $\pm$ 0.58 (66.67%)
Superior Insert		-0.46 $\pm$ 1.20			-0.39 $\pm$ 0.53 (25.00%)	
Tibial		-0.86 $\pm$ 1.38			-1.29 $\pm$ 2.70 (-50.00%)	

\*Indicates statistically significant difference in topographic measurements ( $p \leq 0.05$ ) between the simulator input conditions.

Table 49. Mean ( $\pm$  95% CL) surface kurtosis ( $R_{ku}$ ) measurements for each articulating surface of the medium sized implants after 2 Mc of ISO 22622:2019 loading and kinematic input profiles.

$R_{ku}$ ( $\mu\text{m}$ )	UoL (0-3 Mc)			ISO 22622:2019 (3-5 Mc)		
	Medial	Central	Lateral	Medial	Central	Lateral
Talar	12.51 $\pm$ 4.71	7.87 $\pm$ 3.86	9.82 $\pm$ 5.92	18.44 $\pm$ 10.18 (47.40%)	33.46 $\pm$ 7.71* (325.16%)	20.06 $\pm$ 7.78* (104.28%)
Inferior Insert	5.92 $\pm$ 2.17	8.92 $\pm$ 8.76	8.35 $\pm$ 8.79	5.57 $\pm$ 2.73 (-5.91%)	5.48 $\pm$ 2.39 (-38.57%)	5.12 $\pm$ 2.30 (-38.68%)
Superior Insert		19.71 $\pm$ 7.48			13.08 $\pm$ 6.38 (-33.64%)	
Tibial		33.93 $\pm$ 15.55			40.00 $\pm$ 10.48 (17.89%)	

\*Indicates statistically significant difference in topographic measurements ( $p \leq 0.05$ ) between the simulator input conditions.

**APPENDIX F**

**ETHICAL APPROVAL**

## APPENDIX F: ETHICAL APPROVAL

### F.1 University of Leeds Ethics Committee Approval

The Secretariat  
Level 11, Worsley Building  
University of Leeds  
Leeds, LS2 9NL  
Tel: 0113 343 4873  
Email: [ResearchEthics@leeds.ac.uk](mailto:ResearchEthics@leeds.ac.uk)



James Hopwood  
Institute of Medical and Biological Engineering  
University of Leeds  
Leeds, LS2 9JT

**MaPS and Engineering joint Faculty Research Ethics Committee (MEEC FREC)  
University of Leeds**

15 October 2021

Dear James

**Title of study**            **Biomechanical comparison of two marker motion capture systems during activities of daily living**  
**Ethics reference**        **MEEC 17-037**

I am pleased to inform you that the application listed above has been reviewed by the MaPS and Engineering joint Faculty Research Ethics Committee (MEEC FREC) and I can confirm a favourable ethical opinion as of the date of this letter. The following documentation was considered:

Document	Version	Date
MEEC 17-037 University Ethical Review JDH V0.1.pdf	1	25/05/18
MEEC 17-037 Participant Recruitment Poster JDH V0.1.pdf	1	25/05/18
MEEC 17-037 Recruitment email JDH V0.1.pdf	1	25/05/18
MEEC 17-037 Participant Information Sheet JDH v0.1.pdf	1	25/05/18
MEEC 17-037 Participant Consent Form JDH v0.1.pdf	1	25/05/18
MEEC 17-037 University pre exercise questionnaire JDH v0.1.pdf	1	25/05/18
MEEC 17-037 Risk-assessment JDH v0.1.pdf	1	25/05/18

Reviewers made the following comments:

Application section	Comment
Participant information sheet	The exclusion criteria should be listed in the participant information sheet.
Participant information sheet	You indicated that the data will be kept for a period of minimum 5 years in section "Will taking part in this study be kept confidential". However, it's described as "Up to 10 years" in the ethical review application form and consent form. A more consistent declaration should be made.

Please notify the committee if you intend to make any amendments to the information in your ethics application as submitted at date of this approval as all changes must receive ethical approval prior to implementation. The amendment form is available at <http://ris.leeds.ac.uk/EthicsAmendment>.

Please note: You are expected to keep a record of all your approved documentation and other documents relating to the study, including any risk assessments. This should be kept in your study file, which should be readily available for audit purposes. You will be given a two week notice period if your project is to be audited. There is a checklist listing examples of documents to be kept which is available at <http://ris.leeds.ac.uk/EthicsAudits>.

We welcome feedback on your experience of the ethical review process and suggestions for improvement. Please email any comments to [ResearchEthics@leeds.ac.uk](mailto:ResearchEthics@leeds.ac.uk).

Yours sincerely

Jennifer Blaikie  
Senior Research Ethics Administrator, the Secretariat  
On behalf of Dr Dawn Groves, Chair, [MEEC FREC](#)

CC: Student's supervisor(s)

## F.2 Nottingham Trent University Ethics Committee Approval

**NOTTINGHAM TRENT UNIVERSITY**  
**COLLEGE OF SCIENCE AND TECHNOLOGY**  
**ETHICAL COMMITTEE (HUMANS)**

---

**Application No:** 640  
**Title:** Biomechanical Performance of Ankle Fusion and Total Ankle Replacements During Activities of Daily Living.  
**Applicants:** Dr Cleveland Barnett  
**Date of Meeting:** 19<sup>th</sup> March 2020 (updated 18<sup>th</sup> November 2020)

---

With regard to your application to the recent meeting of the Ethical Committee (Humans), the Committee have reviewed this and the following action has been decided:

- Approved
- Approved, subject to the following information being provided/clarified.
- Decision deferred, pending further receipt of further information.
- Not approved



\_\_\_\_\_  
Professor Sergio Rutella  
Chair  
Ethical Review Committee (Humans)

Date: 1 December 2020

## F.3 NHS East of Scotland Research Ethics Service Approval



East of Scotland Research Ethics Service (EoSRES)

Research Ethics Service

Tayside medical Science Centre  
Residency Block Level 3  
George Pirie Way  
Ninewells Hospital and Medical School  
Dundee DD1 9SY

Mr James Hopwood  
Desk 12, X302,  
Institute of Medical and Biological Engineering  
Faculty of Mechanical Engineering  
University of Leeds  
LS2 9JT

Date: 23 April 2020  
Your Ref:  
Our Ref: LR/AG19/ES/0070  
Enquiries to: Arlene Grubb  
Direct Line: 01382 383848  
Email: [eosres.tayside@nhs.net](mailto:eosres.tayside@nhs.net)

Dear Mr Hopwood

**Study title:** Biomechanical Performance of Ankle Fusion and Total Ankle Replacements During Activities of Daily Living.  
**REC reference:** 19/ES/0070  
**Protocol number:** 2.0  
**Amendment number:** AM01(AM04 REC reference only)  
**Amendment date:** 23 March 2020  
**IRAS project ID:** 244600

The above amendment was reviewed at the meeting of the Sub-Committee held on 23 April 2020 in correspondence.

### Ethical opinion

The members of the Committee taking part in the review gave a favourable ethical opinion of the amendment on the basis described in the notice of amendment form and supporting documentation.

### Approved documents

The documents reviewed and approved at the meeting were:

Document	Version	Date
Notice of Substantial Amendment (non-CTIMP)	AM01	23 March 2020
Email with amendment]		06 April 2020
summary of changes to exclusion criteria		
Research protocol or project proposal	2.0	23 March 2020

### Membership of the Committee

The members of the Committee who took part in the review are listed on the attached sheet.

## F.4 NHS Health Research Authority (HRA) and Health and Care Research Wales (HCRW) Approval Letter



Ymchwil Iechyd  
a Gofal **Cymru**  
Health and Care  
Research **Wales**



Prof Anthony Redmond  
PhD Researcher  
University of Leeds  
Leeds Institute of Rheumatic and Musculoskeletal  
Medicine  
Chapel Allerton Hospital  
Harehills Lane, Leeds  
LS7 4SA

Email: [hra.approval@nhs.net](mailto:hra.approval@nhs.net)  
[HCRW.approvals@wales.nhs.uk](mailto:HCRW.approvals@wales.nhs.uk)

19 August 2019

Dear Prof Redmond

**HRA and Health and Care  
Research Wales (HCRW)  
Approval Letter**

<b>Study title:</b>	Biomechanical Performance of Ankle Fusion and Total Ankle Replacements During Activities of Daily Living.
<b>IRAS project ID:</b>	244600
<b>Protocol number:</b>	2.0
<b>REC reference:</b>	19/ES/0070
<b>Sponsor</b>	University of Leeds

I am pleased to confirm that [HRA and Health and Care Research Wales \(HCRW\) Approval](#) has been given for the above referenced study, on the basis described in the application form, protocol, supporting documentation and any clarifications received. You should not expect to receive anything further relating to this application.

Please now work with participating NHS organisations to confirm capacity and capability, in line with the instructions provided in the "Information to support study set up" section towards the end of this letter.

**How should I work with participating NHS/HSC organisations in Northern Ireland and Scotland?**

HRA and HCRW Approval does not apply to NHS/HSC organisations within Northern Ireland and Scotland.

If you indicated in your IRAS form that you do have participating organisations in either of these devolved administrations, the final document set and the study wide governance report (including this letter) have been sent to the coordinating centre of each participating nation. The relevant national coordinating function/s will contact you as appropriate.

Please see [IRAS Help](#) for information on working with NHS/HSC organisations in Northern Ireland and Scotland.

**How should I work with participating non-NHS organisations?**

HRA and HCRW Approval does not apply to non-NHS organisations. You should work with your non-NHS organisations to [obtain local agreement](#) in accordance with their procedures.

**What are my notification responsibilities during the study?**

The document "*After Ethical Review – guidance for sponsors and investigators*", issued with your REC favourable opinion, gives detailed guidance on reporting expectations for studies, including:

- Registration of research
- Notifying amendments
- Notifying the end of the study

The [HRA website](#) also provides guidance on these topics, and is updated in the light of changes in reporting expectations or procedures.

**Who should I contact for further information?**

Please do not hesitate to contact me for assistance with this application. My contact details are below.

Your IRAS project ID is 244600. Please quote this on all correspondence.

Yours sincerely,

Kevin Ahmed  
HRA Approvals Manager

Telephone: 0207 104 8171  
Email: [hra.approval@nhs.net](mailto:hra.approval@nhs.net)

Copy to: *Faculty NHS Research Ethics Officer*

## F.5 Integrated Research Application System (IRAS) Final Document Checklist for HRA Approval

### List of Documents

The final document set assessed and approved by HRA and HCRW Approval is listed below.

<i>Document</i>	<i>Version</i>	<i>Date</i>
Copies of advertisement materials for research participants [Appendix H TARADL Controls Recruitment Poster]	2.0	26 June 2019
Copies of advertisement materials for research participants [Appendix N Controls Recruitment Email]	2.0	26 June 2019
Covering letter on headed paper [TARADL Cover Letter]	1.0	24 May 2019
Evidence of Sponsor insurance or indemnity (non NHS Sponsors only) [TARADL Sponsor Insurance]		17 September 2018
IRAS Application Form [IRAS_Form_22072019]		22 July 2019
Letter from funder [TARADL Letter of Funding]		16 April 2016
Letter from sponsor [TARADL Letter from Sponsor]		23 May 2019
Letter from statistician [TARADL Letter from Statistician]		24 May 2019
Letters of invitation to participant [Appendix F TARADL Controls Invitation Letter]	1.0	23 May 2019
Letters of invitation to participant [Appendix A TARADL Ankle Fusion Group Invitation Letter]	1.0	23 May 2019
Letters of invitation to participant [Appendix B TARADL Ankle Replacement Group Invitation Letter]	1.0	23 May 2019
Organisation Information Document [TARADL Organisation Information Document]	1.0	24 May 2019
Other [Appendix M TARADL Case Report Form]	2.0	26 June 2019
Other [Response to Provisional Opinion]	3.0	08 July 2019
Other [Surgeon Peer Review Letter]		22 July 2019
Other [Surgeon Peer Review Letter]		02 July 2019
Other [Appendix E TARADL Consent to Contact Form]	1.0	23 May 2019
Other [Appendix M TARADL Case Report Form]	1.0	23 May 2019
Participant consent form [Appendix I TARADL ICF Ankle Fusion Group]	1.0	23 May 2019
Participant consent form [Appendix J TARADL ICF Ankle Replacement Group]	1.0	23 May 2019
Participant consent form [Appendix K TARADL ICF Control Group]	1.0	23 May 2019
Participant information sheet (PIS) [Appendix C TARADL PIS Ankle Fusion Group]	2.0	26 May 2019
Participant information sheet (PIS) [Appendix D TARADL PIS Ankle Replacement Group]	2.0	26 May 2019
Participant information sheet (PIS) [Appendix G TARADL PIS Control Group]	2.0	26 May 2019
Research protocol or project proposal [TARADL LBRC Research Protocol]	1.0	23 May 2019
Schedule of Events or SoECAT	1.0	19 August 2019
Summary CV for Chief Investigator (CI) [TARADL CI Summary CV]	1.0	23 May 2019
Summary CV for student [TARADL Student CV]		29 May 2019
Summary CV for supervisor (student research) [Academic Supervisor (AR) CV]	1.0	23 May 2019
Summary CV for supervisor (student research) [Academic Supervisor (GJC) CV]	1.0	22 May 2019
Summary CV for supervisor (student research) [Academic Supervisor (CLB) CV]	1.0	29 May 2019

**APPENDIX G**

**PILOT GAIT STUDY**

## APPENDIX G: GAIT PILOT STUDY

### Reliability of Three-Dimensional Gait Data between Two Motion Capture Laboratories

#### G.1 Introduction

Clinical gait analysis has successfully been used for the functional assessment of patients, in order to quantify improvements or dysfunctions in locomotion after surgical intervention (Andriacchi and Alexander, 2000; Sutherland, 2002). The inherent variability and uncertainties in gait have to be properly evaluated (Schwartz et al., 2004) and depend on a number of factors, which include: (1) the motion capture system (Chiari et al., 2005; Windolf et al., 2008); (2) marker set model (Ferrari et al., 2008; Yoo et al., 2022); (3) experience of the researcher (Gorton et al., 2009; Leigh et al., 2014); (4) calibration volume and location of the gait analysis (Benedetti et al., 2013; Di Marco et al., 2016); (5) intra-subject stride to stride variability (Meldrum et al., 2014); and (6) STA (Leardini et al., 2005). Whilst the final two causes of variability cannot be eliminated due to being patient-related, the first four sources of variability are a result of the chosen methodological approach (Scalona et al., 2019).

Perhaps one of the largest sources of gait variability, stems from the collection of data at different research sites. Noonan et al. (2003) evaluated 11 ambulatory patients with spastic cerebral palsy at four different gait analysis laboratories and demonstrated that there was, on average, 21% (8-34%) variance in 5% of the gait cycle between research sites. The authors also reported that there was increased variability in the transverse and frontal planes, which may be attributed to differences in marker placement between sites. The variance in gait within this study however, was likely a result of the innate differences in cerebral palsy patients, which makes it difficult to compare the results from this study to healthy participants.

Gorton et al. (2009) assessed the variability of nine kinematic parameters within twelve laboratories and twenty four operators, when conducting overground level walking trials on one healthy participant. The results demonstrated an average maximum difference of 15° across each research site. Variability was high between both testing sessions at a single site, with five of the eight gait parameters being significantly different (Gorton et al., 2009). Furthermore, the authors concluded that using a standardised protocol across research sites reduced variability by as much as 20% (Gorton et al., 2009). A similar study measuring the consistency of one healthy participant's gait mechanics across seven different motion capture laboratories, determined that joint angles and moments of the foot and lower limb were generally consistent (Benedetti et al., 2013). However, a limitation of both of the above studies was that they only measured the effect different gait laboratories had on one participant. In addition to this, each research site used different examiners with varying levels of experience with marker placement, which has also been identified as a large source of variability in gait (Leigh et al., 2014).

Most recently, Kaufman et al. (2016) collected kinematic and kinetic parameters of five walking trials at three research centres of excellence for 10 healthy participants. Inter-lab kinematic errors were  $< 5.0^\circ$  for all joint angle measurements in all three planes of motion, whereas kinetic error differed significantly between walking speeds. The data from this study suggested that it is feasible to attain repeatable and reliable gait data across multiple gait laboratories, particularly when gait speed, anatomical placement and segment definitions is standardised between testing sessions (Kaufman et al., 2016). Each of the previous studies mentioned, highlighted the importance of reliability and repeatability when attempting to compare data between research sites, and should be considered when evaluating patient progression post-operatively.

The work presented in this section acted as a pilot study to the post-operative exploratory gait study (Chapter 5), which compared the patient reported outcomes, spatiotemporal and biomechanical differences between patients implanted with AA and TAR, at an intermediate follow-up period. Due to geographical location, availability of the patients and inability to travel to the same gait laboratory, two research sites were selected to give the best coverage to collate data from the selected patient populations. Thus, the aim of this pilot study was to collect consistent 3D gait data using two different motion capture systems at two different research sites. The study used a similar method for the calibration of the motion capture equipment, a single experienced evaluator for marker placement and a uniform fundamental biomechanical model, to ensure that if variability in the gait data was measured, then it would be due to differences between the two motion capture systems

## G.2 Methods

A total of 12 participants volunteered to participate, which corresponds to the recommended sample size for a pilot study (Julious, 2005). The mean ( $\pm$  95% CL) age, height, weight and BMI of the participants are presented in Table 50. Inclusion criteria were individuals aged 18 years and over at the point of data collection, who demonstrated good health status as recognised by a health screen questionnaire. Individuals were excluded from the study if they had a current neuromuscular and/or musculoskeletal injury, had been diagnosed with medical conditions that may affect normal locomotion, or had an injury to the foot or lower body in the past six months. Prior to testing, each participant gave their written consent, with their health screening questionnaire being obtained from all participants at both site visits. The procedures used for the pilot study were approved by the UoL Human Research Ethics Committee (Appendix E1).

Table 50. Mean ( $\pm$  95% CL) demographic data of the participants at both research sites.

	CAH	NTU	<i>p</i> value
<b>Age (years)</b>	24.18 $\pm$ 1.47	24.27 $\pm$ 1.35	0.564
<b>Height (m)</b>	1.78 $\pm$ 0.09	1.78 $\pm$ 0.09	0.655
<b>Weight (kg)</b>	77.05 $\pm$ 7.31	76.95 $\pm$ 7.55	0.838
<b>BMI (kg/m<sup>2</sup>)</b>	24.32 $\pm$ 2.44	24.30 $\pm$ 2.51	0.929

Gait analyses were performed at the Biomedical, Life and Health Sciences Research Centre at the Nottingham Trent University (NTU; Nottingham, UK) and at the Leeds Biomedical Research Centre at Chapel Allerton Hospital (CAH; Leeds, UK). Both sites used force platforms from the same manufacturer (AMTI, Watertown, MA) and same data collection rate of 100 Hz. The only differences between sites, related to the motion capture systems, the number of cameras used and the force plate sampling rate (Table 51). Each participant visited both research sites within a three month period. The order in which the participants visited each laboratory was not randomised, but instead was based on their availability to travel.

Table 51. Gait laboratory motion capture and force platform systems used at each research site.

		CAH	NTU
Motion Capture System	Manufacturer	Vicon	Qualisys Track Manager
	Camera	Vicon MX	Qualisys Oqus
	Number of Cameras	10	13
	Data Collection Rate (Hz)	100	100
Force Platforms	Manufacturer	AMTI (Watertown, MA)	AMTI (Watertown, MA)
	Model	BP400600	BP400600
	Number of Platforms	2	2
	Data Collection Rate (Hz)	1000	500

The experimental conditions used in this pilot study were also used as the methodology for the post-operative comparative gait study between AA and TAR (Chapter 5). Participants were asked to wear form fitting shorts and top, whilst footwear was removed. Participant's height was measured using a stadiometer and weight was determined during the static trials, when the participant stood with both feet on one of the force platforms. Thirty six reflective markers (Qualisys™ Medical AB, Goteborg, Sweden) were placed directly on the skin of the participants. The IOR foot model was used to determine multi-segment ankle kinematic gait data from the participant's dominant foot, whilst a basic SFM was used on the non-dominant foot. The dominant foot was determined as the one the participant would use to kick a ball as far as they could. The IOR allowed for 3D joint rotations to be calculated for the hindfoot, midfoot and forefoot segments. A final segment defined the metatarsus with respect to the calcaneus and is here after referred to as forefoot-to-hindfoot.

The anatomical landmarks were identified through manual palpation in accordance with the Colour Atlas of Skeletal Landmark Definitions (van Sint Jan, 2007). All markers were placed by the same investigator, whom had five years' experience in gait analysis. The tracking markers followed the CAST marker set, which involved the attachment of semi-rigid thermoplastic shells to the pelvis, thigh, and shank of the participants, to determine segment position and orientation. Following the application of the reflective marker set, data was collected while the participant walked over level ground, along an 8 m walkway at a self-selected walking speed, until five successful trials were obtained. The participants walked over two force platforms, which were positioned in the middle of the walkway and were arranged in succession to allow simultaneous

collection of the dominant and non-dominant limbs. Data from the force platforms from both sites were time synchronised with the motion cameras.

Marker position reconstruction and kinetic and kinematic computation were performed at the two research sites using Vicon Nexus 2.9.2 (Vicon Motion Systems, Oxford, UK) for NTU and Qualisys Track Manager Version 2019.3 (Qualisys™ Medical AB, Goteborg, Sweden) for CAH. Data was then exported and processed within Visual3D (C-Motion, Germantown, MD, USA). This process involved developing the biomechanical models for the body segments, filtering the data using a low-pass Butterworth filter with a cut-off frequency of 6 Hz and 25 Hz for the kinematic and force data, respectively (Robertson and Dowling, 2003) as well as determining the gait events of heel strike and toe-off. Importantly, the underlying biomechanical and segmental models were the same between research sites. At each site, spatiotemporal parameters of step length (m), walking speed (m/s) and cadence (steps/min) of the dominant and non-dominant limb were calculated from the determined gait events. Joint angles, moments and power of the hip, knee and ankle were determined for the dominant foot, while the MFEM was used to determine kinematic differences of the hindfoot, midfoot and forefoot segments. Vertical GRF was also compared between both research sites.

Variability of the gait data was determined through descriptive statistics, including the mean and standard deviation of the 3D kinematic, kinetic, moment and power parameters of the hip, knee and ankle during overground walking at both research sites. A Shapiro-Wilk test of normality was conducted to determine if the data was normally distributed. As some of parameters were not normally distributed, the non-parametric Wilcoxon signed-rank test was used, with a significance accepted at the ( $p \leq 0.05$ ) level. This was also deemed appropriate due to the small sample size used within the pilot study. All statistical analyses was conducted using SPSS version 26.0 (SPSS Inc, Chicago, USA).

### G.3 Results

One participant's data was removed after the completion of the study due to significant marker drop out during post-processing, leaving a total of 11 participants. There was no statistically significant differences between walking speed, step length and cadence of the dominant and non-dominant limbs of the participants between the two research sites (Table 52).

Table 52. Mean ( $\pm$  95% CL) spatiotemporal parameters for the participants at the two research sites.

<b>Spatiotemporal Parameters</b>	<b>CAH</b>	<b>NTU</b>	<b><i>p</i> value</b>
Walking Speed (m/s)	1.17 $\pm$ 0.14	1.19 $\pm$ 0.10	0.790
Step Length (m) - DL	0.68 $\pm$ 0.01	0.66 $\pm$ 0.02	0.168
Step Length (m) - NDL	0.67 $\pm$ 0.02	0.67 $\pm$ 0.02	0.477
Cadence (steps/min) - DL	108.52 $\pm$ 7.23	108.43 $\pm$ 7.87	0.824
Cadence (steps/min) - NDL	106.33 $\pm$ 6.51	105.34 $\pm$ 7.45	1.000

\*DL = Dominant Limb; NDL = Non-dominant Limb

The mean ( $\pm$  95% CL) hip, knee and SFM ankle kinematic waveforms for the healthy participants at both research sites are displayed in Figures 92-94. The greatest variability was found in the transverse plane of motion at both the hip and knee joints (Table 53), with greater hip external rotation at NTU and increased knee external rotation at CAH. However, these differences were marginal, with the comparable variability within the participant cohort at both research sites meaning that there was no significant differences in transverse plane motion (Table 53).

Table 53. Mean ( $\pm$  95% CL) hip, knee and single-segment ankle kinematic parameters for the participants at the two research sites.

	<b>Kinematic Parameters (°)</b>	<b>CAH</b>	<b>NTU</b>	<b><i>p</i> value</b>
<b>Hip</b>	Peak Hip Flexion	26.53 $\pm$ 3.99	29.40 $\pm$ 3.67	0.328
	Peak Hip Extension	-8.51 $\pm$ 3.47	-5.88 $\pm$ 2.99	0.424
	Sagittal Hip ROM	35.03 $\pm$ 3.16	35.29 $\pm$ 2.62	0.790
	Peak Hip Adduction	6.68 $\pm$ 2.21	6.69 $\pm$ 2.76	0.722
	Peak Hip Abduction	-6.41 $\pm$ 2.03	-6.00 $\pm$ 3.13	0.929
	Frontal Hip ROM	13.09 $\pm$ 1.97	12.69 $\pm$ 1.58	0.859
	Minimum External Rotation	-1.94 $\pm$ 4.07	-0.47 $\pm$ 5.51	0.657
	Peak Hip External Rotation	-11.27 $\pm$ 4.26	-11.46 $\pm$ 5.73	0.929
	Transverse Hip ROM	9.32 $\pm$ 1.62	10.98 $\pm$ 1.57	0.075
<b>Knee</b>	Peak Knee Flexion	65.60 $\pm$ 2.40	64.53 $\pm$ 3.45	0.594
	Peak Knee Extension	2.55 $\pm$ 2.25	1.41 $\pm$ 3.44	0.534
	Sagittal Knee ROM	63.05 $\pm$ 2.35	63.12 $\pm$ 2.33	0.859
	Peak Knee Adduction	7.13 $\pm$ 2.15	6.41 $\pm$ 4.30	0.534
	Peak Knee Abduction	-1.95 $\pm$ 1.52	-3.70 $\pm$ 2.37	0.182
	Frontal Knee ROM	9.07 $\pm$ 1.48	10.11 $\pm$ 2.77	0.657
	Peak Knee Internal Rotation	1.50 $\pm$ 2.76	1.35 $\pm$ 3.73	0.929
	Peak Knee External Rotation	-15.77 $\pm$ 3.84	-12.50 $\pm$ 4.10	0.182
	Transverse Knee ROM	17.27 $\pm$ 2.96	13.85 $\pm$ 2.70	0.053
<b>Ankle</b>	Peak Ankle Dorsiflexion	17.89 $\pm$ 1.64	16.86 $\pm$ 1.63	0.241
	Peak Ankle Plantarflexion	-8.23 $\pm$ 2.73	-9.58 $\pm$ 2.76	0.594
	Sagittal Ankle ROM	26.12 $\pm$ 3.49	26.44 $\pm$ 3.16	1.000
	Peak Ankle Eversion	2.92 $\pm$ 1.38	2.60 $\pm$ 0.85	0.374
	Peak Ankle Inversion	-11.06 $\pm$ 1.90	-11.50 $\pm$ 1.93	0.859
	Frontal Ankle ROM	13.97 $\pm$ 1.99	14.10 $\pm$ 2.18	0.534
	Peak Adduction	2.96 $\pm$ 3.19	2.89 $\pm$ 3.11	0.657
	Peak Abduction	-11.23 $\pm$ 3.78	-11.56 $\pm$ 3.78	0.790
	Transverse Ankle ROM	14.19 $\pm$ 2.25	14.45 $\pm$ 2.74	1.000

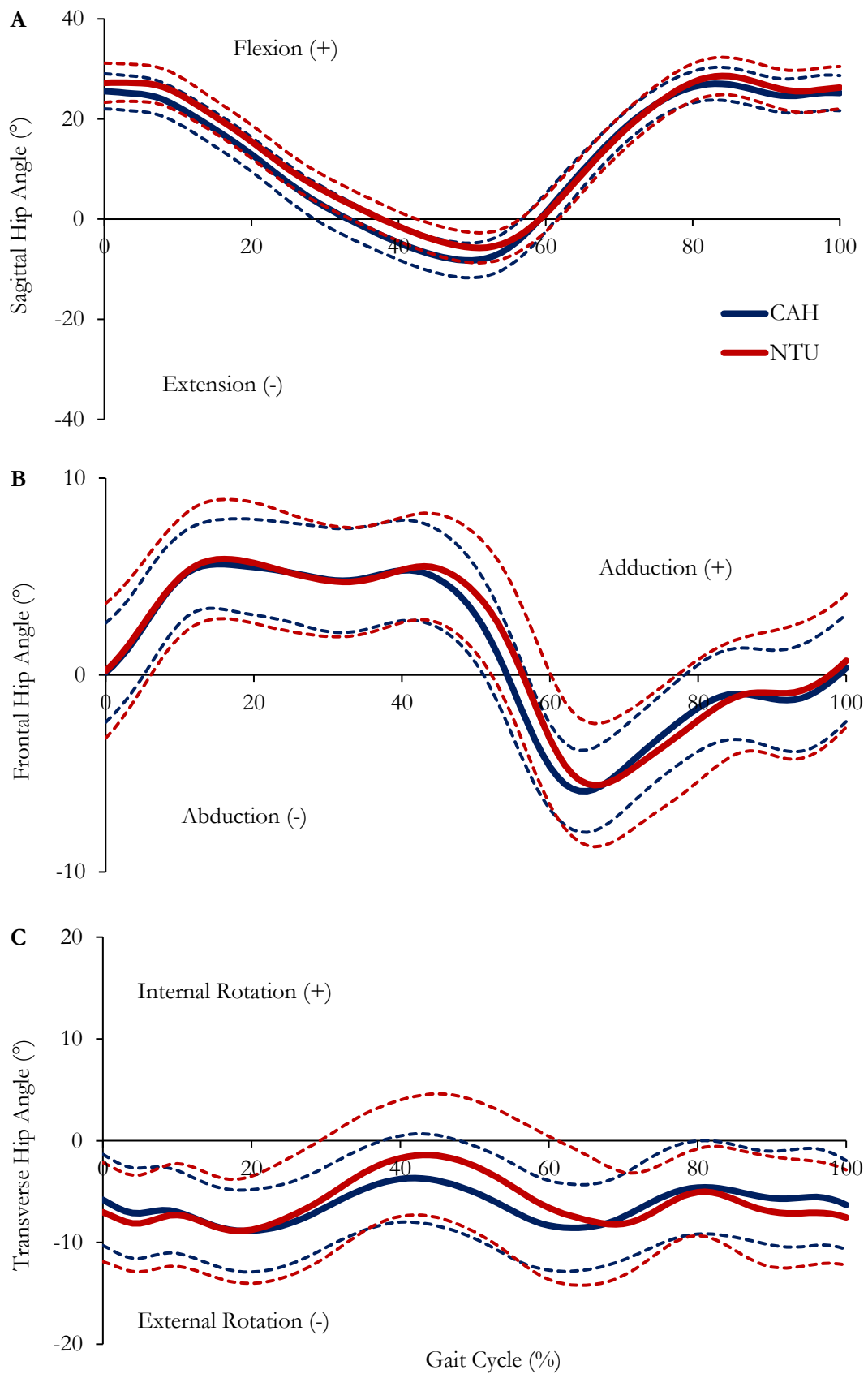


Figure 92. Mean ( $\pm$  95% CL) hip flexion (+)/extension (-) (A), adduction (+)/abduction (-) (B) and internal (+)/external (-) rotation (C) kinematic waveforms during the gait cycle, of the participants at the Chapel Allerton Hospital (CAH; blue) and Nottingham Trent University (NTU; red) research sites

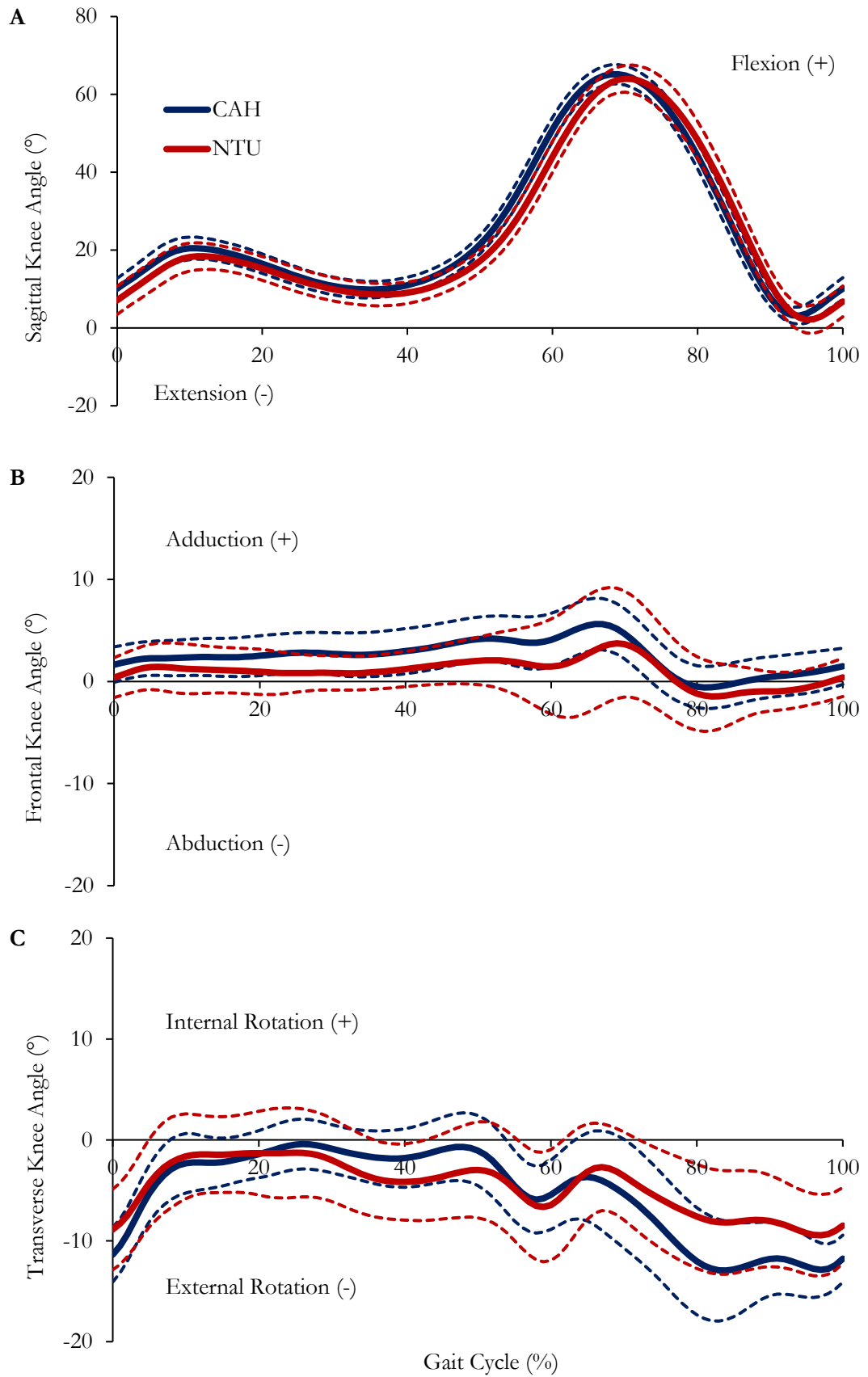


Figure 93. Mean ( $\pm$  95% CL) knee flexion (+)/extension (-) (A), adduction (+)/abduction (-) (B) and internal (+)/external (-) rotation (C) kinematic waveforms during the gait cycle, of the participants at the Chapel Allerton Hospital (CAH; blue) and Nottingham Trent University (NTU; red) research sites.

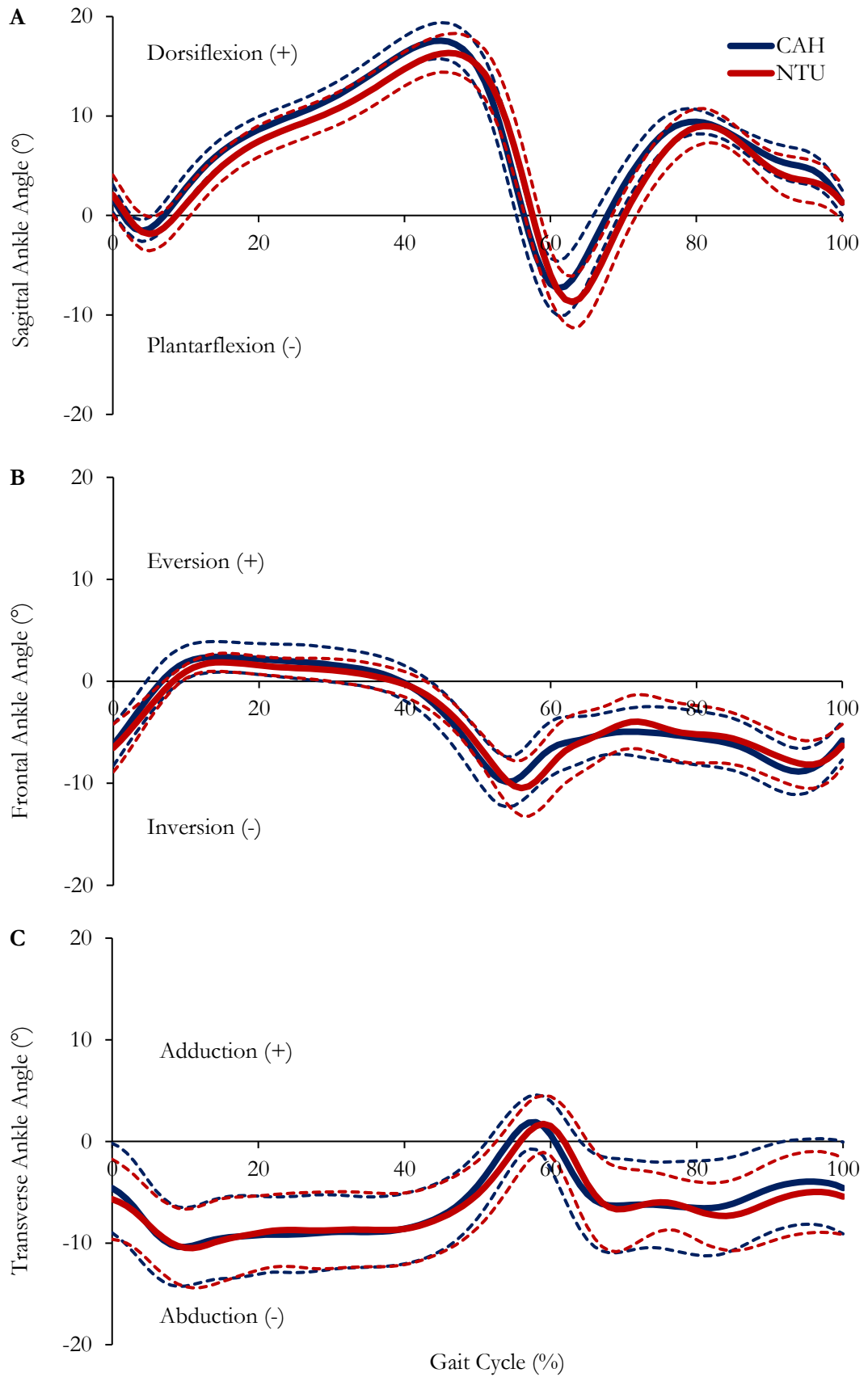


Figure 94. Mean ( $\pm$  95% CL) single-segment ankle dorsiflexion (+)/plantarflexion (-) (A), eversion (+)/inversion (-) (B) and adduction (+)/abduction (-) (C) kinematic waveforms during the gait cycle, of the participants at the Chapel Allerton Hospital (CAH; blue) and Nottingham Trent University (NTU; red) research sites.

There was also no significant differences identified for mean peak or ROM parameters in the sagittal and frontal planes of motion at the proximally located joints (Table 53). SFM ankle kinematics were comparable between the two research sites throughout the gait cycle (Figure 94) and no significant differences were found in all three planes of motion for mean peak and ROM parameters (Table 53).

The mean ( $\pm$  95% CL) kinematic waveforms for hindfoot, midfoot, forefoot and forefoot-to-hindfoot segments of the participants at both research sites are presented in Figures 95-98. Each of the MFM segments were comparable throughout the gait cycle and resulted in no significant differences in the mean peak and ROM parameters between research sites (Table 54).

Table 54. Mean ( $\pm$  95% CL) multi-segment foot segment kinematic parameters for the participants at the two research sites.

	<b>Kinematic Parameters (°)</b>	<b>CAH</b>	<b>NTU</b>	<b><i>p</i> value</b>
<b>Hindfoot</b>	Peak Dorsiflexion	7.57 $\pm$ 2.83	10.48 $\pm$ 3.98	0.790
	Peak Plantarflexion	-12.00 $\pm$ 3.56	-9.69 $\pm$ 2.64	0.155
	Sagittal Hindfoot ROM	19.57 $\pm$ 2.62	20.17 $\pm$ 2.64	1.000
	Minimum Inversion	-1.96 $\pm$ 4.47	0.56 $\pm$ 5.13	0.594
	Peak Inversion	-12.02 $\pm$ 4.49	-10.71 $\pm$ 5.39	0.722
	Frontal Hindfoot ROM	10.06 $\pm$ 1.17	11.27 $\pm$ 2.36	0.328
	Peak Adduction	8.92 $\pm$ 3.38	7.35 $\pm$ 3.78	0.374
	Peak Abduction	-1.38 $\pm$ 3.91	-3.97 $\pm$ 4.82	0.424
	Transverse Hindfoot ROM	10.30 $\pm$ 1.43	11.32 $\pm$ 2.25	0.424
<b>Midfoot</b>	Peak Dorsiflexion	43.46 $\pm$ 4.19	42.29 $\pm$ 4.63	1.000
	Minimum Dorsiflexion	32.00 $\pm$ 4.07	29.20 $\pm$ 5.07	0.424
	Sagittal Midfoot ROM	11.46 $\pm$ 1.27	13.09 $\pm$ 2.60	0.445
	Minimum Inversion	-7.90 $\pm$ 4.20	-10.42 $\pm$ 5.03	0.534
	Peak Inversion	-15.59 $\pm$ 4.74	-19.11 $\pm$ 5.40	0.594
	Frontal Midfoot ROM	7.68 $\pm$ 1.13	8.69 $\pm$ 1.69	0.230
	Peak Adduction	5.58 $\pm$ 3.19	2.67 $\pm$ 6.34	0.374
	Peak Abduction	2.00 $\pm$ 3.35	-2.74 $\pm$ 6.95	0.131
	Transverse Midfoot ROM	3.58 $\pm$ 0.96	5.41 $\pm$ 2.25	0.131
<b>Forefoot</b>	Minimum Plantarflexion	-63.02 $\pm$ 3.87	-63.60 $\pm$ 3.80	0.894
	Peak Plantarflexion	-71.53 $\pm$ 5.00	-73.45 $\pm$ 4.45	0.534
	Sagittal Forefoot ROM	8.51 $\pm$ 1.89	9.85 $\pm$ 1.71	0.131
	Minimum Inversion	-7.12 $\pm$ 3.34	-8.01 $\pm$ 6.12	0.722
	Peak Inversion	-12.67 $\pm$ 3.28	-14.12 $\pm$ 5.75	0.594
	Frontal Forefoot ROM	5.55 $\pm$ 0.84	6.11 $\pm$ 0.91	0.328
	Peak Adduction	10.42 $\pm$ 5.47	17.61 $\pm$ 7.89	0.155
	Minimum Adduction	6.93 $\pm$ 5.58	13.49 $\pm$ 7.43	0.155
	Transverse Forefoot ROM	3.49 $\pm$ 0.91	4.12 $\pm$ 0.93	0.213
<b>Forefoot-to-Hindfoot</b>	Minimum Plantarflexion	-22.81 $\pm$ 4.07	-27.44 $\pm$ 3.70	0.110
	Peak Plantarflexion	-42.09 $\pm$ 4.27	-45.82 $\pm$ 3.18	0.131
	Sagittal Forefoot-to-Hindfoot ROM	19.28 $\pm$ 2.41	18.38 $\pm$ 1.97	0.534
	Minimum Inversion	-13.54 $\pm$ 2.30	-11.77 $\pm$ 3.47	0.248
	Peak Inversion	-21.82 $\pm$ 3.46	-20.49 $\pm$ 4.32	0.534
	Frontal Forefoot-to-Hindfoot ROM	8.28 $\pm$ 1.45	8.72 $\pm$ 1.39	0.929
	Peak External Rotation	3.36 $\pm$ 6.05	2.13 $\pm$ 4.76	0.286
	Peak Internal Rotation	-6.62 $\pm$ 6.13	2.19 $\pm$ 4.88	0.477
Transverse Forefoot-to-Hindfoot ROM	9.98 $\pm$ 1.22	10.02 $\pm$ 1.62	0.790	

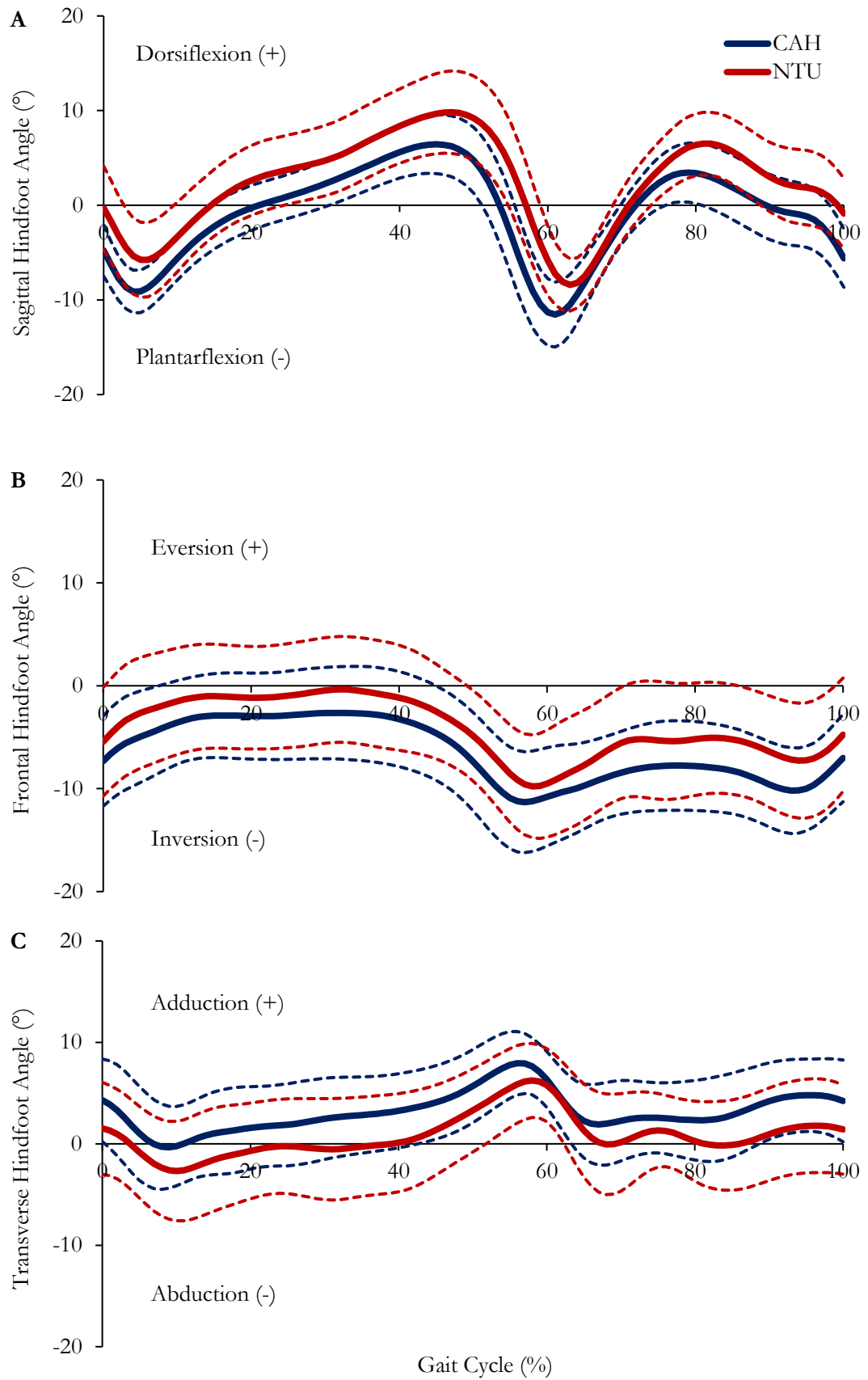


Figure 95. Mean ( $\pm$  95% CL) hindfoot segment dorsiflexion (+)/plantarflexion (-) (A), eversion (+)/inversion (-) (B) and adduction (+)/abduction (-) (C) kinematic waveforms during the gait cycle, of the participants at the Chapel Allerton Hospital (CAH; blue) and Nottingham Trent University (NTU; red) research sites.

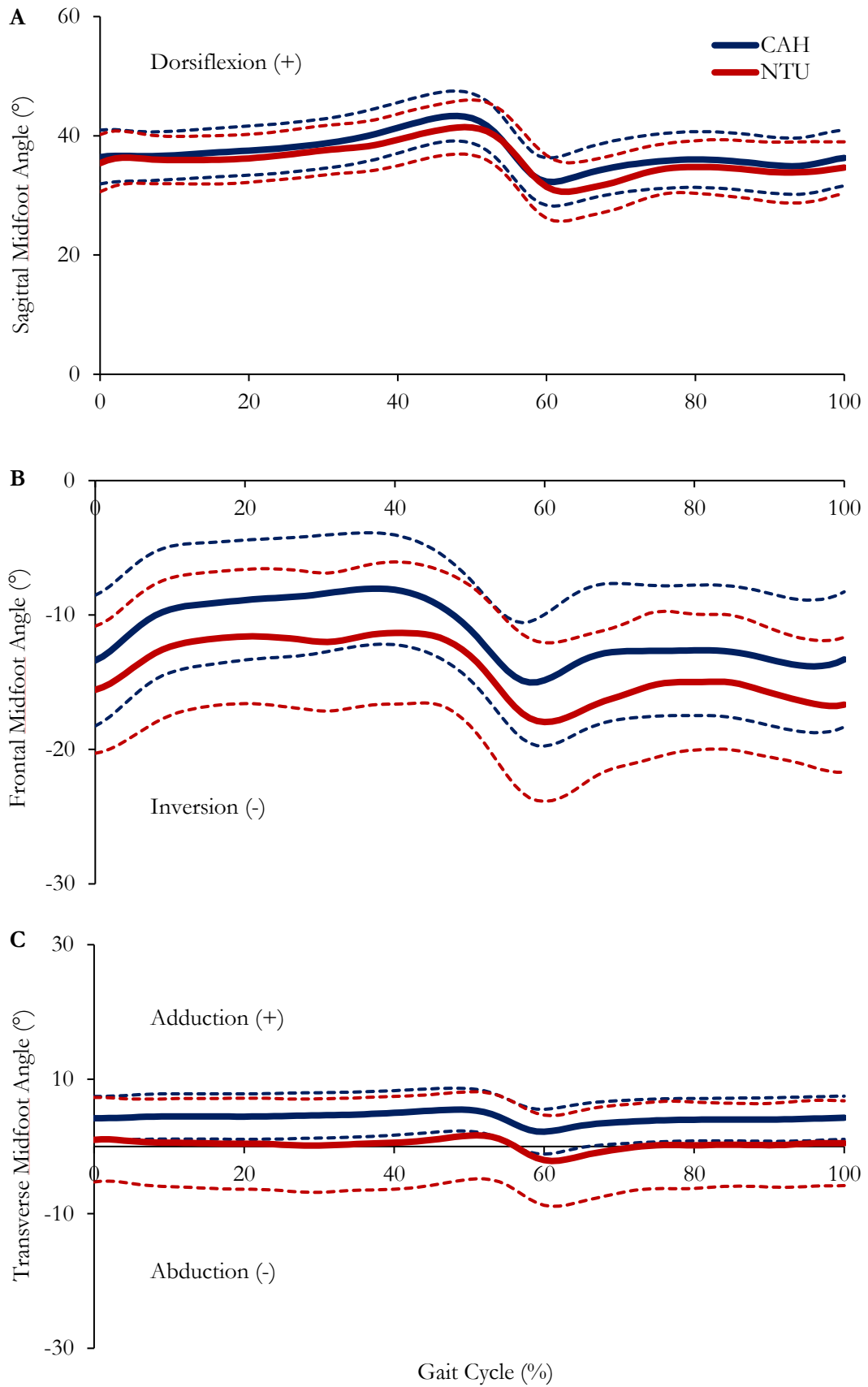


Figure 96. Mean ( $\pm$  95% CL) midfoot segment dorsiflexion (+) (A), inversion (-) (B) and adduction (+)/abduction (-) (C) kinematic waveforms during the gait cycle, of the participants at the Chapel Allerton Hospital (CAH; blue) and Nottingham Trent University (NTU; red) research sites.

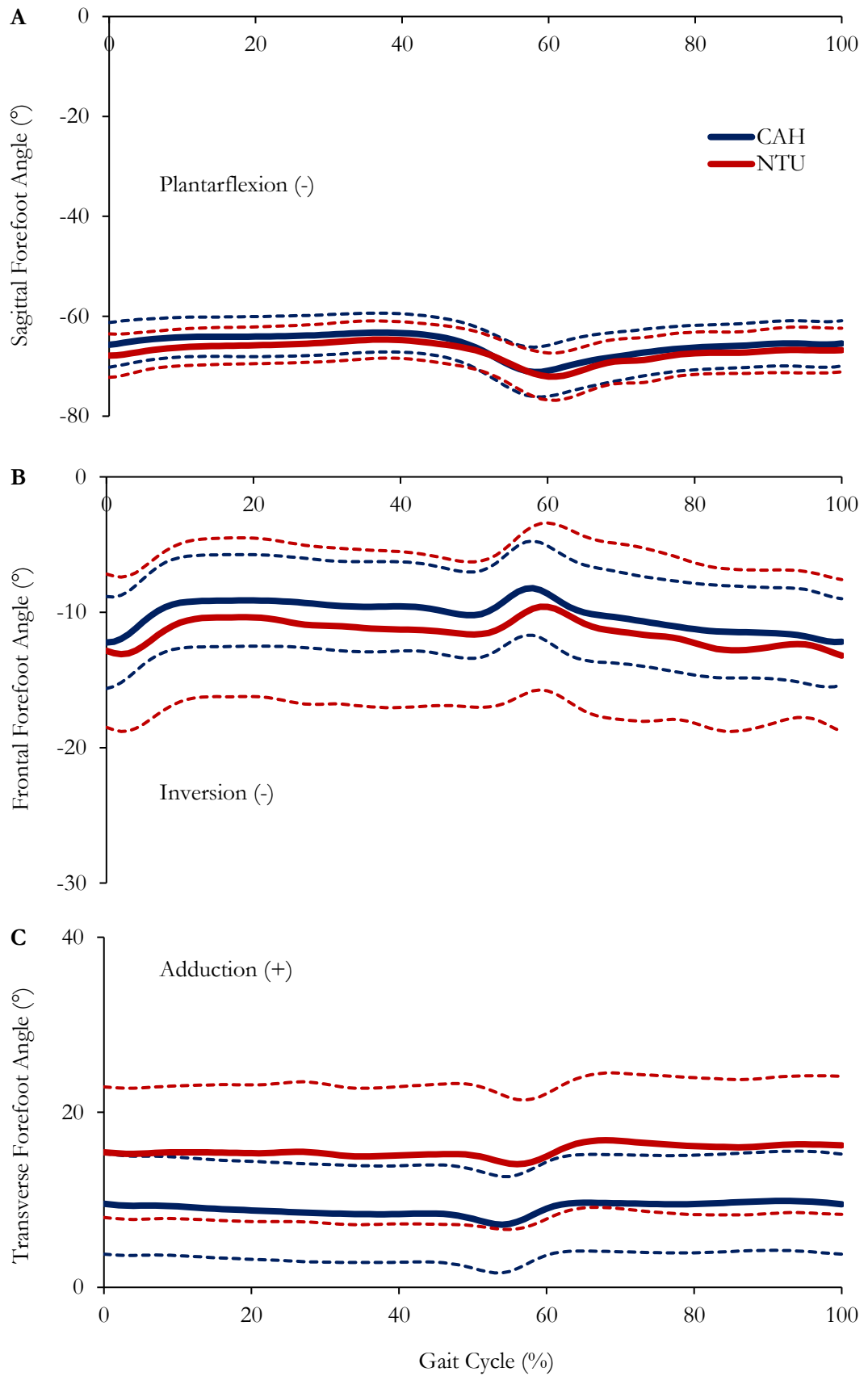


Figure 97. Mean ( $\pm$  95% CL) forefoot segment plantarflexion (-) (A), inversion (-) (B) and adduction (+) (C) kinematic waveforms during the gait cycle, of the participants at Chapel Allerton Hospital (CAH; blue) and Nottingham Trent University (NTU; red) research sites.

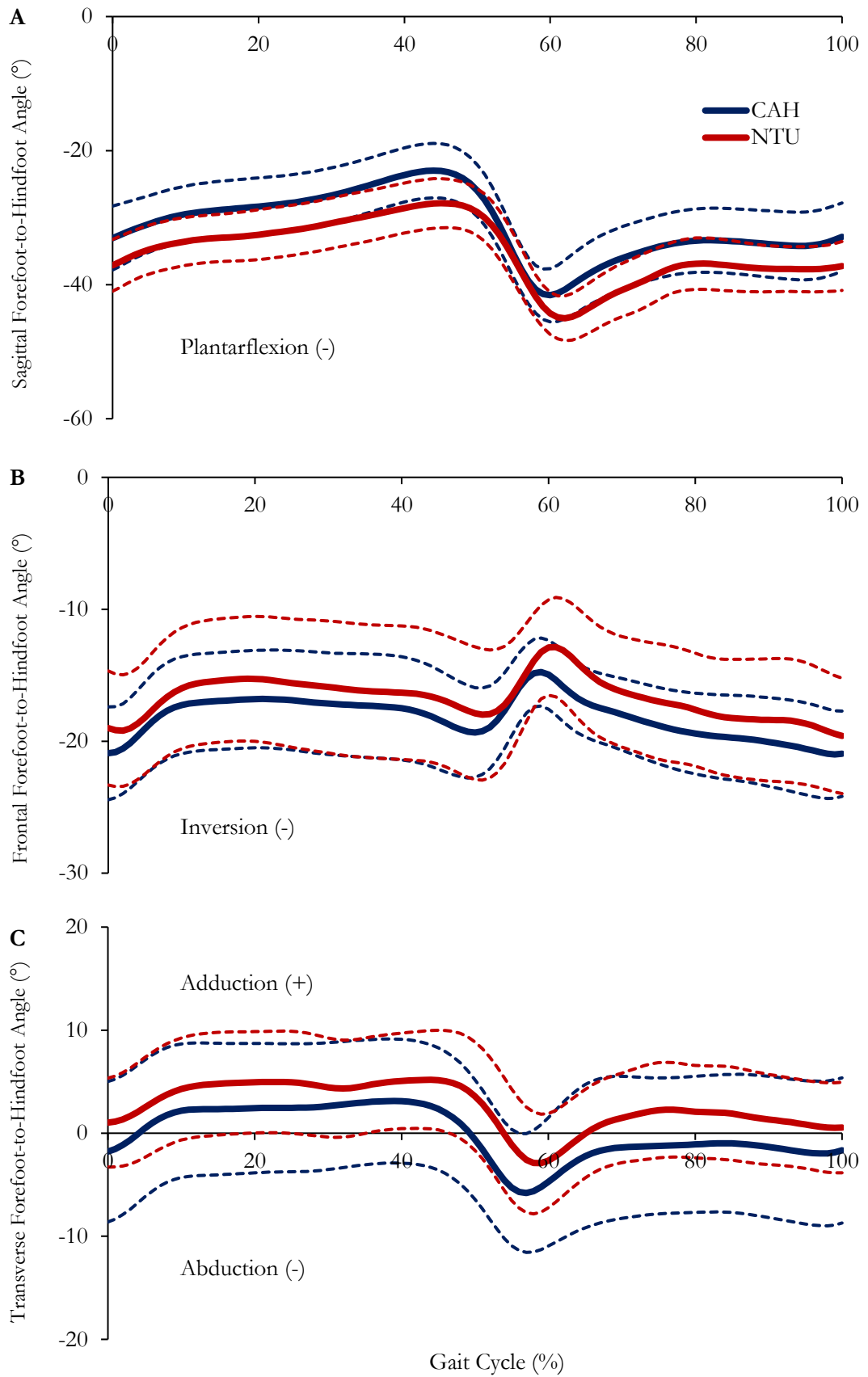


Figure 98. Mean ( $\pm$  95% CL) forefoot-to-hindfoot segment plantarflexion (-) (A), inversion (-) (B) and adduction (+)/abduction (-) (C) kinematic waveforms during the gait cycle, of the participants at Chapel Allerton Hospital (CAH; blue) and Nottingham Trent University (NTU; red) research sites.

The variability ( $\pm$  95% CL) within the participant group at both research sites were relatively comparable throughout the kinematic waveforms for each foot segment, which confirmed the non-significant findings in kinematics at the varying foot segments (Table 54). The hindfoot ROM was approximately 6-7° lower than the measured motion using the SFM, which suggested that the SFM overestimated the ROM at the ankle joint.

The vertical GRF waveform was comparable throughout the stance phase between research sites (Figure 99). The mean peak values ( $GRF1_{max}$  and  $GRF2_{max}$ ) were not significantly different within the healthy participants between the two research sites (Table 55). Peak joint moments of the hip, knee and ankle are presented in Figures 100-102. Whilst attending CAH, patients tended to produce a slightly greater hip internal flexion and abduction moments throughout the stance phase (Figure 100). However, no significant differences were found between peak internal moments in the sagittal and frontal planes of motion at the hip joint (Table 56). A similar trend was also found at the knee and ankle joints, with no significant differences in peak moments (Table 56). The generated sagittal plane power for the hip, knee and ankle during the stance phase is displayed in Figure 103. The participants tended to generate more power in each of the joints around late stance at the CAH motion laboratory (Figure 103). However, there was no significant differences in peak generated power values at each of the lower limb joints (Table 57).

Table 55. Mean ( $\pm$  95% CL) vertical ground reaction force parameters for the participants at the two research sites.

Vertical GRF (BW)	CAH	NTU	<i>p</i> value
$GRF1_{max}$	1.15 $\pm$ 0.05	1.10 $\pm$ 0.04	0.197
$GRF2_{max}$	1.15 $\pm$ 0.03	1.13 $\pm$ 0.02	0.357

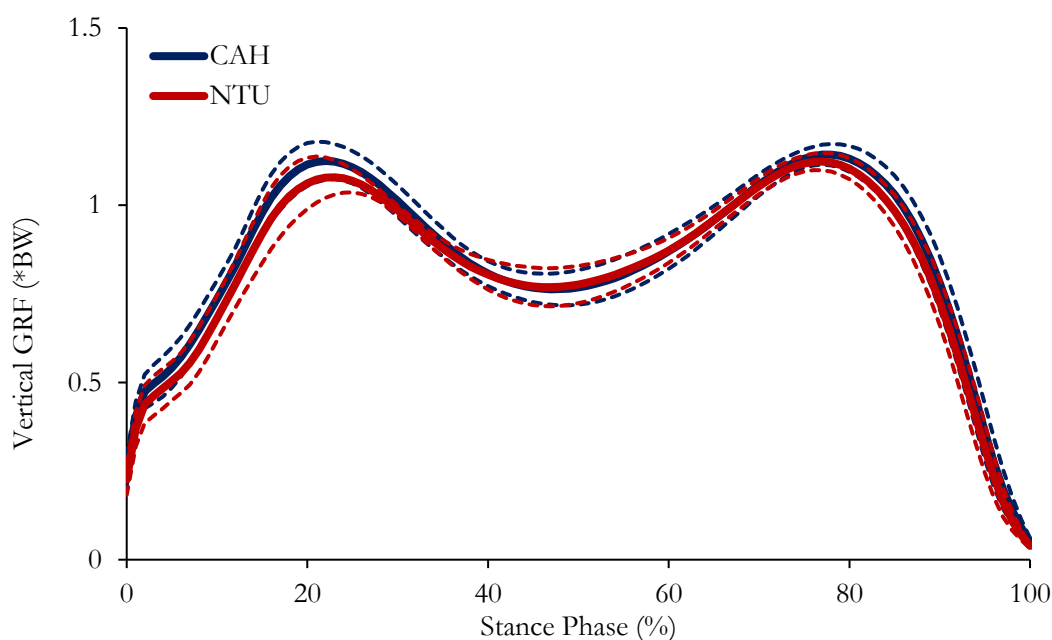


Figure 99. Mean ( $\pm$  95% CL) vertical GRF during the stance phase, of the participants at Chapel Allerton Hospital (CAH; blue) and Nottingham Trent University (NTU; red) research sites.

Table 56. Mean ( $\pm$  95% CL) joint moment parameters for the participants at the two research sites.

Peak Joint Moments (Nm/kg)	CAH	NTU	<i>p</i> value
Hip Flexion	-1.16 $\pm$ 0.18	-0.87 $\pm$ 0.15	0.068
Hip Abduction	1.02 $\pm$ 0.08	0.93 $\pm$ 0.07	0.100
Knee Extension	1.00 $\pm$ 0.15	0.82 $\pm$ 0.14	0.110
Knee Adduction	-0.35 $\pm$ 0.07	-0.37 $\pm$ 0.07	0.894
Ankle Plantarflexion	1.51 $\pm$ 0.07	1.53 $\pm$ 0.07	0.575
Ankle Inversion	0.16 $\pm$ 0.06	0.18 $\pm$ 0.07	0.504

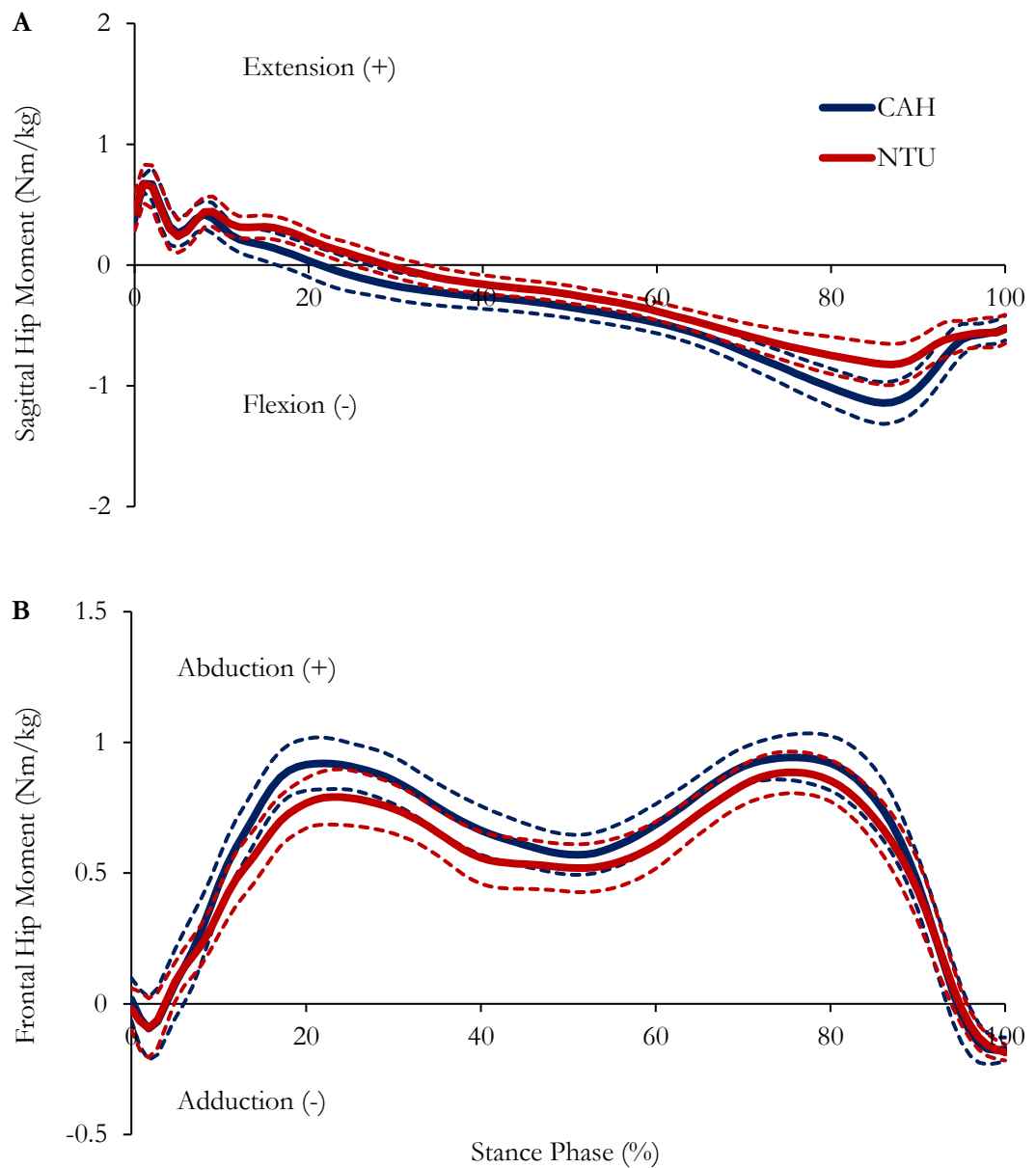


Figure 100. Mean ( $\pm$  95% CL) sagittal (A) and frontal (B) hip internal moments during the stance phase, of the participants at Chapel Allerton Hospital (CAH; blue) and Nottingham Trent University (NTU; red) research sites.

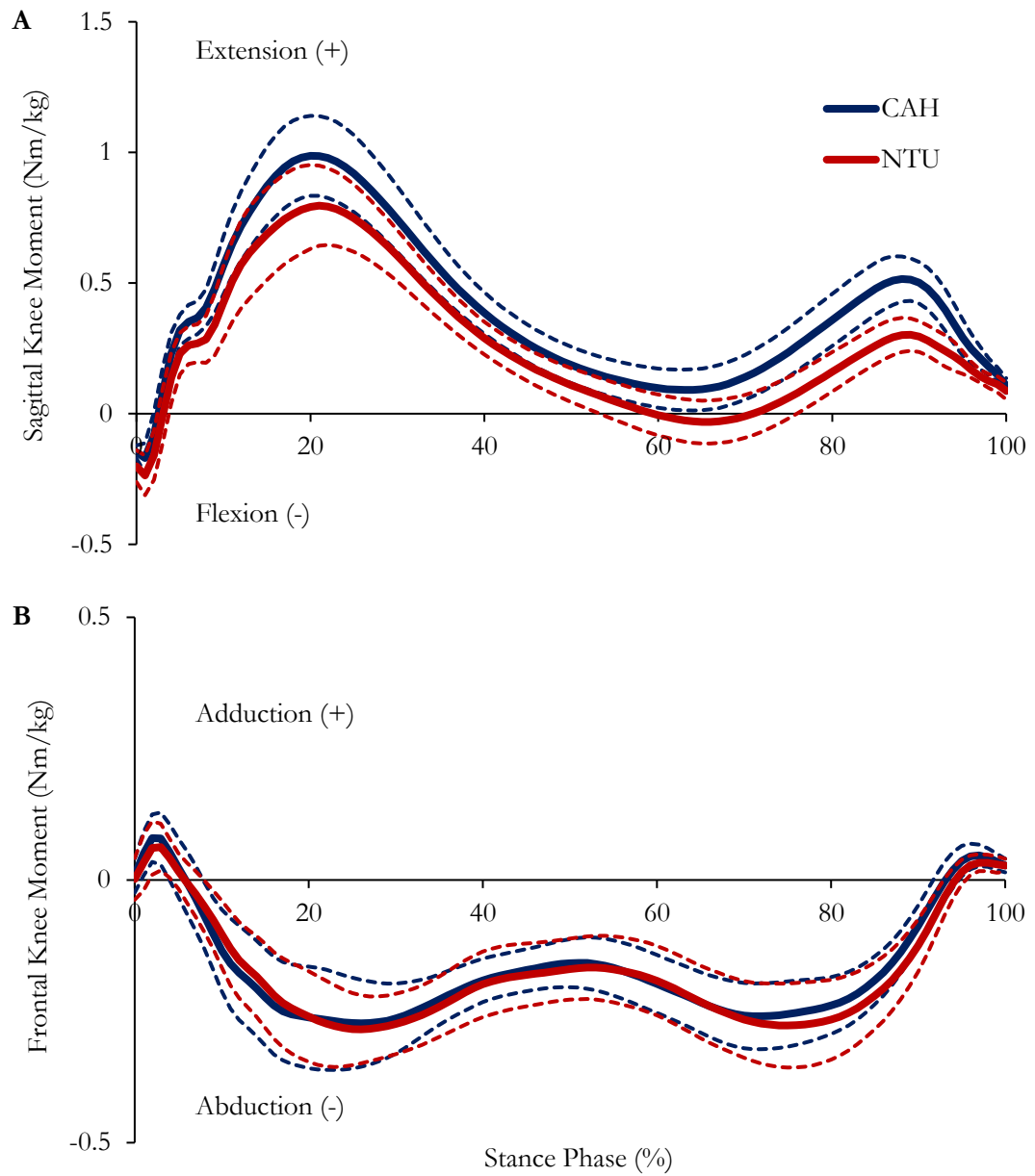


Figure 101. Mean ( $\pm$  95% CL) sagittal (A) and frontal (B) knee internal moments during the stance phase, of the participants at Chapel Allerton Hospital (CAH; blue) and Nottingham Trent University (NTU; red) research sites.

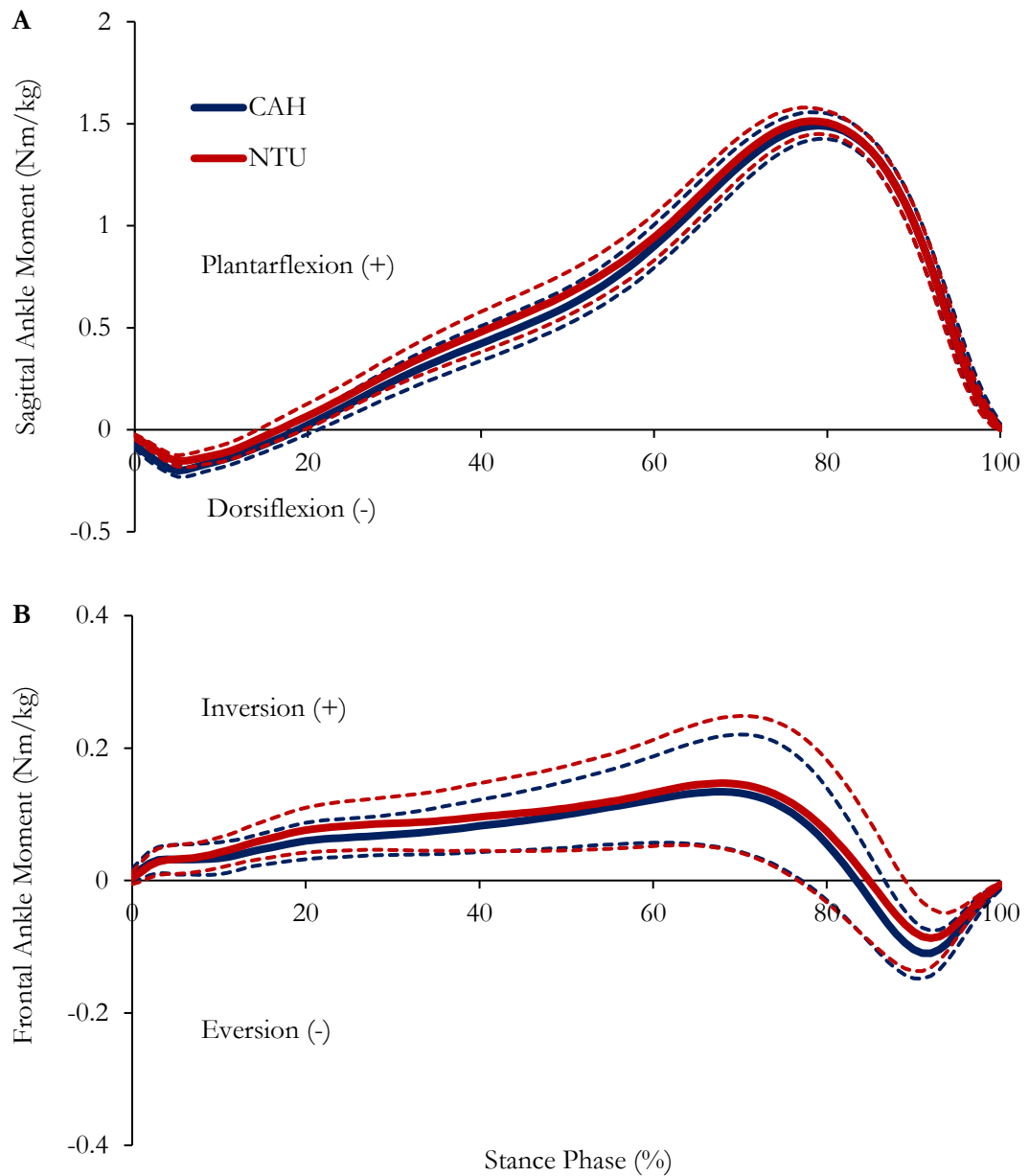


Figure 102. Mean ( $\pm$  95% CL) sagittal (A) and frontal (B) ankle internal moments during the stance phase, of the participants at Chapel Allerton Hospital (CAH; blue) and Nottingham Trent University (NTU; red) research sites.

Table 57. Mean ( $\pm$  95% CL) joint power parameters for the participants at the two research sites.

Peak Generated Power (W/kg)	CAH	NTU	<i>p</i> value
Hip	1.48 $\pm$ 0.36	1.27 $\pm$ 0.27	0.533
Knee	0.78 $\pm$ 0.21	0.77 $\pm$ 0.22	0.790
Ankle	3.56 $\pm$ 0.39	3.13 $\pm$ 0.34	0.155

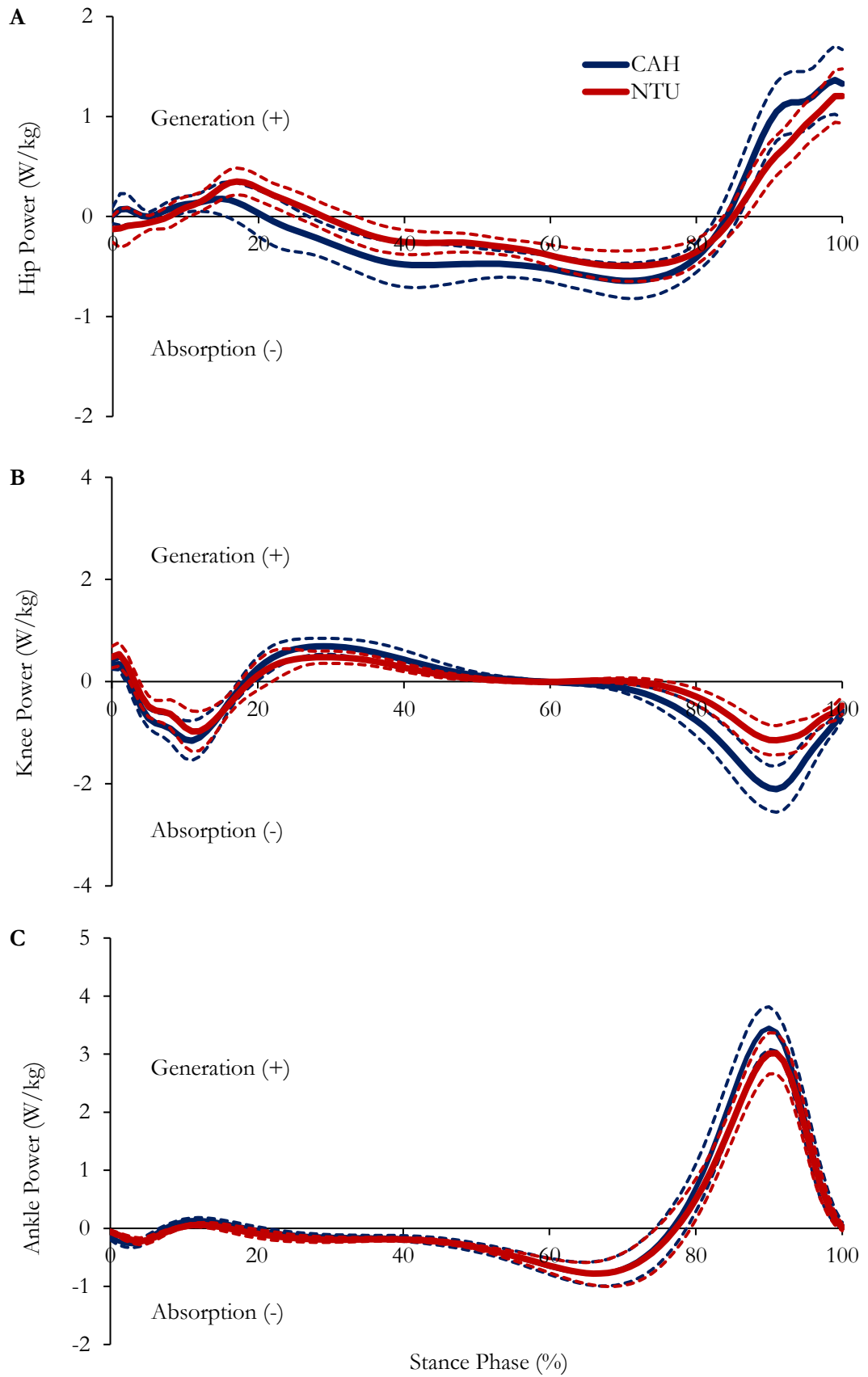


Figure 103. Mean ( $\pm$  95% CL) sagittal hip (A), knee (B) and ankle (C) joint power during the stance phase, of the participants at Chapel Allerton Hospital (CAH; blue) and Nottingham Trent University (NTU; red) research sites.

## **G.4 Discussion and Conclusion**

The pilot study aimed to evaluate the inter-laboratory reproducibility of spatiotemporal, kinetic and kinematic data obtained from healthy participants. There were no statistically significant differences found between the two research sites for any of the measured gait parameters. Therefore, the study demonstrated that it is possible to obtain high quality, reliable data across two different research sites, even when using different motion capture hardware configurations, calibration equipment and instrumentation from different manufacturers. This finding was supported by a previous study, which compared the gait variability across three laboratories (Kaufman et al., 2016).

The kinematic parameters evaluated in the transverse plane of motion differed more between the two research sites, when compared to the sagittal and frontal planes. This is also in accordance with earlier studies, which focused on assessing gait variability between different motion capture laboratories (Gorton et al., 2009; Scalona et al., 2019). However, this difference was not statistically significant for peak or ROM parameters in the transverse plane between the research sites. It should be noted that the transverse plane of motion is associated with the smallest ROM and greatest variability in all three joints of the lower limb (Røislien et al., 2012). The ankle joint was also found to be more comparable than those of the hip and knee between research sites, which is likely due to the smaller joint ROM (Røislien et al., 2012).

Marker misplacement between the two research sites, particularly at the hip and knee joints, may have led to the small differences in peak sagittal moments and peak generated power. Misplacement of markers has previously been shown to cause a misalignment of the FE axis with the anatomical one, generating cross-talk between motion in the sagittal plane and the other planes of motion (Ferrari et al., 2008). It has also been shown that the reproducibility of hip and knee moments was lower than at the ankle joint (Scalona et al., 2019), which could be related to the inherent uncertainties in the estimation of lower limb joint centres (Kadaba et al., 1989). The authors suggested that the propagation of uncertainties along the biomechanical chain of the lower limb may have caused cumulative effects in determining the moments moving from the ankle to the proximally located joints (Scalona et al., 2019).

The non-significant differences in gait mechanics between the two research sites was likely a result of using the identical anatomical segment definitions for the biomechanical model, alongside the standardised protocol, experimental conditions and same examiner who placed the markers on each participant. The results from this study strongly support the importance of standardising these factors, to ensure the most reliable data can be collected across motion capture laboratories. Most importantly, the repeatable data collected, demonstrated that it is possible to compare between the AA and TAR patient cohorts within the post-operative exploratory gait study between the two research sites.

## **APPENDIX H**

### **VISUAL 3D PIPELINE COMMANDS**

## APPENDIX H: VISUAL 3D PIPELINE COMMANDS

### (Example of an operated right foot model)

#### File Open

```
File_Open
!/FILE_NAME=
!/SUFFIX=
/SET_PROMPT=Open all walking files
!/FILTER=
```

#### Interpolate

```
Interpolate
/SIGNAL_TYPES= TARGET
/SIGNAL_FOLDER=ORIGINAL
!/SIGNAL_NAMES=
!/RESULT_FOLDER=PROCESSED
!/RESULT_SUFFIX=
!/MAXIMUM_GAP=10
!/NUM_FIT=3
!/POLYNOMIAL_ORDER=3
```

#### Kinematic Low-pass Filter

```
Lowpass_Filter
/SIGNAL_TYPES=TARGET
!/SIGNAL_FOLDER=ORIGINAL
!/SIGNAL_NAMES=
!/RESULT_FOLDER=PROCESSED
!/RESULT_SUFFIX=
!/FILTER_CLASS=BUTTERWORTH
!/FREQUENCY_CUTOFF=6.0
!/NUM_REFLECTED=6
!/NUM_EXTRAPOLATED=0
!/TOTAL_BUFFER_SIZE=6
!/NUM_BIDIRECTIONAL_PASSES=1
```

#### Kinetic Low-pass Filter

```
Lowpass_Filter
/SIGNAL_TYPES=ANALOG+FORCE+COFF
/SIGNAL_FOLDER=ORIGINAL+ORIGINAL+ORIGINAL
!/SIGNAL_NAMES=
!/RESULT_FOLDER=PROCESSED
!/RESULT_SUFFIX=
!/FILTER_CLASS=BUTTERWORTH
/FREQUENCY_CUTOFF=25.0
!/NUM_REFLECTED=6
!/NUM_EXTRAPOLATED=0
!/TOTAL_BUFFER_SIZE=6
!/NUM_BIDIRECTIONAL_PASSES=1
```

#### Assign Tags to Files

```
Assign_Tags_To_Files
!/MOTION_FILE_NAMES=
!/QUERY=
/TAGS= Walk
```

#### Create Hybrid Model

```
Create_Hybrid_Model
!/CALIBRATION_FILE=
!/SUFFIX=
!/RANGE=ALL_FRAMES
!/SET_PROMPT=Open standing file
```

#### Model Template

```
Apply_Model_Template
!/CALIBRATION_FILE=
```

```
!/MODEL_TEMPLATE=
!/SET_PROMPT=Open model file
!/VIEW_BUILDMODEL_RESULTS=2
```

#### Set Participant Height

```
Set_Participant_Height
!/CALIBRATION_FILE
!/PROMPT=
!/PROMPT_SIZE=90
/HEIGHT= XXX
!/UNITS=m
```

#### Set Participant Mass

```
Set_Participant_Mass
!/CALIBRATION_FILE=
!/PROMPT=
!/PROMPT_SIZE=90
/WEIGHT= XXX
/UNITS=kg
```

#### Build Model

```
Build_Model
/CALIBRATION_FILE= ::STATIC
!/REBUILD_ALL_MODELS=FALSE
!/DISPLAY_RESULTS=TRUE
```

#### Assign Model File

```
Assign_Model_File
!/CALIBRATION_FILE=
!/MOTION_FILE_NAMES=
!/REMOVE_EXISTING_ASSIGNMENTS=FALSE
```

#### Select Active File

```
Select_Active_File
/FILE_NAME= WALK
!/QUERY=
```

#### Automatic Gait Events

```
Automatic_Gait_Events
!/FRAME_WINDOW=8
!/USE_TPR=TRUE
```

#### Right Pelvis Angle

```
Compute_Model_Based_Data
/RESULT_NAME=R_Pelvis
/FUNCTION=JOINT_ANGLE
/SEGMENT=RPV
/REFERENCE_SEGMENT=Virtual Lab
/RESOLUTION_COORDINATE_SYSTEM=
!/USE_CARDAN_SEQUENCE=FALSE
!/NORMALIZATION=FALSE
!/NORMALIZATION_METHOD=
!/NORMALIZATION_METRIC=
!/NEGATEX=FALSE
/NEGATEY=TRUE
!/NEGATEZ=FALSE
!/AXIS1=X
!/AXIS2=Y
!/AXIS3=Z
!/TREADMILL_DATA=FALSE
!/TREADMILL_DIRECTION=UNIT_VECTOR(0,1,0)
!/TREADMILL_SPEED=0.0
```

### Left Pelvis Angle

```
Compute_Model_Based_Data
/RESULT_NAME=L_Pelvis
/FUNCTION=JOINT_ANGLE
/SEGMENT=RPV
/REFERENCE_SEGMENT=Virtual Lab
/RESOLUTION_COORDINATE_SYSTEM=
!/USE_CARDAN_SEQUENCE=FALSE
!/NORMALIZATION=FALSE
!/NORMALIZATION_METHOD=
!/NORMALIZATION_METRIC=
!/NEGATEX=FALSE
!/NEGATEY=FALSE
/NEGATEZ=TRUE
!/AXIS1=X
!/AXIS2=Y
!/AXIS3=Z
!/TREADMILL_DATA=FALSE
!/TREADMILL_DIRECTION=UNIT_VECTOR(0,1,0)
!/TREADMILL_SPEED=0.0
```

### Right Hip Angle

```
Compute_Model_Based_Data
/RESULT_NAME=RHip_Angle
/FUNCTION=JOINT_ANGLE
/SEGMENT=RTH
/REFERENCE_SEGMENT=RPV
/RESOLUTION_COORDINATE_SYSTEM=
!/USE_CARDAN_SEQUENCE=FALSE
!/NORMALIZATION=FALSE
!/NORMALIZATION_METHOD=
!/NORMALIZATION_METRIC=
!/NEGATEX=FALSE
!/NEGATEY=FALSE
!/NEGATEZ=FALSE
!/AXIS1=X
!/AXIS2=Y
!/AXIS3=Z
!/TREADMILL_DATA=FALSE
!/TREADMILL_DIRECTION=UNIT_VECTOR(0,1,0)
!/TREADMILL_SPEED=0.0
```

### Left Hip Angle

```
Compute_Model_Based_Data
/RESULT_NAME=LHip_Angle
/FUNCTION=JOINT_ANGLE
/SEGMENT=LTH
/REFERENCE_SEGMENT=RPV
/RESOLUTION_COORDINATE_SYSTEM=
!/USE_CARDAN_SEQUENCE=FALSE
!/NORMALIZATION=FALSE
!/NORMALIZATION_METHOD=
!/NORMALIZATION_METRIC=
!/NEGATEX=FALSE
/NEGATEY=TRUE
/NEGATEZ=TRUE
!/AXIS1=X
!/AXIS2=Y
!/AXIS3=Z
!/TREADMILL_DATA=FALSE
!/TREADMILL_DIRECTION=UNIT_VECTOR(0,1,0)
!/TREADMILL_SPEED=0.0
```

### Right Knee Angle

```
Compute_Model_Based_Data
/RESULT_NAME=RKnee_Angle
/FUNCTION=JOINT_ANGLE
/SEGMENT=RS
/REFERENCE_SEGMENT=H
/RESOLUTION_COORDINATE_SYSTEM=
!/USE_CARDAN_SEQUENCE=FALSE
!/NORMALIZATION=FALSE
!/NORMALIZATION_METHOD=
!/NORMALIZATION_METRIC=
/NEGATEX=TRUE
/NEGATEY=TRUE
!/NEGATEZ=FALSE
!/AXIS1=X
!/AXIS2=Y
!/AXIS3=Z
!/TREADMILL_DATA=FALSE
!/TREADMILL_DIRECTION=UNIT_VECTOR(0,1,0)
!/TREADMILL_SPEED=0.0
```

### Left Knee Angle

```
Compute_Model_Based_Data
/RESULT_NAME=LKnee_Angle
/FUNCTION=JOINT_ANGLE
/SEGMENT=LSK
/REFERENCE_SEGMENT=LTH
/RESOLUTION_COORDINATE_SYSTEM=
!/USE_CARDAN_SEQUENCE=FALSE
!/NORMALIZATION=FALSE
!/NORMALIZATION_METHOD=
!/NORMALIZATION_METRIC=
/NEGATEX=TRUE
!/NEGATEY=FALSE
/NEGATEZ=TRUE
!/AXIS1=X
!/AXIS2=Y
!/AXIS3=Z
!/TREADMILL_DATA=FALSE
!/TREADMILL_DIRECTION=UNIT_VECTOR(0,1,0)
!/TREADMILL_SPEED=0.0
```

### Right Ankle Angle (single-segment)

```
Compute_Model_Based_Data
/RESULT_NAME=RAnkle_Angle
/FUNCTION=JOINT_ANGLE
/SEGMENT=RMF
/REFERENCE_SEGMENT=RSK
/RESOLUTION_COORDINATE_SYSTEM=
!/USE_CARDAN_SEQUENCE=FALSE
!/NORMALIZATION=FALSE
!/NORMALIZATION_METHOD=
!/NORMALIZATION_METRIC=
!/NEGATEX=FALSE
/NEGATEY=TRUE
/NEGATEZ=TRUE
!/AXIS1=X
!/AXIS2=Y
!/AXIS3=Z
!/TREADMILL_DATA=FALSE
!/TREADMILL_DIRECTION=UNIT_VECTOR(0,1,0)
/TREADMILL_SPEED=0.0
```

### **Left Ankle Angle (single-segment)**

```
Compute_Model_Based_Data
/RESULT_NAME=LAnkle_Angle
/FUNCTION=JOINT_ANGLE
/SEGMENT=LMPF
/REFERENCE_SEGMENT=LSK
/RESOLUTION_COORDINATE_SYSTEM=
!/USE_CARDAN_SEQUENCE=FALSE
!/NORMALIZATION=FALSE
!/NORMALIZATION_METHOD=
!/NORMALIZATION_METRIC=
!/NEGATEX=FALSE
!/NEGATEY=FALSE
!/NEGATEZ=FALSE
!/AXIS1=X
!/AXIS2=Y
!/AXIS3=Z
!/TREADMILL_DATA=FALSE
!/TREADMILL_DIRECTION=UNIT_VECTOR(0,1,0)
!/TREADMILL_SPEED=0.0
```

### **Right Shank-Calc Angle (IOR)**

```
Compute_Model_Based_Data
/RESULT_NAME=RSha_Cal_Angle
/FUNCTION=JOINT_ANGLE
/SEGMENT=RCal
/REFERENCE_SEGMENT=RSK_2
/RESOLUTION_COORDINATE_SYSTEM=
!/USE_CARDAN_SEQUENCE=FALSE
!/NORMALIZATION=FALSE
!/NORMALIZATION_METHOD=
!/NORMALIZATION_METRIC=
/NEGATEX=TRUE
/NEGATEY=TRUE
!/NEGATEZ=FALSE
/AXIS1=Z
/AXIS2=X
/AXIS3=Y
!/TREADMILL_DATA=FALSE
!/TREADMILL_DIRECTION=UNIT_VECTOR(0,1,0)
!/TREADMILL_SPEED=0.0
```

### **Right Calc-Mid Angle (IOR)**

```
Compute_Model_Based_Data
/RESULT_NAME=RCal_Mid_Angle
/FUNCTION=JOINT_ANGLE
/SEGMENT=RMid
/REFERENCE_SEGMENT=RCal
/RESOLUTION_COORDINATE_SYSTEM=
!/USE_CARDAN_SEQUENCE=FALSE
!/NORMALIZATION=FALSE
!/NORMALIZATION_METHOD=
!/NORMALIZATION_METRIC=
/NEGATEX=TRUE
/NEGATEY=TRUE
!/NEGATEZ=FALSE
/AXIS1=Z
/AXIS2=X
/AXIS3=Y
!/TREADMILL_DATA=FALSE
!/TREADMILL_DIRECTION=UNIT_VECTOR(0,1,0)
!/TREADMILL_SPEED=0.0
```

### **Right Mid-Met Angle (IOR)**

```
Compute_Model_Based_Data
/RESULT_NAME=RMid_MetAngle
/FUNCTION=JOINT_ANGLE
/SEGMENT=RMe
/REFERENCE_SEGMENT=RMid
/RESOLUTION_COORDINATE_SYSTEM=
!/USE_CARDAN_SEQUENCE=FALSE
!/NORMALIZATION=FALSE
!/NORMALIZATION_METHOD=
!/NORMALIZATION_METRIC=
/NEGATEX=TRUE
/NEGATEY=TRUE
!/NEGATEZ=FALSE
/AXIS1=Z
/AXIS2=X
/AXIS3=Y
!/TREADMILL_DATA=FALSE
!/TREADMILL_DIRECTION=UNIT_VECTOR(0,1,0)
!/TREADMILL_SPEED=0.0
```

### **Right Calc-Met Angle (IOR)**

```
Compute_Model_Based_Data
/RESULT_NAME=RCal_Met_Angle
/FUNCTION=JOINT_ANGLE
/SEGMENT=RMet
/REFERENCE_SEGMENT=RCal
/RESOLUTION_COORDINATE_SYSTEM=
!/USE_CARDAN_SEQUENCE=FALSE
!/NORMALIZATION=FALSE
!/NORMALIZATION_METHOD=
!/NORMALIZATION_METRIC=
/NEGATEX=TRUE
/NEGATEY=TRUE
!/NEGATEZ=FALSE
/AXIS1=Z
/AXIS2=X
/AXIS3=Y
!/TREADMILL_DATA=FALSE
!/TREADMILL_DIRECTION=UNIT_VECTOR(0,1,0)
!/TREADMILL_SPEED=0.0
```

### **GRF (Force Platform 1: Right Foot)**

```
Compute_Model_Based_Data
/RESULT_NAME=FP1
/FUNCTION=GRF_DATA
/SEGMENT=RFT
/REFERENCE_SEGMENT=
/RESOLUTION_COORDINATE_SYSTEM=Virtual
Lab
!/USE_CARDAN_SEQUENCE=FALSE
/NORMALIZATION=TRUE
/NORMALIZATION_METHOD=DEFAULT_NORM
ALIZATION
!/NORMALIZATION_METRIC=
/NEGATEX=TRUE
!/NEGATEY=FALSE
!/NEGATEZ=FALSE
!/AXIS1=X
!/AXIS2=Y
!/AXIS3=Z
!/TREADMILL_DATA=FALSE
!/TREADMILL_DIRECTION=UNIT_VECTOR(0,1,0)
!/TREADMILL_SPEED=0.0
```

### **GRF (Force Platform 2: Left Foot)**

```
Compute_Model_Based_Data
/RESULT_NAME=FP2
/FUNCTION=GRF_DATA
/SEGMENT=LFT
/REFERENCE_SEGMENT=
/RESOLUTION_COORDINATE_SYSTEM=Virtual
Lab
!/USE_CARDAN_SEQUENCE=FALSE
/NORMALIZATION=TRUE
/NORMALIZATION_METHOD=DEFAULT_NORMALIZATION
!/NORMALIZATION_METRIC=
!/NEGATEX=FALSE
!/NEGATEY=FALSE
!/NEGATEZ=FALSE
!/AXIS1=X
!/AXIS2=Y
!/AXIS3=Z
!/TREADMILL_DATA=FALSE
!/TREADMILL_DIRECTION=UNIT_VECTOR(0,1,0)
!/TREADMILL_SPEED=0.0
```

### **Right Hip Moment**

```
Compute_Model_Based_Data
/RESULT_NAME=RHip_Moment
/FUNCTION=JOINT_MOMENT
/SEGMENT=RTH
/REFERENCE_SEGMENT=
/RESOLUTION_COORDINATE_SYSTEM=RPV
!/USE_CARDAN_SEQUENCE=FALSE
/NORMALIZATION=TRUE
/NORMALIZATION_METHOD=DEFAULT_NORMALIZATION
!/NORMALIZATION_METRIC=
/NEGATEX=TRUE
/NEGATEY=TRUE
/NEGATEZ=TRUE
!/AXIS1=X
!/AXIS2=Y
!/AXIS3=Z
!/TREADMILL_DATA=FALSE
!/TREADMILL_DIRECTION=UNIT_VECTOR(0,1,0)
!/TREADMILL_SPEED=0.0
```

### **Left Hip Moment**

```
Compute_Model_Based_Data
/RESULT_NAME=LHip_Moment
/FUNCTION=JOINT_MOMENT
/SEGMENT=LTH
/REFERENCE_SEGMENT=
/RESOLUTION_COORDINATE_SYSTEM=RPV
!/USE_CARDAN_SEQUENCE=FALSE
/NORMALIZATION=TRUE
/NORMALIZATION_METHOD=DEFAULT_NORMALIZATION
!/NORMALIZATION_METRIC=
/NEGATEX=TRUE
!/NEGATEY=FALSE
!/NEGATEZ=FALSE
!/AXIS1=X
!/AXIS2=Y
!/AXIS3=Z
!/TREADMILL_DATA=FALSE
!/TREADMILL_DIRECTION=UNIT_VECTOR(0,1,0)
!/TREADMILL_SPEED=0.0
```

### **Right Knee Moment**

```
Compute_Model_Based_Data
/RESULT_NAME=RKnee_Moment
/FUNCTION=JOINT_MOMT
/SEGMENT=R
/REFERENCE_SEGMENT=
/RESOLUTION_COORDINATE_SYSTEM=RTH
!/USE_CARDAN_SEQUENCE=FALSE
/NORMALIZATION=TRUE
/NORMALIZATION_METHOD=DEFAULT_NORMALIZATION
!/NORMALIZATION_METRIC=
!/NEGATEX=FALSE
!/NEGATEY=FALSE
/NEGATEZ=TRUE
!/AXIS1=X
!/AXIS2=Y
!/AXIS3=Z
!/TREADMILL_DATA=FALSE
!/TREADMILL_DIRECTION=UNIT_VECTOR(0,1,0)
!/TREADMILL_SPEED=0.0
```

### **Left Knee Moment**

```
Compute_Model_Based_Data
/RESULT_NAME=LKnee_Moment
/FUNCTION=JOINT_MOMENT
/SEGMENT=LSK
/REFERENCE_SEGMENT=
/RESOLUTION_COORDINATE_SYSTEM=LTH
!/USE_CARDAN_SEQUENCE=FALSE
/NORMALIZATION=TRUE
/NORMALIZATION_METHOD=DEFAULT_NORMALIZATION
!/NORMALIZATION_METRIC=
!/NEGATEX=FALSE
/NEGATEY=TRUE
!/NEGATEZ=FALSE
!/AXIS1=X
!/AXIS2=Y
!/AXIS3=Z
!/TREADMILL_DATA=FALSE
!/TREADMILL_DIRECTION=UNIT_VECTOR(0,1,0)
!/TREADMILL_SPEED=0.0
```

### **Right Ankle Moment**

```
Compute_Model_Based_Data
/RESULT_NAME=RAnkle_Moment
/FUNCTION=JOINT_MOMENT
/SEGMENT=RFT
/REFERENCE_SEGMENT=
/RESOLUTION_COORDINATE_SYSTEM=RSK
!/USE_CARDAN_SEQUENCE=FALSE
/NORMALIZATION=TRUE
/NORMALIZATION_METHOD=DEFAULT_NORMALIZATION
!/NORMALIZATION_METRIC=
/NEGATEX=TRUE
!/NEGATEY=FALSE
!/NEGATEZ=FALSE
!/AXIS1=X
!/AXIS2=Y
!/AXIS3=Z
!/TREADMILL_DATA=FALSE
!/TREADMILL_DIRECTION=UNIT_VECTOR(0,1,0)
!/TREADMILL_SPEED=0.0
```

### Left Ankle Moment

```
Compute_Model_Based_Data
/RESULT_NAME=LAnkle_Moment
/FUNCTION=JOINT_MOMENT
/SEGMENT=LFT
/REFERENCE_SEGMENT=
/RESOLUTION_COORDINATE_SYSTEM=LSK
!/USE_CARDAN_SEQUENCE=FALSE
/NORMALIZATION=TRUE
/NORMALIZATION_METHOD=DEFAULT_NORM
ALIZATION
!/NORMALIZATION_METRIC=
/NEGATEX=TRUE
/NEGATEY=TRUE
/NEGATEZ=TRUE
!/AXIS1=X
!/AXIS2=Y
!/AXIS3=Z
!/TREADMILL_DATA=FALSE
!/TREADMILL_DIRECTION=UNIT_VECTOR(0,1,0)
!/TREADMILL_SPEED=0.0
```

### Right Hip Power

```
Compute_Model_Based_Data
/RESULT_NAME=RHip_Moment
/FUNCTION=JOINT_MOMENT
/SEGMENT=RTH
/REFERENCE_SEGMENT=
/RESOLUTION_COORDINATE_SYSTEM=RPV
!/USE_CARDAN_SEQUENCE=FALSE
/NORMALIZATION=TRUE
/NORMALIZATION_METHOD=DEFAULT_NORM
ALIZATION
!/NORMALIZATION_METRIC=
/NEGATEX=TRUE
/NEGATEY=TRUE
/NEGATEZ=TRUE
!/AXIS1=X
!/AXIS2=Y
!/AXIS3=Z
!/TREADMILL_DATA=FALSE
!/TREADMILL_DIRECTION=UNIT_VECTOR(0,1,0)
!/TREADMILL_SPEED=0.0
```

### Left Hip Power

```
Compute_Model_Based_Data
/RESULT_NAME=LHip_Power
/FUNCTION=JOINT_POWER
/SEGMENT=LTH
/REFERENCE_SEGMENT=
/RESOLUTION_COORDINATE_SYSTEM=RPV
!/USE_CARDAN_SEQUENCE=FALSE
/NORMALIZATION=TRUE
/NORMALIZATION_METHOD=DEFAULT_NORM
ALIZATION
!/NORMALIZATION_METRIC=
!/NEGATEX=FALSE
!/NEGATEY=FALSE
!/NEGATEZ=FALSE
!/AXIS1=X
!/AXIS2=Y
!/AXIS3=Z
!/TREADMILL_DATA=FALSE
!/TREADMILL_DIRECTION=UNIT_VECTOR(0,1,0)
!/TREADMILL_SPEED=0.0
```

### Right Knee Power

```
Compute_Model_Based_Data
/RESULT_NAME=RKnee_Power
/FUNCTION=JOINT_POWE
/SEGMENT=RSK
/REFERENCE_SEGMENT
/RESOLUTION_COORDINATE_SYSTEM=RTH
!/USE_CARDAN_SEQUENC=FALSE
/NORMALIZATION=TRUE
/NORMALIZATION_METHOD=DEFAULT_NORM
ALIZATION
!/NORMALIZATION_METRIC=
!/NEGATEX=FALSE
!/NEGATEY=FALSE
!/NEGATEZ=FALSE
!/AXIS1=X
!/AXIS2=Y
!/AXIS3=Z
!/TREADMILL_DATA=FALSE
!/TREADMILL_DIRECTION=UNIT_VECTOR(0,1,0)
!/TREADMILL_SPEED=0.0
```

### Left Knee Power

```
Compute_Model_Based_Data
/RESULT_NAME=LKnee_Power
/FUNCTION=JOINT_POWER
/SEGMENT=LSK
/REFERENCE_SEGMENT=
/RESOLUTION_COORDINATE_SYSTEM=LTH
!/USE_CARDAN_SEQUENCE=FALSE
/NORMALIZATION=TRUE
/NORMALIZATION_METHOD=DEFAULT_NORM
ALIZATION
!/NORMALIZATION_METRIC=
!/NEGATEX=FALSE
!/NEGATEY=FALSE
!/NEGATEZ=FALSE
!/AXIS1=X
!/AXIS2=Y
!/AXIS3=Z
!/TREADMILL_DATA=FALSE
!/TREADMILL_DIRECTION=UNIT_VECTOR(0,1,0)
!/TREADMILL_SPEED=0.0
```

### Right Ankle Power

```
Compute_Model_Based_Data
/RESULT_NAME=RAnkle_Power
/FUNCTION=JOINT_POWER
/SEGMENT=RFT
/REFERENCE_SEGMENT=
/RESOLUTION_COORDINATE_SYSTEM=RSK
!/USE_CARDAN_SEQUENCE=FALSE
/NORMALIZATION=TRUE
/NORMALIZATION_METHOD=DEFAULT_NORM
ALIZATION
!/NORMALIZATION_METRIC=
!/NEGATEX=FALSE
!/NEGATEY=FALSE
!/NEGATEZ=FALSE
!/AXIS1=X
!/AXIS2=Y
!/AXIS3=Z
!/TREADMILL_DATA=FALSE
!/TREADMILL_DIRECTION=UNIT_VECTOR(0,1,0)
!/TREADMILL_SPEED=0.0
```

## Left Ankle Power

[Compute\\_Model\\_Based\\_Data](#)

```
/RESULT_NAME=LAnkle_Power  
/FUNCTION=JOINT_POWER  
/SEGMENT=LFT  
/REFERENCE_SEGMENT=  
/RESOLUTION_COORDINATE_SYSTEM=LSK  
!/USE_CARDAN_SEQUENCE=FALSE  
/NORMALIZATION=TRUE  
/NORMALIZATION_METHOD=DEFAULT_NORMALIZATION  
!/NORMALIZATION_METRIC=  
!/NEGATEX=FALSE  
!/NEGATEY=FALSE  
!/NEGATEZ=FALSE  
!/AXIS1=X  
!/AXIS2=Y  
!/AXIS3=Z  
!/TREADMILL_DATA=FALSE  
!/TREADMILL_DIRECTION=UNIT_VECTOR(0,1,0)  
!/TREADMILL_SPEED=0.0
```

## Recalc

[Recalc](#)

## Open Report Template

[Open\\_Report\\_Template](#)

```
!/REPORT_TEMPLATE=  
!/SET_PROMPT=Open report template
```

## File Save

[File\\_Save](#)

```
!/SET_PROMPT=Save CMO file
```

